Univerzita Hradec Králové
Přírodovědecká fakulta
Katedra biologie

Mitochondriální modulace pro studium neurodegenerace

Disertační práce

Autor:	Mgr. Michaela Hanzlová, rozená Vašková
Studijní program:	P1501 Biologie
Studijní obor:	Aplikovaná biologie a ekologie
Vedoucí práce:	prof. PharmDr. Kamil Musílek, Ph.D.
Odborný konzultant:	Mgr. Monika Schmidt, Ph.D.
	doc. RNDr. Lucie Zemanová, Ph.D.

Hradec Králové leden 2024

Univerzita Hradec Králové
Přírodovědecká fakulta

Zadání disertační práce

Autor:	**Mgr. Michaela Hanzlová**
Studium:	S23BI001DK
Studijní program:	P1501 Biologie
Studijní obor:	Aplikovaná biologie a ekologie
Název disertační práce:	**Mitochondriální modulace pro studium neurodegenerace**
Název disertační práce AJ:	Mitochondrial modulation to study a neurodegeneration

Cíl, metody, literatura, předpoklady:

Lidské mitochondriální enzymy 17β-HSD10 a CypD jsou považovány za potenciální cíle terapii neurodegenerativních onemocnění, zejména Alzheimerovy choroby, neboť přispívají k patologický procesům jako je buněčný stres vyvolaný amyloidem β a celková mitochondriální dysfunkce. Ovlivnění jejich enzymatické aktivity s využitím nízkomolekulárních inhibitorů se proto zdá být slibným přístupem ve výzkumu možné terapie těchto onemocnění.

V rámci disertační práce budou zavedeny a biochemicky charakterizovány fluorescenční metody pro stanovení enzymatické aktivity rekombinantních enzymů 17β-HSD10 a CypD, které zohledňují roli těchto enzymů v organismu. Pomocí zavedených metod bude studován inhibiční potenciál vybraných sloučenin na aktivitu cílových enzymů. Teplotní stabilita 17β-HSD10 a CypD bude studována pomocí diferenční skenovací fluorimetrie. Dále budou připraveny buněčné linie se zvýšenou expresí 17β-HSD10 pro testování nejúčinnějších inhibitorů *in cellulo*.

Lim, J. W.; Lee, J.; Pae, A. N. Mitochondrial Dysfunction and Alzheimer's Disease: Prospects for Therapeutic Intervention. *BMB Rep.* **2020**, *53* (1), 47–55. https://doi.org/10.5483/BMBRep.2020.53.1.279.

Benek, O.; Aitken, L.; Hroch, L.; Kuca, K.; Gunn-Moore, F.; Musilek, K. A Direct Interaction Between Mitochondrial Proteins and Amyloid-β Peptide and Its Significance for the Progression and Treatment of Alzheimer's Disease. *Curr. Med. Chem.* **2015**, *22* (9), 1056–1085. https://doi.org/10.2174/0929867322666150114163051.

Yang, S.-Y.; He, X.-Y.; Miller, D. Hydroxysteroid (17β) Dehydrogenase X in Human Health and Disease. *Mol. Cell. Endocrinol.* **2011**, *343* (1–2), 1–6. https://doi.org/10.1016/j.mce.2011.06.011.

Rao, V. K.; Carlson, E. A.; Yan, S. S. Mitochondrial Permeability Transition Pore Is a Potential Drug Target for Neurodegeneration. *Biochim. Biophys. Acta BBA - Mol. Basis Dis.* **2014**, *1842* (8), 1267–1272. https://doi.org/10.1016/j.bbadis.2013.09.003.

Haleckova, A.; Benek, O.; Zemanová, L.; Dolezal, R.; Musilek, K. Small-Molecule Inhibitors of Cyclophilin D as Potential Therapeutics in Mitochondria-Related Diseases. *Med. Res. Rev.* **2022**, *42* (5), 1822–1855. https://doi.org/10.1002/med.21892.

Zadávající pracoviště:	Katedra biologie, Přírodovědecká fakulta
Vedoucí práce:	prof. PharmDr. Kamil Musílek, Ph.D.
Datum zadání závěrečné práce:	23.1.2020

Prohlášení

Prohlašuji, že jsem disertační práci vypracovala samostatně a že jsem v seznamu použité literatury uvedla citace všech použitých zdrojů. Práce nebyla použita k získání jiného nebo stejného titulu.

V Hradci Králové, dne Mgr. Michaela Hanzlová

Poděkování

Ráda bych na tomto místě poděkovala svému školiteli prof. PharmDr. Kamilu Musílkovi, Ph.D. a odborným konzultantkám Mgr. Monice Schmidt, Ph.D. a doc. RNDr. Lucii Zemanové, Ph.D. Velice děkuji za odborné vedení a veškerou pomoc, trpělivost, cenné rady a předané zkušenosti, které provázely mé doktorské studium a byly stěžejním pilířem pro dokončení této práce.

Děkuji PharmDr. Ondřeji Benkovi, Ph.D. a Mgr. Markétě Sedláček Miškeříkové za návrh a syntézu testovaných sloučenin a za veškerou spolupráci při jejich *in vitro* evaluaci. Dále děkuji Mgr. Evě Kudové, Ph.D. a ÚOCHB za poskytnutí steroidních sloučenin a součinnost při přípravě publikace. Děkuji též RNDr. Lucii Vinklářové, Ph.D., na jejíž práci jsem mohla plynule navázat, a Mgr. Anetě Rotterové za týmovou spolupráci a za přátelské vztahy v našem týmu.

Též děkuji kolegům z Katedry chemie PřF UHK za jejich pomoc, podporu a vytvoření přátelského prostředí. Jsem vděčná za přátele, která jsem zde získala.

Chtěla bych velmi poděkovat svému mentorovi na zahraniční stáži na MedUni Wien Mag. Dr. Thomasu Steinkellnerovi, Ph.D. a celému jeho týmu za možnost uskutečnění této stáže a za vřelé přijetí a předání nových znalostí a zkušeností a též projektu Erasmus+ za její financování.

Dále děkuji za finanční podporu projektům Specifického výzkumu PřF UHK (SV 2105-2020; SV-2104-2021; SV-2103-2022; SV-2108-2023) a Projektu „Rozvoj interní grantové agentury Univerzity Hradec Králové“ (IGRA-TYM-2021002).

Závěrem bych chtěla velice poděkovat mým nejbližším – mé milované rodině, mému úžasnému manželovi a mým přátelům, kteří mi byli po celou dobu mého studia láskyplnou oporou, vždy mě podporovali a věřili ve mě.

Anotace

Hanzlová, M. *Mitochondriální modulace pro studium neurodegenerace*. Hradec Králové, 2024. Disertační práce na Přírodovědecké fakultě Univerzity Hradec Králové. Vedoucí disertační práce prof. PharmDr. Kamil Musílek, Ph.D. 70 s.

V předložené disertační práci je prezentován komentovaný soubor pěti experimentálních publikací, které jsou zaměřeny na studium mitochondriálních enzymů 17β-hydroxysteroiddehydrogenasy typu 10 (17β-HSD10) a cyklofilinu D (CypD). Práce je rozčleněna na teoretickou část a komentovaný přehled publikovaných prací.

Teoretická část práce se věnuje charakterizaci, fyziologické funkci a roli studovaných enzymů v rozvoji a progresi patofyziologických procesů spojených s Alzheimerovou chorobou (AD), neboť se má za to, že oba tyto enzymy přispívají k patologiím pozorovaným u AD jako je poškození mitochondrií a buněčný stres. Za jeden z potenciálních přístupů při vývoji nové terapie AD se považuje inhibice jejich enzymatické aktivity, která je hlavním předmětem studia předkládané práce.

Komentovaný přehled publikovaných prací je strukturován jako soubor pěti komentářů shrnujících klíčové poznatky a získané experimentální výsledky dílčích původních publikací vztahujících se k této disertační práci. Publikace jsou věnovány studiu enzymatické aktivity rekombinantních enzymů 17β-HSD10 a CypD a jejich inhibice, přičemž jedna publikace je tematicky zaměřena na CypD a čtyři publikace jsou zaměřeny na 17β-HSD10.

Klíčová slova

17β-hydroxysteroiddehydrogenasa typu 10, cyklofilin D, Alzheimerova choroba, mitochondrie, 17β-estradiol, allopregnanolon, inhibitory, vztah struktura-aktivita

Annotation

Hanzlova, M. *Mitochondrial modulation to study a neurodegeneration*. Hradec Kralove, 2024. Dissertation thesis at the Faculty of Science of the University of Hradec Kralove. Supervisor prof. Kamil Musilek, Ph.D. 70 p.

The dissertation is designed as an annotated collection of five experimental publications that focus on the study of mitochondrial enzymes 17β-hydroxysteroid dehydrogenase type 10 (17β-HSD10) and cyclophilin D (CypD). The thesis is divided into a theoretical part and an annotated review of the published articles.

The theoretical part of the thesis deals with the characterization, physiological function, and role of the studied enzymes in the development and progression of the pathophysiological processes associated with Alzheimer's disease (AD), as both enzymes are thought to contribute to pathologies observed in AD such as mitochondrial damage and cellular stress. The main focus of the thesis is the inhibition of the enzymatic activity of these enzymes, which is considered to be one of the potential approaches in the development of new AD therapy.

The annotated review of published papers is structured as a set of five commentaries summarizing the key findings and experimental results obtained in the original publications related to this dissertation. The publications focus on the study of the enzymatic activity of the recombinant enzymes 17β-HSD10 and CypD and their inhibition, with one publication thematically focused on CypD and four publications focused on 17β-HSD10.

Keywords

17β-hydroxysteroid dehydrogenase type 10, cyclophilin D, Alzheimer's disease, mitochondria, 17β-estradiol, allopregnanolone, inhibitors, structure-activity relationship

Seznam použitých zkratek

(−)-CHANA	cyklohexenyl aminonaftalen alkohol
17β-HSD10	17β-hydroxysteroiddehydrogenasa typu 10
AAC	acetoacetyl-CoA
Aβ	amyloid β
ABAD	amyloid β vázající alkoholdehydrogenasa
AD	Alzheimerova choroba
ALLOP	allopregnanolon
APP	amyloidový prekurzorový protein
ATP	adenosintrifosfát
CoA	koenzym A
CsA	cyklosporin A
CypA	cyklofilin A
CypD	cyklofilin D
DSF	diferenční skenovací fluorimetrie
E2	17β-estradiol
FDA	Úřad pro kontrolu potravin a léčiv v USA
GABA	kyselina γ-aminomáselná
HEK293	lidská buněčná linie odvozená z embryonálních buněk ledvin
HEK293-17β-HSD10	buněčná linie HEK293 s nadměrnou expresí 17β-HSD10
IC_{50}	poloviční inhibiční koncentrace
K_d	disociační konstanta
kDa	kilodalton
K_i	inhibiční konstanta
K_m	Michaelisova konstanta
miRNA	mikro ribonukleová kyselina
mPTP	mitochondriální pór přechodné propustnosti
MRPP	protein mitochondriální RNasy P
NAD^+/NADH	nikotinamidadenindinukleotid oxidovaná/redukovaná forma
RNasa	ribonukleasa
ROS	reaktivní formy kyslíku
SAR	vztah struktura-aktivita
SDR	dehydrogenasa/reduktasa s krátkým řetězcem
SH-SY5Y	lidská neuroblastomová buněčná linie
Tg mAPP/ABAD	transgenní zvířecí model s nadměrnou expresí mutantní formy lidského APP a 17β-HSD10, resp. ABAD
tRNA	transferová ribonukleová kyselina
V_{max}	maximální rychlost reakce

Obsah

1 Úvod 9
2 Cíle práce 10
3 Teoretická část 11
3.1 Neurodegenerace a Alzheimerova choroba 11
3.2 Mitochondrie a AD 11
3.3 Mitochondriální enzym 17β-HSD10 14
3.3.1 Struktura, lokalizace a exprese 17β-HSD10 14
3.3.2 Fyziologická funkce 17β-HSD10 15
3.4 Role 17β-HSD10 v AD 17
3.4.1 Interakce 17β-HSD10 s Aβ 17
3.4.2 Nadměrná exprese 17β-HSD10 a homeostasa E2 a ALLOP při AD 19
3.4.3 Inhibice enzymatické aktivity 17β-HSD10 22
3.5 Mitochondriální enzym CypD 25
3.5.1 Fyziologická funkce CypD 25
3.6 CypD jako terapeutický cíl AD 26
3.6.1 Inhibice enzymatické aktivity CypD 28
4 Komentáře k publikovaným pracím 31
4.1 Metoda využívající znovusložení RNasy T1 pro stanovení aktivity mitochondriálního cyklofilinu D: Nová *in vitro* metoda použitelná při výzkumu a vývoji léčiv 32
4.2 Vývoj submikromolárních inhibitorů 17β-HSD10 a jejich *in vitro* a *in vivo* hodnocení 35
4.3 Fyziologicky relevantní fluorescenční metoda pro identifikaci inhibitorů 17β-HSD10 37
4.4 Nanomolární inhibitory 17β-HSD10 na bázi benzothiazolylových derivátů s bioaktivitou v buněčném prostředí 40
4.5 C-3 steroidní hemiestery jako inhibitory 17β-HSD10 43
5 Seznam publikovaných prací 46
5.1 Seznam publikací vztahujících se k disertační práci 46
5.2 Seznam publikací nevztahujících se k disertační práci 48
6 Závěr 49
7 Seznam použité literatury 50
8 Příspěvky na konferencích 67
8.1 Přednášky 67
8.2 Posterová sdělení 67
9 Účast na projektech a stážích 69
10 Přílohy 70

1 Úvod

Alzheimerova choroba (AD) je nejčastější formou demence a s rostoucím věkem populace se předpokládá značný nárůst pacientů s tímto onemocněním. V současnosti je dostupná zejména symptomatická léčba této nemoci, přičemž nejnovější terapeutická strategie využívající jako léčiva monoklonální protilátky proti amyloidu β (Aβ) dosud nebyla v Evropě kvůli kontroverzním výsledkům schválena, proto je vývoj efektivní terapie aktuální a potřebný (Cummings et al., 2023, 2022; GBD 2019 Dementia Forecasting Collaborators, 2022; Rayathala et al., 2022). Při vývoji účinné terapie je nicméně zásadní výzkum patřičných molekulárních cílů a výběr vhodných metod a modelových systémů pro testování a design nových sloučenin s terapeutickým potenciálem.

Mitochondriální enzymy 17β-hydroxysteroiddehydrogenasa typu 10 (17β-HSD10) a cyklofilin D (CypD) studované v rámci této disertační práce jsou považovány za potenciální terapeutické cíle AD, neboť různou mírou a různými mechanismy přispívají k patologiím pozorovaným u AD, jako je mitochondriální dysfunkce a buněčný stres vyvolaný Aβ. V posledních letech je proto věnována pozornost výzkumu a objasnění jejich rolí v tomto progresivním neurodegenerativním onemocnění (Benek et al., 2015; Lim et al., 2020).

Předkládaná práce je věnována studiu enzymatické aktivity rekombinantních enzymů 17β-HSD10 a CypD a jejich inhibice, s větším důrazem na 17β-HSD10. Pro tento účel byly v rámci disertační práce zavedeny a optimalizovány metody pro stanovení enzymatické aktivity obou studovaných enzymů využívající přirozenější substráty a reakční podmínky než v minulosti využívané metody. Pomocí těchto *in vitro* metod byl studován inhibiční potenciál vybraných sloučenin na aktivitu cílových enzymů.

2 Cíle práce

Hlavním cílem předkládané práce bylo testování a *in vitro* hodnocení inhibičního potenciálu vybraných sloučenin, které ovlivňují enzymatickou aktivitu 17β-HSD10 a CypD, s využitím fyziologicky relevantních metod pro stanovení enzymatické aktivity těchto enzymů.

Dílčí cíle:

- exprese a purifikace rekombinantních enzymů 17β-HSD10 a CypD
- zavedení, optimalizace a charakterizace metod pro stanovení enzymatické aktivity 17β-HSD10 a CypD
- screening sloučenin s inhibičním potenciálem vůči 17β HSD10 a CypD
- charakterizace nejsilnějších inhibitorů, tj. stanovení koncentrace inhibitoru snižující aktivitu enzymu o 50 % (IC_{50}) a typu inhibice
- studium stability 17β-HSD10 a CypD pomocí diferenční skenovací fluorimetrie (DSF)
- příprava monoklonální buněčné linie HEK293 (lidská buněčná linie odvozená z embryonálních buněk ledvin) s nadměrnou expresí 17β-HSD10 (HEK293-17β-HSD10)

3 Teoretická část

3.1 Neurodegenerace a Alzheimerova choroba

Neurodegenerativní onemocnění jsou charakterizována progresivním úbytkem neuronů v důsledku jejich dysfunkce či odumírání, což vede k postižení kognitivních a/nebo motorických funkcí (Dugger a Dickson, 2017). Souhrnné označení pro neurodegenerativní onemocnění s převahou postižení kognitivních funkcí je demence. Neurodegenerativní onemocnění jsou s rostoucím věkem populace stále častější a do roku 2050 se předpokládá téměř trojnásobný nárůst prevalence demence v populaci (GBD 2019 Dementia Forecasting Collaborators, 2022).

Mezi nejčastější formy demence patří AD. Toto progresivní onemocnění vedoucí k nevratnému poškození mozku je v počátečních fázích doprovázené poruchami paměti, následně nastupují kognitivní změny a změny chování. Na ztrátě synaptických funkcí a rozvoji neurodegenerativních změn se podílí dva klíčové patologické znaky – hromadění extracelulárních plaků Aβ a intracelulárních neurofibrilárních spletí hyperfosforylovaného proteinu tau. Onemocnění dále doprovází metabolické, cévní a zánětlivé změny a další komorbidní patologie. V současné době jsou dostupná pouze symptomatická léčiva, která přinášejí krátkodobou a omezenou úlevu od symptomů AD a obvykle se podávají jako paliativní léčba s cílem zpomalit zhoršování kvality života, proto je vývoj účinné terapie AD aktuální, nutný a společensky potřebný (Du et al., 2018; Soria Lopez et al., 2019; Weller a Budson, 2018; Zhang et al., 2021).

3.2 Mitochondrie a AD

Mitochondrie jsou esenciální pro řadu buněčných funkcí. Kromě ústřední role v produkci energie, díky níž se mitochondriím často přezdívá buněčné elektrárny, mají tyto organely zásadní význam v metabolismu mastných kyselin a aminokyselin, udržování homeostasy Ca^{2+} a regulaci apoptosy (Osellame et al., 2012). Neurony jsou na mitochondriích závislé v řadě základních procesů včetně produkce energie ve formě ATP prostřednictvím oxidativní fosforylace, která je však i hlavním zdrojem vzniku reaktivních forem kyslíku (ROS) (Lopez Sanchez et al., 2016). Mitochondrie se též významně podílejí na komplexní regulaci synaptické plasticity a udržení základní funkce synapsí jako takových, a to zejména díky produkci ATP a udržování hladiny Ca^{2+} (Kang et al., 2008; Tang et al., 2019).

S řadou neurodegenerativních onemocnění včetně AD je spojena mitochondriální dysfunkce (Lionaki et al., 2015; Pei a Wallace, 2018). U AD je tato

dysfunkce obvykle připisována zvýšeným hladinám Aβ a obecně se projevuje snížením oxidativní fosforylace, a tím i produkce ATP, zvýšením produkce ROS, narušením homeostasy Ca^{2+} a změnami v morfologii a dynamice mitochondrií. Nadměrná produkce ROS následně vede k poškození membrán v důsledku peroxidace lipidů a následné indukci apoptosy (Afsar et al., 2023; Luque-Contreras et al., 2014) (Obr. 1). Konkrétně byly v mozcích pacientů s AD v průběhu let nalezeny poruchy jako je snížená aktivita a/nebo hladina pyruvátdehydrogenasového komplexu (Sang et al., 2022; Sheu et al., 1985; Sorbi et al., 1983) a α-ketoglutarátdehydrogenasy (Butterworth a Besnard, 1990; Mastrogiacomo et al., 1993; Sang et al., 2022), deficit komplexů I a IV dýchacího řetězce (Holper et al., 2019; Kim et al., 2001; Parker et al., 1994, 1990), výrazná redoxní nerovnováha spojená s narušenou antioxidační ochranou mozku (Fracassi et al., 2021) a snížená mitofagie (Fang et al., 2019). Nálezy u pacientů byly následně potvrzeny i experimentálně s využitím buněčných modelů AD, tzv. cybridního modelu (Khan et al., 2000; Swerdlow, 2007) a neuronů odvozených od indukovaných pluripotentních kmenových buněk pacientů trpících AD (Flannagan et al., 2021), u nichž byly pozorovány patologické změny jako je snížená pohyblivost a velikost mitochondrií, snížená aktivita dýchacího řetězce (zejména komplexu IV), zvýšený oxidační stres, snížený membránový potenciál a mitofagie, a také zvýšená produkce Aβ. Obdobné poškození mitochondriální funkce bylo u pozorováno i u myších modelů AD (Dragicevic et al., 2010; Du et al., 2010). Mnoho výzkumných skupin navíc poukazuje na to, že toxicita vyvolaná Aβ se prohlubuje souběžně s mitochondriální dysfunkcí a celý proces ústí do začarovaného kruhu, který vede k aktivaci mnoha různých mechanismů přispívajících k neurodegeneraci (Fišar, 2022; Silva et al., 2011; Swerdlow et al., 2010; Yao et al., 2011a) (Obr. 1).

V mitochondriální matrix může Aβ interagovat s různými molekulárními cíli a měnit tak jejich fyziologické funkce, což může přispívat k mitochondriální dysfunkci a rozvoji AD (Benek et al., 2015). Mezi interakční partnery Aβ patří i enzymy 17β-HSD10 a CypD (Benek et al., 2015; Du et al., 2008; Yan et al., 1997). Tyto enzymy jsou spolu pravděpodobně schopné interagovat (Carlson et al., 2015) a jsou považovány za potenciální terapeutické cíle AD (Benek et al., 2015; Haleckova et al., 2022; He et al., 2022). Inhibice interakce s Aβ a/nebo inhibice enzymatické aktivity těchto enzymů pomocí selektivních inhibitorů se považuje za jeden z možných přístupů k terapii AD. Předkládaná práce byla věnována studiu enzymatické aktivity těchto dvou enzymů a její inhibice, s větším důrazem na studium 17β-HSD10.

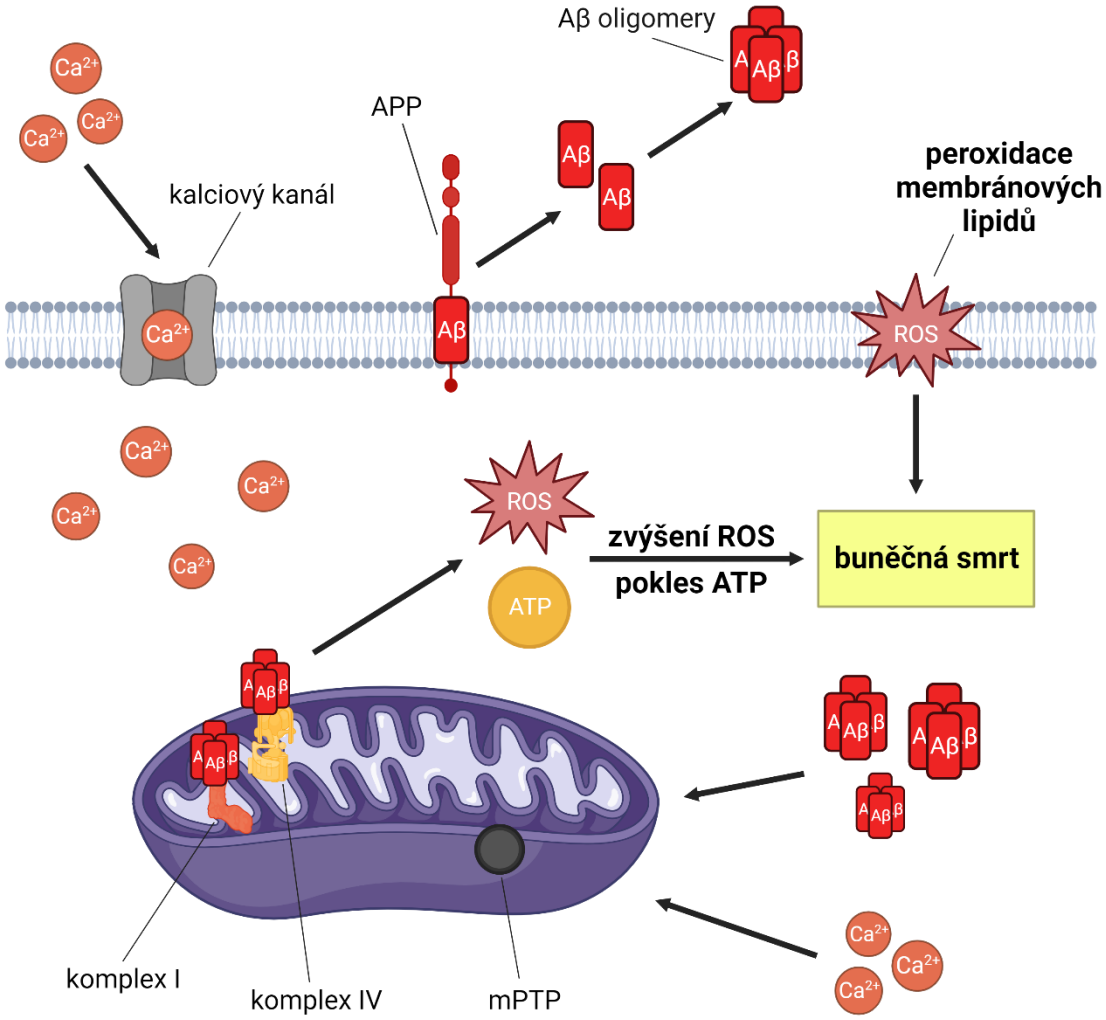

Obr. 1: *Poškození mitochondrie u Alzheimerovy choroby. Nadprodukce amyloidu β (Aβ), který je štěpným produktem amyloidového prekurzorového proteinu (APP), způsobuje dysfunkci komplexů I a IV dýchacího řetězce, což vede ke zvýšené produkci reaktivních forem kyslíku (ROS) a poklesu ATP. Deplece ATP způsobuje dysfunkci iontových kanálů závislých na ATP, čímž dochází k narušení iontové rovnováhy v cytosolu. Zvýšení ROS vede k otevření mitochondriálního póru přechodné propustnosti (mPTP), což umožňuje vstup Ca^{2+} do matrix mitochondrií a dochází ke zvýšenému poškození dýchacího řetězce a oxidativní fosforylace. Nadprodukce ROS má též za následek poškození membrán v důsledku peroxidace lipidů a spuštění apoptosy. Vytvořeno v BioRender.com podle* (Luque-Contreras et al., 2014).

3.3 Mitochondriální enzym 17β-HSD10

Lidská 17β-HSD10 (UniProt: Q99714) je multifunkční mitochondriální enzym, který katalyzuje přeměnu celé řady substrátů, mezi něž patří mastné kyseliny, alkoholy a steroidy (Yang et al., 2005). Díky své výše zmíněné schopnosti vázat Aβ je tento enzym v literatuře často označován též jako amyloid β vázající alkoholdehydrogenasa (ABAD) (Yan et al., 1999), přičemž tento název přímo implikuje jeho spojitost s AD, v souvislosti s níž je dosud také nejvíce diskutován. Kromě toho je 17β-HSD10 spojována i s dalšími onemocněními, konkrétně se jedná o Parkinsonovu chorobu (Tieu et al., 2004) a některé typy nádorových onemocnění, zejména rakovinu prostaty a s ní spojené metastasy do kostí (He et al., 2003; Jernberg et al., 2013). Vzhledem k jeho multifunkčnosti a zapojení do mnoha buněčných procesů se přepokládá, že tento enzym hraje důležitou roli v udržení homeostasy neurosteroidů, strukturní a funkční integritě mitochondrií, a také v buněčné stresové odpovědi (Rauschenberger et al., 2010; Yan et al., 2000; Yan a Stern, 2005).

3.3.1 Struktura, lokalizace a exprese 17β-HSD10

Lidský gen *HSD17B10* kódující protein 17β-HSD10 je mapován na chromosomu Xp11.2. Tento gen je složen ze šesti exonů a pěti intronů, přičemž první tři exony kódují *N*-koncovou oblast proteinu s vazebným místem pro kofaktor NAD^+, tzv. Rossmanův záhyb, a zbylé exony kódují *C*-koncovou oblast s katalytickými residui pro vazbu substrátu obsahující tzv. katalytickou triádu aminokyselin (Ser155, Tyr168, Lys172) (He et al., 1998; Kissinger et al., 2004). Strukturně 17β-HSD10 tvoří homotetramer s celkovou molekulovou hmotností 108 kDa a každá jeho podjednotka se skládá z 261 aminokyselinových zbytků (He et al., 1998) (Obr. 2). 17β-HSD10 patří do nadrodiny dehydrogenas/reduktas s krátkým řetězcem (SDR), čemuž napovídá její nomenklaturní název SDR5C1. S ostatními členy SDR sdílí některé strukturní podobnosti, jako je přítomnost domény s Rossmanovým záhybem či podobná velikost (Persson a Kallberg, 2013). Je však jediným zástupcem této nadrodiny, který ve své struktuře nese jedinečnou sekvenci aminokyselin označovanou jako smyčka D, díky níž je schopen vázat Aβ (Lustbader et al., 2004).

17β-HSD10 je lokalizována v mitochondriální matrix (He et al., 1999; Shafqat et al., 2003) a je exprimována ve všech typech lidských tkání včetně mozku (Yan et al., 1997), kde se její exprese zdá být specifická pro určité oblasti, přičemž nejvyšší hladiny byly nalezeny v hypotalamu, hipokampu a amygdale (He et al., 2005a). Optimální hladina 17β-HSD10 je považována za nutnou pro správný vývoj

mozku, a to zejména kvůli udržení rovnováhy metabolismu neurosteroidů (Yang et al., 2009). Úplná ztráta tohoto proteinu je u člověka pravděpodobně neslučitelná se životem (Zschocke, 2012), neboť kompletní inaktivace genu pro 17β-HSD10 vedla u octomilek (*Drosophila melanogaster*) (Torroja et al., 1998) a drápatek (*Xenopus laevis*) (Rauschenberger et al., 2010) k embryonální letalitě.

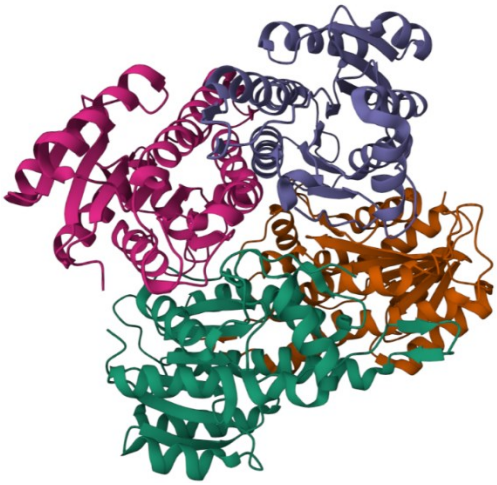

Obr. 2: *Krystalová struktura homotetrameru 17β-HSD10 s barevně odlišenými podjednotkami. Převzato z RCSB PDB (RCSB.org), PDB ID: 1U7T* (Kissinger et al., 2004).

3.3.2 Fyziologická funkce 17β-HSD10

Z hlediska enzymové aktivity je 17β-HSD10 klasifikována pod číslem EC 1.1.1.178 a řadí se to třídy NAD^+-dependentních oxidoreduktas. Z jejího názvu je patrné, že patří do skupiny 17β-hydroxysteroiddehydrogenas, které katalyzují redoxní reakce v pozici C17β steroidního kruhu C_{18}- a C_{19}-steroidů, při nichž dochází ke konverzi hydroxyskupiny na ketoskupinu a naopak, čímž se podílejí na jejich aktivaci a inaktivaci (He et al., 1998; Moeller a Adamski, 2006). Kromě dehydrogenace 17β-OH skupiny estrogenů katalyzuje 17β-HSD10 také dehydrogenaci 3α-OH androgenů a účastní se oxidace hydroxyacyl-CoA v metabolismu mastných kyselin (He et al., 2000b, 2000a, 1999) (Obr. 3). Navzdory četným zavádějícím označením 17β-HSD10 jako alkoholdehydrogenasy (viz alternativní název ABAD) byla tato její aktivita vůči jednoduchým alkoholům v posledních letech označena spíše za zanedbatelnou nebo zcela zpochybněna (He et al., 2023; Yang et al., 2014). V katabolickém metabolismu má 17β-HSD10 významnou funkci ve třetím kroku β-oxidace mastných kyselin s krátkým rozvětveným řetězcem při přeměně L-3-hydroxyacyl-CoA na 3-ketoacyl-CoA

(He et al., 1998; Powell et al., 2000), která je jedním z dílčích kroků degradace isoleucinu, při níž katalyzuje oxidaci 2-methyl-3-hydroxybutyryl-CoA na 2-methyl-acetoacetyl-CoA (Luo et al., 1995). Míra důležitosti a celkové zapojení tohoto enzymu v metabolismu ketolátek je kontroverzní (He et al., 2023), nicméně při jeho deficitu je pozorováno hromadění degradačních produktů tiglylglycinu a 2-methyl-3-hydroxybutyryl-CoA (Zschocke et al., 2000). Zásadní význam má však v metabolismu pohlavních hormonů a neuroaktivních steroidů, kde katalyzuje oxidaci 17β-estradiolu (E2) na estron, allopregnanolonu (ALLOP) na 5α-dihydroprogesteron a 3α-androstandiolu na 5α-dihydrotestosteron (Obr. 3) (He et al., 2000b; Shafqat et al., 2003; Yang et al., 2009).

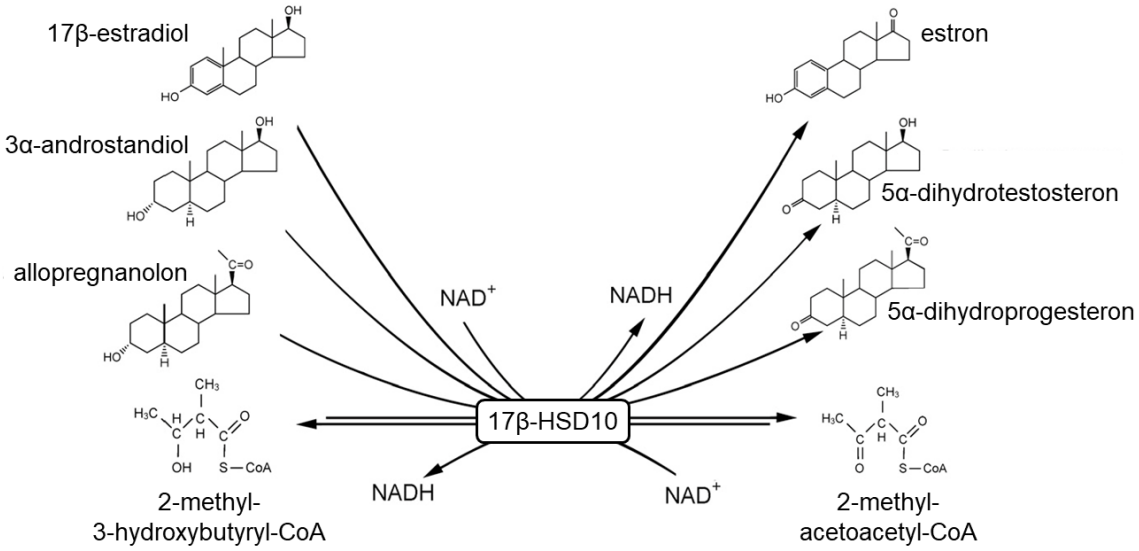

Obr. 3: *Důležité reakce katalyzované lidskou 17β-HSD10. Převzato a upraveno* (Yang et al., 2011).

Kromě enzymatické funkce má 17β-HSD10 také strukturní funkci. Bylo zjištěno, že její neenzymatická funkce je nezbytná pro strukturní a funkční integritu mitochondrií a celkové přežití buňky (Rauschenberger et al., 2010). 17β-HSD10 je také jedním ze tří proteinů tvořících plně funkční komplex mitochondriální ribonukleasy P (RNasa P, EC 3.1.26.5), která je zodpovědná za štěpení 5' konce prekurzorů tRNA (Holzmann et al., 2008). Tento komplex se skládá z tRNA methyltransferasy (MRPP1, protein mitochondriální RNasy P č. 1) a 17β-HSD10 (zde označován jako MRPP2), které spolu tvoří stabilní komplex, na nějž se slabými interakcemi váže Mg^{2+}-dependentní metalonukleasa (MRPP3) (Holzmann et al., 2008; Oerum et al., 2018). Existuje hypotéza, že by narušení aktivity RNasy P

v důsledku akumulace Aβ mohlo ovlivnit translaci a expresi mitochondriálních proteinů, a tím i oxidativní fosforylaci, což by mohlo mít za následek oxidativní stres, mitochondriální dysfunkci a smrt neuronálních buněk (Holzmann a Rossmanith, 2009). Tato hypotéza byla podpořena buněčným modelem, na kterém bylo pozorováno, že hladina 17β-HSD10 je důležitá pro udržení normální hladiny MRPP1 a zachování jejich subkomplexu, přičemž úplná ztráta 17β-HSD10 vedla k poruše zpracování mitochondriálních prekurzorových transkriptů a mitochondriální dysfunkci (Deutschmann et al., 2014).

Vzhledem k výše zmíněným rozmanitým fyziologickým funkcím se 17β-HSD10 řadí do skupiny multifunkčních proteinů označovaných jako tzv. „moonlighting proteins“. Tyto proteiny vykazují více fyziologicky relevantních biochemických či biofyzikálních funkcí najednou a mohou se účastnit více biochemických procesů, ale zároveň bývají často spojeny s různými onemocněními (Jeffery, 2018, 1999). Tato charakteristika zcela odpovídá vlastnostem 17β-HSD10 a je tedy zřejmé, že je její enzymatická i strukturní funkce spolu s její optimální hladinou významná pro udržení homeostasy celé řady fyziologických molekul a správnou regulaci mnoha biochemických i biologických dějů odehrávajících se v buňce.

3.4 Role 17β-HSD10 v AD

Jak již bylo zmíněno, 17β-HSD10 je jedním z potenciálních terapeutických cílů u AD. V literatuře bylo v průběhu let diskutováno několik možných důvodů, proč tento enzym přispívá k mitochondriální dysfunkci a patofyziologii pozorované u AD, přičemž za dva klíčové kritické faktory je považována jeho interakce s Aβ a jeho zvýšená exprese, která byla pozorována v mozcích pacientů s AD i v experimentálních modelech. Zdá se navíc pravděpodobné, že jsou spolu tyto dva faktory úzce propojené (Benek et al., 2015; He et al., 2005; Lustbader et al., 2004; Yan et al., 1997; Yan a Stern, 2005).

3.4.1 Interakce 17β-HSD10 s Aβ

Vazebná interakce 17β-HSD10 a Aβ byla poprvé popsána pomocí kvasinkového dvouhybridního screeningu, avšak v té době byla 17β-HSD10 ještě mylně považována za protein asociovaný s endoplasmatickým retikulem (viz její nesprávné označení ERAB) (Yan et al., 1997). Její lokalizace v mitochondrii byla odhalena až o pár let později (He et al., 2001) a následně byla v mitochondriích mozků pacientů s AD i u myšího modelu potvrzena i její kolokalizace s Aβ (Lustbader et al., 2004).

Interakce 17β-HSD10 a Aβ je vysoce specifická a byla detekována již při nanomolární koncentraci Aβ ($K_d \approx 40–70$ nM), avšak k inhibici enzymatické aktivity 17β-HSD10 dochází až při jeho mikromolární koncentraci: $K_i \approx 1{,}6$ μM pro acetoacetyl-CoA (AAC) a $K_i \approx 3{,}2$ μM pro E2 (Yan et al., 1999). V průběhu dalších let byla ověřena i již dříve navrhovaná domněnka, že oligomerní forma Aβ (Yan et al., 2007), jako makromolekula větší než samotný monomer, deformuje enzym 17β-HSD10 a narušuje tak jeho funkci, neboť vazbou agregátů Aβ na 17β-HSD10 dochází k výraznému narušení katalytické triády aminokyselin a vazebné kapsy pro kofaktor NAD^+, přičemž současná vazba Aβ a NAD^+ na enzym se vzájemně vylučuje (Lustbader et al., 2004; Yan et al., 2007). Vazba peptidů Aβ (1–42, 1–40 a 1–20) na 17β-HSD10 je závislá na dávce (Lustbader et al., 2004) a pro inhibici 17β-HSD10 jsou rozhodující residua 14–24 $Aβ_{40}$, (Oppermann et al., 1999), což bylo podpořeno i pozorováním, že peptid Aβ(25–35) nevykazoval specifickou vazbu na 17β-HSD10 (Lustbader et al., 2004).

V průběhu let byla u buněčných a myších modelů pozorována řada škodlivých důsledků interakce 17β-HSD10 a Aβ vedoucích k mitochondriální toxicitě a dysfunkci, které jsou charakteristické pro AD (Lustbader et al., 2004; Oppermann et al., 1999; Takuma et al., 2005; Yan et al., 1999, 1997; Yan a Stern, 2005). Obecně byly nejčastěji pozorovány projevy mitochondriální dysfunkce jako je oxidační stres a zvýšená hladina ROS, snížená aktivita komplexu IV dýchacího řetězce a tím i hladina ATP, uvolňování laktátdehydrogenasy a cytochromu c z mitochondrií, fragmentace DNA a zvýšená apoptosa. Transgenní myši s nadměrnou expresí mutantní formy lidského amyloidového prekurzorového proteinu (APP) a 17β-HSD10 (Tg mAPP/ABAD) vykazovaly též kognitivní změny jako jsou poruchy prostorové i časové paměti a neschopnost efektivního učení (Lustbader et al., 2004; Takuma et al., 2005). Zdá se, že v rozvoji cytotoxicity způsobené Aβ hraje klíčovou roli enzymatická aktivita 17β-HSD10, neboť neaktivní mutantní enzym toxicitu Aβ nezvýšil, a to i navzdory stejné vazebné afinitě Aβ vůči nemutované i mutované formě 17β-HSD10 (Yan et al., 1999).

V mozcích pacientů s AD a Tg mAPP/ABAD myší byla též zjištěna zvýšená exprese endofilinu I (Ren et al., 2008) a peroxiredoxinu II (Yao et al., 2007), která vzniká v důsledku interakce Aβ a 17β-HSD10 a může tak sloužit jako její indikátor. Endofilin I hraje důležitou roli v regulaci endocytosy synaptických vezikul (Zhang et al., 2015) a jeho zvýšené hladiny v neuronech vedou k aktivaci stresové c-Jun *N*-terminální kinasy a následné buněčné smrti (Ren et al., 2008), umlčení jeho exprese naopak zabraňuje synaptické dysfunkci vyvolané Aβ (Yin et al., 2019). Peroxiredoxin II je antioxidační enzym, který redukuje hladinu peroxidů v buňce a jeho zvýšená exprese se zdá být ochrannou reakcí neuronů před oxidačním

poškozením v přítomnosti Aβ (Yao et al., 2007). Kromě toho tento protein pomáhá zachovávat hipokampální synaptickou plasticitu (Kim et al., 2011) a jeví se jako potenciální biomarker pro diagnostiku AD (Yoshida et al., 2009).

Zabránění interakci Aβ a 17β-HSD10 či její prevence má pozitivní vliv na mitochondriální funkci a buněčný stres vyvolaný Aβ a považuje se proto za jeden z možných terapeutických přístupů pro léčbu AD (Lustbader et al., 2004; Yao et al., 2011b). Dosud bylo publikováno několik inhibitorů vazby 17β-HSD10-Aβ, mezi než patří tzv. návnadový peptid, který je mimetikem smyčky D zodpovědné za vazbu Aβ (Lustbader et al., 2004), a jeho stabilnější varianta fúzovaná s Tat doménou a mitochondriální sekvencí (Yao et al., 2007). Dále byly *in silico* designovány dva účinné nepeptidové inhibitory mimikující pouze residua smyčky D klíčová pro vznik vazby 17β-HSD10-Aβ (Tyr101, Thr108, Thr110), sloučeniny VC15 a VC19 (Viswanath et al., 2017). Ze skupiny nízkomolekulárních inhibitorů prokázaly nejvyšší inhibici sloučeniny **5h** a **5l** publikované Xie et al., které patří do skupiny benzothiazolyl močovinových derivátů (Xie et al., 2006), a dále allopurinolový derivát s označením **14b** a hodnotou IC_{50} 0,74 μM odvozený od významného inhibitoru enzymatické aktivity 17β-HSD10 s názvem AG18051 (Obr. 4). Tento derivát prokázal schopnost obnovit sníženou životaschopnost buněk a mitochondriální dysfunkci vyvolanou $Aβ_{42}$ u neuroblastomové buněčné linie SH-SY5Y a u primárních kortikálních neuronů získaných z transgenních myších modelů měl též pozitivní vliv na mitochondriální metabolismus a morfologii (Morsy et al., 2022).

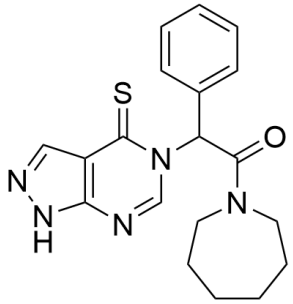

Obr. 4: *Struktura inhibitoru AG18051* (Kissinger et al., 2004).

3.4.2 Nadměrná exprese 17β-HSD10 a homeostasa E2 a ALLOP při AD

Přirozeným kompenzačním nebo možným sekundárním mechanismem pro překonání inhibice 17β-HSD10 v důsledku interakce s Aβ se zdá být její nadměrná exprese (Rauschenberger et al., 2010; Yang et al., 2007) (Obr. 5), která byla nalezena v mozcích pacientů s AD (He et al., 2005a; Kristofiková et al., 2009; Lustbader et al.,

2004; Yan et al., 1997). Zvýšená hladina 17β-HSD10 v mozku exprimujícím Aβ je považována za kritický faktor, který přispívá k mitochondriální dysfunkci a patogenezi AD, neboť vede ke zvýšení mitochondriální toxicity a neuronálního stresu vyvolaného Aβ (Chen a Yan, 2007; Lustbader et al., 2004; Seo et al., 2011; Takuma et al., 2005). Nové poznatky v této oblasti přináší nedávná studie, která s využitím mozkových buněk izolovaných z transgenního myšího modelu AD odhalila účinek přírodního alkaloidu huperzinu A jak na snížení hladiny Aβ, tak i snížení hladiny 17β-HSD10 zvýšené v důsledku jejich vzájemné interakce, čímž došlo ke zlepšení mitochondriální funkce a zvýšení životaschopnosti buněk (Xiao et al., 2019).

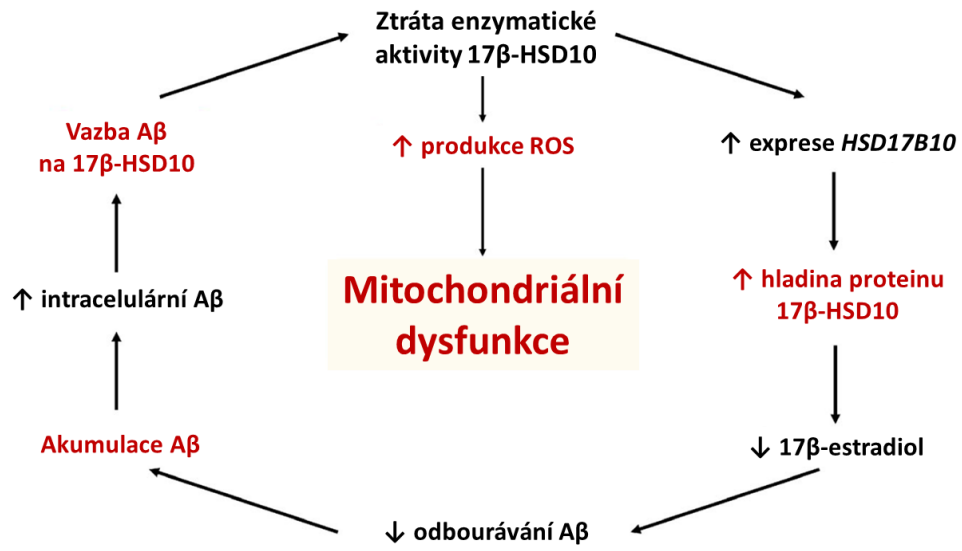

Obr. 5: *Patologická kaskáda způsobená interakcí 17β-HSD10 a Aβ. Interakce Aβ a 17β-HSD10 inhibuje její enzymatickou aktivitu, čímž dochází k přirozené kompenzaci zvýšením její exprese a celkové hladiny v buňce. V důsledku zvýšené exprese je nadměrně metabolizován 17β-estradiol, který je však modulátorem odbourávání Aβ, což vede k jeho akumulaci a kaskáda se opakuje. Celý proces je doprovázen oxidačním stresem a zvýšenou tvorbou reaktivních forem kyslíku (ROS). Výsledkem této patologické kaskády je mitochondriální dysfunkce. (↓ značí pokles, ↑ značí nárůst). Převzato a upraveno* (Vinklarova et al., 2020).

Nadměrná exprese 17β-HSD10 může mít též za následek strukturní změny v mitochondriích, jako je částečná ztráta struktury mitochondriálních krist a kondenzace matrix (Shafqat et al., 2003), a může též narušovat rovnováhu mezi prozánětlivými a protizánětlivými cytokiny, což může vést k zánětu v centrálním nervovém systému a zhoršení kognitivních funkcí (Giatti et al., 2012).

Zvýšená hladina 17β-HSD10 navíc pravděpodobně narušuje homeostasu neurosteroidního metabolismu a může měnit hladiny neuroprotektivních steroidních substrátů tohoto enzymu, zejména E2 a ALLOP, v různých oblastech mozku (He et al., 2018; Yang et al., 2014, 2011). V souladu s tím je i několik publikovaných studií, v nichž byla detekována snížená hladina obou těchto neurosteroidů v mozcích pacientů s AD (Manly et al., 2000; Marx et al., 2006; Yue et al., 2005). U E2 byla navíc pozorována zpětnovazebná smyčka regulace aktivity 17β-HSD10 v důsledku změny hladiny E2 (Yao et al., 2012).

Správná hladina 17β-HSD10 je kritická pro udržení optimální hladiny E2, která je důležitým faktorem pro přežití neuronů (Yang et al., 2007). E2 má řadu protektivních účinků na mitochondrie, mezi něž patří snížení produkce ROS, zvýšení aktivity dýchacího řetězce a produkce ATP, stabilizace mitochondriálního membránového potenciálu a regulace vstupu Ca^{2+} do buněk vyvolaná excitotoxicitou (Amtul et al., 2010; Grimm et al., 2012). E2 může buňku chránit před apoptosou aktivací antioxidačních mechanismů (Guglielmotto et al., 2020; Ozacmak a Sayan, 2009) a svou vazbou na estrogenové receptory α a β může v jádře modulovat transkripci řady významných genů (Marino et al., 2006). Kromě toho má E2 významný vliv na regulaci dvou klíčových patologických znaků AD, Aβ a tau proteinu. Regulací zpracování APP snižuje hladinu Aβ, a tím i jeho agregaci do plaků (Amtul et al., 2010), a zabraňuje též Aβ-indukované dysregulaci homeostasy Ca^{2+} vedoucí k oxidačnímu stresu (Nilsen, 2008). V přítomnosti netoxické koncentrace $Aβ_{42}$ bylo pozorováno zvýšení hladiny E2 v mitochondrii, což naznačuje možnou spojitost se sníženou aktivitou 17β-HSD10 způsobenou interakcí s Aβ, která může mít za následek omezenou přeměnu E2 na estron, naopak opačný efekt, tedy snížení hladiny E2, byl pozorován při použití toxické koncentrace tohoto peptidu (Schaeffer et al., 2008). Toto pozorování se zdá být v souladu s výše zmíněnou kompenzační hypotézou (Obr. 5).

V případě tau patologie může být vlivem E2 indukována fosforylace, resp. deaktivace glykogensynthasy kinasy 3β, což může vést ke snížení a prevenci hyperfosforylace tau proteinu (Alvarez de la Rosa et al., 2005; Goodenough et al., 2005). Dále byl u samic transgenního myšího modelu exprimujícího lidský tau, které byly po ovariektomii vystaveny substituční léčbě E2, pozorován ochranný vliv před vznikem patologické konformace tau způsobené $Aβ_{42}$. Tento protektivní efekt je připisován antioxidační aktivitě E2 a jeho schopnosti modulovat expresi miRNA 218, která je spojena s fosforylací tau (Guglielmotto et al., 2020).

Lidská 17β-HSD10 je též zodpovědná za intracelulární oxidaci ALLOP, pozitivního alosterického modulátoru receptoru kyseliny γ-aminomáselné typu A ($GABA_A$), který má vliv na udržení GABAergní funkce neuronů a reguluje jejich

plasticitu a excitabilitu (Hosie et al., 2006; Schverer et al., 2018). Bylo pozorováno, že léčba ALLOP může eliminovat ztrátu neuronů a zlepšovat kognitivní schopnosti po traumatickém poranění mozku (He et al., 2004) a v literatuře byl též diskutován jeho možný terapeutický potenciál díky jeho vlivu na neurogenesi a díky jeho schopnosti obnovit neuronální populace v mozku postiženém neurodegenerací (Brinton a Wang, 2006; Wang et al., 2005). ALLOP má, stejně jako E2, vliv na patologické znaky spojené s AD. V trojitě transgenním (3xTgAD) myším modelu AD byla vlivem ALLOP eliminována akumulace Aβ a s tím spojená hyperfosforylace tau proteinu (Chen et al., 2011) a v několika studiích byl prokázán jeho antioxidační a neuroprotektivní účinek.

U buněčné linie PC12 odvozené z potkaního feochromocytomu a v myším hipokampu ALLOP významně zvýšil expresi a aktivitu antioxidačního enzymu superoxiddismutasy (Cho et al., 2018; Qian et al., 2015). U lidských fibroblastů získaných od pacientů trpících Niemann-Pickovou chorobou typu C snížil ALLOP hladinu ROS a míru peroxidace lipidů (Zampieri et al., 2009). Nedávná studie dokonce objevila modulační účinek ALLOP na syntézu a opravnou kapacitu enzymů dráhy excisní reparace basí DNA v ovčí amygdale a hipokampu, a to za přirozených i stresových podmínek (Misztal et al., 2020). V roce 2019 byl ALLOP schválen Úřadem pro kontrolu potravin a léčiv v USA (FDA) jako lék brexanolon (obchodní název Zulresso) pro léčbu poporodní deprese (Meltzer-Brody et al., 2018) a aktuálně probíhají druhé fáze klinických studií pro využití ALLOP k léčbě chronického komplexního traumatickém poranění mozku (VA Office of Research and Development, 2023) a pro regenerativní léčbu mírné formy AD (Brinton, 2023).

Neurosteroidy E2 a ALLOP mají významný vliv jak na funkci, bioenergetiku a antioxidační procesy mitochondrií, tak i na patologické změny u AD, jako je akumulace Aβ a hyperfosforylovaného tau (Grimm et al., 2016, 2014). Za jeden z potenciálních přístupů při vývoji terapie AD se považuje inhibice enzymatické aktivity 17β-HSD10, která by měla obnovit narušenou homeostasu způsobenou nadměrnou expresí tohoto enzymu, a tedy i hladiny neuroprotektivních steroidů E2 a ALLOP.

3.4.3 Inhibice enzymatické aktivity 17β-HSD10

Dosud publikované inhibitory enzymatické aktivity 17β-HSD10 lze dle struktury rozdělit do tří skupin. První skupinou jsou sloučeniny na bázi pyrazolopyrimidinu, které jsou prvotními, a také velmi účinnými inhibitory 17β-HSD10. V posledním desetiletí se na ně však výzkum tolik nezaměřuje (Vinklarova et al., 2020). Mezi početnější dvě skupiny a též hojně publikované

inhibitory patří steroidní deriváty a benzothiazolylové deriváty, které byly studovány i v rámci překládané disertační práce.

Do skupiny sloučenin na bázi pyrazolopyrimidinu patří jeden z dosud nejúčinnějších inhibitorů AG18051 (IC_{50} 92 nM; Obr. 4) (Kissinger et al., 2004). Nevýhodou tohoto inhibitoru je jeho ireversibilní mechanismus inhibice, který je pravděpodobně způsoben tvorbou kovalentního aduktu AG18051 s NAD^+ v aktivním místě 17β-HSD10 (Kissinger et al., 2004; Marques et al., 2008). Navzdory tomu vykazoval tento inhibitor na buněčné linii SH-SY5Y účinné snížení toxických účinků $A\beta_{42}$ spolu s pozitivním vlivem na přežití buněk, neboť byl schopen zabránit tvorbě ROS a obnovit hladiny E2 (Lim et al., 2011), a u primárních astrocytů s nadměrnou expresí 17β-HSD10 obnovil narušenou buněčnou respiraci a inhiboval zvýšenou tvorbu superoxidu způsobenou $A\beta_{42}$ (Metodieva et al., 2022). Skupina Abreo et al. identifikovala sérii 18 pyrazolylpyrimidinových derivátů, z nichž 7 nejúčinnějších vykazovalo hodnoty IC_{50} 51–97 nM, tyto deriváty však byly až do minulého roku pod patentovou ochranou (Abreo et al., 2005).

Steroidní deriváty se intuitivně nabízí jako potenciální inhibitory 17β-HSD10 díky své analogii s jejími přirozenými steroidními substráty. Dosud byla publikována řada sloučenin patřící se do této skupiny, nejúčinnější z nich však vykazují nízkou selektivitu nebo poskytují diametrálně rozdílné výsledky při použití odlišných metod testování, resp. použití rekombinantního enzymu *vs.* buněčných linií (Ayan et al., 2012; Boutin et al., 2018). Nejúčinnějším publikovaným steroidním derivátem je sloučenina **D-3,7** (Obr. 6) s hodnotou IC_{50} 0,14 μM naměřenou s využitím buněčné linie HEK293-17β-HSD10 (Boutin et al., 2021).

Nejpočetnější, nejhojněji publikovanou a nejvíce prostudovanou skupinou jsou benzothiazolylové deriváty, případně benzothiazolyl močovinové deriváty. Strukturně tyto sloučeniny vychází z léku frentizolu schváleného FDA (Obr. 6), který je zároveň slabým inhibitorem vazby Aβ a 17β-HSD10 (IC_{50} = 200 μM) (Xie et al., 2006). K dnešnímu dni bylo publikováno velké množství derivátů těchto látek s odlišnými inhibičními a farmako-chemickými vlastnostmi, přičemž vývoj potentnějších inhibitorů je stále předmětem studia několika výzkumných skupin (Aitken et al., 2019; Benek et al., 2018, 2017; Hroch et al., 2017, 2016; Schmidt et al., 2020; Valasani et al., 2014, 2013; Xie et al., 2006). Nejsilnější dosud publikované inhibitory z této skupiny mají hodnoty IC_{50} okolo 0,3 μM (Benek et al., 2023). Výzkumu nových účinnějších benzothiazolylových inhibitorů je věnována značná část předkládané práce.

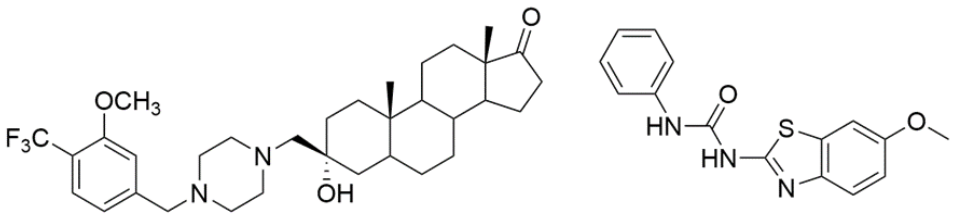

D-3,7 frentizol

Obr. 6: *Struktury významných inhibitorů 17β-HSD10 – sloučenina D-3,7 (steroidní deriváty;* Boutin et al., 2021*) a frentizol (benzothiazolylové deriváty;* Xie et al., 2006*).*

Pro hodnocení inhibičního potenciálu nových sloučenin je klíčová volba použitých metod, neboť výsledky získané z *in vitro* stanovení mohou být zatíženy určitým zkreslením a mohou se též zásadně lišit. V řadě publikací bylo pro stanovení enzymatické aktivity 17β-HSD10 a hodnocení jejích inhibitorů využíváno spektrofotometrické stanovení využívající substrát AAC spolu s kofaktorem NADH (Aitken et al., 2019, 2017, 2016; Hroch et al., 2016; Oppermann et al., 1999; Schmidt et al., 2020), které vychází z metody publikované Binstockem a Schulzem (Binstock a Schulz, 1981). Toto stanovení využívá reduktasové aktivity 17β-HSD10, která však u tohoto enzymu není ve fyziologickém prostředí buňky preferovaná, neboť 17β-HSD10 jako mitochondriální dehydrogenasa preferuje oxidační směr reakce s kofaktorem NAD^+ (Yang et al., 2005). V několika publikacích byl použit tento preferovaný směr reakce s využitím přirozených neurosteroidních substrátů 17β-HSD10 E2 a ALLOP, přičemž nárůst vznikajícího produktu byl nejčastěji stanoven buď pomocí tenkovrstvé chromatografie (Boutin et al., 2018; He et al., 2005b, 1999), nebo byl spektrofotometricky měřen nárůst NADH při 340 nm (Powell et al., 2000; Shafqat et al., 2003; Yan et al., 1999), avšak oba typy stanovení často trpí nedostatečnou citlivostí. Z tohoto důvodu byla značná část předkládané disertační práce věnována zavedení a optimalizaci dostatečně citlivé metody pro stanovení enzymatické aktivity 17β-HSD10 a testování inhibičního potenciálu jejích inhibitorů.

3.5 Mitochondriální enzym CypD

Druhým enzymem studovaným v předkládané práci je lidský CypD (UniProt: P30405) lokalizovaný v mitochondriální matrix (Johnson et al., 1999). Jedná se o protein kódovaný genem *ppif* mapovaném na chromosomu 10q22.3 a jeho správný název by tak měl být cyklofilin F, což je důvod, proč někdy bývá zaměňován s cytosolickým cyklofilinem kódovaných genem *ppid*. CypD je však jedinou isoformou cyklofilinu exprimovanou v mitochondrii. Lidský CypD je cytoplasmaticky translatovaný globulární protein složený z 207 aminokyselinových zbytků s molekulovou hmotností 22 kDa (Obr. 7), jehož mitochondriální cílová sekvence je po transportu do mitochondrií odštěpena, čímž dochází k redukci jeho molekulové hmotnosti na 19 kDa (Bergsma et al., 1991; Gutiérrez-Aguilar a Baines, 2015).

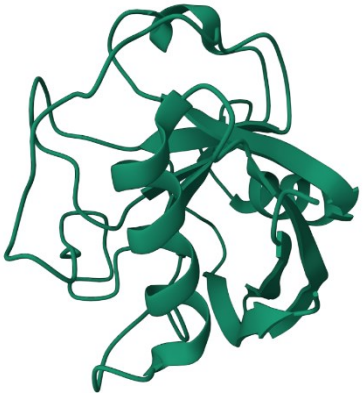

Obr. 7: *Krystalová struktura CypD. Převzato z RCSB PDB (RCSB.org), PDB ID: 3RDC* (Gelin et al., 2015).

3.5.1 Fyziologická funkce CypD

Z hlediska enzymové aktivity patří CypD do nadrodiny peptidyl-prolyl *cis-trans* isomeras (EC 5.2.1.8), které jsou zodpovědné za katalýzu *cis-trans* isomerace peptidových prolin-X vazeb (X může být jakákoliv aminokyselina). Tato funkce je důležitá nejen při skládání proteinů, ale také při sestavování vícedoménových proteinů (Davis et al., 2010; Wang a Heitman, 2005).

Jednou z klíčových mitochondriálních funkcí CypD je regulace mitochondriálního póru přechodné propustnosti (mPTP), který hraje důležitou roli při udržování homeostasy Ca^{2+} a regulaci buněčné smrti (Giorgio et al., 2010). Po otevření mPTP může mít vysoká vodivost tohoto kanálu za následek rychlé nabobtnání mitochondrie způsobené kolapsem chemiosmotického gradientu,

prasknutí vnitřní a vnější mitochondriální membrány, zhroucení mitochondriálního membránového potenciálu a vyčerpání buněčného ATP, což nakonec může vést k buněčné smrti (Halestrap, 2010; Kinnally et al., 2011; Strubbe-Rivera et al., 2021). Přechodné otevření tohoto póru má však i fyziologickou funkci, a to zejména v udržování homeostasy Ca^{2+}, resp. vyplavování nadbytečného Ca^{2+} z mitochondriální matrix (Bernardi a von Stockum, 2012). Přesný mechanismus regulace tohoto póru pomocí CypD však dosud není zcela znám. V regulaci otevření mPTP možná hraje roli i interakční partner CypD, 17β-HSD10, neboť existuje hypotéza, že za normálních podmínek se 17β-HSD10 lokalizovaná v mitochondriální matrix váže na CypD a zabraňuje jeho translokaci a následné tvorbě mPTP, čímž může regulovat otevírání tohoto póru (Carlson et al., 2015). Při zvýšené akumulaci Aβ v mitochondrii však může být tato interakce narušena a regulace CypD pomocí 17β-HSD10 je tak eliminována. CypD je tudíž ve zvýšené míře translokován a interaguje s mPTP, což může vést k apoptose a nekrose (Kristofikova et al., 2020; Muirhead et al., 2010a). Bylo ověřeno, že 17β-HSD10 tvoří s CypD v *in vitro* podmínkách stabilní komplex, avšak vazba 17β-HSD10 může být ovlivněna faktory jako je pH a přítomnost iontů K^+ a Mg^{2+} nebo právě výše zmíněná přítomnost Aβ (Hemmerová et al., 2019).

Kromě účasti při otevírání mPTP má CypD několik dalších důležitých mitochondriálních funkcí, jako je např. regulace exprese mitochondriálních genů, a tím i proliferace a diferenciace buněk (Radhakrishnan et al., 2015), snížení produkce ATP po vazbě na ATP-syntasu (Giorgio et al., 2009), nebo též role v β-oxidaci mastných kyselin skrze interakci s mitochondriálním trifunkčním proteinem (Tavecchio et al., 2015). Při ztrátě či inhibici CypD byly též pozorovány změny ve vyplavování Ca^{2+} zprostředkované mPTP, což vedlo ke zvýšení hladin Ca^{2+} v mitochondriální matrix, aktivaci Ca^{2+}-dependentních dehydrogenas a zvýšení oxidace glukosy namísto mastných kyselin (Elrod et al., 2010).

Řada více či méně prozkoumaných funkcí pojí CypD s patofyziologií několika různých onemocnění, mezi něž patří např. ischemicko-reperfusní poškození nebo též některá neurodegenerativní onemocnění včetně AD (Fayaz et al., 2015; Javadov et al., 2017; Kalani et al., 2018).

3.6 CypD jako terapeutický cíl AD

V souvislosti s AD je dosud nejvíce diskutována klíčová role CypD v modulaci tvorby a otevírání mPTP a z toho plynoucí terapeutické využití jeho selektivních inhibitorů zabraňujících patologickému otevírání mPTP. Zároveň by však tyto inhibitory mohly zasahovat i do dalších fyziologických funkcí CypD zprostředkovaných interakcemi s jinými proteiny (Haleckova et al., 2022; Rao et al.,

2014). V posledních letech je věnována pozornost nalezení účinných nízkomolekulárních inhibitorů enzymatické aktivity CypD s vhodnými terapeutickými vlastnostmi a vysokou selektivitou, návrh takových molekul je však ztížen vysokou mírou podobnosti aktivního místa v rámci různých isoforem cyklofilinů (Davis et al., 2010; Haleckova et al., 2022).

Mezi potenciální terapeutické cíle patří též škodlivá interakce CypD a Aβ, která má za následek zvýšenou tvorbu mPTP a následnou mitochondriální a neuronální dysfunkci (Akhter et al., 2017; Du a Yan, 2010; Rao et al., 2014) (Obr. 8). V mozcích pacientů s AD byla navíc nalezena zvýšená exprese CypD vysvětlovaná jako pravděpodobný důsledek akumulace Aβ v mitochondrii (Du et al., 2008).

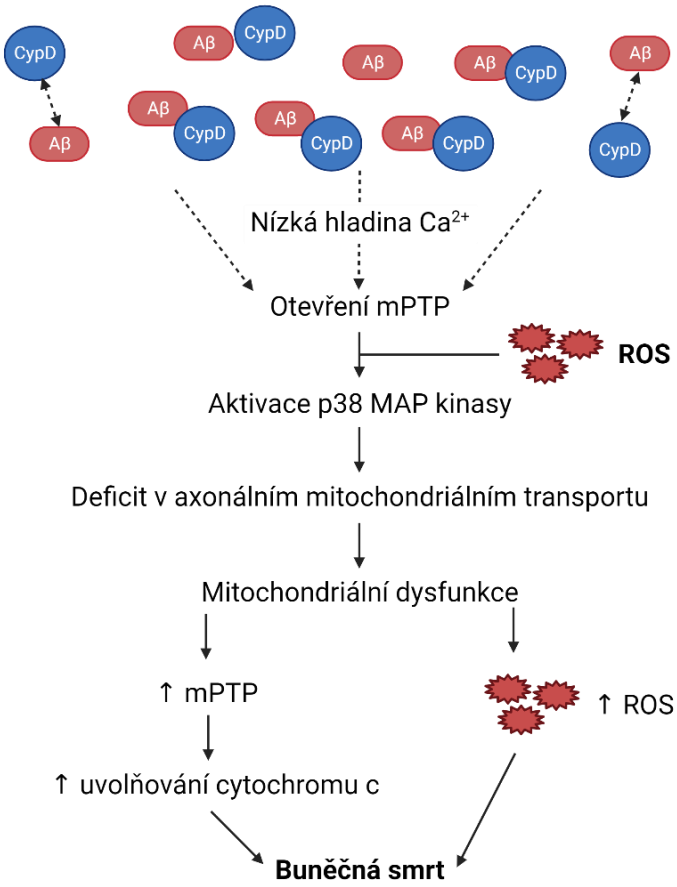

Obr. 8: *Patologické důsledky interakce Aβ a CypD. Vlivem interakce dochází k nadměrnému otevírání mPTP, což vede k narušení rovnováhy Ca^{2+}, která spolu s oxidačním stresem aktivuje navazující signální dráhu p38 MAP kinasy. Následně dochází k poruchám axonálního mitochondriálního transportu a vše přispívá k mitochondriální dysfunkci, která prohlubuje výše zmíněné patologie, a celý proces ústí v buněčnou smrt (↑ značí nárůst). Vytvořeno v BioRender.com podle* (Akhter et al., 2017).

3.6.1 Inhibice enzymatické aktivity CypD

Inhibitory enzymatické aktivity CypD lze dle původu zařadit do dvou základních skupin. První skupinou jsou přírodní makrocyklické inhibitory a jejich analoga a druhou skupinou jsou syntetické nízkomolekulární inhibitory. Inhibitory z druhé skupiny lze strukturně zařadit do tří podskupin: (1) *N*-4-aminobenzyl-*N*′-(2-(2-arylpyrrolidin)-2-oxoethyl)močoviny, (2) 2-(benzyloxy)aryl močoviny a jejich analoga a (3) ostatní nízkomolekulární inhibitory (Haleckova et al., 2022).

Do skupiny přírodních makrocyklických inhibitorů se řadí nejznámější a velmi účinný inhibitor enzymatické aktivity CypD cyklosporin A (CsA; Obr. 9) (Tanveer et al., 1996). Jedná se o cyklický undekapeptid produkovaný vláknitými půdními houbami *Typocladiumum inflatum*, který však vykazuje řadu nežádoucích vlastností, jako jsou imunosupresivní účinky a nízká selektivita, neboť tento peptid inhibuje i další cyklofiliny a právě tato skutečnost dala vzniknout názvu celé této skupiny proteinů (Barbarino et al., 2013; Davis et al., 2010). Ve snaze eliminovat nežádoucí účinky CsA bylo vyvinuto několik jeho neimunosupresivních derivátů, např. alisporivir (Hansson et al., 2004) a NIM811 (Waldmeier et al., 2002), kvůli své peptidické struktuře mají však tyto struktury nepříznivý farmakokinetický profil. Nevhodný farmakokinetický profil a nízká selektivita jsou bohužel společnými omezujícími negativy pro celou tuto skupinu přírodních inhibitorů (Haleckova et al., 2022).

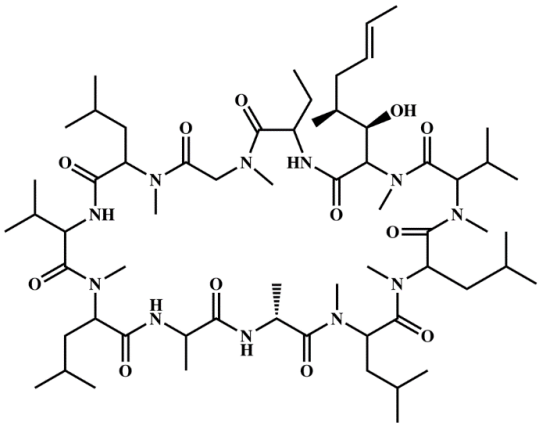

Obr. 9: *Struktura cyklosporinu A. Převzato z* (Varache et al., 2020).

Syntetické sloučeniny podskupiny (1) patřící do skupiny syntetických nízkomolekulárních inhibitorů jsou strukturně odvozeny od sloučeniny **22** publikované Ahmed-Belkacem et al. s hodnotou IC_{50} 6,2 μM (Ahmed-Belkacem et al., 2016). Tato podskupina inhibitorů je nejlépe charakterizována a patří do ní nejúčinnější nízkomolekulární inhibitory CypD. Nejsilnější dosud publikovaný

inhibitor CypD je sloučenina **14** (Obr. 10) výzkumné skupiny Grädler et al. s hodnotou IC_{50} 6 nM (Grädler et al., 2019).

Sloučeniny podskupiny (2) jsou strukturně modifikované inhibitory cyklofilinu A (CypA) publikované Guichou et al. (Guichou et al., 2006). Je zde využito předpokladu, že inhibitory CypA mohou být též účinnými inhibitory CypD, neboť tyto dvě isoformy jsou ze 75 % sekvenčně identické a residua vazebného místa interagující s CsA jsou u obou enzymů konzervována (Kajitani et al., 2008). Nejúčinnějším inhibitorem řadícím se do této podskupiny je sloučenina **9w** (Obr. 10) publikovaná skupinou Park et al., která při koncentraci 5 μM dokázala inhibovat otevírání mPTP z 95 %, přičemž molekulární dokování odhalilo několik možných způsobů vazby této sloučeniny v aktivním místě CypD (Park et al., 2017a).

Podskupina (3) zahrnuje různé strukturně odlišné inhibitory CypD, jako jsou analoga dimedonu (Walkinshaw et al., 2002), chinoxalinové deriváty (Guo et al., 2005), sloučeniny odvozené od myorelaxantu dantrolenu (Murasawa et al., 2012) a inhibitory se 4-aminobenzensulfonamidovými a tetrahydropyrimidinovými skelety (Valasani et al., 2016, 2014b). Lze sem zařadit i několik nepeptidových nízkomolekulárních inhibitorů CypD odhalených Parkem et al. s využitím virtuálního screeningu a molekulárního dokování, z nichž se jako nejúčinnější inhibitor CypD ukázala sloučenina **29** (Obr. 10) s hodnotou K_d 88,2 nM a neuroprotektivními účinky, která byla schopna chránit mitochondrie před toxicitou vyvolanou Aβ prostřednictvím inhibice mPTP (Park et al., 2017b).

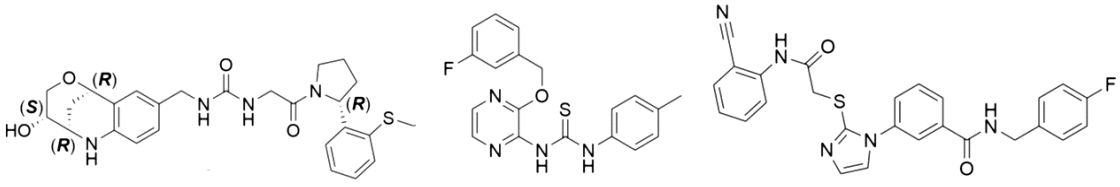

Sloučenina **14** Sloučenina **9w** Sloučenina **29**

Obr. 10: *Významné sloučeniny z různých strukturních podskupin inhibitorů CypD – sloučenina **14** (N-4-aminobenzyl-N′-(2-(2-arylpyrrolidin)-2oxoethyl)močoviny;* Grädler et al., 2019*), sloučenina **9w** (2-(benzyloxy)aryl močoviny a jejich analoga;* Park et al., 2017a*), sloučenina **29** (ostatní nízkomolekulární inhibitory;* Park et al., 2017b*).*

Pro identifikaci a evaluaci inhibitorů je zásadní volba vhodných metod. Pro hodnocení inhibitorů CypD lze využít funkční testy pro sledování mPTP, při kterých se obvykle stanovují parametry jako je ztráta mitochondriálního

membránového potenciálu (využití fluorescenčního barviva JC-1) (Sivandzade et al., 2019) nebo mitochondriální retenční kapacita Ca^{2+} (stanovení mitochondriálního bobtnání) (Li et al., 2018), které nepřímo stanovují míru otevírání mPTP. Tyto funkční testy se provádějí na izolovaných mitochondriích nebo na buněčných kulturách, získané výsledky tudíž nemusí vždy svědčit o inhibici samotného CypD, neboť může docházet k inhibici mPTP jinými, na CypD nezávislými, mechanismy.

Pro stanovení enzymatické aktivity rekombinantního CypD byla řadu let využívána metoda publikovaná Kofronem et al. (Kofron et al., 1991). Principem této metody je isomerace prolinové peptidové vazby tetrapeptidu Suc-AAPF-pNA z *cis* na *trans* konformaci katalyzovaná CypD. Následuje štěpení produktu reakce, *trans*-isomeru, chymotrypsinem a výsledný degradační produkt je detekován spektrofotometricky. Na stejném principu jsou založeny i některé fluorescenční metody (Caporale et al., 2016; Mori et al., 2009; Vivoli et al., 2017; Zoldák et al., 2009), souhrnně však tato stanovení trpí řadou omezení, jako je spontánní a teplotně citlivá *cis*-*trans* isomerace substrátu nebo degradace samotného CypD chymotrypsinem. Součástí překládané práce bylo zavedení nové, více fyziologicky relevantní a robustnější metody pro stanovení enzymatické aktivity CypD *in vitro*, která by byla vhodná pro přesnější hodnocení nových nízkomolekulárních inhibitorů CypD.

4 Komentáře k publikovaným pracím

Tato disertační práce je předkládána jako komentovaný soubor pěti publikací, z nichž 4 jsou publikovány v mezinárodních impaktovaných časopisech a 1 je t.č. rukopisem v pokročilé fázi recenzního řízení. Všechny publikace jsou původní experimentální práce zaměřené na lidské mitochondriální enzymy spojené s neurodegenerací, resp. AD. Jedna publikace je zaměřena na studium enzymatické aktivity CypD a její inhibici (Kapitola 4.1, str. 32–34). Čtyři publikace jsou zaměřeny na studium enzymatické aktivity 17β-HSD10 a evaluaci jejích inhibitorů *in vitro* (Kapitola 4.2–4.5, str. 35–45).

4.1 Metoda využívající znovusložení RNasy T1 pro stanovení aktivity mitochondriálního cyklofilinu D: Nová *in vitro* metoda použitelná při výzkumu a vývoji léčiv

Zemanova, L., **Vaskova, M.**, Schmidt, M., Roubalova, J., Haleckova, A., Benek, O., Musilek, K., 2020. RNase T1 Refolding Assay for Determining Mitochondrial Cyclophilin D Activity: A Novel *In Vitro* Method Applicable in Drug Research and Discovery. Biochemistry 59, 1680–1687.
https://doi.org/10.1021/acs.biochem.9b01025

Lidský mitochondriální enzym CypD je klíčovým komponentem při modulaci tvorby mPTP, který je významným regulátorem buněčné smrti (Giorgio et al., 2010). CypD je proto považován za jeden z terapeutických cílů onemocnění spojených s nadměrným otevíráním mPTP, mezi něž patří i AD, a proto je v poslední době věnována pozornost vývoji účinných selektivních inhibitorů tohoto enzymu (Haleckova et al., 2022; Rao et al., 2014).

Volba vhodných metod zohledňujících fyziologické podmínky a úlohu daného enzymu v organismu hraje důležitou roli při identifikaci a evaluaci inhibitorů s terapeutickým potenciálem. Vzhledem k řadě omezení, kterými trpí v literatuře často používaná Kofronova metoda (Kofron et al., 1991), bylo cílem této studie zavedení nové, robustnější a fyziologicky relevantní *in vitro* metody pro stanovení enzymatické aktivity CypD. Tato metoda je založena na jeho katalytické účasti při znovusložení modelového proteinu, v tomto případě RNasy T1, jako substrátu, která je inspirována metodou Bose et al. (Bose et al., 1994). Stejného principu, ale s použitím různých modelových proteinů, využívá i několik dalších studií, které byly věnovány studiu enzymatické aktivity různých isoforem cyklofilinů a jejich peptidyl-prolyl *cis-trans* isomerasové aktivity, neboť právě účast při skládání proteinů se zdá být hlavní fyziologickou funkcí těchto enzymů (např. Matouschek et al., 1995; Rassow et al., 1995; Zhang et al., 2013).

V rámci této studie byla nejprve experimentálně vyloučena vhodnost použití Kofronovy metody, neboť přítomnost chymotrypsinu v reakční směsi vede jak ke štěpení vzniklého produktu, tak i k degradaci samotného CypD.

Následně byla zavedena a optimalizována nová metoda využívající RNasu T1 jako substrát pro CypD (Obr. 11). RNasa T1 byla denaturována v 8 M močovině a její znovusložení doprovázené nárůstem fluorescence tryptofanů probíhalo po následném zředění reakčním pufrem, přičemž bylo ověřeno, že CypD urychluje opětovné skládání RNasy T1 ve srovnání se spontánním procesem (Obr. 12A). Nejprve bylo nutné optimalizovat složení reakční směsi (50 μM RNasa T1

a 25 nM CypD), aby byla zajištěna optimální odezva a doba trvání reakce, a s využitím metody DSF byl zvolen vhodný pufr zajišťující dobrou stabilitu CypD při skladování a stanovení jeho enzymatické aktivity. Pomocí nové metody byly následně stanoveny hodnoty IC_{50} třech vybraných inhibitorů (Obr. 12B): **CsA** (22,9 nM); **JC-9** (1,26 μM); sloučenina **4** (10,2 μM). Výsledky získané v naší studii korelují s publikovanými daty, čímž potvrzují relevanci zavedené metody.

Nová metoda pro stanovení enzymatické aktivity CypD lépe odpovídá jeho předpokládané fyziologické úloze při skládání proteinů a je vhodná pro identifikaci a hodnocení nových inhibitorů CypD při výzkumu a objevování léčiv. V současné době je na našem pracovišti tato metoda hojně využívána při testování vybraných inhibitorů CypD.

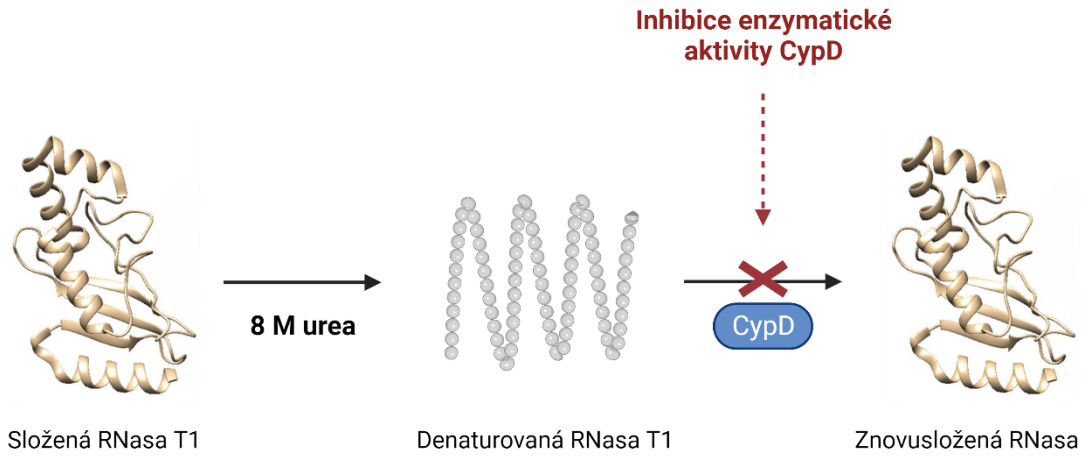

Obr. 11: *Schématické znázornění nové metody pro stanovení enzymatické aktivity rekombinantního CypD využitelné pro testování inhibitorů tohoto enzymu. Principem metody je denaturace RNasy T1 v 8 M močovině a její opětovné složení s využitím katalytické aktivity CypD. Vytvořeno v BioRender.com podle* (Zemanova et al., 2020).

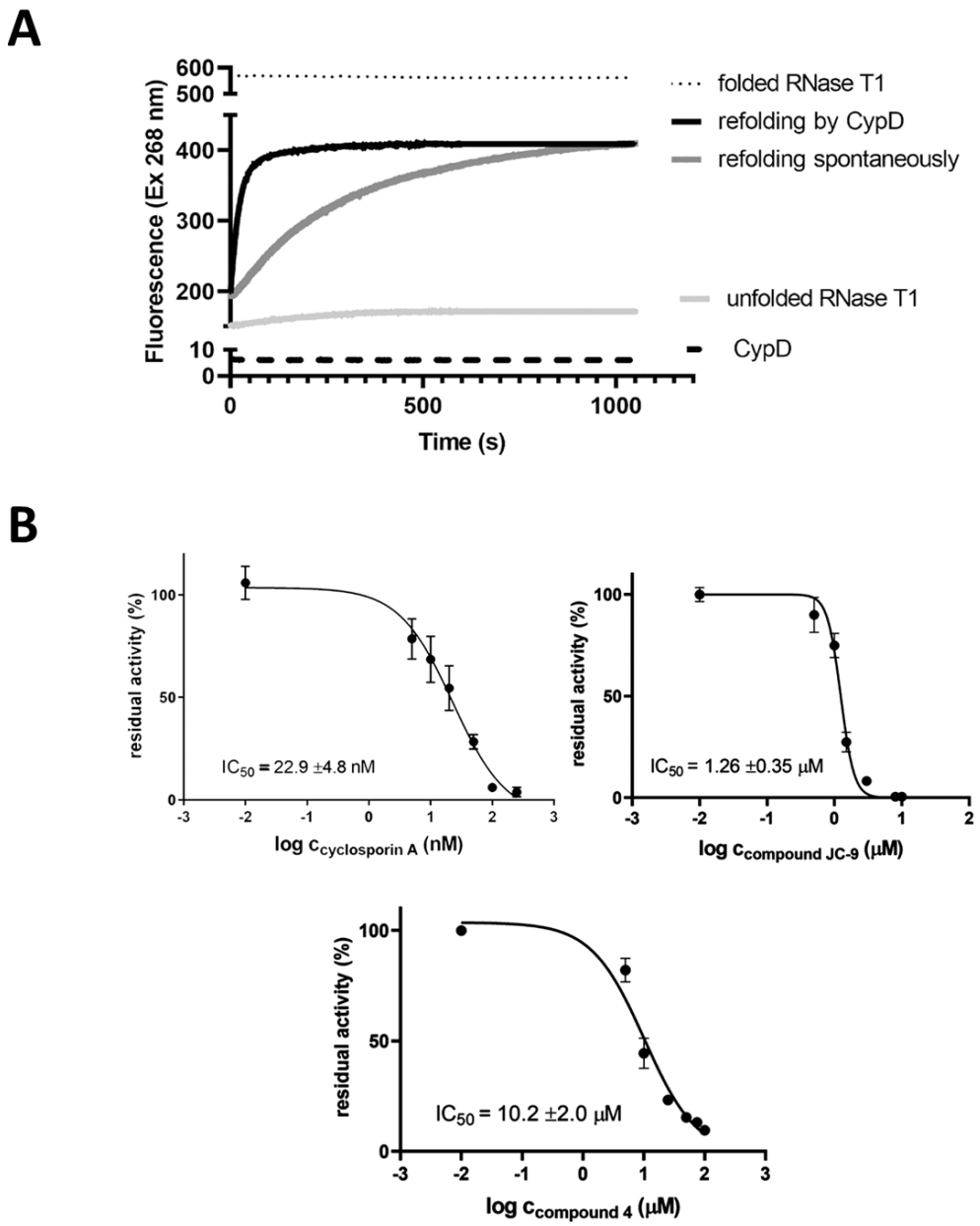

Obr. 12: *Klíčové výsledky publikace I. (**A**) Spontánní znovusložení RNasy T1 (tmavě šedá křivka) a znovusložení RNasy T1 katalyzované CypD (černá křivka). (**B**) Křivky závislosti zbytkové aktivity CypD na koncentraci testovaných sloučenin **CsA**, **JC-9** a **4** a výsledné hodnoty IC_{50}.*

4.2 Vývoj submikromolárních inhibitorů 17β-HSD10 a jejich *in vitro* a *in vivo* hodnocení

Benek, O., **Vaskova, M.**, Miskerikova, M., Schmidt, M., Andrys, R., Rotterova, A., Skarka, A., Hatlapatkova, J., Karasova, J.Z., Medvecky, M., Hroch, L., Vinklarova, L., Fisar, Z., Hroudova, J., Handl, J., Capek, J., Rousar, T., Kobrlova, T., Dolezal, R., Soukup, O., Aitken, L., Gunn-Moore, F., Musilek, K., 2023. Development of submicromolar 17β-HSD10 inhibitors and their *in vitro* and *in vivo* evaluation. Eur. J. Med. Chem. 258, 115593. https://doi.org/10.1016/j.ejmech.2023.115593

Zvýšená exprese multifunkčního mitochondriálního enzymu 17β-HSD10 je rizikovým faktorem u některých typů nádorových onemocnění a též u AD, neboť podporuje nádorové bujení a odolnost nádorových buněk vůči oxidačnímu stresu (Carlson et al., 2015) a u AD vede k narušení homeostasy neuroaktivních steroidů a přispívá k mitochondriální dysfunkci (Yang et al., 2014). Inhibice enzymatické aktivity 17β-HSD10 má terapeutický význam pro léčbu těchto onemocnění, přičemž dosud nejpublikovanější skupinou inhibitorů 17β-HSD10 jsou benzothiazolylové deriváty (Vinklarova et al., 2020).

V této studii byla publikována série 15 nových inhibitorů na bázi benzothiazolylmočoviny, které byly navrženy na základě studia vztahu struktura-aktivita (SAR) dříve publikovaných sloučenin a předpovědí jejich fyzikálně-chemických vlastností. S využitím rekombinantní 17β-HSD10 a AAC jako substrátu bylo identifikováno několik submikromolárních inhibitorů, z nichž dva nejsilnější inhibitory vykazovaly hodnoty IC_{50} ~ 0,3 μM, konkrétně se jednalo o sloučeninu **9** s IC_{50} 0,34 μM a sloučeninu **11** s IC_{50} 0,31 μM (Obr. 13A). Obě sloučeniny ve své struktuře obsahují močovinový spojovací řetězec se 3-Cl, 4-OH substituovaným fenylem, který je považován za rozhodující pro silnou inhibici enzymu, a liší se substituenty na pozici 6 benzothiazolové části (sloučenina **9** obsahuje acetamidovou skupinu a sloučenina **11** karboxylovou; Obr. 13B). Interakce těchto dvou sloučenin se 17β-HSD10 byla potvrzena pomocí DSF (Obr. 13C) a dále bylo na buněčné linii HEK293 pozorováno, že nejsou cytotoxické až do vysokých mikromolárních koncentrací. Na izolovaných mitochondriích byla ověřena jejich selektivita vůči potenciálním mitochondriálním necílovým enzymům (citrátsynthasa, komplexy I–III dýchacího řetězce, monoaminooxidasy A a B) a u sloučeniny **9**, na rozdíl od sloučeniny **11**, byla predikována průchodnost přes hematoencefalickou bariéru. Při *in vivo* testování na potkanech bylo u sloučeniny **9** zjištěno, že je perorálně biologicky dostupná a při intravenózním podání proniká do mozku, sloučenina **11** naopak vykazovala nevyhovující farmakokinetický profil.

Výsledky *in vitro* a *in vivo* potvrzují, že je sloučenina **9** slibnou strukturou pro další vývoj a hodnocení na zvířecích modelech.

A

Compound	17β-HSD10 inhibition					
	10 μM screening	*p* value	1 μM screening	*p* value	IC_{50} (μM)	K_i (μM)
	Residual activity (%)		Residual activity (%)			
control	100 ± 4.3		100 ± 4.8			
6	13.0 ± 2.4	<0.0001	39.8 ± 4.5	<0.0001	0.57 ± 0.12	0.44
7	79.4 ± 2.8	0.0022				
8	27.0 ± 1.4	<0.0001	62.7 ± 8.0	0.0023		
9	22.0 ± 3.4	<0.0001	49.5 ± 9.9	0.0014	0.34 ± 0.07	0.25
10	58.6 ± 2.1	0.0001				
11	17.5 ± 4.0	<0.0001	50.0 ± 11.4	0.0022	0.31 ± 0.09	0.23
12	38.3 ± 2.1	<0.0001	50.0 ± 6.2	0.0004	0.84 ± 0.18	0.65
13	31.0 ± 2.1	<0.0001	70.0 ± 11.2	0.013		
14	68.7 ± 4.0	0.0008				
15	72.1 ± 4.8	0.0017				
16	76.6 ± 2.9	0.0014				
17	33.2 ± 5.2	<0.0001	74.4 ± 9.0	0.0122		
18	54.1 ± 1.4	<0.0001				
19	67.6 ± 5.0	0.001				
20	73.8 ± 3.2	0.0011				

B

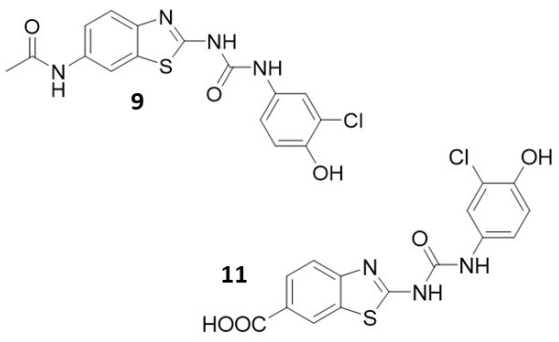

C

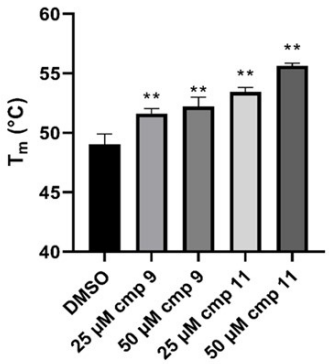

Obr. 13: *Klíčové výsledky publikace II.* ***(A)*** *Výsledky screeningu inhibice 17β-HSD10, hodnoty* IC_{50} *a vypočtené hodnoty* K_i. ***(B)*** *Struktury sloučenin* ***9*** *a* ***11***. ***(C)*** *Ověření interakce sloučenin se 17β-HSD10 metodou DSF.*

4.3 Fyziologicky relevantní fluorescenční metoda pro identifikaci inhibitorů 17β-HSD10

Schmidt, M.†; **Vaskova, M.**†; Rotterova, A.; Fiandova, P.; Miskerikova, M.; Zemanova, L.; Benek, O.; Musilek, K., 2023. Physiologically Relevant Fluorescent Assay for Identification of 17β-hydroxysteroid dehydrogenase type 10 Inhibitors. J. Neurochem. 167, 154–167. https://doi.org/10.1111/jnc.15917
(† autoři přispěli k publikaci ekvivalentním podílem)

Volba vhodného enzymového substrátu je klíčovým předpokladem pro zisk relevantních experimentálních dat při identifikaci a hodnocení testovaných inhibitorů. 17β-HSD10 jako mitochondriální NAD^+-dependentní dehydrogenasa preferuje oxidační směr katalyzované reakce, proto se hojně využívané spektrofotometrické stanovení její enzymatické aktivity využívající substrát AAC spolu s kofaktorem NADH jeví jako fyziologicky méně relevantní. Vzhledem k účasti tohoto enzymu v metabolismu neuroaktivních steroidů je též vhodné využít jeho nativní steroidní substráty. V rámci této studie byla optimalizována fluorescenční metoda pro stanovení enzymatické aktivity 17β-HSD10 využívající substráty E2 a ALLOP, která byla použita pro prověření 38 účinných publikovaných inhibitorů 17β-HSD10 odhalených dříve používanou metodou se substrátem AAC, a nejúčinnější inhibitory byly následně evaluovány *in cellulo* s využitím syntetické fluorogenní sondy (−)-CHANA (cyklohexenyl aminonaftalen alkohol), která slouží jako substrát pro 17β-HSD10 a umožňuje stanovení její aktivity uvnitř živých buněk (Muirhead et al., 2010b).

Nejprve bylo nutné optimalizovat množství enzymu v reakční směsi (42,5 nM) a stanovit kinetické parametry pro 17β-HSD10, jako je Michaelisova konstanta (K_m) a maximální rychlost reakce (V_{max}): K_m 13,11 μM pro E2; K_m 6,86 μM pro ALLOP; K_m 84,36 μM pro NAD^+ (Obr. 14A). Během tohoto stanovení bylo odhaleno, že glycerol, běžně používaný jako kryoprotektant pro uchování proteinů, je rozpoznávaný 17β-HSD10 jako substrát, a proto byl vyloučen ze všech experimentálních kroků.

Následně byl proveden screening 38 vybraných benzothiazolylových derivátů při 10 μM a 1 μM koncentraci s využitím substrátu E2 a pro nejsilnějších 13 z nich byly stanoveny hodnoty IC_{50}. Sloučenina **26** (Aitken at al., 2019; Obr. 14E) s nekompetitivním typem inhibice (IC_{50} 70 nM s E2; 19 nM s ALLOP) a sloučenina **34** (Aitken at al., 2019; Obr. 14E) s akompetitivním typem inhibice (IC_{50} 346 nM s E2; 191 nM s ALLOP) disponovaly nejvyšším inhibičním potenciálem, přičemž sloučenina **26** vykázala nižší hodnotu IC_{50} než dosud nejúčinnější

experimentálně ověřený inhibitor 17β-HSD10, AG18051 (Obr. 14B). Interakce obou sloučenin se 17β-HSD10 byla ověřena metodou DSF (Obr. 14C). U obou sloučenin byla též s využitím fluorogenní sondy (–)-CHANA ověřena jejich schopnost pronikat do buňky a inhibovat cílový enzym v buněčné linii HEK293-17β-HSD10 (Obr. 14D). Na buněčné linii HEK293 byl dále vyloučen cytotoxický vliv sloučeniny **34** a sloučenina **26** vykázala zvýšenou cytotoxicitu až při dlouhodobé expozici při vyšší koncentraci.

Publikovaná metoda využívající preferovaného směru katalýzy a nativních substrátů 17β-HSD10 přináší rozšířené poznatky a hodnotná data, která mohou pomoci při designu slibných sloučenin pro vývoj klinicky relevantních inhibitorů 17β-HSD10.

A

	E2	ALLOP	NAD⁺	glycerol
K_m (μM)	13.11 ± 0.26	6.86 ± 0.11	84.36 ± 5.47	360.43 x 10^3
V_{max} (nmol min^{-1} mg^{-1})	6.34 ± 0.07	8.46 ± 0.06	8.06 ± 0.09	11.88 ± 0.35
k_{cat} (min^{-1})	0.178	0.238	0.227	0.334
k_{cat}/K_m (M^{-1} min^{-1})	13.6 x 10^3	34.7 x 10^3	2.7 x 10^3	0.93

B

	IC_{50} (nM) ± SEM		Type of inhibition	
Compound	E2	ALLOP	E2	ALLOP
AG18051	89 ± 9	20 ± 1.9	Covalent	Covalent
26	70 ± 10	19 ± 1.5	Non-competitive	Non-competitive
34	346 ± 53	191 ± 28	Uncompetitive	Uncompetitive

C

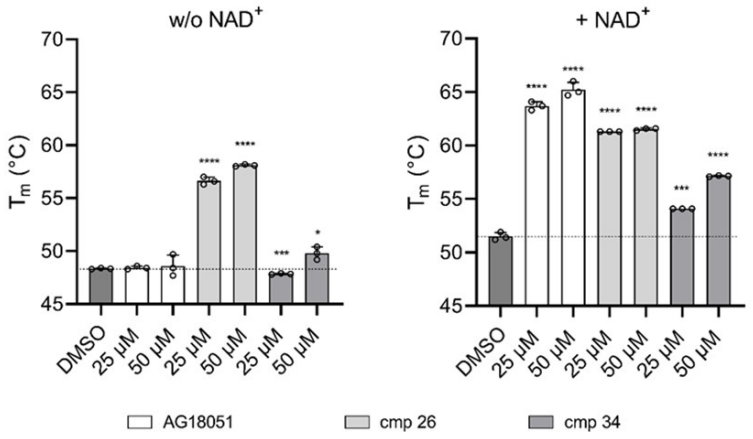

D

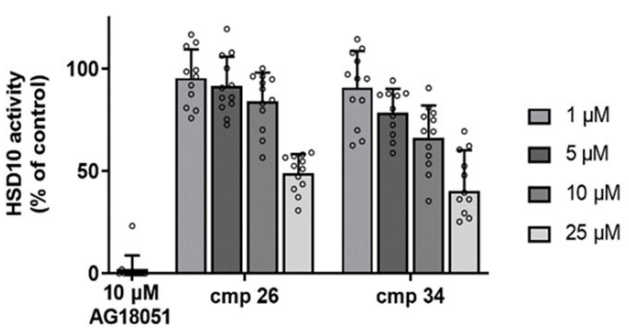

E

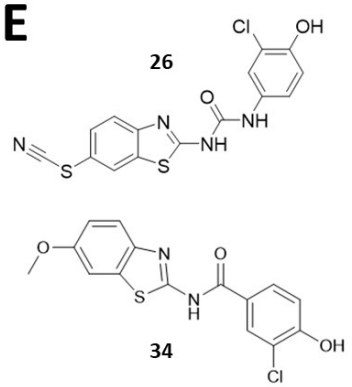

Obr. 14: *Klíčové výsledky publikace III. (**A**) Kinetické parametry enzymu 17β-HSD10. (**B**) Hodnoty IC_{50} a typy inhibic sloučenin **26** a **34** s použitím substrátů E2 a ALLOP. (**C**) Ověření interakce sloučenin se 17β-HSD10 metodou DSF. (**D**) Inhibice 17β-HSD10 v buněčné linii HEK293-HSD10 stanovená s využitím fluorogenní sondy (–)-CHANA. (**E**) Struktury nejúčinnějších sloučenin **26** a **34**.*

4.4 Nanomolární inhibitory 17β-HSD10 na bázi benzothiazolylových derivátů s bioaktivitou v buněčném prostředí

Hanzlova, M.†; Miskerikova, M.†; Rotterova, A.†; Jurkova, K.; Hamsikova, M.; Haleckova, A.; Andrys R.; Schmidt, M.; Benek, O.; Musilek, K., 2023. Nanomolar benzothiazolyl-based inhibitors of 17β-HSD10 with cellular bioactivity. ACS Med. Chem. Lett. 14, 1724−1732. https://doi.org/10.1021/acsmedchemlett.3c00355
(† autoři přispěli k publikaci ekvivalentním podílem)

Tato studie byla stejně jako studie v Kapitole 4.2 a 4.3 (str. 35–39) věnována inhibici enzymatické aktivity 17β-HSD10. Na základě SAR analýzy dříve publikovaných inhibitorů (Benek et al., 2023) byla navržena série nových benzothiazolylových derivátů, které byly testovány *in vitro* s využitím několika enzymatických a buněčných metod.

Celkem bylo navrženo a připraveno 14 sloučenin, které ve svých strukturách obsahují různou kombinaci substituentu na pozici 3 fenylové části, substituentu na pozici 6 benzothiazolové části a různě dlouhého spojovacího řetězce (Obr. 15D). Jako parentální struktury sloužily toho času nejúčinnější publikované benzothiazolové inhibitory, sloučeniny **9** a **11** uvedené v Kapitole 4.2 (str. 35–36).

Screening sloučenin při 10 μM a 1 μM koncentraci na rekombinantní 17β-HSD10 byl proveden s využitím AAC a E2 jako substrátů. Všechny sloučeniny vykazovaly dobrý inhibiční potenciál, proto jim byly stanoveny hodnoty IC_{50} s využitím fyziologicky relevantnějšího substrátu E2. Šest sloučenin vykazovalo submikromolární hodnoty IC_{50} a u nejsilnějších inhibitorů (sloučenina **3**: IC_{50} 0,41 μM; **5**: IC_{50} 0,27 μM; **6**: IC_{50} 0,52 μM; **7**: IC_{50} 0,34 μM) byl určen smíšený typ inhibice a byly jim též stanoveny hodnoty IC_{50} se substrátem ALLOP (sloučenina **3**: IC_{50} 0,095 μM; **5**: IC_{50} 0,33 μM; **6**: IC_{50} 0,29 μM; **7**: IC_{50} 0,25 μM) (Obr. 15A). Pro ověření interakce těchto čtyřech inhibitorů se 17β-HSD10 použita metoda DSF, která potvrdila stabilizaci konformace 17β-HSD10 v závislosti na dávce přidaného inhibitoru (Obr. 15B). Pro stanovení inhibice aktivity 17β-HSD10 uvnitř živých buněk HEK293-17β-HSD10 byla použita fluorogenní sonda (−)-CHANA (Obr. 15C), přičemž sloučeniny **13** (IC_{50} 5,45 μM), **14** (IC_{50} 4,39 μM) a **15** (IC_{50} 4,76 μM) s alifatickými spojovacími řetězci a 6-acetamidovou substitucí na benzothiazolové části molekuly se při testování *in cellulo* ukázaly jako nejpotentnější inhibitory 17β-HSD10. Toto zjištění však bylo v kontrastu s výsledky enzymatického testování, kde byly nejsilnějšími inhibitory sloučeniny s močovinovými spojovacími řetězci, nicméně tyto rozdíly byly pravděpodobně

způsobeny nižší průchodností benzothiazolylmočovinových sloučenin do buněk. U všech testovaných sloučenin byla vyloučena cytotoxicita na buněčné linii HEK293.

Výsledky *in vitro* a *in cellulo* ukázaly, že benzothiazolylové deriváty s alifatickými spojovacími řetězci mohou být vhodnější pro budoucí vývoj nových inhibitorů 17β-HSD10 než dříve publikované a dosud favorizované benzothiazolylmočoviny.

A

compound	E2		ALLOP
	IC_{50} (μM)	inhibition type	IC_{50} (μM)
1	1.81 ± 0.19	–	–
2	1.15 ± 0.11	–	–
3	0.41 ± 0.04	mixed	0.095 ± 0.006
4	0.78 ± 0.05	–	–
5	0.27 ± 0.02	mixed	0.33 ± 0.02
6	0.52 ± 0.04	mixed	0.29 ± 0.03
7	0.34 ± 0.04	mixed	0.25 ± 0.03
9	1.98 ± 0.17	–	–
10	1.34 ± 0.16	–	–
11	6.56 ± 0.69	–	–
12	1.01 ± 0.11	–	–
13	2.38 ± 0.16	–	–
14	1.69 ± 0.12	–	–
15	0.93 ± 0.11	–	–
16	1.38 ± 0.09	–	–

B

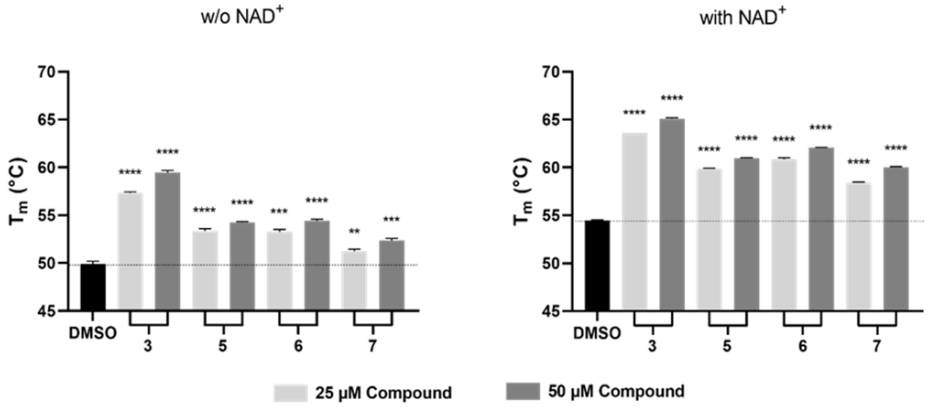

C

Compound	(-)-CHANA IC_{50} values (µM)
4	10.40 ± 1.02
6	6.21 ± 0.44
13	5.45 ± 0.76
14	4.39 ± 0.63
15	4.76 ± 0.25
16	9.03 ± 1.37

D

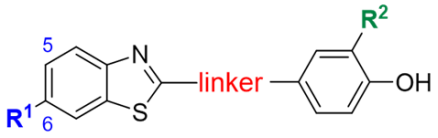

Obr. 15: *Klíčové výsledky publikace IV. (**A**) Hodnoty IC_{50} a typy inhibic testovaných sloučenin s použitím substrátů E2 a ALLOP. (**B**) Ověření interakce sloučenin se 17β-HSD10 metodou DSF. (**C**) Hodnoty IC_{50} pro inhibici 17β-HSD10 v buněčné linii HEK293-HSD10 stanovené s využitím fluorogenní sondy (–)-CHANA. (**D**) Obecná struktura nových benzothiazolylových derivátů.*

4.5 C-3 steroidní hemiestery jako inhibitory 17β-HSD10

Hanzlova, M., Slavikova, B., Morozovova, M., Musilek, K., Rotterova, A., Zemanova, L., Kudova, E., 2024. The C-3 steroidal hemiesters as inhibitors of 17β-hydroxysteroid dehydrogenase type 10. Manuskript v pokročilé fázi recenzního řízení v ACS Omega.

Tato studie byla věnována inhibici enzymatické aktivity 17β-HSD10 s využitím inhibitorů se steroidní strukturou. Steroidní deriváty, analoga nativních substrátů 17β-HSD10, jsou druhou nejhojněji zastoupenou skupinou inhibitorů tohoto enzymu, nejúčinnější publikované inhibitory však disponují nízkou selektivitou a poskytují rozporuplné výsledky při testování *in vitro* (Ayan et al., 2012; Boutin et al., 2018). Publikovaná studie byla proto věnována vývoji nových inhibitorů patřících do této skupiny a jejich testování *in vitro*.

Nejsilnějšími dosud popsanými steroidními inhibitory jsou RM-532-46 (Ayan 2012) a D-3,7 (Boutin 2021). Je zajímavé, že tyto sloučeniny, stejně jako benzothiazolylmočovinové deriváty, obsahující dusík, a tudíž se mohou chovat jako protonový akceptor, resp. báze. S přihlédnutím k tomuto faktu byla pro porovnání navržena a připravena série 24 nových záporně nabitých steroidních sloučenin, které obsahují kyselý hemiesterový substituent v poloze C-3 steroidního kruhu.

Pro testování nových sloučenin byla využita fluorescenční metoda popsaná v Kapitole 4.3 (str. 37–39) využívající E2 jako substrát. Výsledky 10 μM screeningu ukázaly, že sloučeniny **10**, **14**–**16** a **21**–**24** vykazují inhibici ≥ 50 % (Obr. 16A), a proto byly pro těchto osm sloučenin stanoveny hodnoty IC_{50} (Obr. 16B). Studie SAR odhalila, že nejaktivnějšími sloučeninami jsou sloučeniny **14**–**16** a **21**–**24** s lipofilní substitucí v poloze C-17 steroidního kruhu, přičemž nejvyšší inhibici prokázaly sloučeniny **22** (IC_{50} 6,95 μM) a **23** (IC_{50} 5,59 μM). Nejsilnějším inhibitorem byla sloučenina **23** (Obr. 16E)**,** která vykazovala kompetitivní typ inhibice a se substrátem ALLOP vykazovala hodnotu IC_{50} 15,25 μM, čímž byla ověřena její schopnost inhibovat aktivitu 17β-HSD10 bez ohledu na substrát. U sloučenin **14**–**16** a **21**–**24** byly navíc zjištěny příznivé biologické vlastnosti, konkrétně dobrá permeabilita přes monovrstvu buněk Caco-2 a vysoká *in vitro* stabilita v potkaní a lidské plasmě (Obr. 16C). S využitím buněčné linie HEK293 bylo následně ověřeno, že sloučenina **23** neovlivňuje životaschopnost buněk a nevykazuje cytotoxicitu ani při nejvyšší testované koncentraci 20 μM. Pro ověření schopnosti sloučeniny **23** inhibovat cílový enzym uvnitř živých buněk HEK293-HSD10 byla použita fluorogenní sonda (–)-CHANA. Inhibice vykazovala

závislost na dávce (Obr. 16D), přičemž nejvyšší použitá koncentrace 25 μM vedla k ~ 50% inhibici aktivity 17β-HSD10 uvnitř buněk.

Výsledky této studie přináší rozšíření poznatků o steroidních inhibitorech 17β-HSD10 spolu s hodnotnými experimentálními výsledky. Příznivé biologické a inhibiční vlastnosti vybraných steroidních sloučenin, zejména sloučeniny **23**, naznačují, že se jedná o slibné kandidáty pro další vývoj.

A

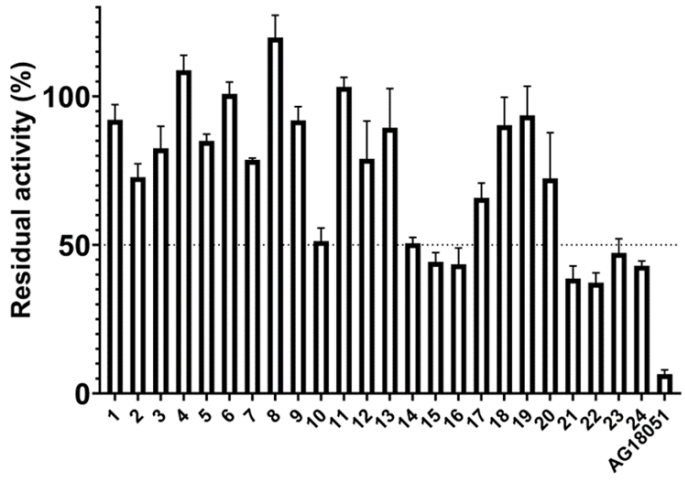

B

Compound	IC_{50} (μM)
10	16.89 ± 1.33
14	9.94 ± 0.23
15	9.01 ± 0.43
16	9.29 ± 0.28
21	7.33 ± 0.45
22	6.95 ± 0.35
23	5.59 ± 0.25
24	7.17 ± 0.40

C

Compound	Caco-2 cell permeability (50 μM)	Rat plasma stability	Human plasma stability
	Papp (cm/s)	% remaining after 8 hours	
14	5.7×10^{-6}	55	100
15	1.9×10^{-6}	99	100
16	1.2×10^{-6}	43	94
21	1.0×10^{-4}	88	99
22	1.2×10^{-5}	57	98
23	3.1×10^{-6}	32	100
24	1.3×10^{-6}	38	100

D

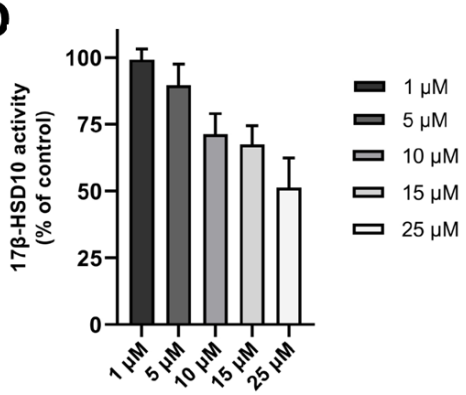

E

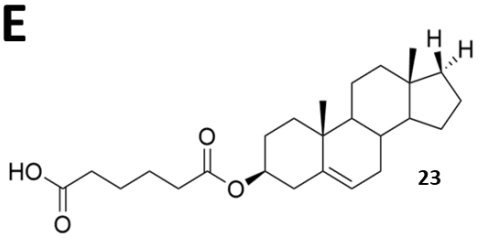

Obr. 16: *Klíčové výsledky publikace V. (**A**) Screening inhibičního potenciálu sloučenin při koncentraci 10 μM se substrátem E2. (**B**) Hodnoty IC_{50} pro nejsilnější inhibitory. (**C**) Stanovení zdánlivého permeačního koeficientu (Papp) přes monovrstvu buněk Caco-2 a in vitro stability v potkaní a lidské plasmě u vybraných inhibitorů. (**D**) Inhibice 17β-HSD10 uvnitř buněk HEK293-HSD10. (**E**) Struktura sloučeniny **23**.*

5 Seznam publikovaných prací

5.1 Seznam publikací vztahujících se k disertační práci

Zemanova, L., **Vaskova, M.**, Schmidt, M., Roubalova, J., Haleckova, A., Benek, O., Musilek, K., 2020. RNase T1 Refolding Assay for Determining Mitochondrial Cyclophilin D Activity: A Novel *In Vitro* Method Applicable in Drug Research and Discovery. Biochemistry 59, 1680–1687. https://doi.org/10.1021/acs.biochem.9b01025

WoS IF_{2020} = 3,163; Biochemistry & Molecular Biology: 193/295 (Q3)
AIS_{2020} = 1,032; Biochemistry & Molecular Biology: 113/313 (Q2)

- Podíl autora: exprese a purifikace rekombinantního CypD (analýza metodou Western blot), zavedení a optimalizace metody pro stanovení enzymatické aktivity CypD, stanovení IC_{50} vybraných inhibitorů, provedení DSF, zpracování dat (vyhodnocení a grafické zpracování), příprava a revize publikace

Benek, O., **Vaskova, M.**, Miskerikova, M., Schmidt, M., Andrys, R., Rotterova, A., Skarka, A., Hatlapatkova, J., Karasova, J.Z., Medvecky, M., Hroch, L., Vinklarova, L., Fisar, Z., Hroudova, J., Handl, J., Capek, J., Rousar, T., Kobrlova, T., Dolezal, R., Soukup, O., Aitken, L., Gunn-Moore, F., Musilek, K., 2023. Development of submicromolar 17β-HSD10 inhibitors and their *in vitro* and *in vivo* evaluation. Eur. J. Med. Chem. 258, 115593. https://doi.org/10.1016/j.ejmech.2023.115593

WoS IF_{2022} = 6,7; Medicinal Chemistry: 7/60 (Q1)
AIS_{2022} = 0,965; Medicinal Chemistry: 11/70 (Q1)

- Podíl autora: exprese a purifikace rekombinantní 17β-HSD10, biochemická evaluace inhibitorů (10 μM a 1 μM screening a stanovení IC_{50}; DSF), zpracování dat (vyhodnocení, statistické a grafické zpracování), příprava a revize publikace

Schmidt, M.†, **Vaskova, M.**†, Rotterova, A., Fiandova, P., Miskerikova, M., Zemanova, L., Benek, O., Musilek, K., 2023. Physiologically Relevant Fluorescent Assay for Identification of 17β-hydroxysteroid dehydrogenase type 10 Inhibitors. J. Neurochem. 167, 154–167. https://doi.org/10.1111/jnc.15917

(† autoři přispěli k publikaci ekvivalentním podílem)

WoS IF_{2022} = 4,7; Biochemistry & Molecular Biology: 92/285 (Q2)
Neurosciences: 85/272 (Q2)
AIS_{2022} = 1,177; Biochemistry & Molecular Biology: 86/315 (Q2)
Neurosciences: 111/306 (Q2)

- Podíl autora: exprese a purifikace rekombinantní 17β-HSD10, zavedení a optimalizace metody pro stanovení enzymatické aktivity 17β-HSD10, charakterizace metody a stanovení kinetických parametrů, biochemická evaluace inhibitorů (10 μM a 1 μM screening, stanovení IC_{50} a typu inhibice; DSF), příprava buněčné linie HEK293-17β-HSD10, zpracování dat (vyhodnocení, statistické a grafické zpracování), příprava a revize publikace

Hanzlova, M.†; Miskerikova, M.†; Rotterova, A.†; Jurkova, K.; Hamsikova, M.; Haleckova, A.; Andrys R.; Schmidt, M.; Benek, O.; Musilek, K., 2023. Nanomolar benzothiazolyl-based inhibitors of 17β-HSD10 with cellular bioactivity. ACS Med. Chem. Lett. 14, 1724−1732. https://doi.org/10.1021/acsmedchemlett.3c00355

(† autoři přispěli k publikaci ekvivalentním podílem)

WoS IF_{2022} = 4,2; Medicinal Chemistry: 21/60 (Q2)
AIS_{2022} = 0,998; Medicinal Chemistry: 10/70 (Q1)

- Podíl autora: exprese a purifikace rekombinantní 17β-HSD10, biochemická evaluace inhibitorů (10 μM a 1 μM screening, stanovení IC_{50} a typu inhibice; DSF), zpracování dat (vyhodnocení, statistické a grafické zpracování), příprava a revize publikace

Hanzlova, M., Slavikova, B., Morozovova, M., Musilek, K., Rotterova, A., Zemanova, L., Kudova, E., 2024. The C-3 steroidal hemiesters as inhibitors of 17β-hydroxysteroid dehydrogenase type 10. Manuskript v pokročilé fázi recenzního řízení v ACS Omega.

WoS IF_{2022} = 4.1; Multidisciplinary Chemistry: 69/178 (Q2)
AIS_{2022} = 0.626; Multidisciplinary Chemistry: 85/230 (Q2)

- Podíl autora: exprese a purifikace rekombinantní 17β-HSD10, biochemická evaluace inhibitorů (10 μM screening, stanovení IC_{50} a typu inhibice), zpracování dat (vyhodnocení a grafické zpracování), příprava a revize publikace

5.2 Seznam publikací nevztahujících se k disertační práci

Lee, H.M., Andrys, R., Jonczyk, J., Kim, K., Vishakantegowda, A.G., Malinak, D., Skarka, A., Schmidt, M., **Vaskova, M.**, Latka, K., Bajda, M., Jung, Y.-S., Malawska, B., Musilek, K., 2021. Pyridinium-2-carbaldoximes with quinolinium carboxamide moiety are simultaneous reactivators of acetylcholinesterase and butyrylcholinesterase inhibited by nerve agent surrogates. J. Enzyme Inhib. Med. Chem. 36, 437–449. https://doi.org/10.1080/14756366.2020.1869954

WoS IF_{2021} = 5,756; Biochemistry & Molecular Biology: 82/297 (Q2)
Medicinal Chemistry: 13/63 (Q1)
AIS_{2021} = 0,634; Biochemistry & Molecular Biology: 197/322 (Q3)
Medicinal Chemistry: 31/72 (Q2)

Maříková, J., Mamun, A.A., Shammari, L.A., Korábečný, J., Kučera, T., Hulcová, D., Kuneš, J., Malaník, M., **Vašková, M.**, Kohelová, E., Nováková, L., Cahlíková, L., Pour, M., 2021. Structure Elucidation and Cholinesterase Inhibition Activity of Two New Minor Amaryllidaceae Alkaloids. Molecules 26, 1279. https://doi.org/10.3390/molecules26051279

WoS IF_{2021} = 4,927; Biochemistry & Molecular Biology: 114/297 (Q2)
Multidisciplinary Chemistry: 65/179 (Q2)
AIS_{2021} = 0,671; Biochemistry & Molecular Biology: 177/322 (Q3)
Multidisciplinary Chemistry: 81/266 (Q2)

Malinovská, L., Le, S.T., Herczeg, M., **Vašková, M.**, Houser, J., Fujdiarová, E., Komárek, J., Hodek, P., Borbás, A., Wimmerová, M., Csávás, M., 2019. Synthesis of β-d-galactopyranoside-Presenting Glycoclusters, Investigation of Their Interactions with Pseudomonas aeruginosa Lectin A (PA-IL) and Evaluation of Their Anti-Adhesion Potential. Biomolecules 9, 686. https://doi.org/10.3390/biom9110686

WoS IF_{2019} = 4,082; Biochemistry & Molecular Biology 98/297 (Q2)

Thai Le, S., Malinovska, L., Vašková, M., Mező, E., Kelemen, V., Borbás, A., Hodek, P., Wimmerová, M., Csávás, M., 2019. Investigation of the Binding Affinity of a Broad Array of l-Fucosides with Six Fucose-Specific Lectins of Bacterial and Fungal Origin. Molecules 24, 2262. https://doi.org/10.3390/molecules24122262

WoS IF_{2019} = 3,267; Biochemistry & Molecular Biology: 142/297 (Q2)
Multidisciplinary Chemistry: 70/177 (Q2)
AIS_{2019} = 0,599; Biochemistry & Molecular Biology: 184/297 (Q3)
Multidisciplinary Chemistry: 69/177 (Q2)

6 Závěr

V současné době je léčba AD pouze symptomatická nebo založená na kontroverzním použití monoklonálních protilátek, proto je v posledních letech věnována pozornost výzkumu této nemoci a nalezení nové účinné terapie. Studované mitochondriální enzymy 17β-HSD10 a CypD představují potenciální terapeutické cíle tohoto neurodegenerativního onemocnění (Lim et al., 2020).

Vývoj nových nízkomolekulárních inhibitorů 17β-HSD10 a CypD je předmětem zájmu mnoha výzkumných skupin. Pro testování nových sloučenin *in vitro* je však klíčová volba vhodných metod pro relevantní stanovení enzymatické aktivity a potažmo inhibičních vlastností a charakterizaci testovaných sloučenin. Proto byly v rámci předkládané práce zavedeny, optimalizovány a charakterizovány robustnější metody pro stanovení enzymatické aktivity studovaných enzymů, které zohledňují fyziologické podmínky a úlohu daného enzymu v organismu: pro 17β-HSD10 byly použity neurosteroidní substráty E2 a ALLOP, pro CypD byla využita jako substrát RNasa T1. Tyto metody byly následně využity k testování inhibitorů daných enzymů. V rámci publikací vztahujících se k této disertační práci byla testována celá řada inhibitorů 17β-HSD10, které se strukturně řadí do skupin benzothiazolylových derivátů a steroidních derivátů, u CypD byly při evaluaci metody testovány tři jeho známé inhibitory. Interakce 17β-HSD10 s vybranými sloučeninami byla ověřena metodou DSF, přičemž u CypD byla touto metodou studována jeho stabilita v pufrech o různém složení. Součástí překládané práce byla též příprava monoklonálních buněčných linií HEK293-17β-HSD10, které byly využity pro testování vybraných inhibitorů 17β-HSD10 v buněčném prostředí.

Hlavním přínosem předkládané práce je zavedení a optimalizace metod pro stanovení enzymatické aktivity obou studovaných enzymů, které jsou robustnější, citlivější a využívají více fyziologické substráty a reakční podmínky pro dané enzymy než dosud používané metody. Získané experimentální výsledky poskytují rozšířené poznatky a hodnotná data nejen pro již publikované inhibitory, ale také pro design a vývoj nových klinicky relevantních inhibitorů s lepším inhibičním potenciálem a vhodnějšími vlastnostmi.

7 Seznam použité literatury

Abreo, M.A., Meng, J.J., Agree, C.S., 2005. Fused pyrazole compounds, pharmaceutical compositions, and methods for modulating or inhibiting ERAB or HADH2 activity. US6964957B2. https://patents.google.com/patent/US6964957B2/en

Afsar, A., Chacon Castro, M. del C., Soladogun, A.S., Zhang, L., 2023. Recent Development in the Understanding of Molecular and Cellular Mechanisms Underlying the Etiopathogenesis of Alzheimer's Disease. Int. J. Mol. Sci. 24, 7258. https://doi.org/10.3390/ijms24087258

Ahmed-Belkacem, A., Colliandre, L., Ahnou, N., Nevers, Q., Gelin, M., Bessin, Y., Brillet, R., Cala, O., Douguet, D., Bourguet, W., Krimm, I., Pawlotsky, J.-M., Guichou, J.-F., 2016. Fragment-based discovery of a new family of non-peptidic small-molecule cyclophilin inhibitors with potent antiviral activities. Nat. Commun. 7, 12777. https://doi.org/10.1038/ncomms12777

Aitken, L., Baillie, G., Pannifer, A., Morrison, A., Jones, P.S., Smith, T.K., McElroy, S.P., Gunn-Moore, F.J., 2017. In Vitro Assay Development and HTS of Small-Molecule Human ABAD/17β-HSD10 Inhibitors as Therapeutics in Alzheimer's Disease. SLAS Discov. Adv. Life Sci. R&D 22, 676–685. https://doi.org/10.1177/2472555217697964

Aitken, L., Benek, O., McKelvie, B.E., Hughes, R.E., Hroch, L., Schmidt, M., Major, L.L., Vinklarova, L., Kuca, K., Smith, T.K., Musilek, K., Gunn-Moore, F.J., 2019. Novel Benzothiazole-Based Ureas as 17β-HSD10 Inhibitors, A Potential Alzheimer's Disease Treatment. Molecules 24, 2757. https://doi.org/10.3390/molecules24152757

Aitken, L., Quinn, S.D., Perez-Gonzalez, C., Samuel, I.D.W., Penedo, J.C., Gunn-Moore, F.J., 2016. Morphology-Specific Inhibition of β-Amyloid Aggregates by 17β-Hydroxysteroid Dehydrogenase Type 10. ChemBioChem 17, 1029–1037. https://doi.org/10.1002/cbic.201600081

Akhter, F., Chen, D., Yan, S.F., Yan, S.S., 2017. Mitochondrial Perturbation in Alzheimer's Disease and Diabetes. Prog. Mol. Biol. Transl. Sci. 146, 341–361. https://doi.org/10.1016/bs.pmbts.2016.12.019

Alvarez de la Rosa, M., Silva, I., Nilsen, J., Pérez, M.M., García-Segura, L.M., Ávila, J., Naftolin, F., 2005. Estradiol Prevents Neural Tau Hyperphosphorylation Characteristic of Alzheimer's Disease. Ann. N. Y. Acad. Sci. 1052, 210–224. https://doi.org/10.1196/annals.1347.016

Amtul, Z., Wang, L., Westaway, D., Rozmahel, R.F., 2010. Neuroprotective mechanism conferred by 17beta-estradiol on the biochemical basis of Alzheimer's disease. Neuroscience 169, 781–786. https://doi.org/10.1016/j.neuroscience.2010.05.031

Ayan, D., Maltais, R., Poirier, D., 2012. Identification of a 17β-Hydroxysteroid Dehydrogenase Type 10 Steroidal Inhibitor: A Tool to Investigate the Role of Type 10 in Alzheimer's Disease and Prostate Cancer. ChemMedChem 7, 1181–1184. https://doi.org/10.1002/cmdc.201200129

Barbarino, J.M., Staatz, C.E., Venkataramanan, R., Klein, T.E., Altman, R.B., 2013. PharmGKB summary: cyclosporine and tacrolimus pathways. Pharmacogenet. Genomics 23, 563–585. https://doi.org/10.1097/FPC.0b013e328364db84

Benek, O., Aitken, L., Hroch, L., Kuca, K., Gunn-Moore, F., Musilek, K., 2015. A Direct Interaction Between Mitochondrial Proteins and Amyloid-β Peptide and its Significance for the Progression and Treatment of Alzheimer's Disease. Curr. Med. Chem. 22, 1056–1085. https://doi.org/10.2174/0929867322666150114163051

Benek, O., Hroch, L., Aitken, L., Dolezal, R., Guest, P., Benkova, M., Soukup, O., Musil, K., Kuca, K., Smith, T.K., Gunn-Moore, F., Musilek, K., 2017. 6-Benzothiazolyl Ureas, Thioureas and Guanidines are Potent Inhibitors of ABAD/17β-HSD10 and Potential Drugs for Alzheimer. Med. Chem. 13, 345–358. https://doi.org/10.2174/1573406413666170109142725

Benek, O., Hroch, L., Aitken, L., Gunn-Moore, F., Vinklarova, L., Kuca, K., Perez, D.I., Perez, C., Martinez, A., Fisar, Z., Musilek, K., 2018. 1-(Benzo[d]thiazol-2-yl)-3-phenylureas as dual inhibitors of casein kinase 1 and ABAD enzymes for treatment of neurodegenerative disorders. J. Enzyme Inhib. Med. Chem. 33, 665–670. https://doi.org/10.1080/14756366.2018.1445736

Benek, O., Vaskova, M., Miskerikova, M., Schmidt, M., Andrys, R., Rotterova, A., Skarka, A., Hatlapatkova, J., Karasova, J.Z., Medvecky, M., Hroch, L., Vinklarova, L., Fisar, Z., Hroudova, J., Handl, J., Capek, J., Rousar, T., Kobrlova, T., Dolezal, R., Soukup, O., Aitken, L., Gunn-Moore, F., Musilek, K., 2023. Development of submicromolar 17β-HSD10 inhibitors and their in vitro and in vivo evaluation. Eur. J. Med. Chem. 258, 115593. https://doi.org/10.1016/j.ejmech.2023.115593

Bergsma, D.J., Eder, C., Gross, M., Kersten, H., Sylvester, D., Appelbaum, E., Cusimano, D., Livi, G.P., McLaughlin, M.M., Kasyan, K., 1991. The cyclophilin multigene family of peptidyl-prolyl isomerases. Characterization of three separate human isoforms. J. Biol. Chem. 266, 23204–23214. https://doi.org/10.1016/S0021-9258(18)54484-7

Bernardi, P., von Stockum, S., 2012. The permeability transition pore as a Ca2+ release channel: New answers to an old question. Cell Calcium 52, 22–27. https://doi.org/10.1016/j.ceca.2012.03.004

Binstock, J.F., Schulz, H., 1981. Fatty acid oxidation complex from Escherichia coli. Methods Enzymol. 71, 403–411. https://doi.org/10.1016/0076-6879(81)71051-6

Bose, S., Mücke, M., Freedman, R.B., 1994. The characterization of a cyclophilin-type peptidyl prolyl cis-trans-isomerase from the endoplasmic-reticulum lumen. Biochem. J. 300, 871–875. https://doi.org/10.1042/bj3000871

Boutin, S., Maltais, R., Roy, J., Poirier, D., 2021. Synthesis of 17β-hydroxysteroid dehydrogenase type 10 steroidal inhibitors: Selectivity, metabolic stability and enhanced potency. Eur. J. Med. Chem. 209, 112909. https://doi.org/10.1016/j.ejmech.2020.112909

Boutin, S., Roy, J., Maltais, R., Alata, W., Calon, F., Poirier, D., 2018. Identification of steroidal derivatives inhibiting the transformations of allopregnanolone and estradiol by 17β-hydroxysteroid dehydrogenase type 10. Bioorg. Med. Chem. Lett. 28, 3554–3559. https://doi.org/10.1016/j.bmcl.2018.09.031

Brinton, R., 2023. Allopregnanolone Regenerative Therapeutic for Mild Alzheimer's Disease (REGEN-BRAIN©). Identification No. NCT04838301. https://clinicaltrials.gov/study/NCT04838301 (citováno 9. 1. 2024)

Brinton, R.D., Wang, J.M., 2006. Therapeutic Potential of Neurogenesis for Prevention and Recovery from Alzheimer's Disease: Allopregnanolone as a Proof of Concept Neurogenic Agent. Curr. Alzheimer Res. 3, 185–190. https://doi.org/10.2174/156720506777632817

Butterworth, R.F., Besnard, A.M., 1990. Thiamine-dependent enzyme changes in temporal cortex of patients with Alzheimer's disease. Metab. Brain Dis. 5, 179–184. https://doi.org/10.1007/BF00997071

Caporale, A., Mascanzoni, F., Farina, B., Sturlese, M., Di Sorbo, G., Fattorusso, R., Ruvo, M., Doti, N., 2016. FRET-Protease-Coupled Peptidyl-Prolyl cis-trans Isomerase Assay: New Internally Quenched Fluorogenic Substrates for High-Throughput Screening. J. Biomol. Screen. 21, 701–712. https://doi.org/10.1177/1087057116650402

Carlson, E.A., Marquez, R.T., Du, F., Wang, Y., Xu, L., Yan, S.S., 2015. Overexpression of 17β-hydroxysteroid dehydrogenase type 10 increases pheochromocytoma cell growth and resistance to cell death. BMC Cancer 15, 166. https://doi.org/10.1186/s12885-015-1173-5

Chen, J.X., Yan, S.D., 2007. Amyloid-β-Induced Mitochondrial Dysfunction. J. Alzheimers Dis. 12, 177–184. https://doi.org/10.3233/JAD-2007-12208

Chen, S., Wang, J.M., Irwin, R.W., Yao, J., Liu, L., Brinton, R.D., 2011. Allopregnanolone promotes regeneration and reduces β-amyloid burden in a preclinical model of Alzheimer's disease. PloS ONE 6, e24293. https://doi.org/10.1371/journal.pone.0024293

Cho, I., Kim, W.-J., Kim, H.-W., Heo, K., Lee, B.I., Cho, Y.-J., 2018. Increased Superoxide Dismutase 2 by Allopregnanolone Ameliorates ROS-Mediated Neuronal Death in Mice with Pilocarpine-Induced Status Epilepticus. Neurochem. Res. 43, 1464–1475. https://doi.org/10.1007/s11064-018-2561-4

Cummings, J., Apostolova, L., Rabinovici, G.D., Atri, A., Aisen, P., Greenberg, S., Hendrix, S., Selkoe, D., Weiner, M., Petersen, R.C., Salloway, S., 2023. Lecanemab: Appropriate Use Recommendations. J. Prev. Alzheimers Dis. 10, 362–377. https://doi.org/10.14283/jpad.2023.30

Cummings, J., Rabinovici, G.D., Atri, A., Aisen, P., Apostolova, L.G., Hendrix, S., Sabbagh, M., Selkoe, D., Weiner, M., Salloway, S., 2022. Aducanumab: Appropriate Use Recommendations Update. J. Prev. Alzheimers Dis. 9, 221–230. https://doi.org/10.14283/jpad.2022.34

Davis, T.L., Walker, J.R., Campagna-Slater, V., Jr, P.J.F., Paramanathan, R., Bernstein, G., MacKenzie, F., Tempel, W., Ouyang, H., Lee, W.H., Eisenmesser, E.Z., Dhe-Paganon, S., 2010. Structural and Biochemical Characterization of the Human Cyclophilin Family of Peptidyl-Prolyl Isomerases. PLoS Biol. 8, e1000439. https://doi.org/10.1371/journal.pbio.1000439

Deutschmann, A.J., Amberger, A., Zavadil, C., Steinbeisser, H., Mayr, J.A., Feichtinger, R.G., Oerum, S., Yue, W.W., Zschocke, J., 2014. Mutation or knock-down of 17β-hydroxysteroid dehydrogenase type 10 cause loss of MRPP1 and impaired processing of mitochondrial heavy strand transcripts. Hum. Mol. Genet. 23, 3618–3628. https://doi.org/10.1093/hmg/ddu072

Dragicevic, N., Mamcarz, M., Zhu, Y., Buzzeo, R., Tan, J., Arendash, G.W., Bradshaw, P.C., 2010. Mitochondrial amyloid-beta levels are associated with the extent of mitochondrial dysfunction in different brain regions and the degree of cognitive impairment in Alzheimer's transgenic mice. J. Alzheimers Dis. 20, S535-550. https://doi.org/10.3233/JAD-2010-100342

Du, H., Guo, L., Fang, F., Chen, D., A Sosunov, A., M McKhann, G., Yan, Y., Wang, C., Zhang, H., Molkentin, J.D., Gunn-Moore, F.J., Vonsattel, J.P., Arancio, O., Chen, J.X., Yan, S.D., 2008. Cyclophilin D deficiency attenuates mitochondrial and neuronal perturbation and ameliorates learning and memory in Alzheimer's disease. Nat. Med. 14, 1097–1105. https://doi.org/10.1038/nm.1868

Du, H., Guo, L., Yan, S., Sosunov, A.A., McKhann, G.M., Yan, S.S., 2010. Early deficits in synaptic mitochondria in an Alzheimer's disease mouse model. Proc. Natl. Acad. Sci. U. S. A. 107, 18670–18675. https://doi.org/10.1073/pnas.1006586107

Du, H., Yan, S.S., 2010. Unlocking the Door to Neuronal Woes in Alzheimer's Disease: Aβ and Mitochondrial Permeability Transition Pore. Pharm. Basel Switz. 3, 1936–1948. https://doi.org/10.3390/ph3061936

Du, X., Wang, X., Geng, M., 2018. Alzheimer's disease hypothesis and related therapies. Transl. Neurodegener. 7, 2. https://doi.org/10.1186/s40035-018-0107-y

Dugger, B.N., Dickson, D.W., 2017. Pathology of Neurodegenerative Diseases. Cold Spring Harb. Perspect. Biol. 9, a028035. https://doi.org/10.1101/cshperspect.a028035

Elrod, J.W., Wong, R., Mishra, S., Vagnozzi, R.J., Sakthievel, B., Goonasekera, S.A., Karch, J., Gabel, S., Farber, J., Force, T., Brown, J.H., Murphy, E., Molkentin, J.D., 2010. Cyclophilin D controls mitochondrial pore–dependent Ca^{2+} exchange, metabolic flexibility, and propensity for heart failure in mice. J. Clin. Invest. 120, 3680–3687. https://doi.org/10.1172/JCI43171

Fang, E.F., Hou, Y., Palikaras, K., Adriaanse, B.A., Kerr, J.S., Yang, B., Lautrup, S., Hasan-Olive, M.M., Caponio, D., Dan, X., Rocktäschel, P., Croteau, D.L., Akbari, M., Greig, N.H., Fladby, T., Nilsen, H., Cader, M.Z., Mattson, M.P., Tavernarakis, N., Bohr, V.A., 2019. Mitophagy inhibits amyloid-β and tau pathology and reverses cognitive deficits in models of Alzheimer's disease. Nat. Neurosci. 22, 401–412. https://doi.org/10.1038/s41593-018-0332-9

Fišar, Z., 2022. Linking the Amyloid, Tau, and Mitochondrial Hypotheses of Alzheimer's Disease and Identifying Promising Drug Targets. Biomolecules 12, 1676. https://doi.org/10.3390/biom12111676

Flannagan, K., Stopperan, J.A., Troutwine, B.M., Lysaker, C.R., Strope, T., Draper, J., Shaddy-Gouvion, C., Vivian, J., Haeri, M., Wilkins, H.M., 2021. Mitochondrial phenotypes in iPSC AD models. Alzheimers Dement. 17, e058489. https://doi.org/10.1002/alz.058489

Fracassi, A., Marcatti, M., Zolochevska, O., Tabor, N., Woltjer, R., Moreno, S., Taglialatela, G., 2021. Oxidative Damage and Antioxidant Response in Frontal Cortex of Demented and Nondemented Individuals with Alzheimer's Neuropathology. J. Neurosci. 41, 538–554. https://doi.org/10.1523/JNEUROSCI.0295-20.2020

GBD 2019 Dementia Forecasting Collaborators, 2022. Estimation of the global prevalence of dementia in 2019 and forecasted prevalence in 2050: an analysis for the Global Burden of Disease Study 2019. Alzheimer's Dement. 7, e105–e125. https://doi.org/10.1016/S2468-2667(21)00249-8

Gelin, M., Delfosse, V., Allemand, F., Hoh, F., Sallaz-Damaz, Y., Pirocchi, M., Bourguet, W., Ferrer, J.L., Labesse, G., Guichou, J.F., 2015. Combining "dry" co-crystallization and in situ diffraction to facilitate ligand screening by X-ray crystallography. Acta Crystallogr. D Biol. Crystallogr. 71, 1777–1787. https://doi.org/10.1107/S1399004715010342

Giatti, S., Boraso, M., Melcangi, R.C., Viviani, B., 2012. Neuroactive steroids, their metabolites, and neuroinflammation. J. Mol. Endocrinol. 49, R125–R134. https://doi.org/10.1530/JME-12-0127

Giorgio, V., Bisetto, E., Soriano, M.E., Dabbeni-Sala, F., Basso, E., Petronilli, V., Forte, M.A., Bernardi, P., Lippe, G., 2009. Cyclophilin D Modulates Mitochondrial F0F1-ATP Synthase by Interacting with the Lateral Stalk of the Complex. J. Biol. Chem. 284, 33982–33988. https://doi.org/10.1074/jbc.M109.020115

Giorgio, V., Soriano, M.E., Basso, E., Bisetto, E., Lippe, G., Forte, M.A., Bernardi, P., 2010. Cyclophilin D in mitochondrial pathophysiology. Biochim. Biophys. Acta 1797, 1113–1118. https://doi.org/10.1016/j.bbabio.2009.12.006

Goodenough, S., Schleusner, D., Pietrzik, C., Skutella, T., Behl, C., 2005. Glycogen synthase kinase 3β links neuroprotection by 17β-estradiol to key Alzheimer processes. Neuroscience 132, 581–589. https://doi.org/10.1016/j.neuroscience.2004.12.029

Grädler, U., Schwarz, D., Blaesse, M., Leuthner, B., Johnson, T.L., Bernard, F., Jiang, X., Marx, A., Gilardone, M., Lemoine, H., Roche, D., Jorand-Lebrun, C., 2019. Discovery of novel Cyclophilin D inhibitors starting from three dimensional fragments with millimolar potencies. Bioorg. Med. Chem. Lett. 29, 126717. https://doi.org/10.1016/j.bmcl.2019.126717

Grimm, A., Biliouris, E.E., Lang, U.E., Götz, J., Mensah-Nyagan, A.G., Eckert, A., 2016. Sex hormone-related neurosteroids differentially rescue bioenergetic deficits induced by amyloid-β or hyperphosphorylated tau protein. Cell. Mol. Life Sci. 73, 201–215. https://doi.org/10.1007/s00018-015-1988-x

Grimm, A., Lim, Y.-A., Mensah-Nyagan, A.G., Götz, J., Eckert, A., 2012. Alzheimer's disease, oestrogen and mitochondria: an ambiguous relationship. Mol. Neurobiol. 46, 151–160. https://doi.org/10.1007/s12035-012-8281-x

Grimm, A., Schmitt, K., Lang, U.E., Mensah-Nyagan, A.G., Eckert, A., 2014. Improvement of neuronal bioenergetics by neurosteroids: implications for age-related neurodegenerative disorders. Biochim. Biophys. Acta 1842, 2427–2438. https://doi.org/10.1016/j.bbadis.2014.09.013

Guglielmotto, M., Manassero, G., Vasciaveo, V., Venezia, M., Tabaton, M., Tamagno, E., 2020. Estrogens Inhibit Amyloid-β-Mediated Paired Helical Filament-Like Conformation of Tau Through Antioxidant Activity and miRNA 218 Regulation in hTau Mice. J. Alzheimers Dis. 77, 1339–1351. https://doi.org/10.3233/JAD-200707

Guichou, J.-F., Viaud, J., Mettling, C., Subra, G., Lin, Y.-L., Chavanieu, A., 2006. Structure-Based Design, Synthesis, and Biological Evaluation of Novel Inhibitors of Human Cyclophilin A. J. Med. Chem. 49, 900–910. https://doi.org/10.1021/jm050716a

Guo, H., Wang, F., Yu, K., Chen, J., Bai, D., Chen, K., Shen, X., Jiang, H., 2005. Novel cyclophilin D inhibitors derived from quinoxaline exhibit highly inhibitory activity against rat mitochondrial swelling and Ca2+ uptake/release. Acta Pharmacol. Sin. 26, 1201–1211. https://doi.org/10.1111/j.1745-7254.2005.00189.x

Gutiérrez-Aguilar, M., Baines, C.P., 2015. Structural mechanisms of cyclophilin D-dependent control of the mitochondrial permeability transition pore. Biochim. Biophys. Acta 1850, 2041–2047. https://doi.org/10.1016/j.bbagen.2014.11.009

Haleckova, A., Benek, O., Zemanová, L., Dolezal, R., Musilek, K., 2022. Small-molecule inhibitors of cyclophilin D as potential therapeutics in mitochondria-related diseases. Med. Res. Rev. 42, 1822–1855. https://doi.org/10.1002/med.21892

Halestrap, A.P., 2010. A pore way to die: the role of mitochondria in reperfusion injury and cardioprotection. Biochem. Soc. Trans. 38, 841–860. https://doi.org/10.1042/BST0380841

Hansson, M.J., Mattiasson, G., Månsson, R., Karlsson, J., Keep, M.F., Waldmeier, P., Ruegg, U.T., Dumont, J.-M., Besseghir, K., Elmér, E., 2004. The Nonimmunosuppressive Cyclosporin Analogs NIM811 and UNIL025 Display Nanomolar Potencies on Permeability Transition in Brain-Derived Mitochondria. J. Bioenerg. Biomembr. 36, 407–413. https://doi.org/10.1023/B:JOBB.0000041776.31885.45

He, J., Hoffman, S.W., Stein, D.G., 2004. Allopregnanolone, a progesterone metabolite, enhances behavioral recovery and decreases neuronal loss after traumatic brain injury. Restor. Neurol. Neurosci. 22, 19–31.

He, X.-Y., Dobkin, C., Brown, W.T., Yang, S.-Y., 2023. Infantile Neurodegeneration Results from Mutants of 17β-Hydroxysteroid Dehydrogenase Type 10 Rather Than Aβ-Binding Alcohol Dehydrogenase. Int. J. Mol. Sci. 24, 8487. https://doi.org/10.3390/ijms24108487

He, X.-Y., Dobkin, C., Brown, W.T., Yang, S.-Y., 2022. 3-Hydroxyacyl-CoA and Alcohol Dehydrogenase Activities of Mitochondrial Type 10 17β-Hydroxysteroid Dehydrogenase in Neurodegeneration Study. J. Alzheimers Dis. 88, 1487–1497. https://doi.org/10.3233/JAD-220481

He, X.-Y., Isaacs, C., Yang, S.-Y., 2018. Roles of Mitochondrial 17β-Hydroxysteroid Dehydrogenase Type 10 in Alzheimer's Disease. J. Alzheimers Dis. 62, 665–673. https://doi.org/10.3233/JAD-170974

He, X.-Y., Merz, G., Mehta, P., Schulz, H., Yang, S.-Y., 1999. Human Brain Short Chain l-3-Hydroxyacyl Coenzyme A Dehydrogenase Is a Single-domain Multifunctional Enzyme: characterization of a novel 17β-hydroxysteroid dehydrogenase. J. Biol. Chem. 274, 15014–15019. https://doi.org/10.1074/jbc.274.21.15014

He, X.-Y., Merz, G., Yang, Y.Z., Mehta, P., Schulz, H., Yang, S.Y., 2001. Characterization and localization of human type10 17beta-hydroxysteroid dehydrogenase. Eur. J. Biochem. 268, 4899–4907. https://doi.org/10.1046/j.0014-2956.2001.02421.2421.x

He, X.-Y., Merz, G., Yang, Y.Z., Pullakart, R., Mehta, P., Schulz, H., Yang, S.Y., 2000a. Function of human brain short chain L-3-hydroxyacyl coenzyme A dehydrogenase in androgen metabolism. Biochim. Biophys. Acta 1484, 267–277. https://doi.org/10.1016/s1388-1981(00)00014-7

He, X.-Y., Schulz, H., Yang, S.Y., 1998. A human brain L-3-hydroxyacyl-coenzyme A dehydrogenase is identical to an amyloid beta-peptide-binding protein involved in Alzheimer's disease. J. Biol. Chem. 273, 10741–10746. https://doi.org/10.1074/jbc.273.17.10741

He, X.-Y., Wegiel, J., Yang, S.-Y., 2005a. Intracellular oxidation of allopregnanolone by human brain type 10 17beta-hydroxysteroid dehydrogenase. Brain Res. 1040, 29–35. https://doi.org/10.1016/j.brainres.2005.01.022

He, X.-Y., Wegiel, J., Yang, Y.-Z., Pullarkat, R., Schulz, H., Yang, S.-Y., 2005b. Type 10 17beta-hydroxysteroid dehydrogenase catalyzing the oxidation of steroid modulators of gamma-aminobutyric acid type A receptors. Mol. Cell. Endocrinol. 229, 111–117. https://doi.org/10.1016/j.mce.2004.08.011

He, X.-Y., Yang, Y.-Z., Peehl, D.M., Lauderdale, A., Schulz, H., Yang, S.-Y., 2003. Oxidative 3α-hydroxysteroid dehydrogenase activity of human type 10 17β-hydroxysteroid dehydrogenase. J. Steroid Biochem. Mol. Biol. 87, 191–198. https://doi.org/10.1016/j.jsbmb.2003.07.007

He, X.-Y., Yang, Y.Z., Schulz, H., Yang, S.Y., 2000b. Intrinsic alcohol dehydrogenase and hydroxysteroid dehydrogenase activities of human mitochondrial short-chain L-3-hydroxyacyl-CoA dehydrogenase. Biochem. J. 345, 139–143. https://doi.org/10.1042/bj3450139

Hemmerová, E., Špringer, T., Krištofiková, Z., Homola, J., 2019. In vitro study of interaction of 17β-hydroxysteroid dehydrogenase type 10 and cyclophilin D and its potential implications for Alzheimer's disease. Sci. Rep. 9, 16700. https://doi.org/10.1038/s41598-019-53157-7

Holper, L., Ben-Shachar, D., Mann, J.J., 2019. Multivariate meta-analyses of mitochondrial complex I and IV in major depressive disorder, bipolar disorder, schizophrenia, Alzheimer disease, and Parkinson disease. Neuropsychopharmacology 44, 837–849. https://doi.org/10.1038/s41386-018-0090-0

Holzmann, J., Frank, P., Löffler, E., Bennett, K.L., Gerner, C., Rossmanith, W., 2008. RNase P without RNA: identification and functional reconstitution of the human mitochondrial tRNA processing enzyme. Cell 135, 462–474. https://doi.org/10.1016/j.cell.2008.09.013

Holzmann, J., Rossmanith, W., 2009. tRNA recognition, processing, and disease: Hypotheses around an unorthodox type of RNase P in human mitochondria. Mitochondrion 9, 284–288. https://doi.org/10.1016/j.mito.2009.03.008

Hosie, A.M., Wilkins, M.E., da Silva, H.M.A., Smart, T.G., 2006. Endogenous neurosteroids regulate GABAA receptors through two discrete transmembrane sites. Nature 444, 486–489. https://doi.org/10.1038/nature05324

Hroch, L., Benek, O., Guest, P., Aitken, L., Soukup, O., Janockova, J., Musil, K., Dohnal, V., Dolezal, R., Kuca, K., Smith, T.K., Gunn-Moore, F., Musilek, K., 2016. Design, synthesis and in vitro evaluation of benzothiazole-based ureas as potential ABAD/17β-HSD10 modulators for Alzheimer's disease treatment. Bioorg. Med. Chem. Lett. 26, 3675–3678. https://doi.org/10.1016/j.bmcl.2016.05.087

Hroch, L., Guest, P., Benek, O., Soukup, O., Janockova, J., Dolezal, R., Kuca, K., Aitken, L., Smith, T.K., Gunn-Moore, F., Zala, D., Ramsay, R.R., Musilek, K., 2017. Synthesis and evaluation of frentizole-based indolyl thiourea analogues as MAO/ABAD inhibitors for Alzheimer's disease treatment. Bioorg. Med. Chem. 25, 1143–1152. https://doi.org/10.1016/j.bmc.2016.12.029

Jeffery, C.J., 2018. Protein moonlighting: what is it, and why is it important? Philos. Trans. R. Soc. B Biol. Sci. 373, 20160523. https://doi.org/10.1098/rstb.2016.0523

Jeffery, C.J., 1999. Moonlighting proteins. Trends Biochem. Sci. 24, 8–11. https://doi.org/10.1016/s0968-0004(98)01335-8

Jernberg, E., Thysell, E., Ylitalo, E.B., Rudolfsson, S., Crnalic, S., Widmark, A., Bergh, A., Wikström, P., 2013. Characterization of Prostate Cancer Bone Metastases According to Expression Levels of Steroidogenic Enzymes and Androgen Receptor Splice Variants. PLoS ONE 8, e77407. https://doi.org/10.1371/journal.pone.0077407

Johnson, N., Khan, A., Virji, S., Ward, J.M., Crompton, M., 1999. Import and processing of heart mitochondrial cyclophilin D. Eur. J. Biochem. 263, 353–359. https://doi.org/10.1046/j.1432-1327.1999.00490.x

Kajitani, K., Fujihashi, M., Kobayashi, Y., Shimizu, S., Tsujimoto, Y., Miki, K., 2008. Crystal structure of human cyclophilin D in complex with its inhibitor, cyclosporin A at 0.96-Å resolution. Proteins Struct. Funct. Bioinforma. 70, 1635–1639. https://doi.org/10.1002/prot.21855

Kang, J.-S., Tian, J.-H., Pan, P.-Y., Zald, P., Li, C., Deng, C., Sheng, Z.-H., 2008. Docking of axonal mitochondria by syntaphilin controls their mobility and affects short-term facilitation. Cell 132, 137–148. https://doi.org/10.1016/j.cell.2007.11.024

Khan, S.M., Cassarino, D.S., Abramova, N.N., Keeney, P.M., Borland, M.K., Trimmer, P.A., Krebs, C.T., Bennett, J.C., Parks, J.K., Swerdlow, R.H., Parker, W.D., Bennett, J.P., 2000. Alzheimer's disease cybrids replicate beta-amyloid abnormalities through cell death pathways. Ann. Neurol. 48, 148–155. https://doi.org/10.1002/1531-8249(200008)48:2<148::AID-ANA3>3.0.CO;2-7

Kim, S.H., Vlkolinsky, R., Cairns, N., Fountoulakis, M., Lubec, G., 2001. The reduction of NADH ubiquinone oxidoreductase 24- and 75-kDa subunits in brains of patients with Down syndrome and Alzheimer's disease. Life Sci. 68, 2741–2750. https://doi.org/10.1016/s0024-3205(01)01074-8

Kim, S.-U., Jin, M.-H., Kim, Y.S., Lee, S.-H., Cho, Y.S., Cho, K.-J., Lee, K.-S., Kim, Y.I., Kim, G.W., Kim, J.-M., Lee, T.-H., Lee, Y.-H., Shong, M., Kim, H.-C., Chang, K.-T., Yu, D.-Y., Lee, D.-S., 2011. Peroxiredoxin II preserves cognitive function against age-linked hippocampal oxidative damage. Neurobiol. Aging 32, 1054–1068. https://doi.org/10.1016/j.neurobiolaging.2009.05.017

Kinnally, K.W., Peixoto, P.M., Ryu, S.-Y., Dejean, L.M., 2011. Is mPTP the gatekeeper for necrosis, apoptosis, or both? Biochim. Biophys. Acta 1813, 616–622. https://doi.org/10.1016/j.bbamcr.2010.09.013

Kissinger, C.R., Rejto, P.A., Pelletier, L.A., Thomson, J.A., Showalter, R.E., Abreo, M.A., Agree, C.S., Margosiak, S., Meng, J.J., Aust, R.M., Vanderpool, D., Li, B., Tempczyk-Russell, A., Villafranca, J.E., 2004. Crystal structure of human ABAD/HSD10 with a bound inhibitor: implications for design of Alzheimer's disease therapeutics. J. Mol. Biol. 342, 943–952. https://doi.org/10.1016/j.jmb.2004.07.071

Kofron, J.L., Kuzmic, P., Kishore, V., Colón-Bonilla, E., Rich, D.H., 1991. Determination of kinetic constants for peptidyl prolyl cis-trans isomerases by an improved spectrophotometric assay. Biochemistry 30, 6127–6134. https://doi.org/10.1021/bi00239a007

Kristofiková, Z., Bocková, M., Hegnerová, K., Bartos, A., Klaschka, J., Rícný, J., Rípová, D., Homola, J., 2009. Enhanced levels of mitochondrial enzyme 17beta-hydroxysteroid dehydrogenase type 10 in patients with Alzheimer disease and multiple sclerosis. Mol. Biosyst. 5, 1174–1179. https://doi.org/10.1039/b904799a

Kristofikova, Z., Springer, T., Gedeonova, E., Hofmannova, A., Ricny, J., Hromadkova, L., Vyhnalek, M., Laczo, J., Nikolai, T., Hort, J., Petrasek, T., Stuchlik, A., Vales, K., Klaschka, J., Homola, J., 2020. Interactions of 17β-Hydroxysteroid Dehydrogenase Type 10 and Cyclophilin D in Alzheimer's Disease. Neurochem. Res. 45, 915–927. https://doi.org/10.1007/s11064-020-02970-y

Li, W., Zhang, C., Sun, X., 2018. Mitochondrial Ca2+ Retention Capacity Assay and Ca2+-triggered Mitochondrial Swelling Assay. J. Vis. Exp. 135, e56236. https://doi.org/10.3791/56236

Lim, J.W., Lee, J., Pae, A.N., 2020. Mitochondrial dysfunction and Alzheimer's disease: prospects for therapeutic intervention. BMB Rep. 53, 47–55. https://doi.org/10.5483/BMBRep.2020.53.1.279

Lim, Y.-A., Grimm, A., Giese, M., Mensah-Nyagan, A.G., Villafranca, J.E., Ittner, L.M., Eckert, A., Götz, J., 2011. Inhibition of the Mitochondrial Enzyme ABAD Restores the Amyloid-β-Mediated Deregulation of Estradiol. PLoS ONE 6, e28887. https://doi.org/10.1371/journal.pone.0028887

Lionaki, E., Markaki, M., Palikaras, K., Tavernarakis, N., 2015. Mitochondria, autophagy and age-associated neurodegenerative diseases: New insights into a complex interplay. Biochim. Biophys. Acta 1847, 1412–1423. https://doi.org/10.1016/j.bbabio.2015.04.010

Lopez Sanchez, M.I.G., Crowston, J.G., Mackey, D.A., Trounce, I.A., 2016. Emerging Mitochondrial Therapeutic Targets in Optic Neuropathies. Pharmacol. Ther. 165, 132–152. https://doi.org/10.1016/j.pharmthera.2016.06.004

Luo, M.J., Mao, L.F., Schulz, H., 1995. Short-chain 3-hydroxy-2-methylacyl-CoA dehydrogenase from rat liver: purification and characterization of a novel enzyme of isoleucine metabolism. Arch. Biochem. Biophys. 321, 214–220. https://doi.org/10.1006/abbi.1995.1388

Luque-Contreras, D., Carvajal, K., Toral-Rios, D., Franco-Bocanegra, D., Campos-Peña, V., 2014. Oxidative Stress and Metabolic Syndrome: Cause or Consequence of Alzheimer's Disease? Oxid. Med. Cell. Longev. 2014, e497802. https://doi.org/10.1155/2014/497802

Lustbader, J.W., Cirilli, M., Lin, C., Xu, H.W., Takuma, K., Wang, N., Caspersen, C., Chen, X., Pollak, S., Chaney, M., Trinchese, F., Liu, S., Gunn-Moore, F., Lue, L.-F., Walker, D.G., Kuppusamy, P., Zewier, Z.L., Arancio, O., Stern, D., Yan, S.S., Wu, H., 2004. ABAD directly links Abeta to mitochondrial toxicity in Alzheimer's disease. Science 304, 448–452. https://doi.org/10.1126/science.1091230

Manly, J.J., Merchant, C.A., Jacobs, D.M., Small, S.A., Bell, K., Ferin, M., Mayeux, R., 2000. Endogenous estrogen levels and Alzheimer's disease among postmenopausal women. Neurology 54, 833–837. https://doi.org/10.1212/WNL.54.4.833

Marino, M., Galluzzo, P., Ascenzi, P., 2006. Estrogen Signaling Multiple Pathways to Impact Gene Transcription. Curr. Genomics 7, 497–508. https://doi.org/10.2174/138920206779315737

Marques, A.T., Antunes, A., Fernandes, P.A., Ramos, M.J., 2008. Computational optimization of AG18051 inhibitor for amyloid-β binding alcohol dehydrogenase enzyme. Int. J. Quantum Chem. 108, 1982–1991. https://doi.org/10.1002/qua.21716

Marx, C.E., Trost, W.T., Shampine, L.J., Stevens, R.D., Hulette, C.M., Steffens, D.C., Ervin, J.F., Butterfield, M.I., Blazer, D.G., Massing, M.W., Lieberman, J.A., 2006. The neurosteroid allopregnanolone is reduced in prefrontal cortex in Alzheimer's disease. Biol. Psychiatry 60, 1287–1294. https://doi.org/10.1016/j.biopsych.2006.06.017

Mastrogiacomo, F., Bergeron, C., Kish, S.J., 1993. Brain α-Ketoglutarate Dehydrotenase Complex Activity in Alzheimer's Disease. J. Neurochem. 61, 2007–2014. https://doi.org/10.1111/j.1471-4159.1993.tb07436.x

Matouschek, A., Rospert, S., Schmid, K., Glick, B.S., Schatz, G., 1995. Cyclophilin catalyzes protein folding in yeast mitochondria. Proc. Natl. Acad. Sci. U. S. A. 92, 6319–6323. https://doi.org/10.1073/pnas.92.14.6319

Meltzer-Brody, S., Colquhoun, H., Riesenberg, R., Epperson, C.N., Deligiannidis, K.M., Rubinow, D.R., Li, H., Sankoh, A.J., Clemson, C., Schacterle, A., Jonas, J., Kanes, S., 2018. Brexanolone injection in post-partum depression: two multicentre, double-blind, randomised, placebo-controlled, phase 3 trials. Lancet 392, 1058–1070. https://doi.org/10.1016/S0140-6736(18)31551-4

Metodieva, V., Smith, T., Gunn-Moore, F., 2022. The Mitochondrial Enzyme 17βHSD10 Modulates Ischemic and Amyloid-β-Induced Stress in Primary Mouse Astrocytes. eNeuro 9, ENEURO.0040-22.2022. https://doi.org/10.1523/ENEURO.0040-22.2022

Misztal, T., Kowalczyk, P., Młotkowska, P., Marciniak, E., 2020. The Effect of Allopregnanolone on Enzymatic Activity of the DNA Base Excision Repair Pathway in the Sheep Hippocampus and Amygdala under Natural and Stressful Conditions. Int. J. Mol. Sci. 21, 7762. https://doi.org/10.3390/ijms21207762

Moeller, G., Adamski, J., 2006. Multifunctionality of human 17beta-hydroxysteroid dehydrogenases. Mol. Cell. Endocrinol. 248, 47–55. https://doi.org/10.1016/j.mce.2005.11.031

Mori, T., Itami, S., Yanagi, T., Tatara, Y., Takamiya, M., Uchida, T., 2009. Use of a Real-Time Fluorescence Monitoring System for High-Throughput Screening for Prolyl Isomerase Inhibitors. J. Biomol. Screen. 14, 419–424. https://doi.org/10.1177/1087057109333979

Morsy, A., Maddeboina, K., Gao, J., Wang, H., Valdez, J., Dow, L.F., Wang, X., Trippier, P.C., 2022. Functionalized Allopurinols Targeting Amyloid-Binding Alcohol Dehydrogenase Rescue Aβ-Induced Mitochondrial Dysfunction. ACS Chem. Neurosci. 13, 2176–2190. https://doi.org/10.1021/acschemneuro.2c00246

Muirhead, K.E.A., Borger, E., Aitken, L., Conway, S.J., Gunn-Moore, F.J., 2010a. The consequences of mitochondrial amyloid beta-peptide in Alzheimer's disease. Biochem. J. 426, 255–270. https://doi.org/10.1042/bj20091941

Muirhead, K. E. A., Froemming, M., Li, X., Musilek, K., Conway, S.J., Sames, D., Gunn-Moore, F.J., 2010b. (-)-CHANA, a fluorogenic probe for detecting amyloid binding alcohol dehydrogenase HSD10 activity in living cells. ACS Chem. Biol. 5, 1105–1114. https://doi.org/10.1021/cb100199m

Murasawa, S., Iuchi, K., Sato, S., Noguchi-Yachide, T., Sodeoka, M., Yokomatsu, T., Dodo, K., Hashimoto, Y., Aoyama, H., 2012. Small-molecular inhibitors of Ca2+-induced mitochondrial permeability transition (MPT) derived from muscle relaxant dantrolene. Bioorg. Med. Chem. 20, 6384–6393. https://doi.org/10.1016/j.bmc.2012.08.062

Nilsen, J., 2008. Estradiol and neurodegenerative oxidative stress. Front. Neuroendocrinol. 29, 463–475. https://doi.org/10.1016/j.yfrne.2007.12.005

Oerum, S., Roovers, M., Rambo, R.P., Kopec, J., Bailey, H.J., Fitzpatrick, F., Newman, J.A., Newman, W.G., Amberger, A., Zschocke, J., Droogmans, L., Oppermann, U., Yue, W.W., 2018. Structural insight into the human mitochondrial tRNA purine N1-methyltransferase and ribonuclease P complexes. J. Biol. Chem. 293, 12862–12876. https://doi.org/10.1074/jbc.ra117.001286

Oppermann, U.C., Salim, S., Tjernberg, L.O., Terenius, L., Jörnvall, H., 1999. Binding of amyloid beta-peptide to mitochondrial hydroxyacyl-CoA dehydrogenase (ERAB): regulation of an SDR enzyme activity with implications for apoptosis in Alzheimer's disease. FEBS Lett. 451, 238–242. https://doi.org/10.1016/s0014-5793(99)00586-4

Osellame, L.D., Blacker, T.S., Duchen, M.R., 2012. Cellular and molecular mechanisms of mitochondrial function. Best Pract. Res. Clin. Endocrinol. Metab. 26, 711–723. https://doi.org/10.1016/j.beem.2012.05.003

Ozacmak, V.H., Sayan, H., 2009. The effects of 17beta estradiol, 17alpha estradiol and progesterone on oxidative stress biomarkers in ovariectomized female rat brain subjected to global cerebral ischemia. Physiol. Res. 58, 909–912. https://doi.org/10.33549/physiolres.931647

Park, I., Londhe, A.M., Lim, J.W., Park, B.-G., Jung, S.Y., Lee, J.Y., Lim, S.M., No, K.T., Lee, J., Pae, A.N., 2017b. Discovery of non-peptidic small molecule inhibitors of cyclophilin D as neuroprotective agents in Aβ-induced mitochondrial dysfunction. J. Comput. Aided Mol. Des. 31, 929–941. https://doi.org/10.1007/s10822-017-0067-9

Park, J.-E., Elkamhawy, A., Hassan, A.H.E., Pae, A.N., Lee, J., Paik, S., Park, B.-G., Roh, E.J., 2017a. Synthesis and evaluation of new pyridyl/pyrazinyl thiourea derivatives: Neuroprotection against amyloid-β-induced toxicity. Eur. J. Med. Chem. 141, 322–334. https://doi.org/10.1016/j.ejmech.2017.09.043

Parker, W.D., Filley, C.M., Parks, J.K., 1990. Cytochrome oxidase deficiency in Alzheimer's disease. Neurology 40, 1302–1303. https://doi.org/10.1212/wnl.40.8.1302

Parker, W.D., Parks, J., Filley, C.M., Kleinschmidt-DeMasters, B.K., 1994. Electron transport chain defects in Alzheimer's disease brain. Neurology 44, 1090–1096. https://doi.org/10.1212/wnl.44.6.1090

Pei, L., Wallace, D.C., 2018. Mitochondrial Etiology of Neuropsychiatric Disorders. Biol. Psychiatry 83, 722–730. https://doi.org/10.1016/j.biopsych.2017.11.018

Persson, B., Kallberg, Y., 2013. Classification and nomenclature of the superfamily of short-chain dehydrogenases/reductases (SDRs). Chem. Biol. Interact. 202, 111–115. https://doi.org/10.1016/j.cbi.2012.11.009

Powell, A.J., Read, J.A., Banfield, M.J., Gunn-Moore, F., Yan, S.D., Lustbader, J., Stern, A.R., Stern, D.M., Brady, R.L., 2000. Recognition of structurally diverse substrates by type II 3-hydroxyacyl-CoA dehydrogenase (HADH II)/amyloid-beta binding alcohol dehydrogenase (ABAD). J. Mol. Biol. 303, 311–327. https://doi.org/10.1006/jmbi.2000.4139

Qian, X., Cao, H., Ma, Q., Wang, Q., He, W., Qin, P., Ji, B., Yuan, K., Yang, F., Liu, X., Lian, Q., Li, J., 2015. Allopregnanolone attenuates Aβ25-35-induced neurotoxicity in PC12 cells by reducing oxidative stress. Int. J. Clin. Exp. Med. 8, 13610–13615.

Radhakrishnan, J., Bazarek, S., Chandran, B., Gazmuri, R.J., 2015. Cyclophilin-D: a resident regulator of mitochondrial gene expression. FASEB J. 29, 2734–2748. https://doi.org/10.1096/fj.14-263855

Rao, V.K., Carlson, E.A., Yan, S.S., 2014. Mitochondrial permeability transition pore is a potential drug target for neurodegeneration. Biochim. Biophys. Acta 1842, 1267–1272. https://doi.org/10.1016/j.bbadis.2013.09.003

Rassow, J., Mohrs, K., Koidl, S., Barthelmess, I.B., Pfanner, N., Tropschug, M., 1995. Cyclophilin 20 is involved in mitochondrial protein folding in cooperation with molecular chaperones Hsp70 and Hsp60. Mol. Cell. Biol. 15, 2654–2662. https://doi.org/10.1128/mcb.15.5.2654

Rauschenberger, K., Schöler, K., Sass, J.O., Sauer, S., Djuric, Z., Rumig, C., Wolf, N.I., Okun, J.G., Kölker, S., Schwarz, H., Fischer, C., Grziwa, B., Runz, H., Nümann, A., Shafqat, N., Kavanagh, K.L., Hämmerling, G., Wanders, R.J.A., Shield, J.P.H., Wendel, U., Stern, D., Nawroth, P., Hoffmann, G.F., Bartram, C.R., Arnold, B., Bierhaus, A., Oppermann, U., Steinbeisser, H., Zschocke, J., 2010. A non-enzymatic function of 17beta-hydroxysteroid dehydrogenase type 10 is required for mitochondrial integrity and cell survival. EMBO Mol. Med. 2, 51–62. https://doi.org/10.1002/emmm.200900055

Rayathala, J., Kumar, K., Venkatesh, P., 2022. Review on Alzheimer's disease: past, present and future. J. Innov. Appl. Pharm. Sci. 7, 28–31. https://doi.org/10.37022/jiaps.v7i1.274

Ren, Y., Xu, H.W., Davey, F., Taylor, M., Aiton, J., Coote, P., Fang, F., Yao, J., Chen, D., Chen, J.X., Yan, S.D., Gunn-Moore, F.J., 2008. Endophilin I expression is increased in the brains of Alzheimer disease patients. J. Biol. Chem. 283, 5685–5691. https://doi.org/10.1074/jbc.M707932200

Sang, C., Philbert, S.A., Hartland, D., Unwin, R.D., Dowsey, A.W., Xu, J., Cooper, G.J.S., 2022. Coenzyme A-Dependent Tricarboxylic Acid Cycle Enzymes Are Decreased in Alzheimer's Disease Consistent With Cerebral Pantothenate Deficiency. Front. Aging Neurosci. 14, 893159. https://doi.org/10.3389/fnagi.2022.893159

Schaeffer, V., Meyer, L., Patte-Mensah, C., Eckert, A., Mensah-Nyagan, A.G., 2008. Dose-dependent and sequence-sensitive effects of amyloid-beta peptide on neurosteroidogenesis in human neuroblastoma cells. Neurochem. Int. 52, 948–955. https://doi.org/10.1016/j.neuint.2008.01.010

Schmidt, M., Benek, O., Vinklarova, L., Hrabinova, M., Zemanova, L., Chribek, M., Kralova, V., Hroch, L., Dolezal, R., Lycka, A., Prchal, L., Jun, D., Aitken, L., Gunn-Moore, F., Kuca, K., Musilek, K., 2020. Benzothiazolyl Ureas are Low Micromolar and Uncompetitive Inhibitors of 17β-HSD10 with Implications to Alzheimer's Disease Treatment. Int. J. Mol. Sci. 21, E2059. https://doi.org/10.3390/ijms21062059

Schverer, M., Lanfumey, L., Baulieu, E.-E., Froger, N., Villey, I., 2018. Neurosteroids: non-genomic pathways in neuroplasticity and involvement in neurological diseases. Pharmacol. Ther. 191, 190–206. https://doi.org/10.1016/j.pharmthera.2018.06.011

Seo, J.-S., Lee, K.-W., Kim, T.-K., Baek, I.-S., Im, J.-Y., Han, P.-L., 2011. Behavioral stress causes mitochondrial dysfunction via ABAD up-regulation and aggravates plaque pathology in the brain of a mouse model of Alzheimer disease. Free Radic. Biol. Med. 50, 1526–1535. https://doi.org/10.1016/j.freeradbiomed.2011.02.035

Shafqat, N., Marschall, H.-U., Filling, C., Nordling, E., Wu, X.-Q., Björk, L., Thyberg, J., Mårtensson, E., Salim, S., Jörnvall, H., Oppermann, U., 2003. Expanded substrate screenings of human and Drosophila type 10 17beta-hydroxysteroid dehydrogenases (HSDs) reveal multiple specificities in bile acid and steroid hormone metabolism: characterization of multifunctional 3alpha/7alpha/7beta/17beta/20beta/21-HSD. Biochem. J. 376, 49–60. https://doi.org/10.1042/BJ20030877

Sheu, K.-F., Kim, Y.-T., Blass, J.P., Weksler, M.E., 1985. An immunochemical study of the pyruvate dehydrogenase deficit in Alzheimer's disease brain. Ann. Neurol. 17, 444–449. https://doi.org/10.1002/ana.410170505

Silva, D.F.F., Esteves, A.R., Oliveira, C.R., Cardoso, S.M., 2011. Mitochondria: the common upstream driver of amyloid-β and tau pathology in Alzheimer's disease. Curr. Alzheimer Res. 8, 563–572. https://doi.org/10.2174/156720511796391872

Sivandzade, F., Bhalerao, A., Cucullo, L., 2019. Analysis of the Mitochondrial Membrane Potential Using the Cationic JC-1 Dye as a Sensitive Fluorescent Probe. Bio Protoc. 9, e3128. https://doi.org/10.21769/BioProtoc.3128

Sorbi, S., Bird, E.D., Blass, J.P., 1983. Decreased pyruvate dehydrogenase complex activity in Huntington and Alzheimer brain. Ann. Neurol. 13, 72–78. https://doi.org/10.1002/ana.410130116

Soria Lopez, J.A., González, H.M., Léger, G.C., 2019. Alzheimer's disease. Handb. Clin. Neurol. 167, 231–255. https://doi.org/10.1016/B978-0-12-804766-8.00013-3

Strubbe-Rivera, J.O., Schrad, J.R., Pavlov, E.V., Conway, J.F., Parent, K.N., Bazil, J.N., 2021. The mitochondrial permeability transition phenomenon elucidated by cryo-EM reveals the genuine impact of calcium overload on mitochondrial structure and function. Sci. Rep. 11, 1037. https://doi.org/10.1038/s41598-020-80398-8

Swerdlow, R.H., 2007. Mitochondria in cybrids containing mtDNA from persons with mitochondriopathies. J. Neurosci. Res. 85, 3416–3428. https://doi.org/10.1002/jnr.21167

Swerdlow, R.H., Burns, J.M., Khan, S.M., 2010. The Alzheimer's disease mitochondrial cascade hypothesis. J. Alzheimers Dis. 20, S265-279. https://doi.org/10.3233/JAD-2010-100339

Takuma, K., Yao, J., Huang, J., Xu, H., Chen, X., Luddy, J., Trillat, A.-C., Stern, D.M., Arancio, O., Yan, S.S., 2005. ABAD enhances Aβ-induced cell stress via mitochondrial dysfunction. FASEB J. 19, 1–25. https://doi.org/10.1096/fj.04-2582fje

Tang, J., Oliveros, A., Jang, M.-H., 2019. Dysfunctional Mitochondrial Bioenergetics and Synaptic Degeneration in Alzheimer Disease. Int. Neurourol. J. 23, S5-10. https://doi.org/10.5213/inj.1938036.018

Tanveer, A., Virji, S., Andreeva, L., Totty, N.F., Hsuan, J.J., Ward, J.M., Crompton, M., 1996. Involvement of Cyclophilin D in the Activation of A mitochondrial Pore by Ca2+ and Oxidant Stress. Eur. J. Biochem. 238, 166–172. https://doi.org/10.1111/j.1432-1033.1996.0166q.x

Tavecchio, M., Lisanti, S., Bennett, M.J., Languino, L.R., Altieri, D.C., 2015. Deletion of Cyclophilin D Impairs β-Oxidation and Promotes Glucose Metabolism. Sci. Rep. 5, 15981. https://doi.org/10.1038/srep15981

Tieu, K., Perier, C., Vila, M., Caspersen, C., Zhang, H.-P., Teismann, P., Jackson-Lewis, V., Stern, D.M., Yan, S.D., Przedborski, S., 2004. L-3-hydroxyacyl-CoA dehydrogenase II protects in a model of Parkinson's disease. Ann. Neurol. 56, 51–60. https://doi.org/10.1002/ana.20133

Torroja, L., Ortuño-Sahagún, D., Ferrús, A., Hämmerle, B., Barbas, J.A., 1998. scully, an Essential Gene of Drosophila, is Homologous to Mammalian Mitochondrial Type II l-3-hydroxyacyl-CoA Dehydrogenase/Amyloid-β Peptide-binding Protein. J. Cell Biol. 141, 1009–1017. https://doi.org/10.1083/jcb.141.4.1009

VA Office of Research and Development, 2023. Allopregnanolone in Chronic Complex Traumatic Brain Injury (ALLO). Identification No. NCT04003285. https://clinicaltrials.gov/study/NCT04003285?term=NCT04003285&rank=1 (citováno 9. 1. 2024)

Valasani, K.R., Hu, G., Chaney, M.O., Yan, S.S., 2013. Structure-based design and synthesis of benzothiazole phosphonate analogues with inhibitors of human ABAD-Aβ for treatment of Alzheimer's disease. Chem. Biol. Drug Des. 81, 238–249. https://doi.org/10.1111/cbdd.12068

Valasani, K.R., Sun, Q., Fang, D., Zhang, Z., Yu, Q., Guo, Y., Li, J., Roy, A., ShiDu Yan, S., 2016. Identification of a Small Molecule Cyclophilin D Inhibitor for Rescuing Aβ-Mediated Mitochondrial Dysfunction. ACS Med. Chem. Lett. 7, 294–299. https://doi.org/10.1021/acsmedchemlett.5b00451

Valasani, K.R., Sun, Q., Hu, G., Li, J., Du, F., Guo, Y., Carlson, E.A., Gan, X., Yan, S.S., 2014a. Identification of Human ABAD Inhibitors for Rescuing Aβ-Mediated Mitochondrial Dysfunction. Curr. Alzheimer Res. 11, 128–136. https://doi.org/10.2174/1567205011666140130150108

Valasani, K.R., Vangavaragu, J.R., Day, V.W., Yan, S.S., 2014b. Structure Based Design, Synthesis, Pharmacophore Modeling, Virtual Screening, and Molecular Docking Studies for Identification of Novel Cyclophilin D Inhibitors. J. Chem. Inf. Model. 54, 902–912. https://doi.org/10.1021/ci5000196

Varache, M., Ciancone, M., Couffin, A.-C., 2020. Optimization of a Solid-Phase Extraction Procedure for the Analysis of Drug-Loaded Lipid Nanoparticles and its Application to the Determination of Leakage and Release Profiles. J. Pharm. Sci. 109, 2527–2535. https://doi.org/10.1016/j.xphs.2020.05.003

Vinklarova, L., Schmidt, M., Benek, O., Kuca, K., Gunn-Moore, F., Musilek, K., 2020. Friend or enemy? Review of 17β-HSD10 and its role in human health or disease. J. Neurochem. 155, 231–249. https://doi.org/10.1111/jnc.15027

Viswanath, A.N.I., Kim, T., Jung, S.Y., Lim, S.M., Pae, A.N., 2017. In silico-designed novel non-peptidic ABAD LD hot spot mimetics reverse Aβ-induced mitochondrial impairments in vitro. Chem. Biol. Drug Des. 90, 1041–1055. https://doi.org/10.1111/cbdd.13065

Vivoli, M., Renou, J., Chevalier, A., Norville, I.H., Diaz, S., Juli, C., Atkins, H., Holzgrabe, U., Renard, P.-Y., Sarkar-Tyson, M., Harmer, N.J., 2017. A miniaturized peptidyl-prolyl isomerase enzyme assay. Anal. Biochem. 536, 59–68. https://doi.org/10.1016/j.ab.2017.08.004

Waldmeier, P.C., Feldtrauer, J.-J., Qian, T., Lemasters, J.J., 2002. Inhibition of the Mitochondrial Permeability Transition by the Nonimmunosuppressive Cyclosporin Derivative NIM811. Mol. Pharmacol. 62, 22–29. https://doi.org/10.1124/mol.62.1.22

Walkinshaw, M.D., Taylor, P., Turner, N.J., Flitsch, S.L., 2002. Cyclophilin-binding ligands. WO2002048178A2. https://patents.google.com/patent/WO2002048178A2/en

Wang, J.M., Johnston, P.B., Ball, B.G., Brinton, R.D., 2005. The Neurosteroid Allopregnanolone Promotes Proliferation of Rodent and Human Neural Progenitor Cells and Regulates Cell-Cycle Gene and Protein Expression. J. Neurosci. 25, 4706–4718. https://doi.org/10.1523/JNEUROSCI.4520-04.2005

Wang, P., Heitman, J., 2005. The cyclophilins. Genome Biol. 6, 226. https://doi.org/10.1186/gb-2005-6-7-226

Weller, J., Budson, A., 2018. Current understanding of Alzheimer's disease diagnosis and treatment. F1000Research 7, 1161. https://doi.org/10.12688/f1000research.14506.1

Xiao, X., Chen, Q., Zhu, X., Wang, Y., 2019. ABAD/17β-HSD10 reduction contributes to the protective mechanism of huperzine a on the cerebral mitochondrial function in APP/PS1 mice. Neurobiol. Aging 81, 77–87. https://doi.org/10.1016/j.neurobiolaging.2019.05.016

Xie, Y., Deng, S., Chen, Z., Yan, S., Landry, D.W., 2006. Identification of small-molecule inhibitors of the Abeta-ABAD interaction. Bioorg. Med. Chem. Lett. 16, 4657–4660. https://doi.org/10.1016/j.bmcl.2006.05.099

Yan, S.D., Fu, J., Soto, C., Chen, X., Zhu, H., Al-Mohanna, F., Collison, K., Zhu, A., Stern, E., Saido, T., Tohyama, M., Ogawa, S., Roher, A., Stern, D., 1997. An intracellular protein that binds amyloid-beta peptide and mediates neurotoxicity in Alzheimer's disease. Nature 389, 689–695. https://doi.org/10.1038/39522

Yan, S.D., Shi, Y., Zhu, A., Fu, J., Zhu, H., Zhu, Y., Gibson, L., Stern, E., Collison, K., Al-Mohanna, F., Ogawa, S., Roher, A., Clarke, S.G., Stern, D.M., 1999. Role of ERAB/L-3-hydroxyacyl-coenzyme A dehydrogenase type II activity in Abeta-induced cytotoxicity. J. Biol. Chem. 274, 2145–2156. https://doi.org/10.1074/jbc.274.4.2145

Yan, S.D., Stern, D.M., 2005. Mitochondrial dysfunction and Alzheimer's disease: role of amyloid-β peptide alcohol dehydrogenase (ABAD). Int. J. Exp. Pathol. 86, 161–171. https://doi.org/10.1111/j.0959-9673.2005.00427.x

Yan, S.D., Zhu, Y., Stern, E.D., Hwang, Y.C., Hori, O., Ogawa, S., Frosch, M.P., Connolly, E.S., McTaggert, R., Pinsky, D.J., Clarke, S., Stern, D.M., Ramasamy, R., 2000. Amyloid beta -peptide-binding alcohol dehydrogenase is a component of the cellular response to nutritional stress. J. Biol. Chem. 275, 27100–27109. https://doi.org/10.1074/jbc.M000055200

Yan, Y., Liu, Y., Sorci, M., Belfort, G., Lustbader, J.W., Yan, S.S., Wang, C., 2007. Surface plasmon resonance and nuclear magnetic resonance studies of ABAD-Abeta interaction. Biochemistry 46, 1724–1731. https://doi.org/10.1021/bi061314n

Yang, S.-Y., He, X.-Y., Isaacs, C., Dobkin, C., Miller, D., Philipp, M., 2014. Roles of 17β-hydroxysteroid dehydrogenase type 10 in neurodegenerative disorders. J. Steroid Biochem. Mol. Biol. 143, 460–472. https://doi.org/10.1016/j.jsbmb.2014.07.001

Yang, S.-Y., He, X.-Y., Miller, D., 2011. Hydroxysteroid (17β) dehydrogenase X in human health and disease. Mol. Cell. Endocrinol. 343, 1–6. https://doi.org/10.1016/j.mce.2011.06.011

Yang, S.-Y., He, X.-Y., Miller, D., 2007. HSD17B10: A gene involved in cognitive function through metabolism of isoleucine and neuroactive steroids. Mol. Genet. Metab. 92, 36–42. https://doi.org/10.1016/j.ymgme.2007.06.001

Yang, S.-Y., He, X.-Y., Olpin, S.E., Sutton, V.R., McMenamin, J., Philipp, M., Denman, R.B., Malik, M., 2009. Mental retardation linked to mutations in the HSD17B10 gene interfering with neurosteroid and isoleucine metabolism. Proc. Natl. Acad. Sci. U. S. A. 106, 14820–14824. https://doi.org/10.1073/pnas.0902377106

Yang, S.-Y., He, X.-Y., Schulz, H., 2005. Multiple functions of type 10 17β-hydroxysteroid dehydrogenase. Trends Endocrinol. Metab. 16, 167–175. https://doi.org/10.1016/j.tem.2005.03.006

Yao, J., Du, H., Yan, S., Fang, F., Wang, C., Lue, L.-F., Guo, L., Chen, D., Stern, D.M., Gunn Moore, F.J., Xi Chen, J., Arancio, O., Yan, S.S., 2011b. Inhibition of amyloid-beta (Abeta) peptide-binding alcohol dehydrogenase-Abeta interaction reduces Abeta accumulation and improves mitochondrial function in a mouse model of Alzheimer's disease. J. Neurosci. Off. J. Soc. Neurosci. 31, 2313–2320. https://doi.org/10.1523/JNEUROSCI.4717-10.2011

Yao, J., Irwin, R., Chen, S., Hamilton, R., Cadenas, E., Brinton, R.D., 2012. Ovarian hormone loss induces bioenergetic deficits and mitochondrial β-amyloid. Neurobiol. Aging 33, 1507–1521. https://doi.org/10.1016/j.neurobiolaging.2011.03.001

Yao, J., Rettberg, J.R., Klosinski, L.P., Cadenas, E., Brinton, R.D., 2011a. Shift in brain metabolism in late onset Alzheimer's disease: Implications for biomarkers and therapeutic interventions. Mol. Aspects Med., Oxidative Damage and Disease 32, 247–257. https://doi.org/10.1016/j.mam.2011.10.005

Yao, J., Taylor, M., Davey, F., Ren, Y., Aiton, J., Coote, P., Fang, F., Chen, J.X., Yan, S.D., Gunn-Moore, F.J., 2007. Interaction of amyloid binding alcohol dehydrogenase/Abeta mediates up-regulation of peroxiredoxin II in the brains of Alzheimer's disease patients and a transgenic Alzheimer's disease mouse model. Mol. Cell. Neurosci. 35, 377–382. https://doi.org/10.1016/j.mcn.2007.03.013

Yin, Y., Cha, C., Wu, F., Li, J., Li, S., Zhu, X., Zhang, J., Guo, G., 2019. Endophilin 1 knockdown prevents synaptic dysfunction induced by oligomeric amyloid β. Mol. Med. Rep. 19, 4897–4905. https://doi.org/10.3892/mmr.2019.10158

Yoshida, Y., Yoshikawa, A., Kinumi, T., Ogawa, Y., Saito, Y., Ohara, K., Yamamoto, H., Imai, Y., Niki, E., 2009. Hydroxyoctadecadienoic acid and oxidatively modified peroxiredoxins in the blood of Alzheimer's disease patients and their potential as biomarkers. Neurobiol. Aging 30, 174–185. https://doi.org/10.1016/j.neurobiolaging.2007.06.012

Yue, X., Lu, M., Lancaster, T., Cao, P., Honda, S.-I., Staufenbiel, M., Harada, N., Zhong, Z., Shen, Y., Li, R., 2005. Brain estrogen deficiency accelerates Aβ plaque formation in an Alzheimer's disease animal model. Proc. Natl. Acad. Sci. U. S. A. 102, 19198–19203. https://doi.org/10.1073/pnas.0505203102

Zampieri, S., Mellon, S.H., Butters, T.D., Nevyjel, M., Covey, D.F., Bembi, B., Dardis, A., 2009. Oxidative stress in NPC1 deficient cells: protective effect of allopregnanolone. J. Cell. Mol. Med. 13, 3786–3796. https://doi.org/10.1111/j.1582-4934.2008.00493.x

Zemanova, L., Vaskova, M., Schmidt, M., Roubalova, J., Haleckova, A., Benek, O., Musilek, K., 2020. RNase T1 Refolding Assay for Determining Mitochondrial Cyclophilin D Activity: A Novel In Vitro Method Applicable in Drug Research and Discovery. Biochemistry 59, 1680–1687. https://doi.org/10.1021/acs.biochem.9b01025

Zhang, H., Wei, W., Zhao, M., Ma, L., Jiang, X., Pei, H., Cao, Y., Li, H., 2021. Interaction between Aβ and Tau in the Pathogenesis of Alzheimer's Disease. Int. J. Biol. Sci. 17, 2181–2192. https://doi.org/10.7150/ijbs.57078

Zhang, J., Tan, M., Yin, Y., Ren, B., Jiang, N., Guo, G., Chen, Y., 2015. Distinct Functions of Endophilin Isoforms in Synaptic Vesicle Endocytosis. Neural Plast. 2015, 371496. https://doi.org/10.1155/2015/371496

Zhang, X.-C., Wang, W.-D., Wang, J.-S., Pan, J.-C., 2013. PPIase independent chaperone-like function of recombinant human Cyclophilin A during arginine kinase refolding. FEBS Lett. 587, 666–672. https://doi.org/10.1016/j.febslet.2013.01.028

Zoldák, G., Aumüller, T., Lücke, C., Hritz, J., Oostenbrink, C., Fischer, G., Schmid, F.X., 2009. A library of fluorescent peptides for exploring the substrate specificities of prolyl isomerases. Biochemistry 48, 10423–10436. https://doi.org/10.1021/bi9014242

Zschocke, J., 2012. HSD10 disease: clinical consequences of mutations in the HSD17B10 gene. J. Inherit. Metab. Dis. 35, 81–89. https://doi.org/10.1007/s10545-011-9415-4

Zschocke, J., Ruiter, J.P.N., Brand, J., Lindner, M., Hoffmann, G.F., Wanders, R.J.A., Mayatepek, E., 2000. Progressive Infantile Neurodegeneration Caused by 2-Methyl-3-Hydroxybutyryl-CoA Dehydrogenase Deficiency: A Novel Inborn Error of Branched-Chain Fatty Acid and Isoleucine Metabolism. Pediatr. Res. 48, 852–855. https://doi.org/10.1203/00006450-200012000-00025

8 Příspěvky na konferencích

8.1 Přednášky

Vaskova, M.; Rotterova, A.; Jurkova, K.; Hamsikova, M. *In vitro* study of 17β-HSD10 activity. Young Scientists Conference – Igráček UHK, Hradec Králové, Czech Republic, 17. 5. 2023

8.2 Posterová sdělení

Miskerikova, M.; Rotterova, A.; **Vaskova, M.**; Benek, O.; Schmidt, M.; Musilek, K. Nanomolar benzothiazolyl-based inhibitors of mitochondrial enzyme 17β-HSD10 with cellular bioactivity. 9th Edition of the European Workshop in Drug Synthesis – EWDSy, Siena, Italy, 21.–24. 5. 2023.

Haleckova, A.; Benek, O.; **Vaskova, M.**; Zemanova, L.; Musilek, K. Synthesis and evaluation of small molecule mPTP/CypD inhibitors. 56th Conference: Advances in Organic, Bioorganic and Pharmaceutical Chemistry – Liblice 2022, Špindlerův Mlýn, Czech Republic, 10.–12. 11. 2022.

Miskerikova, M.; Benek, O.; Schmidt, M.; **Vaskova, M.**; Musilek, K. Synthesis and *in vitro* evaluation of novel inhibitors of mitochondrial enzyme 17β-HSD10 for treatment of Alzheimer's disease. 56th Conference: Advances in Organic, Bioorganic and Pharmaceutical Chemistry – Liblice 2022, Špindlerův Mlýn, Czech Republic, 10.–12. 11. 2022.

Miskerikova, M.; Benek, O.; Schmidt, M.; **Vaskova, M.**; Musilek, K. Synthesis of novel inhibitors of mitochondrial enzyme 17β-HSD10. XXVII EFMC International Symposium on Medicinal Chemistry – EFMC-ISMC 2022, Nice, France, 4.–8. 9. 2022.

Haleckova, A.; Benek, O.; **Vaskova, M.**; Zemanova, L.; Musilek, K. Synthesis and *In vitro* Evaluation of Small Molecule Inhibitors of Cyclophilin D for Treatment of Mitochondrial Dysfunction Related Diseases. XXVII EFMC International Symposium on Medicinal Chemistry – EFMC-ISMC 2022, Nice, France, 4.–8. 9. 2022.

Haleckova, A.; Benek, O.; **Vaskova, M.**; Zemanova, L.; Musilek, K. Synthesis of Small Molecule Inhibitors of Cyclophilin D and Their *In vitro* Evaluation for Neuroprotective Treatment of Alzheimer's Disease. 55th Advances in Organic, Bioorganic and Pharmaceutical Chemistry Conference, – Liblice 2021, Špindlerův Mlýn, Czech Republic, 10.–12. 11. 2021.

Haleckova, A.; Benek, O.; **Vaskova, M.**; Zemanova, L.; Musilek, K. Synthesis of small molecule inhibitors of Cyclophilin D and their *in vitro* evaluation for neuroprotective treatment of alzheimers disease. XXVI EFMC International Symposium on Medicinal Chemistry – EFMC-ISMC 2021, Virtual Event, 29. 8. – 2. 9. 2021.

Schmidt, M.; **Vaskova, M.**; Benek, O.; Zemanova, L.; Musilek, K. Novel biochemical assay for mitochondrial 17β-hydroxysteroid dehydrogenase type 10 inhibitors discovery. XXVI. Annual Congress of Czech and Slovak Societies for Biochemistry and Molecular Biology, České Budějovice, Czech Republic, 29. 8. – 1. 9. 2021.

Vaskova, M.; Schmidt, M.; Benek, O.; Zemanova, L.; Musilek, K. A novel *in vitro* method for determining mitochondrial 17β-HSD10 activity: small-molecule inhibitors screening. The 45th FEBS Virtual Congress, 3.–7. 8. 2021.

9 Účast na projektech a stážích

Výzkum, který je součástí předkládané disertační práce, byl realizován za finanční podpory níže uvedených projektů:

Projekt specifického výzkumu UHK (SV-2108-2023, 2023): Štúdium nových molekúl so schopnosťou ovplyvňovať neurodegeneratívne ochorenia

- spoluřešitel

„Igráček UHK" (4/2022 – 3/2023): *In vitro* study of 17β-HSD10 activity

- hlavní řešitel

Projekt specifického výzkumu UHK (SV-2103-2022, 2022): Výzkum nově připravených sloučenin potenciálně využitelných při terapii Alzheimerovy choroby

- spoluřešitel

Projekt specifického výzkumu UHK (SV-2104-2021, 2021): Výzkum malých molekul využitelných při intoxikacích nebo onemocněních nervové soustavy

- spoluřešitel

Projekt specifického výzkumu UHK (SV-2105-2020): Štúdium a *in vitro* testovanie inhibičnej aktivity novo pripravených zlúčenín optimalizovaných pre inhibíciu a reaktiváciu proteínov

- spoluřešitel

V rámci doktorského studia byla absolvována zahraniční stáž:

20. 8. – 30. 11. 2022: Odborná stáž (Rakousko)

Institut für Pharmakologie, Medizinischen Universität Wien, Vídeň

Téma: Is gamma-amino butyric acid a substrate for the vesicular monoamine transporter VMAT2?

Mentor: Mag. Dr. Thomas Steinkellner, Ph.D.

Financování: projekt Erasmus+

10 Přílohy

Seznam publikačních příloh:

Publikace I: RNase T1 Refolding Assay for Determining Mitochondrial Cyclophilin D Activity: A Novel *In Vitro* Method Applicable in Drug Research and Discovery

Publikace II: Development of submicromolar 17β-HSD10 inhibitors and their *in vitro* and *in vivo* evaluation

Publikace III: Physiologically Relevant Fluorescent Assay for Identification of 17β-hydroxysteroid dehydrogenase type 10 Inhibitors

Publikace IV: Nanomolar benzothiazolyl-based inhibitors of 17β-HSD10 with cellular bioactivity

Publikace V: The C-3 steroidal hemiesters as inhibitors of 17β-hydroxysteroid dehydrogenase type 10

10.1 Publikace I

Zemanova, L., **Vaskova, M.**, Schmidt, M., Roubalova, J., Haleckova, A., Benek, O., Musilek, K., 2020. RNase T1 Refolding Assay for Determining Mitochondrial Cyclophilin D Activity: A Novel In Vitro Method Applicable in Drug Research and Discovery. Biochemistry 59, 1680–1687. https://doi.org/10.1021/acs.biochem.9b01025

Biochemistry

pubs.acs.org/biochemistry Article

RNase T1 Refolding Assay for Determining Mitochondrial Cyclophilin D Activity: A Novel *In Vitro* Method Applicable in Drug Research and Discovery

Lucie Zemanova,* Michaela Vaskova, Monika Schmidt, Jana Roubalova, Annamaria Haleckova, Ondrej Benek, and Kamil Musilek

Cite This: *Biochemistry* 2020, 59, 1680−1687 Read Online

ACCESS | Metrics & More | Article Recommendations | Supporting Information

ABSTRACT: Human cyclophilin D is a mitochondrial peptidyl-prolyl isomerase that plays a role in regulating the opening of the mitochondrial permeability transition pore. It is considered a viable and promising molecular target for the treatment of diseases for which disease development is associated with pore opening, e.g., Alzheimer's disease or ischemia/reperfusion injury. Currently available and widely used *in vitro* methods based on Kofron's assay for determining cyclophilin D activity suffer from serious drawbacks and limitations. In this study, a completely novel approach for an *in vitro* assay of cyclophilin D activity using RNase T1 refolding is introduced. The method is simple and is more in line with the presumed physiological role of cyclophilin D in protein folding than Kofron's assay, which relies on a peptide substrate. The method is applicable for identifying novel inhibitors of cyclophilin D as potential drugs for the treatment of the diseases mentioned above. Moreover, the description of CypD activity in the *in vitro* RNase T1 refolding assay reveals new possibilities for investigating the role of cyclophilin D in protein folding in cells and may lead to a better understanding of its pathological and physiological roles.

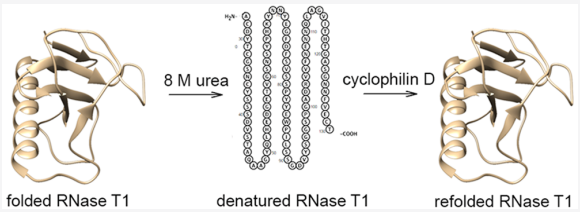

Downloaded via Lucie Zemanova on May 11, 2020 at 06:25:45 (UTC).
See https://pubs.acs.org/sharingguidelines for options on how to legitimately share published articles.

Cyclophilins (Cyps) are ubiquitous enzymes present in almost all forms of life from bacteria to humans. They are peptidyl-prolyl isomerases (PPIase, EC 5.2.1.8) and catalyze the interconversion of *cis* and *trans* conformers of planar peptide bonds preceding internal proline residues.[1−4] This reaction is considered a rate-limiting step in protein folding. However, the reaction can also be catalyzed by structurally unrelated enzymes, such as FK506-binding proteins (FKBPs) and parvulins.[2,5,6]

Seventeen human cyclophilins have been identified, and each contains a PPIase domain (∼109 amino acids) with a sequence similarity of 51−86%. Some Cyps encompass other structural motifs, such as tetratricopeptide (TRP) or RNA-recognition motif (RRM).[2] Cyps can be found in all cellular compartments; however, only one isoform is expressed in mitochondria, namely, cyclophilin D (CypD, encoded by the *ppif* gene so its correct name should be CypF). CypD can also be localized in the cytosol, but such a molecule is a different protein encoded by a different gene (*ppid*). The mitochondrial CypD contains only the PPIase domain and a mitochondrial targeting signal sequence with a molecular weight of 22 kDa, whereas the cytosolic CypD (also named Cyp40) consists of the PPIase domain and a TRP motif with a molecular weight of 40 kDa.[7] The mitochondrial CypD is a protein crucial for mitochondrial function because it is associated with the formation of mitochondrial permeability transition pore (mPTP), which is in turn implicated in mitochondrial swelling and apoptosis/necrosis. Thus, it is involved in the development of several diseases (e.g., Alzheimer's disease and ischemia/reperfusion injury).[8−10] Although components of mPTP (ANT, VDAC, and F-ATP synthase) and the exact mode of its action remain controversial and widely discussed, the role of CypD as a regulator of mPTP opening is relevant and widely accepted.[11,12] Thus, CypD is considered a viable and promising target for the treatment of the diseases mentioned above. Despite intensive research, its exact function in the mitochondria and the opening of mPTP remains not fully understood.[10,13]

As a well-known CypD inhibitor, cyclosporine A (CsA) is potent but not selective for only for CypD; major efforts have been made to find inhibitors with better characteristics for drug research and discovery. In studies of novel inhibitors of CypD, several methods, such as binding assays (e.g., isothermal titration calorimetry and surface plasmon resonance),[14−16]

Received: November 19, 2019
Revised: March 18, 2020
Published: April 10, 2020

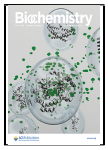

ACS Publications © 2020 American Chemical Society

https://dx.doi.org/10.1021/acs.biochem.9b01025
Biochemistry 2020, 59, 1680−1687

functional assays (e.g., mitochondrial swelling and JC-1 mitochondrial membrane potential assays),[14,17,18] and *in silico* approaches,[15,16,18] have been used. However, there is only one approach for determining the CypD enzymatic activity that uses a short peptide as a substrate as described by Kofron et al. (also used for other Cyps).[19] This method is based on coupling with an indicator enzymatic reaction using chymotrypsin. The method uses a tetrapeptide Suc-AXPF-pNA with the *cis* conformation of the proline peptide bond as a substrate. The *trans* isomer formed by CypD is subsequently degraded by chymotrypsin, and the degradation product is measured spectrophotometrically.

Although this method has been used for more than 25 years,[15,20] it is associated with more drawbacks than benefits. Maintaining the X−P peptide bond in the substrate (Suc-AAPF-pNA) in the *cis* conformation is problematic, and 0.5 M LiCl in anhydrous trifluoroethanol (TFE) must be used as a solvent for the substrate stock solution. When the substrate solution is added to the aqueous environment of the assay, a spontaneous *cis*−*trans* isomerization of the substrate occurs leading to its degradation by chymotrypsin; this effect presents via very high absorbance values. Moreover, the enzymatic reaction itself is very rapid (a reaction plateau is reached within tens of seconds from initiation) even though the assay is performed at temperatures below 10 °C. These issues lead to very complicated implementation and evaluation.

Reported efforts to introduce novel peptide substrates[20−22] with better properties for such an assay have yet to yield significant success. Moreover, the physiological function of CypD is likely not the interconversion of *cis* and *trans* conformers of short peptides but that of proteins in the process of protein folding,[13] as inferred from the functions of other cyclophilins.[3] Cyps were formerly described to play a role as foldases (accelerating slow steps in protein folding, such as the isomerization of the prolyl peptide bond) or chaperones. The folding activity is connected with the PPIase domain,[3] whereas chaperone activity is mainly associated with other parts of Cyps (such as the TRP domain or the linker part in cytosolic CypD[23,24]). The first experimental evidence that human CypD could participate in protein folding in the case of p53 was recently published.[25]

The aim of this study was to develop a novel, simple *in vitro* assay for determining CypD activity using an unfolded model protein as a substrate to prove the ability of CypD at least *in vitro* to participate in protein re/folding. The method should be suitable for the identification and evaluation of novel CypD inhibitors in drug research and discovery.

MATERIALS AND METHODS

Chemicals. Chymotrypsin from bovine pancreas (C7762), *N*-succinyl-Ala-Ala-Pro-Phe *p*-nitroanilide (Suc-AAPF-pNA), trifluoroethanol (TFE), cyclosporine A (CsA), SYPRO Orange, benzonase nuclease, and lysozyme (L6876) were obtained from Sigma-Aldrich. RNase T1 from *Aspergillus oryzae* (EN0542, UniprotKB accession number P00651) was purchased from Thermo Fisher Scientific. The protease inhibitor cocktail cOmplete, Mini, EDTA free was obtained from Roche. All other chemicals and reagents were of the highest commercially available purity.

Syntheses of Compound 4 and JC-9. Compound **4** and JC-9 were synthesized using previously described protocols.[14,15] The identity and purity of prepared compounds were confirmed by ^{1}H and ^{13}C NMR spectroscopy and mass spectrometry. Details of the synthesis protocols are provided in the Supporting Information.

Prediction of Chymotrypsin Activity toward Human CypD. The sequence of CypD (or other PPIases) was extracted from UniProt. Two prediction tools were used: the PeptideCutter tool (https://web.expasy.org/peptide_cutter/) and Prosper.[26] In PeptideCutter, only potential chymotrypsin high-specificity cleavage sites [C-terminus (FYZ), not before P] were evaluated.

Cloning and Expression of Human CypD. The DNA sequence for the truncated version of human CypD (UniprotKB accession number P30405, amino acids 30−207, CypDΔ29)[27] was synthesized as a DNA fragment using the GeneArt gene synthesis service (Thermo Fisher Scientific) after codon optimization for the *Escherichia coli* expression system. The DNA sequence was amplified by polymerase chain reaction (PCR) using specific primers with overlaps for restriction endonucleases *Nco*I and *Xho*I present in the expression vector and cloned into the pCR4-TOPO vector; the coding sequence was confirmed by sequencing. The coding sequence was subcloned into the pET28b(+) expression vector in frame with an upstream His-tag sequence to generate N-terminal His-tagged truncated CypD and then transformed into the *E. coli* BL21(DE3) expression strain (Novagen). The transformed bacterial cells were grown in LB medium. The protein expression was subsequently induced by transferring the bacteria into autoinduction Overnight Express TB medium (Novagen) and incubated at 25 °C in a shaking incubator (200 rpm) for 16 h.

Purification of Human Recombinant CypD. Bacterial cells expressing human CypD were harvested by centrifugation; the bacterial pellet was resuspended in a lysis buffer [50 mM sodium phosphate buffer, 150 mM NaCl, and 10 mM imidazole (pH 8.0) with added 1 mg/mL lysozyme, 250 units/mL benzonase, and 1 tablet of protease inhibitor cocktail/10 mL] and incubated for 20 min on ice. Sonication was used to disrupt the cells followed by centrifugation (12000*g* for 10 min). The supernatant was transferred onto 1 mL of Ni-NTA resin and incubated for 1 h at 4 °C. His-tagged CypD bound on resin was washed three times with 10 mL of washing buffer 1 [50 mM sodium phosphate buffer, 150 mM NaCl, and 10 mM imidazole (pH 8.0)], followed by 3 × 10 mL of washing buffer 2 [50 mM sodium phosphate buffer, 150 mM NaCl, and 20 mM imidazole (pH 8.0)], and eluted by elution buffer [50 mM sodium phosphate buffer, 150 mM NaCl, and 250 mM imidazole (pH 8.0)]. The elution buffer was exchanged using Amicon Ultra-4 into 50 mM Tris, 150 mM NaCl (pH 8.0), or 20 mM Tris (pH 8.0). Glycerol was added to a concentration of 30% (v/v), and the final CypD solution was stored at −20 °C. The purification process was monitored by 12.5% sodium dodecyl sulfate−polyacrylamide gel electrophoresis (SDS−PAGE), and the presence of CypD was confirmed by Western blot. The protein concentration was determined by the Bradford assay.[28]

Western Blot. Samples were separated on a 12.5% SDS−polyacrylamide gel and transferred to an Immobilon P PVDF membrane (Merck Millipore) at 25 V and 1 mA for 15 min using the Trans-Blot Turbo system (Bio-Rad) in blotting buffer [25 mM Tris, 192 mM glycine, and 20% (v/v) methanol]. The membrane was rinsed for 90 min in blocking buffer comprising 3% (w/v) nonfat dry milk (Bio-Rad) in TBS-T buffer [0.1% (v/v) Tween-20 in TBS]. The blocked membrane was incubated overnight with mouse anti-cyclo-

https://dx.doi.org/10.1021/acs.biochem.9b01025
Biochemistry 2020, 59, 1680−1687

philin F antibody (sc-376061; 1:500; Santa Cruz Biotechnology). After the membrane had been extensively washed, m-IgκBP-HRP (sc-516102; 1:5000; Santa Cruz Biotechnology) was applied for 90 min. Antibody and binding protein were diluted in 3% (w/v) nonfat dry milk in TBS-T buffer. After being extensively washed, the membrane was incubated with Amersham ECL Prime reagent (GE Healthcare Lifesciences). Chemiluminescence was detected by Azure C400 (Azure Biosystems).

Assay of Chymotrypsin Activity. Purified recombinant CypD (1 μg) was incubated with chymotrypsin (5 μg, dissolved in 1 mM HCl) with or without 20 μg of substrate (Suc-AAPF-pNA, dissolved in 0.5 M LiCl in TFE) in 50 mM HEPES and 100 mM NaCl (pH 8.0) (total volume of 10 μL). The reaction was started by adding chymotrypsin and incubating the mixture on ice or at room temperature for 10, 30, or 60 s. The reaction was stopped by adding 2.5 μL of SDS sample buffer for electrophoresis. Samples were incubated at 95 °C for 3 min and loaded onto a 20% SDS−PAGE gel.

Buffer Screening by Differential Scanning Fluorimetry. SYPRO Orange was mixed with particular buffers at 1:1000 dilutions and added to white PCR tubes containing 1.4 μg of CypD (total volume of 40 μL). The samples were vortexed, briefly centrifuged, and heated in a qPCR machine qTower^3/G (Analytic Jena) from 25 to 90 °C (1 °C/min). Fluorescence was monitored at excitation and emission wavelengths of 490 and 575 nm, respectively. Obtained melting curves were analyzed, and melting temperatures (T_m) were determined by qPCRsoft 4.0.

Folding Activity of CypD. RNase T1 unfolding (50 μM; 100, 75, 25, and 10 μM in the initial experiments) was performed in the presence of 20 mM Tris buffer and 8 M urea (pH 8.0) for 2 h at room temperature. CypD was first diluted in 20 mM Tris buffer and 30% glycerol (pH 8.0) to a concentration of 1 μM and further with 20 mM Tris buffer (pH 8.0) to a final concentration of 25 nM (10, 50, 75, and 100 nM in the initial experiments). After a 5 min incubation on ice, 390 μL of 25 nM CypD (or buffer without CypD as a control) was added to a cuvette containing 10 μL of 50 μM unfolded RNase T1 to start the refolding of RNase T1. The mixture was briefly mixed using a pipet, and the measurement started immediately. The refolding of RNase T1 was monitored by tryptophan fluorescence (excitation wavelength of 268 nm, slit of 10 nm, and emission wavelength of 325 nm, slit of 5 nm) at 10 °C using a PerkinElmer LS55 spectrofluorometer (PerkinElmer). The folding enzyme activity of CypD was calculated from a linear part of the obtained graph (as explained in Table S2) and expressed as ΔF/min.

Determination of the Emission Spectra of RNase T1. Emission spectra from 290 to 450 nm (slit of 5 nm) at an excitation wavelength of 268 nm (slit of 10 nm) were measured at 10 °C using a PerkinElmer LS44 spectrofluorometer (PerkinElmer) for different samples: 50 μM RNase T1 in 20 mM Tris buffer and 8 M urea (pH 8.0) (unfolded RNase T1), 50 μM RNase T1 in 20 mM Tris buffer (pH 8.0) (folded RNase T1), 50 μM unfolded RNase T1 in the presence 25 nM Cyp D after 1000 s from the reaction start (refolded by CypD), and 50 μM unfolded RNase T1 in buffer after 1000 s from the reaction start (refolded spontaneously). Samples refolded by CypD or refolded spontaneously were prepared in the same way as described in Folding Activity of CypD.

Determining the Effect of the Efficiency of CsA, Compound JC-9, and Compound 4 Inhibition on Folding Activity of CypD. The unfolding of RNase T1 was performed in the same way as described in Folding Activity of CypD. CsA, compound JC-9, and compound **4** were dissolved in anhydrous DMSO to prepare stock solutions with concentrations of 100, 40, 20, 8, 4, and 2 μM for CsA or 40, 30, 20, 10, 4, and 2 mM for compound JC-9 and compound **4**. CypD was first diluted in 20 mM Tris buffer and 30% glycerol (pH 8.0) to a concentration of 1 μM and further with 20 mM Tris buffer (pH 8.0) containing 0.25% anhydrous DMSO (noninhibited control), CsA, compound JC-9, or compound **4** to a final concentration of 25 nM. After a 5 min incubation on ice, 390 μL of 25 nM CypD with DMSO or CsA (or only buffer as a non-enzymatic control) was added to a cuvette containing 10 μL of 50 μM unfolded RNase T1 to start the refolding. The samples were processed and measured as described in Folding Activity of CypD. The non-enzymatic control was subtracted from the measured values, and the IC_{50} value was determined using GraphPad Prism 8 (GraphPad Software, Inc.).

RESULTS AND DISCUSSION

The method used for assaying CypD activity according to Kofron[19] has many drawbacks as described above. Another important issue is the resistance of CypD to the protease activity of the indicator enzyme, chymotrypsin. For this

Table 1. Prediction of Protease Activity of Chymotrypsin toward CypD by PeptideCutter[a] and Prosper[b,26]

	no. of cleavage sites	position of the cleavage site
PeptideCutter	15	10, 49, 78, 88, 90, 95, 102, 109, 121, 130, 154, 155, 163, 171, 187
Prosper	2	66, 171

[a]https://web.expasy.org/peptide_cutter/. [b]https://prosper.erc.monash.edu.au/home.html.

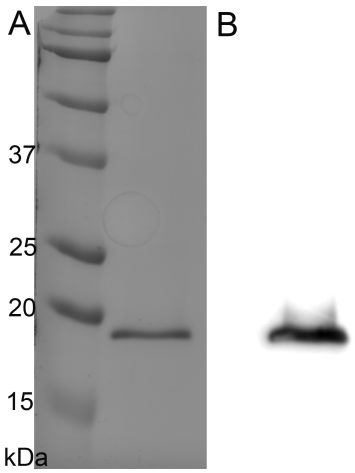

Figure 1. (A) SDS−PAGE of purified recombinant CypD and (B) Western blot to confirm identity using a specific anti-CypD antibody. The molecular weight of CypD was 18 kDa. The DNA sequence without the mitochondrial signal peptide (corresponding to amino acids 1−29, CypDΔ29) was cloned.

https://dx.doi.org/10.1021/acs.biochem.9b01025
Biochemistry 2020, 59, 1680−1687

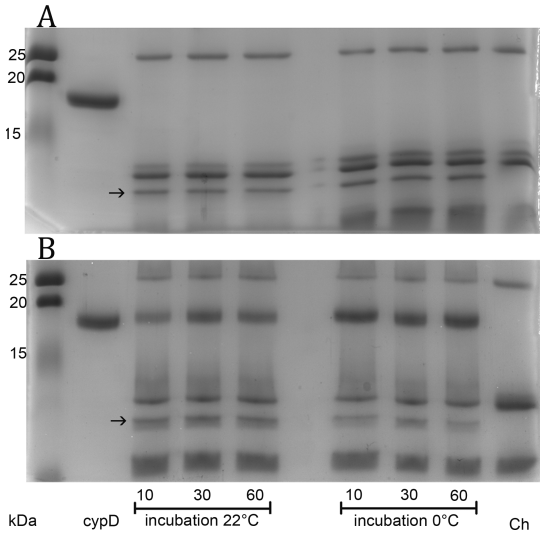

Figure 2. Experimental evaluation of chymotrypsin (Ch) activity toward CypD (A) without and (B) with peptide substrate Suc-AAPF-pNA for CypD. The CypD:substrate:chymotrypsin ratio was 1:20:5 (w/w/w) for the 10, 30, and 60 s incubation times. Some degradation products of CypD are marked by arrows.

purpose, software predictions were performed by two distinct tools. Both indicated that CypD was likely to be degraded by chymotrypsin (Table 1).

However, software predictions could be misleading; experimental confirmation would be necessary. For this reason, human recombinant CypD was prepared in *E. coli* and purified to homogeneity using a His-tag affinity matrix (Figure 1). Our experiments showed that CypD was completely cleaved by chymotrypsin within the first 10 s after mixing even at 0 °C (Figure 2A). Using an experimental setup with CypD and substrate Suc-AXPF-pNA closer to Kofron's assay[19] [1:20:5 (w/w/w) CypD:substrate:chymotrypsin ratio], CypD degradation was slower but still present (Figure 2B). However, in the original Kofron's assay, the chymotrypsin excess was several orders of magnitude higher (7 nM cyclophilin vs 0.234 mM chymotrypsin[19]). Thus, the rate of degradation of CypD in the original setup would be more rapid, and CypD would likely degrade as soon as the first seconds of the assay.

Software predictions of protease activity of chymotrypsin that seemed to be in accordance with experimental evaluation were used for other Cyps and PPIases (Table S1). Kofron's assay was likely inappropriate for determining their activity.

The aim of our study was to introduce a novel, simple *in vitro* assay that could be used for the determination of CypD enzymatic activity. Because CypD is predicted to play rate-limiting roles in the isomerization of peptidyl−proline bonds in protein folding, an *in vitro* assay from this area was considered. Several different model proteins have been used to determine PPIase activity in protein folding *in vitro*, e.g., RNase T1,[29−31] dihydrofolate reductase,[32,33] arginine kinase,[34] and carbonic anhydrase.[35,36] In this study, RNase T1 was selected because it is a relatively small protein with 104 residues containing four prolyl−peptide bonds, two of which (bonds preceding Pro39 and Pro55) are in the *cis* conformation in its native form (Figure S1).[37] Moreover, in the proximity of the aforementioned *cis* prolyl−peptide bonds, RNase T1 contains Trp (Trp59), which can be used to monitor the assay[30,31,37,38] and is commercially available.

The first test of CypD refolding activity was inspired by Bose et al.;[29] i.e., 100 μM RNase T1 was unfolded in 8 M urea and refolded by dilution in the presence or absence of 25 nM human CypD (Figure 3A). Human CypD was found to accelerate the refolding of RNase T1 in comparison with spontaneous processes. To the best of our knowledge, the activity of human CypD in the refolding of RNase T1 *in vitro* is described here for the first time. The used concentration of RNase T1 is quite high for routine assays, so different concentrations of RNase T1 in the presence of 25 nM CypD were tested. It was necessary to balance between low RNase T1 concentrations and sufficient differences in the time change of fluorescence between the catalyzed and spontaneous refolding of RNase T1 due to the intended use of this method in CypD inhibitor testing. Thus, 50 μM RNase T1 was selected as a reasonable compromise (Figure 3B).

The concentration of CypD in the reaction mixture was also optimized (Figure 4B) because higher concentrations of CypD were associated with faster refolding. The 25 nM concentration of CypD was selected as optimal because only the linear part of the curve was used to evaluate CypD refolding activity (Table

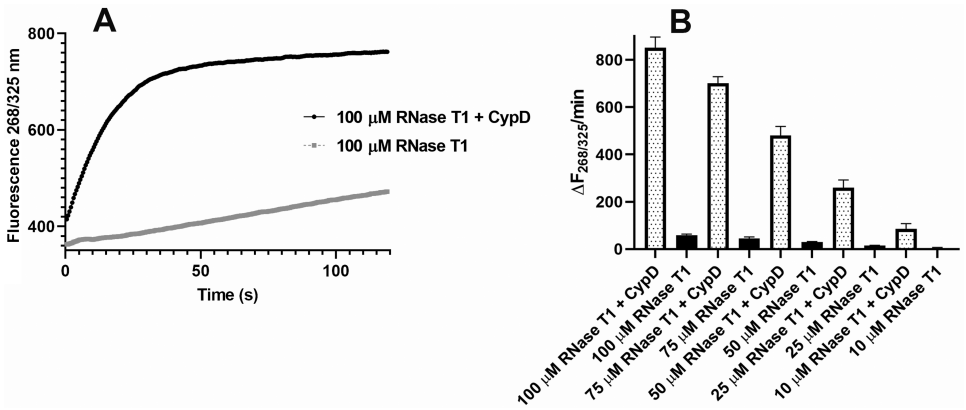

Figure 3. (A) Initial test of refolding 100 μM RNase T1 in the absence or presence of human CypD. (B) Dependence of the fluorescence signal corresponding to folding activity on the concentration of RNase T1 in the absence or presence of 25 nM human CypD.

https://dx.doi.org/10.1021/acs.biochem.9b01025
Biochemistry 2020, 59, 1680−1687

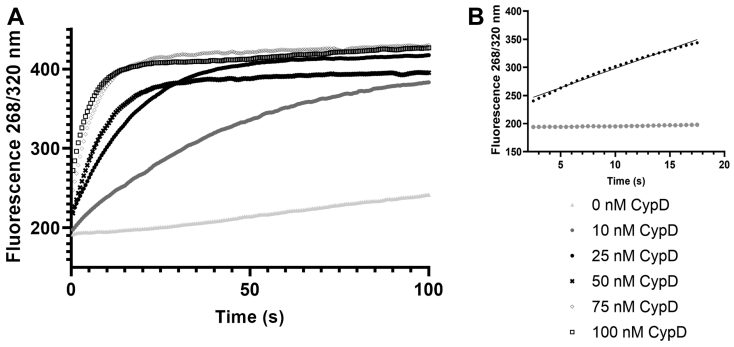

Figure 4. (A) Refolding of 50 μM RNase T1 treated with 8 M urea after dilution in the absence (light gray circles) or presence [(dark gray circles) 10, (●) 25, (×) 50, (◇) 75, and (□) 100 nM] of various concentrations of CypD. (B) Linear part of the graph used to evaluate the refolding activity of CypD.

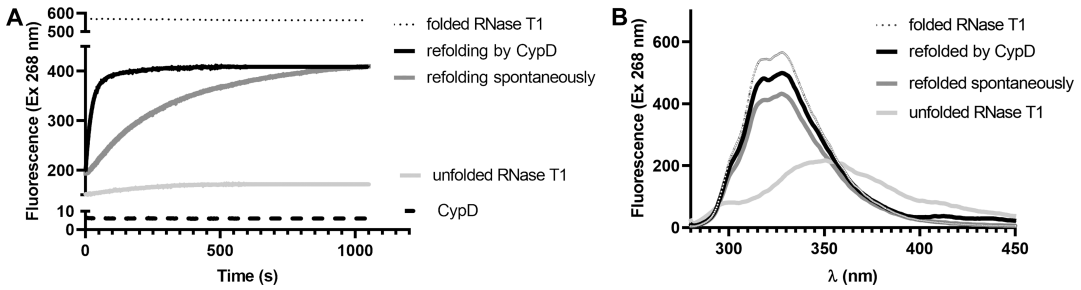

Figure 5. (A) Spontaneous refolding (dark gray squares) and refolding of RNase T1 catalyzed by CypD (■). Fluorescence values of these samples were compared with those of folded RNase T1 (···), unfolded RNase T1 in 8 M urea (light gray squares), and CypD itself (---). (B) Emission spectra of RNase T1 refolded by CypD (■) and refolded spontaneously (dark gray squares) were measured after 1000 s.

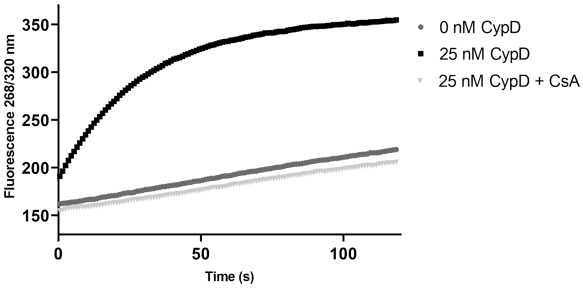

Figure 6. Refolding of RNase T1 catalyzed by CypD is inhibited by the inhibitor cyclosporine A (CsA) at 2 μM.

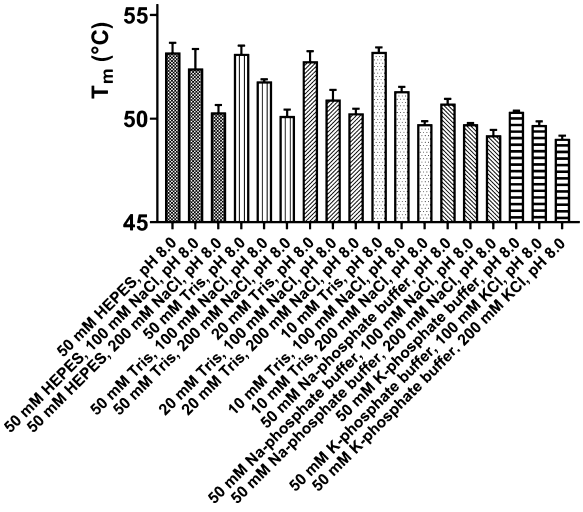

Figure 7. Melting temperatures (T_m) for recombinant human CypD in the presence of different buffers. Values are given as means ± the standard deviation from three experiments.

S2). In this case, the linear part was sufficiently long (Figure 4B).

The emission spectra of folded and unfolded RNase T1 were studied to monitor the refolding reaction. In both cases (i.e., when the reaction was spontaneous or catalyzed by CypD), unfolded RNase T1 (at an emission maximum of 350 nm) in 8 M urea refolded to the folded state (at an emission maximum of 325 nm). However, the refolding of RNase T1 was approximately 8 times faster in the presence of CypD (Figure 5A) than in buffer alone (Figure 5B). The contribution of the intrinsic fluorescence of CypD was negligible.

A similar folding activity has been previously described for yeast mitochondrial cyclophilin Cpr3.[33,39] In this case, Scholz et al.[39,40] reported that expression in a bacterial system may lead to contamination of pure His-tagged Cpr3 with bacterial protein SlyD, which possesses a high PPIase activity because of the high content of His in the SlyD sequence. To avoid this issue, an extra washing step was added to the purification protocol to further reduce the level of binding of low-affinity proteins to Ni-NTA. Moreover, SlyD belongs to FKBPs not inhibited by CsA. However, in our experiment, CypD refolding activity was inhibited by CsA (Figure 6). Altogether, we can conclude that human CypD could catalyze refolding of RNase

https://dx.doi.org/10.1021/acs.biochem.9b01025
Biochemistry 2020, 59, 1680−1687

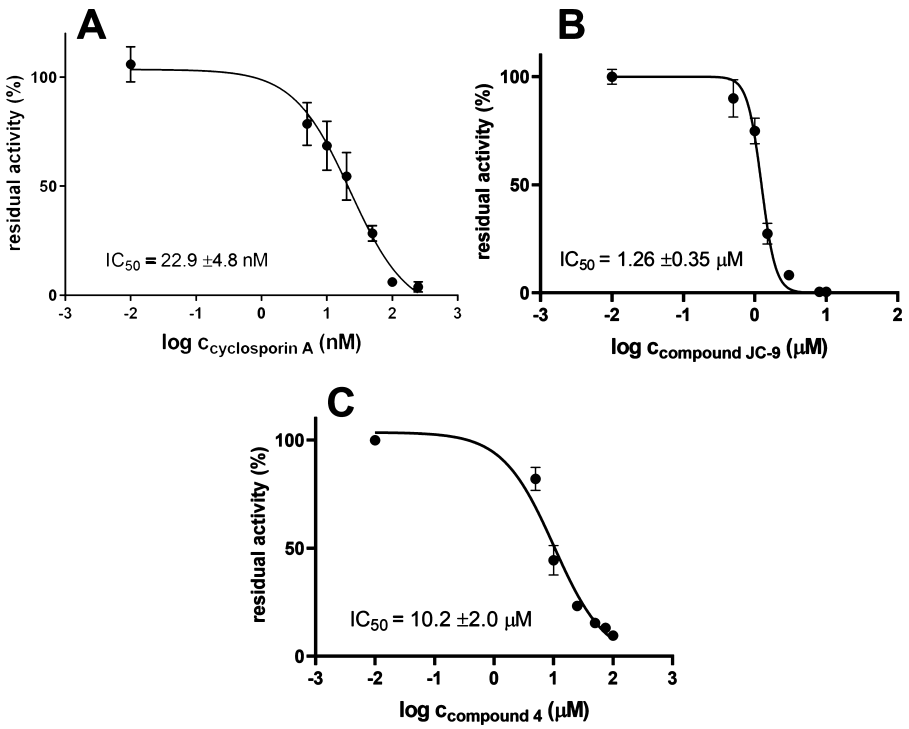

Figure 8. Half-inhibition concentrations (IC_{50}) for (A) CsA, (B) compound JC-9,[14] and (C) compound **4**[16] for the RNase T1 refolding assay catalyzed by human CypD. Values are given as means ± the standard deviation for three or four experiments.

T1 *in vitro*, and such activity is inhibited by the well-known Cyp inhibitor CsA (Figure 6).

Human CypD is very sensitive to the environment and handling. For this reason, a suitable buffer for CypD was determined by differential scanning fluorimetry (DSF).[41,42] General buffers used for biochemical purposes were tested at pH 8.0 because CypD is an enzyme physiologically localized in the mitochondrial matrix at higher pH values.[43] CypD stability was determined using T_m values (Figure 7); an increased T_m corresponded to better stability. CypD was generally found to be less stable in phosphate buffers than in Tris or HEPES. The influence of salt on CypD stability was also tested (Figure 7) because Kofron's assay uses a buffer with 100 mM NaCl. Surprisingly, NaCl was shown to be a destabilizing agent in all tested buffers. Decreased CypD activity in the presence of NaCl was also observed during the optimization of the refolding assay (data not shown).

The 20 mM Tris buffer (pH 8.0) was selected as the optimal buffer for the refolding assay. With the addition of 30% (v/v) glycerol, this buffer proved to be suitable for short-term storage (approximately months) at approximately 1 mg/mL. For long-term storage (approximately one year), the presence of 150 mM NaCl was found to be favorable for preserving refolding activity. CypD was also sensitive to dilution; it was necessary to dilute it gradually (see Materials and Methods) to maintain stability for at least 180 min on ice. Such a time span was sufficient for screening the inhibition ability of several compounds or for determining half-inhibition concentration (IC_{50}) of CypD inhibitors even if the measurement was carried out in cuvettes.

As shown in Figure 6, CsA could inhibit CypD refolding activity at a concentration of 2 μM. The half-inhibition concentration (IC_{50}) of CsA was determined in an RNase T1 refolding assay catalyzed by CypD (Figure 8A). Although it is not possible to directly compare IC_{50} values among diverse studies and methods, data determined in this study for CypD and CsA in the refolding assay ($IC_{50} \sim 23$ nM) corresponded well with previous results (approximately nanomolar IC_{50} or K_i).[14,15] The refolding assay was also tested with weaker inhibitors of CypD. Two structurally different inhibitors (approximately micromolar IC_{50}, K_i, and K_d) from Valasani et al.[14] (compound **JC-9**) and Shore et al.[16] (compound **4**) were utilized. The results obtained in our study (IC_{50} = 1−10 μM) again corresponded well with the published data (Figure 8B,C), demonstrating that the RNase T1 refolding assay could be widely applicable for studying diverse CypD inhibitors.

A possible drawback of the refolding assay lies is its dependence on measurements in cuvettes. If a reaction is rapid, it could be difficult to convert the assay to a high-throughput screening format. However, it is possible to adapt the assay with a simple high-throughput screening method that captures the interaction of the compound or ligand with the target protein. As such, DSF has been used in similar applications and could be an option here.[44−48] In any case, the introduction of an *in vitro* protein refolding assay catalyzed by CypD opens new opportunities for CypD studies and helps reveal the role of CypD in the cell and its involvement in the development of Alzheimer's disease or ischemia/reperfusion injury.

CONCLUSION

CypD is a novel molecular target for the treatment of diseases associated with mPTP opening. One research direction involving CypD focuses on the search for new potent and selective inhibitors. However, currently available methods for

https://dx.doi.org/10.1021/acs.biochem.9b01025
Biochemistry 2020, 59, 1680−1687

determining CypD activity based on the standard Kofron's assay are inappropriate for many reasons, including the degradation of CypD by the indicator enzyme chymotrypsin. This paper introduced a completely novel *in vitro* approach for determining CypD activity using the RNase T1 refolding assay. It is a very simple method using unfolded model proteins; such a reaction better simulates probable CypD physiological functions in the cell than Kofron's assay with peptide substrates. This method improves the investigation of novel CypD inhibitors (optimally in tandem with a high-throughput screening method) in drug research and development and presents new possibilities for investigating CypD pathological and physiological functions in the cell.

■ ASSOCIATED CONTENT

Supporting Information

The Supporting Information is available free of charge at https://pubs.acs.org/doi/10.1021/acs.biochem.9b01025.

> Prediction of protease activity of chymotrypsin (Table S1), examples of raw data from the refolding assay and their evaluation (Table S2), structure of RNase T1 with displayed prolines (Figure S1), and synthesis of compound **4** and compound JC-9 (PDF)

Accession Codes

RNase T1 from *A. oryzae*, UniprotKB accession number P00651; RNase T1 from *A. oryzae*, PDB accession number 1BU4; human cyclophilin D, UniprotKB accession number P30405.

■ AUTHOR INFORMATION

Corresponding Author

Lucie Zemanova − *University of Hradec Kralove, Faculty of Science, Department of Chemistry, 500 03 Hradec Kralove, Czech Republic;* orcid.org/0000-0002-2732-5935; Email: lucie.zemanova@uhk.cz

Authors

Michaela Vaskova − *University of Hradec Kralove, Faculty of Science, Department of Chemistry, 500 03 Hradec Kralove, Czech Republic*

Monika Schmidt − *University of Hradec Kralove, Faculty of Science, Department of Chemistry, 500 03 Hradec Kralove, Czech Republic;* orcid.org/0000-0003-4984-9155

Jana Roubalova − *University of Hradec Kralove, Faculty of Science, Department of Chemistry, 500 03 Hradec Kralove, Czech Republic*

Annamaria Haleckova − *University of Hradec Kralove, Faculty of Science, Department of Chemistry, 500 03 Hradec Kralove, Czech Republic*

Ondrej Benek − *University of Hradec Kralove, Faculty of Science, Department of Chemistry, 500 03 Hradec Kralove, Czech Republic*

Kamil Musilek − *University of Hradec Kralove, Faculty of Science, Department of Chemistry, 500 03 Hradec Kralove, Czech Republic; University Hospital Hradec Kralove, Biomedical Research Center, 500 05 Hradec Kralove, Czech Republic;* orcid.org/0000-0002-7504-4062

Complete contact information is available at: https://pubs.acs.org/10.1021/acs.biochem.9b01025

Funding

This work was supported by the Ministry of Education, Youth and Sports of the Czech Republic (Project ESF CZ.02.1.01/0.0/0.0/18_069/0010054) and the University of Hradec Kralove (Faculty of Science, SV2113-2019, VT2019-2021, and postdoctoral positions).

Notes

The authors declare no competing financial interest.

■ ACKNOWLEDGMENTS

The authors thank Dr. Rudolf Andrys, Ph.D., for the MS analyses of compound **4** and compound JC-9.

■ REFERENCES

(1) Wang, P., and Heitman, J. (2005) The cyclophilins. *Genome Biol. 6*, 226.

(2) Davis, T. L., Walker, J. R., Campagna-Slater, V., Finerty, P. J., Paramanathan, R., Bernstein, G., MacKenzie, F., Tempel, W., Ouyang, H., Lee, W. H., Eisenmesser, E. Z., and Dhe-Paganon, S. (2010) Structural and biochemical characterization of the human cyclophilin family of peptidyl-prolyl isomerases. *PLoS Biol. 8*, No. e1000439.

(3) Kumari, S., Roy, S., Singh, P., Singla-Pareek, S. L., and Pareek, A. (2013) Cyclophilins: proteins in search of function. *Plant Signaling Behav. 8*, No. e22734.

(4) Ünal, C. M., and Steinert, M. (2014) Microbial peptidyl-prolyl cis/trans isomerases (PPIases): virulence factors and potential alternative drug targets. *Microbiol. Mol. Biol. Rev. 78*, 544−571.

(5) Nath, P. R. (2017) Peptidyl-prolyl isomerase (PPIase): an emerging area in tumor biology. *Cancer Res. Front 3* (1), 126−143.

(6) Wedemeyer, W. J., Welker, E., and Scheraga, H. A. (2002) Proline cis-trans isomerization and protein folding. *Biochemistry 41*, 14637−14644.

(7) Perrucci, G. L., Gowran, A., Zanobini, M., Capogrossi, M. C., Pompilio, G., and Nigro, P. (2015) Peptidyl-prolyl isomerases: a full cast of critical actors in cardiovascular diseases. *Cardiovasc. Res. 106*, 353−364.

(8) Fayaz, S. M., Raj, Y. V., and Krishnamurthy, R. G. (2015) CypD: The Key to the Death Door. *CNS Neurol. Disord.: Drug Targets 14*, 654−663.

(9) Kalani, K., Yan, S. F., and Yan, S. S. (2018) Mitochondrial permeability transition pore: a potential drug target for neurodegeneration. *Drug Discovery Today 23*, 1983−1989.

(10) Javadov, S., Jang, S., Parodi-Rullán, R., Khuchua, Z., and Kuznetsov, A. V. (2017) Mitochondrial permeability transition in cardiac ischemia-reperfusion: whether cyclophilin D is a viable target for cardioprotection? *Cell. Mol. Life Sci. 74*, 2795−2813.

(11) Carraro, M., Checchetto, V., Szabó, I., and Bernardi, P. (2019) F-ATP synthase and the permeability transition pore: fewer doubts, more certainties. *FEBS Lett. 593*, 1542−1553.

(12) Bonora, M., and Pinton, P. (2019) A New Current for the Mitochondrial Permeability Transition. *Trends Biochem. Sci. 44*, 559−561.

(13) Porter, G. A., and Beutner, G. (2018) Cyclophilin D, Somehow a Master Regulator of Mitochondrial Function. *Biomolecules 8*, 176.

(14) Valasani, K. R., Sun, Q., Fang, D., Zhang, Z., Yu, Q., Guo, Y., Li, J., Roy, A., and ShiDu Yan, S. (2016) Identification of a Small Molecule Cyclophilin D Inhibitor for Rescuing Aβ-Mediated Mitochondrial Dysfunction. *ACS Med. Chem. Lett. 7*, 294−299.

(15) Ahmed-Belkacem, A., Colliandre, L., Ahnou, N., Nevers, Q., Gelin, M., Bessin, Y., Brillet, R., Cala, O., Douguet, D., Bourguet, W., Krimm, I., Pawlotsky, J. M., and Guichou, J. F. (2016) Fragment-based discovery of a new family of non-peptidic small-molecule cyclophilin inhibitors with potent antiviral activities. *Nat. Commun. 7*, 12777.

(16) Shore, E. R., Awais, M., Kershaw, N. M., Gibson, R. R., Pandalaneni, S., Latawiec, D., Wen, L., Javed, M. A., Criddle, D. N., Berry, N., O'Neill, P. M., Lian, L. Y., and Sutton, R. (2016) Small

Molecule Inhibitors of Cyclophilin D To Protect Mitochondrial Function as a Potential Treatment for Acute Pancreatitis. *J. Med. Chem. 59*, 2596−2611.
(17) Guo, H. X., Wang, F., Yu, K. Q., Chen, J., Bai, D. L., Chen, K. X., Shen, X., and Jiang, H. L. (2005) Novel cyclophilin D inhibitors derived from quinoxaline exhibit highly inhibitory activity against rat mitochondrial swelling and Ca2+ uptake/ release. *Acta Pharmacol. Sin. 26*, 1201−1211.
(18) Park, I., Londhe, A. M., Lim, J. W., Park, B. G., Jung, S. Y., Lee, J. Y., Lim, S. M., No, K. T., Lee, J., and Pae, A. N. (2017) Discovery of non-peptidic small molecule inhibitors of cyclophilin D as neuroprotective agents in Aβ-induced mitochondrial dysfunction. *J. Comput.-Aided Mol. Des. 31*, 929−941.
(19) Kofron, J. L., Kuzmic, P., Kishore, V., Colón-Bonilla, E., and Rich, D. H. (1991) Determination of kinetic constants for peptidyl prolyl cis-trans isomerases by an improved spectrophotometric assay. *Biochemistry 30*, 6127−6134.
(20) Zoldák, G., Aumüller, T., Lücke, C., Hritz, J., Oostenbrink, C., Fischer, G., and Schmid, F. X. (2009) A library of fluorescent peptides for exploring the substrate specificities of prolyl isomerases. *Biochemistry 48*, 10423−10436.
(21) Vivoli, M., Renou, J., Chevalier, A., Norville, I. H., Diaz, S., Juli, C., Atkins, H., Holzgrabe, U., Renard, P. Y., Sarkar-Tyson, M., and Harmer, N. J. (2017) A miniaturized peptidyl-prolyl isomerase enzyme assay. *Anal. Biochem. 536*, 59−68.
(22) Caporale, A., Mascanzoni, F., Farina, B., Sturlese, M., Di Sorbo, G., Fattorusso, R., Ruvo, M., and Doti, N. (2016) FRET-Protease-Coupled Peptidyl-Prolyl cis-trans Isomerase Assay: New Internally Quenched Fluorogenic Substrates for High-Throughput Screening. *J. Biomol. Screening 21*, 701−712.
(23) Freeman, B. C., Toft, D. O., and Morimoto, R. I. (1996) Molecular chaperone machines: chaperone activities of the cyclophilin Cyp-40 and the steroid aporeceptor-associated protein p23. *Science 274*, 1718−1720.
(24) Mok, D., Allan, R. K., Carrello, A., Wangoo, K., Walkinshaw, M. D., and Ratajczak, T. (2006) The chaperone function of cyclophilin 40 maps to a cleft between the prolyl isomerase and tetratricopeptide repeat domains. *FEBS Lett. 580*, 2761−2768.
(25) Lebedev, I., Nemajerova, A., Foda, Z. H., Kornaj, M., Tong, M., Moll, U. M., and Seeliger, M. A. (2016) A Novel In Vitro CypD-Mediated p53 Aggregation Assay Suggests a Model for Mitochondrial Permeability Transition by Chaperone Systems. *J. Mol. Biol. 428*, 4154−4167.
(26) Song, J., Tan, H., Perry, A. J., Akutsu, T., Webb, G. I., Whisstock, J. C., and Pike, R. N. (2012) PROSPER: an integrated feature-based tool for predicting protease substrate cleavage sites. *PLoS One 7*, No. e50300.
(27) Schlatter, D., Thoma, R., Küng, E., Stihle, M., Müller, F., Borroni, E., Cesura, A., and Hennig, M. (2005) Crystal engineering yields crystals of cyclophilin D diffracting to 1.7 A resolution. *Acta Crystallogr., Sect. D: Biol. Crystallogr. 61*, 513−519.
(28) Zor, T., and Selinger, Z. (1996) Linearization of the Bradford protein assay increases its sensitivity: theoretical and experimental studies. *Anal. Biochem. 236*, 302−308.
(29) Bose, S., Mücke, M., and Freedman, R. B. (1994) The characterization of a cyclophilin-type peptidyl prolyl cis-trans-isomerase from the endoplasmic-reticulum lumen. *Biochem. J. 300* (Part 3), 871−875.
(30) Mayr, L. M., Odefey, C., Schutkowski, M., and Schmid, F. X. (1996) Kinetic analysis of the unfolding and refolding of ribonuclease T1 by a stopped-flow double-mixing technique. *Biochemistry 35*, 5550−5561.
(31) Mücke, M., and Schmid, F. X. (1992) Enzymatic catalysis of prolyl isomerization in an unfolding protein. *Biochemistry 31*, 7848−7854.
(32) Rassow, J., Mohrs, K., Koidl, S., Barthelmess, I. B., Pfanner, N., and Tropschug, M. (1995) Cyclophilin 20 is involved in mitochondrial protein folding in cooperation with molecular chaperones Hsp70 and Hsp60. *Mol. Cell. Biol. 15*, 2654−2662.
(33) Matouschek, A., Rospert, S., Schmid, K., Glick, B. S., and Schatz, G. (1995) Cyclophilin catalyzes protein folding in yeast mitochondria. *Proc. Natl. Acad. Sci. U. S. A. 92*, 6319−6323.
(34) Zhang, X. C., Wang, W. D., Wang, J. S., and Pan, J. C. (2013) PPIase independent chaperone-like function of recombinant human Cyclophilin A during arginine kinase refolding. *FEBS Lett. 587*, 666−672.
(35) Kern, G., Kern, D., Schmid, F. X., and Fischer, G. (1994) Reassessment of the putative chaperone function of prolyl-cis/trans-isomerases. *FEBS Lett. 348*, 145−148.
(36) Freskgård, P. O., Bergenhem, N., Jonsson, B. H., Svensson, M., and Carlsson, U. (1992) Isomerase and chaperone activity of prolyl isomerase in the folding of carbonic anhydrase. *Science 258*, 466−468.
(37) Odefey, C., Mayr, L. M., and Schmid, F. X. (1995) Non-prolyl cis-trans peptide bond isomerization as a rate-determining step in protein unfolding and refolding. *J. Mol. Biol. 245*, 69−78.
(38) Schönbrunner, E. R., Mayer, S., Tropschug, M., Fischer, G., Takahashi, N., and Schmid, F. X. (1991) Catalysis of protein folding by cyclophilins from different species. *J. Biol. Chem. 266*, 3630−3635.
(39) Scholz, C., Schindler, T., Dolinski, K., Heitman, J., and Schmid, F. X. (1997) Cyclophilin active site mutants have native prolyl isomerase activity with a protein substrate. *FEBS Lett. 414*, 69−73.
(40) Scholz, C., Maier, P., Dolinski, K., Heitman, J., and Schmid, F. X. (1999) R73A and H144Q mutants of the yeast mitochondrial cyclophilin Cpr3 exhibit a low prolyl isomerase activity in both peptide and protein-folding assays. *FEBS Lett. 443*, 367−369.
(41) Niesen, F. H., Berglund, H., and Vedadi, M. (2007) The use of differential scanning fluorimetry to detect ligand interactions that promote protein stability. *Nat. Protoc. 2*, 2212−2221.
(42) Crowther, G. J., Napuli, A. J., Thomas, A. P., Chung, D. J., Kovzun, K. V., Leibly, D. J., Castaneda, L. J., Bhandari, J., Damman, C. J., Hui, R., Hol, W. G., Buckner, F. S., Verlinde, C. L., Zhang, Z., Fan, E., and Van Voorhis, W. C. (2009) Buffer optimization of thermal melt assays of Plasmodium proteins for detection of small-molecule ligands. *J. Biomol. Screening 14*, 700−707.
(43) Casey, J. R., Grinstein, S., and Orlowski, J. (2010) Sensors and regulators of intracellular pH. *Nat. Rev. Mol. Cell Biol. 11*, 50−61.
(44) Crowther, G. J., Napuli, A. J., Gilligan, J. H., Gagaring, K., Borboa, R., Francek, C., Chen, Z., Dagostino, E. F., Stockmyer, J. B., Wang, Y., Rodenbough, P. P., Castaneda, L. J., Leibly, D. J., Bhandari, J., Gelb, M. H., Brinker, A., Engels, I. H., Taylor, J., Chatterjee, A. K., Fantauzzi, P., Glynne, R. J., Van Voorhis, W. C., and Kuhen, K. L. (2011) Identification of inhibitors for putative malaria drug targets among novel antimalarial compounds. *Mol. Biochem. Parasitol. 175*, 21−29.
(45) Sorrell, F. J., Greenwood, G. K., Birchall, K., and Chen, B. (2010) Development of a differential scanning fluorimetry based high throughput screening assay for the discovery of affinity binders against an anthrax protein. *J. Pharm. Biomed. Anal. 52*, 802−808.
(46) Wan, K. F., Wang, S., Brown, C. J., Yu, V. C., Entzeroth, M., Lane, D. P., and Lee, M. A. (2009) Differential scanning fluorimetry as secondary screening platform for small molecule inhibitors of Bcl-XL. *Cell Cycle 8*, 3943−3952.
(47) Krasavin, M., Stavniichuk, R., Zozulya, S., Borysko, P., Vullo, D., and Supuran, C. T. (2016) Discovery of Strecker-type α-aminonitriles as a new class of human carbonic anhydrase inhibitors using differential scanning fluorimetry. *J. Enzyme Inhib. Med. Chem. 31*, 1707−1711.
(48) Desroses, M., Busker, S., Astorga-Wells, J., Attarha, S., Kolosenko, I., Zubarev, R. A., Helleday, T., Grandér, D., and Page, B. D. G. (2018) STAT3 differential scanning fluorimetry and differential scanning light scattering assays: Addressing a missing link in the characterization of STAT3 inhibitor interactions. *J. Pharm. Biomed. Anal. 160*, 80−88.

https://dx.doi.org/10.1021/acs.biochem.9b01025
Biochemistry 2020, 59, 1680−1687

Supporting information

RNase T1 Refolding Assay for Determining Mitochondrial Cyclophilin D Activity: A Novel in vitro Method Applicable in Drug Research and Discovery

Lucie Zemanova[a]*, Michaela Vaskova[a], Monika Schmidt[a], Jana Roubalova[a], Annamaria Haleckova[a], Ondrej Benek[a], Kamil Musilek[a,b]

[a]University of Hradec Kralove, Faculty of Science, Department of Chemistry, Rokitanskeho 62, 500 03 Hradec Kralove, Czech Republic

[b]University Hospital Hradec Kralove, Biomedical Research Centre, Sokolska 581, 500 05 Hradec Kralove, Czech Republic

Corresponding Author email: lucie.zemanova@uhk.cz

Contents

1. **Prediction of protease activity of chymotrypsin** 2
2. **Raw data from RNaseT1 refolding assay** 3
3. **RNase T1 from *Aspergillus oryzae*** 5
4. **Chemical synthesis of used CypD inhibitors** 6

1. Prediction of protease activity of chymotrypsin

Table S1. Prediction of protease activity of chymotrypsin toward different human cyclophilins and other PPIases (previously measured by Kofron assay) by Peptide cutter.

	Peptide cutter	
	Number of cleavage sites	Position of cleavage site
cypA	20	7, 8, 22, 25, 36, 46, 48, 53, 60, 67, 79, 83, 88, 112, 113, 121, 129, 145, 170, 174
cypB	21	23, 24, 47, 48, 62, 65, 76, 86, 88, 93, 100, 107, 119, 128, 133, 137, 152, 153, 161, 169, 211,
cypC	20	22, 29, 41, 42, 59, 70, 80, 82, 87, 94, 113, 122, 127, 131, 146, 147, 155, 163, 205, 212
cypD cytosolic	26	19, 20, 37, 48, 68, 73, 80, 87, 99, 103, 108, 110, 132, 133, 149, 233, 234, 239, 246, 252, 289, 311, 317, 323, 365, 369
cypE	26	9, 26, 29, 41, 49, 51, 54, 73, 96, 101, 105, 143, 172, 182, 184, 189, 196, 203, 215, 219, 224, 248, 249, 257, 265, 300
pin1	13	11, 23, 24, 25, 34, 73, 92, 103, 110, 125, 134, 139, 151
FKBP12	8	27 37 47 49 60 81 83 100

2. Raw data from RNaseT1 refolding assay

Table S2. Example of raw data from RNaseT1 refolding assay (Figure 4). Only linear part of the graph (values marked in gray) was used for evaluation of CypD activity expressed as ΔF/min.

	0 nM cypD	25 nM cypD		0 nM cypD	25 nM cypD		0 nM cypD	25 nM cypD		0 nM cypD	25 nM cypD		0 nM cypD	25 nM cypD
t (s)	F(268/325)	F(268/325)	t (s)	F(268/325)	F(268/325)	t (s)	F(268/325)	F(268/325)	t (s)	F(268/325)	F(268/325)	t (s)	F(268/325)	F(268/325)
0,5	191,84	219,985	24,5	200,6262	368,5778	48,5	214,003	405,2194	72,5	227,3796	412,9176	96,5	239,3496	416,3344
1	192,6636	225,4074	25	200,8242	370,2112	49	214,294	405,7644	73	227,6882	412,7796	97	239,5754	416,2662
1,5	193,3552	230,7522	25,5	200,797	371,8972	49,5	214,3402	405,6202	73,5	228,0626	412,6768	97,5	240,0052	416,416
2	193,8214	235,6724	26	200,852	373,7574	50	214,4442	406,3902	74	228,3048	413,3732	98	240,5504	416,4758
2,5	193,9388	240,2242	26,5	201,1254	375,2056	50,5	214,408	406,51	74,5	228,3694	413,4552	98,5	240,8356	416,7778
3	194,0868	244,9506	27	201,254	376,6528	51	215,0046	406,941	75	228,7194	413,5686	99	241,2054	417,151
3,5	194,2714	249,3906	27,5	201,6554	378,1532	51,5	215,495	407,4748	75,5	229,266	413,589	99,5	241,5006	417,3314
4	194,4114	253,8602	28	201,9222	379,2274	52	215,9162	408,0004	76	229,391	413,3996	100	241,7656	417,421
4,5	194,187	258,6298	28,5	202,2316	380,1102	52,5	216,4386	407,766	76,5	229,8848	413,1484	100,5	241,9432	417,531
5	194,1074	263,295	29	202,5698	381,1042	53	216,8304	408,246	77	230,2202	413,1954	101	241,7734	417,4344
5,5	194,2184	267,6988	29,5	202,8	382,1836	53,5	216,7266	408,5528	77,5	230,44	412,971	101,5	242,1158	417,0082
6	194,2908	271,9424	30	202,9094	383,3222	54	216,8566	408,4332	78	230,3946	413,2242	102	242,1418	417,2002
6,5	194,5844	276,2654	30,5	203,4396	384,2262	54,5	216,7594	408,7642	78,5	230,5672	413,1582	102,5	242,327	417,2682
7	195,1094	279,9394	31	203,737	385,4558	55	217,026	409,0988	79	230,6844	413,1248	103	242,5164	417,0318
7,5	195,3116	283,867	31,5	204,1206	386,6184	55,5	217,3276	409,016	79,5	231,0378	413,2332	103,5	243,1522	417,2232
8	195,3026	287,5814	32	204,1832	387,6796	56	217,5922	409,2212	80	231,3234	413,3626	104	243,4768	417,3028
8,5	195,1068	291,4352	32,5	204,5086	388,3384	56,5	217,9502	409,3994	80,5	231,8416	413,454	104,5	244,1198	417,2746
9	195,0378	294,8008	33	204,51	389,347	57	218,3914	409,4938	81	232,1456	413,8294	105	244,4646	417,4114
9,5	195,0446	298,3278	33,5	204,8922	390,2384	57,5	218,4792	409,8434	81,5	232,4828	413,8126	105,5	244,573	417,3514
10	195,0688	301,6798	34	205,1338	391,0684	58	218,748	409,9042	82	232,583	413,9824	106	244,7824	417,4356
10,5	195,1598	304,7788	34,5	205,3848	391,8942	58,5	219,2612	410,2294	82,5	233,0186	414,3164	106,5	244,9814	417,5458
11	195,5194	307,839	35	205,5664	392,8462	59	219,541	410,3386	83	233,0598	414,5198	107	245,1536	417,8328
11,5	195,7286	311,2576	35,5	205,8306	393,5548	59,5	219,8406	410,5444	83,5	233,2902	414,5824	107,5	245,13	418,0096
12	195,739	314,5364	36	205,9216	394,1132	60	220,3424	410,675	84	233,4856	414,907	108	245,5134	418,154
12,5	195,8948	317,2734	36,5	206,3182	394,7738	60,5	220,8986	411,0262	84,5	233,7492	414,8948	108,5	245,9174	418,1462
13	196,2616	320,3398	37	206,5936	395,4786	61	221,2116	411,4678	85	233,6996	415,1896	109	246,1534	418,239
13,5	196,5936	323,1704	37,5	206,8944	395,889	61,5	221,3814	411,8498	85,5	233,6736	414,9448	109,5	246,2472	417,6946
14	196,8144	325,6624	38	207,3532	396,332	62	221,6586	411,8614	86	233,9546	415,0414	110	246,6696	417,3502
14,5	197,0346	328,0598	38,5	207,5414	397,0714	62,5	221,7914	411,7858	86,5	234,1496	415,195	110,5	247,2702	417,3986
15	197,2016	330,9136	39	207,499	397,5606	63	221,8244	411,7082	87	234,62	415,3302	111	247,3664	417,6006
15,5	197,1506	333,6992	39,5	207,8068	398,1958	63,5	221,8986	411,5706	87,5	235,0744	414,9972	111,5	247,6722	417,603
16	197,3016	336,4744	40	207,9858	398,7116	64	222,073	411,686	88	235,8612	415,0754	112	248,0846	417,5492

16,5	197,638	339,1814	40,5	208,2482	399,4564	64,5	222,3334	411,716	88,5	236,115	415,1434	112,5	248,5926	417,6912
17	197,737	341,5782	41	208,65	400,0972	65	222,5954	412,0084	89	236,0398	415,2024	113	248,2326	418,0506
17,5	197,97	343,8568	41,5	208,7434	400,6358	65,5	222,9202	412,2198	89,5	236,0374	415,3424	113,5	248,4678	418,0044
18	198,21	345,843	42	209,2784	400,834	66	223,2882	412,4806	90	236,1388	415,64	114	248,694	418,0542
18,5	198,2808	347,7548	42,5	209,7394	401,3562	66,5	223,6268	412,3498	90,5	236,3044	415,765	114,5	248,7554	418,437
19	198,2016	349,5772	43	209,906	401,6828	67	223,926	412,49	91	236,5678	415,8186	115	248,5912	418,2276
19,5	198,355	351,6094	43,5	210,2442	402,0254	67,5	224,2816	412,461	91,5	237,2648	415,8616	115,5	248,8862	417,473
20	198,5858	353,5232	44	210,7698	402,4534	68	224,4196	412,7334	92	237,6774	415,9562	116	249,1096	416,7644
20,5	198,7082	355,46	44,5	210,7916	402,8426	68,5	224,6338	412,6184	92,5	238,054	416,1038	116,5	249,3748	415,877
21	198,7914	357,4732	45	211,3282	403,214	69	225,0818	412,8656	93	237,984	416,5126	117	249,7346	415,714
21,5	198,9838	359,0232	45,5	211,518	403,525	69,5	225,3218	412,902	93,5	238,1034	416,679	117,5	249,9594	416,0388
22	199,3444	360,9878	46	211,8084	403,6424	70	225,3866	413,199	94	238,329	416,7062	118	250,342	416,8746
22,5	199,4584	362,6436	46,5	212,2622	403,6824	70,5	225,8332	413,2886	94,5	238,5442	416,6884	118,5	250,6044	417,45
23	199,857	364,2908	47	213,0252	404,3906	71	226,292	413,4962	95	238,5962	416,4666	119	250,6134	418,3486
23,5	200,1492	365,3828	47,5	213,1338	404,5562	71,5	226,419	413,0956	95,5	238,85	416,4368			
24	200,2402	367,263	48	213,7798	404,9732	72	226,8968	413,0966	96	239,289	416,1826			

	0 nM cypD	**25 nM cypD**
ΔF(17,5-2,5)	4,03	103,63
CypD activity (ΔF/s)		6,64
CypD activity (ΔF/min)		398,41

3. RNase T1 from *Aspergillus oryzae*

Figure S1. RNase T1 from *Aspergillus oryzae* (PDB: 1BU4) with displayed all proline residues (Pro39, Pro55, Pro60, Pro73). Peptide bonds preceding Pro39 and Pro55 (cyan) are in *cis* conformation, Trp59 (green) is in close proximity to these Pro and its fluorescence is used for monitoring of folding reaction.

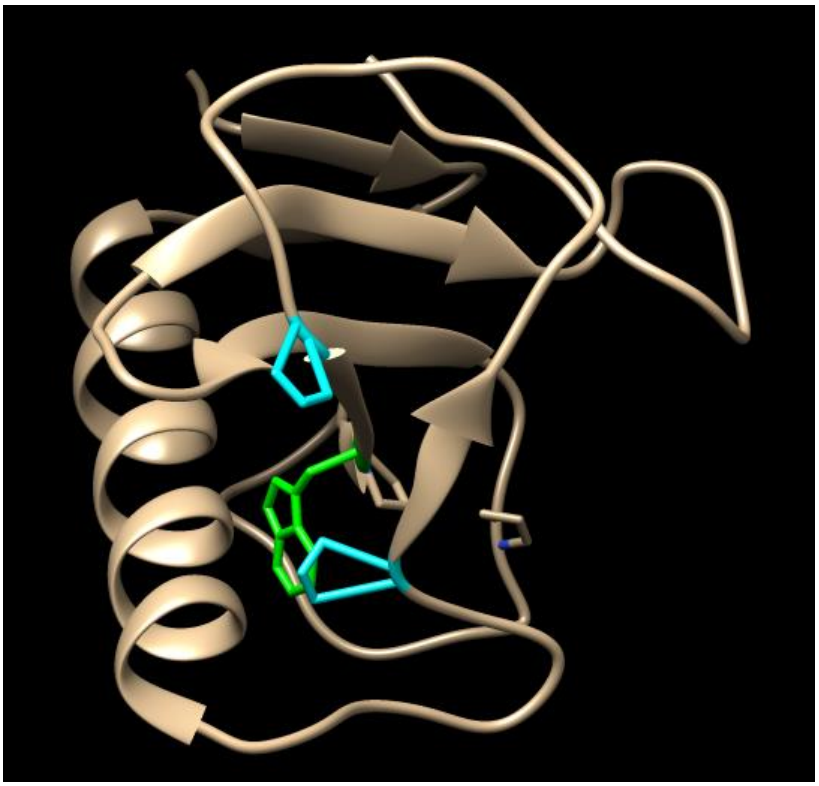

4. Chemical synthesis of used CypD inhibitors

General chemistry

Solvents and reagents were purchased from Fluka and Sigma-Aldrich (Czech Republic) and used without further purification. Reactions were monitored by thin layer chromatography performed on aluminium sheets pre-coated with silica gel 60 F254 (Merck, Czech Republic) and detected under 254 nm UV light. Column chromatography was performed on a silica gel 60 column (230 mesh). Melting points were measured by using a Stuart SMP30 melting point apparatus (Bibby Scientific Limited, Staffordshire, UK) and were uncorrected.

NMR spectra were recorded at Varian S500 spectrometer (1H 500 MHz and 13C 126 MHz, Palo Alto CA, USA). In all cases, the chemical shift values were reported in ppm (δ) relative to residual solvent peak for dimethylsulfoxide-d6 (δ 2.50 and δ 39.52 for 1H and 13C respectively).

LC-MS was determined using Agilent Infinity II 1290 UHPLC system with Agilent 6470 QqQ mass spectrometer (Agilent Technologies, Santa Clara, USA). Chromatographic separation was performed on Zorbax Eclipse C18 column (50 x 2.1 mm, 1.8 µm) with 0.1% formic acid in ultra-pure water as mobile phase A and 0.1% formic acid in acetonitrile as mobile phase B. MS conditions were as follows: gas temp 300 °C, gas flow 8 l/min, nebulizer 35 psi, sheat gas temp 380 °C, sheat gas flow 11 L/min, capillary 3500 V, nozzle voltage 0 V. Positive and negative ions were monitored in the range of 50 – 800 m/z. The purity of final products was >95%.

Chemical synthesis and product characterization

Compound JC-9

2-(3-Cyano-4-isobutoxyphenyl)-4-methyl-N-(4-sulfamoylphenyl)thiazole-5-carboxamide

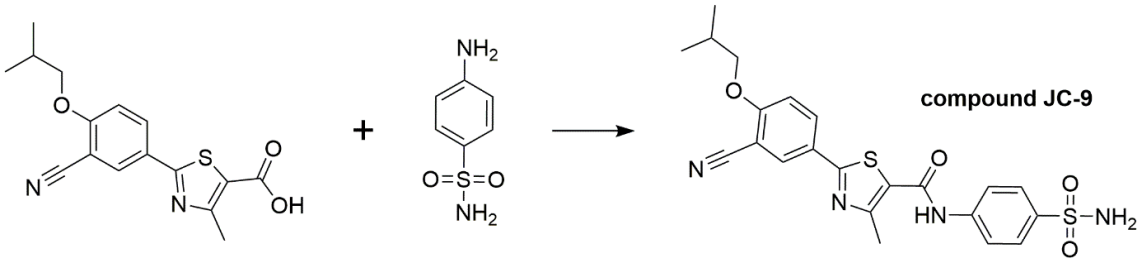

To a solution of 2-(3-cyano-4-isobutoxyphenyl)-4-methylthiazole-5-carboxylic acid (0.5 g, 1.58 mmol) in anhydrous toluene (10 mL) containing catalytic amount of DMF was added dropwise thionyl chloride (115 µl, 1.58 mmol) and the resulting mixture was stirred at room temperature for 30 min and afterwards at 90 °C for 3 h. The reaction mixture was then slowly cooled to room temperature and concentrated to give acyl chloride intermediate as white residue. This residue was dissolved in acetonitrile and an equimolar amount of 4-aminobenzenesulfonamide (0.27 g, 1.58 mmol) was added. This solution was stirred for 4 h at 75 °C to give impure solid. This solid that was separated by filtration, washed with acetonitrile, ice-cold water, and then recrystallized from ethanol (25 mL) to give pure compound 2.

Yield 57%; mp: 285–286 °C; 1H NMR (500 MHz, DMSO-d6) δ (ppm) 10.55 (s, 1H), 8.28 (d, J = 2.3 Hz, 1H), 8.22 (dd, J = 8.9, 2.4 Hz, 1H), 7.95 – 7.73 (m, 4H), 7.39 (d, J = 9.1 Hz, 1H), 7.29 (s, 2H), 4.01 (d, J = 6.5 Hz, 2H), 2.65 (s, 3H), 2.09 (dd, J = 12.9, 6.2 Hz, 1H), 1.02 (d, J = 6.7 Hz, 6H); 13C NMR (126 MHz, DMSO-d6) δ (ppm) 164.46, 161.94, 160.03, 156.25, 141.50,

139.13, 132.88, 131.31, 126.58, 125.88, 125.32, 119.90, 115.36, 113.98, 101.62, 75.13, 27.57, 18.69, 17.16; ESI-MS: m/z 471.1 $[M+H]^+$ (calc. for $C_{22}H_{22}N_4O_4S_2$: 471.1 $[M+H]^+$).

Intermediate S1 in synthesis of compound 4

Ethyl 2-(3-(4-(tert-butoxycarbonylamino)benzyl)ureido)acetate (S1)

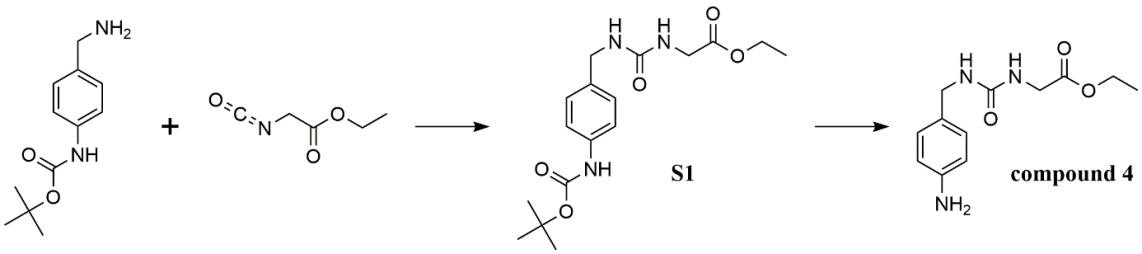

Ethyl isocyanatoacetate (252 µl, 2.25 mmol) was dissolved in THF (6 mL), then 4-(tert-butoxycarbonylamino)benzylamine (500 mg, 2.25 mmol) was added in one portion and the reaction mixture was stirred for 2 h at room temperature. The reaction mixture was concentrated and purified by precipitation in diethyl ether, yielding intermediate S1 (690 mg, 88%) as a white solid.

1H NMR (500 MHz, DMSO-d6) δ (ppm) 9.25 (br s, 1H), 7.37 (d, J = 8.3 Hz, 2H), 7.12 (d, J = 8.5 Hz, 2H), 6.56 (t, J = 6.0 Hz, 1H), 6.23 (t, J = 6.1 Hz, 1H), 4.12 (d, J = 5.9 Hz, 2H), 4.08 (q, J = 7.1 Hz, 2H), 3.77 (d, J = 6.0 Hz, 2H), 1.46 (s, 9H), 1.19 (t, J = 7.1 Hz, 3H).

Compound 4

Ethyl 2-(3-(4-aminobenzyl)ureido)acetate

N-boc protected intermediate S1 (350 mg, 0.99 mmol) was dissolved in 1.75 mL of dichloromethane, then 1.75 mL of trifluoroacetic acid (TFA) was added and the reaction mixture was stirred for 1 h at room temperature. Then the reaction mixture was concentrated and the crude product purified by precipitation using ethyl acetate/ hexane to yield the deprotected amine in form of TFA salt as a yellow solid. The TFA salt was quenched with 10% aq. $NaHCO_3$ solution and the product in form of free amine was extracted into ethyl acetate (4×20 mL). The combined organic layers were dried over Na_2SO_4, filtered and concentrated to yield the product (186 mg, 74%) as a yellow solid.

Yield 74%; mp: 158–160 °C; 1H NMR (500 MHz, DMSO-d6) δ (ppm) 6.90 (d, J = 8.2 Hz, 2H), 6.50 (d, J = 8.4 Hz, 2H), 6.40 (t, J = 5.8 Hz, 1H), 6.17 (t, J = 6.1 Hz, 1H), 4.92 (s, 2H), 4.08 (q, J = 7.1 Hz, 2H), 4.01 (d, J = 5.7 Hz, 2H), 3.77 (d, J = 6.0 Hz, 2H), 1.19 (t, J = 7.1 Hz, 3H); 13C NMR (126 MHz, DMSO-d6) δ (ppm) 171.21, 157.86, 147.36, 128.05, 127.35, 113.68, 60.15, 42.73, 41.55, 14.11; ESI-MS: m/z 252.2 $[M+H]^+$ (calc. for $C_{12}H_{17}N_3O_3$: 252.1 $[M+H]^+$).

10.2 Publikace II

Benek, O., **Vaskova, M.**, Miskerikova, M., Schmidt, M., Andrys, R., Rotterova, A., Skarka, A., Hatlapatkova, J., Karasova, J.Z., Medvecky, M., Hroch, L., Vinklarova, L., Fisar, Z., Hroudova, J., Handl, J., Capek, J., Rousar, T., Kobrlova, T., Dolezal, R., Soukup, O., Aitken, L., Gunn-Moore, F., Musilek, K., 2023. Development of submicromolar 17β-HSD10 inhibitors and their *in vitro* and *in vivo* evaluation. Eur. J. Med. Chem. 258, 115593. https://doi.org/10.1016/j.ejmech.2023.115593

European Journal of Medicinal Chemistry 258 (2023) 115593

Contents lists available at ScienceDirect

European Journal of Medicinal Chemistry

journal homepage: www.elsevier.com/locate/ejmech

Research paper

Development of submicromolar 17β-HSD10 inhibitors and their *in vitro* and *in vivo* evaluation

Ondrej Benek [a,b,*], Michaela Vaskova [a], Marketa Miskerikova [a], Monika Schmidt [a,b], Rudolf Andrys [a], Aneta Rotterova [a], Adam Skarka [a], Jana Hatlapatkova [c], Jana Zdarova Karasova [c], Matej Medvecky [a,d], Lukas Hroch [b], Lucie Vinklarova [a], Zdenek Fisar [e], Jana Hroudova [e], Jiri Handl [f], Jan Capek [f], Tomas Rousar [f], Tereza Kobrlova [b], Rafael Dolezal [b], Ondrej Soukup [b], Laura Aitken [g], Frank Gunn-Moore [g], Kamil Musilek [a,b,**]

[a] University of Hradec Kralove, Faculty of Science, Department of Chemistry, Rokitanskeho 62, 500 03, Hradec Kralove, Czech Republic
[b] University Hospital Hradec Kralove, Biomedical Research Centre, Sokolska 581, 500 05, Hradec Kralove, Czech Republic
[c] University of Defence, Faculty of Military Health Sciences, Department of Toxicology and Military Pharmacy, Trebesska 1575, 500 01, Hradec Kralove, Czech Republic
[d] University of Warwick, Bioinformatics Research Technology Platform, Coventry, CV4 7AL, United Kingdom
[e] Charles University and General University Hospital in Prague, First Faculty of Medicine, Department of Psychiatry, Ke Karlovu 11, 120 00, Prague 2, Czech Republic
[f] University of Pardubice, Faculty of Chemical Technology, Department of Biological and Biochemical Sciences, Studentska 573, Pardubice, 53210, Czech Republic
[g] University of St. Andrews, School of Biology, Biomedical Science Research Complex, North Haugh, St. Andrews KY16 9ST, United Kingdom

ARTICLE INFO

Keywords:
Amyloid-binding alcohol dehydrogenase (ABAD)
Alzheimer's disease
17β-hydroxysteroid dehydrogenase type 10 (17β-HSD10)
Enzyme inhibition
Pharmacokinetics

ABSTRACT

17β-hydroxysteroid dehydrogenase type 10 (17β-HSD10) is a multifunctional mitochondrial enzyme and putative drug target for the treatment of various pathologies including Alzheimer's disease or some types of hormone-dependent cancer. In this study, a series of new benzothiazolylurea-based inhibitors were developed based on the structure-activity relationship (SAR) study of previously published compounds and predictions of their physicochemical properties. This led to the identification of several submicromolar inhibitors (IC_{50} ~0.3 μM), the most potent compounds within the benzothiazolylurea class known to date. The positive interaction with 17β-HSD10 was further confirmed by differential scanning fluorimetry and the best molecules were found to be cell penetrable. In addition, the best compounds weren't found to have additional effects for mitochondrial off-targets and cytotoxic or neurotoxic effects. The two most potent inhibitors **9** and **11** were selected for *in vivo* pharmacokinetic study after intravenous and peroral administration. Although the pharmacokinetic results were not fully conclusive, it seemed that compound **9** was bioavailable after peroral administration and could penetrate into the brain (brain-plasma ratio 0.56).

1. Introduction

17β-hydroxysteroid dehydrogenase type 10 (17β-HSD10), also formerly termed amyloid-binding alcohol dehydrogenase (ABAD), is an oxidoreductase enzyme located in the mitochondrial matrix. It can catalyse the turnover of numerous substrates, especially steroids and neurosteroids. Besides its catalytic activity, it also acts as a structural component of RNase P. Thus, it is involved in many physiological functions. 17β-HSD10 plays an important role in the development of several human diseases and its inhibition is considered a potential treatment strategy for Alzheimer's disease (AD) and hormone-dependent cancer [1].

The development of AD is connected with an elevated level of amyloid-β peptide (Aβ), tauopathy, and mitochondrial dysfunction in the brain [2]. There are several putative mechanisms of Aβ toxicity to neuronal cells [3]. One of the theories focuses on the detrimental effects of Aβ on mitochondrial functions via interaction with mitochondrial proteins. Among other mitochondrial targets, Aβ is known to interact with 17β-HSD10, which compromises its function and contributes to mitochondrial dysfunction seen in AD. Blocking the interaction of

* Corresponding author. University of Hradec Kralove, Faculty of Science, Department of Chemistry, Rokitanskeho 62, 500 03 Hradec Kralove, Czech Republic.
** Corresponding author. University of Hradec Kralove, Faculty of Science, Department of Chemistry, Rokitanskeho 62, 500 03 Hradec Kralove, Czech Republic.
E-mail addresses: ondrej.benek@uhk.cz (O. Benek), kamil.musilek@uhk.cz (K. Musilek).

https://doi.org/10.1016/j.ejmech.2023.115593
Received 23 December 2022; Received in revised form 13 May 2023; Accepted 23 June 2023
Available online 24 June 2023
0223-5234/© 2023 Elsevier Masson SAS. All rights reserved.

17β-HSD10 with Aβ or inhibition of 17β-HSD10 enzymatic function suppresses Aβ toxicity and ameliorates mitochondrial dysfunction, and thus presents a potential AD treatment strategy [1,4,5].

Due to its important role in steroid metabolism, 17β-HSD10 is implicated in some cancer types. In prostate cancer, 17β-HSD10 enables steroid synthesis, catalysing the alternative synthesis pathway of androgen by generating dihydrotestosterone (DHT) in the absence of testosterone [6,7]. It was also suggested that 17β-HSD10 overexpression supports cancer growth and makes the cancer cells more resistant to oxidative stress [8,9]. Based on these findings, inhibition of 17β-HSD10 could be considered a potential treatment strategy for cancer [1,7].

There is only a limited number of 17β-HSD10 inhibitors known to date. Based on their structure, the inhibitors can be sorted into three main classes, i.e., pyrazoles [10,11], steroids [7,12,13], and benzothiazolylureas. Benzothiazolylureas and their analogues are the largest class of 17β-HSD10 inhibitors and their development was described in a number of studies [14–22]. The most potent benzothiazolylurea inhibitors known to date (**1**–**5**) have IC_{50} values ~1 μM (Fig. 1) [21,22].

The intention of this study was to design and develop new benzothiazolylurea inhibitors with improved activity and/or physico-chemical properties that would be suitable for *in vivo* experiments.

2. Results and discussion

2.1. Structural design

Formerly, our research group has published several articles on the development of 1-benzothiazolyl-3-phenylurea 17β-HSD10 inhibitors [17–22]. SAR analysis of previous results highlighted several key structural motifs important for inhibition activity. Firstly, the 3-halogen-4-hydroxy substitution pattern on phenyl moiety was crucial for potent enzyme inhibition [17,18,21,22]. It seems that halogens, with their electron-withdrawing inductive (-I) effect, could increase the acidity and/or hydrogen bond donor (HBD) capacity of the neighbouring hydroxyl group, which resulted in improved binding and inhibition. However, electron-withdrawing groups with negative mesomeric (-M) effect (e.g., carboxyl, carbonyl) were not tolerated except for the nitrile group. This could be due to their ability to create an intramolecular hydrogen bond with the neighbouring hydroxyl group while creating a 6-membered ring. This would result in a decreased acidity/HBD capability of the neighbouring hydroxyl, which consequently manifested in the lower activity of the corresponding inhibitor. In contrast, the nitrile group (-M effect) possess linear geometry, thus could not form a hydrogen bond with the neighbouring hydroxyl. To further probe this theory, we decided to prepare compounds **6** and **7** (Fig. 2A) substituted with strongly electron-withdrawing trifluoromethyl group (-I effect) and nitro group (-M effect, the potential for intramolecular H-bonding), respectively.

Secondly, the substitution in position 6 of benzothiazolyl moiety affected the inhibition potency. The best-known inhibitors bear either a larger HBA group (ethoxy in compound **2**, methanesulfonyl in **3**) or a small HBD group (hydroxyl in **4** and primary amine in **5**) [21,22]. Therefore, we decided to prepare a series of compounds containing larger substituents with combined HBA/HBD properties (Fig. 2B). Further, the synthetic precursor of compound **11** (ester **10**) was also isolated and evaluated. To assess the importance of HBD properties, we prepared *N*-methylated analogues of **5** and **12** devoid of HBD character (compounds **8** and **13**, respectively; Fig. 2B).

The ability to pass cell membranes is a necessary pre-requisite for drugs acting via intracellular effectors (e.g., 17β-HSD10). The ability to pass cell membranes (via passive diffusion) can be assessed by *in silico* predictions of their physico-chemical properties. Even more strict physico-chemical criteria are required from CNS-targeted drugs that need to pass blood–brain barrier (BBB) to exert their effect in the brain [23,24]. Thus, we have calculated the physico-chemical properties [25] of the designed compounds and used the CNS multiparameter optimization (MPO) developed by Wager et al. [23] to predict and compare the likeliness of BBB-permeation. As can be seen, the benzothiazolylureas have rather suboptimal physico-chemical properties with the exception of compounds **7** and **12** (Table 1).

To address this issue, we have designed compounds with urea linker replaced by two- or three-membered aliphatic linker (compounds **15**, **17**, and **18**; Fig. 2C) and benzothiazolyl moiety replaced by isosteric benzoxazole or indole heterocycles (compounds **19** and **20**; Fig. 2C). Further, two imine precursors, **14** and **16**, were also isolated and evaluated (Fig. 2C). All the "non-urea" compounds, with the exception of **15** (MPO = 3.9), comply with the MPO score for CNS bioavailable drugs (MPO ≥4; Table 1). In addition, solubility is another important physico-chemical parameter predictive for BBB penetration, with most CNS drugs having aqueous solubility at pH 7.4 higher than 100 μmol/L [24]. The previously published urea inhibitors showed, in some cases, low solubility, which hampered theirs *in vitro* assessment [18]. Therefore, we have accounted for solubility when designing the non-urea compounds. As seen in Table 1, compounds **17**–**20** have improved Clog$S_{7.4}$ values

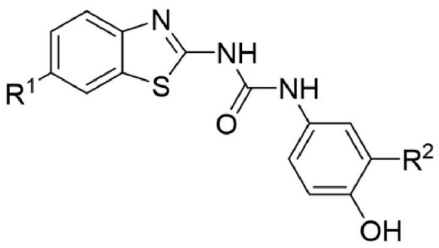

Compound	R^1	R^2	IC_{50} (μM)
1	OMe	Br	1.3
2	OEt	Cl	1.6
3	SO_2Me	Cl	0.9
4	OH	Cl	1.2
5	NH_2	Cl	1.6

Fig. 1. The most potent benzothiazolylurea 17β-HSD10 inhibitors discovered to date (**1**–**5**).

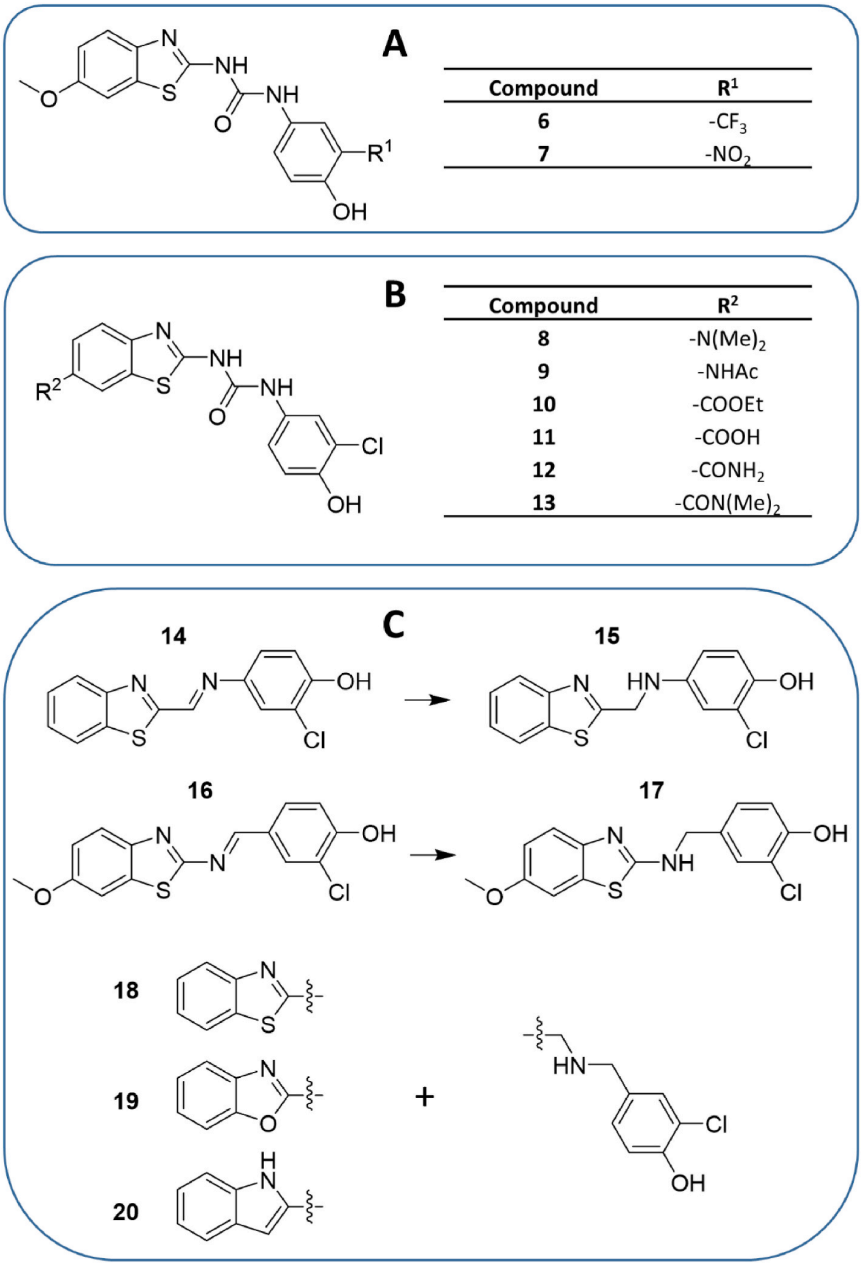

Fig. 2. Prepared compounds could be divided into three series. **A**) Compounds **6** and **7** with halogen in position 3 of phenyl moiety replaced with alternative electron-withdrawing groups. **B**) Compounds **8**–**13** with different substitutions in position 6 of benzothiazolyl moiety. **C**) Compounds **14**–**20** with non-urea linkers.

compared to urea compounds (with the exception of likely highly soluble compound **11**).

2.2. Synthesis

Compounds containing urea linker in their structure were generally prepared via a two-step synthesis. Firstly, the corresponding benzothiazole-2-amine was treated with 1,1′-carbonyldiimidazole to form an imidazolyl intermediate, which was then treated with the corresponding aniline derivative to yield the 1,3-disubstituted urea as a final product. Final product **11** substituted in position 6 of benzothiazole with carboxyl group was prepared via basic hydrolysis of ethyl ester **10** (Fig. 3).

In several cases, the required 2-aminobenzothiazole and 4-aminophenol precursors were not commercially available, thus, they were synthesized. 4-amino-2-(trifluoromethyl)phenol (**25a**) was prepared by de-methylation of 4-methoxy-3-(trifluoromethyl)aniline using hydrobromic acid (Fig. 3). Benzothiazole-2-amines substituted in position 6 with acetamide (**22b**) or dimethylcarboxamide group (**22g**) were prepared from corresponding *para*-substituted anilines in reaction with potassium thiocyanate and tetramethylammonium dichloroiodate(I) (Fig. 3).

However, using above-mentioned process didn't yield desired N^6,N^6-dimethylbenzo[*d*]thiazole-2,6-diamine (**30**). Therefore, it was prepared from 6-nitrobenzo[*d*]thiazole-2-amine via 4-step synthesis (Fig. 4). Firstly, the amine group of 6-nitrobenzo[*d*]thiazole-2-amine was protected with di-*tert*-butyl dicarbonate. Secondly, the nitro group was reduced with Pd/C catalysed hydrogenation. Consequently, the 6-amine

Table 1
Calculated physico-chemical properties of new inhibitors. MPO score ≥4 indicates that the compound is likely to be CNS bioavailable.

Compound	Clog*P*	Clog*D*	TPSA	MW	HBD	pK_a	MPO	Clog$S_{7.4}$
optimal score	≤3	≤2	40–90	≤360	≤0.5	≤8	4–6	≥ (−4)
6	3.92	3.57	111.72	383.35	3	2.31	3.0	−4.86
7	2.97	1.97	157.54	360.35	3	2.22	4.2	−4.13
8	3.90	3.74	105.73	362.83	3	3.6	3.3	−4.86
9	2.82	2.29	131.59	376.82	4	1.72	3.7	−4.06
10	4.18	2.95	128.79	391.83	3	0.38	2.9	−3.95
11	3.44	−0.16	139.79	363.78	4	0.38	3.8	−1.36
12	2.36	1.27	145.58	362.79	5	0.52	4.0	−3.43
13	2.79	1.67	122.80	390.84	3	0.69	3.9	−3.98
14	4.35	4.32	73.72	288.75	1	1.79	4.2	−4.86
15	4.17	4.16	73.39	290.77	2	2.94	3.9	−4.55
16	4.02	3.36	82.95	318.78	1	3.91	4.6	−3.77
17	3.90	3.84	82.62	320.79	2	3.83	4.1	−4.72
18	3.61	3.58	73.39	304.80	2	5.46	4.4	−2.87
19	3.06	3.02	58.29	288.73	2	6.33	5.0	−2.88
20	3.67	1.71	48.05	286.76	3	9.24	4.2	−1.63

Notes: *In silico* predictions of physico-chemical properties using ACS Percepta software. The multiparameter optimization (MPO) scoring function is based on six fundamental physico-chemical parameters – calculated partition coefficient (Clog*P*); calculated distribution coefficient at pH 7.4 (Clog*D*); molecular weight (MW); topological polar surface area (TPSA); number of HBD; most basic centre (pK_a). All properties are weighted equally, with a desirability score ranging from 0.0 to 1.0 and therefore a total CNS MPO desirability score ranges from 0.0 to 6.0. The MPO score for CNS available drugs is ≥ 4. Further, aqueous solubility at pH 7.4 was predicted (Clog$S_{7.4}$).

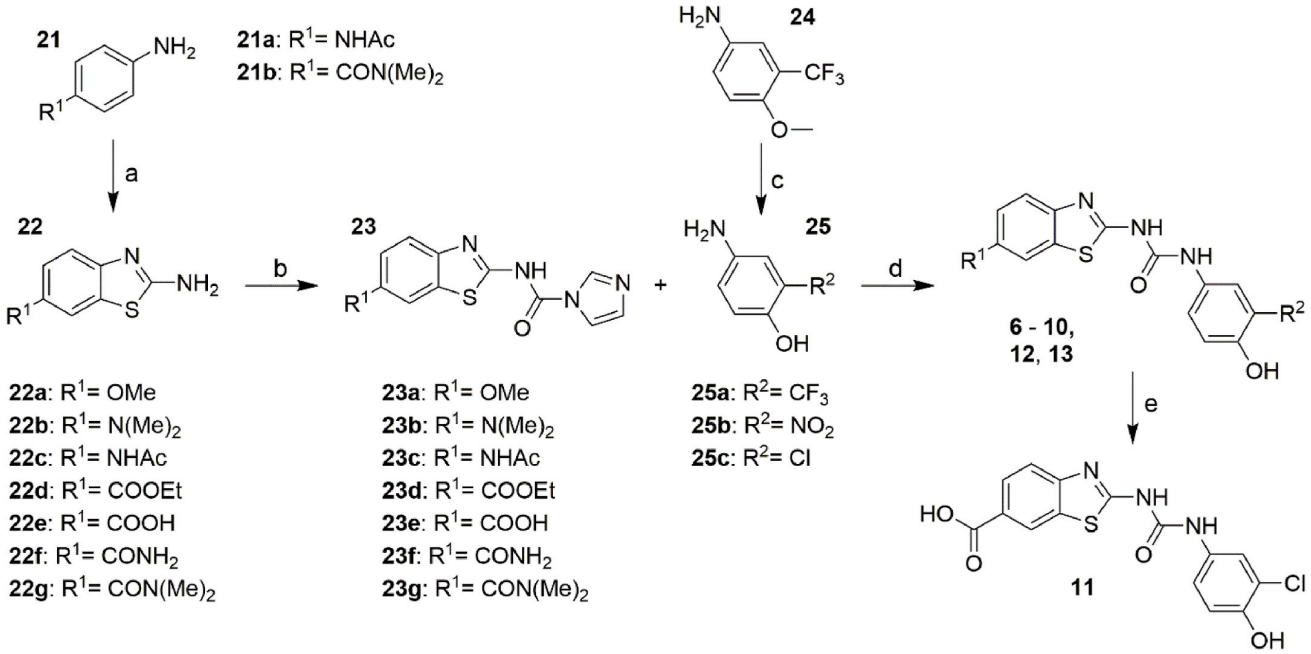

Fig. 3. General method for synthesis of 1-(benzo[*d*]thiazol-2-yl)-3-phenylurea derivatives **6**–**13**. Reagents and conditions: (a) KSCN, tetramethylammonium dichloroiodate(I), DMSO/H_2O, RT – 70 °C; (b) CDI, DCM, RT; (c) HBr, acetic acid, reflux; (d) MeCN, reflux; (e) NaOH, H_2O/MeOH, 50 °C.

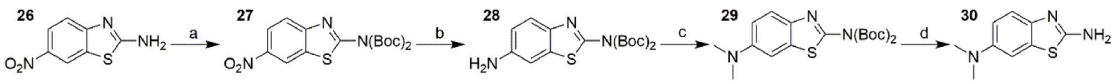

Fig. 4. Synthesis of N^6,N^6-dimethylbenzo[*d*]thiazole-2,6-diamine (**30**). Reagents and conditions: (a) $(Boc)_2O$, DMAP, THF, RT; (b) Pd/C, H_2, EtOH, RT; (c) methyl iodide, K_2CO_3, DMF, RT; (d) 4 M HCl, dioxane, RT.

group was di-methylated with methyl iodide, and finally, *N*-Boc acidic deprotection yielded N^6,N^6-dimethylbenzo[*d*]thiazole-2,6-diamine.

Inhibitors with two-membered aliphatic linker (**15**, **17**) were prepared from corresponding aldehyde and amine starting materials via reductive amination. Imine intermediates **14** and **16** were also isolated and evaluated (Fig. 5).

Benzothiazole derivative with three-membered aliphatic linker (**18**) was prepared in two steps via nucleophilic substitution from 2-(bromomethyl)benzo[*d*]thiazole and (3-chloro-4-methoxyphenyl)methanamine and by consequent de-methylation of methoxy group from the resulting intermediate (Fig. 6). The corresponding benzoxazole derivative (**19**) was prepared in three steps (Fig. 6). First, 2-aminophenol was

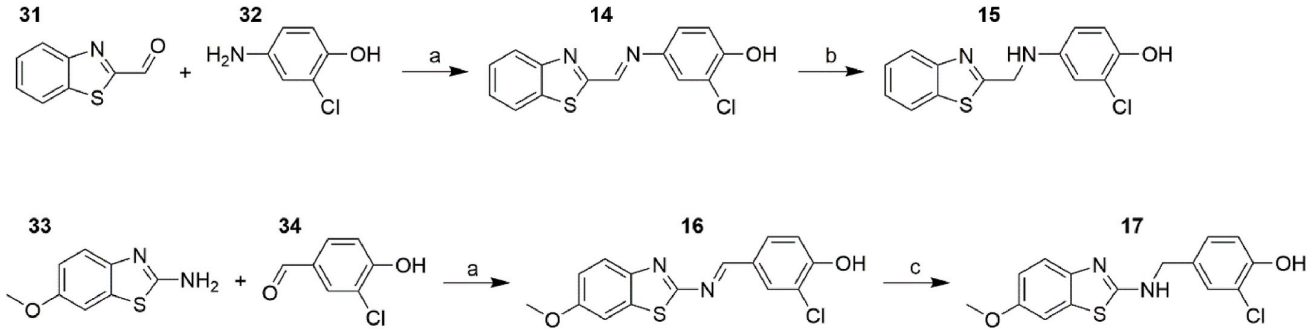

Fig. 5. Synthesis of inhibitors with two-atom linkers. Reagents and conditions: (a) toluene, reflux; (b) Pd/C, MeOH, RT; (c) $NaBH_4$, MeOH, RT.

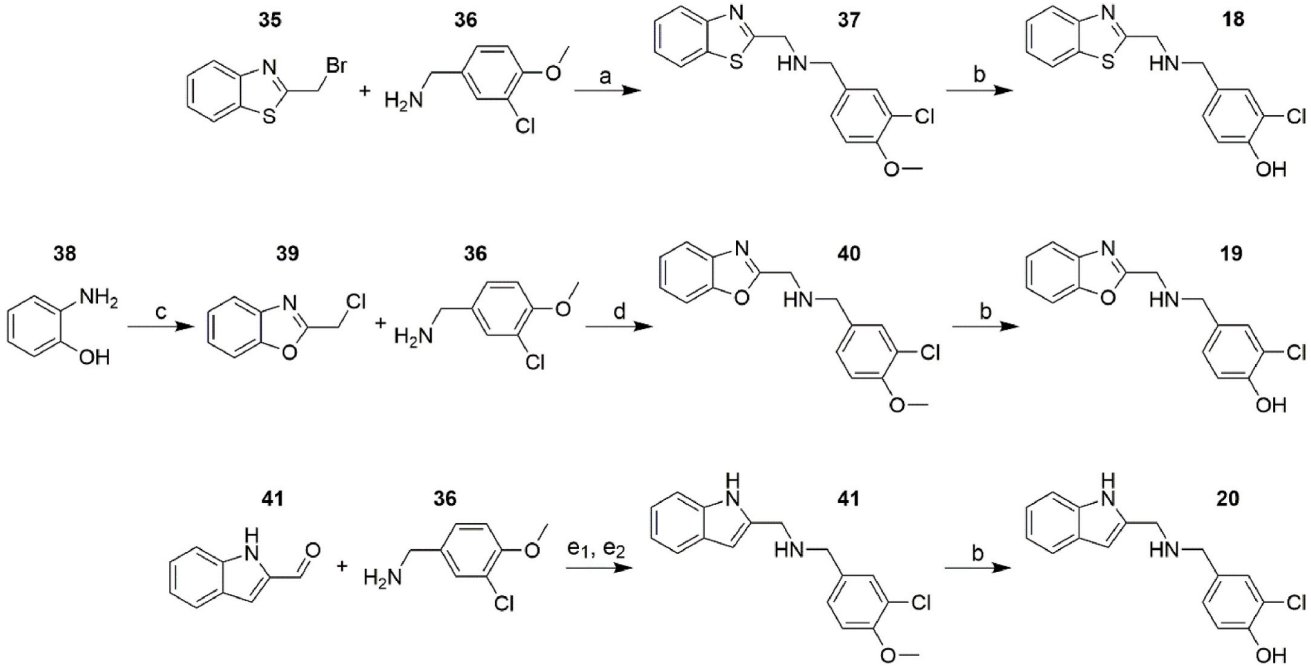

Fig. 6. Synthesis of inhibitors with three-atom aliphatic linkers (**18**–**20**). Reagents and conditions: (a) DIEA, DCM, RT; (b) $AlCl_3$; DCE, 60 °C; (c) 2-chloroacetyl chloride, Et_3N, *o*-xylene, 145 °C; (d) DIEA, MeCN, 70 °C; (e_1) MeOH, 0 °C – RT; (e_2) $NaBH_3CN$, MeOH, 0 °C – RT.

converted to 2-(chloromethyl)benzo[*d*]oxazole in reaction with 2-chloroacetyl chloride. Then, 2-(chloromethyl)benzo[*d*]oxazole reacted with 4-(aminomethyl)-2-chlorophenol to obtain 1-(benzo[*d*]oxazol-2-yl)-*N*-(3-chloro-4-methoxybenzyl)methanamine, which was consequently de-methylated to obtain final product **19**. The corresponding indole derivative (**20**) was prepared in two steps. Reductive amination of 1*H*-indole-2-carbaldehyde and (3-chloro-4-methoxyphenyl)methanamine yielded the methoxy intermediate that was consequently de-methylated to obtain compound **20** (Fig. 6).

The details of chemical synthesis are described in the Experimental Section of the manuscript (Chapter 4). All final products were characterized by $^{1}H/^{13}C$ NMR and HRMS techniques (spectral data are provided in the Supporting Information).

2.3. Experimental physico-chemical parameters

To validate the predicted physico-chemical properties of prepared compounds, we have measured the log*P*, log*D*, pK_a, and log$S_{7.4}$ values (Table 2). The distribution coefficient of prepared compounds between water – octanol (log*P*) and PBS buffer (pH 7.4) – octanol (log*D*) was

Table 2
Experimental physico-chemical properties of prepared compounds.

Compound	log*P*	log*D*	pK_a	log$S_{7.4}$
6	4.28 ± 0.05	5.06 ± 0.24	11.23 ± 0.33	−4.48
7	3.47 ± 0.01	3.44 ± 0.01	10.43 ± 0.14	−4.78
8	4.09 ± 0.03	4.08 ± 0.05	4.61 ± 0.11	−4.08
9	3.66 ± 0.19	3.35 ± 0.09	9.83 ± 0.06	−4.55
10	4.58 ± 0.02	4.64 ± 0.02	9.26 ± 0.18	−4.81
11	1.19 ± 0.01	0.75 ± 0.10	9.75 ± 0.23	−4.36
12	3.32 ± 0.05	3.34 ± 0.12	9.35 ± 0.05	−4.78
13	2.94 ± 0.01	2.95 ± 0.08	9.51 ± 0.15	−4.81
14	2.94 ± 0.03	2.73 ± 0.06	9.14 ± 0.14	−4.68
15	3.77 ± 0.02	3.88 ± 0.04	9.07 ± 0.04	−4.69
16	3.79 ± 0.04	3.95 ± 0.01	11.57 ± 0.02	−4.73
17	4.19 ± 0.03	4.17 ± 0.03	8.40 ± 0.08	−4.73
18	4.03 ± 0.05	4.04 ± 0.01	8.79 ± 0.14	−3.99
19	3.14 ± 0.06	3.19 ± 0.02	8.74 ± 0.21	−3.38
20	2.84 ± 0.06	2.73 ± 0.10	7.60 ± 0.06	−3.39

determined by UHPLC-DAD-MS measurement of analyte concentration in a particular solvent. The negative decimal logarithms of the dissociation constants (pK_a) of prepared compounds were determined spectrophotometrically using buffers of given pH (range from 3.0 to 11.5 with 0.5-unit increment).

Generally, the *in silico* predictions of log*P*, log*D*, and log$S_{7.4}$ correlated plausibly with the experimental results, showing similar trends when comparing the compounds. However, the experimental values were generally shifted in a less-desired direction (i.e., higher log*P* and log*D*, and lower log$S_{7.4}$ values). The pK_a (most basic center) measurements were limited by the assay pH window 3–12, as most urea derivatives were predicted to have pK_a less than 3. Therefore, the comparison was possible only for urea **8** and non-urea compounds **16**–**20**. However, the predicted and experimental values did not correlate very well, showing the limitations in the prediction of pK_a for this particular set of compounds. Taken together, the experimental measurement of physico-chemical parameters confirmed that the non-urea compounds generally had better "CNS drug-like" properties than their urea counterparts and, thus, are more likely to penetrate the BBB.

2.4. Enzyme inhibition

The prepared compounds were initially screened for their inhibition activity towards 17β-HSD10 at 10 μM concentration (Table 3). Compounds that showed inhibition higher than 50% (i.e., residual activity lower than 50% of uninhibited enzymatic reaction) were consequently forwarded for 1 μM screening. Compounds that showed inhibition higher than 40% at 1 μM (i.e., residual activity lower than 60%) were consequently forwarded for IC_{50} measurement. K_i values were calculated from IC_{50} data using method by Cer et al. [26].

Table 3
Results of 17β-HSD10 inhibition screening, IC_{50} measurements, and K_i calculations.

Compound	17β-HSD10 inhibition					
	10 μM screening	*p* value[a]	1 μM screening	*p* value[a]	IC_{50} (μM)	K_i[b]
	Residual activity (%)		Residual activity (%)			(μM)
control	100 ± 4.3		100 ± 4.8			
6	13.0 ± 2.4	<0.0001	39.8 ± 4.5	<0.0001	0.57 ± 0.12	0.44
7	79.4 ± 2.8	0.0022				
8	27.0 ± 1.4	<0.0001	62.7 ± 8.0	0.0023		
9	22.0 ± 3.4	<0.0001	49.5 ± 9.9	0.0014	0.34 ± 0.07	0.25
10	58.6 ± 2.1	0.0001				
11	17.5 ± 4.0	<0.0001	50.0 ± 11.4	0.0022	0.31 ± 0.09	0.23
12	38.3 ± 2.1	<0.0001	50.0 ± 6.2	0.0004	0.84 ± 0.18	0.65
13	31.0 ± 2.1	<0.0001	70.0 ± 11.2	0.013		
14	68.7 ± 4.0	0.0008				
15	72.1 ± 4.8	0.0017				
16	76.6 ± 2.9	0.0014				
17	33.2 ± 5.2	<0.0001	74.4 ± 9.0	0.0122		
18	54.1 ± 1.4	<0.0001				
19	67.6 ± 5.0	0.001				
20	73.8 ± 3.2	0.0011				

Notes: All reactions were measured in triplicate, and the values are expressed as mean ± SD.
[a] Versus control by Student's *t*-test.
[b] Values calculated based on the models described in Cer et al. (2009) [26].

Out of fifteen new compounds, four were found to be highly potent inhibitors with submicromolar IC_{50} values (namely **6**, **9**, **11** and **12**). The most potent inhibitors **9** and **11** had IC_{50} of 0.34 μM and 0.31 μM, respectively. Unfortunately, none of the non-urea compounds have been found very active in the 10 μM screening except compound **16**, which advanced for the 1 μM screen, but it did not advance further for IC_{50} measurement.

From the structure-activity point of view, we have identified or verified several important features that affect inhibitory activity. Replacement of chlorine in position 3 of phenyl moiety with trifluoromethyl (compound **6**) led to a significant increase in activity compared to fluorinated and chlorinated analogues (presented in Schmidt et al. [22]). Nitro-substituted analogue **7**, on the other hand, was found inactive. This complies with our theory that this position is ideal for an electron-withdrawing substituent that, at the same time, cannot create an intramolecular H-bond to neighbouring hydroxyl, so that the hydroxyl stays available for H-bonding (as a H-bond donor) or eventually salt-bridge interaction with the target enzyme. The other three potent (submicromolar) inhibitors bear an HBD group at position 6 of benzothiazolyl moiety (acetamide **9**, carboxyl **11,** and amide **12**), while analogues devoid of HBD character (dimethylamine **8**, ester **10**, and dimethylamide **13**) were found less potent. Finally, replacing of the urea linker with a two- or three-membered linker led to a decrease in activity (analogic ureas presented in Schmidt et al. [22]).

2.5. Molecular docking

The molecular docking study was performed with two different protein structures (PDB: 1E6W and 1U7T) and using two docking softwares (AutoDock: Vina [27] and MOE [28]). The docking was performed with all the prepared compounds, so that calculated binding energies (Table 4) could be compared to experimental inhibition data. Further, the inspection of ligands orientation within the active site and their binding interactions with protein residues were studied. The key findings were demonstrated for the most potent inhibitor out of each of the three structural series (Fig. 2), i.e. compound **6** for class A, compound **11** for class B and compound **17** for class C (Fig. 7). A 2D depiction of individual ligands within the active site can be found in Supporting Information (Figs. S1, S2, S3).

The best correlation between estimated binding energy and inhibition results was obtained for 1E6W receptor using MOE (Table 4). In this setup, the urea-linked compounds (**6**–**13**) performed better to non-urea analogues. Similar trend, though less pronounced, was observed also for MOE with 1U7T receptor. On the other hand, results from AutoDock: Vina (AD: Vina) with either receptor did not pick up this trend.

Table 4
Calculated binding energies in various docking setups (receptor 1E6W or 1U7T; docking software AD: Vina or MOE).

Compound	Binding energy estimate [kcal/mol]			
	AD: Vina		MOE	
	1U7T	1E6W	1U7T	1E6W
6	−7,3	−6,6	−6	−7,1
7	−6,8	−5,9	−6,1	−7,2
8	−6,0	−1,9	−6,1	−7
9	−6,3	−1,2	−6,6	−7,1
10	−6,5	−1,6	−6,3	−7,6
11	−6,9	−6,7	−6	−6,8
12	−6,5	−2,3	−5,8	−7,1
13	−6,4	0,4	−6,3	−7,6
14	−6,1	−5,6	−5	−5,9
15	−6,4	−7,0	−5,7	−6,5
16	−6,4	−3,5	−5,6	−6,2
17	−6,7	−7,1	−5,7	−6,8
18	−6,2	−7,5	−6	−6,4
19	−6,3	−7,4	−5,8	−7,1
20	−6,6	−7,8	−5,6	−6,6

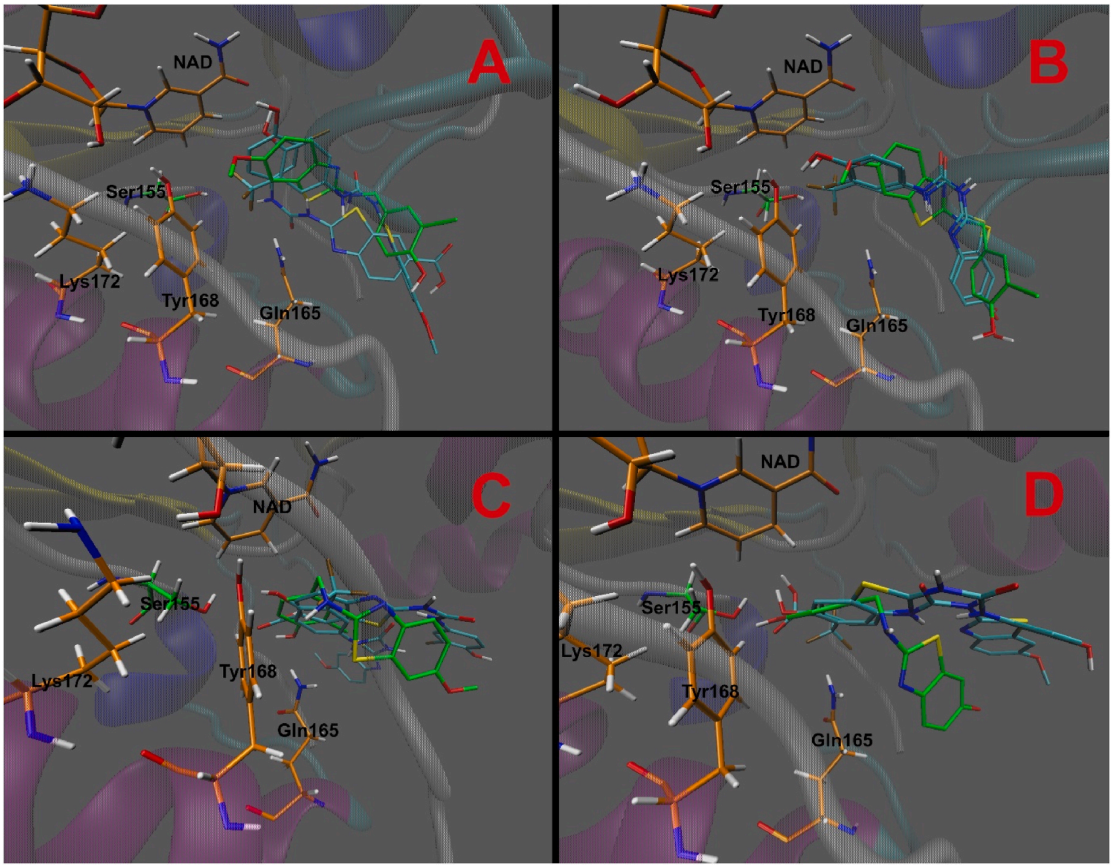

Fig. 7. Superimposition of the top-scoring binding modes of compounds with **6**, **11** and **17** in 1E6W (A, C) and 1U7T (B, D) as predicted by MOE (A, B) and AD: Vina (C, D). Inhibitors **6** and **11** are shown in cyan, serine 155 residue along with inhibitor **17** are shown in green, other protein residues and NAD^+ cofactor are shown in orange.

However, none of the docking setups could predict the differences in inhibitor potency in regard to different substitutions of benzothiazolyl of phenyl moieties. Resulting Gibbs binding energies from AD: Vina with 1U7T receptor correctly predicted compounds **6**, **11** and **17** as the best hits within their structural series, while they showed lower binding energy values for other two highly active compounds **9** and **12**.

The overall orientation of ligands within the binding site differed for AD: Vina and MOE as depicted for the exemplary inhibitors **6**, **11** and **17** (Fig. 7). In MOE (both receptors) the urea linked compounds **6** and **11** were oriented with their phenyl moiety facing inside, towards the NAD^+ cofactor, while the benzothiazolyl moiety pointed towards entrance of the active site. On the other hand, compound **17** with aliphatic linker was oriented in opposite direction. This could possibly explain the better docking score as well as experimental inhibition results of urea-linked compounds (**6**–**13**) compared to non-urea analogues (**14**–**20**). In AD: Vina (both receptors), however, the orientation of the three sample inhibitors did not show any regular pattern offering no particular explanation for the experimental inhibition data.

Analysis of individual inhibitors and their interactions within the active site showed highly variable results and did not show any particular interaction responsible for good binding affinity/inhibition. Despite high variability of the ligand binding interactions, the docking results showed recurrent involvement of residues Gln162, Gln165, Lys212, Tyr168 as well as Ser155, especially if lower-scoring ligand poses were included in the analysis (see Figs. 7 and 8 and Supplementary Figs. S1, S2, S3). Gln162 and Gln165 often showed van der Waals and possible H-bond interaction with NH or CO groups of the linker moiety. Lys212 showed either van der Waals or H-bond interaction with urea linker or

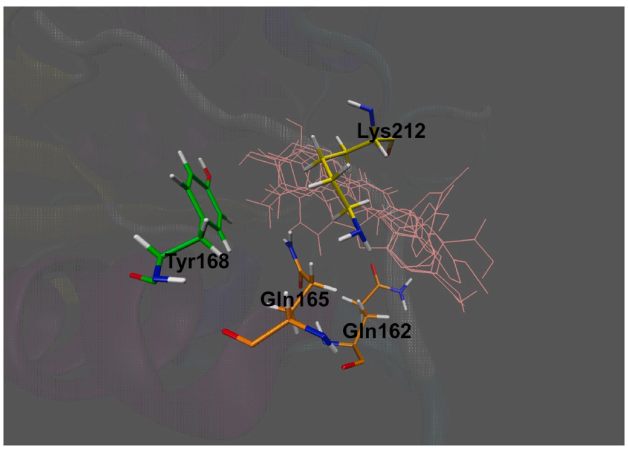

Fig. 8. Residues that may play an important role in stabilization of ligands in the substrate-binding site of 17β-HSD10 enzyme (illustrated in 1E6W structure). The superimposed inhibitors are highlighted in pink.

phenyl ring substituents and also H-arene interaction with thiazolyl ring. Tyr168 and Ser155 from the catalytic site also seemed to frequently participate to ligand stabilization, although the nature of the interaction with ligands was not consistent. A specific interaction was frequently observed for inhibitor **11** - an H-bond between its carboxyl substituent and the C-terminal carboxyl of Pro261.

Taken together, the docking results showed high variability in ligands orientation within the active site and in their interaction patterns with the particular amino acid residues, and thus the reliability of docking results seems rather low. An experimentally obtained 3D structure of a benzothiazolylurea inhibitor complexed together with 17β-HSD10 enzyme would be of great benefit for understanding the interactions that are taking place between this type of inhibitors and 17β-HSD10, thus providing a solid starting ground for the future docking studies.

2.6. Mitochondrial off-targets

As the compounds are supposed to act on 17β-HSD10 within mitochondria, we assessed their effect on several potential mitochondrial off-targets, namely citrate synthase (CS), complexes I, II, and III of electron-transport chain, and monoamine oxidases A and B (MAO-A and MAO-B). For this evaluation, we have selected the four most potent 17β-HSD10 inhibitors **6**, **9**, **11**, and **12**.

The activity of mitochondrial CS, Complex I, and the couple Complex II + III was measured spectrophotometrically on isolated pig brain mitochondria at a drug concentration of 50 μM (Table 5). CS activity was measured as the colour change of 5,5′-dithiobis-(2-nitrobenzoic) acid (DTNB) according to a method published by Srere [29]. The activity of respiratory Complex I was measured based on the rotenone-sensitive rate of the NADH oxidation; a slightly modified previously published method [30] was used [31]. The Complex II + III activity was measured as the antimycin A-sensitive rate of cytochrome *c* reduction upon addition of succinate [32]. The activity of citrate synthase was not significantly affected by any tested compound. The activity of Complex I was inhibited significantly by three compounds (**6**, **9** and **12**). Complex II + III activity was partially inhibited by the compound **6** only. Thus, Complex I represents a potential off-target for these compounds, especially compound **6** (residual activity 5.3% at 50 μM).

The *in vitro* effects on the overall activity of the electron-transport chain (expressed as Complex I-linked respiration and Complex II-linked respiration) were measured using high-resolution respirometry as drug-induced changes in the oxygen consumption rate of the isolated mitochondria in state 3 respiration as described previously [33]. The obtained IC_{50} values for all compounds were in the mid-micromolar range (Table 6), which was about two orders of magnitude higher than the IC_{50} values for inhibition of their primary target 17β-HSD10. The effects of the tested compounds on mitochondrial respiration are in good correlation with the above-mentioned effects on the activity of individual mitochondrial complexes, confirming that Complex I represents a potential off-target for compound **6**.

The activities of MAO-A and MAO-B in isolated mitochondria were assayed using a radiochemical method by the modification of a previously published experimental protocol [34] with either radiolabelled serotonin ([^{3}H]5-HT) as the MAO-A substrate and radiolabelled phenylethylamine ([^{14}C]PEA) as the MAO-B substrate. The obtained IC_{50} values for MAO-A and MAO-B (Table 7) were found in the mid-micromolar range except for the inhibition of MAO-A by compound **9** (IC_{50} = 5.8 μM). Therefore, MAO-A should be considered a potential off-target for compound **9**, although its IC_{50} value for 17β-HSD10 inhibition is still 10-times lower.

Table 6
Drug-induced inhibition of mitochondrial respiration.

Compound	Complex I-linked respiration	Complex II-linked respiration
	IC_{50} (μM)	IC_{50} (μM)
6	28.0 ± 1.1	98 ± 19
9	36.4 ± 3.2	27 ± 47
11	93 ± 15	260 ± 143
12	88 ± 21	ND[a]

Notes: Mitochondrial respiration was measured in isolated pig brain mitochondria using protocols for the O2k-Respirometer (Oroboros). Inhibitory curves were analysed by the four-parameter logistic regression and the half-maximal inhibitory concentrations (IC_{50}) were established. Data are presented as mean ± standard error (SE) of at least three independent measurements.
[a] Compound **12** caused an increase in respiratory rate associated with Complex II.

Table 7
Drug effects on monoamine oxidase (MAO) activity.

Compound	MAO-A IC_{50} (μM)	MAO-B IC_{50} (μM)
6	79 ± 17	ND[a]
9	5.8 ± 1.1	120 ± 23
11	85 ± 58	81 ± 8.9
12	ND[a]	84 ± 39

Notes: Monoamine oxidase (MAO) activity was assayed radiochemically in isolated pig brain mitochondria. Inhibitory curves were analysed by the four-parameter logistic regression and the half-maximal inhibitory concentrations (IC_{50}) were established. Data are presented as mean ± standard error (SE) of at least two independent measurements.
[a] Compounds **6** and **12** showed no inhibition for MAO-B and MAO-A, respectively.

Together, the tested compounds exhibited inhibitory effects on the activity of mitochondrial enzymes up to relatively high concentrations that mostly exceeded the expected therapeutic plasma concentrations. On the other hand, due to the positive effects of MAO-A inhibition on depression (frequent comorbidity in AD) and MAO-B inhibition on neurodegeneration [35], it may be actually appropriate to include the effect on MAO activity for novel AD lead molecules [36]. Targeting several pathological mechanisms with one molecule for the treatment of complex diseases like AD is a well-established approach, also termed as "multi-target drug design" [37]. Notably, compounds with a combined effect on 17β-HSD10 and MAOs had been previously developed by Hroch et al. [18].

2.7. Cytotoxicity and cell viability

A set of cellular assays was used to evaluate the cytotoxic potential of prepared compounds. Firstly, the four most potent inhibitors (**6**, **9**, **11**, **12**) were assessed for their toxic effects on HEK293 and SH-SY5Y cell lines. Cytotoxic effect and effect on cell viability were measured at two concentrations (1 and 10 μM) and expressed as normalized % of control values (1% DMSO and 100 μM valinomycin, respectively). The cell viability was determined as changes in ATP level by measuring

Table 5
Effects on citrate synthase and respiratory chain complexes activity at drug concentration of 50 μM.

Compound	Citrate synthase activity (%)	*p* value[a]	Complex I activity (%)	*p* value[a]	Complex II + III activity (%)	*p* value[a]
control	100.0 ± 5.5		100.0 ± 3.3		100.0 ± 5.6	
6	92.7 ± 0.3	0.0834	5.3 ± 7.5	<0.0001	52.2 ± 8.7	0.0013
9	99.9 ± 0.1	0.9764	24.3 ± 7.1	<0.0001	97.4 ± 1.1	0.4742
11	100.3 ± 0.3	0.9294	87.7 ± 12.3	0.1697	ND	
12	94.4 ± 5.4	0.2767	25.2 ± 18.1	0.0021	99.7 ± 9.5	0.9647

Notes: Values are expressed as mean ± SD for at least three independent measurements.
[a] Versus control by Student's *t*-test.

luminescence in CellTitre-Glo® assay. The cytotoxicity of compounds was determined as changes in membrane integrity by measuring fluorescence in CellTox™ Green assay. None of the tested compounds showed significant toxicity at either concentration (Fig. 9). A slight cytotoxic effect, as well as slightly decreased viability, were observed in both cell lines for compound **6** at 10 μM.

For further evaluation, we decided to discard compound **6**, due to its cytotoxicity and effects on mitochondrial off-targets, and also the less potent inhibitor **12**, and we continued with the two most promising compounds **9** and **11**. The cytotoxicity of the two most promising inhibitors was tested on neuronal cell line SH-SY5Y by measuring the glutathione levels (GSH assay) and dehydrogenase activity (WST-1 assay). The testing was performed at four concentrations (0.1–100 μM) and at two time-points (incubation for 4 and 24 h). A significant decrease of glutathione levels was found only in cells treated with 100 μM compound **9** after 4 h incubation, however, after 24 h incubation this effect was less distinct (Fig. 10A). Transient decrease of intracellular glutathione could be related to increased oxidative stress caused by incubation with tested compound. A significant decrease of dehydrogenase activity was found in cells treated with 100 μM compound **9** in both time intervals (Fig. 10B). The decreased dehydrogenase activity of cells correlated with their decreased metabolic activity and viability. Notably, no signs of cytotoxicity were observed for compound **11**, even at the highest concentration tested. Taken together, the two most potent 17β-HSD10 inhibitors **9** and **11** showed low cytotoxicity up to 10 μM concentration, when assessed via different methods and under various conditions, which is about two orders of magnitude above their IC_{50} values for 17β-HSD10 inhibition. Additional cytotoxicity data were obtained via the lactate dehydrogenase (LDH) assay and can be found in the Supporting Information (Table S1).

2.8. Differential scanning fluorimetry

Differential Scanning Fluorimetry (DSF) was employed as an orthogonal assay to confirm the best hits (**9**, **11**) identified in the enzymatic assay. DSF is used to detect the molecular binding between ligand and protein based on the change in the protein's denaturation temperature [38]. Both compounds significantly increased the denaturation temperature of the protein, and thus were confirmed to bind to the enzyme (Fig. 11). The measurement was conducted at two different concentrations of the inhibitor, and the results were found concentration-dependent, which indicates specific binding (opposite to non-specific binding events based on ligand aggregation, etc.).

2.9. PAMPA-BBB

In order to further explore the capacity of the two most promising compounds **9** and **11** to penetrate into the brain, we used the Parallel Artificial Membrane Permeability Assay (PAMPA–BBB) described by Di et al. [39]. Further, we included the rather inactive compound **19**, which was however favoured for the BBB penetration by having the highest CNS-MPO score. An assay validation was made comparing the reported permeability values of commercial drugs. Based on the obtained results (Table 8) compounds **9** and **19** are expected to cross the BBB by passive diffusion, while compound **11** was predicted not to penetrate BBB.

In correspondence to their physico-chemical properties and CNS-MPO score, compounds **11** and **19** showed positive and negative results in the PAMPA assay, respectively. Compound **19**, which obtained the highest CNS-MPO score, was also found superior in the PAMPA-BBB model with Pe value comparable with the best reference drugs donepezil and rivastigmine. On the other hand, compound **9** was found to be BBB permeable in PAMPA assay despite its calculated (Table 1) as well as experimentally determined (Table 2) physico-chemical properties did not fully meet the criteria suggested by CNS-MPO model.

2.10. Pharmacokinetics

Firstly, a pharmacokinetic study after intravenous (i.v.) administration was performed with compounds **9** and **11**. The 20 μM solution of **9** or 25 μM solution of **11** was applied to the tail-vein of male wild-type rats (0.1 mL per 100 g of weight = overall dose 0.013 mg/kg for **9** and 0.018 mg/kg for **11**). The inhibitors were dissolved in saline containing 3% DMSO, the dosing was based on the maximal solubility of compounds in water. Animals were sacrificed at 9 time-points (5, 15, 30, 60, 90, 180, 240, 360, and 1440 min; 3 animals per time-point). Animals were exsanguinated, plasma and brain samples were collected, and the concentration of inhibitor in samples was quantified using HPLC-MS.

Consequently, pharmacokinetic study after peroral (p.o.) administration was performed with compounds **9** and **11**. The inhibitor was dissolved in a vehicle comprising of 10% NMP, 25% Kolliphor EL and 65% saline. The 16 mM inhibitor solution was applied with a blunt needle via the oesophagus into the stomach of male wild-type rats (overall dose 60 mg/kg). Animals were sacrificed at 15 time-points (5, 15, 30, 45, 60, 120, 180, 240, 300, 360, 420, 480, 540, 600, and 1440 min; 3 animals per time-point). Animals were exsanguinated, plasma and brain samples were collected, and analysed by HPLC-MS. Treated animals (both administration routes) displayed normal behaviour without side effects for the entire period of experiments. The

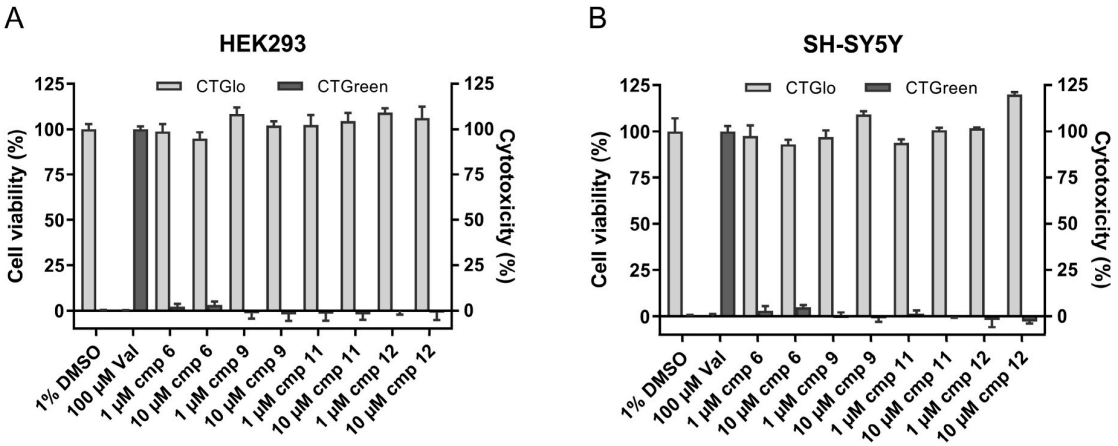

Fig. 9. Cell viability and compound cytotoxicity determination. Cell viability was determined using CellTitre-Glo (Promega) in HEK293 (**A**) and SH-SY5Y (**B**) cell lines in multiplex with measurement of compounds cytotoxicity assayed by CellTox Green (Promega). Data are presented as mean ± standard error of at least two independent experiments in tetraplicate.

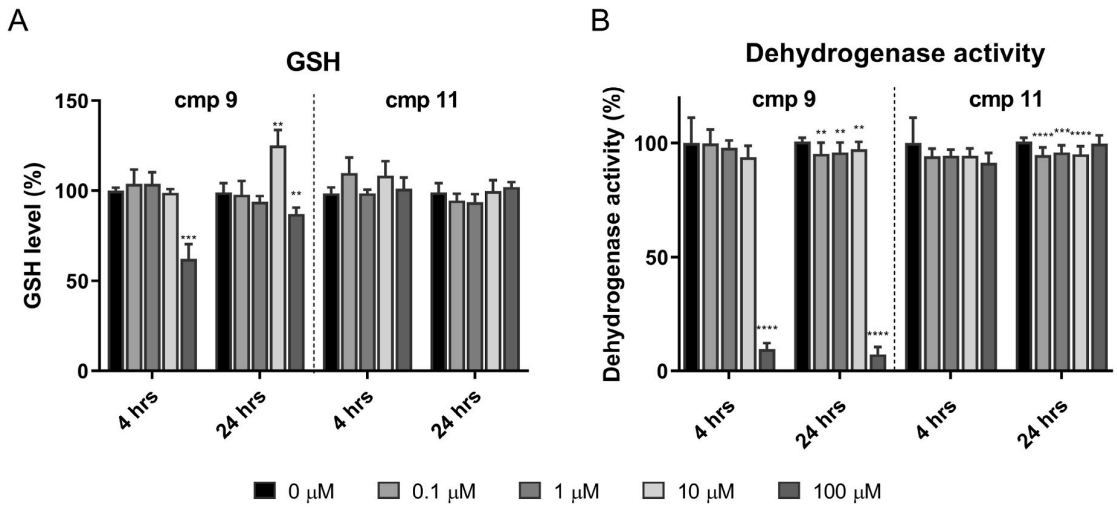

Fig. 10. Effects of compounds on glutathione levels (**A**) and intracellular dehydrogenase activity (**B**). SH-SY5Y cells were incubated with inhibitors **9** and **11** (0.1–100 μM), for 4 and 24 h. After treatment, dehydrogenase activity using WST-1 test and glutathione levels using monochlorobimane assay were measured. Data are presented as mean ± SD of triplicate of at least three independent experiments and differences between groups are determined by the Student's unpaired *t*-test. $^{*}p \leq 0.05$, $^{**}p \leq 0.01$, $^{***}p \leq 0.001$, $^{****}p \leq 0.0001$.

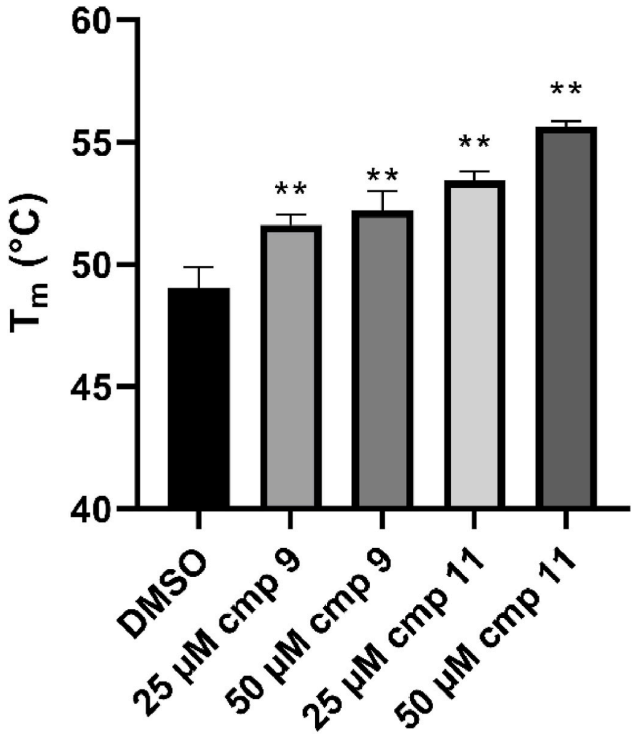

Fig. 11. Results of DSF experiments. Inhibitors **9** and **11** were both found to interact with the protein, significantly increasing its denaturation temperature in a concentration-dependent manner. Values are given as means ± SD (n = 3) and differences between groups are determined by the Student's unpaired *t*-test. $^{*}p \leq 0.05$, $^{**}p \leq 0.01$, $^{***}p \leq 0.001$, $^{****}p \leq 0.0001$.

experimental data were analysed using standard non-compartmental analysis in the Kinetica software, version 4.0. The obtained results are summarized in Table 9.

After i.v. administration, both compounds were successfully detected in plasma. Compound **11** was detected in higher concentrations and with higher AUC in plasma compared to **9**, otherwise both compounds showed similar pharmacokinetic profiles. Regarding brain bioavailability after i.v. administration, compound **9** showed significantly higher exposure (0.57 brain/plasma ratio) compared to **11** (0.02 ratio), which was in accordance with the PAMPA assay (Table 8).

Table 8
Prediction of BBB penetration of 17β-HSD10 inhibitors and standard drugs using PAMPA–BBB assay.

Compound	BBB Penetration Estimation	
	Pe ± SEM (× 10^{-6} cm s^{-1})	CNS (±)
9	7.81 ± 1.00	+
11	0.39 ± 0.22	–
19	23.71 ± 5.41	+
Furosemide	0.19 ± 0.07	–
Chlorothiazide	1.15 ± 0.54	–
Ranitidine	0.35 ± 0.31	–
Donepezil	21.93 ± 2.06	+
Tacrine	5.96 ± 0.59	+
Rivastigmine	20.00 ± 2.07	+

Notes: 'CNS (+)' (high BBB permeability predicted); Pe (10^{-6} cm s^{-1}) > 4.0. 'CNS (–) (low BBB permeability predicted); Pe (10^{-6} cm s^{-1}) < 2.0. 'CNS (±) (BBB permeability uncertain); Pe (10^{-6} cm s^{-1}) from 4.0 to 2.0. Data are presented as the mean ± SEM of three independent measurements.

After p.o. administration, compound **9** reached a higher C_{max} than **11** and had significantly higher AUC, while the T_{max} values were similar for both compounds. Although the exact peroral bioavailability could not be assessed due to the different i.v. and p.o. dosage, it is obvious that compound **9** has a higher p.o. bioavailability compared to **11**. This is in agreement with the higher Pe value for compound **9** in the PAMPA assay and overall better physico-chemical properties, i.e. it is more likely to permeate through cellular membranes and absorb from the GIT. Regarding their IC_{50} values, both compounds reached the effective concentration in plasma but only for a limited time (approx. 1 h and 0.5 h for **9** and **11**, respectively). Both compounds showed two plasma peaks after p.o. administration, which could indicate enterohepatic circulation. Contrary to i.v. results, the brain exposure was very low for both compounds after p.o. administration (less than 0.1 brain/plasma ratio), and their concentration did not reach effective levels, which would be a subject of further investigation.

Table 9
Pharmacokinetic parameters in plasma and brain following a single intravenous (dose 0.013 and 0.018 mg kg^{-1} for **9** and **11** respectively) and oral (dose: 60 mg kg^{-1}) administration in male wild-type rats.

PLASMA (i.v.)	Compound 9	Compound 11
C_{max} (pM)	389.00 ± 60.66	1540.33 ± 246.06
T_{max} (min)	5.00 ± 0.00	5.00 ± 0.00
$AUC_{0\text{-}1440}$ (min × pM)	5832 ± 895	18 961 ± 4978
λ_z (L/min)	0.049 ± 0.009	0.025 ± 0.003
Half-life (min)	15.80 ± 2.91	29.37 ± 3.74
MRT (min)	24.53 ± 3.76	15.70 ± 2.83
CL (L/min/kg)	6.67 ± 0.79	3.10 ± 0.62
V_z (L/kg)	147.33 ± 26.92	134.97 ± 35.31
BRAIN (i.v.)	**Compound 9**	**Compound 11**
C_{max} (pM)	12.61 ± 6.97	0.41 ± 0.34
T_{max} (min)	956.00 ± 388.30	90.00 ± 0.00
$AUC_{0\text{-}1440}$ (min × pM)	3299 ± 900	34.00 ± 28.00
Kp brain (AUCbrain/AUCplasma)	0.566	0.002
PLASMA (p.o.)	**Compound 9**	**Compound 11**
C_{max} (pM)	13 529.33 ± 1261.49	6854.00 ± 923.33
T_{max} (min)	35.00 ± 4.09	25.00 ± 4.09
$AUC_{0\text{-}1440}$ (min × pM)	1 431 047 ± 211 968	212 993 ± 30 083
BRAIN (p.o.)	**Compound 9**	**Compound 11**
C_{max} (pM)	205.83 ± 124.37	154.33 ± 58.88
T_{max} (min)	35.00 ± 4.09	40.00 ± 8.17
$AUC_{0\text{-}1440}$ (min × pM)	15 749 ± 7917	20 135 ± 12 942
Kp brain (AUCbrain/AUCplasma)	0.011	0.095

Notes: C_{max}, maximal plasma or brain concentration; T_{max}, time to C_{max}; $AUC_{0\text{-}1440}$, area under curve/bioavailability; λ_z, elimination constant in terminal phase of curve, half-life in elimination phase; MRT, mean residence time; CL, clearance; V_z, elimination rate constant. All values are expressed as mean ± standard error (SE) of three independent measurements.

3. Conclusion

Inhibition of mitochondrial enzyme 17β-HSD10 is a potential treatment strategy for AD or hormone-dependent cancer. In this study, we have developed a series of new benzothiazolylurea-based inhibitors. Several compounds were found to be submicromolar inhibitors and their interaction with 17β-HSD10 enzyme was further confirmed using DSF. Selected inhibitors **9** and **11** were extensively assessed *in vitro* and they were found non-cytotoxic up to high-micromolar concentrations, had good selectivity profile over potential mitochondrial off-targets, and compound **9** was predicted to pass BBB. Finally, a pharmacokinetic study of the two best inhibitors **9** and **11** was performed after i.v. and p.o. administration. While compound **11** showed an inappropriate pharmacokinetic profile, compound **9** was found to be perorally bioavailable and likely to penetrate to the brain, however, the brain bioavailability results were not fully conclusive, as brain penetration was observed only after i.v. but not after p.o. administration. Together, the *in vitro* and *in vivo* results highlighted compound **9** as a promising lead compound for further development and evaluation on animal models.

4. Experimental Section

4.1. General chemistry

All reagents and solvents were purchased from commercial sources (Sigma Aldrich, Activate Scientific, Alfa Aesar, Merck, Penta Chemicals and VWR) and they were used without any further purification. Low boiling point (≥90% 40–60 °C) petroleum ether (PE) was used if not stated otherwise. Thin-layer chromatography (TLC) for reaction monitoring was performed on Merck aluminium sheets, silica gel 60 F_{254}. Visualisation was performed either via UV (254 nm) or appropriate stain reagent solutions (alternatively in a combination of both). Preparative column chromatography was performed on silica gel 60 (70–230 mesh, 63–200 μm, 60 Å pore size). Melting points were determined on a Stuart SMP30 melting point apparatus and are uncorrected.

Nuclear magnetic resonance (NMR) spectra were acquired at 500/126 MHz (^{1}H, ^{13}C) on a Varian S500 spectrometer or at 300/75 MHz (^{1}H and ^{13}C) on a Varian Gemini 300 spectrometer. Chemical shifts δ are given in ppm and referenced to the signal center of solvent peaks (DMSO-d_6: δ 2.50 ppm and 39.52 ppm for ^{1}H and ^{13}C, respectively; Chloroform-*d*: δ 7.26 ppm and 77.16 ppm for ^{1}H and ^{13}C, respectively), thus indirectly correlated to TMS standard (δ 0 ppm). Coupling constants are expressed in Hz. Spectra acquisitions were performed by assoc. prof. Jiri Kunes workgroup, Department of Inorganic and Organic Chemistry, Faculty of Pharmacy in Hradec Kralove, Charles University in Prague.

High-resolution mass spectra (HRMS) were recorded by coupled LC-MS system consisting of Dionex UltiMate 3000 analytical LC system and Q Exactive Plus hybrid quadrupole-orbitrap spectrometer. As an ion-source, heated electro-spray ionization (HESI) was utilised (setting: sheath gas flow rate 40, aux gas flow rate 10, sweep gas flow rate 2, spray voltage 3.2 kV, capillary temperature 350 °C, aux gas temperature 300 °C, S-lens RF level 50. Positive ions were monitored in the range of 100–1500 *m/z* with the resolution set to 140 000. Obtained mass spectra were processed in Xcalibur 3.0.63 software.

4.2. Chemical synthesis

4.2.1. 4-Amino-2-(trifluoromethyl)phenol (25a)

4-Methoxy-3-(trifluoromethyl)aniline (1 eq) was dissolved in glacial acetic acid (3 mL/mmol) and hydrobromic acid (40%, 3 mL/mmol). The reaction mixture was heated at reflux for the next 20 h. The solution was neutralized with saturated $NaHCO_3$ solution. The aqueous layer was extracted with EtOAc (3 × 25 mL). Combined organic layers were washed with brine, dried over anhydrous Na_2SO_4 and the solvent was removed under reduced pressure. The crude residue was purified by column chromatography ($CHCl_3$:MeOH, 30:1) to yield 4-amino-2-(trifluoromethyl)phenol as an off-white solid (65%).

^{1}H NMR (500 MHz, DMSO-d_6) δ 9.30 (s, 1H), 6.75–6.70 (m, 2H), 6.67 (dd, J = 8.6, 2.6 Hz, 1H), 4.95 (br s, 2H); HRMS (ESI) calcd for $C_7H_7F_3NO$ $[M+H]^+$ 178.0474, found 178.0473.

4.2.2. Procedure A (general conditions): 6-substituted-benzo[d]thiazol-2-amines (22b, 22g)

N-(4-Aminophenyl)acetamide or 4-amino-*N*,*N*-dimethylbenzamide (1 eq) and potassium thiocyanate (7 eq) were dissolved in DMSO:water (5 mL/mmol, 9:1) and stirred for 15 min. Tetramethylammonium dichloroiodate(I) (3 eq) was added and the reaction mixture was heated at 70 °C for 16 h [40]. The reaction mixture was diluted with H_2O, alkalized with 1 M NaOH and extracted with EtOAc (3 × 25 mL). Organic layers were combined, dried over anhydrous Na_2SO_4 and the solvent was removed under reduced pressure. The residue was recrystallized (Et_2O:EtOAc) to obtain 6-(substituted)benzo[*d*]thiazol-2-amine.

4.2.3. N-(2-Aminobenzo[d]thiazol-6-yl)acetamide (22b)

Beige solid; yield 89%; ^{1}H NMR (500 MHz, DMSO-d_6) δ 9.86 (s, 1H), 8.00 (t, J = 1.3 Hz, 1H), 7.33 (s, 2H), 7.25–7.22 (m, 2H), 2.02 (s, 3H).

4.2.4. 2-Amino-N,N-dimethylbenzo[d]thiazole-6-carboxamide (22g)

Beige solid; yield 81%; ^{1}H NMR (500 MHz, DMSO-d_6) δ 7.74 (d, J = 1.5 Hz, 1H), 7.64 (s, 2H), 7.32 (d, J = 8.2 Hz, 1H), 7.26 (dd, J = 8.2, 1.6 Hz, 1H), 2.96 (s, 6H).

4.2.5. N,N-di(Boc)-6-nitrobenzo[d]thiazol-2-amine (27)

The mixture of 6-nitrobenzo[*d*]thiazol-2-amine (1 eq) and DMAP (0.05 eq) in anhydrous THF (5 mL/mmol) was cooled to 0 °C and the solution of *tert*-butyl-dicarbonate (2.05 eq) in anhydrous THF (2 mL/mmol) was added drop-wise. The reaction mixture was allowed to reach RT, stirred overnight and heated at 65 °C for 2 h to complete the reaction [41]. The solvent was removed under reduced pressure, the residue was

diluted with EtOAc (25 mL), washed with citric acid (15%, 2 × 5 mL), water (5 mL) and brine (5 mL). The organic layer was dried over anhydrous Na_2SO_4, the solvent was removed under reduced pressure and the crude residue was subsequently recrystallized (PE:Et_2O) to yield *N*,*N*-di(Boc)-6-nitrobenzo[*d*]thiazol-2-amine as a light yellow solid (97%).

^{1}H NMR (500 MHz, DMSO-d_6) δ 9.11 (d, J = 2.4 Hz, 1H), 8.29 (dd, J = 8.9, 2.4 Hz, 1H), 7.92 (d, J = 8.9 Hz, 1H), 1.57 (s, 18H).

4.2.6. N^2,N^2-di(Boc)-benzo[d]thiazole-2,6-diamine (28)

N,*N*-di(Boc)-6-nitrobenzo[*d*]thiazol-2-amine (27; 1 eq) was dissolved in EtOH (10 mL/mmol) and palladium on activated carbon (Pd/C, 10%, 0.05 eq) was added. The hydrogen atmosphere was introduced and the mixture was stirred at RT overnight [42]. The mixture was filtered through cellite pad and evaporated to dryness. The crude product was subsequently recrystallized (PE:Et_2O) to yield N^2,N^2-di(Boc)-benzo[*d*]thiazole-2,6-diamine as a white solid (97%).

^{1}H NMR (500 MHz, DMSO-d_6) δ 7.48 (d, J = 8.7 Hz, 1H), 7.01 (d, J = 2.2 Hz, 1H), 6.73 (dd, J = 8.7, 2.2 Hz, 1H), 5.36 (s, 2H), 1.48 (s, 18H).

4.2.7. N^2,N^2-di(Boc)-N^6,N^6-dimethylbenzo[d]thiazole-2,6-diamine (29)

The mixture of N^2,N^2-di(Boc)-benzo[*d*]thiazole-2,6-diamine (28; 1 eq), methyl iodide (2.05 eq) and potassium carbonate (2.05 eq) in DMF (5 mL) was stirred at RT overnight. The reaction mixture was diluted with H_2O, filtered and the crude residue was purified by column chromatography (heptane:EtOAc) to yield N^2,N^2-di(Boc)-N^6,N^6-dimethylbenzo[*d*]thiazole-2,6-diamine as a colourless oil (38%).

^{1}H NMR (500 MHz, DMSO-d_6) δ 7.62 (d, J = 8.9 Hz, 1H), 7.25 (d, J = 2.5 Hz, 1H), 6.94 (dd, J = 9.0, 2.5 Hz, 1H), 2.95 (s, 6H), 1.49 (s, 18H).

4.2.8. N^6,N^6-dimethylbenzo[d]thiazole-2,6-diamine (30)

N^2,N^2-di(Boc)-N^6,N^6-dimethylbenzo[*d*]thiazole-2,6-diamine (29; 1 eq) was stirred for 24 h in 4 M HCl-dioxane solution (10 mL/mmol) [41]. The reaction mixture was diluted with Et_2O (50 mL) to achieve complete hydrochloride salt precipitation, which was collected by suction filtration. The solution of 1 M NaOH was added to the mixture of hydrochloride salt in H_2O to achieve a neutral pH value and the mixture was stirred for the next 2 h. Finally, the precipitate was collected by suction filtration, dried and recrystallized (PE:Et_2O) to yield N^6,N^6-dimethylbenzo[*d*]thiazole-2,6-diamine as a white solid (95%).

^{1}H NMR (500 MHz, DMSO-d_6) δ 7.17 (d, J = 8.8 Hz, 1H), 7.05 (d, J = 2.6 Hz, 1H), 7.03 (s, 2H), 6.70 (dd, J = 8.8, 2.6 Hz, 1H), 2.83 (s, 6H).

4.2.9. Procedure B (general conditions): N-(6-substituted-benzo[d]thiazol-2-yl)-1H-imidazole-1-carboxamides (23a-23g)

N,*N*′-Carbonyldiimidazole (1.2 eq) was added to a solution of 6-substituted-benzo[*d*]thiazol-2-amine (1 eq) in anhydrous DCM (5 mL/mmol) and the reaction was heated at reflux for 20 h. The reaction mixture was cooled down to 2–8 °C, the precipitate was collected by suction filtration and washed with cold DCM [154]. The crude product was dried under reduced pressure to yield *N*-(6-substituted-benzo[*d*]thiazol-2-yl)-1*H*-imidazole-1-carboxamide as a white solid and used in the next reaction step without further purification.

4.2.10. Procedure C (general conditions): 1-aryl-3-(6-(substituted)benzo[d]thiazol-2-yl)ureas (6–10, 12, 13)

An aniline derivative (1.1 eq) was added to the suspension of *N*-(6-substituted-benzo[*d*]thiazol- 2-yl)-1*H*-imidazole-1-carboxamide (1 eq) in anhydrous acetonitrile (15 mL/mmol) and the reaction was heated at reflux for 20 h [154]. The reaction was cooled to RT, quenched with 1 M HCl (15 mL/mmol) and the precipitate was collected by filtration. The crude product was recrystallized from Et_2O:MeOH and dried to constant weight yielding the corresponding 1-aryl-3-(6-substituted-benzobenzo[*d*]thiazol-2-yl)ureas (**6**–**10**, **12**, **13**).

4.2.11. 1-(4-Hydroxy-3-(trifluoromethyl)phenyl)-3-(6-methoxybenzo[d]thiazol-2-yl)urea (6)

White solid; yield 64%; m.p. 260.5–262.5 °C; ^{1}H NMR (500 MHz, DMSO-d_6) δ 10.35 (br s, 1H), 9.74 (s, 1H), 7.74 (s, 1H), 7.55 (d, J = 9.0 Hz, 1H), 7.51 (s, 1H), 7.47 (d, J = 9.1 Hz, 1H), 7.03 (d, J = 8.9 Hz, 1H), 6.98 (d, J = 9.1 Hz, 1H), 3.79 (s, 3H); ^{13}C NMR (126 MHz, DMSO-d_6) δ 157.77, 155.77, 152.25, 151.45, 141.75, 132.25, 129.91, 124.82, 123.91 (q, J = 270.5 Hz), 119.85, 117.49, 117.15 (q, J = 5.3 Hz), 115.17 (q, J = 30.3 Hz), 114.49, 105.01, 55.66; HRMS (ESI) calcd for $C_{16}H_{13}F_3N_3O_3S$ $[M+H]^+$ 384.0624, found 384.0611.

4.2.12. 1-(4-Hydroxy-3-nitrophenyl)-3-(6-methoxybenzo[d]thiazol-2-yl)urea (7)

Beige solid; yield 99%; m.p. 263–264.5 °C; ^{1}H NMR (500 MHz, DMSO-d_6) δ 10.90 (s, 2H), 9.26 (s, 1H), 8.22 (d, J = 2.7 Hz, 1H), 7.59 (dd, J = 9.0, 2.7 Hz, 1H), 7.53 (d, J = 8.8 Hz, 1H), 7.50 (d, J = 2.6 Hz, 1H), 7.12 (d, J = 9.0 Hz, 1H), 6.98 (dd, J = 8.8, 2.6 Hz, 1H), 3.79 (s, 3H); ^{13}C NMR (126 MHz, DMSO-d_6) δ 158.16, 155.74, 152.69, 148.06, 141.39, 135.86, 132.13, 130.51, 127.12, 119.61 (two non-equivalent carbons), 114.79, 114.45, 105.04, 55.63; HRMS (ESI) calcd for $C_{15}H_{13}N_4O_5S$ $[M+H]^+$ 361.0601, found 361.0595.

4.2.13. 1-(3-Chloro-4-hydroxyphenyl)-3-(6-(dimethylamino)benzo[d]thiazol-2-yl)urea (8)

Beige solid, yield 92%, m.p. 130–132 °C; ^{1}H NMR (500 MHz, DMSO-d_6) δ 10.56 (br s, 1H), 9.89 (s, 1H), 8.98 (s, 1H), 7.60 (d, J = 2.6 Hz, 1H), 7.46 (d, J = 8.8 Hz, 1H), 7.19 (d, J = 2.6 Hz, 1H), 7.17 (dd, J = 8.8, 2.6 Hz, 1H), 6.93 (d, J = 8.7 Hz, 1H), 6.86 (dd, J = 8.9, 2.6 Hz, 1H), 2.91 (s, 6H). ^{13}C NMR (126 MHz, DMSO-d_6) δ 156.08, 152.15, 148.79, 147.47, 139.62, 132.72, 130.92, 120.65, 119.33, 118.04, 116.65, 115.30, 112.69, 103.97, 40.89. HRMS (ESI) calcd for $C_{16}H_{16}ClN_4O_2S$ $[M+H]^+$ 363.0677, found 363.0673.

4.2.14. N-(2-(3-(3-chloro-4-hydroxyphenyl)ureido)benzo[d]thiazol-6-yl)acetamide (9)

Beige solid; yield 71%; m.p. 190.5–191.5 °C; ^{1}H NMR (500 MHz, DMSO-d_6) δ 10.06 (s, 1H), 9.33 (s, 1H), 8.23 (d, J = 2.1 Hz, 1H), 7.59 (d, J = 2.6 Hz, 1H), 7.56 (d, J = 8.7 Hz, 1H), 7.44 (dd, J = 8.7, 2.1 Hz, 1H), 7.18 (dd, J = 8.8, 2.6 Hz, 1H), 6.94 (d, J = 8.7 Hz, 1H), 2.06 (s, 3H); ^{13}C NMR (126 MHz, DMSO-d_6) δ 168.15, 158.61, 152.17, 148.89, 143.73, 134.88, 131.43, 130.82, 120.59, 119.35, 119.26, 119.17, 118.21, 116.70, 111.40, 23.96; HRMS (ESI) calcd for $C_{16}H_{14}ClN_4O_3S$ $[M+H]^+$ 377.0470, found 377.0465.

4.2.15. Ethyl 2-(3-(3-chloro-4-hydroxyphenyl)ureido)benzo[d]thiazole-6-carboxylate (10)

Beige solid; yield 78%; m.p. 233–234 °C; ^{1}H NMR (500 MHz, DMSO-d_6) δ 11.08 (br s, 1H), 9.95 (s, 1H), 9.04 (s, 1H), 8.54 (s, 1H), 7.96 (dd, J = 8.5, 1.8 Hz, 1H), 7.70 (d, J = 8.5 Hz, 1H), 7.61 (d, J = 2.6 Hz, 1H), 7.20 (dd, J = 8.8, 2.6 Hz, 1H), 6.94 (d, J = 8.7 Hz, 1H), 4.33 (q, J = 7.1 Hz, 2H), 1.34 (t, J = 7.1 Hz, 3H); ^{13}C NMR (126 MHz, DMSO-d_6) δ 165.50, 162.93, 151.97, 149.09, 131.39, 130.53, 127.09, 124.14, 123.41, 121.18, 120.92, 119.58, 119.34, 116.64, 60.66, 14.24; HRMS (ESI) calcd for $C_{17}H_{15}ClN_3O_4S$ $[M+H]^+$ 392.0466, found 392.0463.

4.2.16. 2-(3-(3-Chloro-4-hydroxyphenyl)ureido)benzo[d]thiazole-6-carboxylic acid (11)

Ethyl 2-(3-(3-chloro-4-hydroxyphenyl)ureido)benzo[*d*]thiazole-6-carboxylate (**10**) was suspended in a mixture of 1 M NaOH and MeOH (1:1) and the reaction mixture was heated at 50 °C overnight. After the reaction was completed (monitored by TLC), the reaction mixture was concentrated under reduced pressure and neutralized with 1 M HCl. The resulting precipitate was collected by filtration and recrystallized (MeCN) to obtain 2-(3-(3-chloro-4-hydroxyphenyl)ureido) benzo[*d*]thiazole-6-carboxylic acid as a beige solid (0.34 g, 94%).

Beige solid; yield 94%; m.p. 265 °C (decomp.); ^{1}H NMR (500 MHz,

DMSO-d_6) δ 9.95 (br s, 1H), 9.36 (s, 1H), 8.52 (s, 1H), 7.95 (dd, J = 8.4, 1.2 Hz, 1H), 7.68 (d, J = 8.4 Hz, 1H), 7.60 (d, J = 2.3 Hz, 1H), 7.20 (dd, J = 8.7, 2.3 Hz, 1H), 6.95 (d, J = 8.7 Hz, 1H); ^{13}C NMR (126 MHz, DMSO-d_6) δ 167.09, 162.63, 152.26, 149.05, 131.23, 130.65, 127.31, 125.08, 123.54, 120.75, 119.41, 119.37, 118.77, 116.71; HRMS (ESI) calcd for $C_{15}H_{11}ClN_3O_4S$ $[M+H]^+$ 364.0153, found 364.0149.

4.2.17. 2-(3-(3-Chloro-4-hydroxyphenyl)ureido)benzo[d]thiazole-6-carboxamide (12)

Beige solid; yield 42%; m.p. 185–186 °C; ^{1}H NMR (500 MHz, DMSO-d_6) δ 9.93 (br s, 1H), 9.25 (s, 1H), 8.42 (d, J = 1.8 Hz, 1H), 7.97 (br s, 1H), 7.91 (dd, J = 8.4, 1.8 Hz, 1H), 7.66 (d, J = 8.4 Hz, 1H), 7.61 (d, J = 2.6 Hz, 1H), 7.33 (br s, 1H), 7.20 (dd, J = 8.7, 2.6 Hz, 1H), 6.94 (d, J = 8.7 Hz, 1H); ^{13}C NMR (126 MHz, DMSO-d_6) δ 167.49, 161.67, 152.34, 150.03, 149.01, 130.86, 130.67, 128.90, 125.71, 121.24, 120.76, 119.43, 119.35, 118.46, 116.68; HRMS (ESI) calcd for $C_{15}H_{12}ClN_4O_3S$ $[M+H]^+$ 363.0313, found 363.0308.

4.2.18. 2-(3-(3-Chloro-4-hydroxyphenyl)ureido)-N,N-dimethylbenzo[d]thiazole-6-carboxamide (13)

Beige solid; yield 92%; m.p. 266–267 °C; ^{1}H NMR (500 MHz, DMSO-d_6) δ 11.08 (br s, 1H), 9.94 (s, 1H), 9.06 (s, 1H), 7.99 (d, J = 1.7 Hz, 1H), 7.65 (d, J = 8.3 Hz, 1H), 7.61 (d, J = 2.6 Hz, 1H), 7.42 (dd, J = 8.3, 1.8 Hz, 1H), 7.20 (dd, J = 8.8, 2.6 Hz, 1H), 6.94 (d, J = 8.7 Hz, 1H), 2.98 (s, 6H); ^{13}C NMR (126 MHz, DMSO-d_6) δ 169.87, 161.21, 152.36, 149.01, 148.39, 130.85, 130.79, 130.66, 125.29, 120.84, 119.53, 119.33, 119.33, 118.56, 116.65, 34.99; HRMS (ESI) calcd for $C_{17}H_{16}ClN_4O_3S$ $[M+H]^+$ 391.0626, found 391.0620.

4.2.19. Procedure D (general conditions): Schiff bases synthesis (14, 16)

Equimolar amounts of amine and aldehyde were dissolved in toluene (10 mL/mmol) and heated at reflux for 48 h. The solvent was removed under reduced pressure and the crude residue was recrystallized (PE: Et_2O) to yield the corresponding product as a yellow solid.

4.2.20. (E)-4-((Benzo[d]thiazol-2-ylmethylene)amino)-2-chlorophenol (14)

Yellow solid; yield 95%; m.p. 242–243 °C; ^{1}H NMR (500 MHz, DMSO-d_6) δ 10.62 (s, 1H), 8.99 (s, 1H), 8.19–8.15 (m, 1H), 8.14–8.10 (m, 1H), 7.65 (d, J = 2.6 Hz, 1H), 7.61–7.53 (m, 2H), 7.41 (dd, J = 8.6, 2.6 Hz, 1H), 7.06 (d, J = 8.6 Hz, 1H); ^{13}C NMR (126 MHz, DMSO-d_6) δ 167.46, 153.55, 153.50, 151.59, 140.62, 134.54, 126.95, 126.78, 123.82, 123.40, 123.10, 122.65, 120.41, 116.82; HRMS (ESI) calcd for $C_{14}H_{10}ClN_2OS$ $[M+H]^+$ 289.0197, found 289.0195.

4.2.21. (E)-2-Chloro-4-(((6-methoxybenzo[d]thiazol-2-yl)imino)methyl)phenol (16)

Yellow solid; yield 84%; m.p. 260.5–261.5 °C; ^{1}H NMR (500 MHz, DMSO-d_6) δ 11.34 (s, 1H), 8.99 (s, 1H), 8.07 (d, J = 2.1 Hz, 1H), 7.90 (dd, J = 8.5, 2.1 Hz, 1H), 7.80 (d, J = 8.8 Hz, 1H), 7.64 (d, J = 2.6 Hz, 1H), 7.14 (d, J = 8.5 Hz, 1H), 7.10 (dd, J = 8.9, 2.6 Hz, 1H), 3.84 (s, 3H); ^{13}C NMR (126 MHz, DMSO-d_6) δ 168.94, 164.36, 157.82, 157.18, 145.55, 135.28, 131.85, 130.29, 127.05, 123.08, 120.64, 117.06, 115.64, 105.09, 55.70; HRMS (ESI) calcd for $C_{15}H_{12}ClN_2O_2S$ $[M+H]^+$ 319.0303, found 319.0302.

4.2.22. 4-((Benzo[d]thiazol-2-ylmethyl)amino)-2-chlorophenol (15)

(*E*)-4-((benzo[*d*]thiazol-2-ylmethylene)amino)-2-chlorophenol (**14**; 1eq) was dissolved in MeOH (10 mL/mmol) and palladium on activated carbon (10% Pd/C; 0.1 eq) was added. The hydrogen atmosphere was introduced and the mixture was stirred at RT overnight [42]. The mixture was filtered through cellite pad and evaporated to dryness. The crude residue was recrystallized (Et_2O:EtOH) to obtain 4-((benzo[*d*] thiazol-2-ylmethyl)amino)-2- chlorophenol as a white solid (69%).

White solid; yield 69%; m.p. 188.5–189.5 °C; ^{1}H NMR (500 MHz, DMSO-d_6) δ 9.10 (s, 1H), 8.02 (d, J = 7.8 Hz, 1H), 7.94 (d, J = 8.1 Hz, 1H), 7.51–7.45 (m, 1H), 7.42–7.36 (m, 1H), 6.73 (d, J = 8.7 Hz, 1H), 6.62 (d, J = 2.8 Hz, 1H), 6.47 (dd, J = 8.7, 2.8 Hz, 1H), 6.40 (t, J = 6.1 Hz, 1H), 4.62 (d, J = 6.1 Hz, 2H); ^{13}C NMR (126 MHz, DMSO-d_6) δ 174.86, 153.13, 144.46, 141.51, 134.53, 125.95, 124.76, 122.25 (two non-equivalent carbons), 120.00, 117.47, 113.54, 112.62, 46.38; HRMS (ESI) calcd for $C_{14}H_{12}ClN_2OS$ $[M+H]^+$ 291.0353, found 291.0349.

4.2.23. 2-Chloro-4-(((6-methoxybenzo[d]thiazol-2-yl)amino)methyl)phenol (17)

(*E*)-2-chloro-4-(((6-methoxybenzo[*d*]thiazol-2-yl)imino)methyl) phenol (**16**; 1 eq) and $NaBH_4$ (1.1 eq) were added to anh. MeOH (10 mL/mmol) and the mixture was stirred at RT overnight. The mixture was diluted with H_2O and extracted with EtOAc (3 × 15 mL), dried over anhydrous Na_2SO_4 and the solvent was removed under reduced pressure. The crude residue was recrystallized (Et_2O:EtOH) to yield 2-chloro-4-(((6- methoxybenzo[*d*]thiazol-2-yl)amino)methyl)phenol as a white solid (83%).

White solid; yield 83%; m.p. 163.5–164.5 °C; ^{1}H NMR (500 MHz, DMSO-d_6) δ 10.08 (s, 1H), 8.18 (t, J = 5.7 Hz, 1H), 7.33 (d, J = 2.1 Hz, 1H), 7.31 (d, J = 2.7 Hz, 1H), 7.29 (d, J = 8.7 Hz, 1H), 7.14 (dd, J = 8.4, 2.2 Hz, 1H), 6.92 (d, J = 8.3 Hz, 1H), 6.82 (dd, J = 8.7, 2.6 Hz, 1H), 4.43 (d, J = 5.4 Hz, 2H), 3.73 (s, 3H); ^{13}C NMR (126 MHz, DMSO-d_6) δ 164.48, 154.36, 152.04, 146.46, 131.40, 130.82, 128.87, 127.30, 119.35, 118.42, 116.48, 112.97, 105.60, 55.54, 46.24; HRMS (ESI) calcd for $C_{15}H_{14}ClN_2O_2S$ $[M+H]^+$ 321.0459, found 321.0454.

4.2.24. 1-(Benzo[d]thiazol-2-yl)-N-(3-chloro-4-methoxybenzyl)methanamine (37)

2-(Bromomethyl)benzo[*d*]thiazole (1 eq), (3-chloro-4-methoxyphenyl) methanamine (1.7 eq, 0.51 g) and DIEA (1.7 eq) were dissolved in DCM (10 mL/mmol) and the mixture was stirred at RT for next 24 h. The solvent was removed under reduced pressure and the residue was purified by column chromatography (PE:$CHCl_3$, 1:1) to yield 1-(benzo[*d*]thiazol-2-yl)-*N*-(3-chloro-4-methoxybenzyl)methanamine as a light yellow oil (96%).

^{1}H NMR (500 MHz, Chloroform-*d*) δ 7.99–7.95 (m, 1H), 7.91–7.87 (m, 1H), 7.49–7.44 (m, 1H), 7.42 (d, J = 2.1 Hz, 1H), 7.40–7.35 (m, 1H), 7.23 (dd, J = 8.4, 2.1 Hz, 1H), 6.90 (d, J = 8.4 Hz, 1H), 4.23 (s, 2H), 3.90 (s, 3H), 3.84 (s, 2H).

4.2.25. 4-(((Benzo[d]thiazol-2-ylmethyl)amino)methyl)-2-chlorophenol (18)

1-(Benzo[*d*]thiazol-2-yl)-*N*-(3-chloro-4-methoxybenzyl)methanamine (**37**; 1 eq) was dissolved in anhydrous DCE (6 mL/mmol) and nitrogen atmosphere was introduced. Aluminium chloride (3 eq) was added portion-wise and the mixture was heated at 60 °C overnight. The reaction mixture was cooled down to RT, quenched with H_2O, partitioned between H_2O:EtOAc and extracted with EtOAc (3 × 25 mL). The organic layers were combined, dried over anhydrous Na_2SO_4 and the solvent was removed under reduced pressure. The residue was purified by column chromatography (PE:EtOAc, 2:1) to yield 4-(((benzo[*d*] thiazol-2-ylmethyl)amino)methyl)- 2-chlorophenol as a white solid (45%).

White solid; yield 45%; m.p. 120–121 °C; ^{1}H NMR (500 MHz, Chloroform-*d*) δ 8.00–7.95 (m, 1H), 7.90–7.86 (m, 1H), 7.49–7.44 (m, 1H), 7.40–7.36 (m, 1H), 7.35 (d, J = 2.1 Hz, 1H), 7.13 (dd, J = 8.3, 2.1 Hz, 1H), 6.94 (d, J = 8.3 Hz, 1H), 4.23 (s, 2H), 3.82 (s, 2H); ^{13}C NMR (126 MHz, Chloroform-*d*) δ 173.26, 153.36, 150.94, 135.10, 132.71, 129.03, 128.39, 126.14, 125.06, 122.83, 121.91, 120.18, 116.43, 52.38, 50.68; HRMS (ESI) calcd for $C_{15}H_{14}ClN_2OS$ $[M+H]^+$ 305.0510, found 305.0508.

4.2.26. 2-(Chloromethyl)benzo[d]oxazole (39)

2-aminophenol (1 eq) and chloroacetyl chloride (1.5 eq) were dissolved in *o*-xylene (6 mL/mmol) under nitrogen atmosphere. TEA (1.1 eq) was added dropwise and the reaction mixture was stirred at 145 °C

overnight. The mixture was diluted with 20 mL sat. aq. NH_4Cl and extracted with EtOAc (3 × 6 mL), The organic phase was dried over anhydrous Na_2SO_4 and solvents were removed under reduced pressure. The residue was purified by column chromatography (PE:EtOAc, 6:1) to yield 2-(chloromethyl)benzo[*d*]oxazole as a yellow oil (71%).

^{1}H NMR (500 MHz, DMSO-d_6) δ 7.78 (t, J = 7.4 Hz, 2H), 7.51–7.37 (m, 2H), 5.08 (s, 2H).

4.2.27. 1-(Benzo[d]oxazol-2-yl)-N-(3-chloro-4-methoxybenzyl) methanamine (40)

2-(Chloromethyl)benzo[*d*]oxazole (**39**; 1 eq), (3-chloro-4-methoxyphenyl)methanamine (1.5 eq) and DIEA (2 eq) were dissolved in anh. MeCN (8 mL/mmol) under nitrogen atmosphere. The reaction mixture was stirred at 70 °C overnight. The reaction mixture was concentrated at reduced pressure. The crude residue was purified by column chromatography ($CHCl_3$:MeOH, 100:1) to yield 1-(benzo[*d*]oxazol-2-yl)-*N*-(3-chloro-4-methoxybenzyl)methanamine as a yellow oil (79%).

^{1}H NMR (500 MHz, DMSO-d_6) δ 7.76–7.63 (m, 2H), 7.44–7.30 (m, 3H), 7.25 (dd, J = 8.4, 2.1 Hz, 1H), 7.06 (d, J = 8.4 Hz, 1H), 3.94 (s, 2H), 3.81 (s, 3H), 3.72 (s, 2H), 3.00 (br s, 1H).

4.2.28. 4-(((Benzo[d]oxazol-2-ylmethyl)amino)methyl)-2-chlorophenol (19)

1-(Benzo[*d*]oxazol-2-yl)-*N*-(3-chloro-4-methoxybenzyl)methanamine (**40**; 1 eq) was dissolved in anh. DCE (10 mL/mmol) under nitrogen atmosphere, aluminium trichloride (3.5 eq) was added and the reaction mixture was stirred at 60 °C overnight. The reaction mixture was concentrated at reduced pressure. The residue was diluted with H_2O, pH was adjusted to 7 using sat. aq. $NaHCO_3$ solution. The product was extracted with EtOAc (3 × 10 mL), dried over anhydrous Na_2SO_4 and the solvent was removed under reduced pressure. The crude residue was purified by column chromatography ($CHCl_3$:MeOH, 30:1). Resulting oily compound was recrystallized from PE to yield 4-(((benzo[*d*]oxazol-2-ylmethyl)amino)methyl)-2-chlorophenol as white solid (46%).

White solid; yield 46%; m.p. 99–100.5 °C; ^{1}H NMR (500 MHz, Chloroform-*d*) δ 7.74–7.69 (m, 1H), 7.54–7.49 (m, 1H), 7.36–7.31 (m, 3H), 7.12 (dd, J = 8.3, 2.0 Hz, 1H), 6.92 (d, J = 8.3 Hz, 1H), 4.08 (s, 2H), 3.81 (s, 2H); ^{13}C NMR (126 MHz, Chloroform-*d*) δ 165.08, 150.97, 150.93, 140.97, 132.37, 129.16, 128.47, 125.18, 124.57, 120.20, 120.03, 116.47, 110.75, 52.19, 45.70; HRMS (ESI) calcd for $C_{15}H_{14}ClN_2O_2$ $[M+H]^+$ 289.0738, found 289.0733.

4.2.29. N-((1H-indol-2-yl)methyl)-1-(3-chloro-4-methoxyphenyl) methanamine (41)

1*H*-indole-2-carbaldehyde (1 eq) was dissolved in anh. MeOH (7 mL/mmol) under nitrogen atmosphere and the solution was cooled to 0 °C. (3-chloro-4-methoxyphenyl)methanamine (1 eq) was dissolved in anh. MeOH (1 mL/mmol) and was added dropwise to the reaction mixture at 0 °C. The reaction was warmed up to RT and stirred overnight. Then the reaction mixture was cooled to 0 °C and $NaBH_3CN$ (1.5 eq) was added. The reaction mixture was stirred at RT overnight. The solvent was evaporated and the residue was diluted with H_2O. The product was extracted with EtOAc (3 × 10 mL), dried over anhydrous Na_2SO_4 and the solvent was removed under reduced pressure. The crude residue was purified by column chromatography ($CHCl_3$ mobile phase) to yield *N*-((1*H*-indol-2-yl)methyl)-1-(3-chloro-4-methoxyphenyl)methanamine as a yellow oil (43%).

^{1}H NMR (300 MHz, DMSO-d_6) δ 10.93 (br s, 1H), 7.48–7.39 (m, 2H), 7.35–7.29 (m, 1H), 7.26 (dd, J = 8.4, 2.1 Hz, 1H), 7.08 (d, J = 8.5 Hz, 1H), 7.04–6.96 (m, 1H), 6.96–6.88 (m, 1H), 6.25 (d, J = 1.1 Hz, 1H), 3.83 (s, 3H), 3.78 (s, 2H), 3.64 (s, 2H), 2.63 (br s, 1H).

4.2.30. 4-((((1H-indol-2-yl)methyl)amino)methyl)-2-chlorophenol (20)

N-((1*H*-indol-2-yl)methyl)-1-(3-chloro-4-methoxyphenyl)methanamine (**41**; 1 eq) was dissolved in anh. DCE (12 mL/mmol) under nitrogen atmosphere, aluminium trichloride (3.5 eq) was added and the reaction mixture was stirred at 60 °C for 7 h. The reaction mixture was concentrated at reduced pressure. The residue was diluted with H_2O and the product was extracted with EtOAc (3 × 10 mL), dried over anhydrous Na_2SO_4 and the solvent was removed under reduced pressure. The crude residue was purified by column chromatography ($CHCl_3$:MeOH, 20:1 + 1% TEA) to yield 4-((((1*H*-indol-2-yl)methyl)amino)methyl)-2-chlorophenol as a light-beige solid (30%).

Light-beige solid; yield 30%; m.p. 136–138 °C; ^{1}H NMR (500 MHz, DMSO-d_6) δ 10.92 (s, 1H), 7.43 (d, J = 7.8 Hz, 1H), 7.37–7.28 (m, 2H), 7.09 (dd, J = 8.3, 2.0 Hz, 1H), 7.04–6.98 (m, 1H), 6.96–6.88 (m, 2H), 6.25 (d, J = 1.1 Hz, 2H), 3.78 (s, 2H), 3.60 (s, 2H); ^{13}C NMR (126 MHz, DMSO-d_6) δ 151.66, 138.79, 136.12, 132.44, 129.25, 128.01, 127.68, 120.29, 119.37, 119.31, 118.57, 116.26, 110.91, 99.15, 51.08, 45.37; HRMS (ESI) calcd for $C_{16}H_{16}ClN_2O$ $[M+H]^+$ 287.0946, found 287.0945.

4.3. LogP and LogD determination

The distribution coefficient of prepared compounds between water – octanol (log*P*) and PBS buffer of pH 7.4 – octanol (log*D*) was determined by UHPLC-DAD-MS measurement of analyte concentration in particular solvent using Agilent 1290 Infinity II chromatography system coupled with Agilent 6470 OqQ mass spectrometer (Agilent Technologies, Santa Clara, USA). Compounds were weighed (0.25 mg) and dissolved in 500 μL of water/buffer – octanol mixture (1:1 (v/v) ratio). Samples were shaken for 30 min and subsequently centrifuged for 10 min at 10,000 rcf. Aqueous and octanol phases were transferred into vials and analysed. The concentration of analyte in a particular phase was determined according to an adequate calibration line.

4.4. pK_a determination

The negative decimal logarithms of the dissociation constants (pK_a) of prepared compounds were determined spectrophotometrically using buffers of given pH (range from 3.0 to 11.5 with 0.5 unit increment). Ten microliters of tested compound (1 mg/mL) were dissolved in 490 μL of particular buffer and absorbance spectra of various dissociation states were scanned in the range 200–400 nm using Carry-60 UV-VIS spectrophotometer (Agilent Technologies, Santa Clara, USA) at 20 °C. The pK_a values were calculated from the sigmoidal dependence of the absorbance of the dissociated form of the substance on the pH value using GraphPad Prism 8.2 software (San Diego, USA).

4.5. Solubility

Compound solubility determination was performed using nephelometry assays on NEPHELOstar microplate instrument (BMG Labtech, Offenburg, Germany). Stock solutions of analysed compounds were prepared in a concentration 160 μg/mL in phosphate buffer (pH = 7.4). Each suspension was sonicated at full power with Hielscher UP100H needle ultrasonic processor (Teltow, Germany) to achieve uniform dispersion of particles. Immediately after sonication, the suspension was loaded into NEPHELOstar instrument injector A, together with phosphate buffer (pH = 7.4) loaded into injector B. Compound dilution was then performed automatically in 48 wells in range 0–160 μg/mL. After 30 s of shaking, each well was scanned with 80% laser power in matrix 3 × 3, beam width 2 mm. If necessary, the process was repeated with a higher concentration of stock solution (640 μg/mL and 2.54 mg/mL). Obtained data were evaluated in Graphpad Prism 7.03 using segmental linear regression.

4.6. Enzyme inhibition

The recombinant 17β-HSD10 was expressed in *Escherichia coli* BL21 (DE3) strain and purified as described previously [22]. For the compounds' inhibitory potency and IC_{50} determination, the SAAC method using acetoacetyl-CoA (AAC) as a substrate and absorbance readout at

340 nm was used [22]. In brief, 0.15 μg of recombinant 17β-HSD10 was mixed with 320 μmol/L nicotinamide adenine dinucleotide (NADH) as an enzyme cofactor in assay buffer (10 mM Tris-HCl, pH 7.4, 150 mM NaCl, 1 mM dithiothreitol (DTT), 0.001% Tween 20 and 0.01% bovine serum albumin) and the mixture was preincubated for 5 min at 37 °C with the tested inhibitor (or vehicle control). The reaction was started by the addition of 320 μmol/L AAC and monitored as a change in absorbance at 340 nm for 5 min in 10-sec intervals. Inhibitors were dissolved in anhydrous DMSO and further diluted in DMSO and assay buffer to reach the final inhibitor concentrations. All data were analysed in GraphPad Prism 7 software using non-linear regression, and IC_{50} values were calculated for each inhibitor from at least three independent measurements, all in triplicate. The data are expressed as the mean ± SD.

4.7. Molecular docking

For the purposes of molecular docking, two crystal structures of 17β-HSD10 (PDB ID: 1U7T with resolution 2.00 Å and PDB ID: 1E6W with resolution 1.70 Å) were obtained from the online PDB database (www.rcsb.org). The ligands under investigation were generated by Avogadro v1.2.0 [43] and consequently geometrically optimized using MMFF94 force field. Two docking methods, AutoDock: Vina v1.1.3 [27] and MOE v2022.02 [28] respectively, were employed in the molecular docking experiment.

Following procedure was adopted to conduct the flexible docking in AD: Vina: UCSF Chimera v1.16 [44] was used for the initial process of removal of the surplus copies of the enzyme chains, non-bonded inhibitors and other small molecules (except for NAD). AutoDockFR suite v1.0 [45] and OpenBabel library v2.4.1 [46] were used to add hydrogen atoms and to assign the partial charges to all atoms in both enzymes. Residues Ser155, Tyr168 and Lys172 from the active site were selected as flexible. The rotatable bonds in the flexible residues were detected automatically by AutoDock Tools v1.5.4. Centre of the grid box was selected as the centre of an estrone molecule that was co-crystallized with 1E6W, or center of the cavity in the active site of 1U7T respectively. Size of x, y, and z sides of the grid box was set to 25 Å. AD: Vina docking was then performed using exhaustiveness parameter of 32, employing 12 CPUs in parallel multithreading. 10 replicate dockings were conducted for every ligand. Resulting complexes with minimal predicted Gibbs binding energy were selected as the top-scoring.

In MOE, the initial process of removal of the surplus copies of the enzyme chains, non-bonded inhibitors and other small molecules (except for NAD) was followed by receptor preparation using MOE-QuickPrep, which included addition of hydrogen atoms and assigning the partial charges to all atoms in both enzymes. Ligand placement was performed using the Triangle Matcher protocol, which defines the active site using α-spheres, that were generated using the MOE-SiteFinder application. The top 1000 poses produced from placement were then scored using the London dG scoring function. The top 30 poses as ranked by London dG were kept and minimized using MMFF94x within a flexible receptor. The resulting poses were then scored using the GBVI/WSA dG scoring function.

Superpositions of selected top-scoring ligands were visualised by VMD v1.9.4 [47] and edited in GIMP v2.10 (www.gimp.org).

4.8. Mitochondrial assays

4.8.1. Pig brain mitochondria

A crude mitochondrial fraction was isolated from the brain cortex of slaughtered pigs by the standard differential centrifugation technique. Purified mitochondria were separated from the crude mitochondrial fraction by centrifugation with a sucrose gradient and used for the assays [48]. A cytochrome *c* test was used to evaluate the intactness of the outer mitochondrial membrane in mitochondrial preparations. Damage to the inner mitochondrial membrane was assessed by measuring the release of the matrix enzyme citrate synthase (CS). Mitochondria were stored in a preservation medium on the ice at a total protein concentration of 20–50 mg/mL. The concentration of proteins was determined by the Lowry method [49] with bovine serum albumin as a standard.

4.8.2. Citrate synthase and complex I and complex II + III activity

The activity of CS (E.C. 2.3.3.1) and mitochondrial Complex I (E.C. 7.1.1.2) and the couple Complex II (E.C. 1.3.5.1) and III (E.C. 7.1.1.8) was measured spectrophotometrically using an Uvikon XL spectrophotometer (Secomam, Ales, France). Isolated pig brain mitochondria were diluted in hypotonic buffer (25 mM potassium phosphate and 5 mM $MgCl_2$, pH 7.2) and shortly ultrasonicated three times to stimulate the enzyme to the highest activity. The drug was incubated with mitochondria at 30 °C for 30 min. The drug-free solvent (DMSO) was added to the control sample. The total sample volume was 1 mL; the measurement temperature was 30 °C.

CS activity was measured as the color change of 5,5′-dithiobis-(2-nitrobenzoic acid) (DTNB) according to a method published by Srere [29]. The incubation medium was composed of 0.2 mM DTNB, 0.1 mM acetyl-CoA, 0.1% Triton X-100, 100 mM Tris/HCl (pH 8.1), mitochondria (20 μg/mL mitochondrial protein), and 50 μM of drug. The reaction was initiated by adding the oxaloacetate (0.5 mM) and measured at 412 nm for 3 min.

The activity of respiratory Complex I was measured based on the rotenone-sensitive rate of the NADH oxidation; a slightly modified previously published method [30] was used. The incubation medium was composed of phosphate buffer (25 mM KH_2PO_4, 5 mM $MgCl_2$, pH 7.2), 2 mM KCN, mitochondria (1 mg/mL of mitochondrial protein), and 50 μM drug. The reaction was initiated by coenzyme Q_{10} (100 μM) and NADH (100 μM) and measured at 340 nm for 5 min. A background correction was verified, which was measured under the same conditions after inhibition of the Complex I by 10 μM rotenone.

The couple Complex II + III activity was determined as the rate of reduction of cytochrome *c* measured at 550 nm for 3 min [32,50]. The final mitochondrial protein concentration was 0.5 mg/ml. The medium contained 50 mM KH_2PO_4, 0.625 mM EDTA, 20 mM succinate, 0.1 mM rotenone (Complex I inhibitor that ensured that cytochrome *c* reduction occurs via Complex II), 2 mM KCN (cytochrome *c* oxidase inhibitor that prevented the re-oxidation of cytochrome *c*), and 50 μM drug. The reaction is started by the addition of 30 μmol/L cytochrome *c*.

4.8.3. Mitochondrial respiration

In vitro effects of the test compounds on electron transport system activity were measured by high-resolution respirometry as drug-induced changes in the rate of oxygen consumption in isolated mitochondria in state 3 respiration, as previously described [33,48]. The Oxygraph-2k equipped with two tempered chambers and Clark-type electrodes and an automatic titration-injection micropump TIP2k (Oroboros Instruments, Innsbruck, Austria) was used [51]. Briefly, following substrate addition was made (malate + pyruvate + ADP for Complex I-linked respiration and ADP + rotenone + succinate for Complex II-linked respiration), the sample was titrated with a drug in one chamber and with DMSO in the second chamber. Drug-induced changes in oxygen flow were determined with 10–20 different drug concentrations (the final concentrations were set within the range of 1.25–500 μM).

4.8.4. Monoamine oxidase assay

The activities of MAO-A and MAO-B were assayed using radiochemical method by the modification of a previously published experimental protocol [34] with either tritium-labelled serotonin ([^{3}H]5-HT) as the MAO-A substrate and ^{14}C-labelled phenylethylamine ([^{14}C]PEA) as the MAO-B substrate. The reaction mixture containing the mitochondria and a drug at 5–7 various concentrations (final drug concentrations ranged from 1 μM to 1000 μM) was preincubated at 37 °C for 60 min. The reaction was initiated by the addition of the radiolabelled

substrate and terminated after 20 min (MAO-A activity) or 1 min (MAO-B activity) incubation. The MAO activities were determined by measuring the radioactivity levels of the corresponding aldehyde, resulting from oxidative deamination of [^{3}H]5-HT or [^{14}C]PEA, using an LS 6100IC liquid scintillation counter (Beckman Instruments, Inc., Fullerton, CA, USA).

4.8.5. Data analysis

DatLab software (Oroboros Instruments, Innsbruck, Austria) was used for respirometry data acquisition and analysis. To correct for a slight decrease in respiratory rate during experiments lasting more than 1 h, the relative respiratory rate was calculated as the ratio of the oxygen consumption rate in the sample titrated with a drug to the oxygen consumption rate in the sample titrated with the solvent (DMSO).

Plotted dose-response curves of the activity were analysed by four-parameter logistic regression using SigmaPlot software (Inpixon HQ, Palo Alto, CA 94303, USA), and the half-maximal inhibitory concentration (IC_{50}) was established, which represents the drug concentration required to inhibit by 50% the difference between baseline (no drug) and residual value (drug overdose) of mitochondrial respiratory rate or MAO activity.

Statistical analyses were performed using a Statistica data analysis software system (TIBCO Software Inc., Palo Alto, CA, USA). Data are presented as the mean ± standard error (SE) or the mean ± standard deviation (SD).

4.9. CellTox Green Cytotoxicity Assay and CellTiter-Glo cell viability assay

HEK293 and SH-SY5Y cells were maintained in DMEM (Capricorn) supplemented with 10% fetal bovine serum (Gibco), 2 mM L-glutamine (Lonza) and non-essential amino acids additives (Gibco) at 37 °C, under a humidified atmosphere of 5% CO_2. Selected compounds (**6**, **9**, **11**, **12**) were tested on HEK293 and SH-SY5Y cell lines to determine their cytotoxic effects and impact on cell viability using CellTox Green and CellTiter-Glo 2.0 kits (Promega G8741 and G9241, respectively), respectively. The measurements were performed as endpoint methods in the multiplex using a TECAN SPARK® instrument. For multiplex measurement, 7500 cells were seeded per well in 50 μL of culture media and cultured for 24 h before adding selected compounds. The compounds were dissolved in anhydrous DMSO, further diluted in DMSO and added to the wells at a final compound concentration of 1 μM and 10 μM (1% DMSO concentration). The cells treated with 1% DMSO only were used as a vehicle control and 100 μM valinomycin treatment was used as a positive control. After the treatment, the cells were cultured for additional 48 h followed by the multiplex measurement. The measurements were performed in a white solid bottom 96 well microplates (Grainer Bio-One 655083) following the manufacturer's protocol. The fluorescent CellTox Green Cytotoxicity Assay was measured first (ex 485 nm and em 530 nm wavelengths) followed by the CellTiter-Glo Luminescent Cell Viability Assay with an integration time of 500 ms.

4.10. Dehydrogenase activity and glutathione assay

SH-SY5Y cells (ATCC CRL-2266), a human neuroblastoma cell line, was cultured in Dulbecco's Modified Eagle's Medium/Nutrient Mixture F-12 w/wo phenol red supplemented with 15% (v/v) fetal bovine serum, 50 μg/mL penicillin, 50 μg/mL streptomycin, 1% (v/v) nonessential amino acids and 2 mM glutamine and maintained at 37 °C in a sterile, humidified atmosphere of 5% CO_2. All the experiments were conducted using SH-SY5Y cells in passages 14–18. The cells were cultured for 4 and 24 h with selected compounds.

Glutathione (GSH) levels were measured using the optimized monochlorobimane spectrofluorometric assay [52]. After cell treatment, 20 μL of the bimane solution was added to cells to obtain the final concentration 40 μmol/L and the spectrofluorometric measurement was started immediately. The fluorescence increase (EX/EM = 394/490 nm) was measured for 10 min using a Tecan Spark fluorescence microplate reader (Tecan, Switzerland). The fluorescence was expressed as the slope of change in fluorescence over time. The glutathione levels were expressed as the percentage relative to the glutathione levels in control cells (= 100%). The results were expressed as mean ± SD.

Dehydrogenase activity was assessed by WST-1 test (Roche, Germany). The WST-1 test measures the activity of intra- and extra-mitochondrial dehydrogenases. After cell treatment, 10 μL of WST-1 reagent was added to the cultured cells. The absorbance change (0–1 h) was measured spectrophotometrically at wavelength of 440 nm using a Tecan Spark fluorescence microplate reader (Tecan, Switzerland). The cell viability was expressed as the percentage of intra- and extra-mitochondrial dehydrogenases activity relative to that in control cells (= 100%). The results were expressed as mean ± SD. The maximal background absorbance was lower than 15% of a signal in untreated cells.

4.11. Thermal shift assay

Melting temperatures (T_m) were measured in 100 mM potassium phosphate buffer (pH 8.0) containing a 1:1000 dilution of SYPRO Orange (Sigma-Aldrich) and 1.43 μM 17β-HSD10. The compounds were tested at two concentrations (25 and 50 μmol/L) in the total reaction volume of 40 μL. The fluorescence melting curve was monitored in a temperature range from 25 to 90 °C in the temperature ramps of 1 °C/min using qTOWER^3 real-time PCR thermal cycler (Analytic Jena; Ex/Em = 490/575). Melting curves were analysed and melting temperatures were determined using qPCRsoft 4.0. All measurements were performed in triplicate.

4.12. Parallel Artificial Membrane Permeability Assay (PAMPA–BBB)

The filter membrane of the donor plate was coated with PBL (Polar Brain Lipid, Avanti, AL, USA) in dodecane (4 μL of 20 mg/mL PBL in dodecane) and the acceptor well was filled with 300 μL of PBS pH 7.4 buffer (V_A). Tested compounds were dissolved first in DMSO and that diluted with PBS pH 7.4 to reach the final concentration in the range between 25 and 100 μM in the donor well. The concentration of DMSO did not exceed 0.5% (*v/v*) in the donor solution. 300 μL of the donor solution was added to the donor wells (V_D) and the donor filter plate was carefully put on the acceptor plate so that coated membrane was "in touch" with both donor solution and acceptor buffer. Test compound diffused from the donor well through the lipid membrane (Area = 0.28 cm^2) to the acceptor well. The concentration of the drug in both donor and the acceptor wells were assessed after 3, 4, 5 and 6 h of incubation in quadruplicate using the UV plate reader Synergy HT (Biotek, Winooski, VT, USA) at the maximum absorption wavelength of each compound. Besides that, the solution of theoretical compound concentration, simulating the equilibrium state established if the membrane were ideally permeable was prepared and assessed as well. The concentration of the compounds in the donor and acceptor well and equilibrium concentration were calculated from the standard curve and expressed as the permeability (Pe) according to the equation:

$$\log Pe = \log\left\{ C \times -\ln\left(1 - \frac{[drug]_{acceptor}}{[drug]_{equilibrium}}\right)\right\}$$

where

$$C = \left(\frac{V_D \times V_A}{(V_D + V_A) \times Area \times Time}\right)$$

4.13. In vivo experiments

4.13.1. Animals

Male albino Wistar rats weighing 220–250 g were purchased from Velaz (Prague, Czech Republic). They were kept in an air-conditioned enclosure with light from 07:00 *a.m.* to 7:00 *p.m.* and were allowed access to standard food and tap water *ad libitum*. During the housing, rats were divided into groups of 6 animals. The pharmacokinetic study was performed following ethical guidelines. The handling of the experimental animals was performed under the supervision of the Ethics Committee of the Faculty of Military Health Sciences, Czech Republic (No. MO 103046/2018–684800, and MO 268874/2018–684800).

4.13.2. Pharmacokinetic study

After intravenous (i.v.) administration of **9** (15.06 μg/kg; 0.2 mL/100 g *b.w.*, *3% DMSO in saline*) and **11** (18.18 μg/kg; 0.2 mL/100 g *b.w.*, *3% DMSO in saline*) blood samples were collected from the rats under deep terminal anaesthesia (CO_2) by cardiac puncture and stored in heparinised 1.5 mL tubes at 0, 5, 15, 30, 60, 90, 180, 240, 360 and 1440 min ($n = 3$). After oral administration of **9** and **11** (both 60 mg/kg; 1 mL/100 g *b.w.*, *25% Kolliphor + 10% NMP in saline*) blood samples were collected in the same way at 0, 5, 15, 30, 45, 60, 120, 180, 240, 300, 360, 420, 480, 540, 600 and 1440 min ($n = 3$). All blood samples were immediately centrifuged at 3000×*g* for 10 min (10 °C), and the plasma was divided into two parts.

As the blood in organ vessels also contained the studied molecules, this would have interfered with the accuracy of the brain concentration assay. Therefore, the animals were perfused transcardially with saline solution (0.9% NaCl) for 5 min (10 mL/min). After perfusion, the skull was opened, and the brain was carefully removed. Brains were stored at −80 °C until analysis.

4.13.3. Sample analysis

Frozen brains were homogenized in cold PBS (w/v 1:4) using Fastprep-24 5G sample disruption instrument. Thawed plasma or homogenized brain in the volume of 100 μL, was mixed with the same volume of methanol and acetonitrile, vortexed for 15 min and centrifuged at 14000 g for 3 min. The supernatant was then filtered through 0.22 μm PTFE syringe filter into the vial and measured.

Detection of **9** and **11** was performed on the Agilent 1290 Infinity II UHPLC system coupled to the Agilent 6470 QqQ mass spectrometer. Chromatographic conditions were maintained at gradient elution of 0.4 mL/min by 0.1% formic acid in water and acetonitrile (0–0.5 70:30, 0.5–3.0 gradient to 10:90, 3.0–3.6 10:90, 3.6–5.0 70:30), thermostated autosampler set to 15 °C and column thermostat equipped with the Zorbax Eclipse plus RRHD C18 2.1 × 50 mm, 1.8 μm (PN 959757–902) column kept to 25 °C. MS source parameters for detection of compound **9** were set to the following: drying gas 320 °C at 4 L/min, sheath gas 400 °C at 12 L/min, nebulizer pressure 35 psi, capillary voltage 3500 V and nozzle voltage 300 V. Transitions of $[M+H]^+$ ions *m/z* were detected with setting of dwell time 200 ms, cell accelerator 4 V, fragmentor 129 V for 377 → 208, 166 and 133 (CE 24, 44 and 60 V). MS source parameters for detection of compound **11** were set to the following: drying gas 260 °C at 12 L/min, sheath gas 400 °C at 12 L/min, nebulizer pressure 30 psi, capillary voltage 3500 V and nozzle voltage 900 V. Transitions of $[M+H]^+$ ions *m/z* were detected with setting of dwell time 200 ms, cell accelerator 4 V, fragmentor 129 V for 364 → 195, 151 and 109 (CE 20, 48 and 60 V).

4.13.4. Data evaluation

Standard non-compartmental analysis was performed using the Kinetica software, version 4.0 (InnaPhase Corporation, Thermo Fisher Scientific Inc., Waltham, MA, USA). The maximum concentration (C_{max}) and the time to the maximum concentration (T_{max}) were determined directly from the observed data. The area under the mean plasma concentration-time curve from zero to 1440 min ($AUC_{0–1440min}$) was defined. The λ_z (terminal rate constant) was estimated using linear regression of the log-transformed concentrations plotted against time. The half-life was calculated as follows: $t_{1/2} = ln(2)/\lambda_z$.

Declaration of competing interest

The authors declare the following financial interests/personal relationships which may be considered as potential competing interests: Ondrej Benek has patent #CZ307796 issued to University of Hradec Kralove. Kamil Musilek has patent #CZ307796 issued to University of Hradec Kralove. Lukas Hroch has patent #CZ307796 issued to University of Hradec Kralove.

Data availability

Data will be made available on request.

Acknowledgement

This study was supported by the Ministry of Education, Youth, and Sports of the Czech Republic (project ESF no. CZ.02.1.01/0.0/0.0/18_069/0010054), by the University of Hradec Kralove (Faculty of Science, no. SV2103-2022), by Charles University, Prague, Czech Republic (project Cooperatio, research area Neurosciences), by the project MH CZ-DRO VFN64165, and by MH CZ - DRO (UHHK, 00179906), by the Ministry of Defence of the Czech Republic (Faculty of Military Health Sciences Hradec Kralove) under the grant entitled the "Long-term organization development plan - Medical Aspects of Weapons of Mass Destruction", and by the RS MacDonald Charitable Trust and Rosetrees Trust.

Appendix A. Supplementary data

Supplementary data to this article can be found online at https://doi.org/10.1016/j.ejmech.2023.115593.

References

[1] L. Vinklarova, M. Schmidt, O. Benek, K. Kuca, F. Gunn-Moore, K. Musilek, Friend or enemy? Review of 17β-HSD10 and its role in human health or disease, J. Neurochem. 155 (2020) 231–249, https://doi.org/10.1111/jnc.15027.
[2] Z. Fišar, Linking the amyloid, Tau, and mitochondrial hypotheses of Alzheimer's disease and identifying promising drug targets, Biomolecules 12 (2022) 1676, https://doi.org/10.3390/biom12111676.
[3] H. Hampel, J. Hardy, K. Blennow, C. Chen, G. Perry, S.H. Kim, V.L. Villemagne, P. Aisen, M. Vendruscolo, T. Iwatsubo, C.L. Masters, M. Cho, L. Lannfelt, J. L. Cummings, A. Vergallo, The amyloid-β pathway in Alzheimer's disease, Mol. Psychiatr. 26 (2021) 5481–5503, https://doi.org/10.1038/s41380-021-01249-0.
[4] A. Morsy, P.C. Trippier, Amyloid-binding alcohol dehydrogenase (ABAD) inhibitors for the treatment of Alzheimer's disease, J. Med. Chem. 62 (2018) 4252–4264, https://doi.org/10.1021/acs.jmedchem.8b01530.
[5] O. Benek, L. Aitken, L. Hroch, K. Kuca, F. Gunn-Moore, K. Musilek, A direct interaction between mitochondrial proteins and amyloid-beta peptide and its significance for the progression and treatment of Alzheimer's disease, Curr. Med. Chem. 22 (2015) 1056–1085, https://doi.org/10.2174/0929867322666150114163051.
[6] X.-Y. He, S.-Y. Yang, Roles of type 10 17beta-hydroxysteroid dehydrogenase in intracrinology and metabolism of isoleucine and fatty acids, Endocr. Metab. Immune Disord. - Drug Targets 6 (2006) 95–102, https://doi.org/10.2174/187153006776056639.
[7] D. Ayan, R. Maltais, D. Poirier, Identification of a 17β-hydroxysteroid dehydrogenase type 10 steroidal inhibitor: a tool to investigate the role of type 10 in Alzheimer's disease and prostate cancer, ChemMedChem 7 (2012) 1181–1184, https://doi.org/10.1002/cmdc.201200129.
[8] X.-Y. He, Y.-Z. Yang, D.M. Peehl, A. Lauderdale, H. Schulz, S.-Y. Yang, Oxidative 3α-hydroxysteroid dehydrogenase activity of human type 10 17β-hydroxysteroid dehydrogenase, J. Steroid Biochem. Mol. Biol. 87 (2003) 191–198, https://doi.org/10.1016/j.jsbmb.2003.07.007.
[9] E.A. Carlson, R.T. Marquez, F. Du, Y. Wang, L. Xu, S.S. Yan, Overexpression of 17β-hydroxysteroid dehydrogenase type 10 increases pheochromocytoma cell growth and resistance to cell death, BMC Cancer 15 (2015) 166, https://doi.org/10.1186/s12885-015-1173-5.
[10] C.R. Kissinger, P.A. Rejto, L.A. Pelletier, J.A. Thomson, R.E. Showalter, M.A. Abreo, C.S. Agree, S. Margosiak, J.J. Meng, R.M. Aust, D. Vanderpool, B. Li, A. Tempczyk-

Russell, J.E. Villafranca, Crystal structure of human ABAD/HSD10 with a bound inhibitor: implications for design of Alzheimer's disease therapeutics, J. Mol. Biol. 342 (2004) 943–952, https://doi.org/10.1016/j.jmb.2004.07.071.
[11] A. Morsy, K. Maddeboina, J. Gao, H. Wang, J. Valdez, L.F. Dow, X. Wang, P. C. Trippier, Functionalized allopurinols targeting amyloid-binding alcohol dehydrogenase rescue aβ-induced mitochondrial dysfunction, ACS Chem. Neurosci. 13 (2022) 2176–2190, https://doi.org/10.1021/acschemneuro.2c00246.
[12] S. Boutin, J. Roy, R. Maltais, W. Alata, F. Calon, D. Poirier, Identification of steroidal derivatives inhibiting the transformations of allopregnanolone and estradiol by 17β-hydroxysteroid dehydrogenase type 10, Bioorg. Med. Chem. Lett 28 (2018) 3554–3559, https://doi.org/10.1016/j.bmcl.2018.09.031.
[13] S. Boutin, R. Maltais, J. Roy, D. Poirier, Synthesis of 17β-hydroxysteroid dehydrogenase type 10 steroidal inhibitors: selectivity, metabolic stability and enhanced potency, Eur. J. Med. Chem. 209 (2021), 112909, https://doi.org/10.1016/j.ejmech.2020.112909.
[14] Y. Xie, S. Deng, Z. Chen, S. Yan, D.W. Landry, Identification of small-molecule inhibitors of the Aβ–ABAD interaction, Bioorg. Med. Chem. Lett 16 (2006) 4657–4660, https://doi.org/10.1016/j.bmcl.2006.05.099.
[15] K.R. Valasani, G. Hu, M.O. Chaney, S.S. Yan, Structure-based design and synthesis of benzothiazole phosphonate analogues with inhibitors of human ABAD-aβ for treatment of Alzheimer's disease, Chem. Biol. Drug Des. 81 (2013) 238–249, https://doi.org/10.1111/cbdd.12068.
[16] K.R. Valasani, Q. Sun, G. Hu, J. Li, F. Du, Y. Guo, E.A. Carlson, X. Gan, S.S. Yan, Identification of human ABAD inhibitors for rescuing aβ-mediated mitochondrial dysfunction, Curr. Alzheimer Res. 11 (2014) 128–136, https://doi.org/10.2174/1567205011666140130150108.
[17] L. Hroch, O. Benek, P. Guest, L. Aitken, O. Soukup, J. Janockova, K. Musil, V. Dohnal, R. Dolezal, K. Kuca, T.K. Smith, F. Gunn-Moore, K. Musilek, Design, synthesis and in vitro evaluation of benzothiazole-based ureas as potential ABAD/17β-HSD10 modulators for Alzheimer's disease treatment, Bioorg. Med. Chem. Lett. 26 (2016) 3675–3678, https://doi.org/10.1016/j.bmcl.2016.05.087.
[18] L. Hroch, P. Guest, O. Benek, O. Soukup, J. Janockova, R. Dolezal, K. Kuca, L. Aitken, T.K. Smith, F. Gunn-Moore, D. Zala, R.R. Ramsay, K. Musilek, Synthesis and evaluation of frentizole-based indolyl thiourea analogues as MAO/ABAD inhibitors for Alzheimer's disease treatment, Bioorg. Med. Chem. 25 (2017) 1143–1152, https://doi.org/10.1016/j.bmc.2016.12.029.
[19] O. Benek, L. Hroch, L. Aitken, R. Dolezal, R. Hughes, P. Guest, M. Benkova, O. Soukup, K. Musil, K. Kuca, T.K. Smith, F. Gunn-Moore, K. Musilek, 6-Benzothiazolyl ureas, Thioureas and Guanidines are potent inhibitors of ABAD/17 beta-HSD10 and potential drugs for Alzheimer's disease treatment: design, synthesis and in vitro evaluation, Med. Chem. 13 (2017) 345–358, https://doi.org/10.2174/1573406413666170109142725.
[20] O. Benek, L. Hroch, L. Aitken, F. Gunn-Moore, L. Vinklarova, K. Kuca, D.I. Perez, C. Perez, A. Martinez, Z. Fisar, K. Musilek, 1-(Benzo[d]thiazol-2-yl)-3-phenylureas as dual inhibitors of casein kinase 1 and ABAD enzymes for treatment of neurodegenerative disorders, J. Enzym. Inhib. Med. Chem. 33 (2018) 665–670, https://doi.org/10.1080/14756366.2018.1445736.
[21] L. Aitken, O. Benek, B.E. McKelvie, R.E. Hughes, L. Hroch, M. Schmidt, L.L. Major, L. Vinklarova, K. Kuca, T.K. Smith, K. Musilek, F.J. Gunn-Moore, Novel benzothiazole-based ureas as 17β-HSD10 inhibitors, A potential Alzheimer's disease treatment, Molecules 24 (2019) 2757, https://doi.org/10.3390/molecules24152757.
[22] M. Schmidt, O. Benek, L. Vinklarova, M. Hrabinova, L. Zemanova, M. Chribek, V. Kralova, L. Hroch, R. Dolezal, A. Lycka, L. Prchal, D. Jun, L. Aitken, F. Gunn-Moore, K. Kuca, K. Musilek, Benzothiazolyl ureas are low micromolar and uncompetitive inhibitors of 17β-HSD10 with implications to Alzheimer's disease treatment, Int. J. Mol. Sci. 21 (2020), https://doi.org/10.3390/ijms21062059, 2059.
[23] T.T. Wager, X. Hou, P.R. Verhoest, A. Villalobos, Moving beyond rules: the development of a central nervous system multiparameter optimization (CNS MPO) approach to enable alignment of druglike properties, ACS Chem. Neurosci. 1 (2010) 435–449, https://doi.org/10.1021/cn100008c.
[24] Z. Rankovic, CNS drug design: balancing physicochemical properties for optimal brain exposure, J. Med. Chem. 58 (2015) 2584–2608, https://doi.org/10.1021/jm501535r.
[25] PhysChem, ADME/Tox Calculations, 1.2, ACD/Labs Percepta Software, 2020. https://www.acdlabs.com/products/percepta/index.php#resources. (Accessed 6 April 2020).
[26] R.Z. Cer, U. Mudunuri, R. Stephens, F.J. Lebeda, IC50-to-Ki: a web-based tool for converting IC50 to Ki values for inhibitors of enzyme activity and ligand binding, Nucleic Acids Res. 37 (2009) W441, https://doi.org/10.1093/nar/gkp253. –W445.
[27] O. Trott, A.J. Olson, AutoDock Vina, Improving the speed and accuracy of docking with a new scoring function, efficient optimization and multithreading, J. Comput. Chem. 31 (2010) 455–461, https://doi.org/10.1002/jcc.21334.
[28] Molecular Operating Environment (MOE), 02 Chemical Computing Group ULC, 1010 Sherbooke St. West, 2R7, Canada, H3A, Montreal, QC, 2022, p. 2023. Suite #910.
[29] P.A. Srere, [1] Citrate synthase: [EC 4.1.3.7. Citrate oxaloacetate-lyase (CoA-acetylating)], in: Methods in Enzymology, Academic Press, 1969, pp. 3–11, https://doi.org/10.1016/0076-6879(69)13005-0.
[30] J. Folbergrová, P. Ješina, R. Haugvicová, V. Lisý, J. Houštěk, Sustained deficiency of mitochondrial complex I activity during long periods of survival after seizures induced in immature rats by homocysteic acid, Neurochem. Int. 56 (2010) 394–403, https://doi.org/10.1016/j.neuint.2009.11.011.
[31] J. Hroudova, Z. Fisar, Activities of respiratory chain complexes and citrate synthase influenced by pharmacologically different antidepressants and mood stabilizers, Neuroendocrinol. Lett. 31 (2010) 336–342.
[32] M. Ľupták, Z. Fišar, J. Hroudová, Effect of novel antipsychotics on energy metabolism — in vitro study in pig brain mitochondria, Mol. Neurobiol. 58 (2021) 5548–5563, https://doi.org/10.1007/s12035-021-02498-4.
[33] Z. Fišar, K. Musílek, O. Benek, L. Hroch, L. Vinklárová, M. Schmidt, J. Hroudová, J. Raboch, Effects of novel 17β-hydroxysteroid dehydrogenase type 10 inhibitors on mitochondrial respiration, Toxicol. Lett. 339 (2021) 12–19, https://doi.org/10.1016/j.toxlet.2020.12.012.
[34] Z. Fišar, Inhibition of monoamine oxidase activity by cannabinoids, Naunyn-Schmied Arch Pharmacol. 381 (2010) 563–572, https://doi.org/10.1007/s00210-010-0517-6.
[35] A.C. Tripathi, S. Upadhyay, S. Paliwal, S.K. Saraf, Privileged scaffolds as MAO inhibitors: retrospect and prospects, Eur. J. Med. Chem. 145 (2018) 445–497, https://doi.org/10.1016/j.ejmech.2018.01.003.
[36] O. Benek, O. Soukup, M. Pasdiorova, L. Hroch, V. Sepsova, P. Jost, M. Hrabinova, D. Jun, K. Kuca, D. Zala, R.R. Ramsay, J. Marco-Contelles, K. Musilek, Design, synthesis and in vitro evaluation of indolotacrine analogues as multitarget-directed ligands for the treatment of Alzheimer's disease, ChemMedChem 11 (2016) 1264–1269, https://doi.org/10.1002/cmdc.201500383.
[37] O. Benek, J. Korabecny, O. Soukup, A perspective on multi-target drugs for Alzheimer's disease, Trends Pharmacol. Sci. 41 (2020) 434–445, https://doi.org/10.1016/j.tips.2020.04.008.
[38] F.H. Niesen, H. Berglund, M. Vedadi, The use of differential scanning fluorimetry to detect ligand interactions that promote protein stability, Nat. Protoc. 2 (2007) 2212–2221, https://doi.org/10.1038/nprot.2007.321.
[39] L. Di, E.H. Kerns, K. Fan, O.J. McConnell, G.T. Carter, High throughput artificial membrane permeability assay for blood–brain barrier, Eur. J. Med. Chem. 38 (2003) 223–232, https://doi.org/10.1016/S0223-5234(03)00012-6.
[40] V.N. Telvekar, H.M. Bachhav, V.K. Bairwa, A novel system for the synthesis of 2-aminobenzthiazoles using sodium dichloroiodate, Synlett 23 (2012) 2219–2222, https://doi.org/10.1055/s-0032-1317080.
[41] D.W. Engers, J.R. Field, U. Le, Y. Zhou, J.D. Bolinger, R. Zamorano, A.L. Blobaum, C.K. Jones, S. Jadhav, C.D. Weaver, P.J. Conn, C.W. Lindsley, C.M. Niswender, C. R. Hopkins, Discovery, synthesis, and Structure−Activity relationship development of a series of N-(4-Acetamido)phenylpicolinamides as positive allosteric modulators of metabotropic glutamate receptor 4 (mGlu4) with CNS exposure in rats, J. Med. Chem. 54 (2011) 1106–1110, https://doi.org/10.1021/jm101271s.
[42] D. Ménard, I. Niculescu-Duvaz, H.P. Dijkstra, D. Niculescu-Duvaz, B.M.J. M. Suijkerbuijk, A. Zambon, A. Nourry, E. Roman, L. Davies, H.A. Manne, F. Friedlos, R. Kirk, S. Whittaker, A. Gill, R.D. Taylor, R. Marais, C.J. Springer, Novel potent BRAF inhibitors: toward 1 nM compounds through optimization of the central phenyl ring, J. Med. Chem. 52 (2009) 3881–3891, https://doi.org/10.1021/jm900242c.
[43] M.D. Hanwell, D.E. Curtis, D.C. Lonie, T. Vandermeersch, E. Zurek, G.R. Hutchison, Avogadro: an advanced semantic chemical editor, visualization, and analysis platform, J. Cheminf. 4 (2012) 17, https://doi.org/10.1186/1758-2946-4-17.
[44] E.F. Pettersen, T.D. Goddard, C.C. Huang, G.S. Couch, D.M. Greenblatt, E.C. Meng, T.E. Ferrin, UCSF Chimera—a visualization system for exploratory research and analysis, J. Comput. Chem. 25 (2004) 1605–1612, https://doi.org/10.1002/jcc.20084.
[45] P.A. Ravindranath, S. Forli, D.S. Goodsell, A.J. Olson, M.F. Sanner, AutoDockFR: advances in protein-ligand docking with explicitly specified binding site flexibility, PLoS Comput. Biol. 11 (2015), e1004586, https://doi.org/10.1371/journal.pcbi.1004586.
[46] N.M. O'Boyle, M. Banck, C.A. James, C. Morley, T. Vandermeersch, G. R. Hutchison, Open Babel: an open chemical toolbox, J. Cheminf. 3 (2011) 33, https://doi.org/10.1186/1758-2946-3-33.
[47] W. Humphrey, A. Dalke, K. Schulten, VMD: visual molecular dynamics, J. Mol. Graph. 14 (1996) 33–38, https://doi.org/10.1016/0263-7855(96)00018-5.
[48] J. Hroudová, Z. Fišar, Assessment of the effects of drugs on mitochondrial respiration, in: V. Weissig, M. Edeas (Eds.), Mitochondrial Medicine: Volume 3: Manipulating Mitochondria and Disease- Specific Approaches, Springer US, New York, NY, 2021, pp. 133–142, https://doi.org/10.1007/978-1-0716-1270-5_9.
[49] O. Lowry, N. Rosebrough, A. Farr, R. Randall, Protein measurement with the folin phenol reagent, J. Biol. Chem. 193 (1951) 265–275, https://doi.org/10.1016/S0021-9258(19)52451-6.
[50] I.A. Trounce, Y.L. Kim, A.S. Jun, D.C. Wallace, [42] Assessment of mitochondrial oxidative phosphorylation in patient muscle biopsies, lymphoblasts, and transmitochondrial cell lines, in: Methods in Enzymology, Academic Press, 1996, pp. 484–509, https://doi.org/10.1016/S0076-6879(96)64044-0.
[51] D. Pesta, E. Gnaiger, High-resolution respirometry: OXPHOS protocols for human cells and permeabilized fibers from small biopsies of human muscle, in: C. M. Palmeira, A.J. Moreno (Eds.), Mitochondrial Bioenergetics: Methods and Protocols, Humana Press, Totowa, NJ, 2012, pp. 25–58, https://doi.org/10.1007/978-1-61779-382-0_3.
[52] J. Čapek, M. Hauschke, L. Brůčková, T. Roušar, Comparison of glutathione levels measured using optimized monochlorobimane assay with those from ortho-phthalaldehyde assay in intact cells, J. Pharmacol. Toxicol. Methods 88 (2017) 40–45, https://doi.org/10.1016/j.vascn.2017.06.001.

Supporting Information

Development of submicromolar 17β-HSD10 inhibitors and their *in vitro* and *in vivo* evaluation

Ondrej Benek[1,2*], Michaela Vaskova[1], Marketa Miskerikova[1], Monika Schmidt[1,2], Rudolf Andrys[1], Aneta Rotterova[1], Adam Skarka[1], Jana Hatlapatkova[3], Jana Zdarova Karasova[3], Matej Medvecky[1,4], Lukas Hroch[2], Lucie Vinklarova[1], Zdenek Fisar[5], Jana Hroudova[5], Jiri Handl[6], Jan Capek[6], Tomas Rousar[6], Tereza Kobrlova[2], Rafael Dolezal[2], Ondrej Soukup[2], Laura Aitken[7], Frank Gunn-Moore[7], Kamil Musilek[1,2*]

[1] *University of Hradec Kralove, Faculty of Science, Department of Chemistry, Rokitanskeho 62, 500 03 Hradec Kralove, Czech Republic*

[2] *University Hospital Hradec Kralove, Biomedical Research Centre, Sokolska 581, 500 05 Hradec Kralove, Czech Republic*

[3] *University of Defence, Faculty of Military Health Sciences, Department of Toxicology and Military Pharmacy, Trebesska 1575, 500 01, Hradec Kralove, Czech Republic*

[4] *University of Warwick, Bioinformatics Research Technology Platform, Coventry CV4 7AL, United Kingdom*

[5] *Charles University and General University Hospital in Prague, First Faculty of Medicine, Department of Psychiatry, Ke Karlovu 11, 120 00, Prague 2, Czech Republic*

[6] *University of Pardubice, Faculty of Chemical Technology, Department of Biological and Biochemical Sciences, Studentska 573, Pardubice 53210, Czech Republic*

[7] *University of St. Andrews, School of Biology, Biomedical Science Research Complex, North Haugh, St. Andrews KY16 9ST, United Kingdom*

* Correspondence: ondrej.benek@uhk.cz and kamil.musilek@uhk.cz

Contents:

1. ^{1}H NMR and ^{13}C NMR spectra of final products **6**-**20**……..S2–16

2. HR-MS spectra of final products **6**-**20**……..S17–24

3. 2D pictures from molecular docking of **6**, **11**, **17**……..S25–27

4. LDH cytotoxicity assay……..S28

^{1}H NMR spectrum of compound **6** (500 MHz, DMSO-d_6)

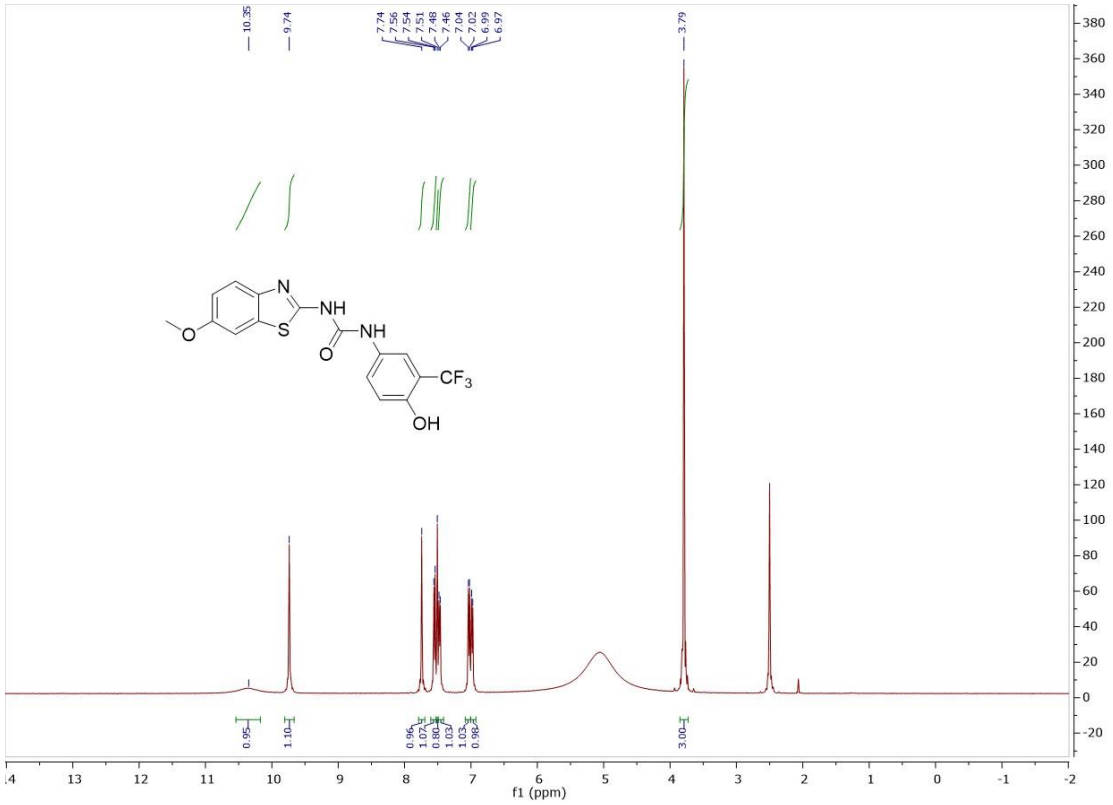

^{13}C NMR spectrum of compound **6** (126 MHz, DMSO-d_6)

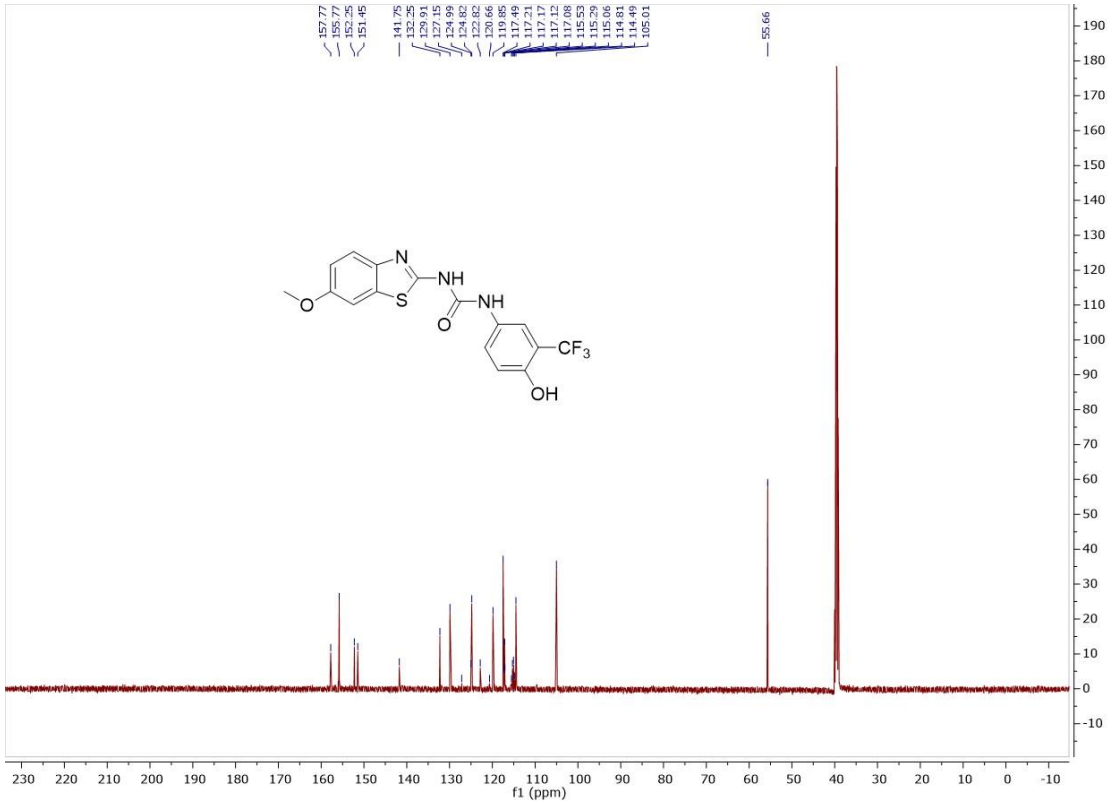

^{1}H NMR spectrum of compound **7** (500 MHz, DMSO-d_6)

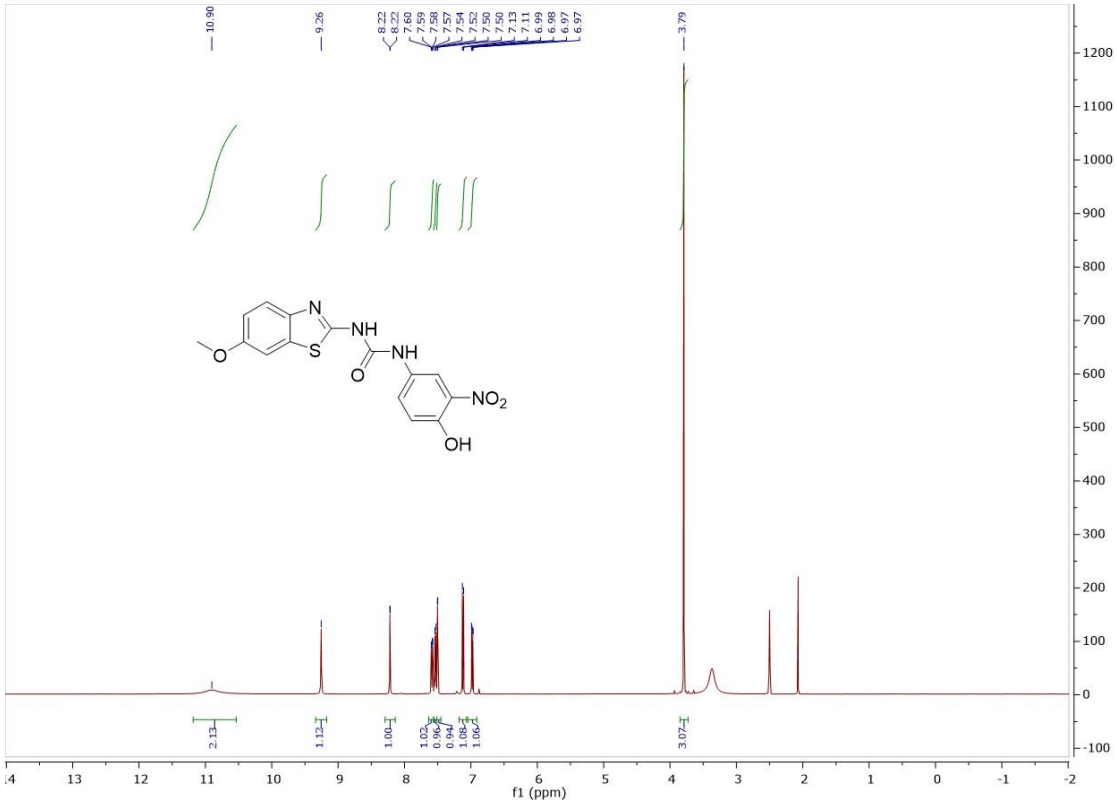

^{13}C NMR spectrum of compound **7** (126 MHz, DMSO-d_6)

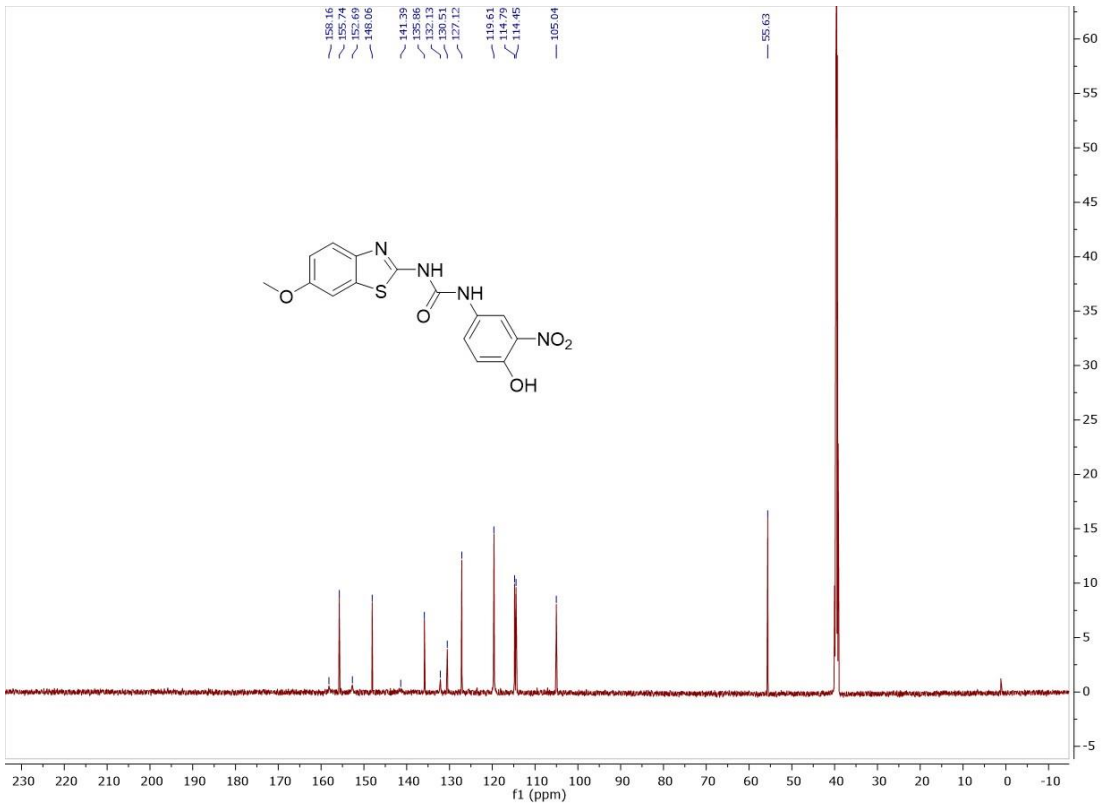

^{1}H NMR spectrum of compound **8** (500 MHz, DMSO-d_6)

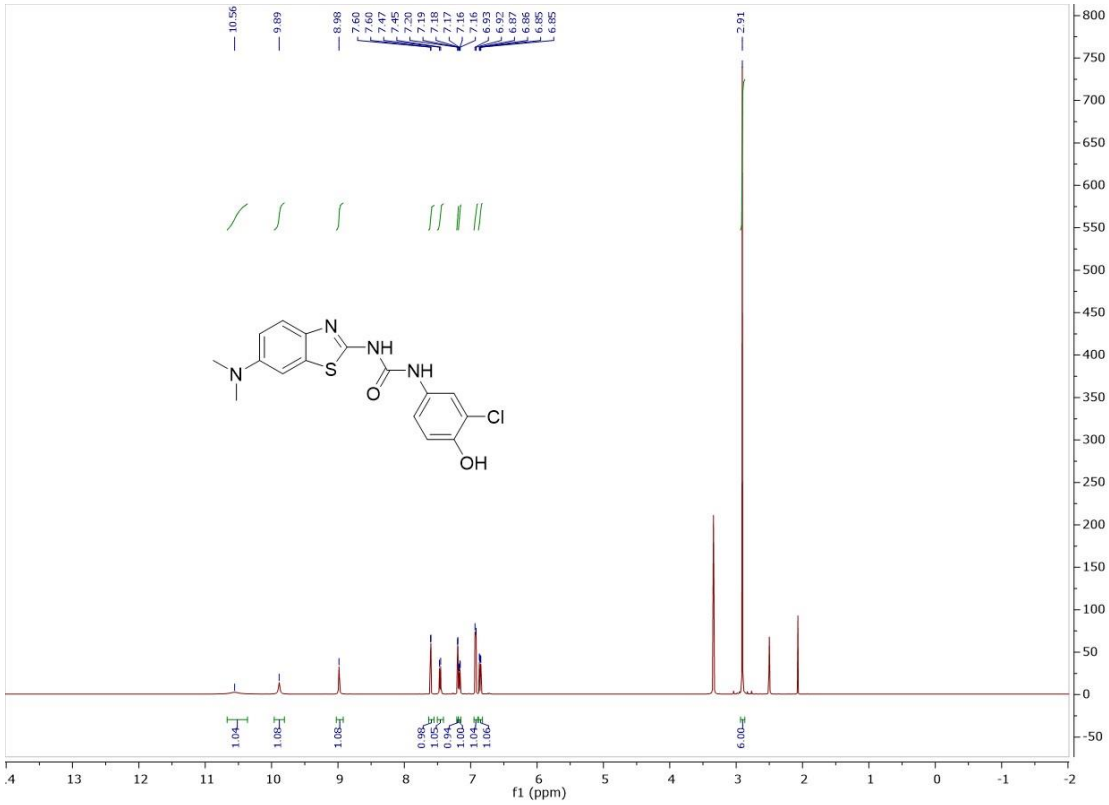

^{13}C NMR spectrum of compound **8** (126 MHz, DMSO-d_6)

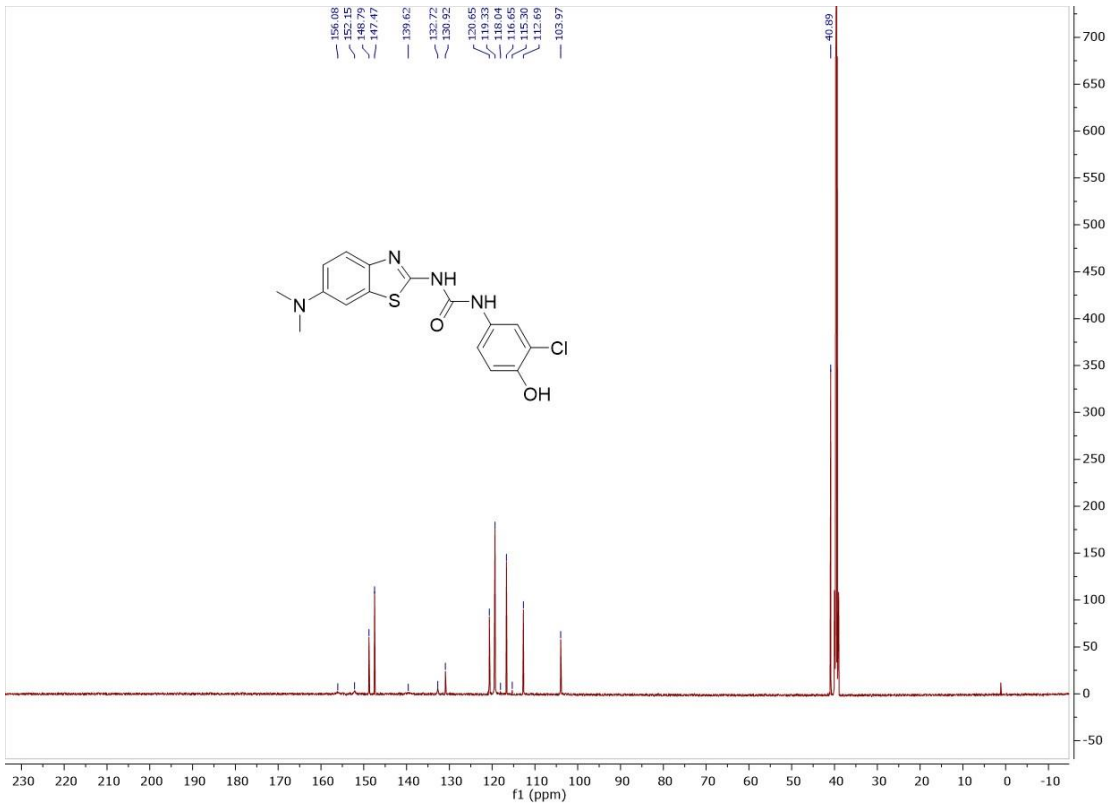

^{1}H NMR spectrum of compound **9** (500 MHz, DMSO-d_6)

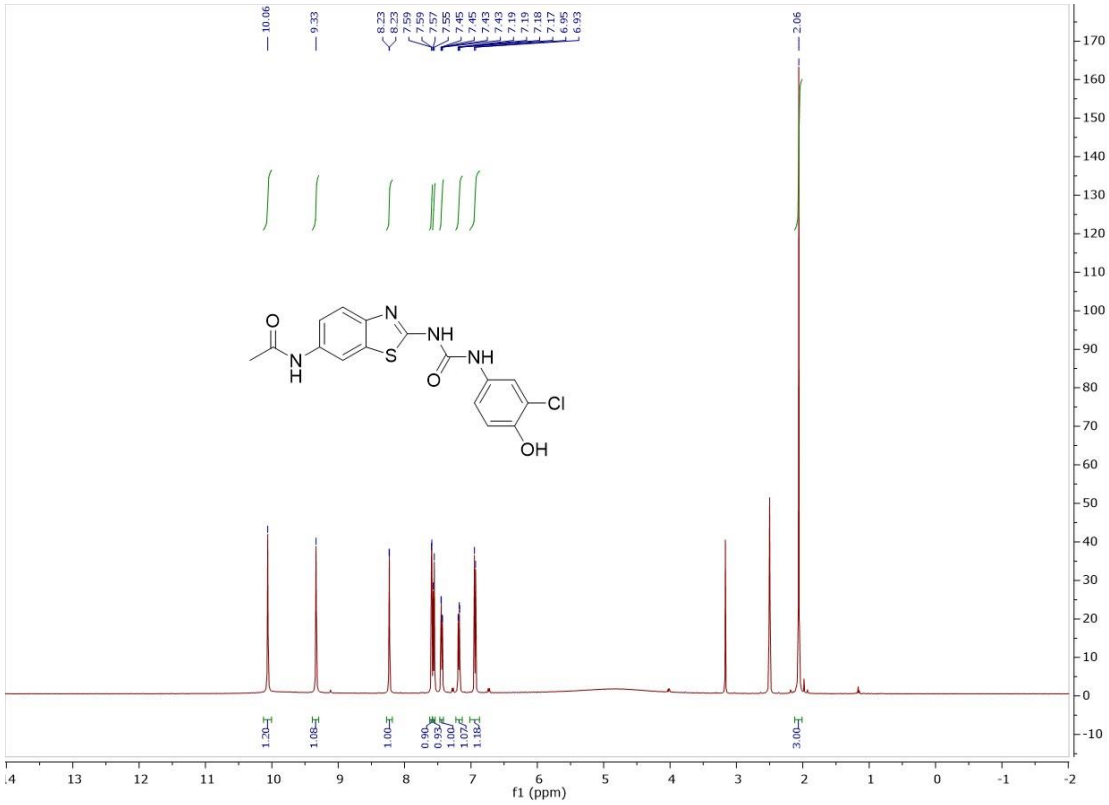

^{13}C NMR spectrum of compound **9** (126 MHz, DMSO-d_6)

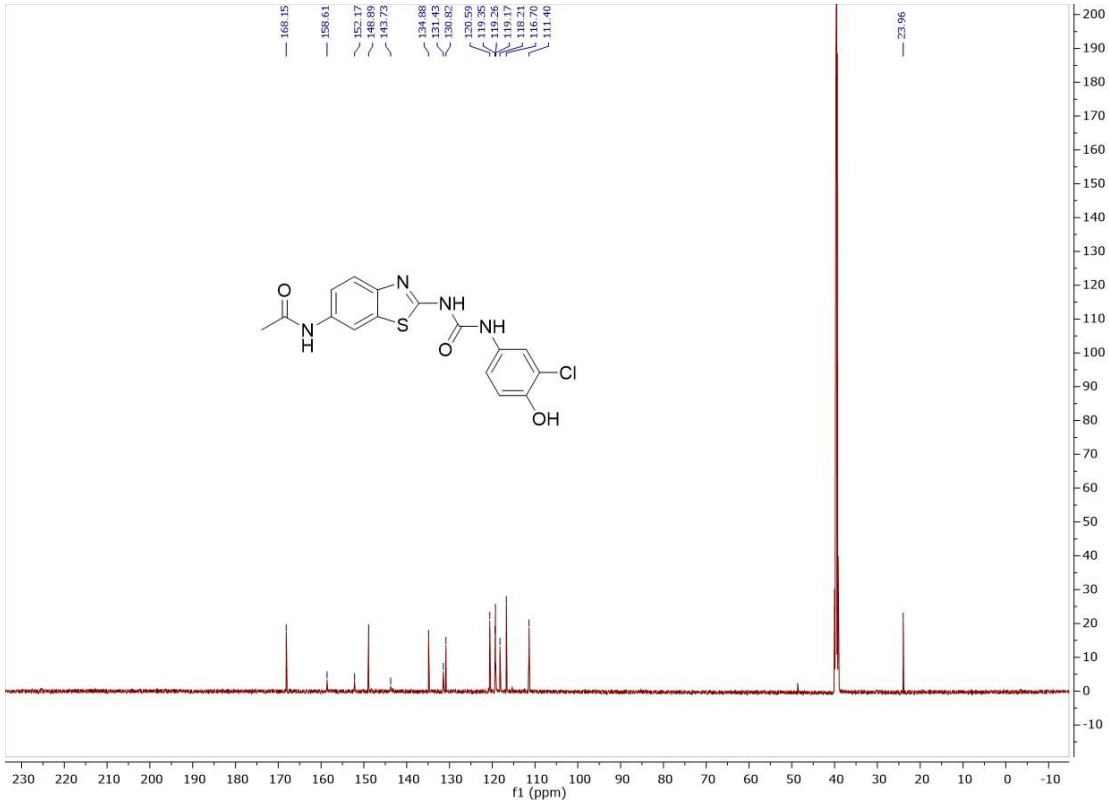

^{1}H NMR spectrum of compound **10** (500 MHz, DMSO-d_6)

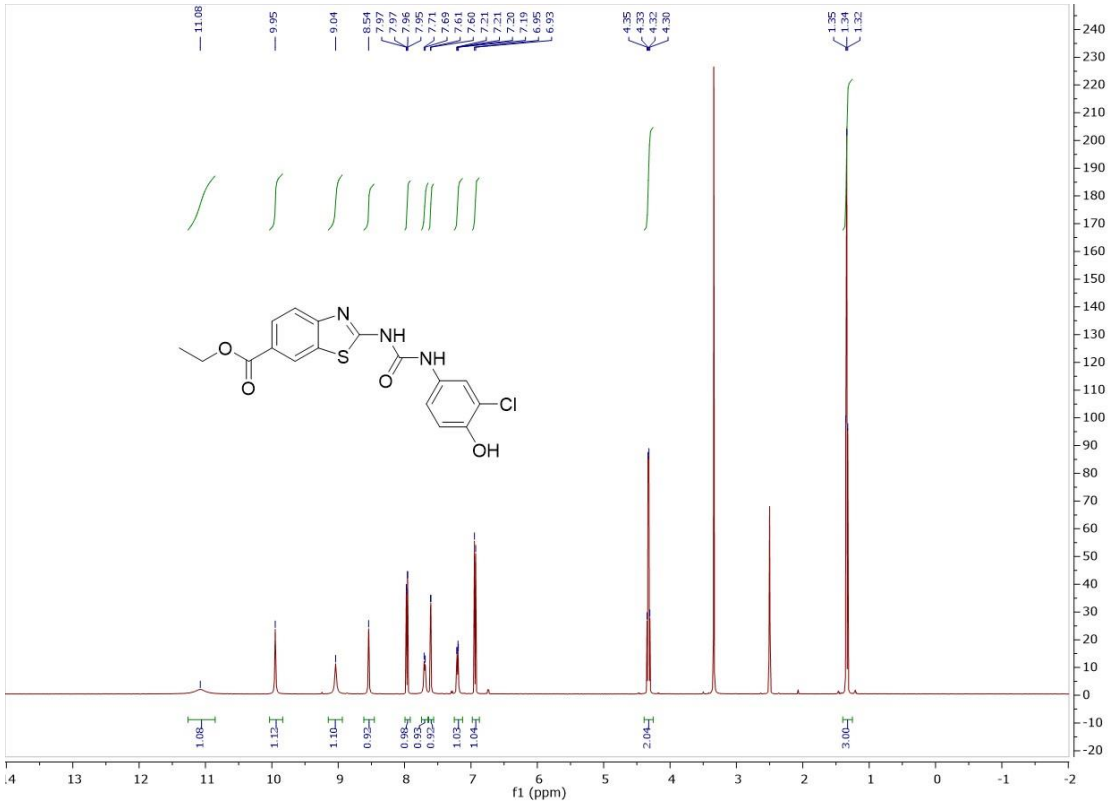

^{13}C NMR spectrum of compound **10** (126 MHz, DMSO-d_6)

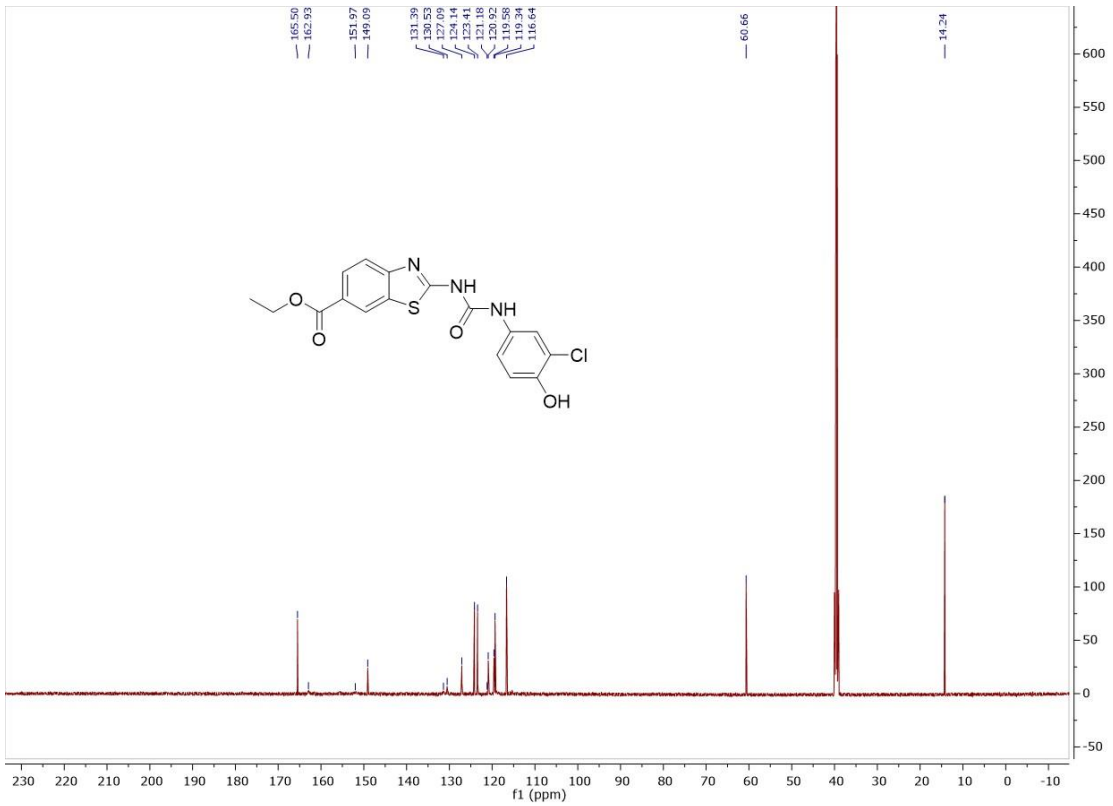

^{1}H NMR spectrum of compound **11** (500 MHz, DMSO-d_6)

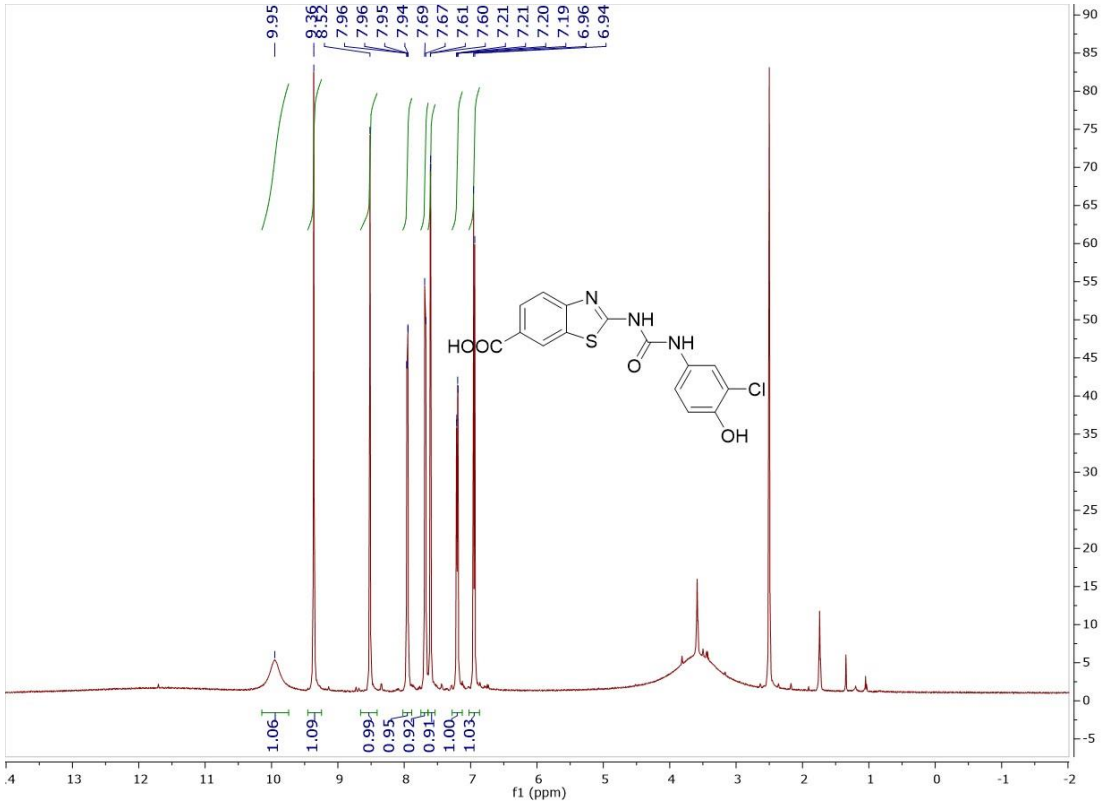

^{13}C NMR spectrum of compound **11** (126 MHz, DMSO-d_6)

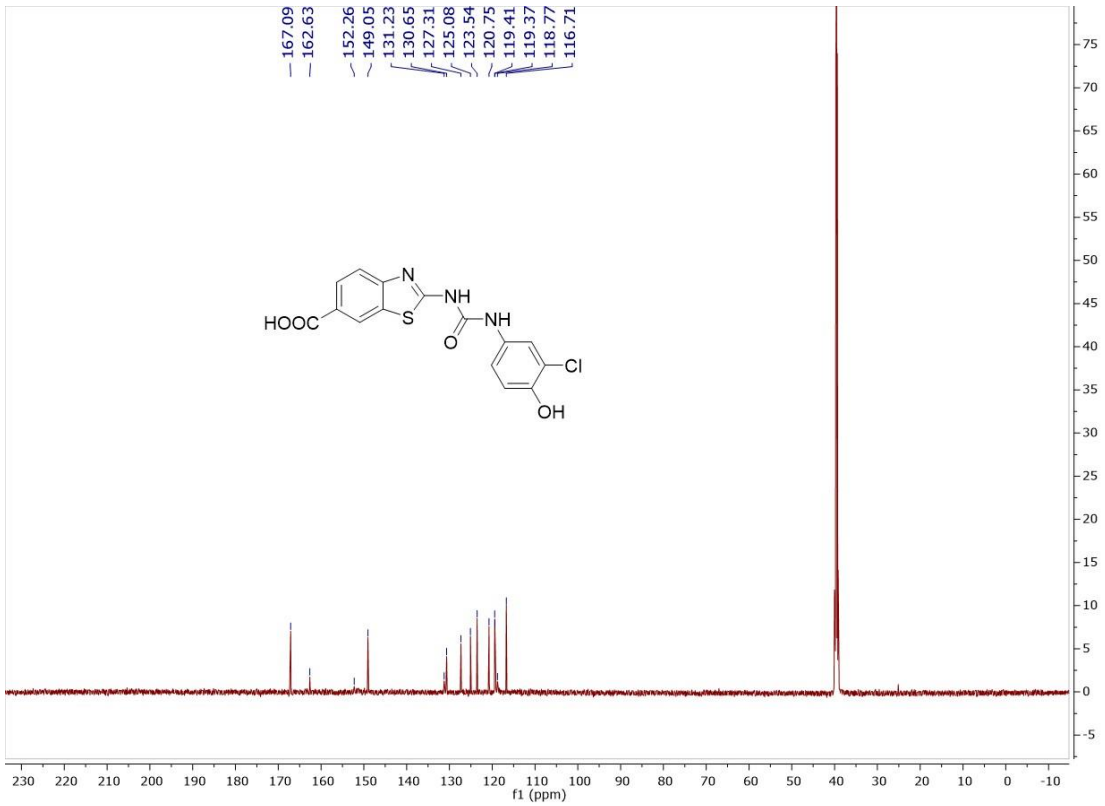

^{1}H NMR spectrum of compound **12** (500 MHz, DMSO-d_6)

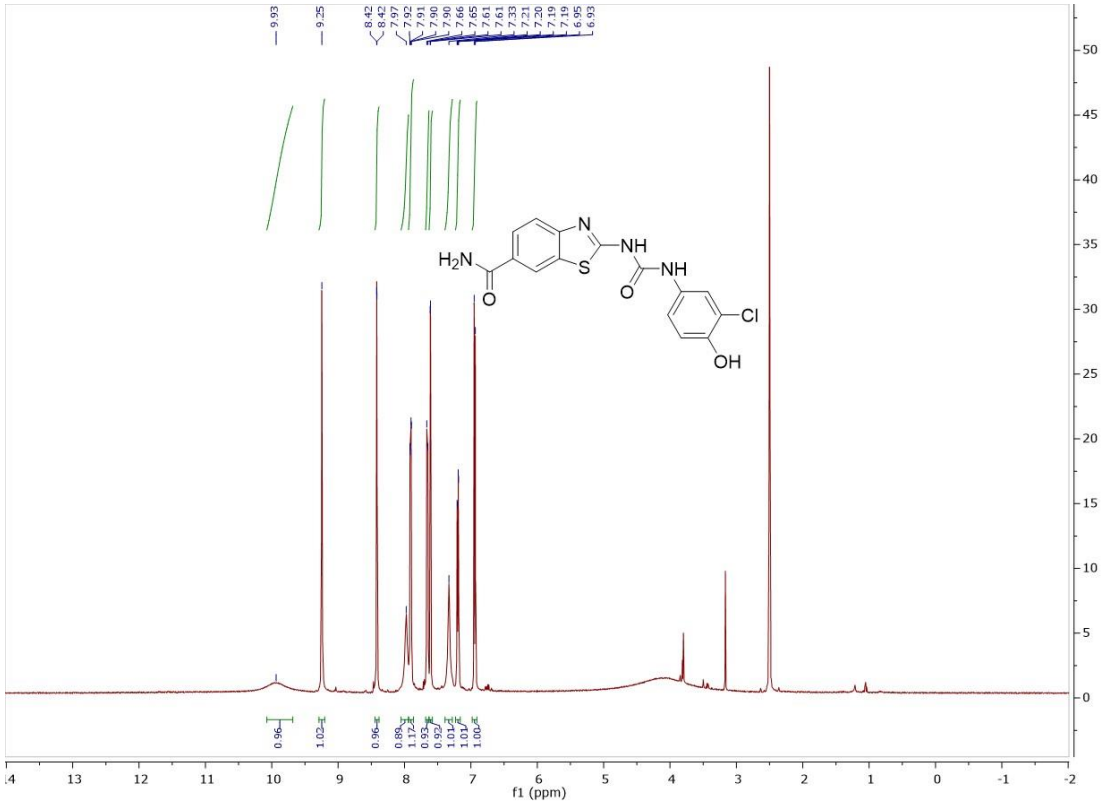

^{13}C NMR spectrum of compound **12** (126 MHz, DMSO-d_6)

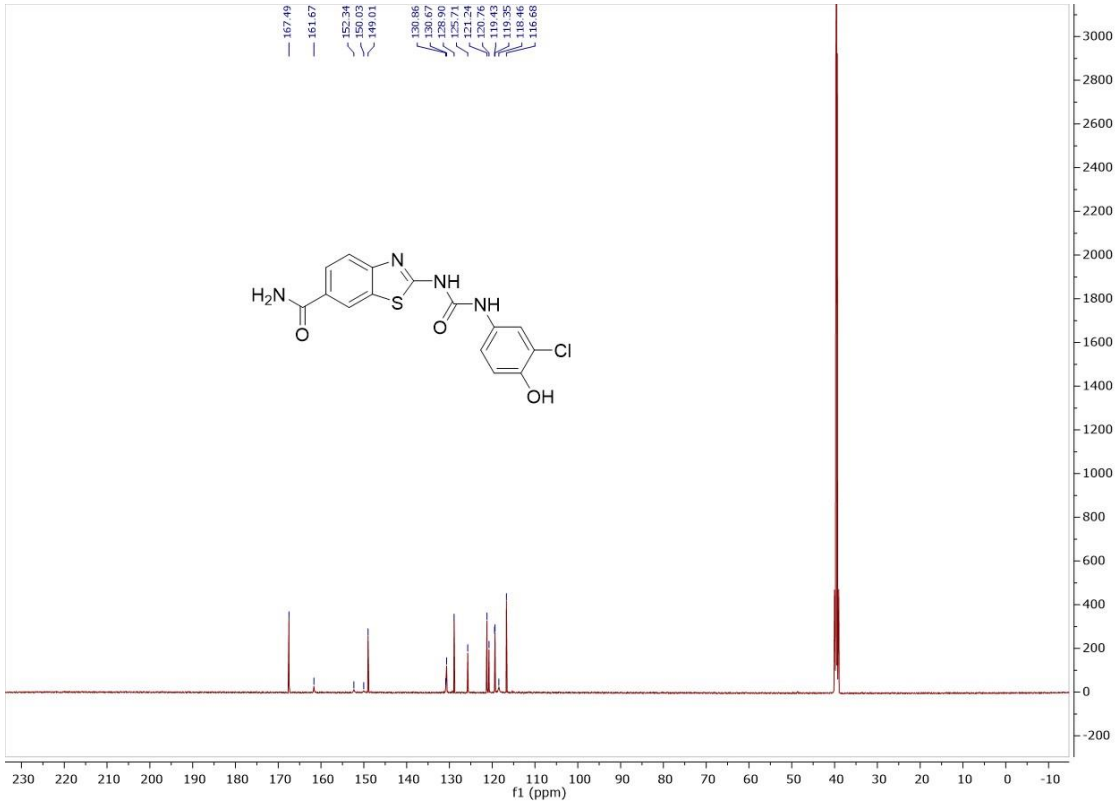

^{1}H NMR spectrum of compound **13** (500 MHz, DMSO-d_6)

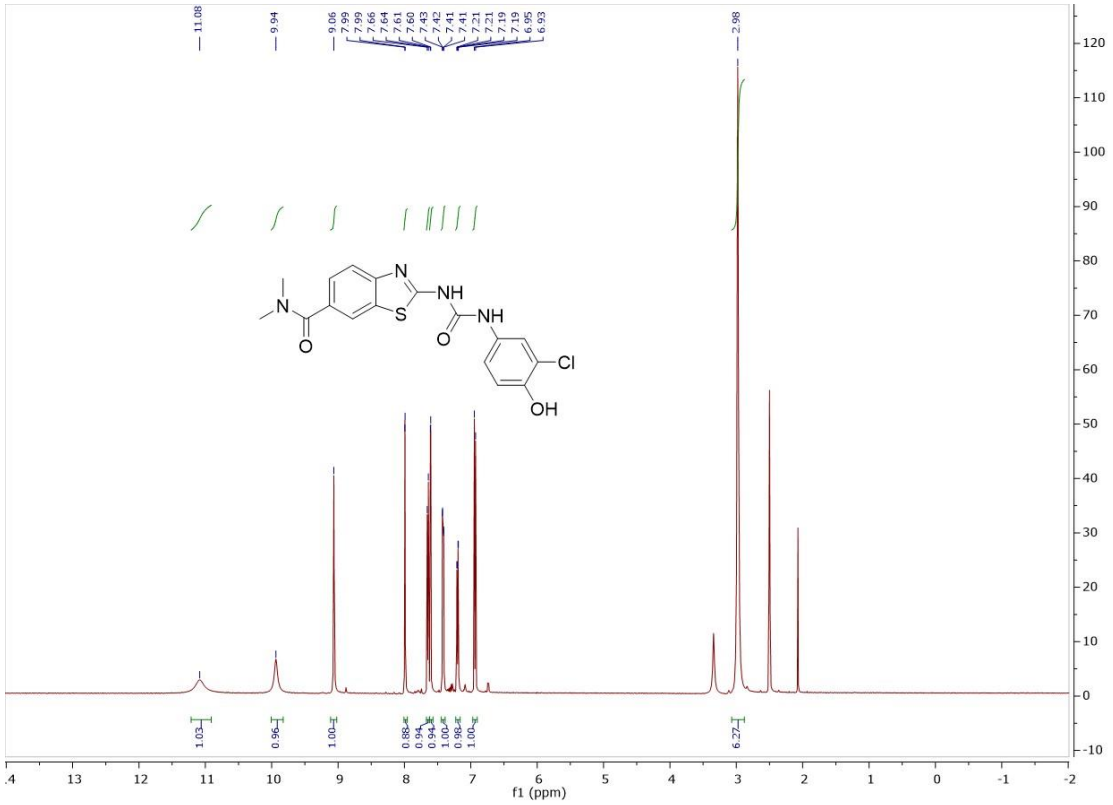

^{13}C NMR spectrum of compound **13** (126 MHz, DMSO-d_6)

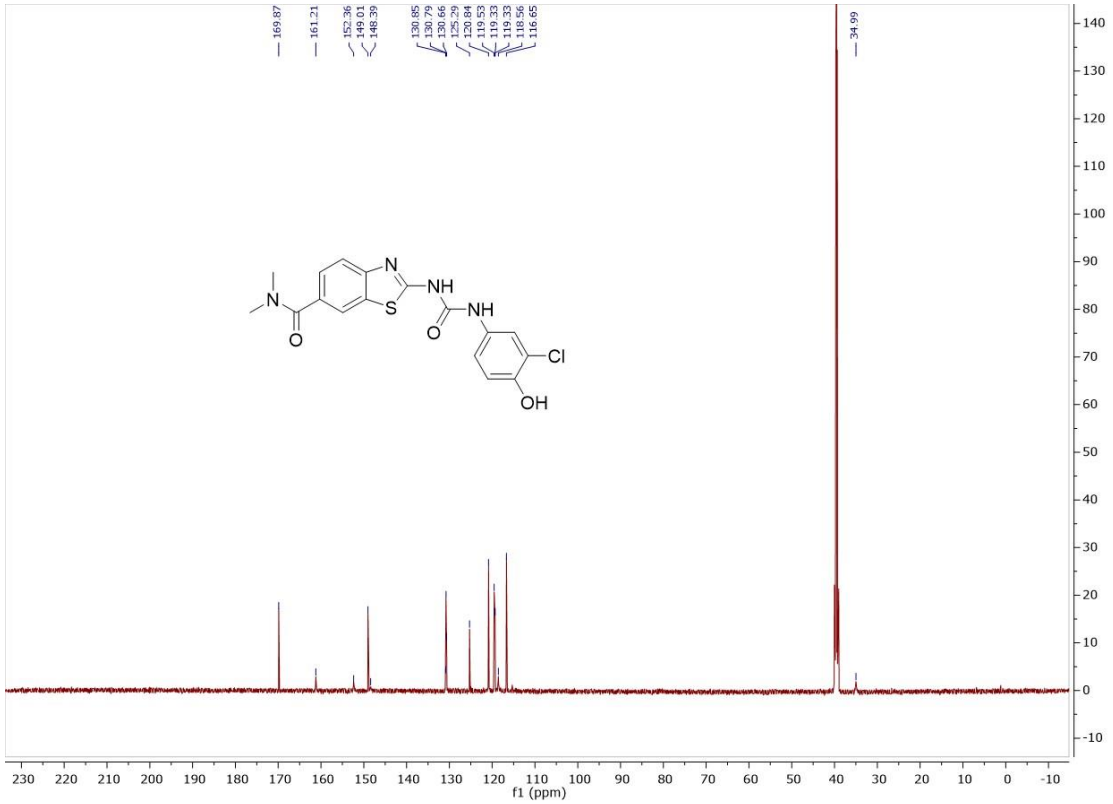

^{1}H NMR spectrum of compound **14** (500 MHz, DMSO-d_6)

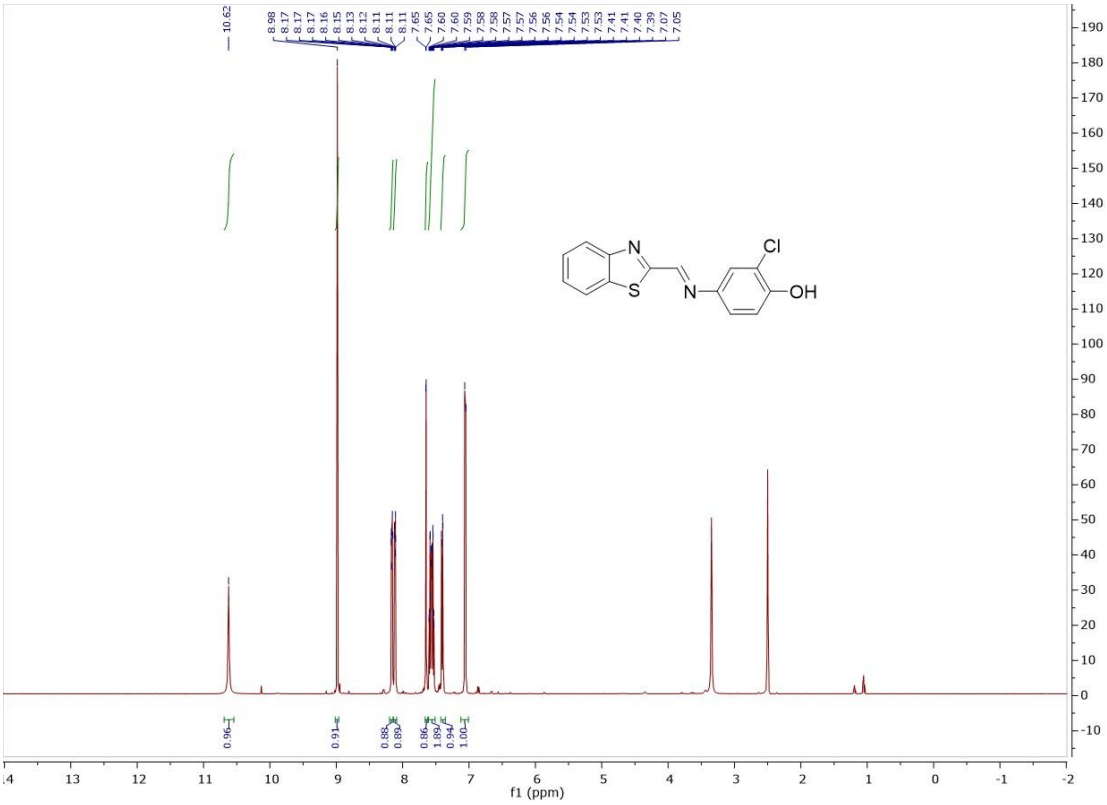

^{13}C NMR spectrum of compound **14** (126 MHz, DMSO-d_6)

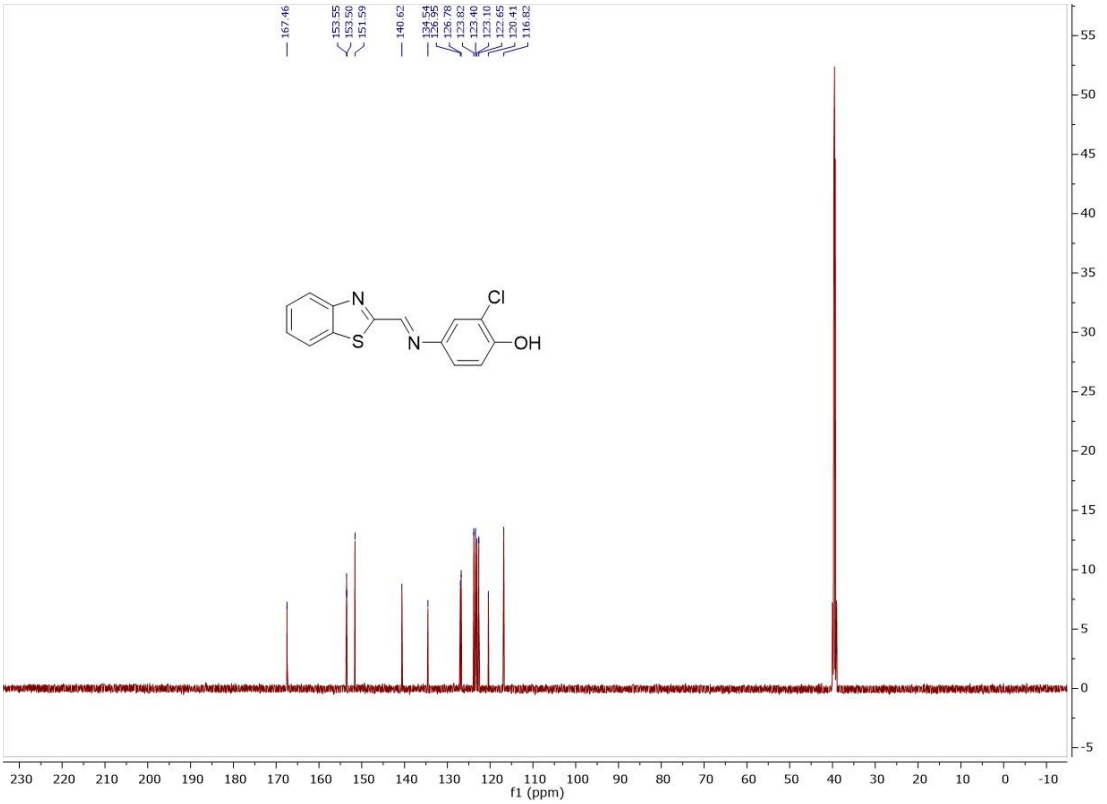

^{1}H NMR spectrum of compound **15** (500 MHz, DMSO-d_6)

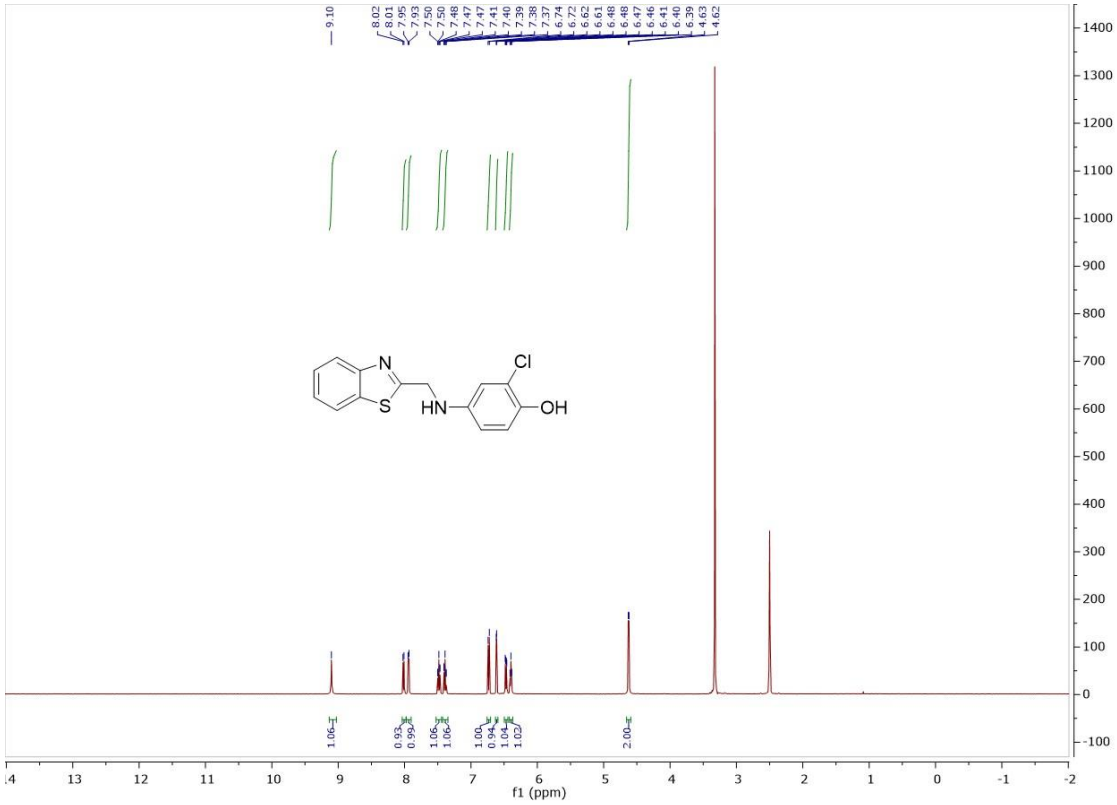

^{13}C NMR spectrum of compound **15** (126 MHz, DMSO-d_6)

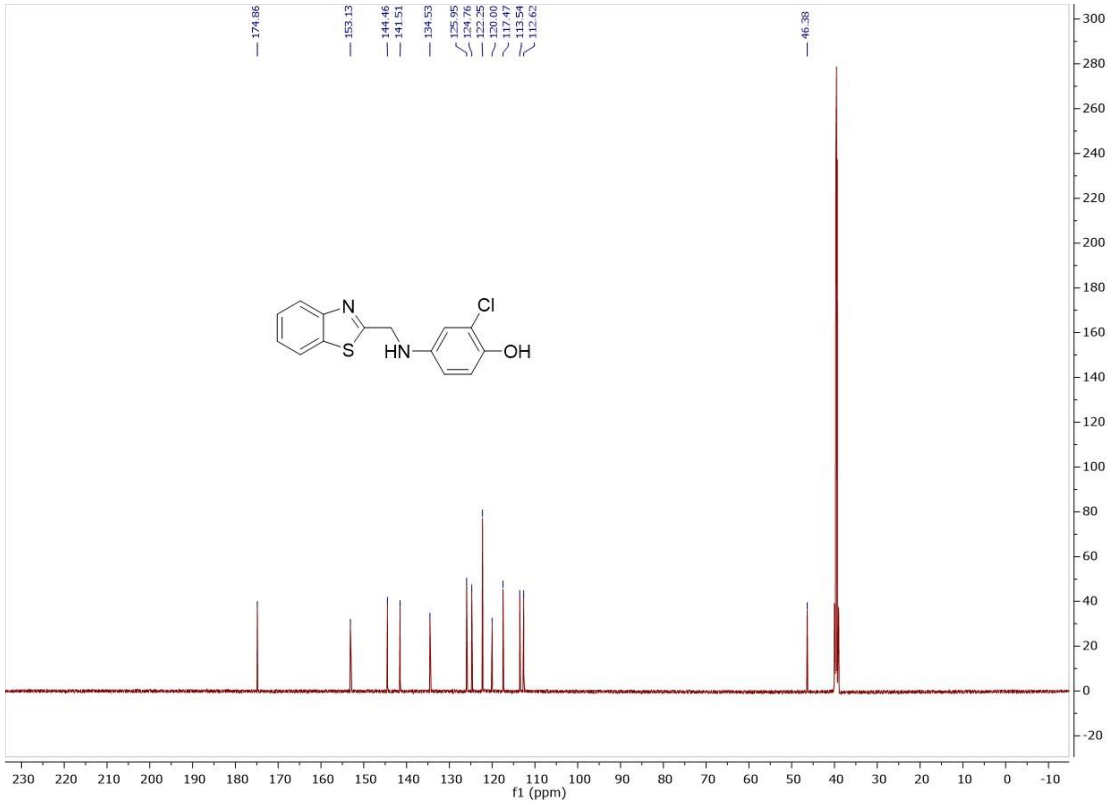

^{1}H NMR spectrum of compound **16** (500 MHz, DMSO-d_6)

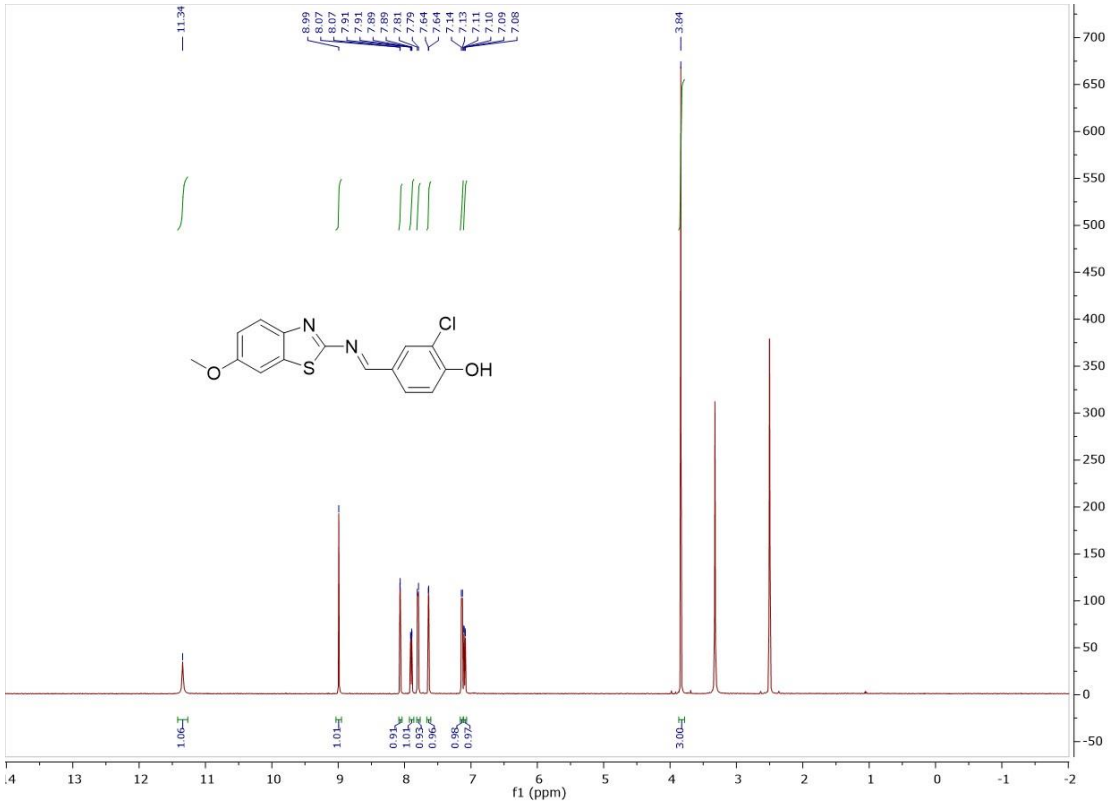

^{13}C NMR spectrum of compound **16** (126 MHz, DMSO-d_6)

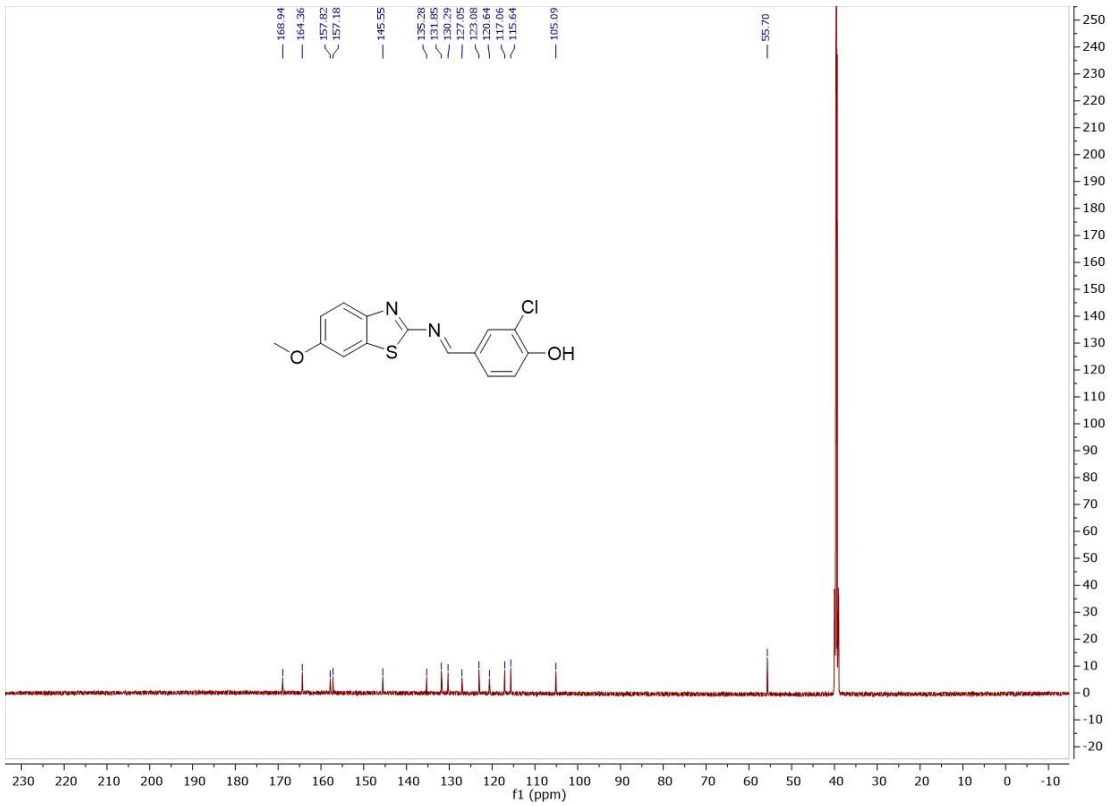

^{1}H NMR spectrum of compound **17** (500 MHz, DMSO-d_6)

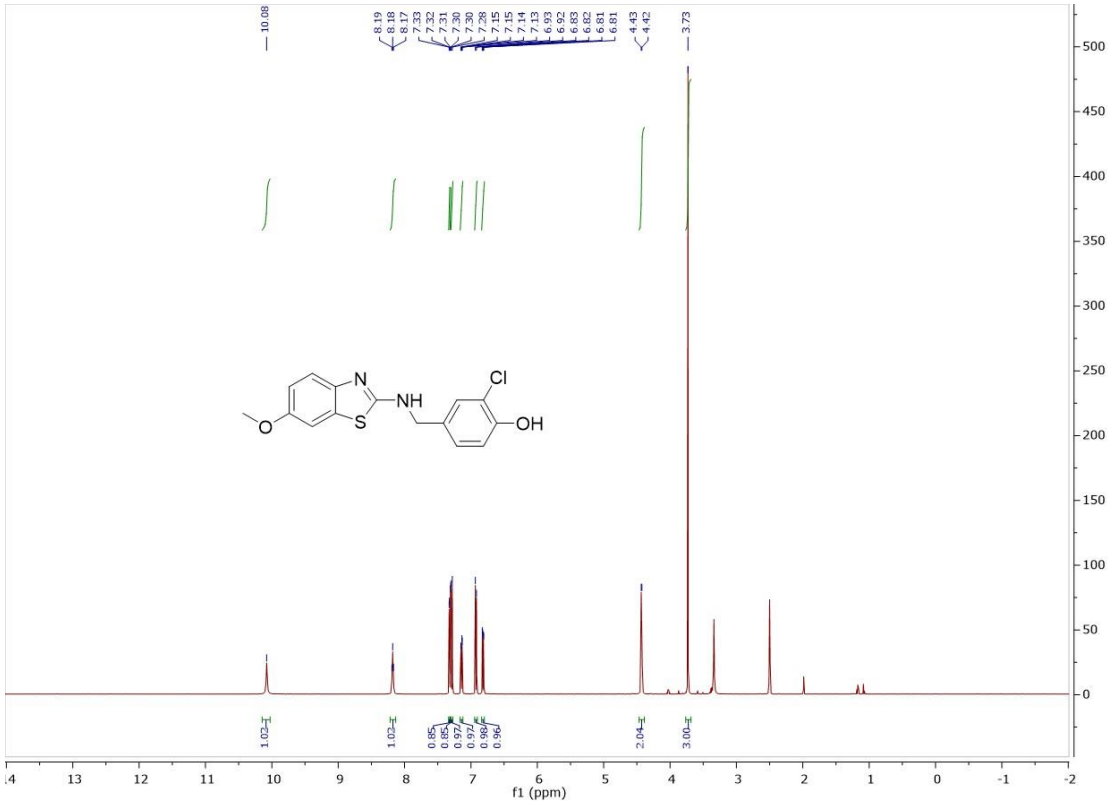

^{13}C NMR spectrum of compound **17** (126 MHz, DMSO-d_6)

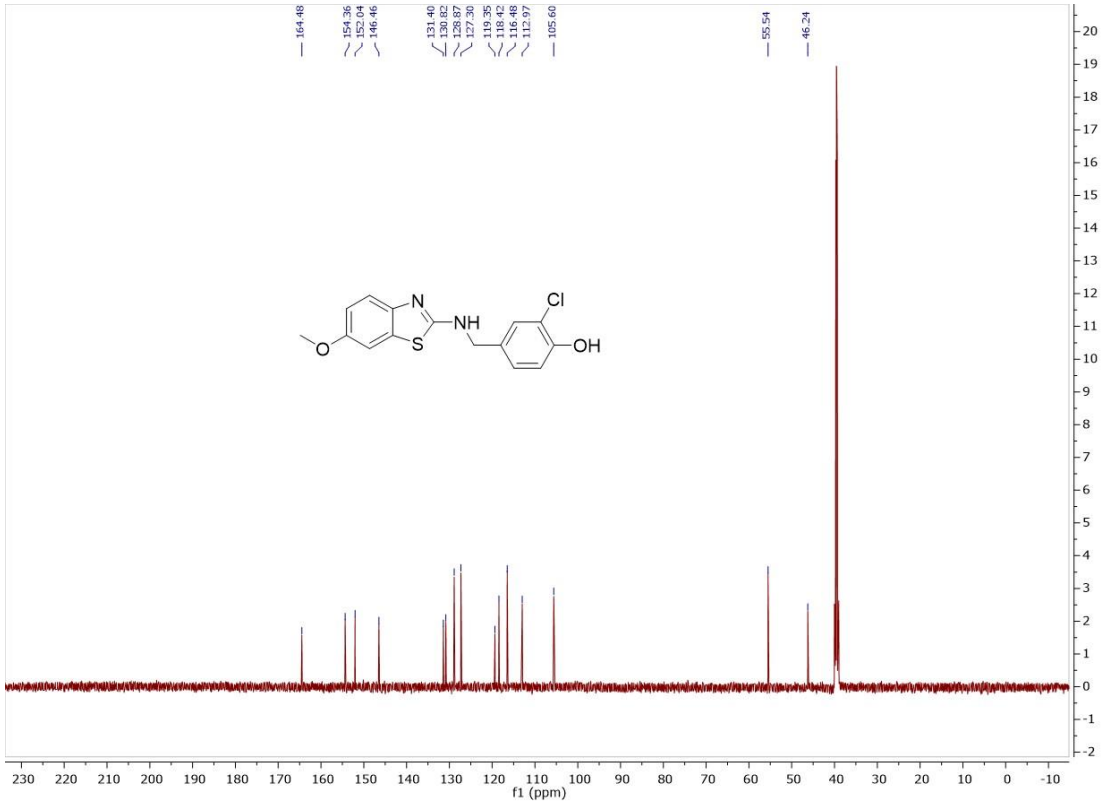

^{1}H NMR spectrum of compound **18** (500 MHz, Chloroform-*d*)

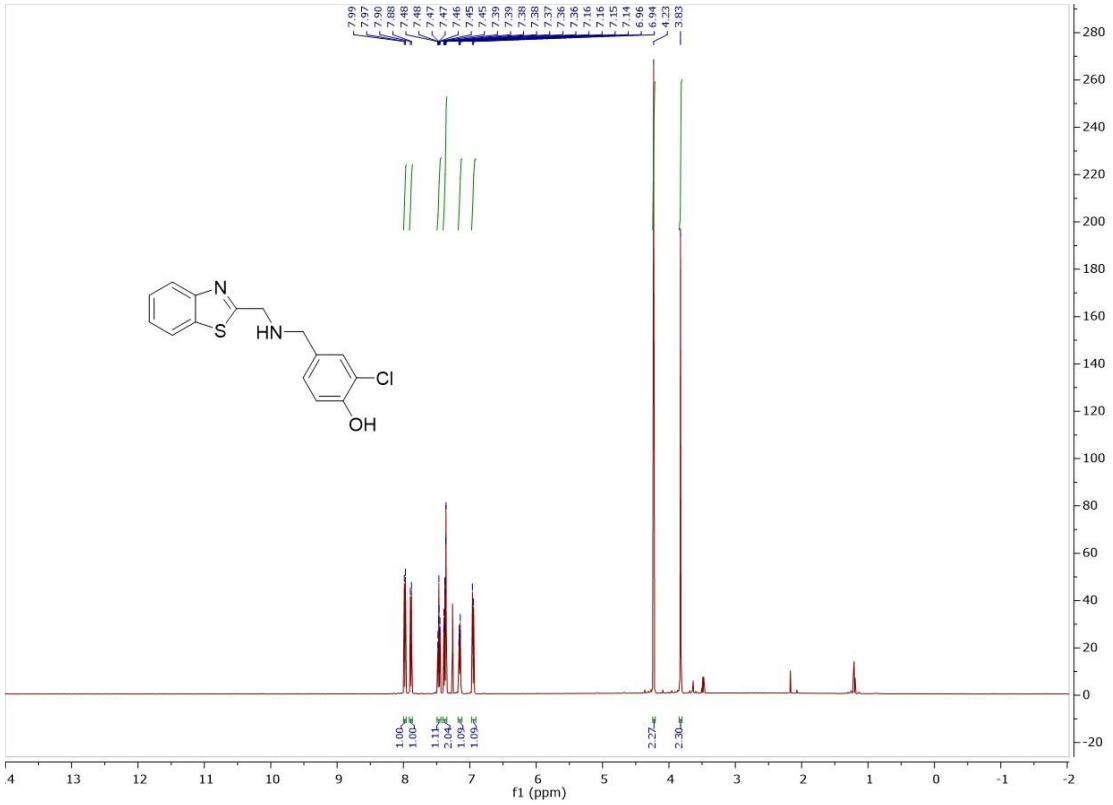

^{13}C NMR spectrum of compound **18** (126 MHz, Chloroform-*d*)

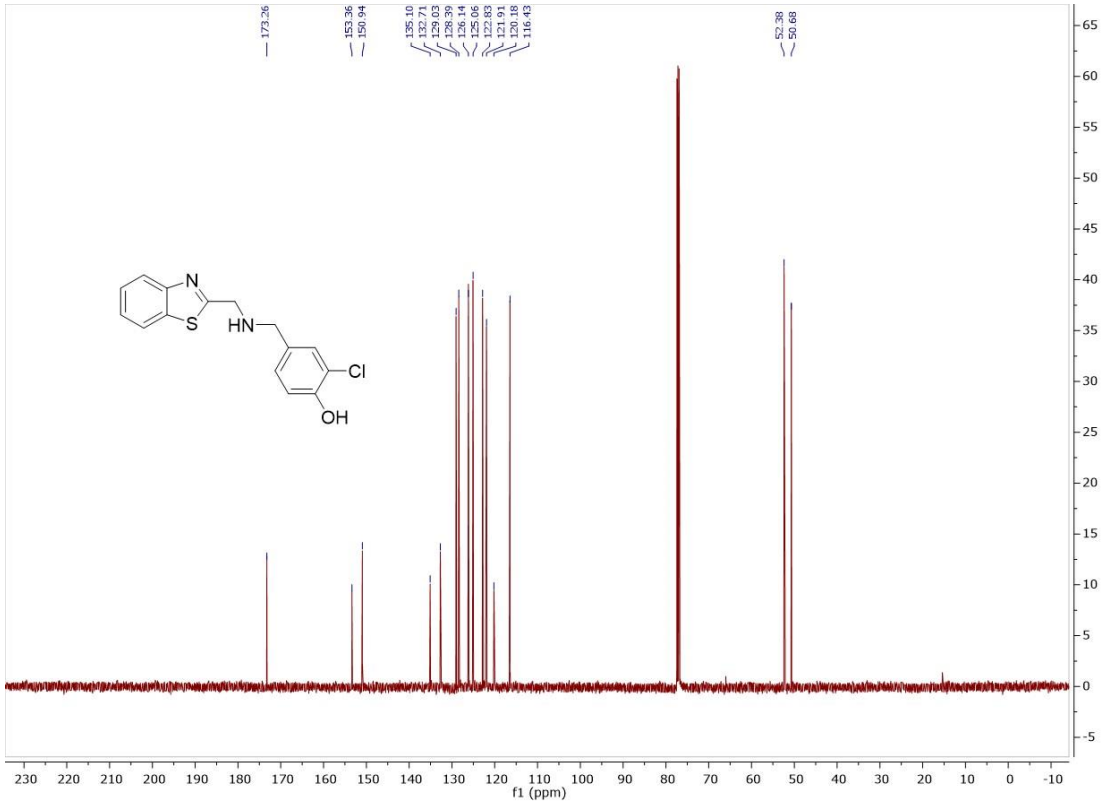

^{1}H NMR spectrum of compound **19** (500 MHz, Chloroform-*d*)

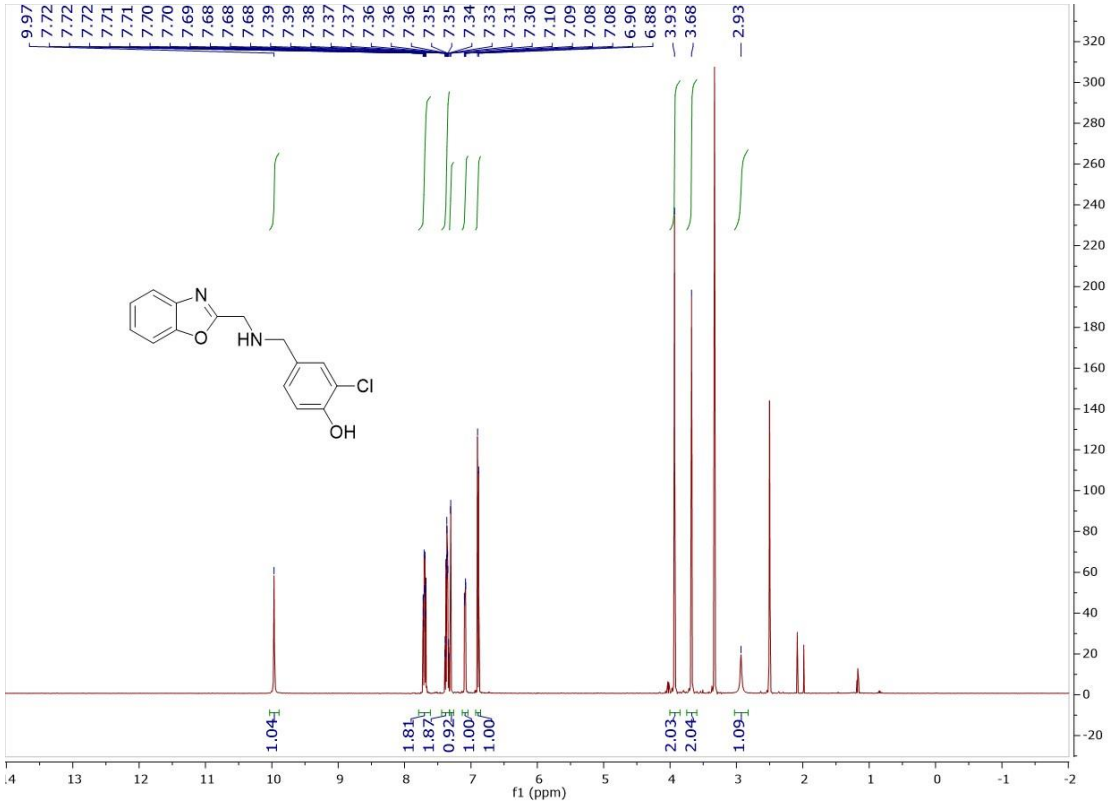

^{13}C NMR spectrum of compound **19** (126 MHz, Chloroform-*d*)

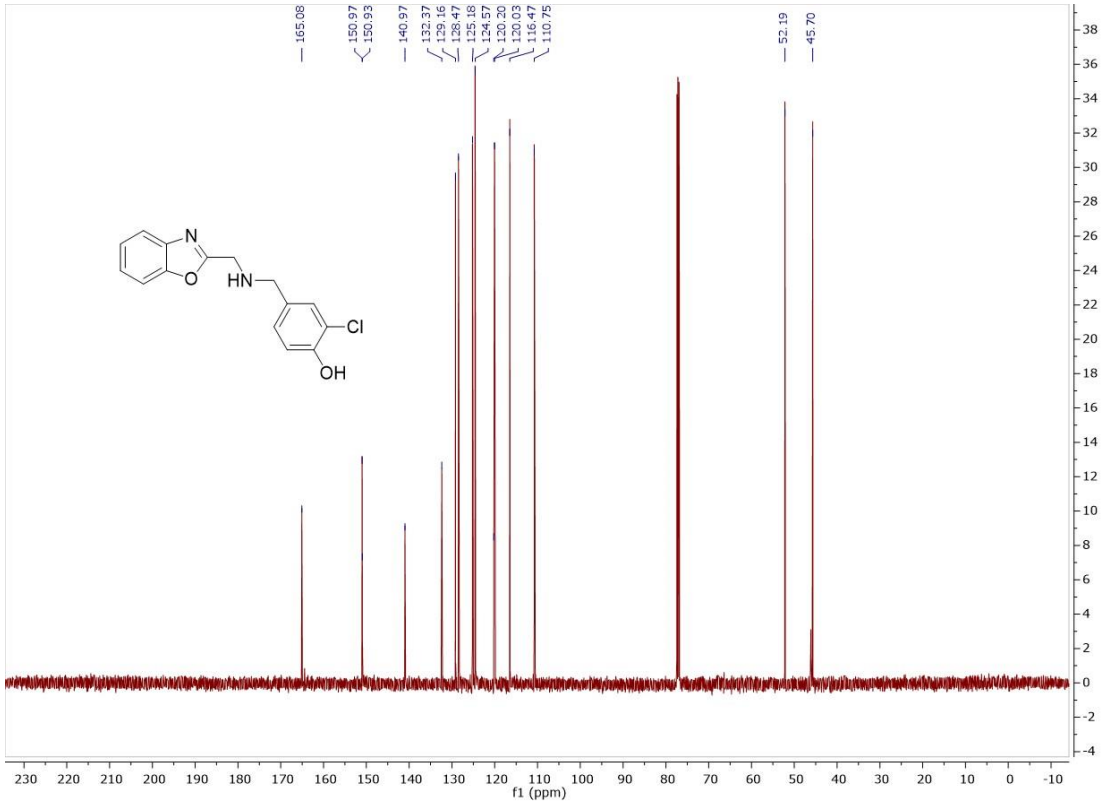

^{1}H NMR spectrum of compound **20** (500 MHz, DMSO-d_6)

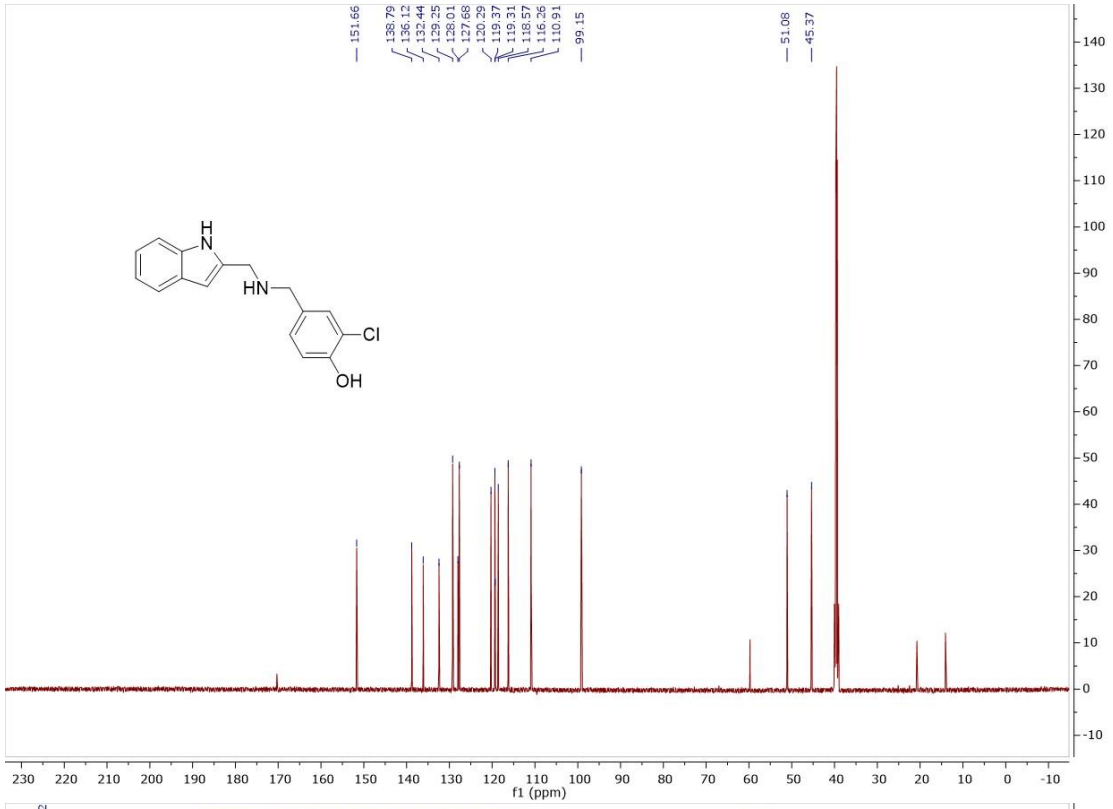

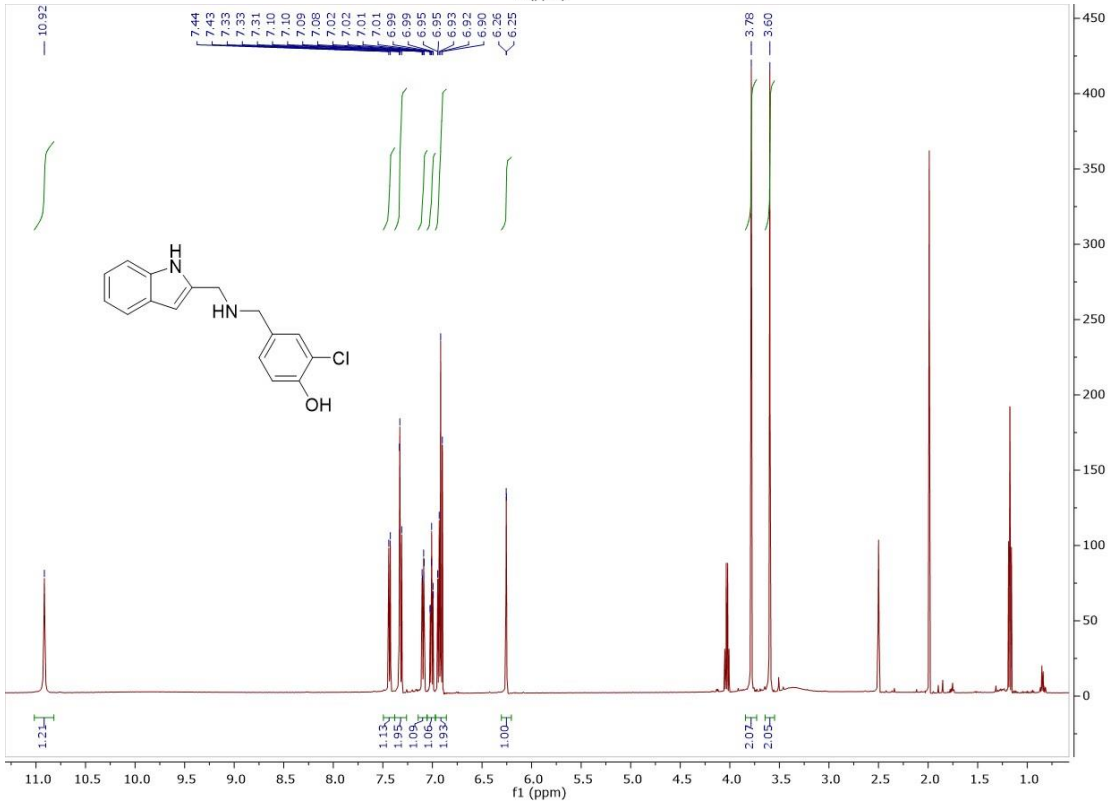

^{13}C NMR spectrum of compound **20** (126 MHz, DMSO-d_6)

HR-MS information of compound **6**

4-OB-40 #390 RT: 4.22 AV: 1 NL: 2.60E9
T: FTMS + p ESI Full ms [100.00-1500.0

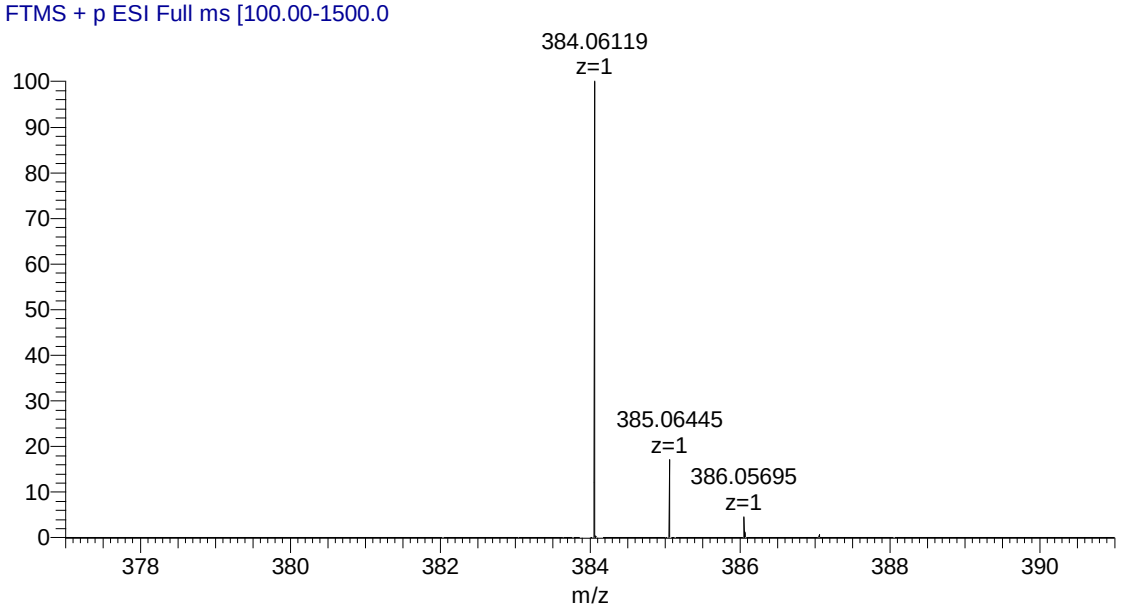

HR-MS information of compound **7**

4-OB-38 #982 RT: 9.43 AV: 1 NL: 3.85E7
T: FTMS + p ESI Full ms [100.00-1500.0

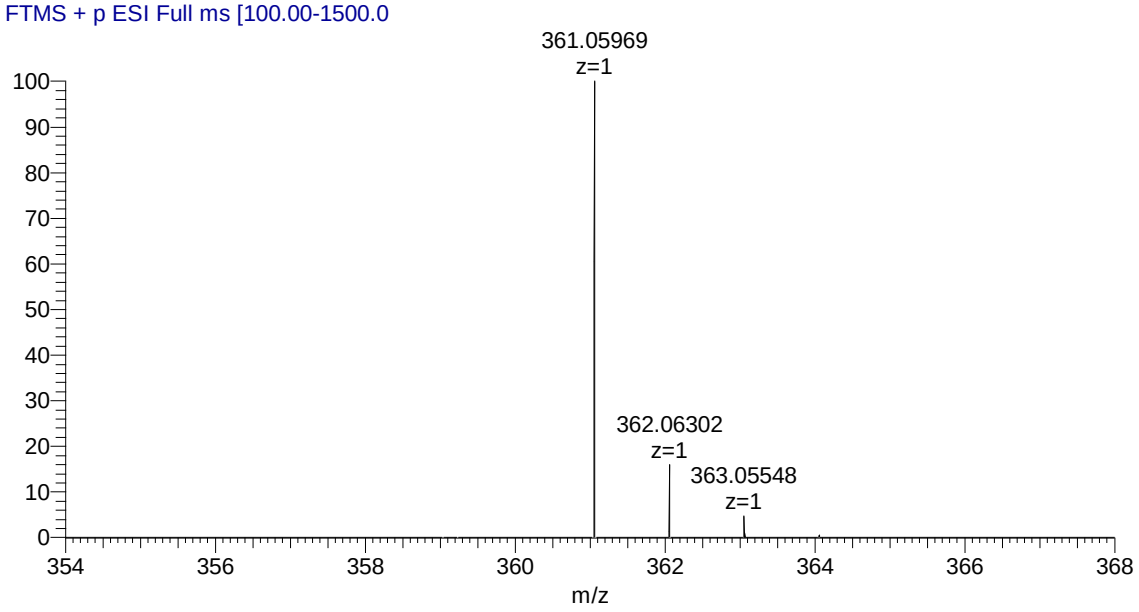

HR-MS information of compound **8**

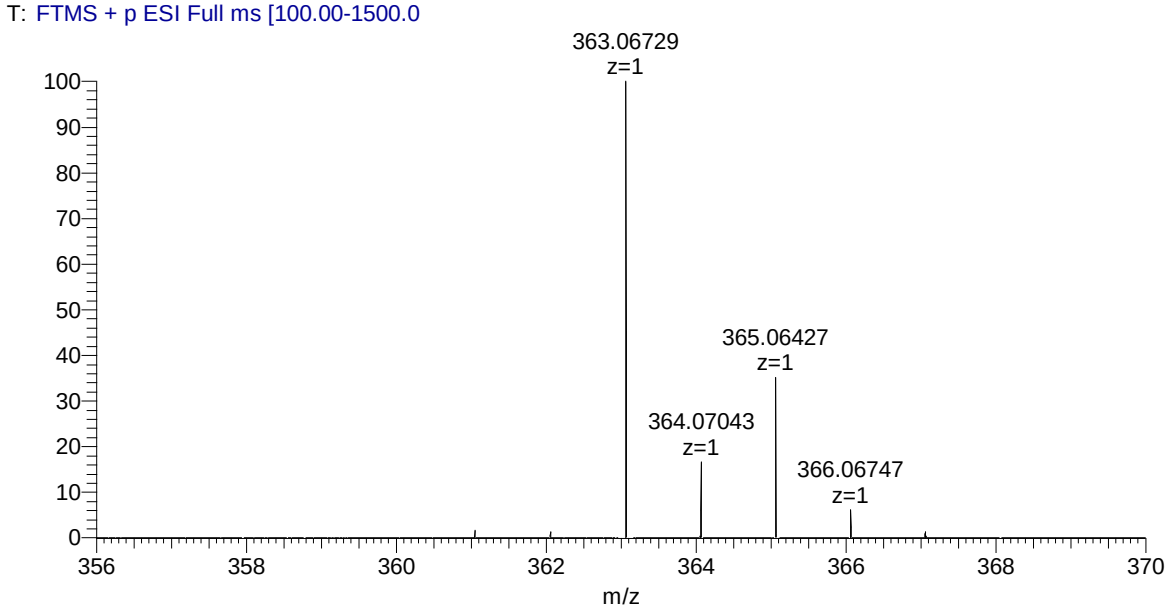

HR-MS information of compound **9**

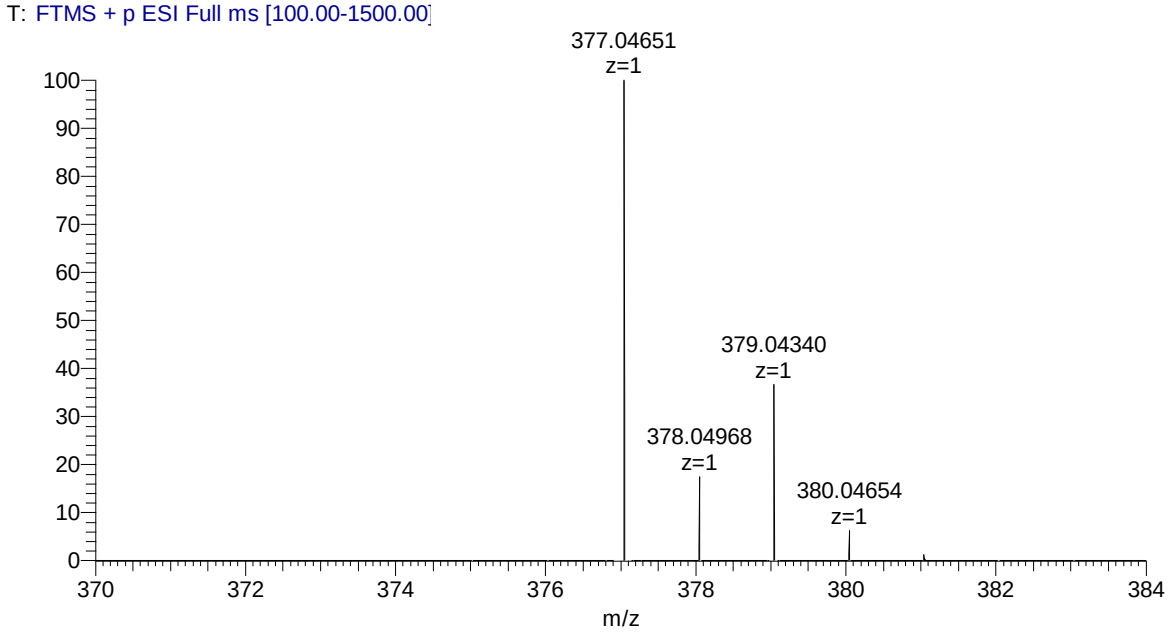

HR-MS information of compound **10**

2-LH-81 #423 RT: 4.58 AV: 1 NL: 2.39E9
T: FTMS + p ESI Full ms [100.00-1500.00]

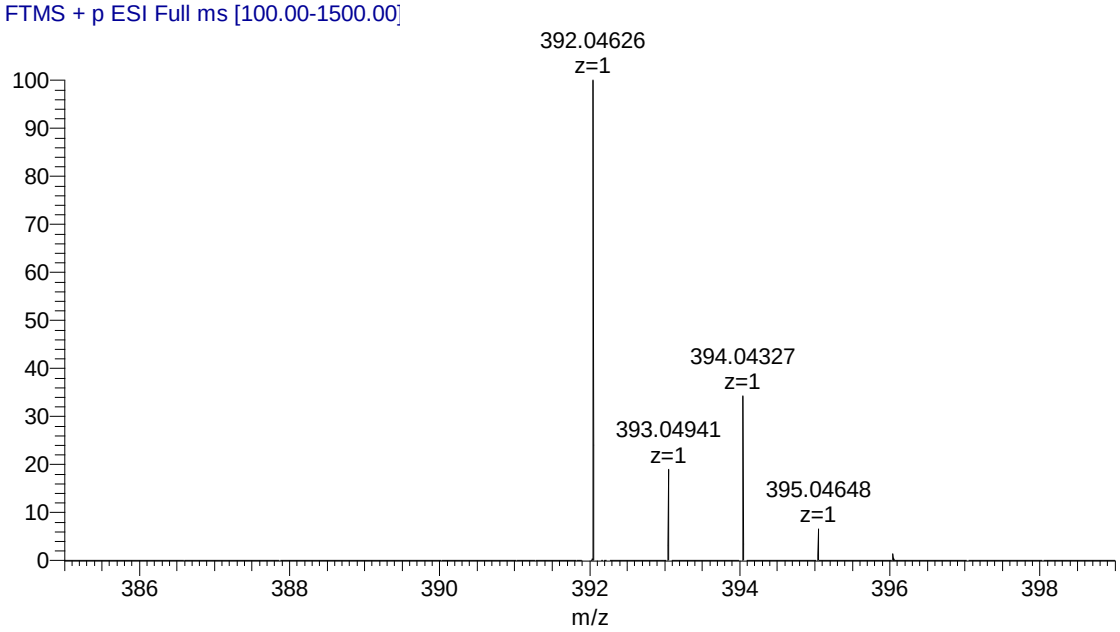

HR-MS information of compound **11**

3-OB-74 #382 RT: 4.05 AV: 1 NL: 5.15E8
T: FTMS + p ESI Full ms [100.00-1500.00]

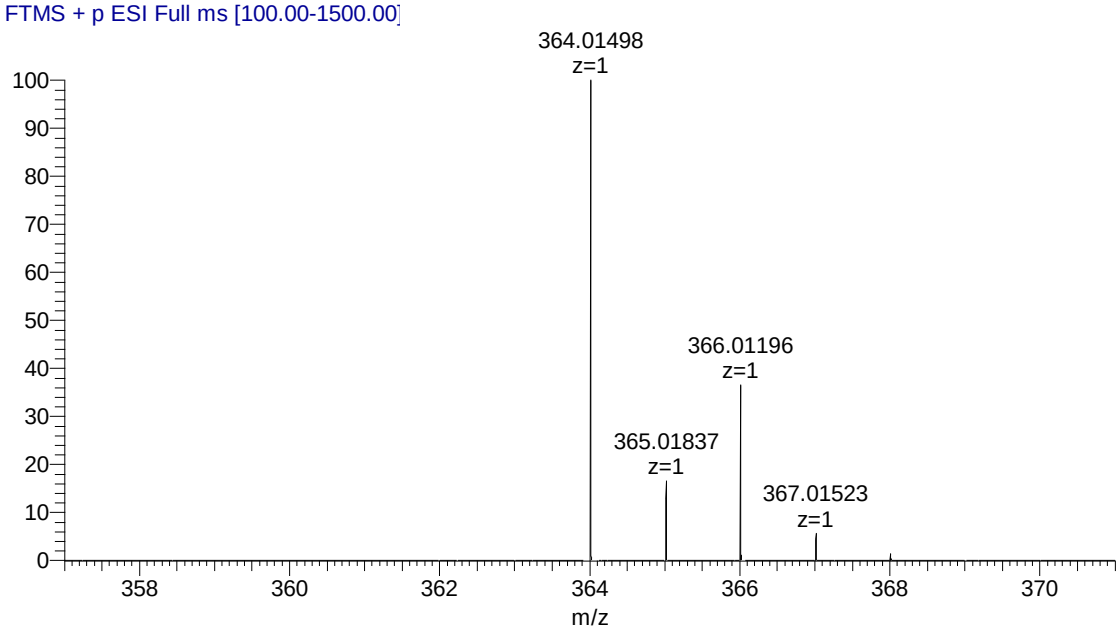

HR-MS information of compound **12**

3-LH-14 #341 RT: 3.72 AV: 1 NL: 5.42E8
T: FTMS + p ESI Full ms [100.00-1500.00]

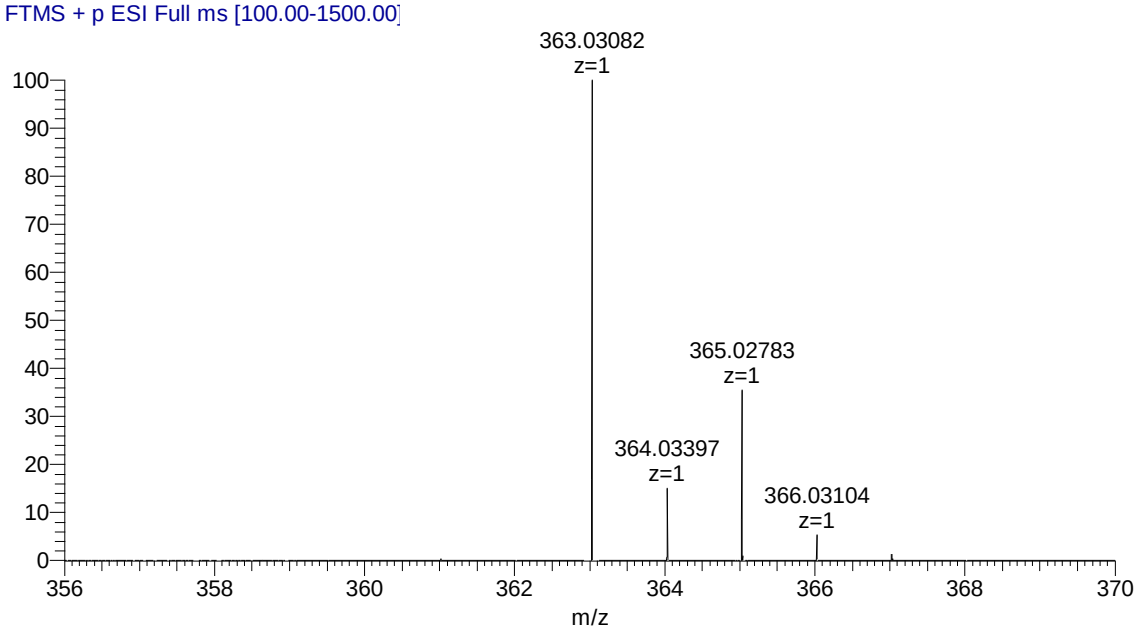

HR-MS information of compound **13**

2-LH-96 #370 RT: 4.02 AV: 1 NL: 1.34E9
T: FTMS + p ESI Full ms [100.00-1500.00]

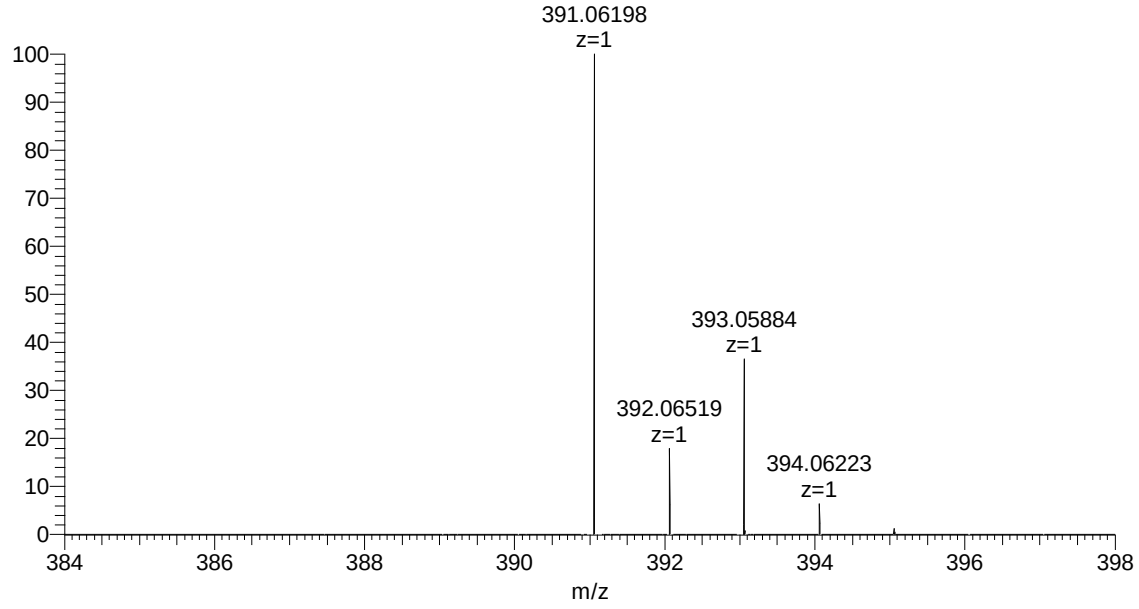

HR-MS information of compound **14**

2-LH-62_1 #677 RT: 4.49 AV: 1 NL: 8.09E7
T: FTMS + p ESI Full lock ms [100.00-150

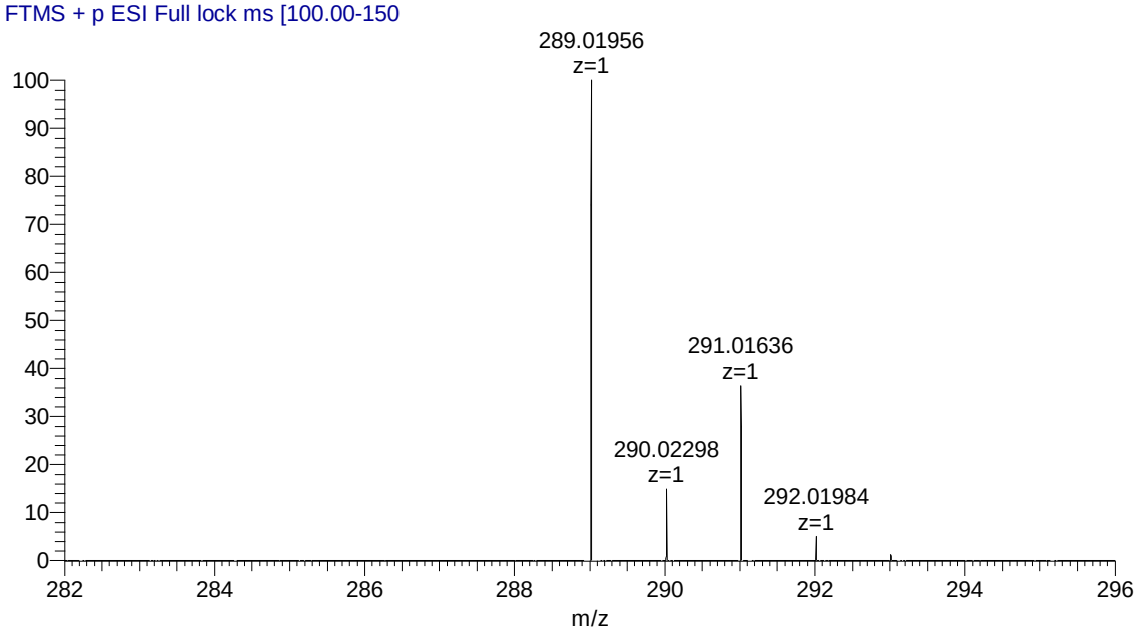

HR-MS information of compound **15**

2-LH-66_2 #378 RT: 4.04 AV: 1 NL: 1.02E9
T: FTMS + p ESI Full ms [100.00-1500.00]

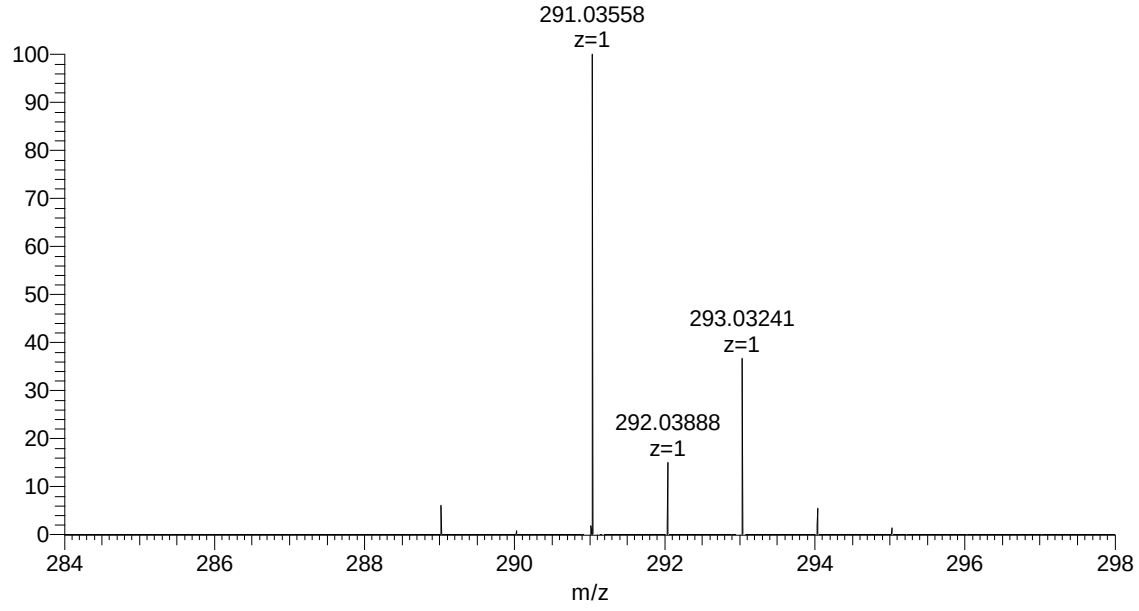

HR-MS information of compound **16**

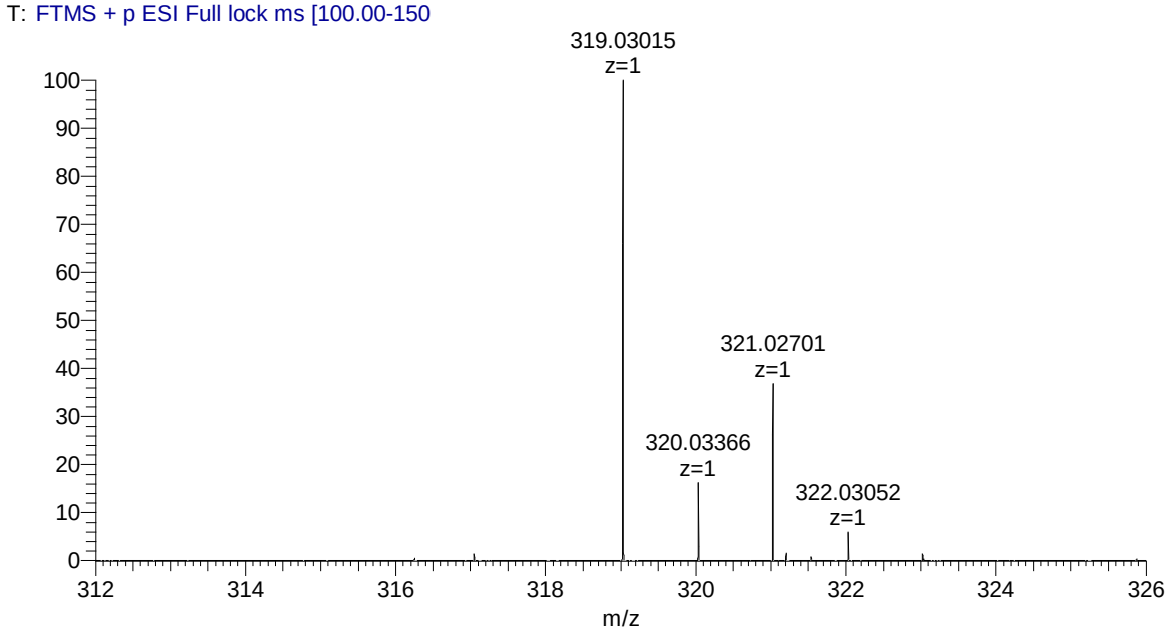

HR-MS information of compound **17**

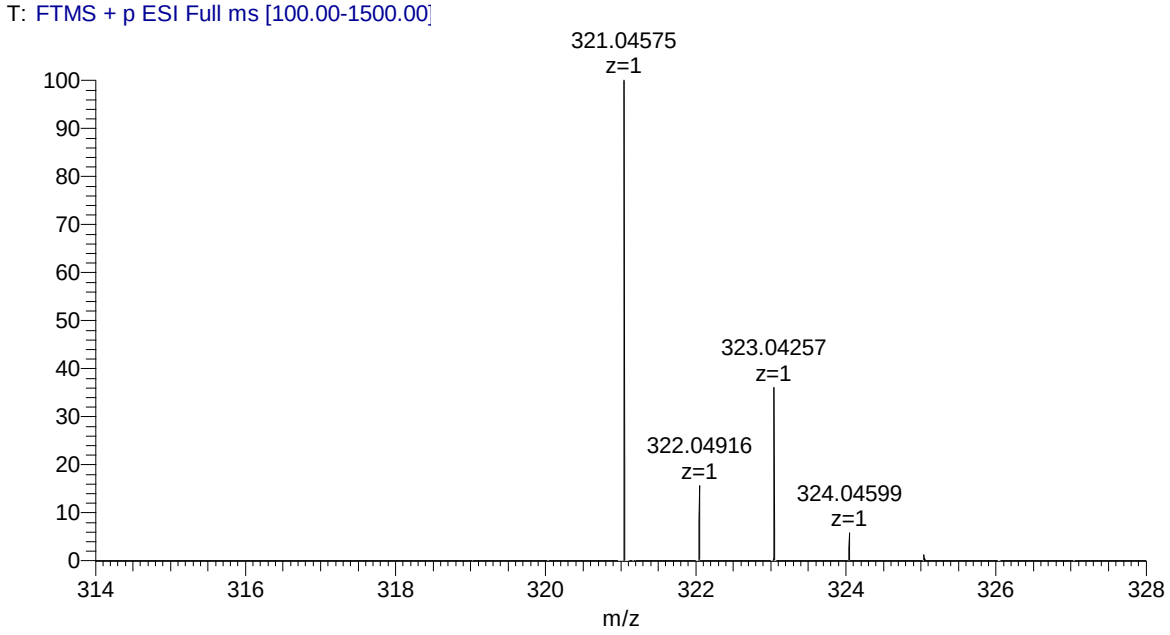

HR-MS information of compound **18**

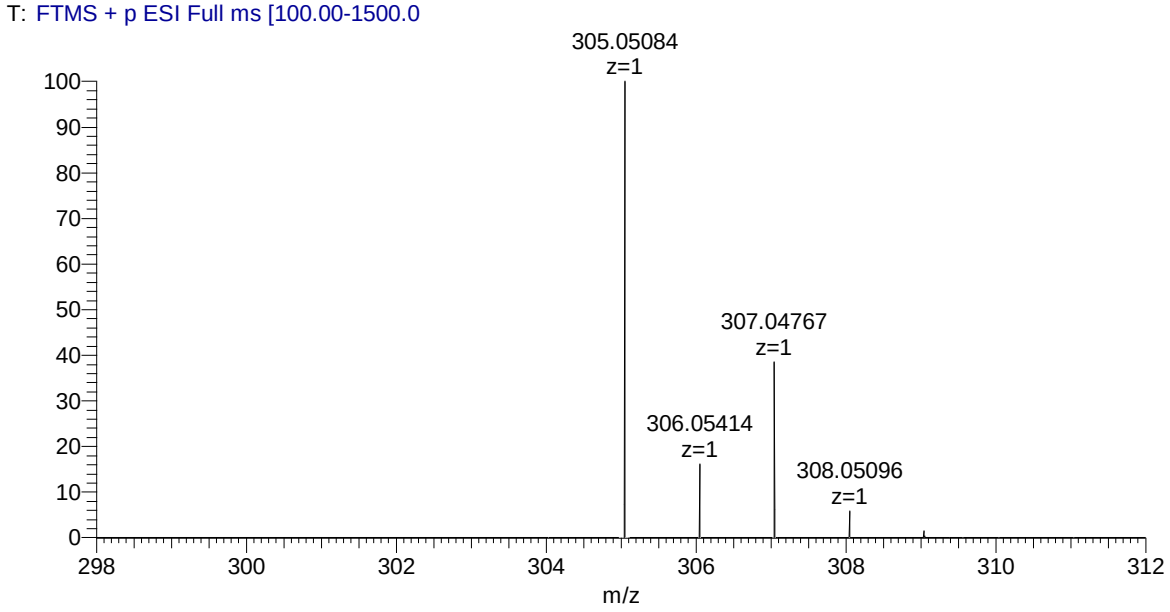

HR-MS information of compound **19**

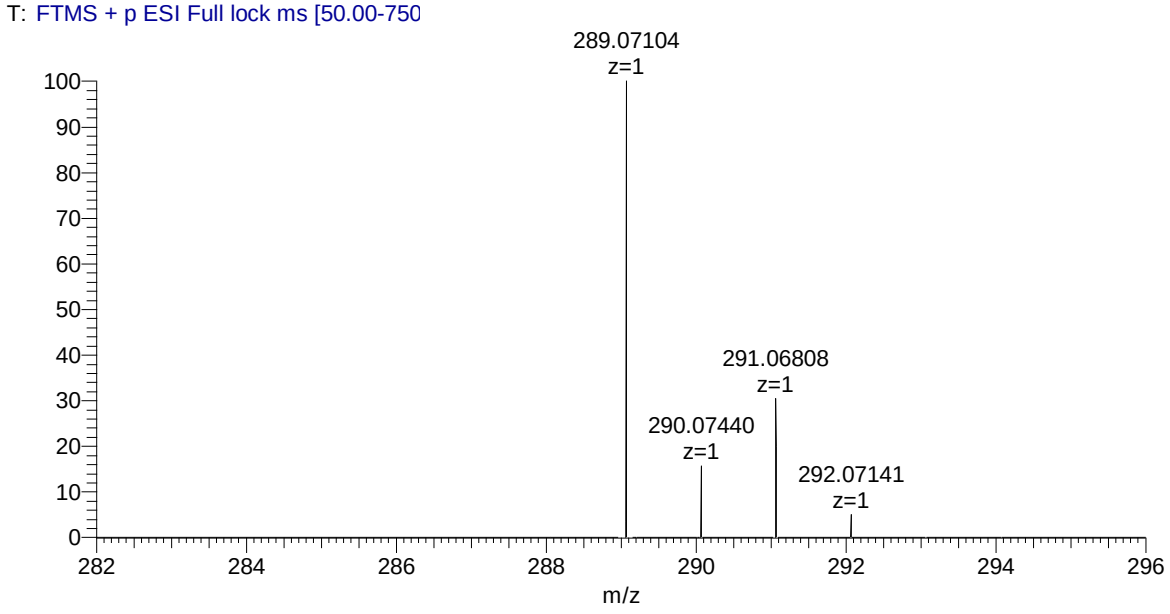

HR-MS information of compound **20**

4-OB-23 #336 RT: 3.47 AV: 1 NL: 1.90E8
T: FTMS + p ESI Full ms [100.00-1500.0

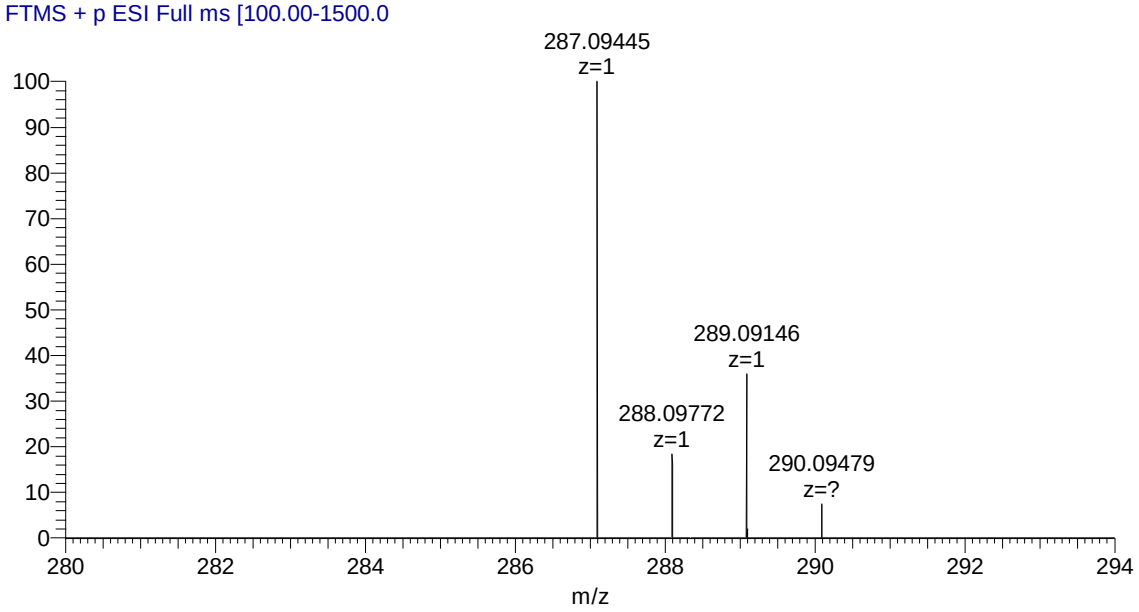

Molecular docking

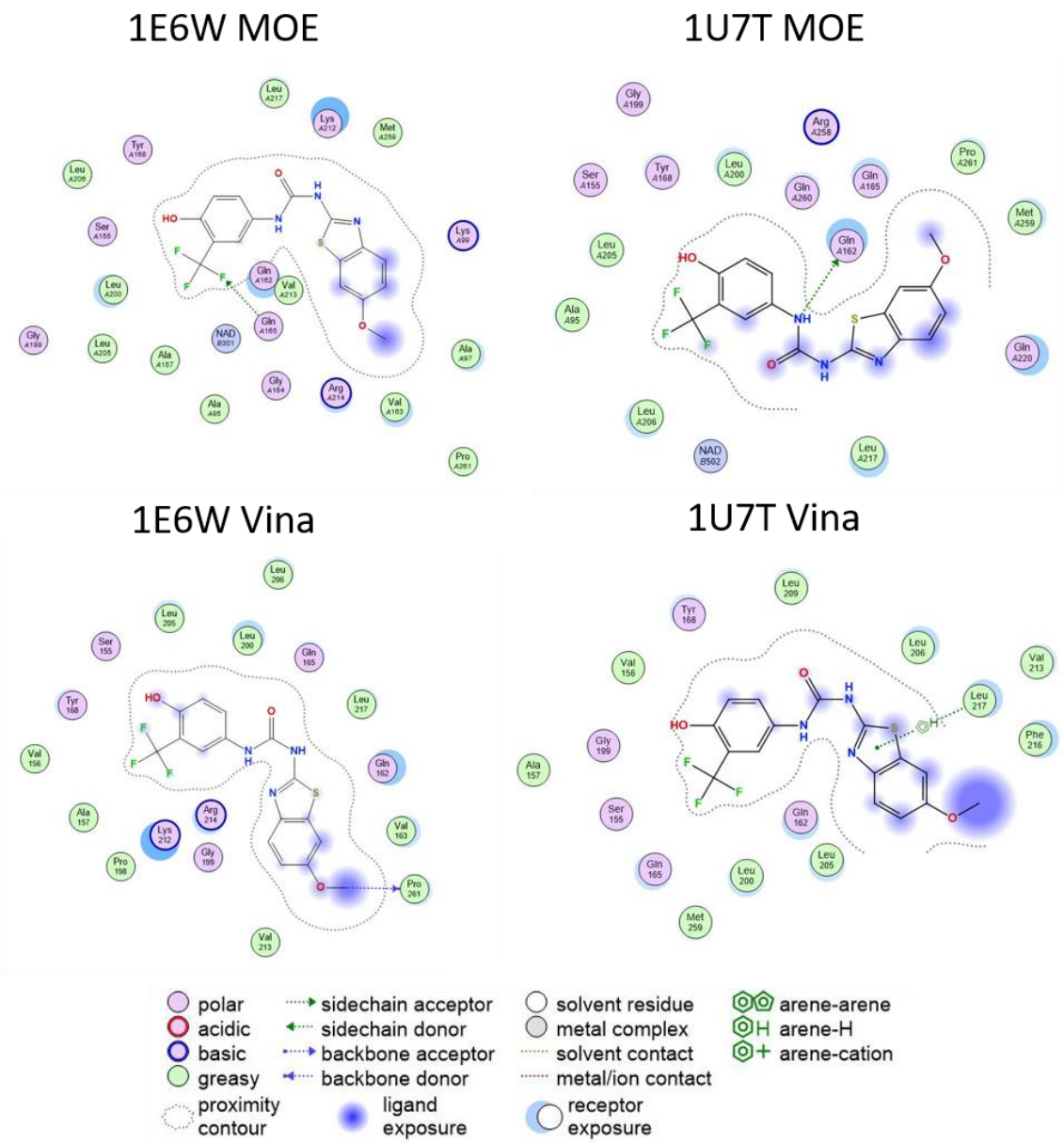

Figure S1: 2D representation of binding interactions of compound **6** within the active site.

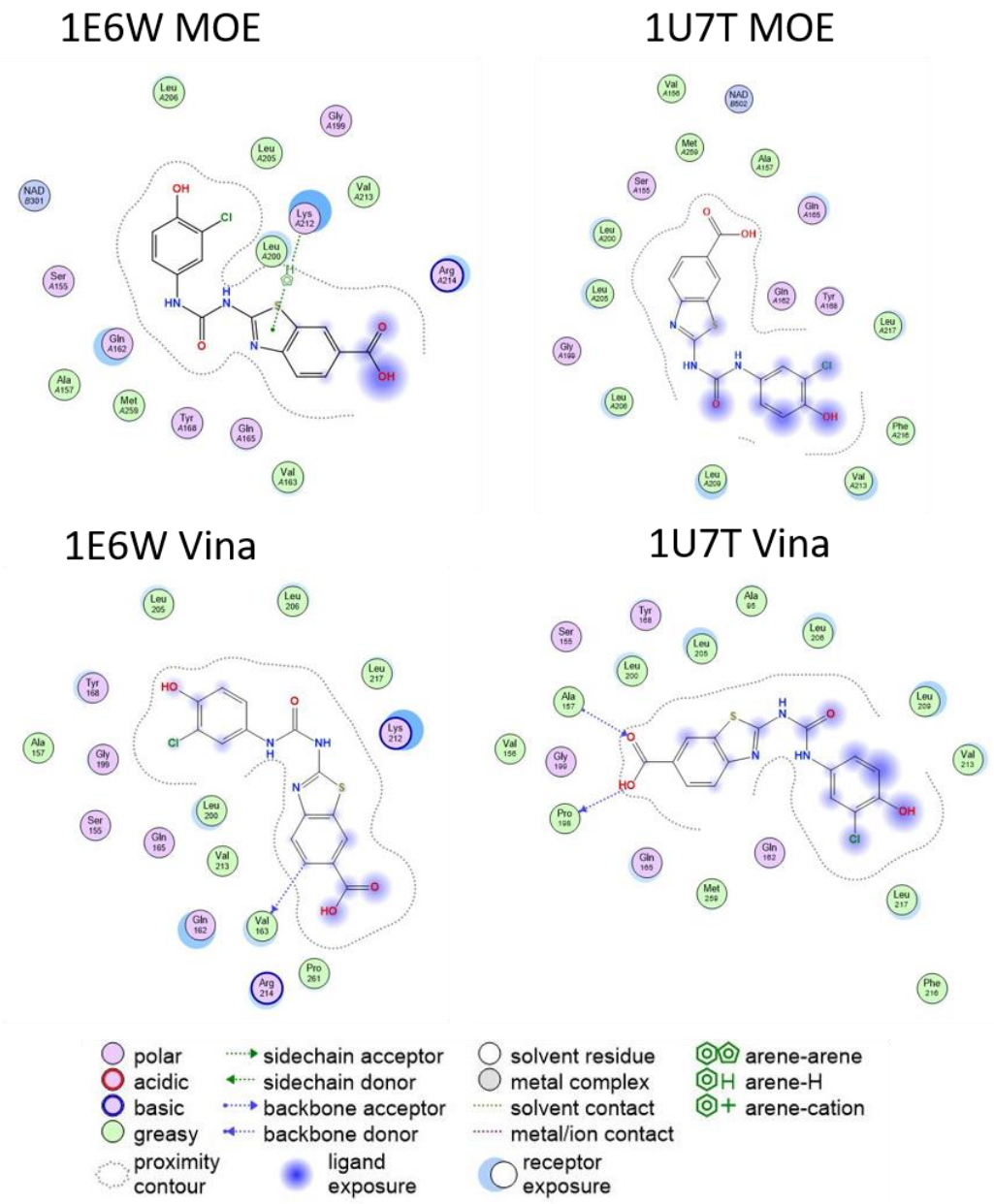

Figure S2: 2D representation of binding interactions of compound **11** within the active site.

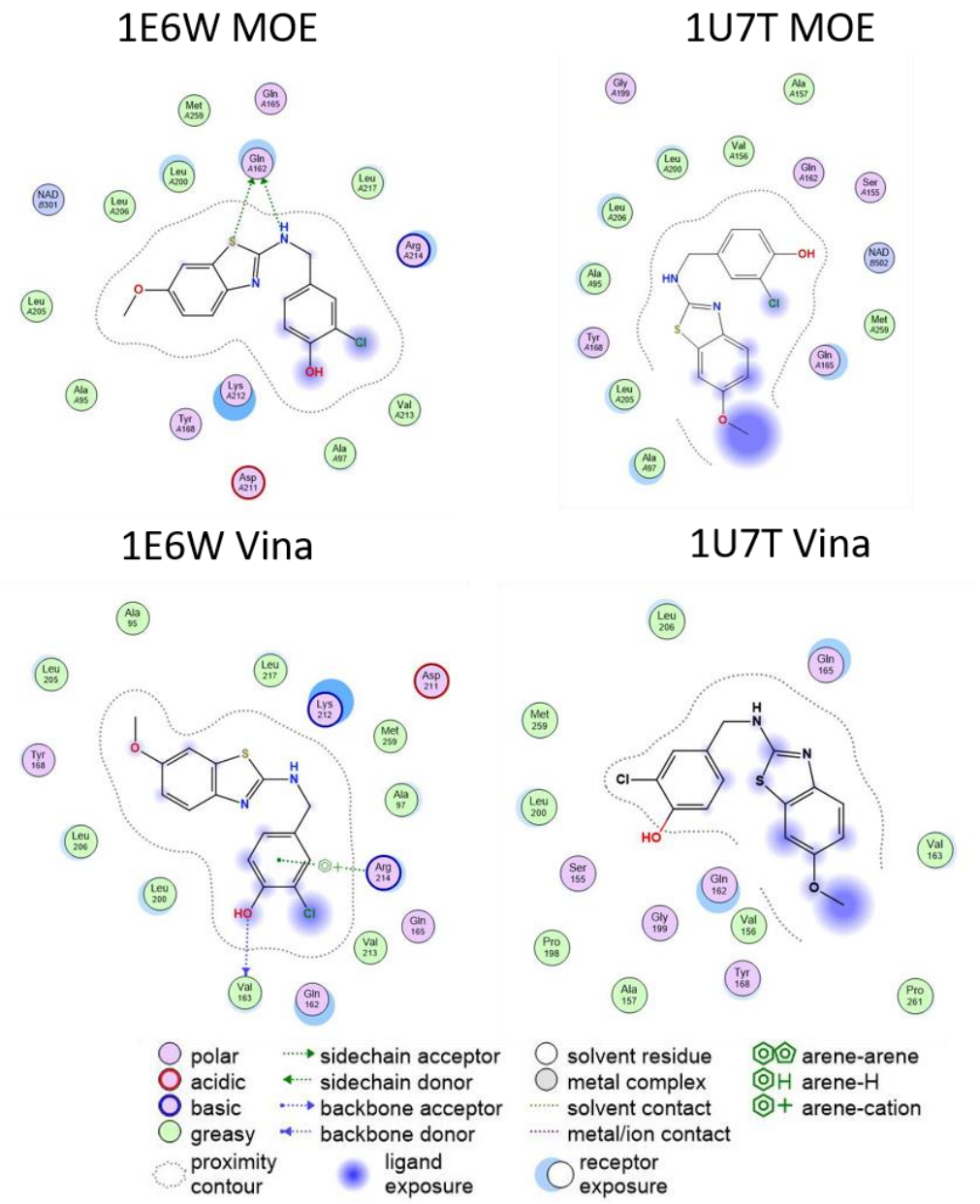

Figure S3: 2D representation of binding interactions of compound **17** within the active site.

Lactate dehydrogenase (LDH) assay

Compounds **9** and **11** were evaluated using lactate dehydrogenase (LDH) assay to further confirm results cytotoxicity testing. LDH assay is a colorimetric assay routinely used to quantitatively measure LDH released into the media from damaged cells as a biomarker for cellular cytotoxicity and cytolysis. Cell cytotoxicity of **9** and **11** at 25µM concentration was assessed on HEK293 cell line after 24 hours incubation. All three compounds showed only slight cytotoxicity (< 15 % increase compared to control; Table S1), which was in accordance with the results from CellTiter-Glo/CellTox Green assay, WST-1 test, and monochlorobimane assay (Figures 9 and 10 in the main manuscript).

Table S1: Cytotoxicity at 25µM concentration measured by LDH assay.

Compound	LDH cytotoxicity (%)
9	14.3 ± 1.8
11	11.4 ± 0.7

Notes: Data are presented as the mean ± standard deviation (SEM).

LDH methodology

Cell cytotoxicity was assessed via the measurement of lactate dehydrogenase leakage into the culture medium using a commercially available kit from Pierce (Thermo Scientific, UK, cat no. 88953). This was carried out in accordance with the kit guidelines, with the activity of LDH being calculated from the change in absorbance at 340 nm as NADH is reduced. HEK293 cells overexpressing mts17β-HSD10 were cultured in phenol-red free media (10% FBS, 1 mM sodium pyruvate, 100 units penicillin, 0.1 mg/mL streptomycin and 2 mM L-glutamine) and seeded at a density of 10,000 cells per well (100 µL, 96-well plates). Cells were then treated with the compound of interest at 25µM concentration in triplicate. Treated cells were then incubated at 37 °C and CO_2 (5%) for 24 h before the LDH assay was performed as per the manufacturer's instructions. Spontaneous control (water) and maximum control (lysis buffer) used in accordance with the kit guide. Absorbance was measured at 490 nm and 680 nm using the SpectraMaxM2e spectrophotometer (Molecular Devices, San Jose, CA, USA). The measured LDH activity was used to calculate % cytotoxicity using the following equation:

$$\%\ \text{cytotoxicity} = \frac{(\text{compound treated LDH Activity} - \text{Spontaneous LDH Activity})}{(\text{Maximum LDH Activity} - \text{Spontaneous LDH Activity})}\ \text{x}100$$

10.3 Publikace III

Schmidt, M.†; **Vaskova, M.**†; Rotterova, A., Fiandova, P., Miskerikova, M., Zemanova, L., Benek, O., Musilek, K., 2023. Physiologically Relevant Fluorescent Assay for Identification of 17β-hydroxysteroid dehydrogenase type 10 Inhibitors. J. Neurochem. 167, 154–167. https://doi.org/10.1111/jnc.15917

Check for updates

Received: 7 March 2023 | Revised: 29 June 2023 | Accepted: 3 July 2023

DOI: 10.1111/jnc.15917

Journal of Neurochemistry JNC WILEY

ORIGINAL ARTICLE

Physiologically relevant fluorescent assay for identification of 17β-hydroxysteroid dehydrogenase type 10 inhibitors

Monika Schmidt | Michaela Vaskova | Aneta Rotterova | Pavlina Fiandova | Marketa Miskerikova | Lucie Zemanova | Ondrej Benek | Kamil Musilek

Department of Chemistry, Faculty of Science, University of Hradec Kralove, Hradec Kralove, Czech Republic

Correspondence
Monika Schmidt and Ondrej Benek, Department of Chemistry, Faculty of Science, University of Hradec Kralove, Rokitanskeho 62, 500 02 Hradec Kralove, Czech Republic.
Email: monika.schmidt@uhk.cz and ondrej.benek@uhk.cz

Funding information
University of Hradec Kralove, Grant/Award Number: SV2103-2022

Abstract

Mitochondrial enzyme 17β-hydroxysteroid dehydrogenase type 10 (HSD10) is a potential molecular target for treatment of mitochondrial-related disorders such as Alzheimer's disease (AD). Its over-expression in AD brains is one of the critical factors disturbing the homeostasis of neuroprotective steroids and exacerbating amyloid beta (Aβ)-mediated mitochondrial toxicity and neuronal stress. This study was focused on revalidation of the most potent HSD10 inhibitors derived from benzothiazolyl urea scaffold using fluorescent-based enzymatic assay with physiologically relevant substrates of 17β-oestradiol and allopregnanolone. The oestradiol-based assay led to the identification of two nanomolar inhibitors (IC_{50} 70 and 346 nM) differing from HSD10 hits revealed from the formerly used assay. Both identified inhibitors were found to be effective also in allopregnanolone-based assay with non-competitive or uncompetitive mode of action. In addition, both inhibitors were confirmed to penetrate the HEK293 cells and they were able to inhibit the HSD10 enzyme in the cellular environment. Both molecules seem to be potential lead structures for further research and development of HDS10 inhibitors.

KEYWORDS
17β-oestradiol, 17β-HSD10, allopregnanolone, Alzheimer's disease, benzothiazole, CHANA

1 | INTRODUCTION

A mitochondrial enzyme 17β-hydroxysteroid dehydrogenase type 10 (HSD10, EC 1.1.1.178) is involved in the oxidation of a wide variety of substrates, for example, alcohols, fatty acids and steroids, and appears to play an essential role in the energy metabolism of mitochondria and cellular response to stress (He et al., 2001). This multifunctional enzyme is expressed in all human tissue types, including the brain (Yang & He, 2001), where its levels seem to be region specific, when high levels were found in the hippocampus, hypothalamus and amygdala (He, Wegiel, & Yang, 2005). Enzyme HSD10 is known to possess multiple essential functions inside the mitochondria (e.g. reviewed in Morsy & Trippier, 2019; Vinklarova et al., 2020), and its complete depletion is connected with embryonic lethality in animals or humans, thus leading to death (Zschocke, 2012).

HSD10 is known to be connected with the pathophysiology of neurodegenerative diseases, in particular Alzheimer's (AD) and Parkinson's disease, as well as certain forms of cancer (He

Abbreviations: AAC, acetoacetyl coenzyme A; AD, Alzheimer's disease; ALLOP, allopregnanolone; Aβ, amyloid beta; CHANA, cyclohexenyl amino naphthalene alcohol; CHANK, cyclohexenyl amino naphthalene ketone; DMSO, dimethyl sulfoxide; DSF, differential scanning fluorimetry; E2, 17β-oestradiol; HEK293-HSD10, HEK293 cell line over-expressing the HSD10; HSD10, 17β-hydroxysteroid dehydrogenase type 10; IC_{50}, half-maximal inhibitory concentration; k_{cat}, turnover number; K_m, Michaelis constant; NAD^+, oxidised form of nicotinamide adenine dinucleotide; NADH, reduced form of nicotinamide adenine dinucleotide; SD, standard deviation; SEM, standard error of the mean; T_m, melting temperature; V_{max}, maximal enzyme reaction velocity.

Monika Schmidt and Michaela Vaskova contributed equally to this work.

et al., 2018; Tieu et al., 2004; Yang et al., 2005). So far, the most discussed is the pathology associated with AD, where HSD10 plays an important role caused by its increased expression in AD brains and its interaction with amyloid beta (Aβ) peptide (He, Wegiel, Yang, Pullarkat, et al., 2005; Lustbader et al., 2004; Yan et al., 1997). It seems that HSD10 up-regulation is one of the critical factors causing mitochondrial dysfunction in AD, as its over-expression exacerbates Aβ-mediated mitochondrial toxicity and neuronal stress (Chen & Yan, 2007; Seo et al., 2011; Takuma et al., 2005). Furthermore, even a non-enzymatic function of HSD10 is required for mitochondrial functional and structural integrity and cell survival (Rauschenberger et al., 2010). Therefore, HSD10 could be one of the major mitochondrial targets for development of anti-AD therapy.

17β-oestradiol (E2; He et al., 1999) and allopregnanolone (ALLOP; He, Wegiel, & Yang, 2005; He, Wegiel, Yang, Pullarkat, et al., 2005) belong among the essential steroids processed by HSD10 when both neurosteroids are involved in the neuronal survival and neuroprotection of the cells. E2 has been shown to have various protective effects on mitochondria, that is, increased electron transport chain activity and ATP production, stabilisation of the mitochondrial membrane potential, decrease in reactive oxygen species production and control of the calcium influx-induced excitotoxicity (Amtul et al., 2010; Grimm et al., 2012). Also, E2 may protect the cell from apoptosis by several mechanisms, such as by activation of antioxidant mechanisms leading to up-regulation of glutathione levels and by its function as a transcription factor after binding to oestrogen receptors α and β (Nilsen, 2008; Pike et al., 2009; Simpkins & Dykens, 2008). Furthermore, E2 significantly affects the regulation of the two most important pathological hallmarks of AD, Aβ and tau proteins (Alvarez-De-La-Rosa et al., 2005; Amtul et al., 2010; Nilsen et al., 2006). A neuroprotective antioxidant effect of ALLOP was demonstrated in different studies, for example, in enhancing superoxide dismutase activity in AD model of PC12 cells or reduction in lipid peroxidation and reactive oxygen species levels in human fibroblasts (Qian et al., 2015; Zampieri et al., 2009).

The over-expression of HSD10 was found in the brains of AD patients (Lustbader et al., 2004; Yan et al., 1997). It may probably affect the homeostasis of the neurosteroid metabolism and it can alter neurosteroid levels in different brain regions (Yang et al., 2011, 2014) when the E2 and ALLOP levels were found reduced in AD brains (Manly et al., 2000; Marx et al., 2006; Yue et al., 2005). The appropriate enzyme level of HSD10 imply to be critical for brain development, cognitive function and neurosteroid homeostasis in a healthy brain (He et al., 1999; Yang et al., 2007, 2009). However, the inhibition of the HSD10 over-expression could increase the level of these neuroprotective steroid levels and thus restore the disturbed homeostasis in the AD brain (He et al., 1999; Lim et al., 2011).

Several classes of HSD10 inhibitors have been developed, for example, benzothiazolyl ureas, steroids and pyrazolopyrimidines (Vinklarova et al., 2020). The most numerous group is benzothiazolyl ureas, whose structure was based on the FDA-approved drug frentizole (Figure 1; Xie et al., 2006). To date, our group has published several series of these compounds, with the best ones having submicromolar IC_{50} values (see compounds **15**, **16**, **21**, **27** and **30**; Aitken et al., 2019; Benek et al., 2017, 2018, 2023; Hroch et al., 2016, 2017; Schmidt et al., 2020). The most in vitro IC_{50} determinations were done via an absorbance assay with recombinant HSD10 enzyme, acetoacetyl-CoA (AAC) as a substrate and reduced form of nicotinamide adenine dinucleotide (NADH) as a co-factor. This assay was derived from a method published in 1981 by Binstock and Schulz (Binstock & Schulz, 1981) and is based on HSD10 reductase activity, whereas HSD10 is basically dehydrogenase which prefers the oxidative reaction with NAD^+ (oxidised form of nicotinamide adenine dinucleotide) as a co-factor (Yang et al., 2005).

In this work, we report the use of fluorescent enzymatic assay and fluorescent cellular assay for HSD10 screening. In enzymatic assay, we have used fluorescence properties of NADH in combination with neurosteroid substrates E2 and ALLOP to determine the best HDS10 inhibitors published by our group in more physiologically relevant in vitro conditions. Moreover, the best hits were evaluated in cellular environment to confirm their cell penetrability and HSD10 inhibitory ability.

2 | MATERIALS AND METHODS

2.1 | Chemicals and compounds

Most of the used chemicals were obtained from Sigma-Aldrich unless otherwise stated. All chemicals and reagents were of the highest commercially available purity. The tested compounds were chosen

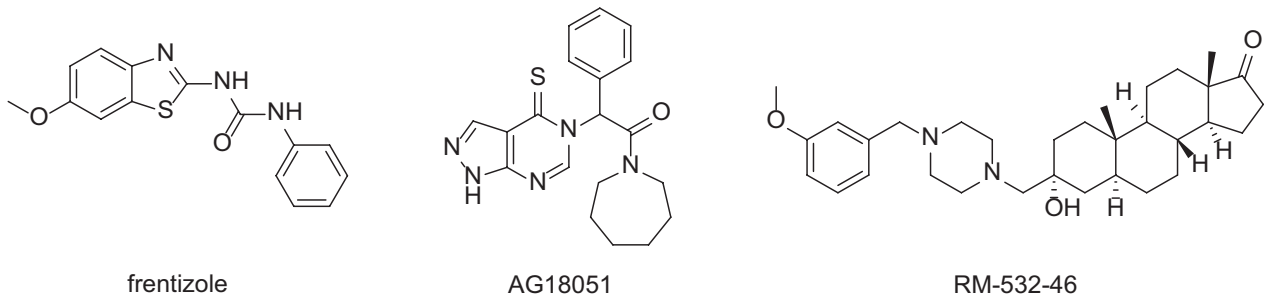

FIGURE 1 Prototypical compounds from different structural classes of HSD10 inhibitors—frentizole (benzothiazolyl ureas), AG18051 (pyrazolopyrimidines) and RM-532-46 (steroids).

14714159, 2023, 2, Downloaded from https://onlinelibrary.wiley.com/doi/10.1111/jnc.15917 by Charles University, Wiley Online Library on [12/11/2023]. See the Terms and Conditions (https://onlinelibrary.wiley.com/terms-and-conditions) on Wiley Online Library for rules of use; OA articles are governed by the applicable Creative Commons License

from the in-house library. The synthetic routes and chemical properties can be found in the published articles (i.e. references in Table 1). All compounds were dissolved in anhydrous dimethyl sulfoxide (DMSO) and further diluted with assay buffers or culture media to the working concentrations to keep the maximum DMSO concentration in all reaction mixtures at 2.2% (v/v) for enzymatic measurements and at 1% (v/v) for cell culture experiments. All buffers were prepared from ultra-pure water and their pH was adjusted for particular buffer.

2.2 | Expression and purification of human recombinant HSD10 enzyme

The recombinant *N*-terminally His-tagged HSD10 (UniProtKB server accession number: Q99714) was expressed in *Escherichia coli* BL21 (DE3) strain harbouring pET28b vector with inserted HSD17B10 gene, and purified as described previously (Schmidt et al., 2020) with minor changes. Briefly, the autoinduction and over-expression were performed at 25°C for 18 h using the Overnight Express™ Instant TB medium (Novagen, Merck). The bacterial pellet harvested by centrifugation (7500 *g*, 10 min, 4°C) was resuspended in lysis buffer (50 mM sodium phosphate buffer, 150 mM NaCl and 10 mM imidazole, pH 8.0) containing 1 mg/mL lysozyme, 150 U/mL benzonase and cOmplete™ EDTA-free protease inhibitor cocktail (Roche, Merck). The suspension was incubated on ice for 20 min and sonicated several times. After centrifugation (16 000 *g*, 10 min, 4°C), the supernatant was loaded onto the Ni-NTA agarose-filled column (Qiagen) and incubated on ice with gentle stirring for 1 h. Affinity purification was performed under native conditions. His-tagged HSD10 bound on the resin was washed three times with 10 mL of washing buffer I (50 mM sodium phosphate buffer, 150 mM NaCl and 20 mM imidazole, pH 8.0), followed by 3 × 10 mL of washing buffer II (50 mM sodium phosphate buffer, 150 mM NaCl and 40 mM imidazole, pH 8.0). Elution was performed using elution buffer (50 mM sodium phosphate buffer, 150 mM NaCl and 250 mM imidazole, pH 8.0), and the elution buffer was subsequently exchanged on Amicon® Ultra-4 Centrifugal Filter Unit (10 000 MWCO) for storage buffer (70 mM Tris–HCl and 215 mM NaCl, pH 8.0). The purified HSD10 enzyme was aliquoted and stored at −80°C. The protein concentration was determined using the Bradford assay using bovine serum albumin as a protein standard and the purification steps and the purity of the enzyme were monitored using SDS-PAGE.

2.3 | Western blot analysis

Sodium dodecyl sulphate-polyacrylamide gel electrophoresis using 15% resolving and 4% stacking gels were used for the recombinant HSD10 purity confirmation. To detect HSD10 by Western blot, samples under reducing conditions were subjected to electrophoresis [1 μg of purified recombinant HSD10 or 10 μg of HEK293 or HEK293 cell line over-expressing the HSD10 (HEK293-HSD10) cell lysate], and subsequently transferred to 0.22 μM PVDF membrane and detected using an anti-HSD10 primary mouse monoclonal antibody (anti-ERAB, clone 5F3, Abcam Cat# ab10260, RRID:AB_296999, dilution 1:1000), followed by the chemiluminescence detection of HRP-conjugated secondary goat anti-mouse IgG antibody (Thermo Fisher Scientific Cat# 32430, RRID:AB_1185566, dilution 1:1000).

2.4 | HSD10 activity assay and enzyme kinetics

The activity of the purified HSD10 was measured fluorometrically using E2 and ALLOP as the substrates and NAD^+ as the enzyme co-factor. The general reaction mixture (200 μL per well) was 50 μM E2 or 20 μM ALLOP (Tocris Bioscience, 0.4 μL, dissolved in anhydrous DMSO), 500 μM NAD^+ (10 μL, dissolved in ultra-pure water) and 42.5 nM purified recombinant HSD10 (1 μL) in assay buffer (188.6 μL, 100 mM potassium phosphate buffer, pH 8.0). The reaction mixture of enzyme and co-factor in the assay buffer was pre-incubated for 5 min at 37°C before adding the substrate. The activity assay was measured in polystyrene black 96-well plates (BRAND, 781608) at 37°C using Tecan Spark 10M instrument (Männedorf), and the HSD10 activity was monitored for 20 min in 30 s intervals as the increase in fluorescence (Ex/Em = 340/460 nm) caused by the enzymatic conversion of NAD^+ to NADH.

The HSD10 kinetic parameters, Michaelis constant (K_m) and maximal enzyme reaction velocity (V_{max}), were determined for enzyme substrates (E2, ALLOP and glycerol) and NAD^+ co-factor, and the concentrations were as follows: 2.3–200 μM for E2, 1.1–100 μM for ALLOP, 62.5–4000 mM for glycerol and 5.3–500 μM for NAD^+. The enzyme reaction rates were determined via the ΔF within the linear range of the measured curves and calculated using a calibration curve of NADH dilution series. For the determination of the kinetic parameters for NAD^+ and glycerol, the saturation curves were fitted using Michaelis–Menten kinetics in GraphPad Prism 8.4.3. As a result of substrate inhibition, the kinetic parameters for E2 and ALLOP were manually calculated from the saturation curve (V_{max} as the highest reaction rate achieved and K_m as the substrate concentration at the one-half of the V_{max}).

2.5 | Small-molecule inhibitors screening and IC_{50} determination

The compounds were screened at 10 and 1 μM concentrations to compare their ability to inhibit HSD10. The general reaction mixture (200 μL per well) consisted of 50 μM E2 or 20 μM ALLOP (0.4 μL, dissolved in anhydrous DMSO), 500 μM NAD^+ (10 μL, dissolved in ultra-pure water), a particular concentration of inhibitor (4 μL) and 42.5 nM purified recombinant HSD10 (1 μL) in assay buffer (184.6 μL, 100 mM potassium phosphate buffer, pH 8.0). The reaction mixture of enzyme, co-factor and inhibitor in the assay buffer was pre-incubated

14714159, 2023, 2, Downloaded from https://onlinelibrary.wiley.com/doi/10.1111/jnc.15917 by Charles University, Wiley Online Library on [12/11/2023]. See the Terms and Conditions (https://onlinelibrary.wiley.com/terms-and-conditions) on Wiley Online Library for rules of use; OA articles are governed by the applicable Creative Commons License

TABLE 1 In vitro inhibitory potency of the tested compounds against human HSD10 in AAC and E2 assay for transformation of AAC to 3-hydroxybutyryl-CoA (taken from previously published data) and E2 to estrone respectively. The measured IC_{50} values (E2 assay) are given as means ± SEM from a single experiment performed in tetraplicate ($n = 4$).

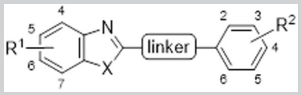

					AAC assay		E2 assay
Cmp	R^1	X	Linker	R^2	IC_{50} (μM) ± SEM/SD	References	IC_{50} (μM) ± SEM
AG18051					0.092	Kissinger et al. (2004)	0.089 ± 0.009
1	–	S	NHCONH	3-Cl, 4-OH	2.2 ± 0.5	Schmidt et al. (2020)	–
2	–	O	NHCONH	3-Cl, 4-OH	4.7 ± 2.3	Schmidt et al. (2020)	–
3	–	NH	NHCONH	3-Cl, 4-OH	2.3 ± 0.5	Schmidt et al. (2020)	–
4	4-Cl	S	NHCONH	3-Cl, 4-OH	–	Schmidt et al. (2020)	–
5	6-Cl	S	NHCONH	3-Cl, 4-OH	–	Hroch et al. (2016)	1.17 ± 0.09
6	7-Cl	S	NHCONH	3-Cl, 4-OH	2.5 ± 0.3	Schmidt et al. (2020)	–
7	6-Cl	O	NHCONH	3-Cl, 4-OH	2.4 ± 0.6	Schmidt et al. (2020)	–
8	6-Cl	NH	NHCONH	3-Cl, 4-OH	1.9 ± 0.4	Schmidt et al. (2020)	–
9	6-F	S	NHCONH	3-Cl, 4-OH	16.8 ± 1.0	Hroch et al. (2016)	–
10	6-Br	S	NHCONH	3-Cl, 4-OH	–	Schmidt et al. (2020)	1.08 ± 0.08
11	6-Me	S	NHCONH	3-Cl, 4-OH	5.5 ± 1.4	Schmidt et al. (2020)	–
12	6-CF_3	S	NHCONH	3-Cl, 4-OH	–	Schmidt et al. (2020)	–
13	6-iPr	S	NHCONH	3-Cl, 4-OH	5.12[c]	Aitken et al. (2019)	0.89 ± 0.05
14	6-tBut	S	NHCONH	3-Cl, 4-OH	5.29[c]	Aitken et al. (2019)	1.01 ± 0.09
15	6-COOH	S	NHCONH	3-Cl, 4-OH	0.31 ± 0.09	Benek et al. (2023)	–
16	6-$CONH_2$	S	NHCONH	3-Cl, 4-OH	0.84 ± 0.18	Benek et al. (2023)	1.61 ± 0.12
17	6-$CONMe_2$	S	NHCONH	3-Cl, 4-OH	–	Benek et al. (2023)	–
18	6-NH_2	S	NHCONH	3-Cl, 4-OH	1.6 ± 0.3	Schmidt et al. (2020)	1.20 ± 0.08
19	6-NMe_2	S	NHCONH	3-Cl, 4-OH	–	Benek et al. (2023)	–
20	6-NO_2	S	NHCONH	3-Cl, 4-OH	5.0 ± 1.2	Schmidt et al. (2020)	–
21	6-NHAc	S	NHCONH	3-Cl, 4-OH	0.34 ± 0.07	Benek et al. (2023)	–
22	6-OH	S	NHCONH	3-Cl, 4-OH	1.2 ± 0.2	Schmidt et al. (2020)	0.71 ± 0.09
23	6-OMe	S	NHCONH	3-Cl, 4-OH	2.4 ± 0.6	Schmidt et al. (2020)	–
24	6-OCF_3	S	NHCONH	3-Cl, 4-OH	–	Hroch et al. (2016)	–
25	6-OEt	S	NHCONH	3-Cl, 4-OH	1.61[c]	Aitken et al. (2019)	0.79 ± 0.07
26	6-SCN	S	NHCONH	3-Cl, 4-OH	2.61[c]	Aitken et al. (2019)	0.07 ± 0.01
27	6-SO_2Me	S	NHCONH	3-Cl, 4-OH	0.93[c]	Aitken et al. (2019)	0.85 ± 0.06
28	6-SO_2CF_3	S	NHCONH	3-Cl, 4-OH	2.69[c]	Aitken et al. (2019)	1.05 ± 0.11
29	6-OMe	S	NHCONH	3-Br, 4-OH	1.28[c]	Aitken et al. (2019)	0.67 ± 0.05
30	6-OMe	S	NHCONH	3-CF_3, 4-OH	0.57 ± 0.12	Benek et al. (2023)	–
31	6-OMe	S	NHCONH	3-CN, 4-OH	–	Aitken et al. (2019)	–
32	6-OCF_3	S	NHCONH	3,5-Cl, 4-OH	–	Hroch et al. (2016)	–
33	6-Cl	S	NHCONH	3,5-F, 4-OH	–	Schmidt et al. (2020)	–
34	6-OMe	S	NHCO	3-Cl, 4-OH	–	Aitken et al. (2019)	0.35 ± 0.05
35	6-OMe	S	$NHCH_2$	3-Cl, 4-OH	–	Benek et al. (2023)	–
36	–	S	CH_2NHCH_2	3-Cl, 4-OH	–	Benek et al. (2023)	–
37	6-OMe	S	NHCNHNH[a]	4-OMe	3.06 ± 0.40	Benek et al. (2017)	–
38	3-Cl-4-OH-Ph[b]		NHCONH	3-Cl, 4-OH	6.83[c]	Aitken et al. (2019)	–

[a]Guanidine.

[b]Replacement of the benzothiazole moiety with 3-chloro-4-hydroxyphenyl.

[c]Confidence intervals can be found in (Aitken et al., 2019).

(Continues)

14714159, 2023, 2, Downloaded from https://onlinelibrary.wiley.com/doi/10.1111/jnc.15917 by Charles University, Wiley Online Library on [12/11/2023]. See the Terms and Conditions (https://onlinelibrary.wiley.com/terms-and-conditions) on Wiley Online Library for rules of use; OA articles are governed by the applicable Creative Commons License

for 5 min at 37°C before adding the substrate. The residual activity was calculated with respect to the uninhibited reaction with DMSO as vehicle control (100% of HSD10 activity). Compound AG18051 (Kissinger et al., 2004) was used as a standard inhibitor from the literature.

For half-maximal inhibitory concentration (IC_{50}) values determination, the residual activity was calculated from a series of reactions measured as dose–response inhibition at nine different concentrations of inhibitors (0.03–40 μM) at fixed enzyme, co-factor and substrate concentrations. The initial rates of the dose–response data were analysed in GraphPad Prism 8.4.3 using non-linear regression analysis, and IC_{50} values (± SEM, standard error of the mean) were calculated.

2.6 | Determination of inhibition type

The activity assay was further used to determine the type of inhibition of the two most potent inhibitors with respect to the substrates, E2 and ALLOP. The inhibitors were used at different concentrations according to their inhibitory ability (compound **34**: 300 and 450 nM for E2 and 127 and 190 nM for ALLOP; compound **26**: 44, 67 and 100 nM for E2 and 5, 10 and 20 nM for ALLOP) in combination with different concentrations of the substrate (3.125–75 μM for E2 and 1.8–20 μM for ALLOP) and a saturated co-factor concentration (500 μM NAD^+). DMSO was used as vehicle control. The data were analysed by GraphPad Prism 8.4.3 using the linearisation of Hanes–Woolf. In addition, the K_m and V_{max} values of inhibited reactions were compared with the control reaction to more precisely determine the inhibition type.

2.7 | Differential scanning fluorimetry (DSF)

Melting temperatures (T_m) were determined in 100 mM potassium phosphate buffer (pH 8.0). The general mixture with a total volume of 40 μL consisted of 1.43 μM HSD10 (0.82 μL), compounds at a final concentration of 25 and 50 μM (0.88 μL) and reaction buffer containing 1:1000 dilution of SYPRO Orange (37.9 μL) with or without the presence of 250 μM NAD^+ (0.39 μL). DMSO was used as vehicle control. The fluorescence melting curve was monitored in a temperature range from 25 to 90°C with the temperature ramps of 1°C/min using qPCR machine qTower^3/G (Analytic Jena; Ex/Em = 490/575 nm). The data were analysed and the melting temperatures were calculated using qPCRsoft 4.0 (Analytic Jena). The differences between groups, that is, between the DMSO vehicle control and the tested inhibitor, were analysed by GraphPad Prism 8.4.3 using the Student's unpaired *t*-test. The normality was conducted using Q-Q analysis with a Shapiro–Wilk assessment to test for normality. The outlier test was not performed.

2.8 | Cell cultures and HSD10 over-expression

HEK293 cells (ECACC Cat# 85120602, RRID:CVCL_0045) were maintained in Dulbecco's modified Eagle medium (Capricorn) supplemented with 10% foetal bovine serum (Gibco), 2 mM L-glutamine and non-essential amino acids additives (Gibco) at 37°C in 5% CO_2 humidified atmosphere. The cells were passaged regularly at 70–80% confluency using the split ratio from 1:6 to 1:10, and all experiments were performed at a maximum passage number of 15 (the passage number counting started at the time of purchasing). All culture preparations were repeatedly tested for *Mycoplasma* contamination (MycoAlert Plus, Promega), authenticated during the preparation of this manuscript and is not listed as a commonly misidentified cell line by the International Cell Line Authentication Committee (ICLAC, https://iclac.org/databases/cross-contaminations/). For HSD10 over-expression, the gene for HSD10 was codon optimised and synthesised de novo as GeneArt Strings DNA fragment (Thermo Fisher). The full-length gene was PCR amplified and inserted into constitutive mammalian expression pcDNA3.4 vector using topoisomerase-based cloning and sequenced. Low-passaged HEK293 cells were nucleofected (Amaxa Nucleofector kit V, Lonza, nucleofector programme A-023) with 3–5 μg of pcDNA3.4-HSD10 plasmid DNA isolated using PureLink HiPure Plasmid MiniPrep kit (Invitrogen). Twenty-four hours after nucleofection, the cells were treated with G418 disulphate salt solution (Roche) at a concentration of 500 μg/mL in culture media to select positive cell clones. After several weeks of clonal selection and expansion, several monoclonal cell lines (HEK293-HSD10) were isolated using limiting dilution. The HSD10 over-expression was confirmed by immunoblotting using an anti-HSD10 primary mouse monoclonal antibody. No institutional ethical approval was required for this work.

2.9 | Cellular HSD10 inhibition

HSD10 inhibition in HEK293-HSD10 cells was performed using (–)-CHANA (cyclohexenyl amino naphthalene alcohol) fluorogenic probe (Muirhead et al., 2010). The cells were seeded at a density of 10^4 cells/well into black 96 clear bottom-well plates (Brand, 781971) in 200 μL cell culture media without phenol red. After 20 h of incubation, the cells were treated with selected compounds (2 μL) in various concentrations (1–25 μM) dissolved in anhydrous DMSO or 2 μL of DMSO only (vehicle control). After 2 h treatment, 2 μL of (–)-CHANA probe was added at the final concentration of 20 μM, and the changes in fluorescent intensities were measured immediately (0 h) and after 2 h after the addition of (–)-CHANA. The fluorescence intensities of the reaction product cyclohexenyl amino naphthalene ketone (CHANK) were measured using TECAN Spark 10 M instrument (Ex/Em = 380/525 nm). The HSD10 activity was calculated as the ΔF between 2 and 0 h after (–)-CHANA addition, and the data were normalised between DMSO-treated HEK293-HSD10 and non-transfected HEK293 controls (using relative response ratio).

2.10 | Cytotoxicity of selected compounds and their influence on cell viability

The selected compounds **26** and **34** were tested on HEK293 cells to determine their cytotoxicity effects and the impact on cell

14714159, 2023, 2, Downloaded from https://onlinelibrary.wiley.com/doi/10.1111/jnc.15917 by Charles University, Wiley Online Library on [12/11/2023]. See the Terms and Conditions (https://onlinelibrary.wiley.com/terms-and-conditions) on Wiley Online Library for rules of use; OA articles are governed by the applicable Creative Commons License

viability using CellTox Green Cytotoxicity Assay and CellTiter-Glo Luminescent Cell Viability Assay kits (Promega). For multiplex measurement, 5×10^3 cells were seeded per well in 50 μL of complete culture media in a white solid flat-bottom 96-well microplates (Nunc, 136102) and cultured for 24 h, followed by the addition of selected compounds (0.5 μL) at a final compound concentration of 10 and 25 μM. The treated cells were cultured for the next 4 or 48 h, followed by the multiplex measurement using a TECAN Spark instrument following the manufacturer protocol with minor changes. For cytotoxicity measurements, 20 μL of complete CellTox Green Reagent (prepared by mixing 20 μL of CellTox Green Dye with 6 mL of CellTox Green Assay Buffer) was used. For viability measurements, 25 μL of CellTiter-Glo 2.0 Reagent was used. The compounds' cytotoxicity was measured fluorometrically (Ex/Em = 485/530 nm), followed by the luminescence-based measurement of the cell viability with an integration time of 500 ms. Cells treated with 1% DMSO only (vehicle control) and 100 μM valinomycin-treated cells (positive control) were used as the controls.

3 | RESULTS

3.1 | Fluorescent E2 and ALLOP assays offer a more relevant point of view on HSD10 inhibition

The importance of the HSD10 enzyme in E2 and ALLOP inactivation and the implications for cell neuroprotection led us to re-investigate the best benzothiazolyl inhibitors and their ability to inhibit HSD10 enzyme using E2 and ALLOP as physiological and thus more relevant enzyme substrates. The assay was based on E2 and ALLOP oxidation by HSD10 leading to inactive estrone or 5α-dihydroprogesterone, respectively. The reaction was continuously monitored as fluorescence increments at 460 nm (Figure 2a) as a result of the formation of NADH.

The amount of HSD10 enzyme (42.5 nM, 1.2 μg/mL) in both assays was adjusted with respect to general considerations for enzymatic assay development, that is, the amount of enzyme should ensure the linearity of product formation in the reaction, depletion of substrate should be up to 10% of its concentration and enzyme concentration should be lower-than-expected inhibitory constants of the most potent inhibitors. This setup provided a sufficient assay window and thus the assay with a relevant screening window coefficient (Z'-factor; Figure 2b; Zhang et al., 1999). The calculated Z'-factors for both substrates were over 0.9, suggesting excellent assays addressing the quality of the assays.

The composition of the reaction mixtures for both substrates was kept as minimalistic as possible. The addition of stabilisers, detergents and other proteins was avoided to exclude their impact on the HSD10 enzymatic activity or ligand binding. To improve the common solubility issues reported previously (Aitken et al., 2019; Hroch et al., 2016), the amount of final DMSO concentration was increased to 2.2% as a safe concentration without much depletion of enzymatic activity.

For both substrates, the relation between the substrate/co-factor concentrations and reaction rate was determined (Figure 3). The K_m values were determined for both neurosteroids, E2 and ALLOP (Figure 3a,b), as well as for the enzyme co-factor NAD^+ and glycerol (Figure 3c,d). The saturation curves of the reactions using E2 and ALLOP as substrates displayed substrate inhibition (Figure 3a,b), showing a decrease in the reaction velocity. The presence of glycerol was also addressed as it is used as a stabiliser for many recombinant enzymes (Vagenende et al., 2009), and glycerol interference was observed in the 17β-HSD14 enzyme experiments (Bertoletti et al., 2016). The glycerol was shown to be a substrate for the HSD10 enzyme and displayed three orders of magnitude higher K_m value compared to E2, ALLOP or NAD^+ (Figure 3d). As this may affect the inhibitory data obtained using both substrates and independently on method readout, glycerol was excluded from

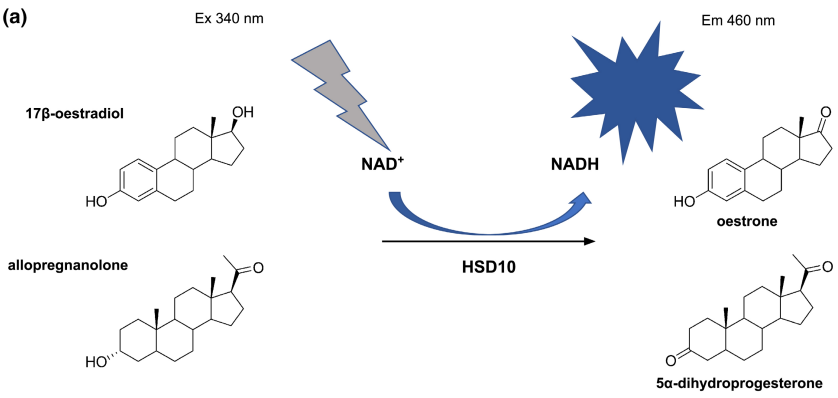

(b)

Substrate	Z´factor
E2 (50 μM)	0.977
ALLOP (20 μM)	0.959

FIGURE 2 Assay characteristics. (a) Schematic presentation of HSD10 enzymatic activity with E2 and ALLOP substrates and (b) Z'-factors for E2 and ALLOP substrates. HSD10, 17β-hydroxysteroid dehydrogenase type 10. ALLOP, allopregnanolone; E2, 17β-oestradiol; NAD^+/NADH, oxidised/reduced form of nicotinamide adenine dinucleotide.

14714159, 2023, 2, Downloaded from https://onlinelibrary.wiley.com/doi/10.1111/jnc.15917 by Charles University, Wiley Online Library on [12/11/2023]. See the Terms and Conditions (https://onlinelibrary.wiley.com/terms-and-conditions) on Wiley Online Library for rules of use; OA articles are governed by the applicable Creative Commons License

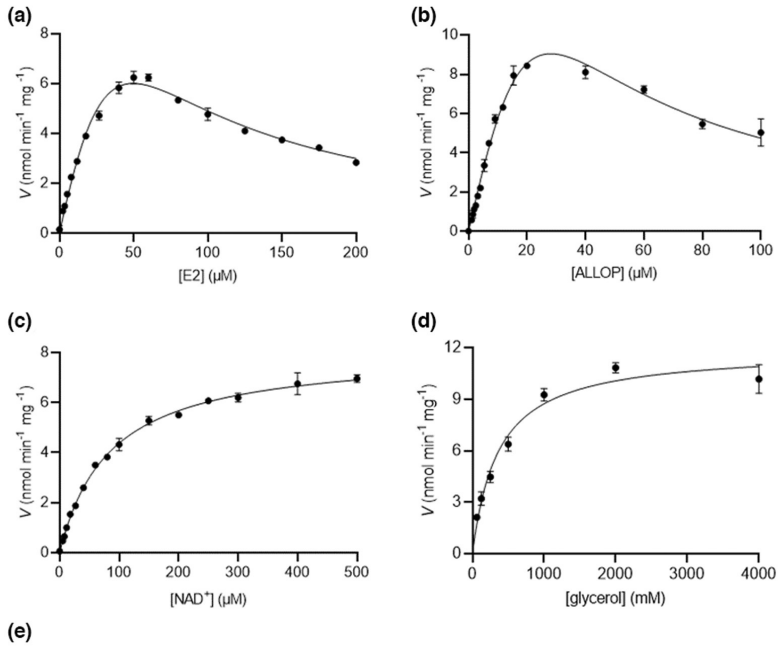

(e)

	E2	ALLOP	NAD+	glycerol
K_m (μM)	13.11 ± 0.26	6.86 ± 0.11	84.36 ± 5.47	360.43 x 10^3
V_{max} (nmol min^{-1} mg^{-1})	6.34 ± 0.07	8.46 ± 0.06	8.06 ± 0.09	11.88 ± 0.35
k_{cat} (min^{-1})	0.178	0.238	0.227	0.334
k_{cat}/K_m (M^{-1} min^{-1})	13.6 x 10^3	34.7 x 10^3	2.7 x 10^3	0.93

FIGURE 3 Determination of kinetic parameters of HSD10 enzyme. HSD10 activity was measured with (a) E2 and (b) ALLOP, both at fixed NAD^+ concentration (500 μM); (c) NAD^+ at fixed E2 concentration (50 μM) or (d) glycerol at fixed NAD^+ concentration (500 μM); and (e) The kinetic parameters of HSD10 enzyme. The K_m and V_{max} values are given as means ± SEM from a single experiment performed in tetraplicate ($n = 4$). ALLOP, allopregnanolone; E2, 17β-oestradiol; NAD^+, oxidised form of nicotinamide adenine dinucleotide; SEM, standard error of the mean.

all steps during enzyme preparation, purification, storage and determinations. The maximum velocities (V_{max}), Michaelis constants (K_m), turnover numbers (k_{cat}) and catalytic efficiencies (k_{cat}/K_m) were calculated for both substrates, NAD^+ co-factor and glycerol from their saturation curves (Figure 3e).

3.2 | Assay with E2 and ALLOP revealed potent HSD10 inhibitors

To date, our group has developed numerous benzothiazole-based HSD10 inhibitors (Aitken et al., 2019; Benek et al., 2017, 2018, 2023; Hroch et al., 2016, 2017; Schmidt et al., 2020). In the formerly published works, the enzymatic activity of HSD10 was determined using acetoacetyl coenzyme A (AAC) as the substrate and NADH as the enzyme co-factor. Based on previous studies, we have selected 38 promising inhibitors that were identified in the AAC assay. These inhibitors were re-evaluated using a novel assay via oxidative NAD^+-dependent route using physiological substrates E2 and ALLOP. All tested compounds were evaluated at 10 μM and 1 μM concentrations (Figure 4, data available in Table S1). Compound AG18051 (Kissinger et al., 2004), the most potent HSD10 inhibitor published so far, was used as the control.

All tested compounds, except for compound **30**, displayed good inhibition activity of HSD10 at 10 μM concentration in the E2 assay (>50% inhibition). The consequent 1 μM screening revealed 13 compounds with more than 50% inhibition ability and they were forwarded to IC_{50} determination (Table 1). Most compounds displayed IC_{50} values around 1 μM. In addition, several screened compounds demonstrated excellent inhibition and showed IC_{50} values in submicromolar concentrations (**26**, **29** and **34**). Compound **26**, having an IC_{50} value of 70 nM, was found slightly more potent than the best experimentally validated HSD10 inhibitor, AG18051 (IC_{50} 89 nM). Interestingly, most of the previously published inhibitors (Table 1, column AAC assay) were confirmed active also in the E2 assay (**5**, **10**, **13**, **14**, **25**, **28** and **29**), while several others were found poorly active and they failed to pass for the IC_{50} determination (**15**, **21** and **30**).

3.3 | Compounds 26 and 34 demonstrated enhanced HSD10 inhibition in vitro

The two best HSD10 inhibitors in E2 assay (**26** and **34**) were previously determined with moderate inhibition ability using AAC assay (Aitken et al., 2019). Compound **34** displayed around 50% inhibition in 25 μM screening using AAC (no IC_{50} data were available) and it was determined as compound acting with the mixed type of inhibition with respect to the AAC substrate or NADH co-factor (Aitken et al., 2019). This compound has the usual 3-chloro-4-hydroxylphenyl substitution in combination with methoxy substituent in position 6 on the benzothiazole moiety. Its uniqueness lies in the linker, where the urea was replaced by the shorter amide moiety. This linker variation seems to be very

14714159, 2023, 2, Downloaded from https://onlinelibrary.wiley.com/doi/10.1111/jnc.15917 by Charles University, Wiley Online Library on [12/11/2023]. See the Terms and Conditions (https://onlinelibrary.wiley.com/terms-and-conditions) on Wiley Online Library for rules of use; OA articles are governed by the applicable Creative Commons License

important, as its analogue **23** containing urea linker was unable to inhibit HSD10 in E2 assay by more than 40% in the 10 μM screening (Figure 4), while compound **34** resulted as nanomolar inhibitor in E2 assay. In addition, compound **34** was acting via the uncompetitive type of inhibition with respect to the E2 substrate (Table 2), which confirmed our previous findings for other benzothiazoles using AAC assay (Schmidt et al., 2020).

Compound **26** demonstrated the highest inhibition towards HSD10 enzyme in E2 assay, but it previously showed only mild enzyme inhibition in AAC assay (Aitken et al., 2019). The compound structure differs from other inhibitors by the thiocyanate substitution in position 6 of the benzothiazole moiety. Unlike compound **34**, compound **26** has shown a non-competitive type of inhibition. Interestingly, this compound was previously published as a mixed-type inhibitor in AAC assay (similarly to **34**; Aitken et al., 2019). The difference in the determined type of inhibition between these two assays may be in the different substrates used or in the methodology used for kinetic measurements (e.g. in concentrations of substrates and inhibitors used).

The two most promising compounds, **26** and **34**, were further forwarded to the assay with ALLOP substrate to confirm their inhibitory effect with another physiologically occurring neurosteroid. Using this substrate, compounds **26** and **34** displayed significantly lower IC_{50} values than with the E2 substrate (Table 2). The control inhibitor AG18051 demonstrated inhibition comparable to that of compound **26**. Furthermore, the same type of inhibition was demonstrated using ALLOP substrate (Table 2), when compound **34** was found to be the uncompetitive inhibitor, while compound **26** showed the non-competitive type of inhibition. These results indicate that these two compounds have different binding mode to the HSD10 within the oxidative conversion of both substrates.

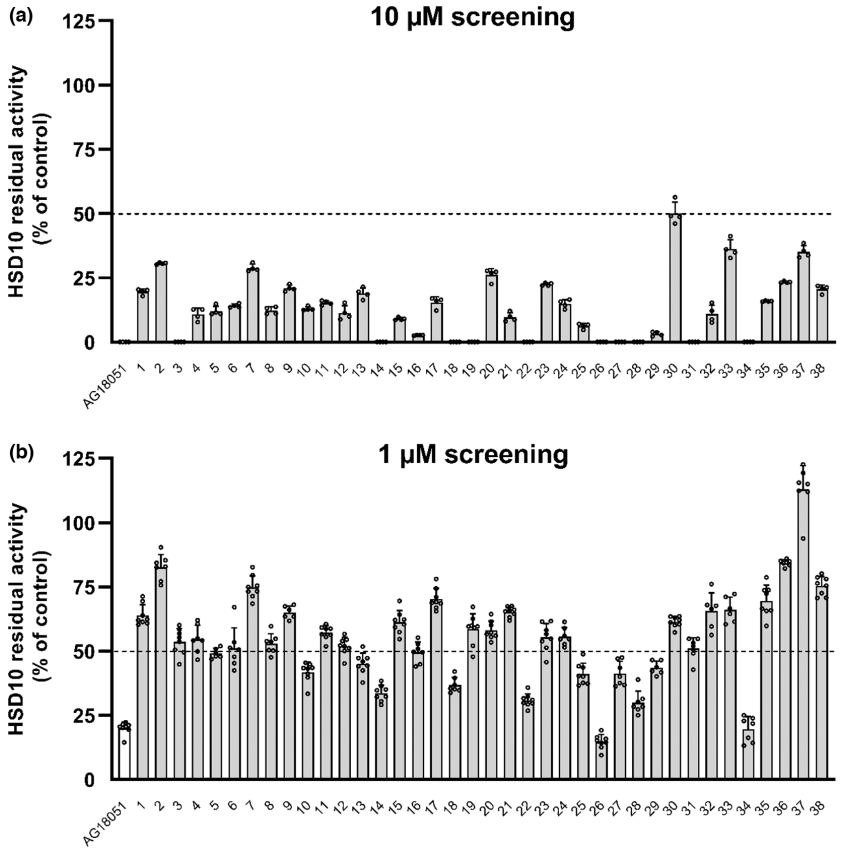

FIGURE 4 10 μM (a) and 1 μM (b) screening of HSD10 inhibitors using E2 assay. Values are given as means ± SD from a single experiment (a) or two independent experiments (b) performed in tetraplicate ($n = 4$ or 8, shown as individual data points). HSD10, 17β-hydroxysteroid dehydrogenase type 10.

TABLE 2 In vitro inhibitory ability and mechanism of action of the most promising compounds using E2 and ALLOP substrates. ALLOP, allopregnanolone; E2, 17β-oestradiol; IC_{50}, half-maximal inhibitory concentration.

	IC_{50} (nM) ± SEM		Type of inhibition	
Compound	E2	ALLOP	E2	ALLOP
AG18051	89 ± 9	20 ± 1.9	Covalent	Covalent
26	70 ± 10	19 ± 1.5	Non-competitive	Non-competitive
34	346 ± 53	191 ± 28	Uncompetitive	Uncompetitive

14714159, 2023, 2, Downloaded from https://onlinelibrary.wiley.com/doi/10.1111/jnc.15917 by Charles University, Wiley Online Library on [12/11/2023]. See the Terms and Conditions (https://onlinelibrary.wiley.com/terms-and-conditions) on Wiley Online Library for rules of use; OA articles are governed by the applicable Creative Commons License

3.4 | DSF confirmed different binding modes of compounds 26 and 34

The shift in the thermal stability of the HSD10 in the presence of selected compounds **26** and **34** was evaluated using the DSF method to confirm the ligand–target interactions (Figure 5, data and statistical reports available in Tables S2 and S3). As the enzyme co-factor NAD^+ can be a very important element in the binding process and thus in the compounds' mode of action, the enzyme thermal stability was examined both in the presence or absence of NAD^+. Control compound AG18051 showed strong binding (increase of T_m) only in the presence of NAD^+, which is in accordance with its known mechanism of action, that is, the covalent binding/interaction with the co-factor within the enzyme's active site (Kissinger et al., 2004). The thermal stability of HSD10 after treatment with inhibitors **26** and **34** showed a positive thermal shift (increase in T_m) and confirmed their interactions with HSD10. In addition, some differences in binding modalities can be assumed from the differences in HSD10 thermal shift profiles in the presence or absence of NAD^+ co-factor. Compound **34** affected the HSD10 thermal stability more in the presence of co-factor, while **26** caused similar increase in T_m under both conditions used. The DSF data thus confirmed the different mechanisms of action for **26** and **34** and they are in agreement with their suggested non-competitive and uncompetitive inhibition mode respectively.

3.5 | Compounds 26 and 34 are HSD10 inhibitors in the cellular environment

The promising results from in vitro determination using recombinant enzyme led us to determine the activity of the best inhibitors **26** and **34** at cellular level. To detect the HSD10 activity inside the cells, the fluorogenic probe (–)-CHANA (cyclohexenyl amino naphthalene alcohol; Figure 6a) in combination with HEK293-HSD10 cells was used. The HSD10 over-expression was analysed by immunoblotting using an anti-HSD10 primary antibody (Figure 6b bottom, original western blot image available in Figure S1), and the HSD10 activity was determined by comparing the (–)-CHANA turnover in HEK293-HSD10 cells and HEK293 cells (Figure 6b top). The inhibitors' ability to affect the enzyme inside the cell was measured as the decrease in fluorescence of CHANK after the inhibitor treatment.

The selected inhibitors **26** and **34** displayed inhibitory activity against HSD10 inside the cells after 4 h treatment and their inhibition ability was found dose dependent (Figure 6c). Although the (–)-CHANA probe is not the physiological substrate of HSD10, it undergoes the alcohol to ketone conversion (oxidation) similar to E2 and ALLOP. The obtained results demonstrate that both inhibitors, **26** and **34**, were able to enter the cells and engage the HSD10 enzyme within.

In addition to HSD10, the compounds may also affect other molecular targets inside cells. For this reason, the cell viability via ATP determination and cytotoxicity were determined after 4 and 48 h post-inhibitor treatment. Compounds **26** and **34** nor the control inhibitor AG18051 displayed a decrease in cell viability measured by ATP levels or in cell membrane integrity after 4 h post-treatment (Figure 7a). These data validate the results from the cellular HSD10 inhibition since the decrease in (–)-CHANA turnover after inhibitors' treatment was not accompanied by the decrease in cell viability. Compound **26** displayed reduced ATP levels and increased cytotoxicity after 48 h at 25 μM concentration (Figure 7b), suggesting impairment of other cellular structures. On the other hand, compound **34** showed no cytotoxicity

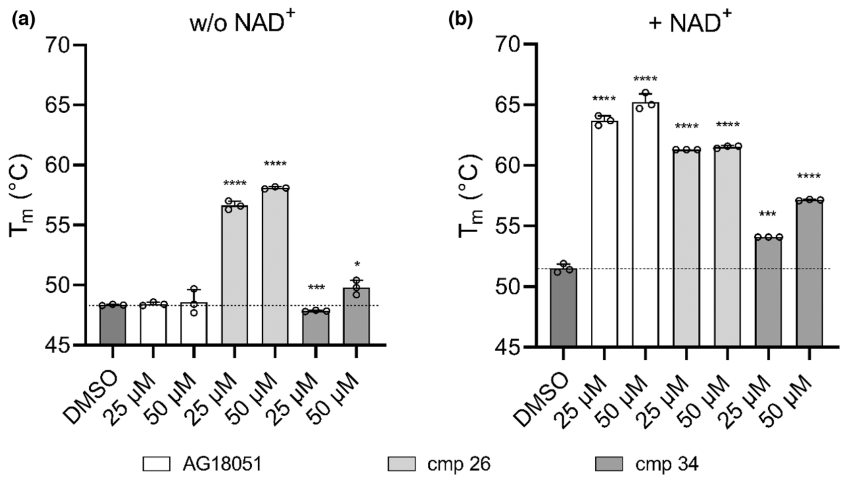

FIGURE 5 Melting temperatures (T_m) for HSD10 in the presence of the compounds **26** and **34**. Enzyme HSD10 treated with inhibitors in the (a) absence or (b) presence of 250 μM NAD^+ co-factor. Values are given as means ± SD from single experiment performed in triplicate ($n = 3$, shown in individual data points), and differences between groups were determined by the Student's unpaired two-tailed *t*-test (*$p \le 0.05$, **$p \le 0.01$, ***$p \le 0.001$ and ****$p \le 0.0001$). The data were normally distributed according to the Shapiro–Wilk test. DMSO, dimethyl sulfoxide; NAD^+, oxidised form of nicotinamide adenine dinucleotide; SEM, standard error of the mean; T_m, melting temperature.

14714159, 2023, 2, Downloaded from https://onlinelibrary.wiley.com/doi/10.1111/jnc.15917 by Charles University, Wiley Online Library on [12/11/2023]. See the Terms and Conditions (https://onlinelibrary.wiley.com/terms-and-conditions) on Wiley Online Library for rules of use; OA articles are governed by the applicable Creative Commons License

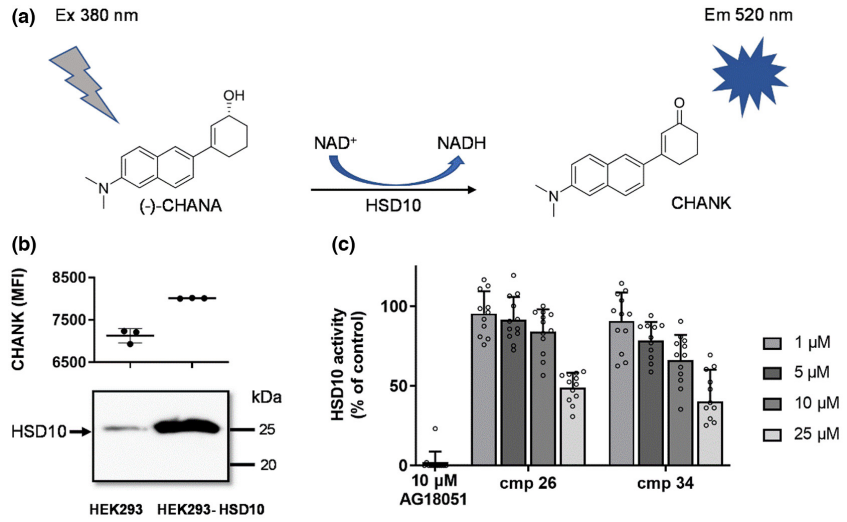

FIGURE 6 HSD10 activity in HEK293-HSD10 cells. (a) The schematic conversion of (−)-CHANA probe by HSD10. (b) (−)-CHANA turnover to CHANK and immunoblotting analysis in HEK293-wt and HEK293-HSD10 cells using an anti-HSD10 antibody. (c) HSD10 inhibition inside the cellular environment was determined using a fluorogenic probe (−)-CHANA and its conversion via HSD10 to fluorescent CHANK inside the HEK293-HSD10. Values are given as means ± SD ($n = 3$) from three independent cell culture preparations with four technical replicates ($n = 12$, shown as individual data points). HSD10, 17β-hydroxysteroid dehydrogenase type 10; CHANA, cyclohexenyl amino naphthalene alcohol; CHANK, cyclohexenyl amino naphthalene ketone; HEK293-HSD10, HEK293 cell line over-expressing the HSD10; NAD^+/NADH, oxidised/reduced forms of nicotinamide adenine dinucleotide; SD, standard deviation.

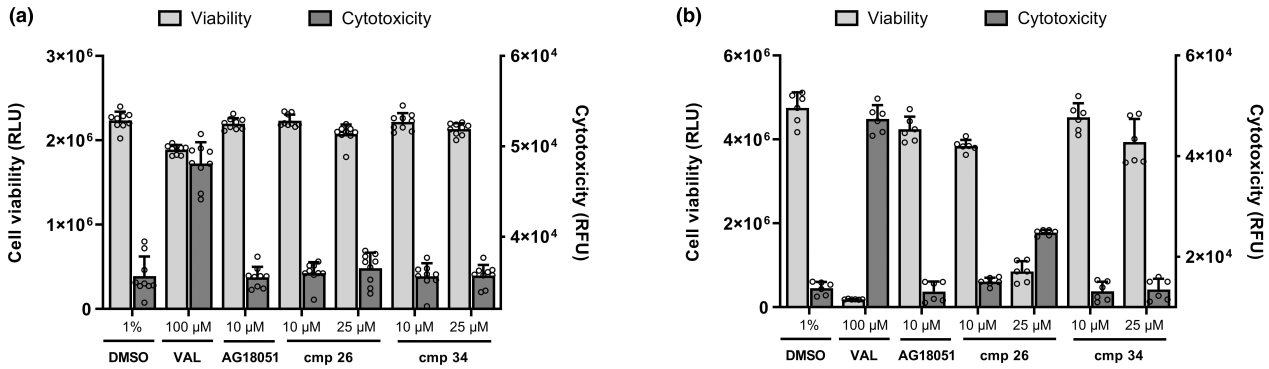

FIGURE 7 Cell viability and cytotoxicity in the HEK293 cell line 4 h (a) or 48 h (b) post-compound exposure. DMSO-treated (1%) and valinomycin-treated cells (100 µM) are used as cell viability and cytotoxicity controls respectively. Values are given as means ± SD from two independent cell culture preparations with three technical replicates ($n = 6$, shown as individual data points). SD, standard deviation.

or altered cell viability after 48 h treatment even at the highest concentration used.

4 | DISCUSSION

Mitochondrial dysfunction has been demonstrated as a fundamental component of AD, and as synaptic plasticity and its function are highly energy-dependent, mitochondria have been considered as a therapeutic target in AD (Swerdlow, 2018; Swerdlow et al., 2014). Many inhibitors of HSD10 were discovered in previous years with the aim to inhibit the enzyme itself or to prevent/disrupt the HSD10-Aβ interaction to reverse the AD-driven pathology (reviewed in Vinklarova et al., 2020). HSD10 was designated as moonlighting protein because of processing several known substrates inside the mitochondria as well as its structural function, role in maintaining the neurosteroid homeostasis, functional and structural integrity of mitochondria and cell survival. The neurosteroids E2 and ALLOP seem to be significant players as the excessive turnover and inactivation of these neuroprotective steroids induced by HSD10 up-regulation may cause the neurons to be more vulnerable/susceptible to AD-related stress (see our latest review Vinklarova et al., 2020). From this point of view, the choice of the appropriate substrate molecule involved in the enzyme inhibitory screenings is crucial with regard to the relevance of the results. We have focused on enzyme inhibition induced by

14714159, 2023, 2, Downloaded from https://onlinelibrary.wiley.com/doi/10.1111/jnc.15917 by Charles University, Wiley Online Library on [12/11/2023]. See the Terms and Conditions (https://onlinelibrary.wiley.com/terms-and-conditions) on Wiley Online Library for rules of use; OA articles are governed by the applicable Creative Commons License

frentizole-based compounds, benzothiazoles, and several structure substitutions capable of inhibiting the HSD10 enzymatic activity discovered using AAC as an enzyme substrate in the reductive reaction direction (Aitken et al., 2019; Benek et al., 2017, 2018, 2023; Hroch et al., 2016, 2017; Schmidt et al., 2020). Here, we present a fluorescent enzymatic and fluorescent cellular assay for HSD10 inhibitors re-screening using E2 and ALLOP as enzyme substrates.

The E2/ALLOP fluorescent method is based on the substrate oxidation associated with the conversion of co-factor NAD^+ to NADH. This reaction setup has several advantages compared to the previously used AAC method. First, HSD10 is the dehydrogenase, thus dehydrogenation/oxidative reaction is more physiologically relevant than the method using AAC which was based on hydrogenation/reduction setup (Aitken et al., 2016, 2017, 2019; Hroch et al., 2016; Oppermann et al., 1999; Schmidt et al., 2020,2023). Furthermore, fluorescence readout is more sensitive than absorbance determination. In addition, the price of AAC itself is relatively high compared to E2/ALLOP and it has to be used in higher concentrations than E2/ALLOP when considering the K_m values. Also, the continuous readout and data collection of the NAD^+ reduction better ensure the initial curve slope determination and is free of the downstream steps necessary for the product determination. Moreover, the exclusion of glycerol from the enzyme preparation and measurements provided more accurate and unbiased data for structure–activity relationship analysis as glycerol was recognised as hydroxysteroid dehydrogenase substrate earlier (Bertoletti et al., 2016). Finally, the assay setup enables easy exchange of substrate molecules, thereby extending the inhibitory data availability.

E2 as an enzyme substrate has been used several times to measure the HSD10 enzymatic activity with different method readouts, including absorbance (Aitken et al., 2017; Powell et al., 2000; Schmidt et al., 2020; Shafqat et al., 2003; Yan et al., 1999), thin-layer chromatography (TLC) method (He et al., 1999), TLC in combination with radioactive-labelled E2 (Ayan et al., 2012; Boutin et al., 2018, 2021; Boutin & Poirier, 2018) or ELISA-based E2 determination (Morsy et al., 2022). TLC detection method was also used for the determination of HSD10 activity using ALLOP as the substrate (Boutin et al., 2018; He, Wegiel, & Yang, 2005; Yang et al., 2009). A similar method using ALLOP substrate in combination with continuous measurement was used to determine MRPP2 protein (alternative name for HSD10 protein; Oerum et al., 2017). Most of the published K_m values for E2 were found to be around 15 μM, which correlates well with our data. Much less information is available for the ALLOP as the HSD10 substrate, but the data from literature (Oerum et al., 2017) were obtained in a similar setup and the determined K_m value is consistent with our findings.

To date, the most potent experimentally validated HSD10 inhibitor is AG18051, a covalent, irreversible inhibitor with IC_{50} 92 nM in AAC assay (Kissinger et al., 2004). In our previous publications, we have described the development of reversible submicromolar HSD10 inhibitors based on the structure based on benzothiazolyl urea structural scaffold (Aitken et al., 2019; Benek et al., 2017, 2023; Hroch et al., 2016; Schmidt et al., 2020). The most potent inhibitors were 1-benzothiazolyl-3-phenylureas harbouring 3-halogen-4-hydroxy substitution on the phenyl ring in combination with different substitutions in position 6 of benzothiazolyl part of the molecule. Here, we have confirmed the inhibition pattern using the E2 assay and discovered several structures with excellent inhibition activity on HSD10 in the nanomolar range. The compounds inhibition potencies obtained from the E2/ALLOP assay are not always in agreement with the previous AAC assay. The discrepancy between the results of the two different assays may originate from the varying spatial size of AAC or E2 substrates. The AAC is much spatially bulkier than E2 and the substrate steric effects may affect the potency of the inhibitor (Powell et al., 2000).

These data also offer the opportunity to analyse structure–activity relationships between the two assays. Most of the potent inhibitors from both assays shared the 3-chloro-4-hydroxy phenyl substitution in combination with urea linker. The best inhibitors in AAC assay (**15**, **16** and **21**) harbour a hydrogen bond donating substitution in position 6 of the benzothiazole moiety. On the other hand, the most potent inhibitors in the E2 assay do not share any particular structural similarity. Although most of the active inhibitors in the E2 assay (with determined IC_{50}) share a hydrogen bond accepting substitution in position 6 of benzothiazolyl moiety, there is not enough data to verify this trend.

Finally, our most potent inhibitors were subjected to cellular fluorescent assay using a fluorogenic (–)-CHANA probe. The probe acts as an artificial substrate for HSD10 and is oxidised to the corresponding fluorescent ketone CHANK (Aitken et al., 2019; Metodieva et al., 2022; Muirhead et al., 2010). Although this probe is not physiological, it is converted by the enzyme in the same manner as E2 and ALLOP substrates. Furthermore, the probe was proved to act selectively on the HSD10 enzyme (Muirhead et al., 2010) and was used in several studies to identify new inhibitors of HSD10 inside living cells (Aitken et al., 2019; Metodieva et al., 2022; Muirhead et al., 2010). The two best inhibitors **26** and **34** showed dose-dependent inhibition of HSD10 in the cellular environment accompanied by low level of cytotoxicity approving the validity of this result. Unfortunately, after 48 h, **26** has shown increased cytotoxicity, perhaps related to the previously described respiratory chain inhibition (mitochondrial complex I; Fišar et al., 2021). Although higher cytotoxicity was apparent only at higher concentrations (two orders of magnitude higher than the IC_{50} values), it should be considered for future in vivo studies.

5 | CONCLUSION

Taken together, the presented experimental data clearly demonstrated the importance of appropriate substrate selection for particular molecular target. HSD10 acts within mitochondria as NAD^+-dependent dehydrogenase and thus the use of substrate undergoing the oxidative reaction course with NAD^+ participation seems to be more physiologically relevant. The use of two native substrates indispensable in homeostasis of neurosteroids provides

14714159, 2023, 2, Downloaded from https://onlinelibrary.wiley.com/doi/10.1111/jnc.15917 by Charles University, Wiley Online Library on [12/11/2023]. See the Terms and Conditions (https://onlinelibrary.wiley.com/terms-and-conditions) on Wiley Online Library for rules of use; OA articles are governed by the applicable Creative Commons License

more accurate data necessary for hit-to-lead optimisation of HSD10 inhibitors. Many inhibitors of HSD10 were formerly discovered with the aim to inhibit the enzyme or to prevent/disrupt the HSD10–Aβ interaction to reverse the AD-driven pathology (see recent reviews Morsy & Trippier, 2019; Vinklarova et al., 2020). Our previous studies on enzyme inhibition by benzothiazolyl ureas resulted in the discovery of several potent inhibitors, while using the AAC assay (Aitken et al., 2019; Benek et al., 2017, 2018, 2023; Hroch et al., 2016, 2017; Schmidt et al., 2020). However, the use of a fluorescent-based assay with the physiologically relevant HSD10 substrates (E2 and ALLOP) allowed us to re-screen the previously identified hits and obtain physiologically relevant data regarding their inhibition ability and mechanism of action. Moreover, we have demonstrated that the inhibitors selected on the basis of these enzymatic assays, compounds **26** and **34**, can penetrate the cell and inhibit the HSD10 enzyme in the cellular environment with no or minor effects on cell viability. These results offer further insights and valuable data that might help to find promising hit compounds for the development of clinically relevant HSD10 inhibitors.

AUTHOR CONTRIBUTIONS

MS, MV, AR, PF and MM: performing the experiments and data analyses; MS and MV: writing original draft; OB, LZ and KM: writing–review and editing; KM: funding acquisition.

ACKNOWLEDGEMENTS

This work was supported by the University of Hradec Kralove (Faculty of Science, no. SV2103-2022).

CONFLICT OF INTEREST STATEMENT

The authors have no conflict of interest to declare.

PEER REVIEW

The peer review history for this article is available at https://www.webofscience.com/api/gateway/wos/peer-review/10.1111/jnc.15917.

DATA AVAILABILITY STATEMENT

Data available in article supplementary material.

ORCID

Monika Schmidt https://orcid.org/0000-0003-4984-9155
Michaela Vaskova https://orcid.org/0000-0001-8858-5434
Aneta Rotterova https://orcid.org/0000-0002-3331-5346
Marketa Miskerikova https://orcid.org/0000-0002-4392-3169
Lucie Zemanova https://orcid.org/0000-0002-2732-5935
Ondrej Benek https://orcid.org/0000-0001-6840-1933
Kamil Musilek https://orcid.org/0000-0002-7504-4062

REFERENCES

Aitken, L., Baillie, G., Pannifer, A., Morrison, A., Jones, P. S., Smith, T. K., McElroy, S. P., & Gunn-Moore, F. J. (2017). In vitro assay development and HTS of small-molecule human ABAD/17β-HSD10 inhibitors as therapeutics in Alzheimer's disease, SLAS Discov. *Advancements in Life Sciences*, *22*, 676–685. https://doi.org/10.1177/2472555217697964

Aitken, L., Benek, O., McKelvie, B. E., Hughes, R. E., Hroch, L., Schmidt, M., Major, L. L., Vinklarova, L., Kuca, K., Smith, T. K., Musilek, K., & Gunn-Moore, F. J. (2019). Novel Benzothiazole-based Ureas as 17β-HSD10 inhibitors, a potential Alzheimer's disease treatment. *Molecules (Basel, Switzerland)*, *24*, 2757. https://doi.org/10.3390/molecules24152757

Aitken, L., Quinn, S. D., Perez-Gonzalez, C., Samuel, I. D. W., Penedo, J. C., & Gunn-Moore, F. J. (2016). Morphology-specific inhibition of β-amyloid aggregates by 17β-Hydroxysteroid dehydrogenase type 10. *Chembiochem*, *17*, 1029–1037. https://doi.org/10.1002/cbic.201600081

Alvarez-De-La-Rosa, M., Silva, I., Nilsen, J., Pérez, M. M., García-Segura, L. M., Ávila, J., & Naftolin, F. (2005). Estradiol prevents neural tau hyperphosphorylation characteristic of Alzheimer's disease. *Annals of the new York Academy of Sciences*, *1052*, 210–224. https://doi.org/10.1196/annals.1347.016

Amtul, Z., Wang, L., Westaway, D., & Rozmahel, R. F. (2010). Neuroprotective mechanism conferred by 17beta-estradiol on the biochemical basis of Alzheimer's disease. *Neuroscience*, *169*, 781–786. https://doi.org/10.1016/j.neuroscience.2010.05.031

Ayan, D., Maltais, R., & Poirier, D. (2012). Identification of a 17β-hydroxysteroid dehydrogenase type 10 steroidal inhibitor: A tool to investigate the role of type 10 in Alzheimer's disease and prostate cancer. *ChemMedChem*, *7*, 1181–1184. https://doi.org/10.1002/cmdc.201200129

Benek, O., Hroch, L., Aitken, L., Dolezal, R., Guest, P., Benkova, M., Soukup, O., Musil, K., Kuca, K., Smith, T. K., Gunn-Moore, F., & Musilek, K. (2017). 6-benzothiazolyl ureas, thioureas and guanidines are potent inhibitors of ABAD/17β-HSD10 and potential drugs for Alzheimer's disease treatment: Design, synthesis and in vitro evaluation. *Medicinal Chemistry*, *13*, 345–358. https://doi.org/10.2174/1573406413666170109142725

Benek, O., Hroch, L., Aitken, L., Gunn-Moore, F., Vinklarova, L., Kuca, K., Perez, D. I., Perez, C., Martinez, A., Fisar, Z., & Musilek, K. (2018). 1-(benzo[d]thiazol-2-yl)-3-phenylureas as dual inhibitors of casein kinase 1 and ABAD enzymes for treatment of neurodegenerative disorders. *Journal of Enzyme Inhibition and Medicinal Chemistry*, *33*, 665–670. https://doi.org/10.1080/14756366.2018.1445736

Benek, O., Vaskova, M., Miskerikova, M., Schmidt, M., Andrys, R., Rotterova, A., Skarka, A., Hatlapatkova, J., Karasova, J. Z., Medvecky, M., Hroch, L., Vinklarova, L., Fisar, Z., Hroudova, J., Handl, J., Capek, J., Rousar, T., Kobrlova, T., Dolezal, R., … Musilek, K. (2023). Development of submicromolar 17β-HSD10 inhibitors and their in vitro and in vivo evaluation. *European Journal of Medicinal Chemistry*, *258*, 115593. https://doi.org/10.1016/j.ejmech.2023.115593

Bertoletti, N., Braun, F., Lepage, M., Möller, G., Adamski, J., Heine, A., Klebe, G., & Marchais-Oberwinkler, S. (2016). New insights into human 17β-hydroxysteroid dehydrogenase type 14: First crystal structures in complex with a steroidal ligand and with a potent non-steroidal inhibitor. *Journal of Medicinal Chemistry*, *59*, 6961–6967. https://doi.org/10.1021/acs.jmedchem.6b00293

Binstock, J. F., & Schulz, H. (1981). Fatty acid oxidation complex from Escherichia coli. *Methods in Enzymology*, *71 Pt C*, 403–411. https://doi.org/10.1016/0076-6879(81)71051-6

Boutin, S., Maltais, R., Roy, J., & Poirier, D. (2021). Synthesis of 17β-hydroxysteroid dehydrogenase type 10 steroidal inhibitors: Selectivity, metabolic stability and enhanced potency. *European Journal of Medicinal Chemistry*, *209*, 112909. https://doi.org/10.1016/j.ejmech.2020.112909

Boutin, S., & Poirier, D. (2018). Structure confirmation and evaluation of a nonsteroidal inhibitor of 17β-hydroxysteroid dehydrogenase type

14714159, 2023, 2, Downloaded from https://onlinelibrary.wiley.com/doi/10.1111/jnc.15917 by Charles University, Wiley Online Library on [12/11/2023]. See the Terms and Conditions (https://onlinelibrary.wiley.com/terms-and-conditions) on Wiley Online Library for rules of use; OA articles are governed by the applicable Creative Commons License

10. *Magnetochemistry*, *4*, 32. https://doi.org/10.3390/magnetochemistry4030032

Boutin, S., Roy, J., Maltais, R., Alata, W., Calon, F., & Poirier, D. (2018). Identification of steroidal derivatives inhibiting the transformations of allopregnanolone and estradiol by 17β-hydroxysteroid dehydrogenase type 10. *Bioorganic & Medicinal Chemistry Letters*, *28*, 3554–3559. https://doi.org/10.1016/j.bmcl.2018.09.031

Chen, J. X., & Yan, S. D. (2007). Amyloid-β-induced mitochondrial dysfunction. *Journal of Alzheimer's Disease*, *12*, 177–184.

Fišar, Z., Musílek, K., Benek, O., Hroch, L., Vinklářová, L., Schmidt, M., Hroudová, J., & Raboch, J. (2021). Effects of novel 17β-hydroxysteroid dehydrogenase type 10 inhibitors on mitochondrial respiration. *Toxicology Letters*, *339*, 12–19. https://doi.org/10.1016/j.toxlet.2020.12.012

Grimm, A., Lim, Y.-A., Mensah-Nyagan, A. G., Götz, J., & Eckert, A. (2012). Alzheimer's disease, oestrogen and mitochondria: An ambiguous relationship. *Molecular Neurobiology*, *46*, 151–160. https://doi.org/10.1007/s12035-012-8281-x

He, X.-Y., Isaacs, C., & Yang, S.-Y. (2018). Roles of mitochondrial 17β-hydroxysteroid dehydrogenase type 10 in Alzheimer's disease. *Journal of Alzheimer's Disease*, *62*, 665–673. https://doi.org/10.3233/JAD-170974

He, X. Y., Merz, G., Mehta, P., Schulz, H., & Yang, S. Y. (1999). Human brain short chain L-3-hydroxyacyl coenzyme a dehydrogenase is a single-domain multifunctional enzyme. Characterization of a novel 17beta-hydroxysteroid dehydrogenase. *The Journal of Biological Chemistry*, *274*, 15014–15019. https://doi.org/10.1074/jbc.274.21.15014

He, X. Y., Merz, G., Yang, Y. Z., Mehta, P., Schulz, H., & Yang, S. Y. (2001). Characterization and localization of human type10 17beta-hydroxysteroid dehydrogenase. *European Journal of Biochemistry*, *268*, 4899–4907. https://doi.org/10.1046/j.0014-2956.2001.02421.2421.x

He, X.-Y., Wegiel, J., & Yang, S.-Y. (2005). Intracellular oxidation of allopregnanolone by human brain type 10 17beta-hydroxysteroid dehydrogenase. *Brain Research*, *1040*, 29–35. https://doi.org/10.1016/j.brainres.2005.01.022

He, X.-Y., Wegiel, J., Yang, Y.-Z., Pullarkat, R., Schulz, H., & Yang, S.-Y. (2005). Type 10 17beta-hydroxysteroid dehydrogenase catalyzing the oxidation of steroid modulators of gamma-aminobutyric acid type a receptors. *Molecular and Cellular Endocrinology*, *229*, 111–117. https://doi.org/10.1016/j.mce.2004.08.011

Hroch, L., Benek, O., Guest, P., Aitken, L., Soukup, O., Janockova, J., Musil, K., Dohnal, V., Dolezal, R., Kuca, K., Smith, T. K., Gunn-Moore, F., & Musilek, K. (2016). Design, synthesis and in vitro evaluation of benzothiazole-based ureas as potential ABAD/17β-HSD10 modulators for Alzheimer's disease treatment. *Bioorganic & Medicinal Chemistry Letters*, *26*, 3675–3678. https://doi.org/10.1016/j.bmcl.2016.05.087

Hroch, L., Guest, P., Benek, O., Soukup, O., Janockova, J., Dolezal, R., Kuca, K., Aitken, L., Smith, T. K., Gunn-Moore, F., Zala, D., Ramsay, R. R., & Musilek, K. (2017). Synthesis and evaluation of frentizole-based indolyl thiourea analogues as MAO/ABAD inhibitors for Alzheimer's disease treatment. *Bioorganic & Medicinal Chemistry*, *25*, 1143–1152. https://doi.org/10.1016/j.bmc.2016.12.029

Kissinger, C. R., Rejto, P. A., Pelletier, L. A., Thomson, J. A., Showalter, R. E., Abreo, M. A., Agree, C. S., Margosiak, S., Meng, J. J., Aust, R. M., Vanderpool, D., Li, B., Tempczyk-Russell, A., & Villafranca, J. E. (2004). Crystal structure of human ABAD/HSD10 with a bound inhibitor: Implications for design of Alzheimer's disease therapeutics. *Journal of Molecular Biology*, *342*, 943–952. https://doi.org/10.1016/j.jmb.2004.07.071

Lim, Y.-A., Grimm, A., Giese, M., Mensah-Nyagan, A. G., Villafranca, J. E., Ittner, L. M., Eckert, A., & Götz, J. (2011). Inhibition of the mitochondrial enzyme ABAD restores the amyloid-β-mediated deregulation of estradiol. *PLoS One*, *6*, e28887. https://doi.org/10.1371/journal.pone.0028887

Lustbader, J. W., Cirilli, M., Lin, C., Xu, H. W., Takuma, K., Wang, N., Caspersen, C., Chen, X., Pollak, S., Chaney, M., Trinchese, F., Liu, S., Gunn-Moore, F., Lue, L.-F., Walker, D. G., Kuppusamy, P., Zewier, Z. L., Arancio, O., Stern, D., … Wu, H. (2004). ABAD directly links Abeta to mitochondrial toxicity in Alzheimer's disease. *Science*, *304*, 448–452. https://doi.org/10.1126/science.1091230

Manly, J. J., Merchant, C. A., Jacobs, D. M., Small, S. A., Bell, K., Ferin, M., & Mayeux, R. (2000). Endogenous estrogen levels and Alzheimer's disease among postmenopausal women. *Neurology*, *54*, 833–837. https://doi.org/10.1212/wnl.54.4.833

Marx, C. E., Trost, W. T., Shampine, L. J., Stevens, R. D., Hulette, C. M., Steffens, D. C., Ervin, J. F., Butterfield, M. I., Blazer, D. G., Massing, M. W., & Lieberman, J. A. (2006). The neurosteroid allopregnanolone is reduced in prefrontal cortex in Alzheimer's disease. *Biological Psychiatry*, *60*, 1287–1294. https://doi.org/10.1016/j.biopsych.2006.06.017

Metodieva, V., Smith, T., & Gunn-Moore, F. (2022). The mitochondrial enzyme 17βHSD10 modulates ischemic and amyloid-β-induced stress in primary mouse astrocytes. *ENeuro*, *9*, ENEURO.0040-22.2022. https://doi.org/10.1523/ENEURO.0040-22.2022

Morsy, A., Maddeboina, K., Gao, J., Wang, H., Valdez, J., Dow, L. F., Wang, X., & Trippier, P. C. (2022). Functionalized Allopurinols targeting amyloid-binding alcohol dehydrogenase rescue Aβ-induced mitochondrial dysfunction. *ACS Chemical Neuroscience*, *13*, 2176–2190. https://doi.org/10.1021/acschemneuro.2c00246

Morsy, A., & Trippier, P. C. (2019). Amyloid-binding alcohol dehydrogenase (ABAD) inhibitors for the treatment of Alzheimer's disease. *Journal of Medicinal Chemistry*, *62*, 4252–4264. https://doi.org/10.1021/acs.jmedchem.8b01530

Muirhead, K. E. A., Froemming, M., Li, X., Musilek, K., Conway, S. J., Sames, D., & Gunn-Moore, F. J. (2010). (–)-CHANA, a fluorogenic probe for detecting amyloid binding alcohol dehydrogenase HSD10 activity in living cells. *ACS Chemical Biology*, *5*, 1105–1114. https://doi.org/10.1021/cb100199m

Nilsen, J. (2008). Estradiol and neurodegenerative oxidative stress. *Frontiers in Neuroendocrinology*, *29*, 463–475. https://doi.org/10.1016/j.yfrne.2007.12.005

Nilsen, J., Chen, S., Irwin, R. W., Iwamoto, S., & Brinton, R. D. (2006). Estrogen protects neuronal cells from amyloid beta-induced apoptosis via regulation of mitochondrial proteins and function. *BMC Neuroscience*, *7*, 74. https://doi.org/10.1186/1471-2202-7-74

Oerum, S., Roovers, M., Leichsenring, M., Acquaviva-Bourdain, C., Beermann, F., Gemperle-Britschgi, C., Fouilhoux, A., Korwitz-Reichelt, A., Bailey, H. J., Droogmans, L., Oppermann, U., Sass, J. O., & Yue, W. W. (2017). Novel patient missense mutations in the HSD17B10 gene affect dehydrogenase and mitochondrial tRNA modification functions of the encoded protein. *Biochimica et Biophysica Acta—Molecular Basis of Disease*, *1863*, 3294–3302. https://doi.org/10.1016/j.bbadis.2017.09.002

Oppermann, U. C., Salim, S., Tjernberg, L. O., Terenius, L., & Jörnvall, H. (1999). Binding of amyloid beta-peptide to mitochondrial hydroxyacyl-CoA dehydrogenase (ERAB): Regulation of an SDR enzyme activity with implications for apoptosis in Alzheimer's disease. *FEBS Letters*, *451*, 238–242. https://doi.org/10.1016/s0014-5793(99)00586-4

Pike, C. J., Carroll, J. C., Rosario, E. R., & Barron, A. M. (2009). Protective actions of sex steroid hormones in Alzheimer's disease. *Frontiers in Neuroendocrinology*, *30*, 239–258. https://doi.org/10.1016/j.yfrne.2009.04.015

Powell, A. J., Read, J. A., Banfield, M. J., Gunn-Moore, F., Yan, S. D., Lustbader, J., Stern, A. R., Stern, D. M., & Brady, R. L. (2000). Recognition of structurally diverse substrates by type II 3-hydroxyacyl-CoA dehydrogenase (HADH II)/amyloid-beta binding alcohol dehydrogenase (ABAD). *Journal of Molecular Biology*, *303*, 311–327. https://doi.org/10.1006/jmbi.2000.4139

Qian, X., Cao, H., Ma, Q., Wang, Q., He, W., Qin, P., Ji, B., Yuan, K., Yang, F., Liu, X., Lian, Q., & Li, J. (2015). Allopregnanolone attenuates Aβ25-35-induced neurotoxicity in PC12 cells by reducing oxidative

14714159, 2023, 2, Downloaded from https://onlinelibrary.wiley.com/doi/10.1111/jnc.15917 by Charles University, Wiley Online Library on [12/11/2023]. See the Terms and Conditions (https://onlinelibrary.wiley.com/terms-and-conditions) on Wiley Online Library for rules of use; OA articles are governed by the applicable Creative Commons License

stress. *International Journal of Clinical and Experimental Medicine*, *8*, 13610–13615.

Rauschenberger, K., Schöler, K., Sass, J. O., Sauer, S., Djuric, Z., Rumig, C., Wolf, N. I., Okun, J. G., Kölker, S., Schwarz, H., Fischer, C., Grziwa, B., Runz, H., Nümann, A., Shafqat, N., Kavanagh, K. L., Hämmerling, G., Wanders, R. J. A., Shield, J. P. H., … Zschocke, J. (2010). A non-enzymatic function of 17beta-hydroxysteroid dehydrogenase type 10 is required for mitochondrial integrity and cell survival. *EMBO Molecular Medicine*, *2*, 51–62. https://doi.org/10.1002/emmm.200900055

Schmidt, M., Benek, O., Vinklarova, L., Hrabinova, M., Zemanova, L., Chribek, M., Kralova, V., Hroch, L., Dolezal, R., Lycka, A., Prchal, L., Jun, D., Aitken, L., Gunn-Moore, F., Kuca, K., & Musilek, K. (2020). Benzothiazolyl Ureas are low micromolar and uncompetitive inhibitors of 17β-HSD10 with implications to Alzheimer's disease treatment. *International Journal of Molecular Sciences*, *21*, E2059. https://doi.org/10.3390/ijms21062059

Seo, J.-S., Lee, K.-W., Kim, T.-K., Baek, I.-S., Im, J.-Y., & Han, P.-L. (2011). Behavioral stress causes mitochondrial dysfunction via ABAD up-regulation and aggravates plaque pathology in the brain of a mouse model of Alzheimer disease. *Free Radical Biology & Medicine*, *50*, 1526–1535. https://doi.org/10.1016/j.freeradbiomed.2011.02.035

Shafqat, N., Marschall, H.-U., Filling, C., Nordling, E., Wu, X.-Q., Björk, L., Thyberg, J., Mårtensson, E., Salim, S., Jörnvall, H., & Oppermann, U. (2003). Expanded substrate screenings of human and drosophila type 10 17beta-hydroxysteroid dehydrogenases (HSDs) reveal multiple specificities in bile acid and steroid hormone metabolism: Characterization of multifunctional 3alpha/7alpha/7beta/17beta/20beta/21-HSD. *The Biochemical Journal*, *376*, 49–60. https://doi.org/10.1042/BJ20030877

Simpkins, J. W., & Dykens, J. A. (2008). Mitochondrial mechanisms of estrogen neuroprotection. *Brain Research Reviews*, *57*, 421–430. https://doi.org/10.1016/j.brainresrev.2007.04.007

Swerdlow, R. H. (2018). Mitochondria and mitochondrial cascades in Alzheimer's disease. *Journal of Alzheimer's Disease*, *62*, 1403–1416. https://doi.org/10.3233/JAD-170585

Swerdlow, R. H., Burns, J. M., & Khan, S. M. (2014). The Alzheimer's disease mitochondrial cascade hypothesis: Progress and perspectives. *Biochimica et Biophysica Acta*, *1842*, 1219–1231. https://doi.org/10.1016/j.bbadis.2013.09.010

Takuma, K., Yao, J., Huang, J., Xu, H., Chen, X., Luddy, J., Trillat, A.-C., Stern, D. M., Arancio, O., & Yan, S. S. (2005). ABAD enhances Abeta-induced cell stress via mitochondrial dysfunction. *FASEB Journal*, *19*, 597–598. https://doi.org/10.1096/fj.04-2582fje

Tieu, K., Perier, C., Vila, M., Caspersen, C., Zhang, H.-P., Teismann, P., Jackson-Lewis, V., Stern, D. M., Yan, S. D., & Przedborski, S. (2004). L-3-hydroxyacyl-CoA dehydrogenase II protects in a model of Parkinson's disease. *Annals of Neurology*, *56*, 51–60. https://doi.org/10.1002/ana.20133

Vagenende, V., Yap, M. G. S., & Trout, B. L. (2009). Mechanisms of protein stabilization and prevention of protein aggregation by glycerol. *Biochemistry*, *48*, 11084–11096. https://doi.org/10.1021/bi900649t

Vinklarova, L., Schmidt, M., Benek, O., Kuca, K., Gunn-Moore, F., & Musilek, K. (2020). Friend or enemy? Review of 17β-HSD10 and its role in human health or disease. *Journal of Neurochemistry*, *155*, 231–249. https://doi.org/10.1111/jnc.15027

Xie, Y., Deng, S., Chen, Z., Yan, S., & Landry, D. W. (2006). Identification of small-molecule inhibitors of the Abeta-ABAD interaction. *Bioorganic & Medicinal Chemistry Letters*, *16*, 4657–4660. https://doi.org/10.1016/j.bmcl.2006.05.099

Yan, S. D., Fu, J., Soto, C., Chen, X., Zhu, H., Al-Mohanna, F., Collison, K., Zhu, A., Stern, E., Saido, T., Tohyama, M., Ogawa, S., Roher, A., & Stern, D. (1997). An intracellular protein that binds amyloid-beta peptide and mediates neurotoxicity in Alzheimer's disease. *Nature*, *389*, 689–695. https://doi.org/10.1038/39522

Yan, S. D., Shi, Y., Zhu, A., Fu, J., Zhu, H., Zhu, Y., Gibson, L., Stern, E., Collison, K., Al-Mohanna, F., Ogawa, S., Roher, A., Clarke, S. G., & Stern, D. M. (1999). Role of ERAB/L-3-hydroxyacyl-coenzyme a dehydrogenase type II activity in Abeta-induced cytotoxicity. *The Journal of Biological Chemistry*, *274*, 2145–2156. https://doi.org/10.1074/jbc.274.4.2145

Yang, S. Y., & He, X. Y. (2001). Role of type 10 17beta-hydroxysteroid dehydrogenase in the pathogenesis of Alzheimer's disease. *Advances in Experimental Medicine and Biology*, *487*, 101–110. https://doi.org/10.1007/978-1-4615-1249-3_8

Yang, S.-Y., He, X.-Y., Isaacs, C., Dobkin, C., Miller, D., & Philipp, M. (2014). Roles of 17β-hydroxysteroid dehydrogenase type 10 in neurodegenerative disorders. *The Journal of Steroid Biochemistry and Molecular Biology*, *143*, 460–472. https://doi.org/10.1016/j.jsbmb.2014.07.001

Yang, S.-Y., He, X.-Y., & Miller, D. (2007). HSD17B10: A gene involved in cognitive function through metabolism of isoleucine and neuroactive steroids. *Molecular Genetics and Metabolism*, *92*, 36–42. https://doi.org/10.1016/j.ymgme.2007.06.001

Yang, S.-Y., He, X.-Y., & Miller, D. (2011). Hydroxysteroid (17β) dehydrogenase X in human health and disease. *Molecular and Cellular Endocrinology*, *343*, 1–6. https://doi.org/10.1016/j.mce.2011.06.011

Yang, S.-Y., He, X.-Y., Olpin, S. E., Sutton, V. R., McMenamin, J., Philipp, M., Denman, R. B., & Malik, M. (2009). Mental retardation linked to mutations in the HSD17B10 gene interfering with neurosteroid and isoleucine metabolism. *Proceedings of the National Academy of Sciences of the United States of America*, *106*, 14820–14824. https://doi.org/10.1073/pnas.0902377106

Yang, S.-Y., He, X.-Y., & Schulz, H. (2005). Multiple functions of type 10 17beta-hydroxysteroid dehydrogenase. *Trends in Endocrinology and Metabolism*, *16*, 167–175. https://doi.org/10.1016/j.tem.2005.03.006

Yue, X., Lu, M., Lancaster, T., Cao, P., Honda, S.-I., Staufenbiel, M., Harada, N., Zhong, Z., Shen, Y., & Li, R. (2005). Brain estrogen deficiency accelerates Abeta plaque formation in an Alzheimer's disease animal model. *Proceedings of the National Academy of Sciences of the United States of America*, *102*, 19198–19203. https://doi.org/10.1073/pnas.0505203102

Zampieri, S., Mellon, S. H., Butters, T. D., Nevyjel, M., Covey, D. F., Bembi, B., & Dardis, A. (2009). Oxidative stress in NPC1 deficient cells: Protective effect of allopregnanolone. *Journal of Cellular and Molecular Medicine*, *13*, 3786–3796. https://doi.org/10.1111/j.1582-4934.2008.00493.x

Zhang, J. H., Chung, T. D., & Oldenburg, K. R. (1999). A simple statistical parameter for use in evaluation and validation of high throughput screening assays. *Journal of Biomolecular Screening*, *4*, 67–73. https://doi.org/10.1177/108705719900400206

Zschocke, J. (2012). HSD10 disease: Clinical consequences of mutations in the HSD17B10 gene. *Journal of Inherited Metabolic Disease*, *35*, 81–89. https://doi.org/10.1007/s10545-011-9415-4

SUPPORTING INFORMATION

Additional supporting information can be found online in the Supporting Information section at the end of this article.

How to cite this article: Schmidt, M., Vaskova, M., Rotterova, A., Fiandova, P., Miskerikova, M., Zemanova, L., Benek, O., & Musilek, K. (2023). Physiologically relevant fluorescent assay for identification of 17β-hydroxysteroid dehydrogenase type 10 inhibitors. *Journal of Neurochemistry*, *167*, 154–167. https://doi.org/10.1111/jnc.15917

14714159, 2023, 2, Downloaded from https://onlinelibrary.wiley.com/doi/10.1111/jnc.15917 by Charles University, Wiley Online Library on [12/11/2023]. See the Terms and Conditions (https://onlinelibrary.wiley.com/terms-and-conditions) on Wiley Online Library for rules of use; OA articles are governed by the applicable Creative Commons License

Supplementary material

Physiologically relevant fluorescent assay for identification of 17β-hydroxysteroid dehydrogenase type 10 inhibitors

Monika Schmidt[1, #, *], Michaela Vaskova [1, #], Aneta Rotterova [1], Pavlina Fiandova [1], Marketa Miskerikova [1], Lucie Zemanova [1], Ondrej Benek[1, *] and Kamil Musilek[1]

[1] Department of Chemistry, Faculty of Science, University of Hradec Kralove, Czech Republic

[#] These authors contributed equally

Table S1. 10 μM and 1 μM screening of HSD10 inhibitors using E2 assay. Values are given as means ± SD from single experiment (10 μM screening, n = 4) or two independent experiments (1 μM screening, n = 8) performed in tetraplicates.

Cmp	HSD10 Residual Activity (%)	
	10 μM Screening	1 μM Screening
AG18051	0.0	20.0 ± 1.2
1	19.5 ± 1.2	63.9 ± 3.3
2	30.6 ± 0.4	82.7 ± 1.1
3	0.0	53.6 ± 4.0
4	10.8 ± 2.4	54.3 ± 3.3
5	12.1 ± 1.9	49.1 ± 2.2
6	14.1 ± 0.7	51.0 ± 0.7
7	28.8 ± 1.5	74.8 ± 3.4
8	12.3 ± 1.4	53.3 ± 4.0
9	21.0 ± 1.2	65.0 ± 3.0
10	13.0 ± 0.8	41.9 ± 1.4
11	15.3 ± 0.8	57.1 ± 1.9
12	11.3 ± 2.8	51.9 ± 1.1
13	18.9 ± 2.1	45.1 ± 4.2
14	0.0	33.6 ± 3.6
15	9.0 ± 0.5	61.2 ± 4.6
16	2.6 ± 0.2	49.5 ± 0.6

17	15.5 ± 2.1	70.3 ± 3.9
18	0.0	37.0 ± 2.4
19	0.0	58.5 ± 5.2
20	26.1 ± 2.4	58.1 ± 2.1
21	9.7 ± 1.7	65.2 ± 0.8
22	0.0	30.8 ± 1.1
23	22.5 ± 0.6	55.4 ± 4.7
24	14.8 ± 1.7	55.3 ± 3.4
25	6.2 ± 1.0	41.1 ± 4.5
26	0.0	14.7 ± 0.4
27	0.0	40.7 ± 5.4
28	0.3 ± 1.9	29.7 ± 2.4
29	3.2 ± 0.8	43.5 ± 0.9
30	50.0 ± 4.4	61.3 ± 1.4
31	0.0	51.0 ± 0.1
32	10.9 ± 3.5	65.7 ± 6.9
33	36.3 ± 3.6	67.5 ± 5.9
34	0.0	19.2 ± 3.9
35	15.9 ± 0.2	69.6 ± 4.4
36	23.3 ± 0.4	84.3 ± 0.3
37	35.1 ± 2.4	113.4 ± 4.5
38	20.6 ± 1.5	75.3 ± 4.2

Table S2. Melting temperatures (T_m) for HSD10 in the presence of the compounds **26** and **34**. Enzyme HSD10 treated with inhibitors in the absence or presence of 250 μM NAD^+ cofactor. Values are given as means ± SD from single experiment performed in triplicate (n = 3).

	T_m values (°C)			
	w/o NAD^+		**with NAD^+**	
DMSO	48.4 ± 0.1		51.5 ± 0.4	
Compound	**25 μM**	**50 μM**	**25 μM**	**50 μM**
AG18051	48.4 ± 0.2	48.6 ± 1.0	63.7 ± 0.6	65.2 ± 0.7
26	56.6 ± 0.4	58.1 ± 0.1	61.3 ± 0.0	61.5 ± 0.1
34	47.9 ± 0.1	49.8 ± 0.6	54.1 ± 0.0	57.2 ± 0.1

Table S3. Statistical reports for Differential Scanning Fluorimetry. Differences between groups were determined by the Student's unpaired two-tailed t-test. Degrees of freedom = 4. The data were normally distributed according to the Shapiro-Wilk test.

Compound	w/o NAD^+		+ NAD^+	
	P value	**t value**	**P value**	**t value**
25 µM AG18051	0.6919	0.4261	<0.0001	39.24
50 µM AG18051	0.4199	0.8980	<0.0001	30.88
25 µM cmp 26	<0.0001	40.45	<0.0001	47.08
50 µM cmp 26	<0.0001	151.0	<0.0001	45.90
25 µM cmp 34	0.0003	12.25	0.0002	12.49
50 µM cmp 34	0.0140	4.171	<0.0001	26.88

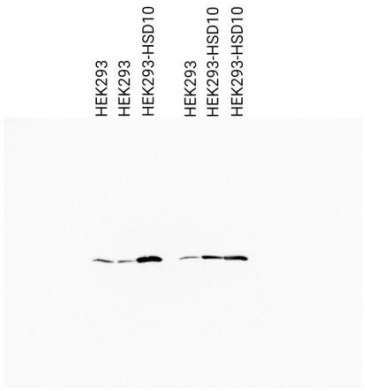

Figure S1: Original full Western blot image of HEK293-wt and HEK293-HSD10 overexpressing cells.

10.4 Publikace IV

Hanzlova, M.†; Miskerikova, M.†; Rotterova, A.†; Jurkova, K.; Hamsikova, M.; Haleckova, A.; Andrys R.; Schmidt, M.; Benek, O.; Musilek, K., 2023. Nanomolar benzothiazolyl-based inhibitors of 17β-HSD10 with cellular bioactivity. ACS Med. Chem. Lett. 14, 1724−1732. https://doi.org/10.1021/acsmedchemlett.3c00355

ACS Medicinal Chemistry Letters

pubs.acs.org/acsmedchemlett Letter

Nanomolar Benzothiazole-Based Inhibitors of 17β-HSD10 with Cellular Bioactivity

Michaela Hanzlova,[#] Marketa Sedlacek Miskerikova,[#] Aneta Rotterova,[#] Katarina Chalupova, Katarina Jurkova, Marie Hamsikova, Rudolf Andrys, Annamaria Haleckova, Jana Svobodova, Monika Schmidt,* Ondrej Benek,* and Kamil Musilek

Cite This: *ACS Med. Chem. Lett.* 2023, 14, 1724−1732 Read Online

ACCESS | Metrics & More | Article Recommendations | Supporting Information

ABSTRACT: Multifunctional mitochondrial enzyme 17β-hydroxysteroid dehydrogenase type 10 (17β-HSD10) is a potential drug target for the treatment of various pathologies. The most discussed is the pathology associated with Alzheimer's disease (AD), where 17β-HSD10 overexpression and its interaction with amyloid-β peptide contribute to mitochondrial dysfunction and neuronal stress. In this work, a series of new benzothiazole-derived 17β-HSD10 inhibitors were designed based on the structure−activity relationship analysis of formerly published inhibitors. A set of enzyme-based and cell-based methods were used to evaluate the inhibitory potency of new compounds, their interaction with the enzyme, and their cytotoxicity. Most compounds exhibited significantly a higher inhibitory potential compared to published benzothiazolyl ureas and good target engagement in a cellular environment accompanied by low cytotoxicity. The best hits displayed mixed-type inhibition with half maximal inhibitory concentration (IC_{50}) values in the nanomolar range for the purified enzyme (**3**−**7**, **15**) and/or low micromolar IC_{50} values in the cell-based assay (**6**, **13**−**16**).

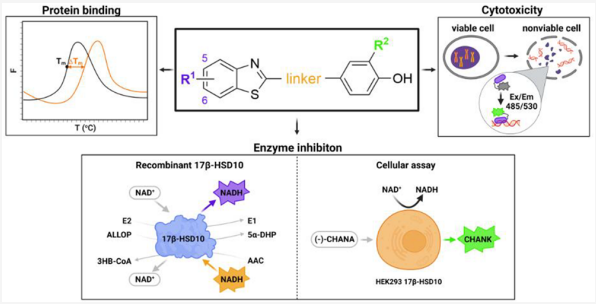

KEYWORDS: *Amyloid-binding alcohol dehydrogenase (ABAD), Alzheimer's disease, Benzothiazole, Enzyme inhibition, 17β-Hydroxysteroid dehydrogenase type 10 (17β-HSD10)*

Downloaded via CHARLES UNIV IN PRAGUE on December 15, 2023 at 13:44:56 (UTC).
See https://pubs.acs.org/sharingguidelines for options on how to legitimately share published articles.

The mitochondrial enzyme 17β-hydroxysteroid dehydrogenase type 10 (17β-HSD10) catalyzes the conversion of a broad range of substrates, e.g., fatty acids, alcohols, neurosteroids, and sex steroids, and is involved in many cellular processes.[1] 17β-HSD10 is considered to play an important role in metabolic homeostasis, mitochondrial structural and functional integrity, and the cellular stress response.[1−3] Thus, its altered functionality and/or expression levels are linked to the pathophysiology of various diseases such as neurodegenerative disorders and certain cancer types.[1,4,5]

The most discussed is the pathology associated with Alzheimer's disease (AD) because 17β-HSD10 is an interaction partner of amyloid-beta peptide (Aβ), and its elevated expression was found in AD brains.[6−9] The overexpression of 17β-HSD10 seems to disrupt the homeostasis of neurosteroid metabolism, and it may alter the levels of neuroprotective steroids, such as 17β-estradiol (E2) and allopregnanolone (ALLOP), in different brain regions.[10,11] Both these neurosteroids have significant effects on mitochondrial function, bioenergetics, and antioxidant processes, as well as AD-related pathologic hallmarks, i.e., accumulation of Aβ and hyperphosphorylated tau protein.[12,13] Therefore, inhibition of the 17β-HSD10 enzymatic activity presents a plausible therapeutic strategy for AD treatment, as the enzyme's inhibition could restore the disturbed homeostasis of E2 and ALLOP neurosteroids.

To date, only a limited number of potent 17β-HSD10 inhibitors have been discovered.[14,15] According to their nature and structure, they can be divided into three main classes: pyrazolopyrimidines,[14,16] steroids,[17−19] and benzothiazolyl ureas.[20−27] The benzothiazolyl urea inhibitors have received the most attention in recent years. The most promising benzothiazolyl ureas were published as submicromolar inhibitors of 17β-HSD10, and they were found to be bioavailable after peroral administration, although they showed uncertain results of penetration into the brain (**1** and **2**; $IC_{50} \approx 0.3$ μM; Figure 1).[27]

Received: August 11, 2023
Revised: November 3, 2023
Accepted: November 7, 2023
Published: November 10, 2023

ACS Publications © 2023 American Chemical Society

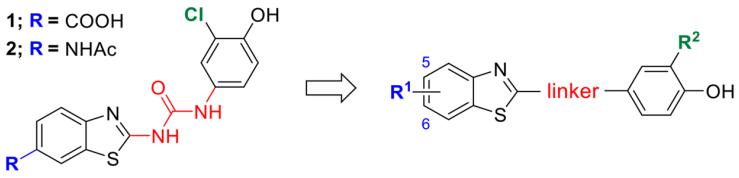

Figure 1. Structural design of new 17β-HSD10 inhibitors based on modifications of parent molecules **1** and **2**.

Table 1. List of Newly Designed Compounds and Their Calculated BBB Score[a]

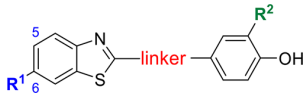

ID	R^1	Linker	R^2	BBB*	ID	R^1	Linker	R^2	BBB*
3	1*H*-tetrazol-5-yl		Cl	1.41	10	COOH		Cl	2.43
4	SO_2NH_2		Cl	2.10	11	COOH		Cl	3.20
5	$NHCONH_2$		Cl	2.10	12	COOH		Cl	3.23
6	$NHSO_2Me$		Cl	2.47	13	NHAc		Cl	4.25
7	COOH		CF_3	2.16	14	NHAc		CF_3	4.26
8	NHAc		CF_3	3.31	15	NHAc		Cl	4.26
9	5-COOH		Cl	2.25	16	NHAc		Cl	4.14

[a]Calculations of the BBB score were performed using MOE 2022.02 software.[30]

The goal of this study was to generate new benzothiazole-based inhibitors with an enhanced inhibitory ability against the 17β-HSD10 enzyme and/or with improved physicochemical properties, that would be active also at the cellular level. For this purpose, we employed the newly established 17β-HSD10 enzymatic assays utilizing physiological substrates E2 and ALLOP,[28] as well as the cellular assay utilizing the (−)-cyclohexenyl amino naphthalene alcohol ((−)−CHANA) fluorogenic probe[29] in the HEK293 cell line overexpressing 17β-HSD10.

The structures of newly designed compounds originate from previously identified submicromolar inhibitors **1** and **2** (Figure 1).[27] The new compounds consist of two aromatic moieties (benzothiazolyl and phenyl) connected via a 2- or 3-membered linker. The carboxyl or the acetamide substitution in position 6 of the benzothiazole moiety of the parent inhibitors (**1**, **2**) was either retained or replaced by substituents that are isosteric or with similar physicochemical properties (i.e., acidic and/or hydrogen bond-donating), namely, tetrazole, sulfonyl amide, methanesulfonamide, and urea. The phenyl moiety always bears a 4-hydroxy substitution, which is necessary for good inhibitory activity,[21,22,25,26] and an electron-withdrawing group in position 3, namely, chlorine (similar to **1**, **2**) or a trifluoromethyl group. The trifluoromethyl group was previously identified as potentially superior in terms of inhibition ability.[27] The linker consists of urea, amide, methyleneamine, or ethyleneamine, and in all cases, the benzothiazolyl moiety was attached to the linker via its nitrogen atom, as this structural feature was found essential for inhibitory activity.[25,27] Finally, two particular modifications were made to broaden the structure−activity relationship study; i.e., the carboxyl group was moved to position 5 of benzothiazolyl moiety, or the ethyleneamine linker was acetylated. The whole list of 14 designed compounds (**3**−**16**) is presented in Table 1.

Crossing the blood-brain barrier (BBB) and entering brain cells are prerequisites for the pharmacological relevance of 17β-HSD10 inhibitors as treatment for AD. The introduction of aliphatic linkers instead of original urea (or amide) was driven by predictions of cell permeability and brain bioavailability performed in a previous study by Benek et al.[27] Here, we have employed the "BBB score" algorithm to predict the brain bioavailability of designed molecules.[31] This algorithm uses several calculated physicochemical descriptors: number of aromatic rings and heavy atoms, molecular weight, number of hydrogen bond donors and hydrogen bond acceptors, topological polar surface area, and pK_a. The final score ranges from 0−6, with compounds scoring ≥4 being predicted to likely permeate via BBB, while compounds scoring ≤2 are unlikely to do so. As can be seen in Table 1, compounds with an aliphatic linker showed a higher BBB score

https://doi.org/10.1021/acsmedchemlett.3c00355
ACS Med. Chem. Lett. 2023, 14, 1724−1732

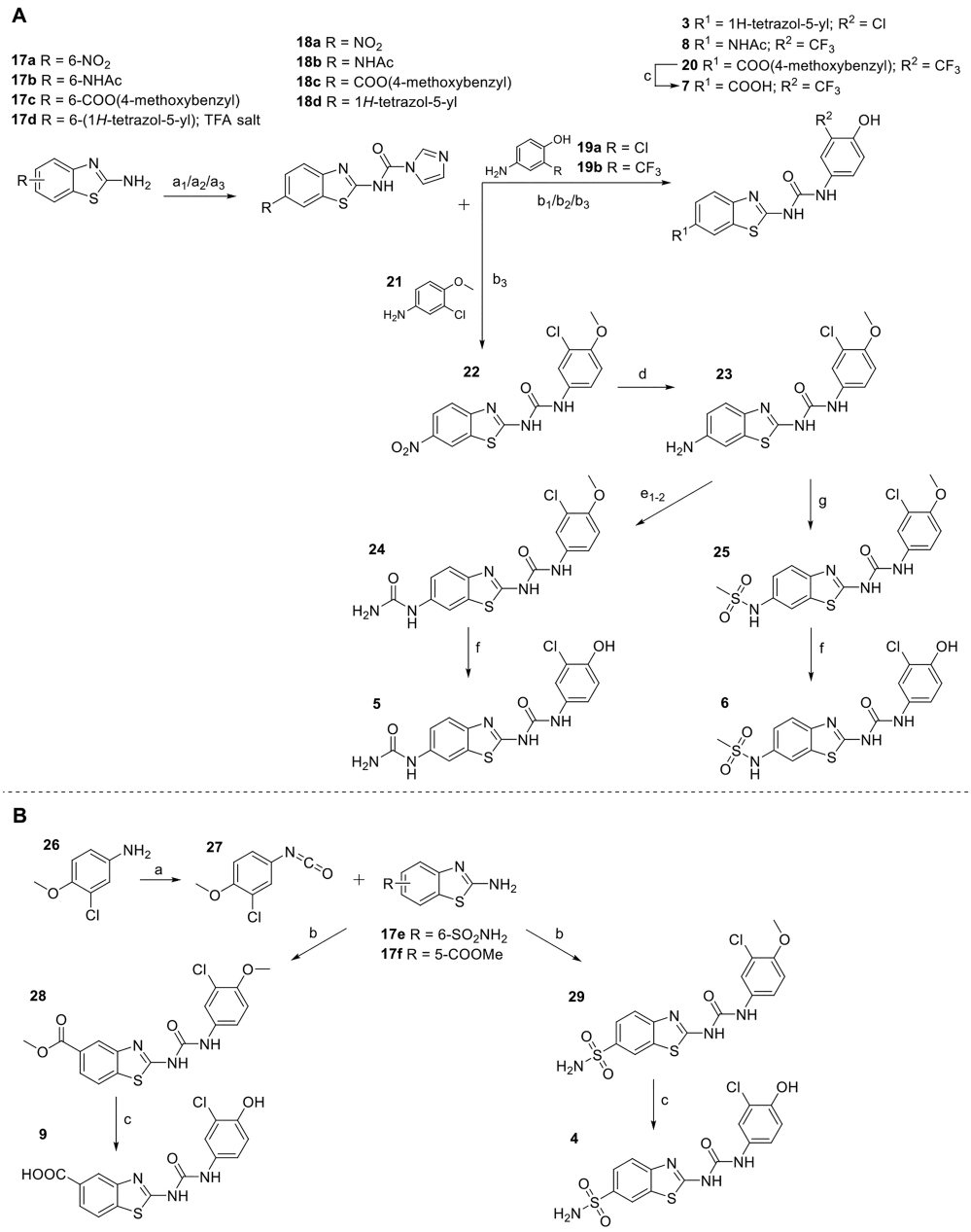

Figure 2. General method for the synthesis of the compounds containing a urea linker in their structure (i.e., **3**–**9**). (A) General synthesis of compounds **3** and **5**–**8** using a synthetic route via CDI. Reagents and conditions: (a_1) CDI, DIPEA, DCM, reflux (for **18d**); (a_2) CDI, MeCN, DMF, 85 °C (for **18c**); (a_3) CDI, DCM, reflux (for **18b** and **18a**); (b_1) MeCN, reflux (for **3**); (b_2) DMF, 60 °C (for **20**); (b_3) MeCN, 70 °C (for **8** and **22**); (c) gl. AcOH, 1 M HCl in AcOH, RT; (d) Fe, NH_4Cl, MeOH:H_2O:THF, 50 °C; (e_1) CDI, DMF, 50 °C; (e_2) 25% aq. sol. NH_3, 50 °C; (f) $AlCl_3$, DCE, 70 °C; (g) MsCl, pyridine, RT. (B) Synthesis of compounds **4** and **9** using a synthetic route via isocyanate. Reagents and conditions: (a) triphosgene, TEA, and DCM, reflux; (b) THF, reflux; (c) $AlCl_3$, DCE, 80 °C.

and thus are predicted to be more likely to enter cells and cross the BBB.

Generally, the urea-linked compounds were prepared via reacting 1,3-benzothiazol-2-amines (**17a**–**d**) with 1,1′-carbonyldiimidazole to give reactive intermediates (**18a**–**d**), which were consequently treated with various aniline derivatives (**19a**–**b** and **21**) to yield the 1-benzothiazol-3-phenylureas (Figure 2A). The resulting ureas were either final products (**3** and **8**) or intermediates (**20** and **22**) for further synthesis. The 4-methoxybenzyl ester derivative **20** was hydrolyzed to yield final product **7**. Nitro derivative **22** was reduced to the corresponding amine **23**. To obtain inhibitor **5**, intermediate **23** was first treated with CDI and subsequently with a 25% aqueous ammonia solution to form a 6-urea substituent (intermediate **24**). Next, intermediate **24** was demethylated to yield the final product **5**. To form inhibitor **6**, intermediate **23**

https://doi.org/10.1021/acsmedchemlett.3c00355
ACS Med. Chem. Lett. 2023, 14, 1724−1732

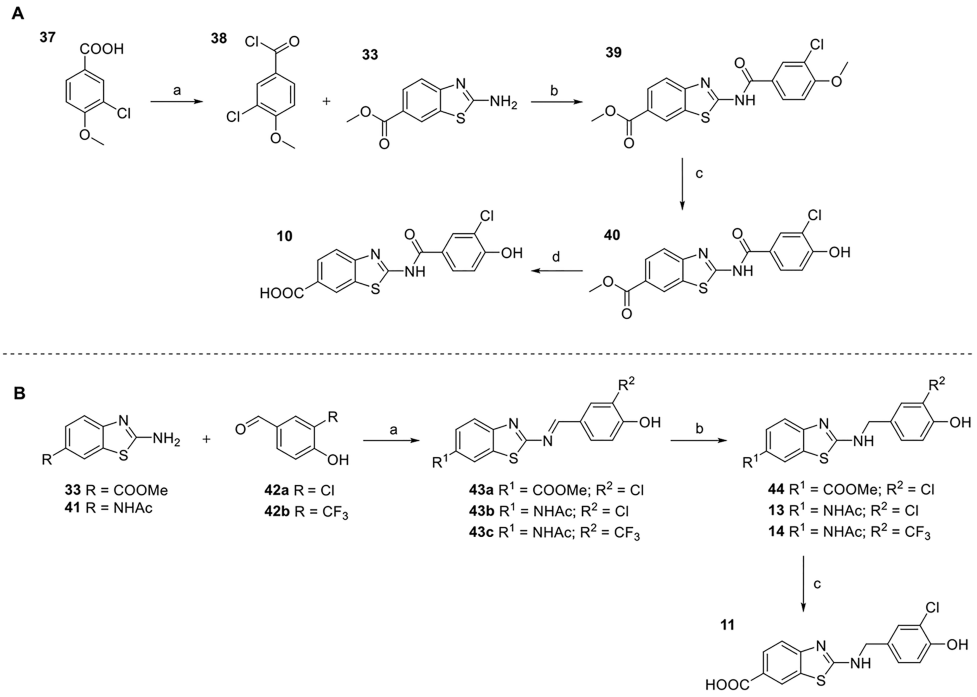

Figure 3. Synthesis of compounds harboring two-membered aliphatic linker (**11**, **13**, and **14**), and compound **10** with amide linker. (A) Synthesis of compound **10**. Reagents and conditions: (a) oxalyl chloride, DCM, RT; (b) toluene, reflux; (c) $AlCl_3$, DCE, 70 °C; (d) 1 M aq. NaOH/EtOH, reflux. (B) Synthesis of compounds **11**, **13**, and **14**. Reagents and conditions: (a) toluene, reflux; (b) $NaBH_3CN$, MeOH, reflux; (c) 1 M aq. NaOH/EtOH, reflux.

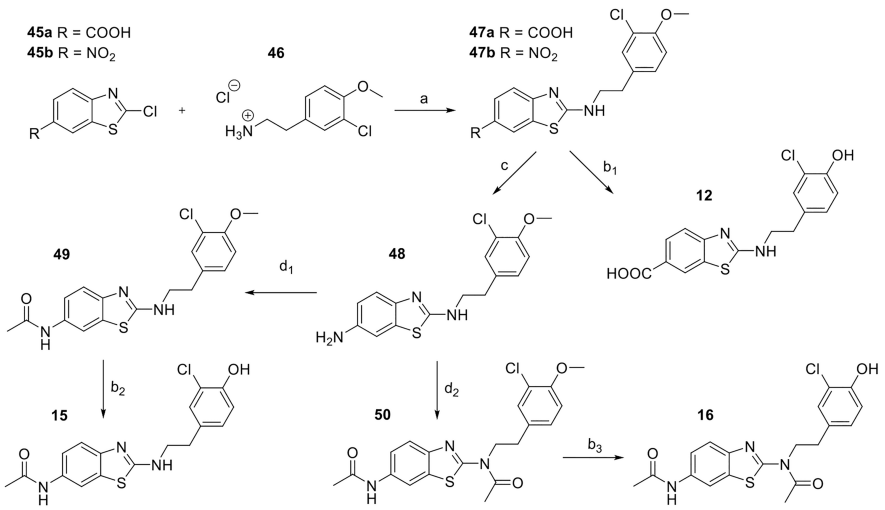

Figure 4. Synthesis of compounds harboring three-membered aliphatic linker (**12**, **15**, and **16**). Reagents and conditions: (a) DIPEA, NMP, 160 °C; (b_1) $AlCl_3$, DCE, 65 °C; (b_2) $AlCl_3$, toluene, 100 °C; (b_3) $AlCl_3$, DCE, 80 °C; (c) Fe, NH_4Cl, MeOH:H_2O:THF, 50 °C; (d_1) Ac_2O (1.05 equiv), TEA, DCM, RT; (d_2) Ac_2O (6 equiv), TEA, DCM, RT.

gradually underwent a reaction with methanesulfonyl chloride and subsequent demethylation.

The urea-linked compounds **4** and **9** were prepared by a different procedure (Figure 2B). First, 3-chloro-4-methoxyaniline was treated with triphosgene to obtain an isocyanate intermediate **27**. Then, intermediate **27** was combined with the corresponding benzothiazol-2-amine (**17e** and **17f**) to yield a urea-linked compound (**28** and **29**). By subsequent demethylation of **29**, the final product **4** was prepared. The same demethylation procedure with **28** led to concurrent methyl ester hydrolysis, thus providing the final product **9** in a single step. In several cases, the required benzothiazole-2-amine and aniline precursors for urea formation were not commercially available, and thus, they were synthesized (description of

https://doi.org/10.1021/acsmedchemlett.3c00355
ACS Med. Chem. Lett. 2023, 14, 1724−1732

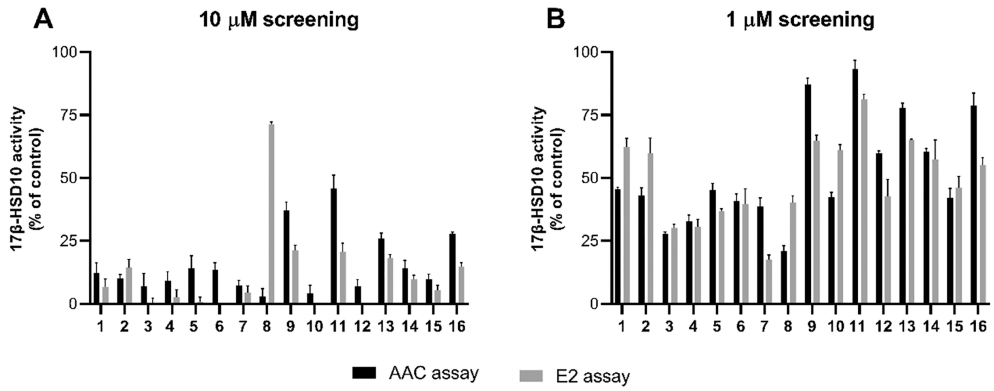

Figure 5. Inhibition screening on purified 17β-HSD10 enzyme. 10 μM (A) and 1 μM (B) screening of the tested compounds against recombinant 17β-HSD10 using AAC and E2 substrates. Values are given as means ± SD (n = 3 for AAC, n = 4 for E2).

syntheses, including compounds **30**−**36**, and corresponding Figure S1 can be found in Supporting Information).

The amide-linked compound **10** was prepared via a four-step synthesis (Figure 3A). First, 3-chloro-4-methoxy benzoic acid was treated with oxalyl chloride to gain an acyl chloride intermediate **38**. Then amine **33** and acyl chloride **38** were combined to yield amide **39**. By gradual demethylation and ester hydrolysis, the final product **10** was obtained. Compounds containing two-membered aliphatic linkers were generally prepared via a two- or three-step synthesis, which is depicted in Figure 3B. First, the corresponding benzothiazole-2-amine was reacted with the corresponding 4-hydroxybenzaldehyde via reductive amination, resulting in final products **13**, **14**, and intermediate **44**. The methyl ester **44** was hydrolyzed to give the final product **11**.

Compounds containing three-membered aliphatic linkers in their structure were generally prepared via the synthesis depicted in Figure 4. First, the corresponding 2-chlorobenzothiazole was treated with 3-chloro-4-methoxyphenethylamine to form intermediates **47a** and **47b**. To form inhibitor **12**, the intermediate **47a** was then demethylated using aluminum trichloride. Nitro derivative **47b** underwent a reduction reaction to obtain amine **48**, which was then treated with different equivalents of acetanhydride (Ac_2O) to yield either monoacetylated intermediate **49** or diacetylated intermediate **50**. Finally, intermediates **49** and **50** were demethylated to yield final products **15** and **16**, respectively. All final products were characterized by H/C NMR and HRMS techniques. The synthetic details and spectral data are listed in the Supporting Information.

The parent inhibitors **1** and **2** were originally identified in an enzymatic assay using acetoacetyl coenzyme A (AAC) as the substrate and NADH as the cofactor (i.e., substrate reduction). However, a more physiological assay with E2 or ALLOP steroid substrates and NAD^+ cofactor (i.e., substrate oxidation) has been recently established.[28] Therefore, the new compounds were initially screened in both assays at 10 and 1 μM concentrations to depict potential differences in inhibition results among the two assays (Figure 5; numerical data in Table S1).

All tested compounds showed good to high inhibition in the AAC assay, as the residual activity at 10 μM did not reach more than 46% for any of the compounds. At 1 μM concentration, more than half of the compounds still showed 17β-HSD10 residual activity lower than 50%. In 10 μM E2 assay screening, all compounds showed even better inhibitory potential compared to the AAC assay results. The only exception was compound **8**, which was found incompatible with the E2 assay at the higher (10 μM) screening concentration due to solubility issues. Similar to the 10 μM screening, the 1 μM E2 assay screening showed comparable or better inhibitory potential of the tested compounds compared to the results from the AAC assay. Despite the difference in absolute inhibition results between both assays, the relative comparisons of inhibition between particular compounds were mostly identical. It is not surprising that the absolute results from the two assays slightly differ as there are significant differences in the reaction conditions, i.e., distinct substrates with opposite conversion (oxidation vs reduction) as well as different composition and pH of the reaction buffers.[28] Nevertheless, the most potent compounds (**3**−**8**, and **15**) exhibited high inhibition in both assays, indicating their suitability for further evaluation.

Further, the more physiologically relevant E2 assay was used to determine IC_{50} values for all newly synthesized compounds as well as for the parent inhibitors (**1** and **2**)[27] (Table 2). As

Table 2. IC_{50} Values and Inhibition Type Were Determined for Purified 17β-HSD10[a]

	E2		ALLOP
compound	IC_{50} (μM)	inhibition type	IC_{50} (μM)
1	1.81 ± 0.19	–	–
2	1.15 ± 0.11	–	–
3	0.41 ± 0.04	mixed	0.095 ± 0.006
4	0.78 ± 0.05	–	–
5	0.27 ± 0.02	mixed	0.33 ± 0.02
6	0.52 ± 0.04	mixed	0.29 ± 0.03
7	0.34 ± 0.04	mixed	0.25 ± 0.03
9	1.98 ± 0.17	–	–
10	1.34 ± 0.16	–	–
11	6.56 ± 0.69	–	–
12	1.01 ± 0.11	–	–
13	2.38 ± 0.16	–	–
14	1.69 ± 0.12	–	–
15	0.93 ± 0.11	–	–
16	1.38 ± 0.09	–	–

[a]Values are given as means ± SEM (n = 4 for IC_{50}, n = 3 for inhibition type).

https://doi.org/10.1021/acsmedchemlett.3c00355
ACS Med. Chem. Lett. 2023, 14, 1724−1732

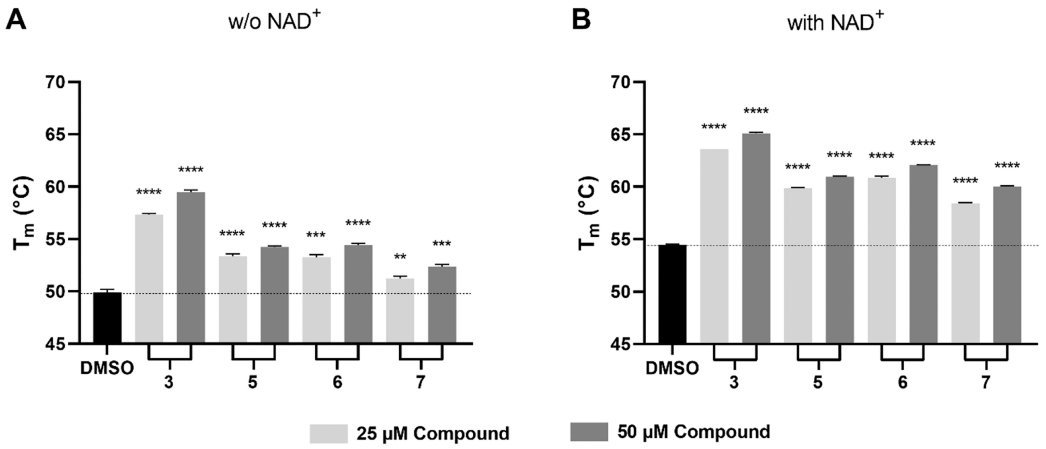

Figure 6. Differential scanning fluorimetry assay. Melting temperatures (T_m) for 17β-HSD10 were measured at 25 and 50 μM inhibitor concentrations in the (A) absence or (B) presence of 250 μM NAD^+ cofactor. Values are given as means ± SD (n = 3), and differences between groups are determined by the Student's unpaired t test. *$P \leq 0.05$, **$P \leq 0.01$, ***$P \leq 0.001$, ****$P \leq 0.0001$.

expected from the 1 μM screening, all compounds showed IC_{50} values in the low micromolar to submicromolar/nanomolar range. When compared to the parent molecules, exactly half of the compounds displayed lower IC_{50} values, thus indicating an improvement in their inhibitory properties. The four most potent inhibitors, **3** (IC_{50} = 0.41 μM), **5** (IC_{50} = 0.27 μM), **6** (IC_{50} = 0.52 μM), and **7** (IC_{50} = 0.34 μM), were further analyzed, and the inhibition type with respect to E2 substrate, as well as IC_{50} values with ALLOP substrate, were determined (Table 2). All four hits exhibited mixed-type inhibition with the E2 substrate, which is in line with previous findings on benzothiazolyl urea inhibitors obtained either in an AAC or E2 assay.[25,26,28] Mixed-type inhibition is a result of a partial competition between the inhibitor and the substrate and thus indicates noncovalent binding of inhibitor within the active site of 17β-HSD10. Compounds **5**, **6**, and **7** showed similar IC_{50} values with the ALLOP substrate compared to E2 results, while compound **3** displayed a significantly lower IC_{50} value of 95 nM. Notably, an even more potent benzothiazolyl urea inhibitor was recently identified using the E2/ALLOP by Schmidt et al. (IC_{50} values of 70 nM in E2 and 19 nM in ALLOP assays).[28] However, this inhibitor contains an atypical thiocyanate substitution that is potentially troublesome from a selectivity point of view, as it was reported to react with cysteine residues of other enzymes.[32]

Structure−activity relationship analysis of new inhibitors revealed several important trends. Comparing the influence of different linkers on the inhibitory potency of the new and the parent compounds (**1** and **2**), the compounds containing amide and ethyleneamine linkers exhibited comparable or slightly better inhibition, while compounds containing a methyleneamine linker were weaker inhibitors. A shift of the original 6-carboxyl on the benzothiazolyl moiety to position 5 (**9**) resulted in inhibition similar to that of the parent compound **1**. However, improvement in inhibitory ability was achieved by replacing the original carboxyl or acetamide substituents with tetrazole (**3**), which is an isostere to carboxylic acid exhibiting similar acidity, planarity, and electronic effects. The same trend was observed for sulfonyl amide (**4**) or methanesulfonamide (**6**) groups, which again exhibit both acidic and HBD/HBA features, as well as for the urea (**5**), which is not acidic but still possess HBD/HBA properties. Finally, replacing chlorine in position 3 of the phenyl ring with an alternative electron-withdrawing group substituent, the trifluoromethyl group (**7**) confirmed the premises of previous works,[24,25] as trifluoromethyl substitution had a positive effect on inhibition ability.

Differential scanning fluorimetry was used as an orthogonal assay to verify the results of enzymatic measurements of the four best inhibitors, **3**, **5**, **6**, and **7**. This method measures the change in melting temperatures (T_m) induced by a shift in the thermal denaturation profile of the protein after inhibitor binding. The compounds were tested in the absence or presence of an NAD^+ cofactor because it can affect the interaction between the inhibitor and 17β-HSD10[16,25,33] depending on the binding mode of the inhibitor. All tested compounds displayed strong binding to the protein in both setups and especially in the presence of NAD^+ (Figure 6; numerical data are listed in Table S2). These findings correlated well with the aforementioned mixed-type inhibition, which implies that the inhibitors bind to the enzyme alone as well as to the enzyme-cofactor complex. The determination was conducted at two different concentrations of the inhibitor, and the readout was found to be concentration-dependent for all the tested compounds, thus indicating specific binding with 17β-HSD10 (opposite to nonspecific binding based on ligand aggregation).

Further evaluation was performed at a cellular level to find out whether the inhibitors can target 17β-HSD10 inside the living cells. First, the cytotoxicity of compounds was assessed to exclude their possible incompatibility with the cellular 17β-HSD10 activity assay. For this purpose, the CellTox Green Cytotoxicity Assay kit was used, a fluorometric method to determine the damaged cells as a biomarker for cellular cytotoxicity and cytolysis. HEK293 cells were treated with compounds at three different concentrations (10 μM, 25 μM, and 50 μM) for 48 h before measurements were performed. No significant cytotoxicity was observed for tested compounds, even at the highest 50 μM concentration (Table S3 in Supporting Information).

To detect the ability of compounds to penetrate into cells and inhibit 17β-HSD10 activity inside the cellular environ-

https://doi.org/10.1021/acsmedchemlett.3c00355
ACS Med. Chem. Lett. 2023, 14, 1724−1732

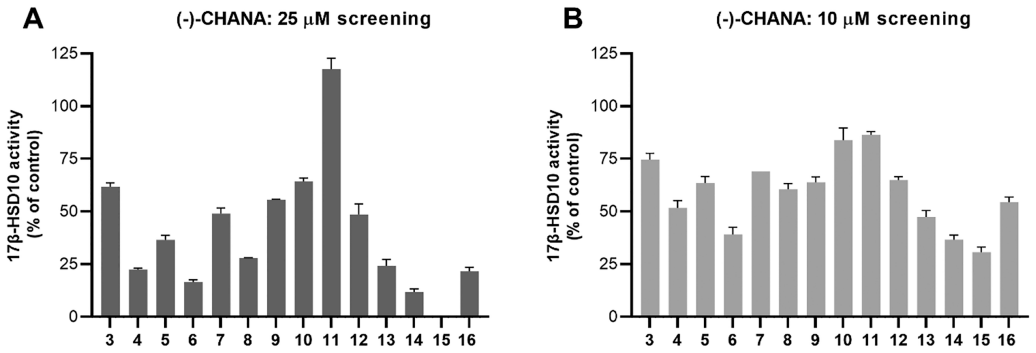

C

Compound	(-)-CHANA IC_{50} values (μM)
4	10.40 ± 1.02
6	6.21 ± 0.44
13	5.45 ± 0.76
14	4.39 ± 0.63
15	4.76 ± 0.25
16	9.03 ± 1.37

Figure 7. Results of 17β-HSD10 inhibition in the cellular environment. Inhibitory screening of compounds at concentrations 25 μM (A) and 10 μM (B) and IC_{50} values (C) using (−)−CHANA fluorogenic probe in HEK293 17β-HSD10 cells. Values are given as mean ± SD from two independent measurements performed in triplicates.

ment, the fluorogenic probe (−)−CHANA was used. This probe is oxidized to the corresponding fluorescent ketone (CHANK), and it was previously shown as a specific substrate for 17β-HSD10.[25,28,29,34] The inhibition inside the HEK293 cells overexpressing 17β-HSD10 (HEK293 17β-HSD10) was determined as the decrease in fluorescence intensity of CHANK production after the inhibitor treatment. All 14 compounds were screened at 10 and 25 μM concentrations, and all of them displayed the ability to penetrate the cells and inhibit 17β-HSD10 activity except for compound **11**, which interfered with the assay (Figure 7A,B; numerical data in Table S4). The six most active inhibitors (**4**, **6**, **13**−**16**) that showed residual activity around or below 50% in 10 μM screening were selected for IC_{50} determination (Figure 7C). Compounds **14** and **15** were found to be the most potent with IC_{50} values less than 5 μM (4.39 and 4.76 μM, respectively). Notably, the inhibition results in the cellular assay did not correspond to the results obtained for a purified enzyme. Differently from the enzymatic assay, compounds containing aliphatic methyleneamine and ethyleneamine linkers (**13**−**15**) were the most potent inhibitors in the cellular assay. Conversely, the urea-linked compounds with submicromolar IC_{50} values on the purified enzyme (**3**−**7**) showed significantly weaker activity in cells. A potential explanation for this discrepancy is that compounds with aliphatic linkers offer better permeability across cell membranes and thus better accessibility to the 17β-HSD10, resulting in higher bioactivity. These findings comply well with the aforementioned structural design of new compounds, which expected (based on the calculated BBB score[31]) that the introduction of aliphatic linkers will improve penetration through BBB, and thus penetration through cellular membranes in general. In addition, the 6-acetamide derivatives **13** and **15** performed significantly better in the cellular assay compared to their 6-carboxyl analogues (**11** and **12**), while there was no significant difference in their activity in the enzymatic E2 assay. Once again, the possible explanation lies in the permeability across the cellular membrane, as carboxylic acids are negatively charged molecules, and thus are less likely to penetrate into cells.

In summary, a series of 14 novel benzothiazole-based 17β-HSD10 inhibitors were prepared and evaluated *in vitro* using various enzymatic and cellular methods. Initially, the compounds were screened in the reductive AAC and the oxidative E2 activity assays on the purified enzyme. All compounds showed good to high inhibitory potency in both screenings and were forwarded to IC_{50} measurement using the more physiologically relevant E2 assay, where six compounds showed submicromolar IC_{50} values. Consequently, the four most potent inhibitors (**3**, **5**−**7**) were assessed in the alternative ALLOP assay, and they were all confirmed as submicromolar to nanomolar inhibitors. Inhibition type assessment revealed mixed-type inhibition for the E2 substrate. Differential scanning fluorimetry was used as an orthogonal assay to exclude potential false positive results from enzymatic assays. All four selected inhibitors (**3**, **5**−**7**) interacted with the protein and stabilized its conformation in a dose-dependent manner, which confirmed the validity of the results from activity assays. Further, the CHANA assay was used to determine the 17β-HSD10 activity inside living cells. Compounds **13**−**15** with aliphatic linkers and 6-acetamide substitution on benzothiazole moiety resulted as the best 17β-HSD10 inhibitors *in cellulo* (low micromolar IC_{50} values). This contrasted with the results of enzymatic assays that highlighted urea-linked compounds as the most potent inhibitors. This discrepancy was likely caused by the lower permeability of urea-linked compounds across the cellular membrane, and it

https://doi.org/10.1021/acsmedchemlett.3c00355
ACS Med. Chem. Lett. 2023, 14, 1724−1732

suggested that the benzothiazole inhibitors with aliphatic linkers could be more relevant for future development compared to formerly pursued benzothiazolyl ureas.

■ ASSOCIATED CONTENT

Supporting Information

The Supporting Information is available free of charge at https://pubs.acs.org/doi/10.1021/acsmedchemlett.3c00355.

A detailed description of methods, experimental procedures, and compounds' characterization (PDF)

■ AUTHOR INFORMATION

Corresponding Authors

Ondrej Benek − *Faculty of Science, Department of Chemistry, University of Hradec Kralove, 500 03 Hradec Kralove, Czech Republic;* orcid.org/0000-0001-6840-1933; Email: ondrej.benek@uhk.cz

Monika Schmidt − *Faculty of Science, Department of Chemistry, University of Hradec Kralove, 500 03 Hradec Kralove, Czech Republic;* orcid.org/0000-0003-4984-9155; Email: monika.schmidt@uhk.cz

Authors

Michaela Hanzlova − *Faculty of Science, Department of Chemistry, University of Hradec Kralove, 500 03 Hradec Kralove, Czech Republic;* orcid.org/0000-0001-8858-5434

Marketa Sedlacek Miskerikova − *Faculty of Science, Department of Chemistry, University of Hradec Kralove, 500 03 Hradec Kralove, Czech Republic;* orcid.org/0000-0002-4392-3169

Aneta Rotterova − *Faculty of Science, Department of Chemistry, University of Hradec Kralove, 500 03 Hradec Kralove, Czech Republic*

Katarina Chalupova − *Faculty of Science, Department of Chemistry, University of Hradec Kralove, 500 03 Hradec Kralove, Czech Republic*

Katarina Jurkova − *Faculty of Science, Department of Chemistry, University of Hradec Kralove, 500 03 Hradec Kralove, Czech Republic;* orcid.org/0000-0001-9981-9179

Marie Hamsikova − *Faculty of Science, Department of Chemistry, University of Hradec Kralove, 500 03 Hradec Kralove, Czech Republic*

Rudolf Andrys − *Faculty of Science, Department of Chemistry, University of Hradec Kralove, 500 03 Hradec Kralove, Czech Republic*

Annamaria Haleckova − *Faculty of Science, Department of Chemistry, University of Hradec Kralove, 500 03 Hradec Kralove, Czech Republic*

Jana Svobodova − *Faculty of Science, Department of Chemistry, University of Hradec Kralove, 500 03 Hradec Kralove, Czech Republic*

Kamil Musilek − *Faculty of Science, Department of Chemistry, University of Hradec Kralove, 500 03 Hradec Kralove, Czech Republic*

Complete contact information is available at: https://pubs.acs.org/10.1021/acsmedchemlett.3c00355

Author Contributions

#M.H., M.S.M., and A.R contributed equally to this work.

Notes

The authors declare the following competing financial interest(s): Ondrej Benek and Kamil Musilek filled patent application no. PCT/CZ2022/050096 issued to University of Hradec Kralove.

■ ACKNOWLEDGMENTS

This work was supported by the Operational Programme "Development of the Internal Grant Agency of the University of Hradec Kralove" (reg. no. CZ.02.2.69/0.0/0.0/19_073/0016949, project IGRA-TYM-2021002) and by the University of Hradec Kralove (Faculty of Science, No. SV2103-2022). The authors are grateful to Patrik Oleksak and Petra Liskova for technical assistance with NMR and HRMS measurements.

■ ABBREVIATIONS

17β-HSD10, 17β-hydroxysteroid dehydrogenase type 10; AAC, acetoacetyl coenzyme A; ABAD, amyloid-binding alcohol dehydrogenase; Aβ, amyloid-beta peptide; AD, Alzheimer's disease; ALLOP, allopregnanolone; BBB, blood-brain barrier; BTMA-ICl_2, benzyltrimethylammonium dichloroiodate(I); CDI, 1,1′-carbonylimidazole; CHANA, cyclohexenyl amino naphthalene alcohol; CHANK, cyclohexenyl amino naphthalene ketone; DCE, 1,2-dichloroethane; DCM, dichloromethane; DIPEA, *N*,*N*-diisopropylethylamine; DMAP, 4-dimethylaminopyridine; DMF, dimethylformamide; DMSO, dimethyl sulfoxide; E2, 17β-estradiol; HBA, hydrogen bond acceptor; HBD, hydrogen bond donor; HRMS, high-resolution mass spectrometry; IC_{50}, half maximal inhibitory concentration; MeCN, acetonitrile; MsCl, methanesulfonyl chloride; NADH/NAD^+, nicotinamide adenine dinucleotide; NMP, *N*-methyl-2-pyrrolidone; NMR, nuclear magnetic resonance; PCR, polymerase chain reaction; SD, standard deviation; SEM, standard error of the mean; TEA, triethylamine; TFA, trifluoroacetic acid; THF, tetrahydrofuran; T_m, melting temperature

■ REFERENCES

(1) Yang, S.-Y.; He, X.-Y.; Schulz, H. Multiple Functions of Type 10 17β-Hydroxysteroid Dehydrogenase. *Trends Endocrinol Metab* **2005**, *16* (4), 167−175.

(2) Du Yan, S.; Zhu, Y.; Stern, E. D.; Hwang, Y. C.; Hori, O.; Ogawa, S.; Frosch, M. P.; Connolly, E. S.; McTaggert, R.; Pinsky, D. J.; Clarke, S.; Stern, D. M.; Ramasamy, R. Amyloid Beta -Peptide-Binding Alcohol Dehydrogenase Is a Component of the Cellular Response to Nutritional Stress. *J. Biol. Chem.* **2000**, *275* (35), 27100−27109.

(3) Rauschenberger, K.; Schöler, K.; Sass, J. O.; Sauer, S.; Djuric, Z.; Rumig, C.; Wolf, N. I.; Okun, J. G.; Kölker, S.; Schwarz, H.; Fischer, C.; Grziwa, B.; Runz, H.; Nümann, A.; Shafqat, N.; Kavanagh, K. L.; Hämmerling, G.; Wanders, R. J. A.; Shield, J. P. H.; Wendel, U.; Stern, D.; Nawroth, P.; Hoffmann, G. F.; Bartram, C. R.; Arnold, B.; Bierhaus, A.; Oppermann, U.; Steinbeisser, H.; Zschocke, J. A Non-Enzymatic Function of 17beta-Hydroxysteroid Dehydrogenase Type 10 Is Required for Mitochondrial Integrity and Cell Survival. *EMBO Mol. Med.* **2010**, *2* (2), 51−62.

(4) Tieu, K.; Perier, C.; Vila, M.; Caspersen, C.; Zhang, H.-P.; Teismann, P.; Jackson-Lewis, V.; Stern, D. M.; Yan, S. D.; Przedborski, S. L-3-Hydroxyacyl-CoA Dehydrogenase II Protects in a Model of Parkinson's Disease. *Ann. Neurol.* **2004**, *56* (1), 51−60.

(5) He, X.-Y.; Isaacs, C.; Yang, S.-Y. Roles of Mitochondrial 17β-Hydroxysteroid Dehydrogenase Type 10 in Alzheimer's Disease. *J. Alzheimers Dis* **2018**, *62* (2), 665−673.

(6) Du Yan, S.; Fu, J.; Soto, C.; Chen, X.; Zhu, H.; Al-Mohanna, F.; Collison, K.; Zhu, A.; Stern, E.; Saido, T.; Tohyama, M.; Ogawa, S.;

Roher, A.; Stern, D. An Intracellular Protein That Binds Amyloid-β Peptide and Mediates Neurotoxicity in Alzheimer's Disease. *Nature* **1997**, *389* (6652), 689−695.
(7) Lustbader, J. W.; Cirilli, M.; Lin, C.; Xu, H. W.; Takuma, K.; Wang, N.; Caspersen, C.; Chen, X.; Pollak, S.; Chaney, M.; Trinchese, F.; Liu, S.; Gunn-Moore, F.; Lue, L.-F.; Walker, D. G.; Kuppusamy, P.; Zewier, Z. L.; Arancio, O.; Stern, D.; Yan, S. S.; Wu, H. ABAD Directly Links Aß to Mitochondrial Toxicity in Alzheimer's Disease. *Science* **2004**, *304* (5669), 448−452.
(8) He, X.-Y.; Wegiel, J.; Yang, S.-Y. Intracellular Oxidation of Allopregnanolone by Human Brain Type 10 17beta-Hydroxysteroid Dehydrogenase. *Brain Res.* **2005**, *1040* (1−2), 29−35.
(9) Seo, J.-S.; Lee, K.-W.; Kim, T.-K.; Baek, I.-S.; Im, J.-Y.; Han, P.-L. Behavioral Stress Causes Mitochondrial Dysfunction via ABAD Up-Regulation and Aggravates Plaque Pathology in the Brain of a Mouse Model of Alzheimer Disease. *Free Radic Biol. and Med.* **2011**, *50* (11), 1526−1535.
(10) Yang, S.-Y.; He, X.-Y.; Miller, D. Hydroxysteroid (17β) Dehydrogenase X in Human Health and Disease. *Mol. Cell. Endocrinol.* **2011**, *343* (1−2), 1−6.
(11) Yang, S.-Y.; He, X.-Y.; Isaacs, C.; Dobkin, C.; Miller, D.; Philipp, M. Roles of 17β-Hydroxysteroid Dehydrogenase Type 10 in Neurodegenerative Disorders. *J. Steroid Biochem Mol. Biol.* **2014**, *143*, 460−472.
(12) Grimm, A.; Schmitt, K.; Lang, U. E.; Mensah-Nyagan, A. G.; Eckert, A. Improvement of Neuronal Bioenergetics by Neurosteroids: Implications for Age-Related Neurodegenerative Disorders. *Biochim. Biophys. Acta* **2014**, *1842* (12 Pt A), 2427−2438.
(13) Grimm, A.; Biliouris, E. E.; Lang, U. E.; Götz, J.; Mensah-Nyagan, A. G.; Eckert, A. Sex Hormone-Related Neurosteroids Differentially Rescue Bioenergetic Deficits Induced by Amyloid-β or Hyperphosphorylated Tau Protein. *Cell. Mol. Life Sci.* **2016**, *73* (1), 201−215.
(14) Morsy, A.; Maddeboina, K.; Gao, J.; Wang, H.; Valdez, J.; Dow, L. F.; Wang, X.; Trippier, P. C. Functionalized Allopurinols Targeting Amyloid-Binding Alcohol Dehydrogenase Rescue Aβ-Induced Mitochondrial Dysfunction. *ACS Chem. Neurosci.* **2022**, *13* (14), 2176−2190.
(15) Vinklarova, L.; Schmidt, M.; Benek, O.; Kuca, K.; Gunn-Moore, F.; Musilek, K. Friend or Enemy? Review of 17β-HSD10 and Its Role in Human Health or Disease. *J. Neurochem* **2020**, *155* (3), 231−249.
(16) Kissinger, C. R.; Rejto, P. A.; Pelletier, L. A.; Thomson, J. A.; Showalter, R. E.; Abreo, M. A.; Agree, C. S.; Margosiak, S.; Meng, J. J.; Aust, R. M.; Vanderpool, D.; Li, B.; Tempczyk-Russell, A.; Villafranca, J. E. Crystal Structure of Human ABAD/HSD10 with a Bound Inhibitor: Implications for Design of Alzheimer's Disease Therapeutics. *J. Mol. Biol.* **2004**, *342* (3), 943−952.
(17) Ayan, D.; Maltais, R.; Poirier, D. Identification of a 17β-Hydroxysteroid Dehydrogenase Type 10 Steroidal Inhibitor: A Tool to Investigate the Role of Type 10 in Alzheimer's Disease and Prostate Cancer. *ChemMedChem.* **2012**, *7* (7), 1181−1184.
(18) Boutin, S.; Roy, J.; Maltais, R.; Alata, W.; Calon, F.; Poirier, D. Identification of Steroidal Derivatives Inhibiting the Transformations of Allopregnanolone and Estradiol by 17β-Hydroxysteroid Dehydrogenase Type 10. *Bioorg. Med. Chem. Lett.* **2018**, *28* (22), 3554−3559.
(19) Boutin, S.; Maltais, R.; Roy, J.; Poirier, D. Synthesis of 17β-Hydroxysteroid Dehydrogenase Type 10 Steroidal Inhibitors: Selectivity, Metabolic Stability and Enhanced Potency. *Eur. J. Med. Chem.* **2021**, *209*, No. 112909.
(20) Valaasani, K.; Sun, Q.; Hu, G.; Li, J.; Du, F.; Guo, Y.; Carlson, E.; Gan, X.; Yan, S. Identification of Human ABAD Inhibitors for Rescuing Aβ-Mediated Mitochondrial Dysfunction. *Curr. Alzheimer Res.* **2014**, *11* (2), 128−136.
(21) Hroch, L.; Benek, O.; Guest, P.; Aitken, L.; Soukup, O.; Janockova, J.; Musil, K.; Dohnal, V.; Dolezal, R.; Kuca, K.; Smith, T. K.; Gunn-Moore, F.; Musilek, K. Design, Synthesis and in Vitro Evaluation of Benzothiazole-Based Ureas as Potential ABAD/17β-HSD10 Modulators for Alzheimer's Disease Treatment. *Bioorg. Med. Chem. Lett.* **2016**, *26* (15), 3675−3678.
(22) Hroch, L.; Guest, P.; Benek, O.; Soukup, O.; Janockova, J.; Dolezal, R.; Kuca, K.; Aitken, L.; Smith, T. K.; Gunn-Moore, F.; Zala, D.; Ramsay, R. R.; Musilek, K. Synthesis and Evaluation of Frentizole-Based Indolyl Thiourea Analogues as MAO/ABAD Inhibitors for Alzheimer's Disease Treatment. *Bioorg. Med. Chem.* **2017**, *25* (3), 1143−1152.
(23) Benek, O.; Hroch, L.; Aitken, L.; Dolezal, R.; Guest, P.; Benkova, M.; Soukup, O.; Musil, K.; Kuca, K.; Smith, T. K.; Gunn-Moore, F.; Musilek, K. 6-Benzothiazolyl Ureas, Thioureas and Guanidines Are Potent Inhibitors of ABAD/17β-HSD10 and Potential Drugs for Alzheimer. *Med. Chem.* **2017**, *13* (4), 345−358.
(24) Benek, O.; Hroch, L.; Aitken, L.; Gunn-Moore, F.; Vinklarova, L.; Kuca, K.; Perez, D. I.; Perez, C.; Martinez, A.; Fisar, Z.; Musilek, K. 1-(Benzo[d]Thiazol-2-Yl)-3-Phenylureas as Dual Inhibitors of Casein Kinase 1 and ABAD Enzymes for Treatment of Neurodegenerative Disorders. *J. Enzyme Inhib Med. Chem.* **2018**, *33* (1), 665−670.
(25) Aitken, L.; Benek, O.; McKelvie, B. E.; Hughes, R. E.; Hroch, L.; Schmidt, M.; Major, L. L.; Vinklarova, L.; Kuca, K.; Smith, T. K.; Musilek, K.; Gunn-Moore, F. J. Novel Benzothiazole-Based Ureas as 17β-HSD10 Inhibitors, A Potential Alzheimer's Disease Treatment. *Molecules* **2019**, *24* (15), 2757.
(26) Schmidt, M.; Benek, O.; Vinklarova, L.; Hrabinova, M.; Zemanova, L.; Chribek, M.; Kralova, V.; Hroch, L.; Dolezal, R.; Lycka, A.; Prchal, L.; Jun, D.; Aitken, L.; Gunn-Moore, F.; Kuca, K.; Musilek, K. Benzothiazolyl Ureas Are Low Micromolar and Uncompetitive Inhibitors of 17β-HSD10 with Implications to Alzheimer's Disease Treatment. *Int. J. Mol. Sci.* **2020**, *21* (6), E2059.
(27) Benek, O.; Vaskova, M.; Miskerikova, M.; Schmidt, M.; Andrys, R.; Rotterova, A.; Skarka, A.; Hatlapatkova, J.; Karasova, J. Z.; Medvecky, M.; Hroch, L.; Vinklarova, L.; Fisar, Z.; Hroudova, J.; Handl, J.; Capek, J.; Rousar, T.; Kobrlova, T.; Dolezal, R.; Soukup, O.; Aitken, L.; Gunn-Moore, F.; Musilek, K. Development of Submicromolar 17β-HSD10 Inhibitors and Their in Vitro and in Vivo Evaluation. *Eur. J. Med. Chem.* **2023**, *258*, No. 115593.
(28) Schmidt, M.; Vaskova, M.; Rotterova, A.; Fiandova, P.; Miskerikova, M.; Zemanova, L.; Benek, O.; Musilek, K. Physiologically Relevant Fluorescent Assay for Identification of 17β-hydroxysteroid Dehydrogenase Type 10 Inhibitors. *J. Neurochem* **2023**, *167* (2), No. 154.
(29) Muirhead, K. E. A.; Froemming, M.; Li, X.; Musilek, K.; Conway, S. J.; Sames, D.; Gunn-Moore, F. J. (−)-CHANA, a Fluorogenic Probe for Detecting Amyloid Binding Alcohol Dehydrogenase HSD10 Activity in Living Cells. *ACS Chem. Biol.* **2010**, *5* (12), 1105−1114.
(30) Molecular Operating Environment (MOE), 02 Chemical Computing Group ULC: Montreal, QC, 2022.
(31) Gupta, M.; Lee, H. J.; Barden, C. J.; Weaver, D. F. The Blood−Brain Barrier (BBB) Score. *J. Med. Chem.* **2019**, *62* (21), 9824−9836.
(32) Mahadevan, S.; Shukla, P. S.; Kalyanaraman, V. S.; Kumar, S. A. The Action of Phenylthiocyanate on Enzymes. *FEBS Lett.* **1969**, *2* (3), 149−153.
(33) Breton, R.; Housset, D.; Mazza, C.; Fontecilla-Camps, J. C. The Structure of a Complex of Human 17β-Hydroxysteroid Dehydrogenase with Estradiol and NADP+ Identifies Two Principal Targets for the Design of Inhibitors. *Structure* **1996**, *4* (8), 905−915.
(34) Metodieva, V.; Smith, T.; Gunn-Moore, F. The Mitochondrial Enzyme 17βHSD10 Modulates Ischemic and Amyloid-β-Induced Stress in Primary Mouse Astrocytes. *eNeuro* **2022**, *9* (5). ENEURO.0040-22.2022.

https://doi.org/10.1021/acsmedchemlett.3c00355
ACS Med. Chem. Lett. 2023, 14, 1724−1732

Supporting Information

Nanomolar benzothiazole-based inhibitors of 17β-HSD10 with cellular bioactivity

Michaela Hanzlova[1†]; Marketa Sedlacek Miskerikova[1†]; Aneta Rotterova[1†]; Katarina Chalupova[1]; Katarina Jurkova[1]; Marie Hamsikova[1]; Rudolf Andrys[1]; Annamaria Haleckova[1]; Jana Svobodova[1]; Monika Schmidt[1]*; Ondrej Benek[1]*; Kamil Musilek[1]

[1]*University of Hradec Kralove, Faculty of Science, Department of Chemistry, Rokitanskeho 62, 500 03 Hradec Kralove, Czech Republic*

† These authors contributed equally to this work.

* Correspondence: ondrej.benek@uhk.cz; monika.schmidt@uhk.cz

Table of Contents

1 Synthesis of benzothiazole-2-amine and aniline precursors 1
2 General Information on Chemical Synthesis 2
3 Detailed description of synthetic procedures and products' characterization 5
4 ^{1}H and ^{13}C NMR spectra of final products 3–16 23
5 HRMS spectra of final products 3–16 38
6 Methods of *in vitro* evaluation 45
6.1 Enzymatic assays 45
6.2 Cell-based assays 46
7 Results of *in vitro* evaluation 48
8 Safety Statement 50
9 References 50

1 Synthesis of benzothiazole-2-amine and aniline precursors

In several cases, the required benzothiazole-2-amine and aniline precursors for urea formation were not commercially available, and thus they were synthesized. 4-amino-2-(trifluoromethyl)phenol (**19b**) was prepared by de-methylation of 4-methoxy-3-(trifluoromethyl)aniline (**30**) using hydrobromic acid (**Figure A**). Benzothiazole-2-amines substituted in position 6 with methyl ester (**33**), cyano (**32**) or sulfonyl amide group (**17e**) were prepared from corresponding *para*-substituted anilines in reaction with potassium thiocyanate and bromine (**31b** and **31c**) or benzyltrimethylammonium dichloroiodate(I) (**31a**) (**Figure B**).

To prepare the tetrazole derivative **17d**, the amine group in 2-aminobenzothiazole-6-carbonitrile (**32**) was protected with Boc-group and its cyano group converted to 1*H*-tetrazol-5-yl in reaction with sodium azide. Consequent de-protection yielded the intended 6-(1*H*-tetrazol-5-yl)benzothiazol-2-amine in the form of salt with trifluoroacetic acid (**17d**; **Figure C**). The 4-methoxybenzyl 2-aminobenzothiazole-6-carboxylate (**17c**) was prepared from methyl 2-aminobenzothiazole-6-carboxylate (**Figure 1D**). Firstly, the methyl ester group of **33** was hydrolyzed to provide carboxylic acid **36**, which was then converted to 4-methoxybenzyl ester (**17c**) in reaction with 4-methoxybenzyl chloride.

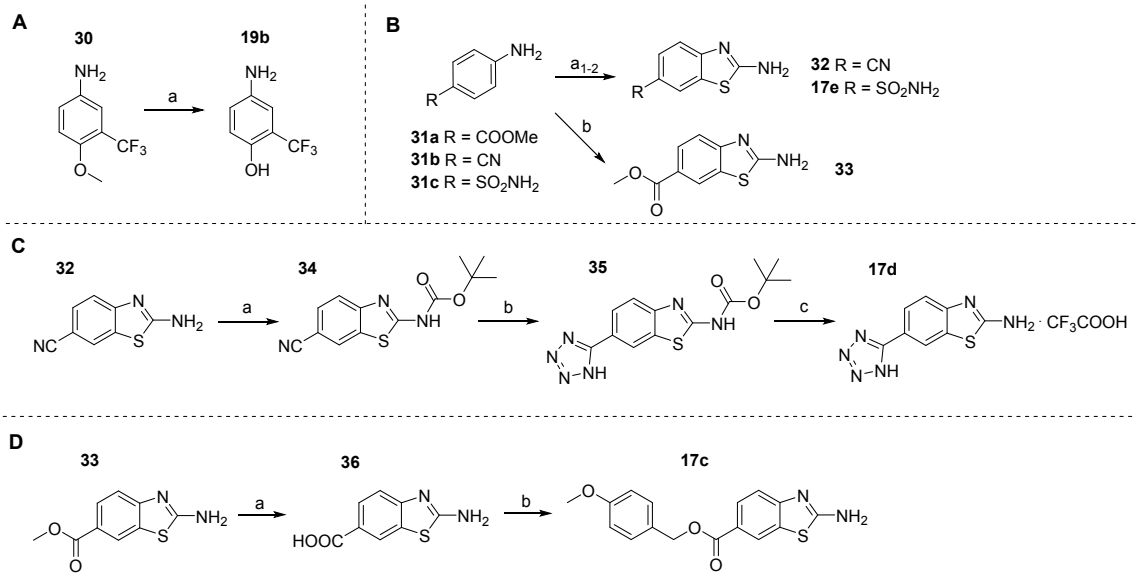

Figure S1: A) Synthesis of compound **19b**. Reagents and conditions: a) gl. AcOH, 48% aq. sol. HBr, reflux; **B)** General method for synthesis of benzothiazole-2-amines. Reagents and conditions: (a_1) Br_2, KSCN, AcOH, RT; (a_2) 25% aq. sol. NH_3, 0 °C; (b) BTMA-ICl_2, KSCN, DMSO/H_2O, 70 °C; **C)** Synthesis of compound **17d**. (a) Boc_2O, DMAP, THF, RT; (b) NaN_3, TEA.HCl, DMF, 100 °C; (c) TFA, DCM, RT; **D)** Synthesis of compound **17c**. Reagents and conditions: (a) 1M aq. NaOH/EtOH, RT; (b) 4-methoxybenzyl chloride, K_2CO_3, DMF, RT.

2 General Information on Chemical Synthesis

All reagents and solvents were purchased from commercial sources (Sigma Aldrich, Activate Scientific, Alfa Aesar, Merck, Penta Chemicals, and VWR) and they were used without any further purification. Thin-layer chromatography (TLC) for reaction monitoring was performed on Merck aluminium sheets, silica gel 60 F_{254}. Visualisation was performed either via UV (254 nm) or appropriate stain reagent solutions (alternatively in a combination of both). Preparative column chromatography

was performed on silica gel 60 (70–230 mesh, 63–200 µm, 60 Å pore size). Melting points were determined on a Büchi M-565 melting point apparatus (BÜCHI Labortechnik AG, Flawil, Switzerland) and are uncorrected.

All synthesized final products (**3-16**) were characterized by ^{1}H and ^{13}C NMR spectroscopy and high-resolution mass spectrometry (HRMS) analyses. Intermediate products were generally characterized by ^{1}H NMR and/or LC-MS. To remove potential aluminium residues (demethylation using aluminium trichloride) or iron residues (Bechamp reduction), corresponding final products and their intermediates were purified by suitable procedures, commonly used for this purpose, e.g., liquid extraction or filtration through Celite followed by column or flash chromatography.

Nuclear magnetic resonance (NMR) spectra were acquired at 500/126 MHz ($^{1}H/^{13}C$) on a Bruker Advance Neo 500 spectrometer. Chemical shifts δ are given in ppm and referenced to the signal centre of solvent peaks (DMSO-d_6: δ 2.50 ppm and 39.52 ppm for ^{1}H and ^{13}C, respectively; THF-d_8: δ 3.58 ppm and 67.57 ppm for ^{1}H and ^{13}C, respectively), thus indirectly correlated to TMS standard (δ 0 ppm). Coupling constants are expressed in Hz.

LC-MS was determined using Agilent Infinity II 1290 UHPLC system coupled with a DAD spectrometer and Agilent 6470 QqQ mass spectrometer (Agilent Technologies, Santa Clara, USA) as detectors. Chromatographic separation was performed on Zorbax Eclipse C18 column (50 x 2.1 mm, 1.8 µm) with 0.1% formic acid in ultra-pure water as mobile phase A and 0.1% formic acid in acetonitrile as mobile phase B. MS conditions were as follows: gas temp 300 °C, gas flow 8 L/min, nebulizer 35 psi, sheat gas temp 380 °C, sheat gas flow 11 L/min, capillary 3500 V, nozzle voltage 0 V. Positive and negative ions were monitored in the range of 50–800 m/z. The purity of the final products was >90%.

For HRMS determination, an Acquity UPLC H-Class analytical LC-MS system coupled with a Vion IMS QTof spectrometer (both produced by Waters, Milford, USA) was used. The LC-MS system consisted of a binary solvent manager and a sample manager FTN-I equipped with a 50 µL loop. A Zorbax Elipse Plus C18 (2.1 × 50 mm/ 1.8 µm) column was used as the stationary phase. Water (MFA) and acetonitrile (MFB) used in the analyses were acidified with 0.1% (*v*/*v*) formic acid. Ions for mass spectrometry were generated by an electro-spray ionization source (ESI) working in positive mode, with the following settings: cone gas flow 50 L/h, desolvation gas flow 600 L/h, capillary voltage 3.00 kV, source temperature 110 °C, desolvation temperature 450 °C, sample cone voltage 40 V, source offset voltage 80 V, resolution mode. The full-scan MS analyses monitored ions within the m/z range 50-1000, scan time 0.500 s. The studied compounds were dissolved in methanol or acetonitrile, and 1 µL of the solution was injected into the LC-MS system. For elution, the following ramp-gradient

program was used: 0–1 min: 5% MFB, 1–4 min: 5–95% MFB, 4–5 min: 95% MFB, 5–5.10 min: 5% MFB. The flow rate in the gradient elution was set to 0.4 mL/min. To increase the accuracy of HRMS, internal lock-mass calibration was employed using leucine enkephalin of m/z = 556.2771 ($[M+H]^+$, $[C_{28}H_{37}N_5O_7]$). The chromatograms and mass spectra were processed in UNIFI software (Waters, Milford, USA).

3 Detailed description of synthetic procedures and products' characterization

Procedure A_3 (general conditions): Synthesis of *N-(6-substituted-benzo[d]thiazol-2-yl)-1H-imidazole-1-carboxamides from corresponding 2-aminobenzo[d]thiazoles* (**18a, 18b**)

The corresponding 6-substituted 2-aminobenzo[*d*]thiazole (1 eq.; **17a** or **17b**, respectively) was dispersed in anhydrous DCM (14 mL/mmol). Subsequently, CDI (1.2 eq.) was added, and the reaction mixture was stirred under reflux overnight. The reaction mixture was then cooled to RT and allowed to precipitate for 30 mins in a refrigerator. The precipitate was filtered off using S4 frit, and dried under reduced pressure at 70 °C, to obtain the crude *N*-(6-substituted-benzo[*d*]thiazol-2-yl)-1*H*-imidazole-1-carboxamide (intermediate **18a** or **18b**, respectively), which was used in the next reaction step without further purification.

N-(6-nitrobenzo[d]thiazol-2-yl)-1H-imidazole-1-carboxamide (**18a**)

Yield 78%.

N-(6-acetamidobenzo[d]thiazol-2-yl)-1H-imidazole-1-carboxamide (**18b**)

Yield 95%.

4-amino-2-(trifluoromethyl)phenol (**19b**)

4-methoxy-3-(trifluoromethyl)aniline (**30**; 1 eq.) was dissolved in glacial AcOH (3 mL/mmol). The same volume of 48% aqueous HBr solution was added, and the reaction mixture was stirred under reflux over the weekend. The reaction mixture was cooled to RT and saturated $NaHCO_3$ solution was added dropwise for neutralization. Subsequently, the reaction mixture was extracted with EtOAc, organic layers were shaken with brine, dried with anhydrous Na_2SO_4, and evaporated under reduced pressure. The crude product was purified by column chromatography ($CHCl_3$/MeOH; 15:1) to obtain 4-amino-2-(trifluoromethyl)phenol (**19b**) in a 66% yield.

^{1}H NMR (500 MHz, DMSO-d_6) δ 9.32 (br s, 1H, OH), 6.75 – 6.70 (m, 2H, ArH), 6.66 (dd, *J* = 8.7, 2.7 Hz, 1H, ArH), 4.78 (br s, 2H, NH_2).

Procedure B_3 (general conditions): Synthesis of *1-phenyl-3-benzo[d]thiazolylureas from corresponding N-(benzo[d]thiazol-2-yl)-1H-imidazole-1-carboxamides* (**22**, **8**)

The corresponding *N*-(6-substituted-benzo[*d*]thiazol-2-yl)-1*H*-imidazole-1-carboxamide (1 eq.; **18a** or **18b**, respectively) was dispersed in anhydrous MeCN (5 mL/mmol). The corresponding aniline (**21**; 1.1 eq.) or phenol (**19b**; 1.1 eq.) was dissolved in anhydrous MeCN (5 mL/mmol), respectively. The two fractions (**18a**+**21** or **18b**+**19b**, respectively) were mixed together and the reaction mixture was stirred at 70 °C overnight. Subsequently, the reaction mixture was cooled to RT and was adjusted

to a slightly acidic pH using 1M aqueous HCl solution and allowed to precipitate for 30 mins in a refrigerator. The precipitate was filtered off using S4 frit, and dried under reduced pressure at 70 °C. The crude product was purified by column chromatography (DCM/MeOH; 10:1) to obtain the intermediate **22** or the final product **8**, respectively.

1-(3-chloro-4-methoxyphenyl)-3-(6-nitrobenzo[d]thiazol-2-yl)urea (**22**)

Yield 73%.

^{1}H NMR (500 MHz, DMSO-d_6) δ 11.41 (br s, 1H, NH), 9.17 (br s, 1H, NH), 8.94 (s, 1H, ArH), 8.22 (dd, *J* = 8.9, 2.5 Hz, 1H, ArH), 7.76 (d, *J* = 8.9 Hz, 1H, ArH), 7.67 (d, *J* = 2.7 Hz, 1H, ArH), 7.37 (dd, *J* = 9.1, 2.6 Hz, 1H, ArH), 7.12 (d, *J* = 8.9 Hz, 1H, ArH), 3.83 (s, 3H, CH_3).

N-{2-[3-(4-hydroxy-3-(trifluoromethyl)phenyl)ureido]benzo[d]thiazol-6-yl}acetamide (**8**)

Beige solid; yield 55%.

Melting point: decomposition at 270 °C

^{1}H NMR (500 MHz, DMSO-d_6) δ 10.32 (br s, 1H), 10.06 (br s, 1H), 9.38 (br s, 1H), 8.23 (d, *J* = 2.1 Hz, 1H, ArH), 7.76 (d, *J* = 2.7 Hz, 1H, ArH), 7.56 (d, *J* = 8.7 Hz, 1H, ArH), 7.48 (dd, *J* = 8.8, 2.7 Hz, 1H, ArH), 7.44 (dd, *J* = 8.7, 2.2 Hz, 1H, ArH), 7.01 (d, *J* = 8.8 Hz, 1H, ArH), 2.06 (s, 3H, CH_3).

^{13}C NMR (126 MHz, DMSO-d_6) δ 168.13, 158.69, 152.43, 151.43, 143.59, 134.89, 131.41, 129.88, 124.97, 123.88 (q, *J* = 271.4 Hz), 119.11, 118.20, 117.42, 117.31 (q, *J* = 5.5 Hz), 115.15 (q, *J* = 29.9 Hz), 111.40, 23.96.

LC-MS: 411.10 $[M+H]^+$ (calc. for $C_{17}H_{14}F_3N_4O_3S$: 411.07 $[M+H]^+$), 98% purity (300 nm).

ESI-HRMS: m/z 411.0730 $[M+H]^+$ (calc. for $C_{17}H_{14}F_3N_4O_3S$: 411.0733 $[M+H]^+$).

1-(6-aminobenzo[d]thiazol-2-yl)-3-(3-chloro-4-methoxyphenyl)urea (**23**)

Iron (10 eq.) and NH_4Cl (4 eq.) were dispersed in a mixture of MeOH/H_2O (1:1; 4 mL/mmol). The solution of 1-(3-chloro-4-methoxyphenyl)-3-(6-nitrobenzo[*d*]thiazol-2-yl)urea (**22**; 1 eq.) dispersed in anhydrous THF (4 mL/mmol) was added dropwise into the solution with iron and was stirred at 50 °C overnight. Subsequently, the reaction mixture was filtered off through Celite pad. The filtrate was concentrated under reduced pressure and then diluted with H_2O. The solution was neutralized with saturated $NaHCO_3$ solution and was allowed to precipitate for 1 hour in a refrigerator. The formed precipitate was filtered off using S4 frit, and dried to obtain the crude 1-(6-aminobenzo[*d*]thiazol-2-yl)-3-(3-chloro-4-methoxyphenyl)urea (**23**) in a 99% yield.

^{1}H NMR (500 MHz, DMSO-d_6) δ 10.50 (br s, 1H, NH), 9.09 (br s, 1H, NH), 7.68 (d, *J* = 2.6 Hz, 1H, ArH), 7.40 – 7.25 (m, 2H, ArH), 7.11 (d, *J* = 8.9 Hz, 1H, ArH), 6.96 (d, *J* = 2.2 Hz, 1H, ArH), 6.66 (dd, *J* = 8.5, 2.2 Hz, 1H, ArH), 5.08 (br s, 2H, NH_2), 3.82 (s, 3H, CH_3).

*1-(3-chloro-4-methoxyphenyl)-3-(6-ureidobenzo[d]thiazol-2-yl)urea (**24**)*

1-(6-aminobenzo[*d*]thiazol-2-yl)-3-(3-chloro-4-methoxyphenyl)urea (**23**; 1 eq.) was dispersed in anhydrous DMF (10 mL/mmol). Subsequently, CDI (1.2 eq.) was added, and the reaction mixture was stirred for 3 hours at RT and 50 °C overnight. Then 25% aqueous NH_3 solution (5 mL/mol) was added, and the reaction mixture was stirred for additional 2 hours at 50 °C. The reaction mixture was then cooled to 0 °C, slightly acidified using 1M aq. HCl and allowed to precipitate for 30 mins in a refrigerator. The precipitate was filtered off using S4 frit to obtain the crude 1-(3-chloro-4-methoxyphenyl)-3-(6-ureidobenzo[*d*]thiazol-2-yl)urea (**24**) in a 39% yield.

^{1}H NMR (500 MHz, DMSO-d_6) δ 10.74 (br s, 1H, NH), 9.23 (br s, 1H, NH), 8.63 (br s, 1H, NH), 8.04 (s, 1H, ArH), 7.69 (d, *J* = 2.7 Hz, 1H, ArH), 7.50 (d, *J* = 8.7 Hz, 1H, ArH), 7.40 – 7.32 (m, 1H, ArH), 7.29 – 7.23 (m, 1H, ArH), 7.12 (d, *J* = 9.0 Hz, 1H, ArH), 5.86 (br s, 2H, NH_2), 3.83 (s, 3H, CH_3).

N-{2-[3-(3-chloro-4-methoxyphenyl)ureido]benzo[d]thiazol-6-yl}methanesulfonamide (**25**)

1-(6-aminobenzo[*d*]thiazol-2-yl)-3-(3-chloro-4-methoxyphenyl)urea (**23**; 1 eq.) was dissolved in anhydrous pyridine (12 mL/mmol). After 5 minutes of stirring at RT, methanesulfonyl chloride (1.1 eq.) was added and the reaction mixture was stirred at RT overnight. After this time, the mixture was diluted with EtOAc, washed with 1M aq. HCl and brine, then dried with anhydrous Na_2SO_4, and concentrated under reduced pressure to obtain the crude *N*-{2-[3-(3-chloro-4-methoxyphenyl)ureido]benzo[*d*]thiazol-6-yl}methanesulfonamide (**25**) that was used in the next reaction step without further purification.

^{1}H NMR (500 MHz, DMSO-d_6) δ 11.41 (br s, 1H, NH), 9.70 (br s, 1H, NH), 9.17 (br s, 1H, NH), 7.73 (d, *J* = 2.2 Hz, 1H, ArH), 7.69 (d, *J* = 2.6 Hz, 1H, ArH), 7.60 (d, *J* = 8.6 Hz, 1H, ArH), 7.36 (dd, *J* = 8.9, 2.7 Hz, 1H, ArH), 7.24 (dd, *J* = 8.6, 2.2 Hz, 1H, ArH), 7.12 (d, *J* = 9.0 Hz, 1H, ArH), 3.83 (s, 3H, CH_3), 2.98 (s, 3H, CH_3).

Procedure F (general conditions): *Demethylation using aluminium trichloride* (**5**-**6**)

The corresponding 1-phenyl-3-benzo[*d*]thiazolylurea (1 eq.; **24** or **25**, respectively) was dispersed in anhydrous DCE (20 mL/mmol), $AlCl_3$ (4 eq.) was added, and the reaction mixture was stirred at 60 °C overnight. The next day, 2 eq. of $AlCl_3$ were added, the temperature was raised to 70 °C and the reaction mixture was stirred overnight again. After the completion of the reaction (monitored by TLC), the reaction mixture was cooled to RT, and DCE was evaporated. The substance was dispersed in H_2O and 1M aq. HCl was used to slightly acidify the solution. The mixture was extracted with EtOAc, washed with brine, dried with anhydrous Na_2SO_4 and concentrated under reduced pressure. The crude product was purified by column chromatography (DCM/MeOH; 20:1) to obtain the final product **5** or **6**, respectively.

1-(3-chloro-4-hydroxyphenyl)-3-(6-ureidobenzo[d]thiazol-2-yl)urea (**5**)

White-beige solid; yield 19%.

Melting point: decomposition at 220 °C

^{1}H NMR (500 MHz, DMSO-d_6) δ 10.62 (br s, 1H), 9.92 (br s, 1H), 8.99 (br s, 1H), 8.60 (br s, 1H), 8.03 (s, 1H, ArH), 7.59 (s, 1H, ArH), 7.50 (d, *J* = 8.8 Hz, 1H, ArH), 7.26 (dd, *J* = 8.7, 2.2 Hz, 1H, ArH), 7.20 – 7.15 (m, 1H, ArH), 6.92 (d, *J* = 8.7 Hz, 1H, ArH), 5.85 (br s, 2H, NH_2).

^{13}C NMR (126 MHz, DMSO-d_6) δ 157.49, 156.12, 151.86, 148.90, 143.54, 136.25, 131.72, 130.83, 120.76, 119.42 (3C), 117.29, 116.68, 109.92.

^{13}C NMR (126 MHz, DMSO-d_6) δ 158.16, 156.40, 152.33, 149.14, 142.18, 136.48, 131.62, 131.00, 120.97, 119.59 (2C), 119.17, 117.64, 116.85, 110.26. (^{13}C NMR was also measured with addition of trifluoroacetic acid (TFA) to improve relaxation of quaternary carbons)

LC-MS: 378.10 $[M+H]^+$ (calc. for $C_{15}H_{13}ClN_5O_3S$: 378.04 $[M+H]^+$), 95% purity (300 nm).

ESI-HRMS: m/z 378.0410 $[M+H]^+$ (calc. for $C_{15}H_{13}ClN_5O_3S$: 378.0422 $[M+H]^+$).

N-{2-[3-(3-chloro-4-hydroxyphenyl)ureido]benzo[d]thiazol-6-yl}methanesulfonamide (**6**)

Brown solid; yield 15%.

Melting point: 161–163 °C

^{1}H NMR (500 MHz, DMSO-d_6) δ 10.76 (br s, 1H), 9.93 (br s, 1H), 9.69 (br s, 1H), 9.01 (br s, 1H), 7.72 (s, 1H, ArH), 7.63 – 7.57 (m, 2H, ArH), 7.24 (dd, *J* = 8.7, 2.3 Hz, 1H, ArH), 7.18 (dd, *J* = 8.8, 2.5 Hz, 1H, ArH), 6.93 (d, *J* = 8.7 Hz, 1H, ArH), 2.97 (s, 3H, CH_3).

^{13}C NMR (126 MHz, DMSO-d_6) δ 159.42, 152.28, 149.04, 145.10, 133.52, 132.06, 130.81, 120.87, 120.30, 119.77, 119.53, 119.42, 116.73, 113.86, 39.10. (^{13}C NMR was measured with addition of trifluoroacetic acid (TFA) to improve relaxation of quaternary carbons)

LC-MS: 410.90 $[M-H]^-$ (calc. for $C_{15}H_{12}ClN_4O_4S_2$: 411.00 $[M-H]^-$), 97% purity (300 nm).

ESI-HRMS: m/z 413.0136 $[M+H]^+$ (calc. for $C_{15}H_{14}ClN_4O_4S_2$: 413.0140 $[M+H]^+$).

Procedure $A_{1\text{-}2}$ (general conditions): *Synthesis of 6-substituted 2-aminobenzo[d]thiazoles from corresponding 4-substituted anilines* (**32**, **17e**)

The corresponding nitrile (**31b**; 1 eq.) or sulfonamide (**31c**; 1 eq.) was dissolved in AcOH (2 mL/mmol), respectively. KSCN (4 eq.) was added, and the reaction mixture was stirred for 20 minutes at RT. After cooling the reaction mixture to 10 °C, Br_2 (2 eq.) dissolved in AcOH (1 mL/mmol) was added dropwise and the mixture was stirred at RT overnight. The reaction mixture was then added to 25% aqueous NH_3 solution (18 mL/mmol) at 0 °C. The reaction mixture was washed with EtOAc and the formed precipitate was filtered off through Celite pad. Subsequently, the filtrate was extracted with EtOAc and organic layers were concentrated under reduced pressure. The crude product was washed

with a 10% aqueous solution of $Na_2S_2O_3$ and brine, dried with anhydrous Na_2SO_4 and concentrated under reduced pressure. The crude product was purified by column chromatography (heptane/THF/EtOAc; 1:1:1) to obtain the corresponding intermediate **32** or **17e**, respectively.

2-aminobenzo[d]thiazole-6-carbonitrile (**32**)

Yield 27%.

^{1}H NMR (500 MHz, DMSO-d_6) δ 8.17 (d, *J* = 1.6 Hz, 1H, ArH), 8.03 (s, 2H, NH_2), 7.60 (dd, *J* = 8.3, 1.5 Hz, 1H, ArH), 7.41 (d, *J* = 8.3 Hz, 1H, ArH).

2-aminobenzo[d]thiazole-6-sulfonamide (**17e**)

Yield 42%.

^{1}H NMR (500 MHz, DMSO-d_6) δ 8.12 (dd, *J* = 2.0, 0.4 Hz, 1H, ArH), 7.90 (s, 2H, NH_2), 7.66 (dd, *J* = 8.4, 2.0 Hz, 1H, ArH), 7.42 (dd, *J* = 8.5, 0.4 Hz, 1H, ArH), 7.21 (s, 2H, SO_2NH_2).

tert-butyl (6-cyanobenzo[d]thiazol-2-yl)carbamate (**34**)

2-aminobenzo[*d*]thiazole-6-carbonitrile (**32**; 1 eq.) and DMAP (0.05 eq.) were dissolved in anhydrous THF (5 mL/mmol) at 0 °C. Boc_2O (1.3 eq.) dissolved in anhydrous THF (2 mL/mmol) was added and the reaction mixture was stirred at RT overnight. The reaction mixture was then extracted with EtOAc. Subsequently, the obtained organic layers were washed with 10% aqueous citric acid solution, saturated $NaHCO_3$ solution, H_2O, and brine. The combined organic layers were dried with anhydrous Na_2SO_4 and concentrated under reduced pressure to obtain the solid *tert*-butyl (6-cyanobenzo[*d*]thiazol-2-yl)carbamate (**34**) in an 87% yield.

tert-butyl [6-(1H-tetrazol-5-yl)benzo[d]thiazol-2-yl]carbamate (**35**)

The protected *tert*-butyl (6-cyanobenzo[*d*]thiazol-2-yl)carbamate (**34**; 1 eq.) was dispersed in anhydrous DMF (2 mL/mmol) together with $Et_3N.HCl$ (10 eq.). Subsequently, NaN_3 (10 eq.) was added, and the reaction mixture was stirred for 16 hours at 100 °C. The reaction mixture was washed with a threefold volume of 0.5M aqueous HCl solution and allowed to precipitate for 30 minutes in a refrigerator. The formed precipitate was filtered off using an S4 frit, and dried under reduced pressure at 70 °C. The crude *tert*-butyl [6-(1*H*-tetrazol-5-yl)benzo[*d*]thiazol-2-yl]carbamate (**35**) was obtained in a 73% yield.

6-(1H-tetrazol-5-yl)benzo[d]thiazole-2-amine trifluoroacetate (**17d**)

The protected *tert*-butyl [6-(1*H*-tetrazol-5-yl)benzo[*d*]thiazol-2-yl]carbamate (**35**; 1 eq.) was dispersed in anhydrous DCM (20 mL/mmol) and cooled to 0 °C. 5 mL of TFA was added and the reaction

mixture was stirred at RT overnight. The organic solvents were evaporated from the reaction mixture, the crude product was flooded with Et_2O and allowed to precipitate for 1 hour in a refrigerator. The formed precipitate was filtered off using S4 frit, and dried to obtain 6-(1*H*-tetrazol-5-yl)benzo[*d*]thiazole-2-amine trifluoroacetate (**17d**) in a 54% yield.

^{1}H NMR (500 MHz, DMSO-d_6) δ 8.40 (s, 1H, ArH), 8.26 (br s, 2H, NH_2), 7.92 (d, *J* = 8.3 Hz, 1H, ArH), 7.54 (d, *J* = 8.3 Hz, 1H, ArH).

^{13}C NMR (126 MHz, DMSO-d_6) δ 168.92, 158.37 (q, *J* = 36.9 Hz), 155.28, 152.61, 133.22 (q, *J* = 290.3 Hz), 130.77, 125.00, 120.23, 117.42, 117.08.

N-[6-(1H-tetrazol-5-yl)benzo[d]thiazol-2-yl]-1H-imidazole-1-carboxamide (**18d**)

6-(1*H*-tetrazole-5-yl)benzo[*d*]thiazole-2-amine trifluoroacetate (**17d**; 1 eq.) was dispersed in anhydrous DCM (15 mL/mmol). DIPEA (1.2 eq.) was added and the reaction mixture was stirred for 5 minutes at RT. Subsequently, CDI (1.2 eq.) was added and the reaction mixture was stirred under reflux overnight. The reaction mixture was then cooled to RT and allowed to precipitate for 1 hour in a refrigerator. The precipitate was filtered off using S4 frit to obtain the crude *N*-[6-(1*H*-tetrazol-5-yl)benzo[*d*]thiazol-2-yl]-1*H*-imidazole-1-carboxamide (**18d**) in an 82% yield.

1-[6-(1H-tetrazol-5-yl)benzo[d]thiazol-2-yl]-3-(3-chloro-4-hydroxyphenyl)urea (**3**)

N-[6-(1*H*-tetrazol-5-yl)benzo[*d*]thiazol-2-yl]-1*H*-imidazole-1-carboxamide (**18d**; 1 eq.) was dispersed in anhydrous MeCN (20 mL/mmol). 4-amino-2-chlorophenol (**19a**; 1.1 eq.) was added and the reaction mixture was stirred under reflux overnight. The reaction mixture was cooled to RT, 1M aqueous HCl solution was added, and the mixture was allowed to precipitate for 30 minutes in a refrigerator. The formed precipitate was filtered off using S4 frit and purified by silica flash chromatography (SiO_2 40 g; 0–20% MeOH in DCM) to obtain 1-[6-(1*H*-tetrazol-5-yl)benzo[*d*]thiazol-2-yl]-3-(3-chloro-4-hydroxyphenyl)urea (**3**) as a dark purple solid in a 30% yield.

Melting point: 202–204 °C

^{1}H NMR (500 MHz, DMSO-d_6) δ 11.18 (br s, 1H), 9.96 (br s, 1H), 9.11 (br s, 1H), 8.59 (d, *J* = 1.7 Hz, 1H, ArH), 8.04 (dd, *J* = 8.5, 1.8 Hz, 1H, ArH), 7.82 (d, *J* = 8.4 Hz, 1H, ArH), 7.61 (d, *J* = 2.6 Hz, 1H, ArH), 7.20 (dd, *J* = 8.8, 2.6 Hz, 1H, ArH), 6.94 (d, *J* = 8.7 Hz, 1H, ArH).

^{13}C NMR (126 MHz, DMSO-d_6) δ 161.77, 155.52, 152.23, 150.11, 149.11, 132.16, 130.57, 124.95, 120.92, 120.54, 119.84, 119.58, 119.37, 118.79, 116.68.

LC-MS: 386.00 $[M-H]^-$ (calc. for $C_{15}H_9ClN_7O_2S$: 386.02 $[M-H]^-$), 99% purity (300 nm).

ESI-HRMS: m/z 388.0364 $[M+H]^+$ (calc. for $C_{15}H_{11}ClN_7O_2S$: 388.0378 $[M+H]^+$).

Methyl 2-aminobenzo[d]thiazole-6-carboxylate (**33**)

Methyl 4-aminobenzoate (**31a**; 1 eq.) and KSCN (7 eq.) were dissolved in a mixture of DMSO/H_2O (9:1; 10 mL/mmol) and the reaction mixture was stirred for 15 minutes at RT. Benzyltrimethylammonium dichloroiodate (3 eq.) was added and the reaction mixture was stirred at 70 °C overnight. The reaction was flooded with H_2O and slightly basified using 4M aqueous NaOH solution. The mixture was extracted with EtOAc, washed with $Na_2S_2O_3$ and brine, dried with anhydrous Na_2SO_4, and concentrated under reduced pressure. The crude product was dispersed in a mixture of Et_2O and EtOAc, allowed to precipitate for 30 mins in a refrigerator, and the precipitate was filtered off using S4 frit, which was subsequently dried under reduced pressure at 70 °C to obtain methyl 2-aminobenzo[*d*]thiazole-6-carboxylate (**33**) in a 60% yield.

^{1}H NMR (500 MHz, DMSO-d_6) δ 8.28 (d, *J* = 1.8 Hz, 1H, ArH), 7.89 (br s, 2H, NH_2), 7.81 (dd, *J* = 8.4, 1.8 Hz, 1H, ArH), 7.37 (d, *J* = 8.4 Hz, 1H, ArH), 3.82 (s, 3H, CH_3).

2-aminobenzo[d]thiazole-6-carboxylic acid (**36**)

Methyl 2-aminobenzo[*d*]thiazole-6-carboxylate (**33**; 1 eq.) was dispersed in a mixture of 1M aq. NaOH and EtOH (1:1; 30 mL/mmol) and the reaction mixture was stirred at RT overnight. Subsequently, EtOH was evaporated, and the reaction mixture was slightly acidified using 1M aq. HCl. The reaction mixture was allowed to precipitate for 30 minutes in a refrigerator and the resulting precipitate was filtered off using S4 frit, which was subsequently dried under reduced pressure at 70 °C. The crude 2-aminobenzo[*d*]thiazole-6-carboxylic acid (**36**) was obtained in a 53% yield.

^{1}H NMR (500 MHz, DMSO-d_6) δ 12.57 (br s, 1H, COOH), 8.24 (s, 1H, ArH), 7.84 (br s, 2H, NH_2), 7.80 (d, *J* = 8.3 Hz, 1H, ArH), 7.35 (d, *J* = 8.4 Hz, 1H, ArH).

4-methoxybenzyl 2-aminobenzo[d]thiazole-6-carboxylate (**17c**)

2-aminobenzo[*d*]thiazole-6-carboxylic acid (**36**; 1 eq.) was dissolved in anhydrous DMF (3 mL/mmol). K_2CO_3 (1.05 eq.) and 4-methoxybenzyl chloride (1.1 eq.) were added, and the reaction mixture was stirred for 4 days at RT. The reaction mixture was flooded with H_2O and allowed to precipitate for 1 hour in a refrigerator. The precipitate was filtered off using S4 frit and dried under reduced pressure at 70 °C to obtain the crude 4-methoxybenzyl 2-aminobenzo[*d*]thiazole-6-carboxylate (**17c**) in a 78% yield.

^{1}H NMR (500 MHz, DMSO-d_6) δ 8.29 (d, *J* = 1.8 Hz, 1H, ArH), 7.89 (br s, 2H, NH_2), 7.82 (dd, *J* = 8.4, 1.8 Hz, 1H, ArH), 7.41 (d, *J* = 8.5 Hz, 2H, ArH), 7.36 (d, *J* = 8.4 Hz, 1H, ArH), 6.95 (d, *J* = 8.5 Hz, 2H, ArH), 5.25 (s, 2H, CH_2), 3.76 (s, 3H, CH_3).

MS (ESI$^+$): calculated for $C_{16}H_{15}N_2O_3S$ $[M+H]^+$ 315.08, found 315.07.

4-methoxybenzyl 2-(1H-imidazole-1-carboxamido)benzo[d]thiazole-6-carboxylate (**18c**)

4-methoxybenzyl 2-aminobenzo[*d*]thiazole-6-carboxylate (**17c**; 1 eq.) was dispersed in anhydrous DMF (2 mL/mmol) and anhydrous MeCN (5 ml/mmol). Subsequently, CDI (5 eq.) was added and the reaction mixture was stirred at 85 °C for 4 hours. The reaction mixture was cooled to RT, flooded with Et_2O and allowed to precipitate for 30 mins in a refrigerator. The precipitate was filtered off using S4 frit and dried under pressure at 70 °C to obtain the crude 4-methoxybenzyl 2-(1*H*-imidazole-1-carboxamido)benzo[*d*]thiazole-6-carboxylate (**18c**) in a 51% yield.

4-methoxybenzyl 2-[3-(4-hydroxy-3-(trifluoromethyl)phenyl)ureido]benzo[d]thiazole-6-carboxylate (**20**)

4-methoxybenzyl 2-(1*H*-imidazole-1-carboxamido)benzo[*d*]thiazole-6-carboxylate (**18c**; 1 eq.) was dispersed in anhydrous DMF (30 mL/mmol) and 4-amino-2-(trifluoromethyl)phenol (**19b**; 1.3 eq.) dissolved in anhydrous DMF (1 mL/mmol) was added. The reaction mixture was stirred at 60 °C overnight. The reaction mixture was cooled to RT, slightly acidified using 1M aq. HCl and allowed to precipitate for 30 minutes in a refrigerator. The precipitate was filtered off using S4 frit and dried under pressure at 70 °C to obtain 4-methoxybenzyl 2-[3-(4-hydroxy-3-(trifluoromethyl)phenyl)ureido]benzo[*d*]thiazole-6-carboxylate (**20**) in a 62% yield.

^{1}H NMR (500 MHz, DMSO-d_6) δ 11.10 (br s, 1H), 10.36 (br s, 1H), 9.10 (br s, 1H), 8.57 (s, 1H, ArH), 7.97 (dd, *J* = 8.5, 1.8 Hz, 1H, ArH), 7.81 – 7.65 (m, 2H, ArH), 7.49 (s, 1H, ArH), 7.43 (d, *J* = 8.7 Hz, 2H, ArH), 7.00 (d, *J* = 8.8 Hz, 1H, ArH), 6.97 (d, *J* = 8.7 Hz, 2H, ArH), 5.29 (s, 2H, CH_2), 3.76 (s, 3H, CH_3).

2-[3-(4-hydroxy-3-(trifluoromethyl)phenyl)ureido]benzo[d]thiazole-6-carboxylic acid (**7**)

4-methoxybenzyl 2-[3-(4-hydroxy-3-(trifluoromethyl)phenyl)ureido]benzo[*d*]thiazole-6-carboxylate (**20**; 1 eq.) was dispersed in glacial AcOH (40 mL/mmol). 1M HCl solution in AcOH (40 eq.) was added dropwise, and the reaction mixture was stirred at RT overnight. The reaction mixture was then concentrated on a rotavapor and purified by silica flash chromatography (SiO_2 24 g; 0–20% MeOH in DCM) to obtain 2-[3-(4-hydroxy-3-(trifluoromethyl)phenyl)ureido]benzo[*d*]thiazole-6-carboxylic acid (**7**) as a light pink solid in a 34% yield.

Melting point: 291–293 °C

^{1}H NMR (500 MHz, DMSO-d_6) δ 12.91 (br s, 1H), 11.51 (br s, 1H), 10.48 (br s, 1H), 8.44 (s, 1H, ArH), 7.99 (d, *J* = 8.3 Hz, 1H, ArH), 7.89 (d, *J* = 2.6 Hz, 1H, ArH), 7.71 – 7.51 (m, 2H, ArH), 7.05 (d, *J* = 8.8 Hz, 1H, ArH).

^{13}C NMR (126 MHz, DMSO-d_6) δ 173.18, 169.98, 162.04, 153.34, 151.05, 150.74, 130.92 (2C), 127.20, 124.41, 124.03 (q, *J* = 271.7 Hz), 122.46, 118.19, 117.38, 116.72, 115.01 (q, *J* = 29.3 Hz).

LC-MS: 396.00 $[M-H]^-$ (calc. for $C_{16}H_9F_3N_3O_4S$: 396.03 $[M-H]^-$), 98% purity (300 nm).

ESI-HRMS: m/z 398.0454 $[M+H]^+$ (calc. for $C_{16}H_{11}F_3N_3O_4S$: 398.0417 $[M+H]^+$).

3-chloro-4-methoxyphenylisocyanate (**27**)

Triphosgene (1 eq.) was dissolved at 0 °C in anhydrous DCM (4 mL/mmol). At the same time, 3-chloro-4-methoxyaniline (**26**; 1 eq.) was dissolved in anhydrous DCM (2 mL/mmol) and then added dropwise to the dissolved triphosgene. The reaction mixture was removed from the ice bath, 1 mL of Et_3N was added dropwise and the reaction mixture was stirred for 1 hour at RT and 1 hour under reflux. Subsequently, DCM was evaporated under reduced pressure and 3-chloro-4-methoxyphenylisocyanate (**27**) was used in the next reaction step without further purification.

Procedure B (general conditions): *Synthesis of 1-phenyl-3-benzo[d]thiazolylureas in reaction with 3-chloro-4-methoxy-phenylisocyanate* (**28**-**29**)

The corresponding 2-aminobenzo[*d*]thiazole (**17e**; 1 eq. or **17f**; 1.05 eq., respectively) was dissolved in anhydrous THF (4 mL/mmol). 3-chloro-4-methoxy-phenylisocyanate (**27**; 1 eq.) was dissolved in anhydrous THF (4 mL/mmol) and added dropwise to the reaction mixture, which was then stirred under reflux overnight. The reaction mixture was cooled to RT, flooded with 1M aqueous HCl solution, followed by evaporation of THF. The crude product was dispersed in MeCN and 1M aqueous HCl solution and was filtered off using S4 frit and dried under reduced pressure at 70 °C. The obtained solid compound was purified by silica flash chromatography (SiO_2 80 g; 0–20% MeOH in DCM) to obtain compound **29** or **28**, respectively.

2-[3-(3-chloro-4-methoxyphenyl)ureido]benzo[d]thiazole-6-sulfonamide (**29**)

Yield 45%.

^{1}H NMR (500 MHz, DMSO-d_6) δ 11.42 (br s, 1H, NH), 9.53 (br s, 1H, NH), 8.41 (s, 1H, ArH), 7.83 (dd, *J* = 8.5, 1.9 Hz, 1H, ArH), 7.77 (d, *J* = 8.6 Hz, 1H, ArH), 7.72 (d, *J* = 2.6 Hz, 1H, ArH), 7.41 (dd, *J* = 8.9, 2.6 Hz, 1H, ArH), 7.33 (s, 2H, NH_2), 7.12 (d, *J* = 9.0 Hz, 1H, ArH), 3.84 (s, 3H, CH_3).

Methyl 2-[3-(3-chloro-4-methoxyphenyl)ureido]benzo[d]thiazole-5-carboxylate (**28**)

Yield 86%.

^{1}H NMR (500 MHz, DMSO-d_6) δ 9.21 (br s, 1H, NH), 8.76 (br s, 1H, NH), 8.46 (d, *J* = 2.3 Hz, 1H, ArH), 7.74 (d, *J* = 2.3 Hz, 1H, ArH), 7.72 (s, 1H, ArH), 7.66 (d, *J* = 2.6 Hz, 1H, ArH), 7.28 (dd, *J* = 8.9, 2.6 Hz, 1H, ArH), 7.09 (d, *J* = 9.0 Hz, 1H, ArH), 3.92 (s, 3H, CH_3), 3.81 (s, 3H, CH_3).

Procedure C (general conditions): *Demethylation using aluminium trichloride* (**4**, **9**)

The corresponding 1-phenyl-3-benzo[*d*]thiazolylurea (1 eq.; **28** or **29**, respectively) was dispersed in anhydrous DCE (20 mL/mmol), $AlCl_3$ (4.5 eq.) was added, and the reaction mixture was stirred at 70 °C overnight. The next day, 2 eq. of $AlCl_3$ were added, the temperature was raised to 80 °C and the reaction mixture was stirred overnight again. The reaction mixture was cooled to RT and DCE was evaporated. The substance was dispersed in H_2O and extracted with EtOAc, washed with brine, dried with anhydrous Na_2SO_4, and concentrated under reduced pressure. The crude product was purified by silica flash chromatography (SiO_2 40 g; 10–50% THF in DCM) to obtain the final product **4** or **9**, respectively.

2-[3-(3-chloro-4-hydroxyphenyl)ureido]benzo[d]thiazole-6-sulfonamide (**4**)

Brow solid; yield 24%.

Melting point: 252–254 °C

^{1}H NMR (500 MHz, DMSO-d_6) δ 11.08 (br s, 1H), 9.95 (br s, 1H), 9.07 (br s, 1H), 8.40 (s, 1H, ArH), 7.82 (dd, *J* = 8.4, 1.9 Hz, 1H, ArH), 7.77 (d, *J* = 8.7 Hz, 1H, ArH), 7.61 (d, *J* = 2.6 Hz, 1H, ArH), 7.32 (br s, 2H, NH_2), 7.20 (dd, *J* = 8.8, 2.6 Hz, 1H, ArH), 6.94 (d, *J* = 8.7 Hz, 1H, ArH).

^{13}C NMR (126 MHz, DMSO-d_6) δ 162.76, 152.34, 150.56, 149.29, 138.51, 131.45, 130.73, 123.97, 121.11, 120.00, 119.73, 119.54, 119.38, 116.81. (^{13}C NMR was measured with addition of trifluoroacetic acid (TFA) to improve relaxation of quaternary carbons)

LC-MS: 399.20 $[M+H]^+$ (calc. for $C_{14}H_{12}ClN_4O_4S_2$: 399.00 $[M+H]^+$), 99% purity (300 nm).

ESI-HRMS: m/z 399.0014 $[M+H]^+$ (calc. for $C_{14}H_{12}ClN_4O_4S_2$: 398.9983 $[M+H]^+$).

2-[3-(3-chloro-4-hydroxyphenyl)ureido]benzo[d]thiazole-5-carboxylic acid (**9**)

Brown solid; yield 30%.

Melting point: 214–216 °C

^{1}H NMR (500 MHz, DMSO-d_6) δ 12.38 (br s, 1H, COOH), 9.80 (br s, 1H), 9.05 (br s, 1H), 8.62 (br s, 1H), 8.43 (d, *J* = 2.5 Hz, 1H, ArH), 7.74 (dd, *J* = 8.7, 2.5 Hz, 1H, ArH), 7.56 (d, *J* = 2.6 Hz, 1H, ArH), 7.48 (d, *J* = 8.6 Hz, 1H, ArH), 7.12 (dd, *J* = 8.8, 2.6 Hz, 1H, ArH), 6.90 (d, *J* = 8.7 Hz, 1H, ArH).

^{13}C NMR (126 MHz, DMSO-d_6) δ 164.09, 163.56, 152.53, 148.36, 139.42, 131.67, 125.99, 124.95, 124.52, 122.84, 120.49, 119.24, 119.11, 118.51, 116.60.

LC-MS: 361.90 $[M-H]^-$ (calc. for $C_{15}H_9ClN_3O_4S$: 362.00 $[M-H]^-$), 94% purity (300 nm).

ESI-HRMS: m/z 364.0137 $[M+H]^+$ (calc. for $C_{15}H_{11}ClN_3O_4S$: 364.0153 $[M+H]^+$).

3-chloro-4-methoxybenzoyl chloride (**38**)

3-chloro-4-methoxy benzoic acid (**37**; 1 eq.) was dissolved in anhydrous DCM (13 mL/mmol). Gradually, oxalyl chloride (6 eq.) was added and the reaction mixture was stirred at RT overnight. DCM was evaporated from the reaction mixture to yield the crude 3-chloro-4-methoxybenzoyl chloride (**38**), which was used in the next reaction step without further purification.

Methyl 2-(3-chloro-4-methoxybenzamido)benzo[d]thiazole-6-carboxylate (**39**)

3-chloro-4-methoxybenzoyl chloride (**38**; 1 eq.) was dissolved in anhydrous toluene (22 mL/mmol) at RT. Methyl 2-aminobenzo[*d*]thiazole-6-carboxylate (**33**; 2.1 eq.) was added and the reaction mixture was stirred under reflux overnight. The precipitate was filtered off using S4 frit and dried under reduced pressure at 70 °C. The crude methyl 2-(3-chloro-4-methoxybenzamido)benzo[*d*]thiazole-6-carboxylate (**39**) was obtained in an 89% yield.

^{1}H NMR (500 MHz, DMSO-d_6) δ 13.03 (br s, 1H, NH), 8.67 (s, 1H, ArH), 8.28 (d, *J* = 2.3 Hz, 1H, ArH), 8.17 (dd, *J* = 8.7, 2.3 Hz, 1H, ArH), 8.04 (dd, *J* = 8.4, 1.8 Hz, 1H, ArH), 7.85 (d, *J* = 8.5 Hz, 1H, ArH), 7.34 (d, *J* = 8.8 Hz, 1H, ArH), 3.97 (s, 3H, CH_3), 3.89 (s, 3H, CH_3).

Methyl 2-(3-chloro-4-hydroxybenzamido)benzo[d]thiazole-6-carboxylate (**40**)

Methyl 2-(3-chloro-4-methoxybenzamido)benzo[*d*]thiazole-6-carboxylate (**39**; 1 eq.) was dissolved in anhydrous DCE (25 mL/mmol). $AlCl_3$ (4.5 eq.) was added, and the reaction mixture was stirred at 70 °C overnight. Subsequently, DCE was evaporated, the crude product was flooded with H_2O, and neutralized by adding saturated $NaHCO_3$ solution. The mixture was extracted with Et_2O and EtOAc, washed with brine, dried with anhydrous Na_2SO_4, and concentrated under reduced pressure. The crude methyl 2-(3-chloro-4-hydroxybenzamido)benzo[*d*]thiazole-6-carboxylate (**40**) was obtained in an 82% yield.

^{1}H NMR (500 MHz, DMSO-d_6) δ 12.11 (br s, 1H), 10.42 (br s, 1H), 7.85 (s, 1H, ArH), 7.42 (d, *J* = 2.2 Hz, 1H, ArH), 7.29 – 7.10 (m, 2H, ArH), 7.02 (d, *J* = 8.5 Hz, 1H, ArH), 6.28 (d, *J* = 8.6 Hz, 1H, ArH), 3.06 (s, 3H, CH_3).

2-(3-chloro-4-hydroxybenzamido)benzo[d]thiazole-6-carboxylic acid (**10**)

Methyl 2-(3-chloro-4-hydroxybenzamido)benzo[*d*]thiazole-6-carboxylate (**40**; 1 eq.) was dispersed in a mixture of 1M aq. NaOH and EtOH (1:1; 30 mL/mmol) and the reaction mixture was stirred under reflux overnight. The reaction mixture was then concentrated under reduced pressure, the residue was neutralized using 1M aqueous HCl solution and was allowed to precipitate for 30 mins in a refrigerator. The precipitate was filtered off using S4 frit, and dried under reduced pressure

at 70 °C. The compound 2-(3-chloro-4-hydroxybenzamido)benzo[*d*]thiazole-6-carboxylic acid (**10**) was obtained as a white-beige solid in a 45% yield.

Melting point: decomposition at 270 °C

^{1}H NMR (500 MHz, DMSO-d_6) δ 12.92 (br s, 1H), 11.24 (br s, 1H), 8.63 (d, *J* = 1.7 Hz, 1H, ArH), 8.24 (d, *J* = 2.3 Hz, 1H, ArH), 8.03 – 7.98 (m, 2H, ArH), 7.82 (d, *J* = 8.5 Hz, 1H, ArH), 7.11 (d, *J* = 8.6 Hz, 1H, ArH).

^{13}C NMR (126 MHz, DMSO-d_6) δ 167.07, 164.64, 162.09, 157.47, 151.60, 131.63, 130.50, 129.12, 127.35, 125.82, 123.86, 123.24, 119.93, 119.88, 116.38.

LC-MS: 346.70 $[M-H]^-$ (calc. for $C_{15}H_8ClN_2O_4S$: 346.99 $[M-H]^-$), 99% purity (300 nm).

ESI-HRMS: m/z 349.0036 $[M+H]^+$ (calc. for $C_{15}H_{10}ClN_2O_4S$: 349.0044 $[M+H]^+$).

Procedure A (general conditions): *Synthesis of imines from corresponding aldehydes and 2-aminobenzo[d]thiazoles* (**43a-c**)

The corresponding 6-substituted 2-aminobenzo[*d*]thiazole (1 eq.; **33** or **41**, respectively) was dissolved in anhydrous toluene (10 mL/mmol), molecular sieves were added, and the reaction mixture was stirred for 5 minutes at RT. The corresponding benzaldehyde (1 eq.; **42a** or **42b**, respectively) was added and the reaction mixture was stirred under reflux overnight. Molecular sieves were filtered off, the filtrate was flooded with Et_2O and allowed to precipitate for 30 mins in a refrigerator. Subsequently, the precipitate was filtered off using S4 frit and dried under reduced pressure to obtain the crude intermediate **43a** or **43b** or **43c**, respectively. The crude intermediates were used in the next reaction step without further purification.

Methyl 2-[(3-chloro-4-hydroxybenzylidene)amino]benzo[d]thiazole-6-carboxylate (**43a**)

Quantitative yield

^{1}H NMR (500 MHz, DMSO-d_6) δ 8.71 (br s, 1H, OH), 8.55 (s, 1H, ArH), 7.97 (d, *J* = 8.7 Hz, 1H, ArH), 7.89 (s, 1H, ArH), 7.81 (d, *J* = 8.4 Hz, 1H, ArH), 7.65 (d, *J* = 8.7 Hz, 1H, ArH), 6.60 (s, 1H, ArH), 3.87 (s, 3H, CH_3), 2.18 (s, 1H, CH).

N-{2-[(3-chloro-4-hydroxybenzylidene)amino]benzo[d]thiazol-6-yl}acetamide (**43b**)

Quantitative yield.

N-{2-[(4-hydroxy-3-(trifluoromethyl)benzylidene)amino]benzo[d]thiazol-6-yl}acetamide (**43c**)

Quantitative yield.

Procedure B (general conditions): *Reduction of imines to corresponding amines* (**44**, **13-14**)

The corresponding 6-substituted benzylidene-2-aminobenzo[d]thiazole (1 eq.; **43a** or **43b** or **43c**, respectively) was dissolved in anhydrous MeOH (13 mL/mmol), $NaBH_3CN$ (2.5 eq.) was added, and the reaction mixture was stirred at 60 °C. After 1 hour another 1 eq. of $NaBH_3CN$ was added and the reaction mixture was stirred under reflux for 48 hours. The reaction mixture was flooded with H_2O,

neutralized with NH_4Cl and extracted with EtOAc. The organic layers were washed with brine, dried with anhydrous Na_2SO_4, and concentrated under reduced pressure. The obtained crude product was then purified by silica flash chromatography (SiO_2 80 g, using EtOAc in heptane as a mobile phase), followed by reversed-phase flash chromatography (C18 80 g, using MeOH in H_2O as a mobile phase) to obtain the intermediate **44** or the final product **13** or **14**, respectively.

Methyl 2-[(3-chloro-4-hydroxybenzyl)amino]benzo[d]thiazole-6-carboxylate (**44**)

Yield 23%.

^{1}H NMR (500 MHz, DMSO-d_6) δ 10.12 (br s, 1H, OH), 8.81 (t, *J* = 5.7 Hz, 1H, NH), 8.31 (d, *J* = 1.7 Hz, 1H, ArH), 7.83 (dd, *J* = 8.5, 1.8 Hz, 1H, ArH), 7.43 (d, *J* = 8.4 Hz, 1H, ArH), 7.34 (d, *J* = 2.1 Hz, 1H, ArH), 7.15 (dd, *J* = 8.3, 2.2 Hz, 1H, ArH), 6.94 (d, *J* = 8.3 Hz, 1H, ArH), 4.51 (d, *J* = 5.7 Hz, 2H, CH_2), 3.83 (d, *J* = 0.5 Hz, 3H, CH_3).

N-{2-[(3-chloro-4-hydroxybenzyl)amino]benzo[d]thiazol-6-yl}acetamide (**13**)

Yellow solid; yield 9%.

Melting point: 183–185 °C

^{1}H NMR (500 MHz, DMSO-d_6) δ 9.89 (br s, 1H), 8.30 (t, *J* = 5.7 Hz, 1H, NH), 8.02 (d, *J* = 2.0 Hz, 1H, ArH), 7.32 – 7.29 (m, 2H, ArH), 7.26 (dd, *J* = 8.7, 2.1 Hz, 1H, ArH), 7.13 (dd, *J* = 8.3, 2.2 Hz, 1H, ArH), 6.91 (d, *J* = 8.3 Hz, 1H, ArH), 4.43 (d, *J* = 5.5 Hz, 2H, CH_2), 2.02 (s, 3H, CH_3).

^{13}C NMR (126 MHz, DMSO-d_6) δ 167.89, 165.27, 152.58, 148.33, 133.26, 130.58, 130.29, 128.88, 127.33, 119.48, 117.82, 117.63, 116.61, 111.63, 46.31, 23.90.

LC-MS: 348.00 $[M+H]^+$ (calc. for $C_{16}H_{15}ClN_3O_2S$: 348.06 $[M+H]^+$), 97% purity (300 nm).

ESI-HRMS: m/z 348.0594 $[M+H]^+$ (calc. for $C_{16}H_{15}ClN_3O_2S$: 348.0568 $[M+H]^+$).

N-{2-[(4-hydroxy-3-(trifluoromethyl)benzyl)amino]benzo[d]thiazol-6-yl}acetamide (**14**)

White solid; yield 6%.

Melting point: 172–174 °C

^{1}H NMR (500 MHz, DMSO-d_6) δ 10.60 (br s, 1H), 9.90 (br s, 1H), 8.33 (t, *J* = 5.7 Hz, 1H, NH), 8.02 (d, *J* = 2.0 Hz, 1H, ArH), 7.51 (d, *J* = 2.2 Hz, 1H, ArH), 7.44 (dd, *J* = 8.6, 2.2 Hz, 1H, ArH), 7.34 – 7.24 (m, 2H, ArH), 6.99 (d, *J* = 8.4 Hz, 1H, ArH), 4.49 (d, *J* = 5.6 Hz, 2H, CH_2), 2.02 (s, 3H, CH_3).

^{13}C NMR (126 MHz, DMSO-d_6) δ 167.86, 165.22, 155.18, 148.29, 133.28, 133.06, 130.56, 128.93, 125.69 (q, *J* = 5.4 Hz), 124.13 (q, *J* = 272.0 Hz), 117.82, 117.61, 117.01, 115.10 (q, *J* = 29.7 Hz), 111.60, 46.35, 23.89.

LC-MS: 382.10 $[M+H]^+$ (calc. for $C_{17}H_{15}F_3N_3O_2S$: 382.08 $[M+H]^+$), 94% purity (300 nm).

ESI-HRMS: m/z 382.0863 $[M+H]^+$ (calc. for $C_{17}H_{15}F_3N_3O_2S$: 382.0832 $[M+H]^+$).

2-[(3-chloro-4-hydroxybenzyl)amino]benzo[d]thiazole-6-carboxylic acid (**11**)

Methyl 2-[(3-chloro-4-hydroxybenzyl)amino]benzo[*d*]thiazole-6-carboxylate (**44**; 1 eq.) was dispersed in a mixture of 1M aq. NaOH and EtOH (1:1; 30 mL/mmol) and the reaction mixture was stirred under reflux overnight. The reaction mixture was then concentrated under reduced pressure and the residue was neutralized using 1M aqueous HCl solution and was allowed to precipitate for 30 mins in a refrigerator. The precipitate was filtered off using S4 frit, and dried under reduced pressure at 70 °C. The compound 2-[(3-chloro-4-hydroxybenzyl)amino]benzo[*d*]thiazole-6-carboxylic acid (**11**) was obtained as a white-beige solid in a 79% yield.

Melting point: 233–235 °C

^{1}H NMR (500 MHz, DMSO-d_6) δ 10.13 (br s, 1H), 8.39 (d, *J* = 1.7 Hz, 1H, ArH), 7.91 (dd, *J* = 8.4, 1.8 Hz, 1H, ArH), 7.57 (d, *J* = 8.4 Hz, 1H, ArH), 7.43 (d, *J* = 2.1 Hz, 1H, ArH), 7.22 (dd, *J* = 8.3, 2.2 Hz, 1H, ArH), 7.01 (d, *J* = 8.3 Hz, 1H, ArH), 4.64 (s, 2H, CH_2).

^{13}C NMR (126 MHz, DMSO-d_6) δ 168.39, 166.80, 152.67, 149.60, 129.40, 128.63, 128.09, 127.77, 127.62, 124.85, 123.78, 119.52, 116.68, 115.77, 47.22.

LC-MS: 333.10 $[M-H]^-$ (calc. for $C_{15}H_{10}ClN_2O_3S$: 333.01 $[M-H]^-$), 94% purity (300 nm).

ESI-HRMS: m/z 335.0236 $[M+H]^+$ (calc. for $C_{15}H_{12}ClN_2O_3S$: 335.0252 $[M+H]^+$).

Procedure A (general conditions): *Synthesis of compounds* **47a-b** *with aminoethylene linker*

3-chloro-4-methoxyphenethylamine hydrochloride (**46**; 1 eq.) was dissolved in NMP (15 mL/mmol). DIPEA (2.5 eq.) was added and the reaction mixture was stirred for 15 minutes at RT. Subsequently, the corresponding 6-substituted 2-chlorobenzo[*d*]thiazole (1 eq.; **45a** or **45b**, respectively) was added, and the reaction mixture was stirred at 160 °C overnight. The reaction mixture was cooled to RT, flooded with H_2O, slightly acidified using 1M aqueous HCl solution and allowed to precipitate for 1 hour in a refrigerator. The precipitate was then filtered off using S4 frit, and dried under reduced pressure at 70 °C to obtain the crude intermediate **47a** or **47b**, respectively.

2-[(3-chloro-4-methoxyphenethyl)amino]benzo[d]thiazole-6-carboxylic acid (**47a**)

Yield 87%.

^{1}H NMR (500 MHz, DMSO-d_6) δ 12.64 (s, 1H, COOH), 8.43 (t, *J* = 5.4 Hz, 1H, NH), 8.26 (d, *J* = 1.8 Hz, 1H, ArH), 7.81 (dd, *J* = 8.4, 1.8 Hz, 1H, ArH), 7.41 (d, *J* = 8.4 Hz, 1H, ArH), 7.35 (d, *J* = 2.1 Hz, 1H, ArH), 7.20 (dd, *J* = 8.4, 2.2 Hz, 1H, ArH), 7.08 (d, *J* = 8.4 Hz, 1H, ArH), 3.82 (s, 3H, CH_3), 3.61 (m, 2H, CH_2), 2.86 (t, *J* = 7.0 Hz, 2H, CH_2).

N-(3-chloro-4-methoxyphenethyl)-6-nitrobenzo[d]thiazol-2-amine (**47b**)

Yield 89%.

^{1}H NMR (500 MHz, DMSO-d_6) δ 8.79 (br s, 1H, NH), 8.70 (d, *J* = 2.5 Hz, 1H, ArH), 8.11 (dd, *J* = 8.9, 2.5 Hz, 1H, ArH), 7.48 (d, *J* = 8.9 Hz, 1H, ArH), 7.36 (d, *J* = 2.1 Hz, 1H, ArH), 7.20 (dd, *J* = 8.4, 2.2 Hz, 1H, ArH), 7.08 (d, *J* = 8.4 Hz, 1H, ArH), 3.82 (s, 3H, CH_3), 3.65 (d, *J* = 7.3 Hz, 2H, CH_2), 2.87 (t, *J* = 7.0 Hz, 2H, CH_2).

2-[(3-chloro-4-hydroxyphenethyl)amino]benzo[d]thiazole-6-carboxylic acid (**12**)

2-[(3-chloro-4-methoxyphenethyl)amino]benzo[*d*]thiazole-6-carboxylic acid (**47a**; 1 eq.) was dispersed in anhydrous DCE (16 mL/mmol), $AlCl_3$ (4.5 eq.) was added and the reaction mixture was stirred at 65 °C overnight. After the completion of the reaction (monitored by TLC), the reaction mixture was cooled to RT, and DCE was evaporated. The substance was dispersed in H_2O and neutralized using 1M aqueous NaOH solution. The mixture was extracted with EtOAc, washed with brine, dried with anhydrous Na_2SO_4, and concentrated under reduced pressure. The obtained crude product was purified by column chromatography (DCM/MeOH; 20:1) to obtain the compound 2-[(3-chloro-4-hydroxyphenethyl)amino]benzo[*d*]thiazole-6-carboxylic acid (**12**) as a white-beige solid in a 14% yield.

Melting point: 250–252 °C

^{1}H NMR (500 MHz, DMSO-d_6) δ 12.57 (br s, 1H, COOH), 9.98 (br s, 1H), 8.42 (br s, 1H), 8.26 (d, *J* = 1.8 Hz, 1H, ArH), 7.81 (dd, *J* = 8.3, 1.8 Hz, 1H, ArH), 7.41 (d, *J* = 8.4 Hz, 1H, ArH), 7.23 (d, *J* = 2.1 Hz, 1H, ArH), 7.02 (dd, *J* = 8.3, 2.1 Hz, 1H, ArH), 6.89 (d, *J* = 8.2 Hz, 1H, ArH), 3.57 (d, *J* = 4.8 Hz, 2H, CH_2), 2.81 (t, *J* = 7.1 Hz, 2H, CH_2).

^{13}C NMR (126 MHz, DMSO-d_6) δ 168.66, 167.28, 156.29, 151.41, 130.86, 130.35, 129.90, 128.31, 127.34, 123.13, 122.68, 119.35, 117.26, 116.55, 45.45, 33.32.

LC-MS: 347.00 $[M-H]^-$ (calc. for $C_{16}H_{12}ClN_2O_3S$: 347.03 $[M-H]^-$), 92% purity (300 nm).

ESI-HRMS: m/z 349.0399 $[M+H]^+$ (calc. for $C_{16}H_{14}ClN_2O_3S$: 349.0408 $[M+H]^+$).

N,N-(3-chloro-4-methoxyphenethyl)benzo[d]thiazole-2,6-diamine (**48**)

Iron (10 eq.) together with NH_4Cl (4 eq.) was dispersed in a mixture of MeOH/H_2O (1:1; 2 mL/mmol). *N*-(3-chloro-4-methoxyphenethyl)-6-nitrobenzo[*d*]thiazol-2-amine (**47b**; 1 eq.) was dispersed in anhydrous THF (2 mL/mmol) and added dropwise to the reaction with iron and was let to stir at 50 °C overnight. Subsequently, the reaction mixture was filtered off through Celite pad. The filtrate was concentrated under reduced pressure and then diluted with H_2O. The filtrate was neutralized with saturated $NaHCO_3$ solution and allowed to precipitate for 1 hour in a refrigerator. The precipitate was extracted with EtOAc and washed with brine, dried with anhydrous Na_2SO_4, and concentrated under reduced pressure. The crude product was purified by silica flash chromatography (SiO_2 80 g; 0–10% MeOH in DCM) to obtain *N,N*-(3-chloro-4-methoxyphenethyl)benzo[*d*]thiazole-2,6-diamine (**48**) in a 57% yield.

^{1}H NMR (500 MHz, DMSO-d_6) δ 7.55 (t, *J* = 5.4 Hz, 1H, NH), 7.31 (d, *J* = 2.1 Hz, 1H, ArH), 7.18 (dd, *J* = 8.4, 2.2 Hz, 1H, ArH), 7.08 (dd, *J* = 12.7, 8.4 Hz, 2H, ArH), 6.81 (d, *J* = 2.2 Hz, 1H, ArH), 6.50 (dd, *J* = 8.4, 2.3 Hz, 1H, ArH), 4.79 (br s, 2H, NH_2), 3.81 (s, 3H, CH_3), 3.51 – 3.44 (m, 2H, CH_2), 2.82 (t, *J* = 7.1 Hz, 2H, CH_2).

N-{2-[(3-chloro-4-methoxyphenethyl)amino]benzo[d]thiazol-6-yl}acetamide (**49**)

N,N-(3-chloro-4-methoxyphenethyl)benzo[*d*]thiazole-2,6-diamine (**48**; 1 eq.) was dissolved in anhydrous DCM (17 mL/mmol), and Ac_2O (1.05 eq.) was added. Subsequently, Et_3N (1.1 eq.) was added dropwise and the reaction mixture was stirred for 10 minutes at 0 °C. The temperature was then increased to RT and the reaction mixture was stirred overnight. The next day, the reaction was washed with 1M aqueous HCl solution and DCM was evaporated. The residue was then flooded with 0.5M aqueous HCl solution, dispersed, and allowed to precipitate for 1 hour in a refrigerator. The precipitate was subsequently filtered off using S4 frit to obtain the crude *N*-{2-[(3-chloro-4-methoxyphenethyl)amino]benzo[*d*]thiazol-6-yl}acetamide (**49**) in a 94% yield.

^{1}H NMR (500 MHz, DMSO-d_6) δ 10.22 (br s, 1H, NH), 10.11 (br s, 1H, NH), 8.22 (d, *J* = 1.9 Hz, 1H, ArH), 7.49 – 7.47 (m, 2H, ArH), 7.43 (d, *J* = 2.2 Hz, 1H, ArH), 7.27 (dd, *J* = 8.4, 2.2 Hz, 1H, ArH), 7.08 (d, *J* = 8.5 Hz, 1H, ArH), 3.81 (s, 3H, CH_3), 3.72 (d, *J* = 9.8 Hz, 2H, CH_2), 2.90 (t, *J* = 7.2 Hz, 2H, CH_2), 2.05 (s, 3H, CH_3).

N-{2-[(3-chloro-4-hydroxyphenethyl)amino]benzo[d]thiazol-6-yl}acetamide (**15**)

N-{2-[(3-chloro-4-methoxyphenethyl)amino]benzo[*d*]thiazol-6-yl}acetamide (**49**; 1 eq.) was dispersed in anhydrous toluene (50 mL/mmol), $AlCl_3$ (6 eq.) was added and the reaction mixture was stirred at 100 °C overnight. The reaction was quenched by adding H_2O. Toluene was evaporated under reduced pressure and the residue was dispersed in MeOH. The residue was then flooded with H_2O and 1M aqueous HCl solution and allowed to precipitate for 30 mins in a refrigerator. The precipitate was filtered off using an S4 frit and the filtrate was slightly basified using a saturated $NaHCO_3$ solution. The filtrate was then extracted with EtOAc and washed with brine, dried with anhydrous Na_2SO_4, and concentrated under reduced pressure. The crude product was purified by column chromatography (DCM/MeOH; 12:1) to obtain *N*-{2-[(3-chloro-4-hydroxyphenethyl)amino]benzo[*d*]thiazol-6-yl}acetamide (**15**) as a white-beige solid in a 39% yield.

Melting point: 218–220 °C

^{1}H NMR (500 MHz, DMSO-d_6) δ 9.92 (br s, 1H), 9.87 (br s, 1H), 8.01 (d, *J* = 2.1 Hz, 1H, ArH), 7.94 (t, *J* = 5.4 Hz, 1H, NH), 7.30 (d, *J* = 8.6 Hz, 1H, ArH), 7.25 (dd, *J* = 8.7, 2.1 Hz, 1H, ArH), 7.22 (d, *J* = 2.1 Hz, 1H, ArH), 7.01 (dd, *J* = 8.3, 2.1 Hz, 1H, ArH), 6.88 (d, *J* = 8.2 Hz, 1H, ArH), 3.51 (q, *J* = 6.7 Hz, 2H, CH_2), 2.79 (t, *J* = 7.1 Hz, 2H, CH_2), 2.02 (s, 3H, CH_3).

^{13}C NMR (126 MHz, DMSO-d_6) δ 167.83, 165.13, 151.34, 148.52, 133.11, 131.08, 130.41, 129.86, 128.28, 119.31, 117.70, 117.55, 116.52, 111.57, 45.33, 33.40, 23.89.

LC-MS: 362.10 $[M+H]^+$ (calc. for $C_{17}H_{17}ClN_3O_2S$: 362.07 $[M+H]^+$), 96% purity (300 nm).

ESI-HRMS: m/z 362.0755 $[M+H]^+$ (calc. for $C_{17}H_{17}ClN_3O_2S$: 362.0725 $[M+H]^+$).

N-(6-acetamidobenzo[d]thiazol-2-yl)-N-(3-chloro-4-methoxyphenethyl)acetamide (**50**)

N,N-(3-chloro-4-methoxyphenethyl)benzo[*d*]thiazole-2,6-diamine (**48**; 1 eq.) was dissolved in anhydrous DCM (6 mL/mmol). Subsequently, Ac_2O (6 eq.) and Et_3N (4 eq.) were added dropwise, and the reaction mixture was stirred at RT overnight. The following day, 4 eq. of Et_3N were added and the reaction mixture was stirred overnight again. After the completion of the reaction (monitored by TLC), the reaction was quenched by the addition of 1M aqueous HCl solution, and DCM was evaporated. The residue was then flooded with H_2O, acidified to the pH of 3 using 1M aqueous HCl solution, dispersed, and allowed to precipitate for 1 hour in a refrigerator. The precipitate was subsequently filtered off using S4 frit to obtain the crude *N*-(6-acetamidobenzo[*d*]thiazol-2-yl)-*N*-(3-chloro-4-methoxyphenethyl)acetamide (**50**) in a 71% yield.

^{1}H NMR (500 MHz, DMSO-d_6) δ 10.10 (br s, 1H, NH), 8.29 (d, *J* = 2.1 Hz, 1H, ArH), 7.77 (d, *J* = 8.7 Hz, 1H, ArH), 7.52 (dd, *J* = 8.8, 2.1 Hz, 1H, ArH), 7.38 (d, *J* = 2.1 Hz, 1H, ArH), 7.20 (dd, *J* = 8.4, 2.1 Hz, 1H, ArH), 7.10 (d, *J* = 8.5 Hz, 1H, ArH), 4.38 (t, *J* = 7.6 Hz, 2H, CH_2), 3.83 (s, 3H, CH_3), 3.03 (t, *J* = 7.5 Hz, 2H, CH_2), 2.30 (s, 3H, CH_3), 2.08 (s, 3H, CH_3).

N-(6-acetamidobenzo[d]thiazol-2-yl)-N-(3-chloro-4-hydroxyphenethyl)acetamide (**16**)

N-(6-acetamidobenzo[*d*]thiazol-2-yl)-*N*-(3-chloro-4-methoxyphenethyl)acetamide (**50**; 1 eq.) was dispersed in anhydrous DCE (11 mL/mmol), $AlCl_3$ (6 eq.) was added, and the reaction mixture was stirred at 80 °C overnight. The reaction was cooled to RT and quenched by adding H_2O. DCE was evaporated by rotavapor, and the residue was dispersed in MeOH. Then H_2O and 1M aq. HCl were added, and the mixture was allowed to precipitate for 30 mins in a refrigerator. The precipitate was filtered off using S4 frit, and dried under reduced pressure at 70 °C. The crude product was purified by silica flash chromatography (SiO_2 40 g; 0–5% MeOH in DCM) to obtain *N*-(6-acetamidobenzo[*d*]thiazol-2-yl)-*N*-(3-chloro-4-hydroxyphenethyl)acetamide (**16**) as a brown solid in a 66% yield.

Melting point: 201–203 °C

^{1}H NMR (500 MHz, DMSO-d_6) δ 10.09 (br s, 1H), 10.03 (br s, 1H), 8.28 (d, *J* = 2.1 Hz, 1H, ArH), 7.76 (d, *J* = 8.7 Hz, 1H, ArH), 7.52 (dd, *J* = 8.7, 2.1 Hz, 1H, ArH), 7.26 (d, *J* = 2.1 Hz, 1H, ArH), 7.02 (dd, *J* = 8.3, 2.1 Hz, 1H, ArH), 6.91 (d, *J* = 8.2 Hz, 1H, ArH), 4.34 (t, *J* = 7.5 Hz, 2H, CH_2), 2.97 (t, *J* = 7.5 Hz, 2H, CH_2), 2.28 (s, 3H, CH_3), 2.07 (s, 3H, CH_3).

^{13}C NMR (126 MHz, DMSO-d_6) δ 171.05, 168.25, 157.38, 151.68, 143.69, 135.61, 133.06, 130.15, 130.01, 128.54, 121.02, 119.52, 118.42, 116.68, 110.91, 49.52, 32.17, 24.00, 22.70.

LC-MS: 404.10 $[M+H]^+$ (calc. for $C_{19}H_{19}ClN_3O_3S$: 404.08 $[M+H]^+$), 96% purity (300 nm).

ESI-HRMS: m/z 404.0867 $[M+H]^+$ (calc. for $C_{19}H_{19}ClN_3O_3S$: 404.0830 $[M+H]^+$).

4 ^{1}H and ^{13}C NMR spectra of final products 3–16

^{1}H NMR spectrum of compound **3** (500 MHz, DMSO-d_6)

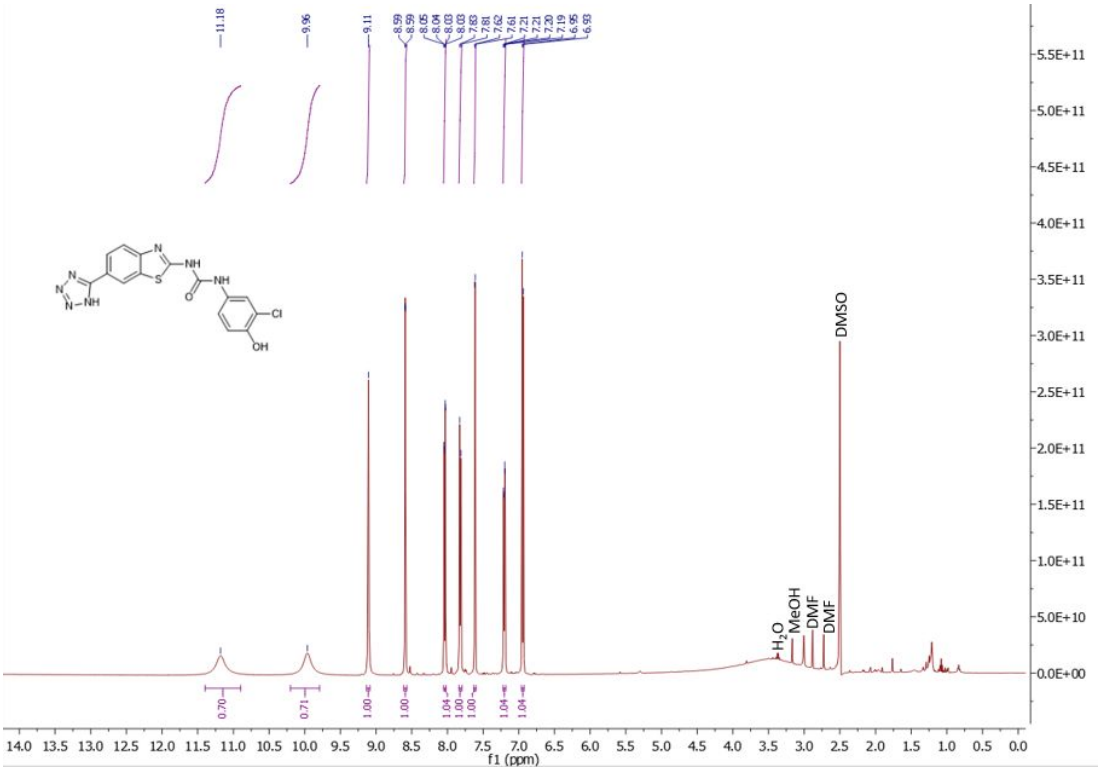

^{13}C NMR spectrum of compound **3** (126 MHz, DMSO-d_6)

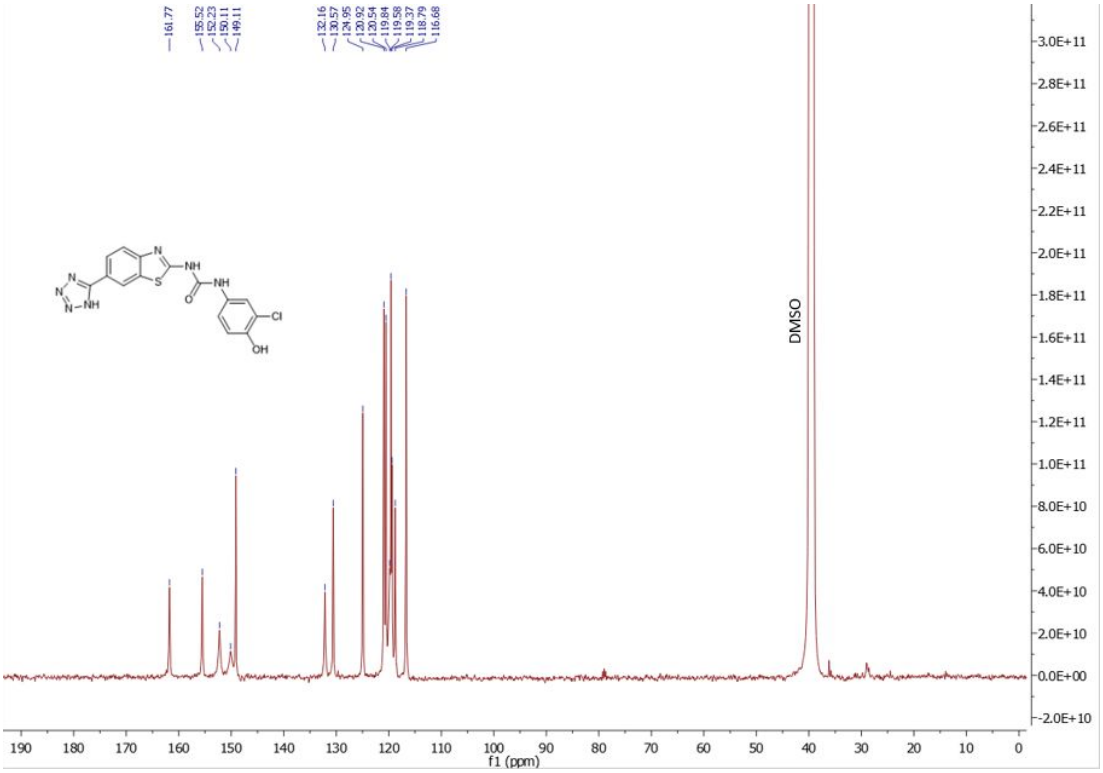

^{1}H NMR spectrum of compound **4** (500 MHz, DMSO-d_6)

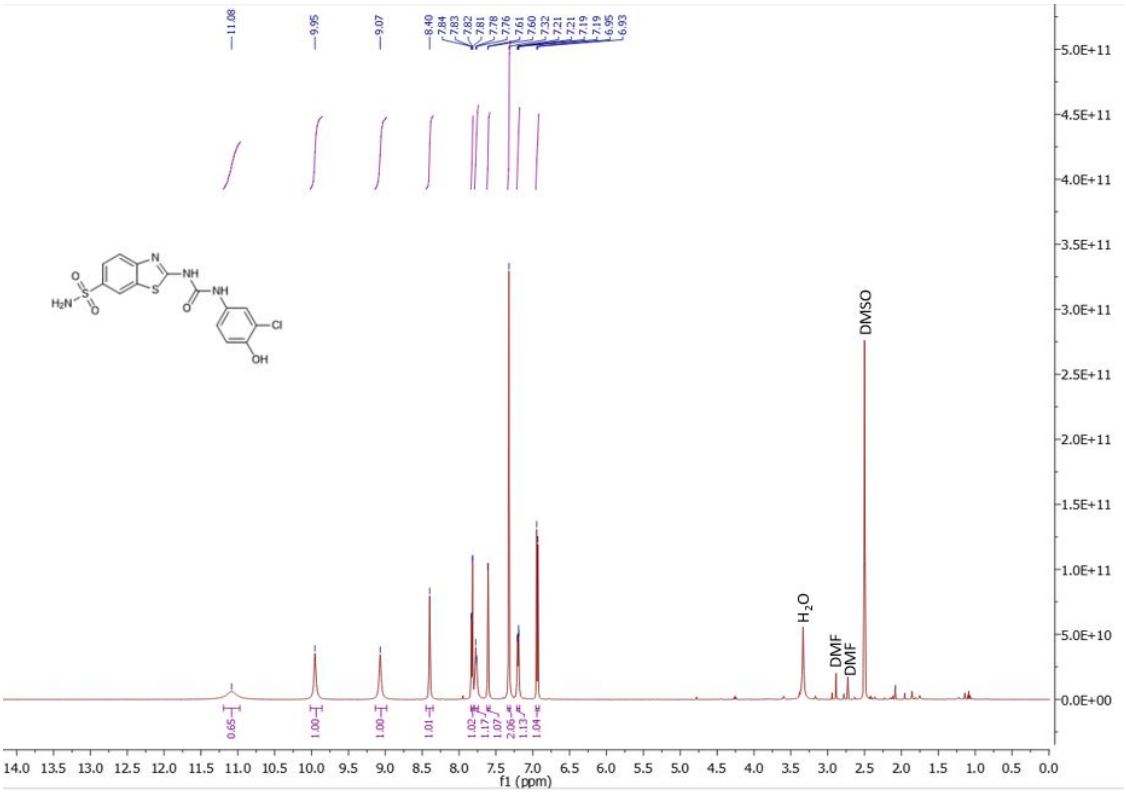

^{13}C NMR spectrum of compound **4** (126 MHz, DMSO-d_6/CF_3COOH)

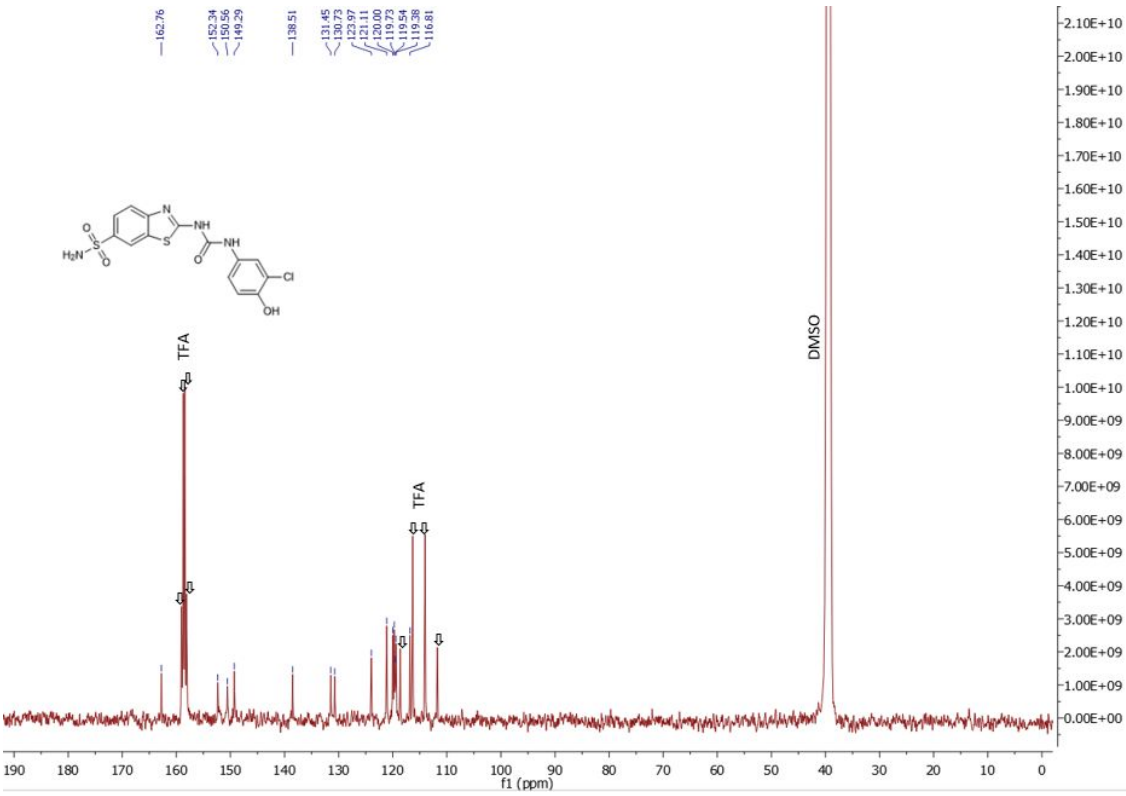

^{1}H NMR spectrum of compound **5** (500 MHz, DMSO-d_6)

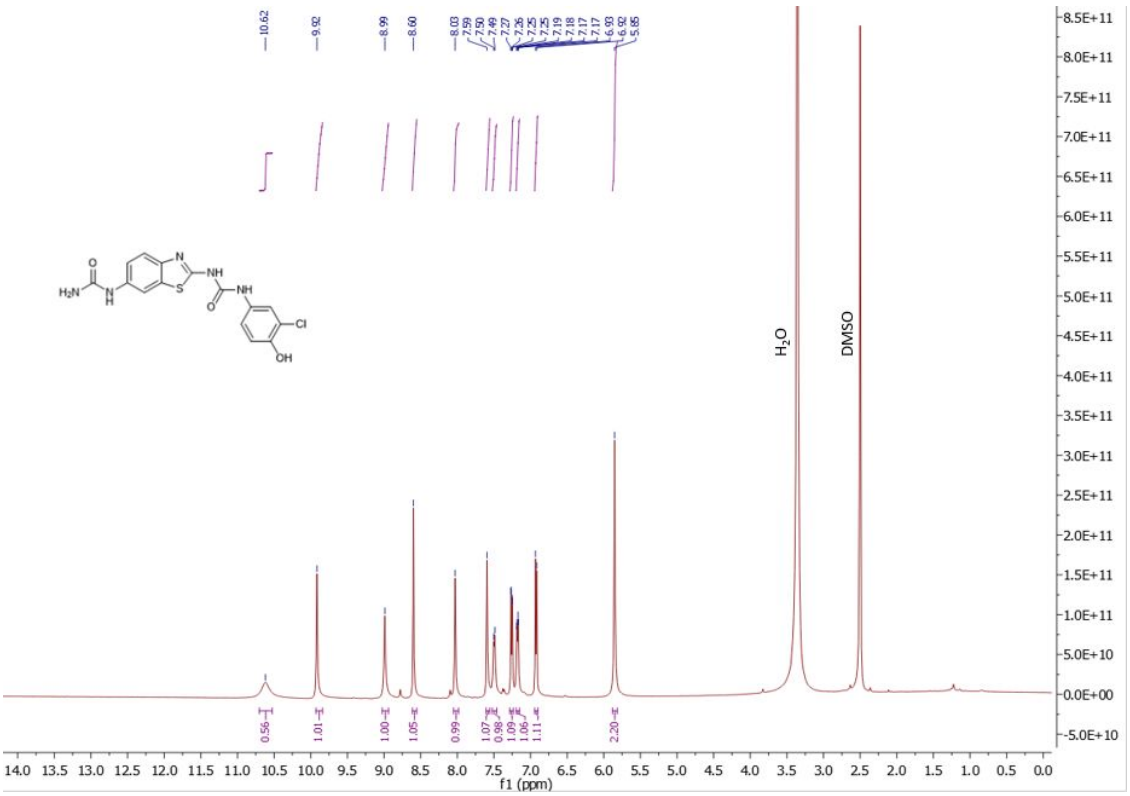

^{13}C NMR spectrum of compound **5** (126 MHz, DMSO-d_6)

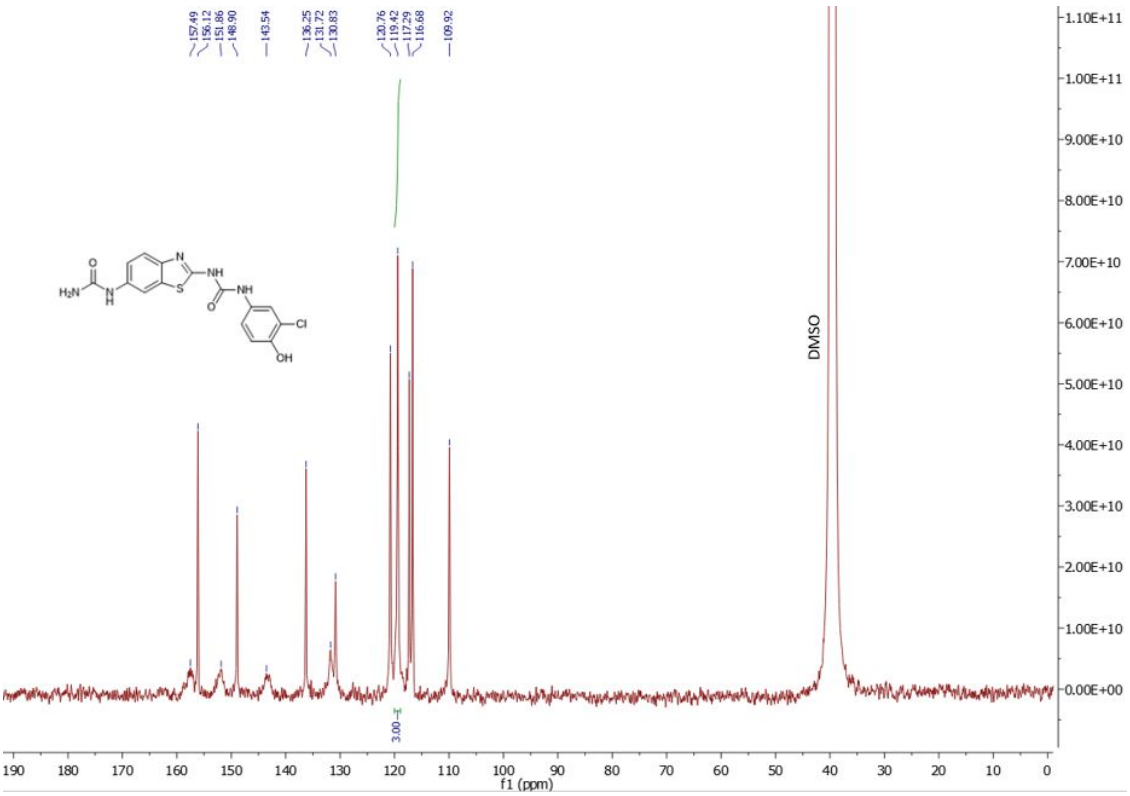

^{13}C NMR spectrum of compound **5** (126 MHz, DMSO-d_6/CF_3COOH)

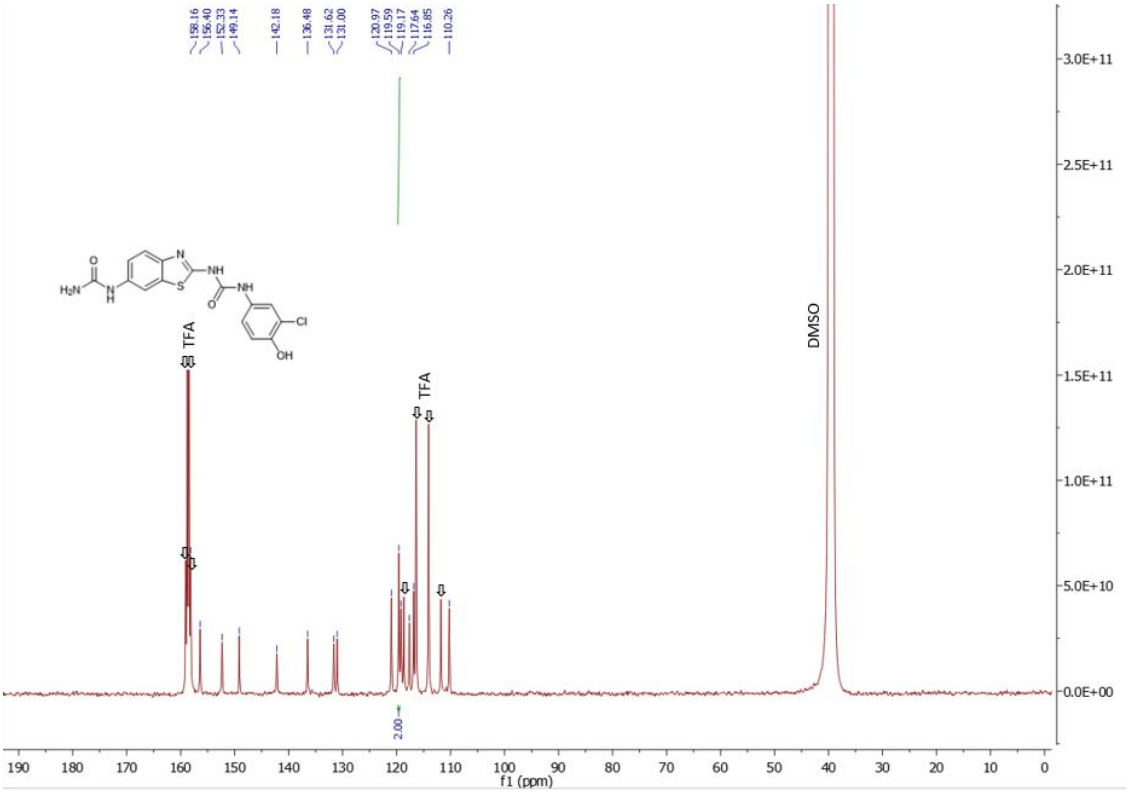

^{1}H NMR spectrum of compound **6** (500 MHz, DMSO-d_6)

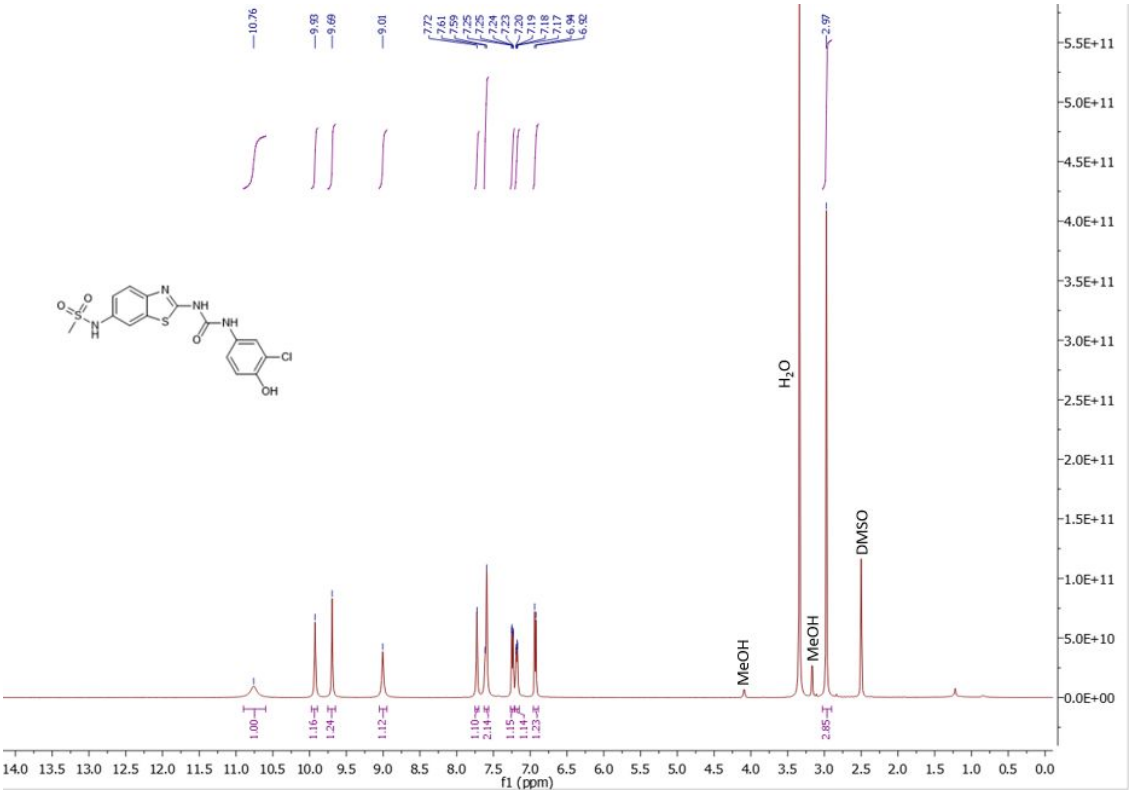

^{13}C NMR spectrum of compound **6** (126 MHz, DMSO-d_6/CF_3COOH)

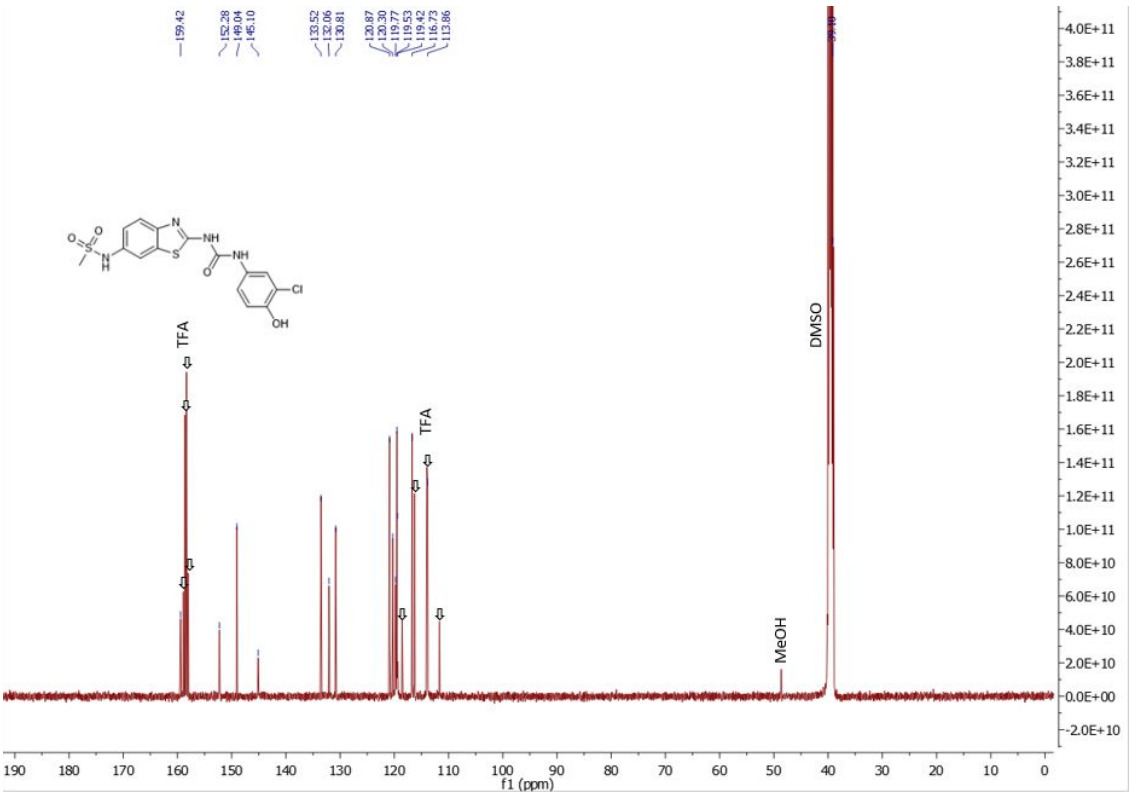

^{1}H NMR spectrum of compound **7** (500 MHz, DMSO-d_6)

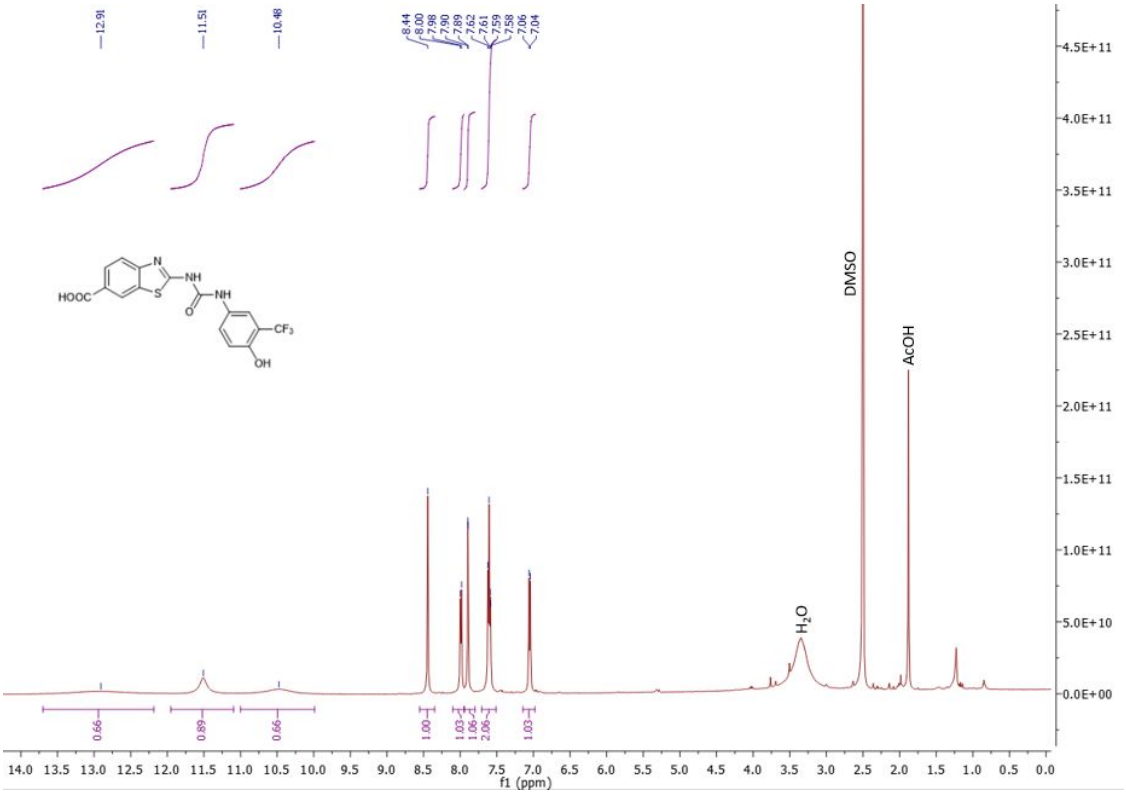

^{13}C NMR spectrum of compound **7** (126 MHz, DMSO-d_6)

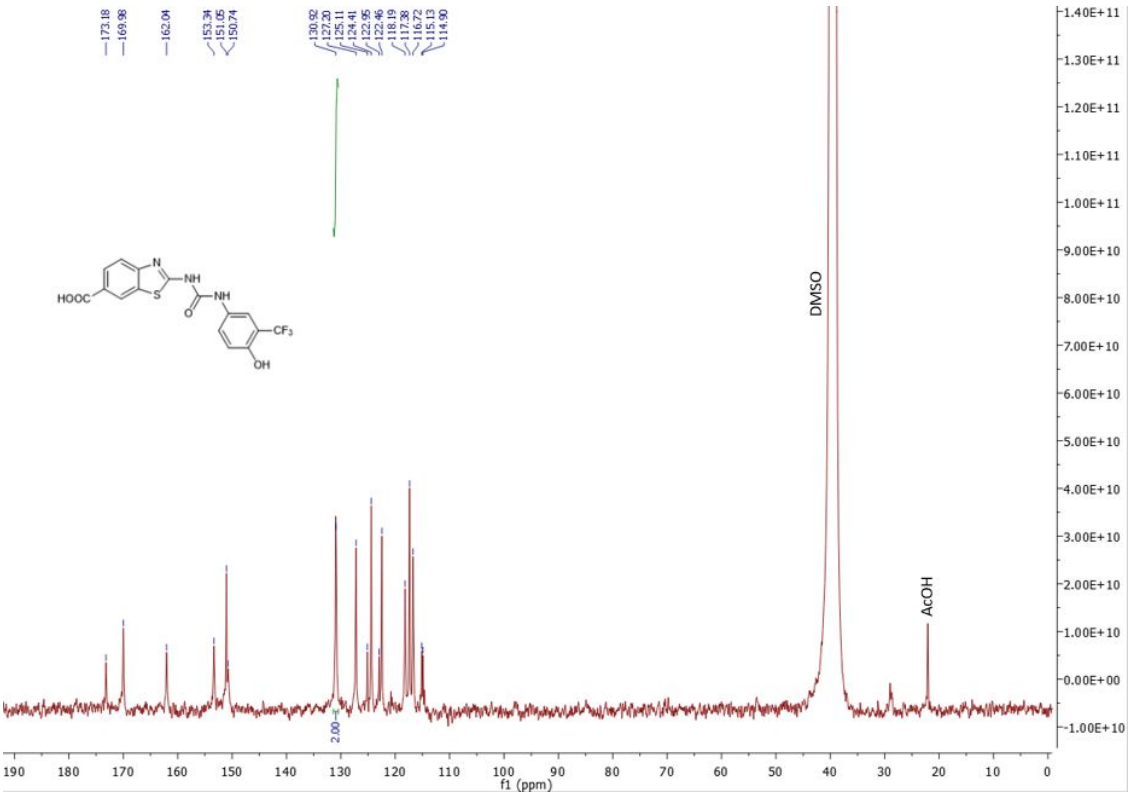

^{1}H NMR spectrum of compound **8** (500 MHz, DMSO-d_6)

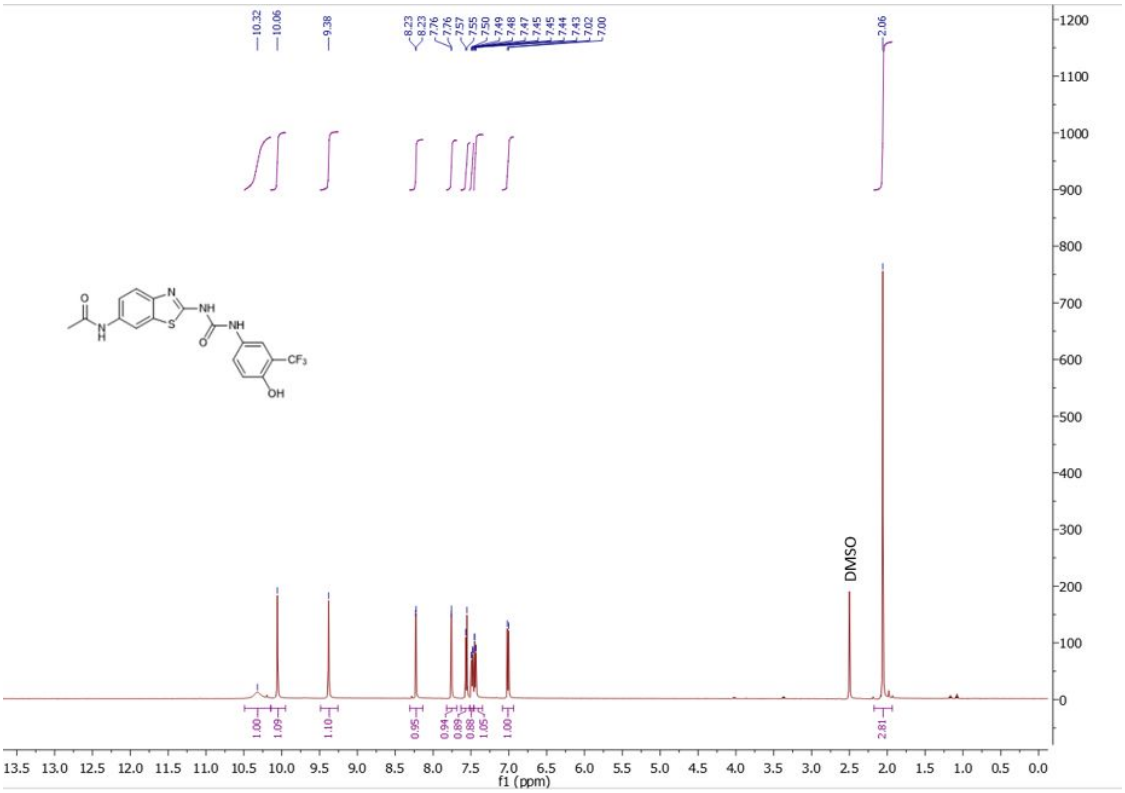

^{13}C NMR spectrum of compound **8** (126 MHz, DMSO-d_6)

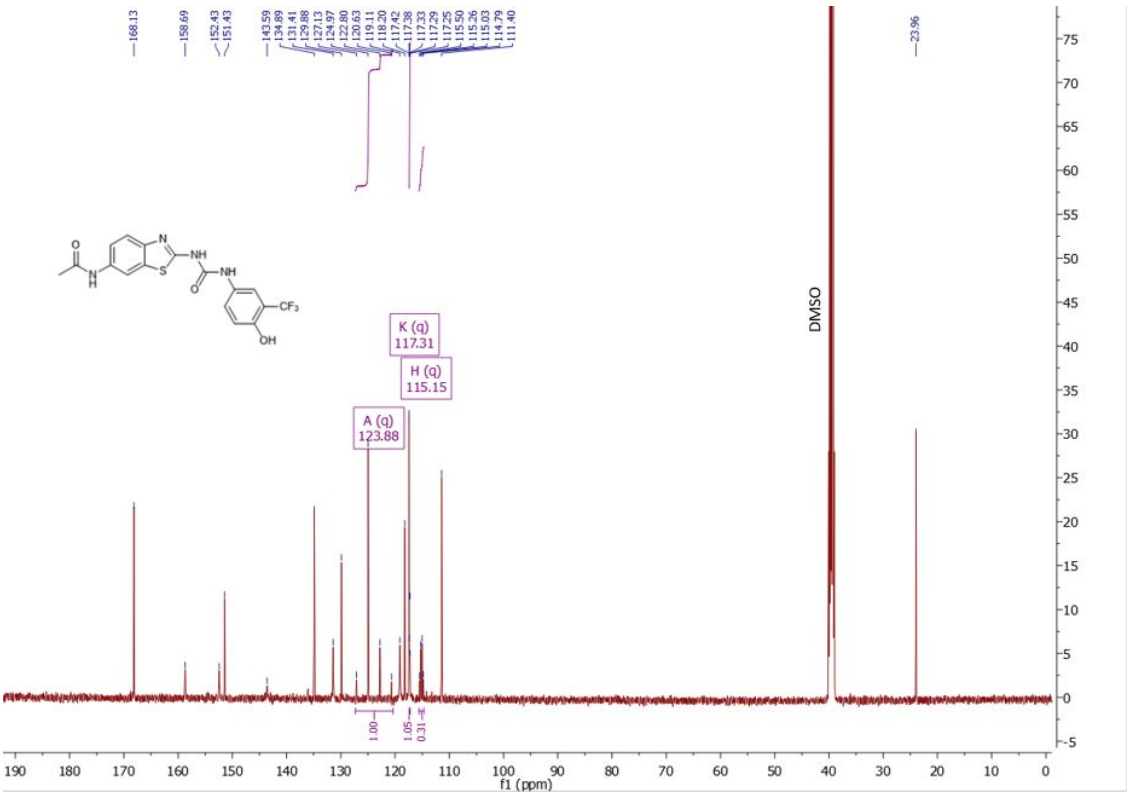

^{1}H NMR spectrum of compound **9** (500 MHz, DMSO-d_6)

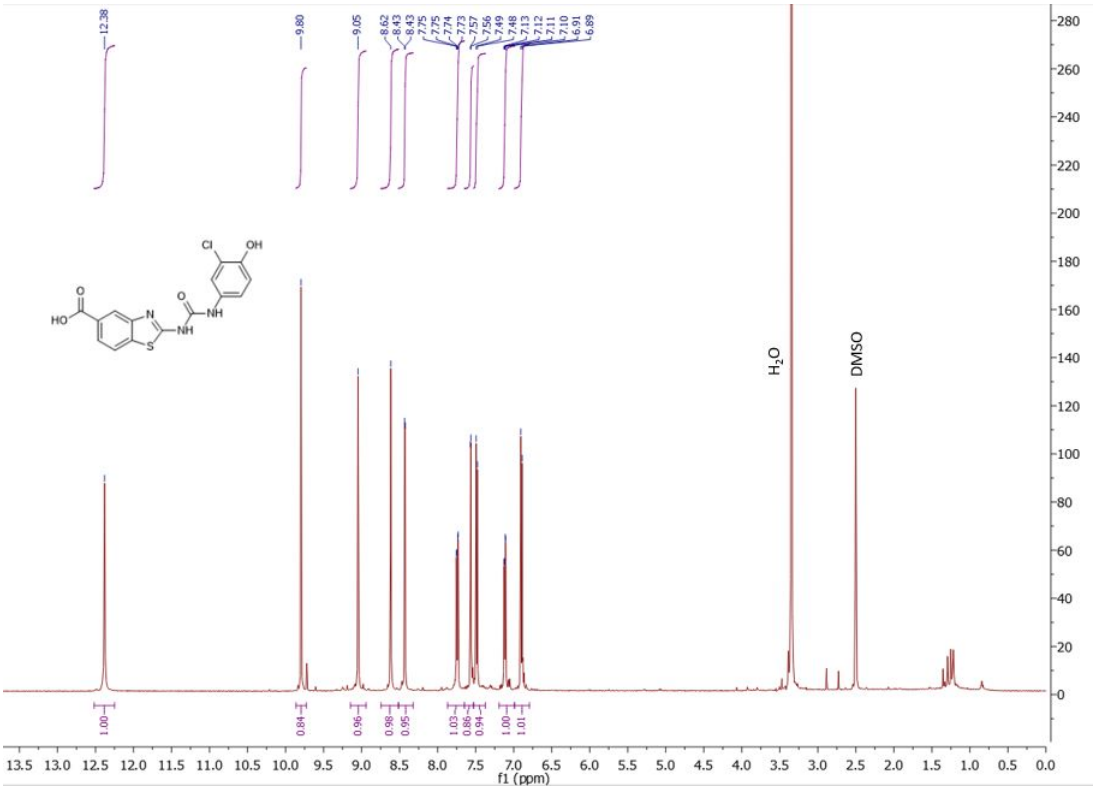

^{13}C NMR spectrum of compound **9** (126 MHz, DMSO-d_6)

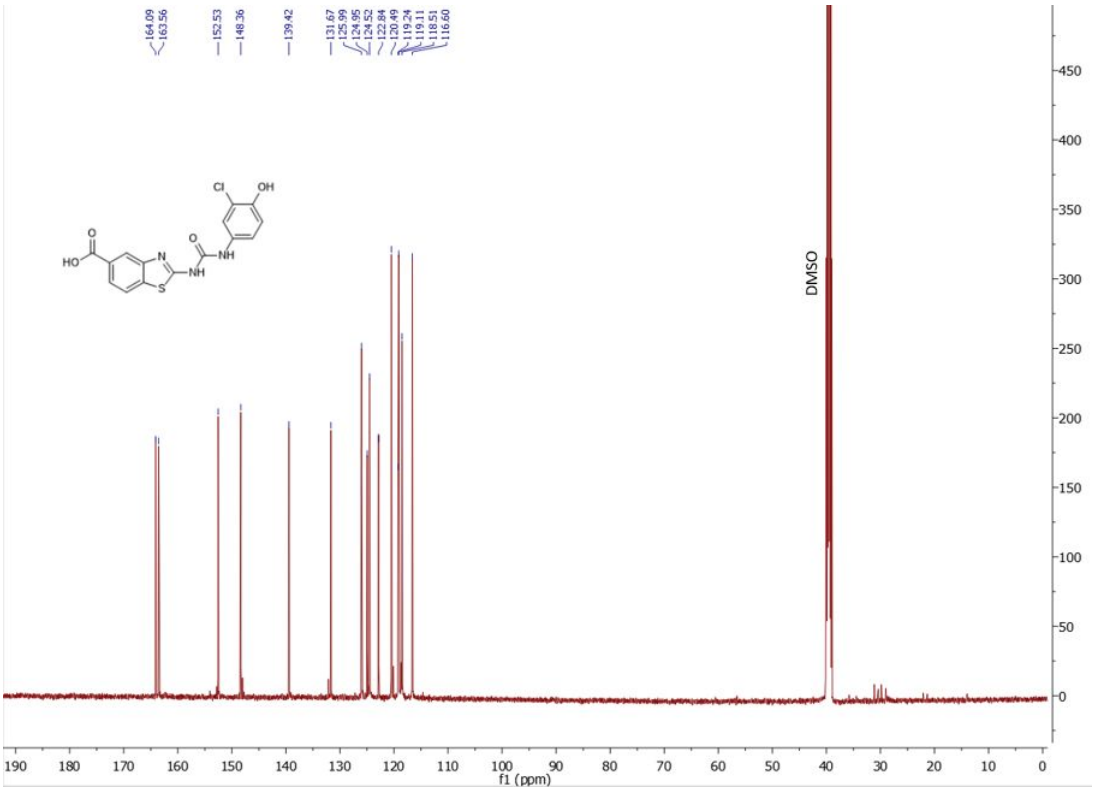

^{1}H NMR spectrum of compound **10** (500 MHz, DMSO-d_6)

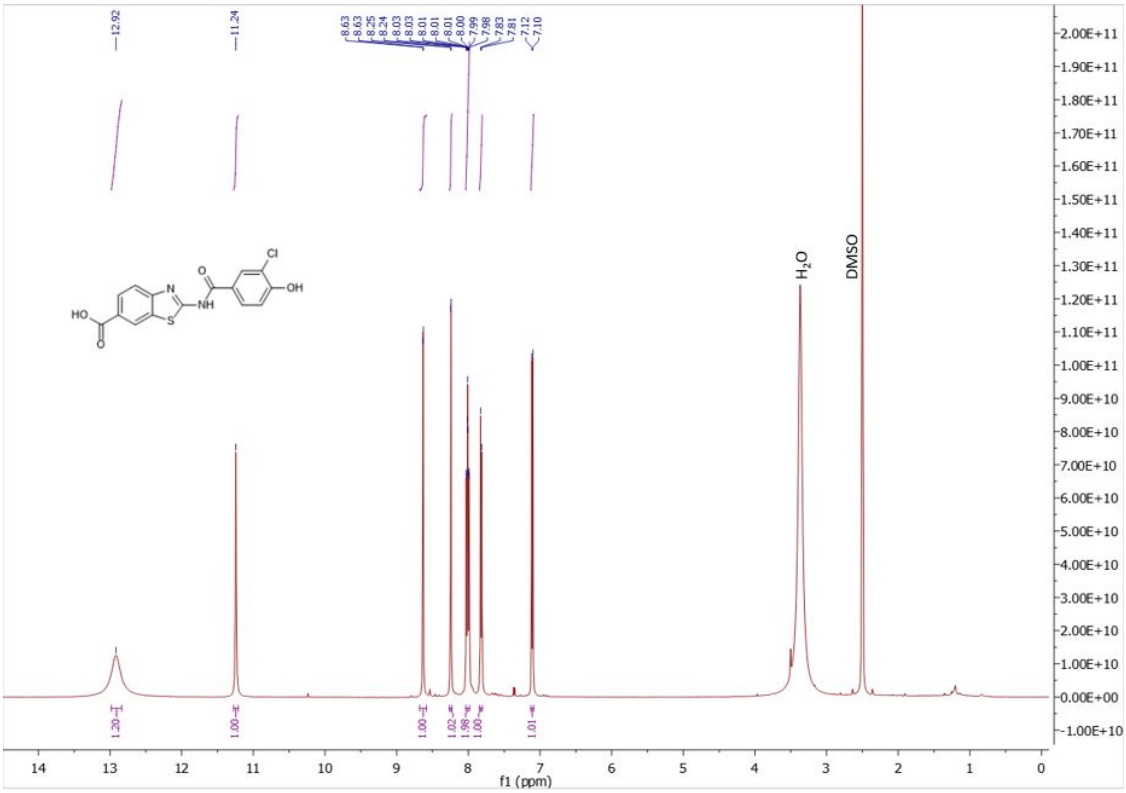

^{13}C NMR spectrum of compound **10** (126 MHz, DMSO-d_6)

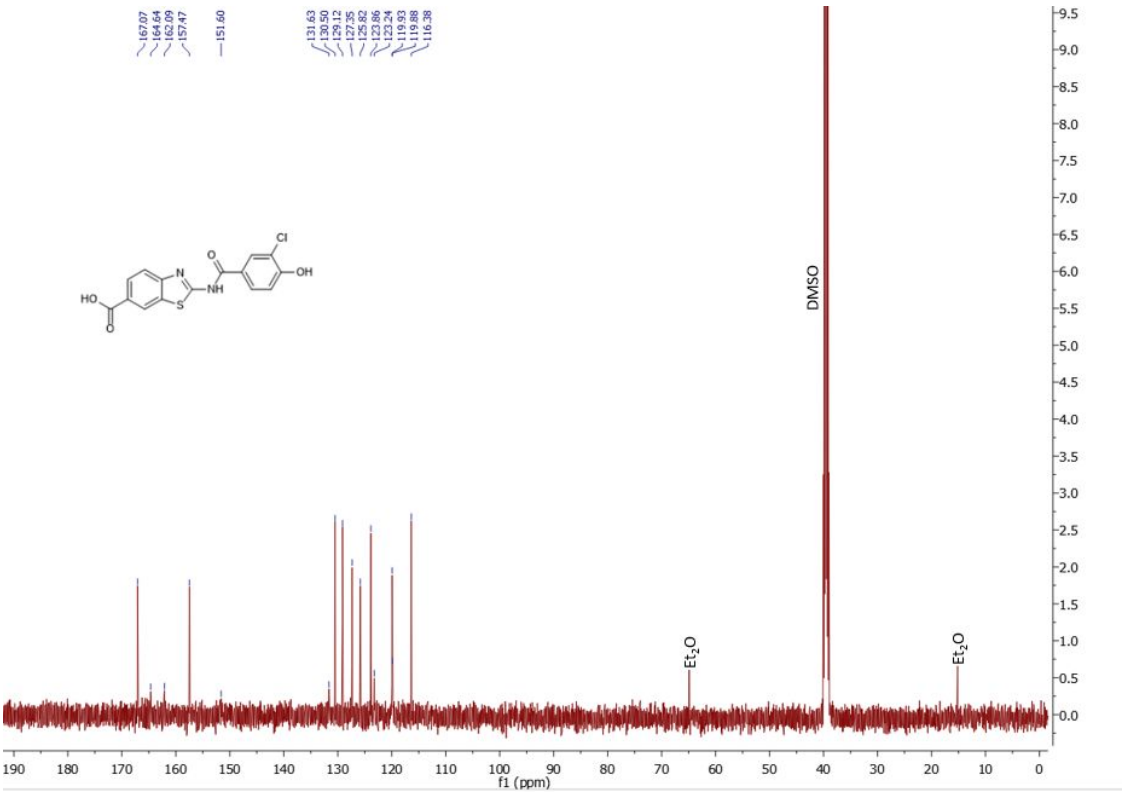

^{1}H NMR spectrum of compound **11** (500 MHz, DMSO-d_6)

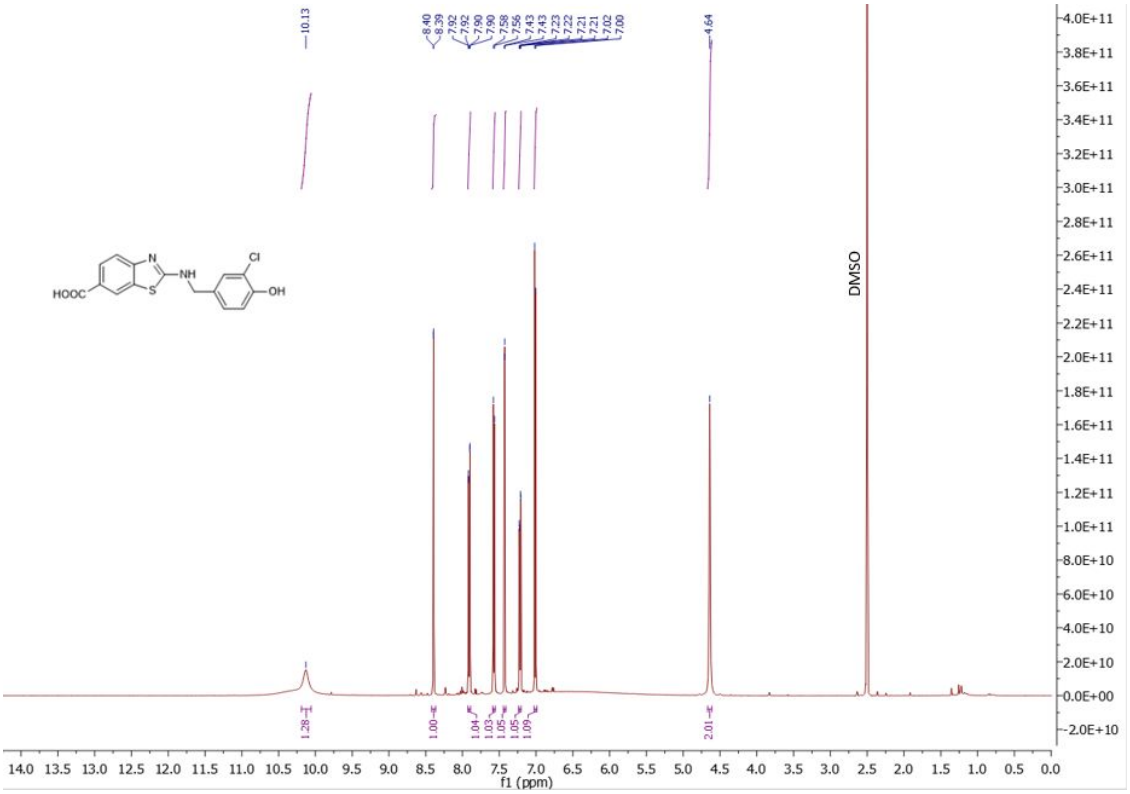

^{13}C NMR spectrum of compound **11** (126 MHz, DMSO-d_6)

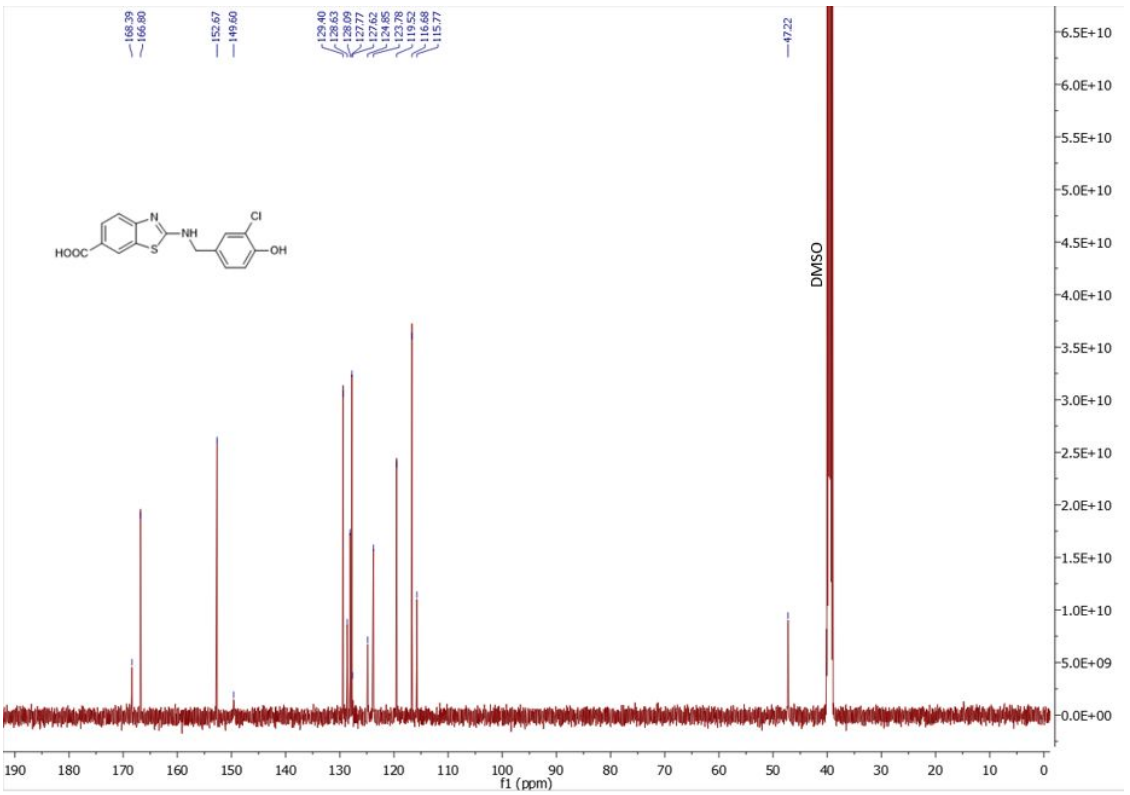

^{1}H NMR spectrum of compound **12** (500 MHz, DMSO-d_6)

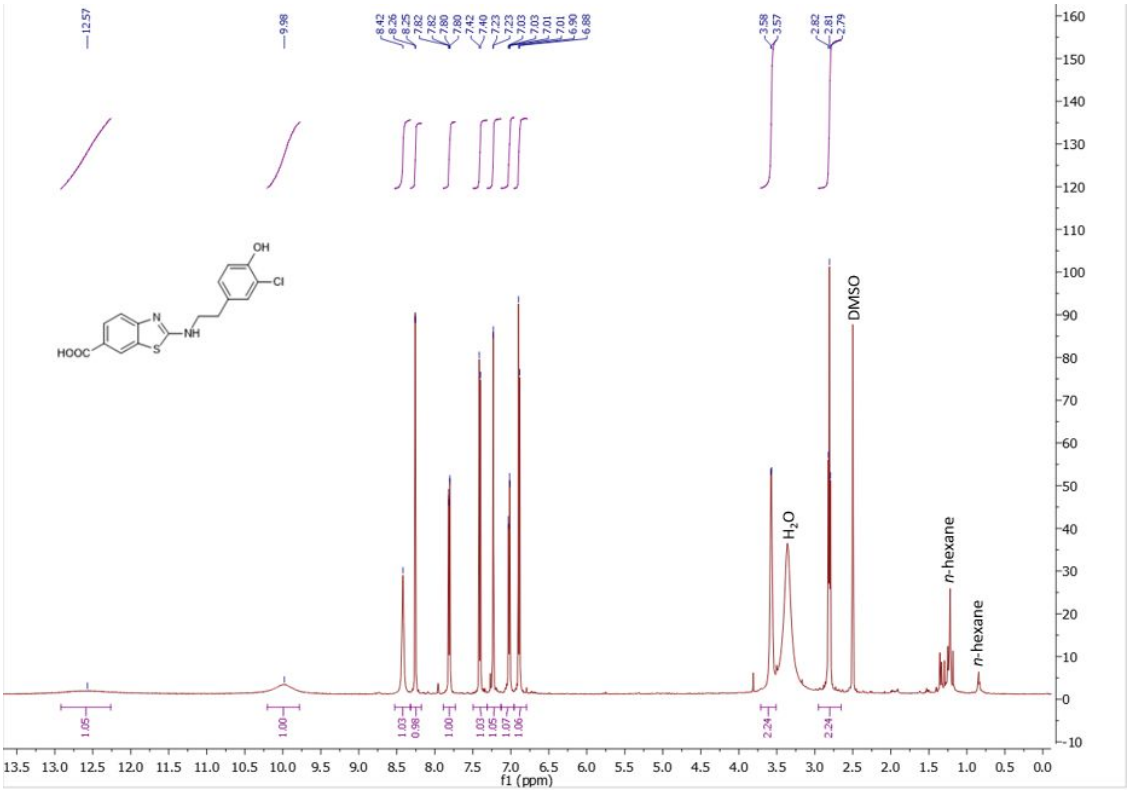

^{13}C NMR spectrum of compound **12** (126 MHz, DMSO-d_6)

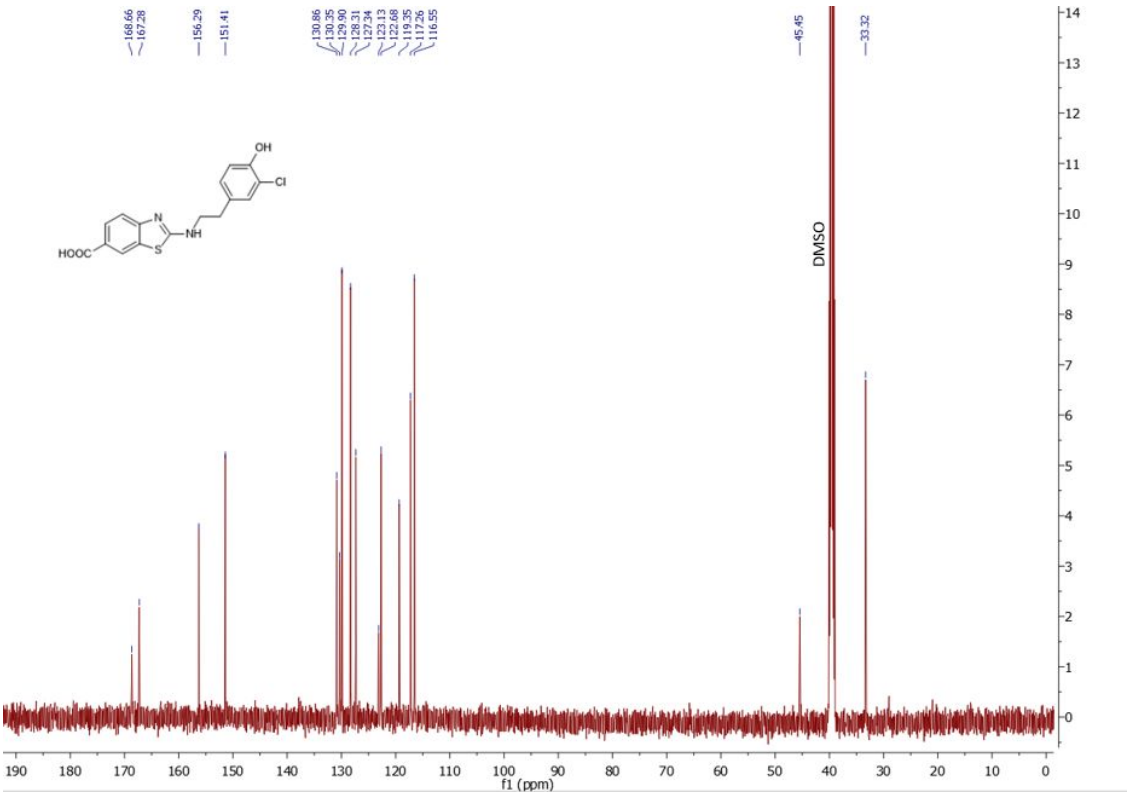

^{1}H NMR spectrum of compound **13** (500 MHz, DMSO-d_6)

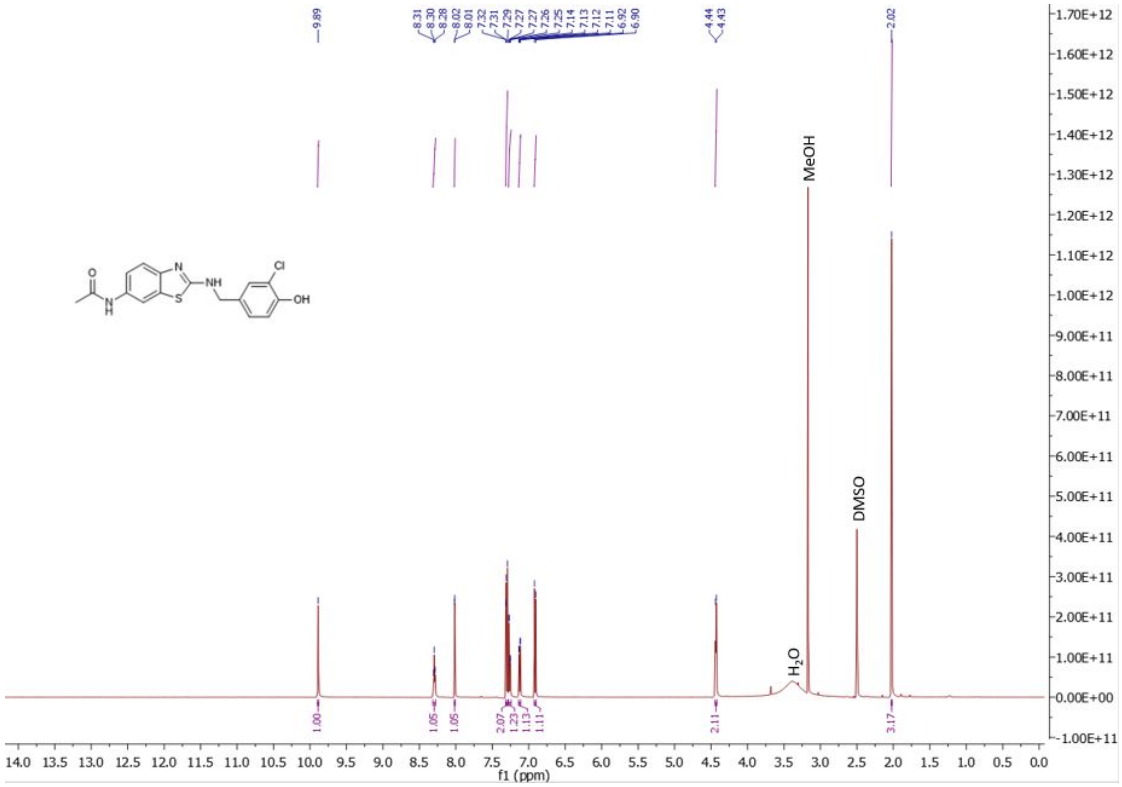

^{13}C NMR spectrum of compound **13** (126 MHz, DMSO-d_6)

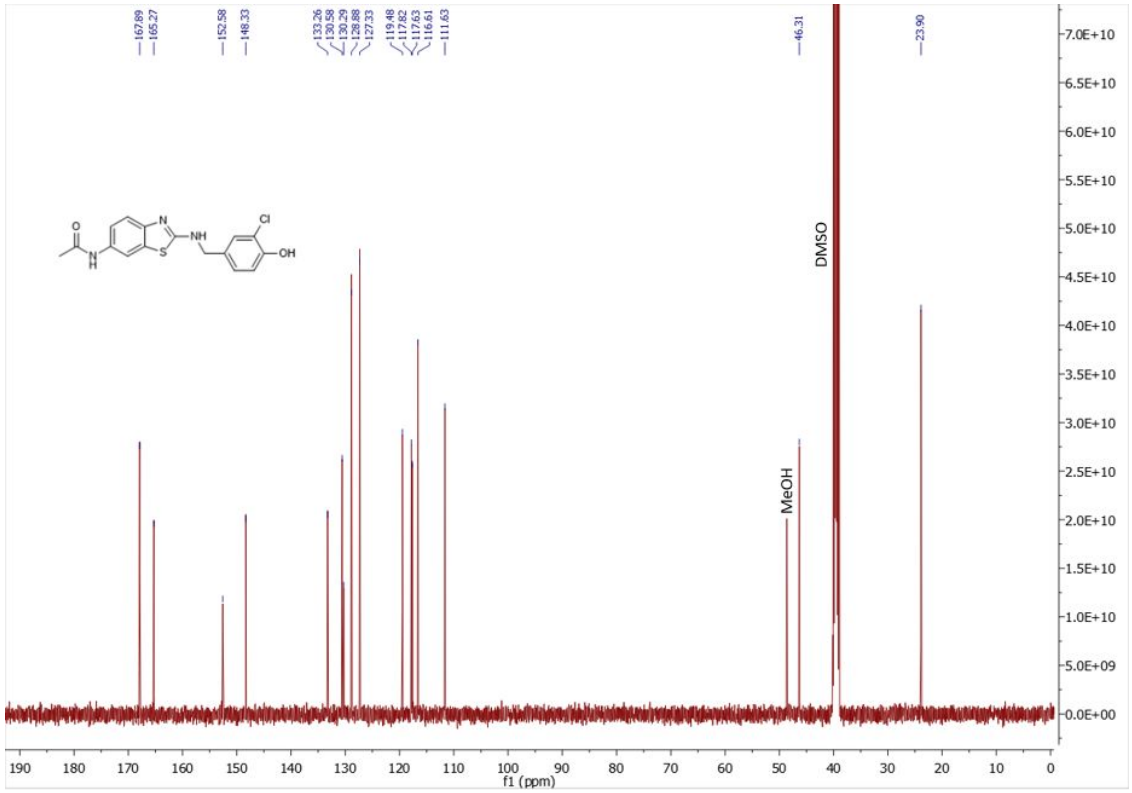

^{1}H NMR spectrum of compound **14** (500 MHz, DMSO-d_6)

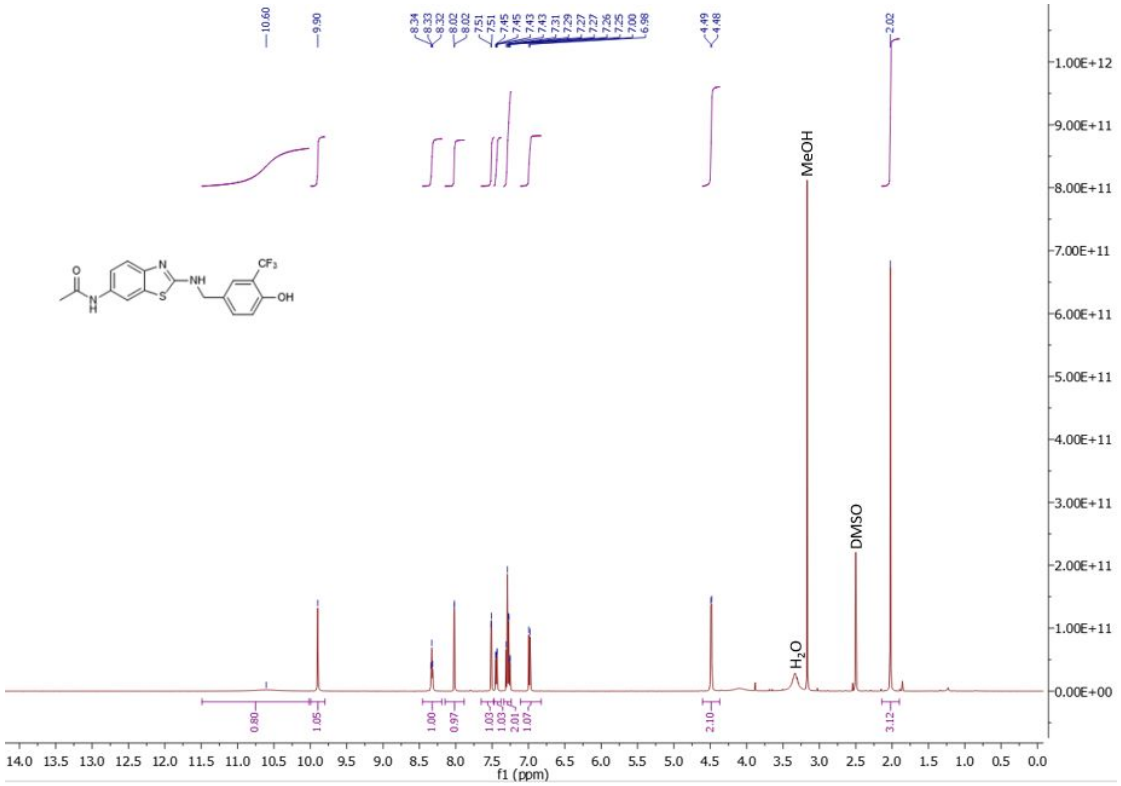

^{13}C NMR spectrum of compound **14** (126 MHz, DMSO-d_6)

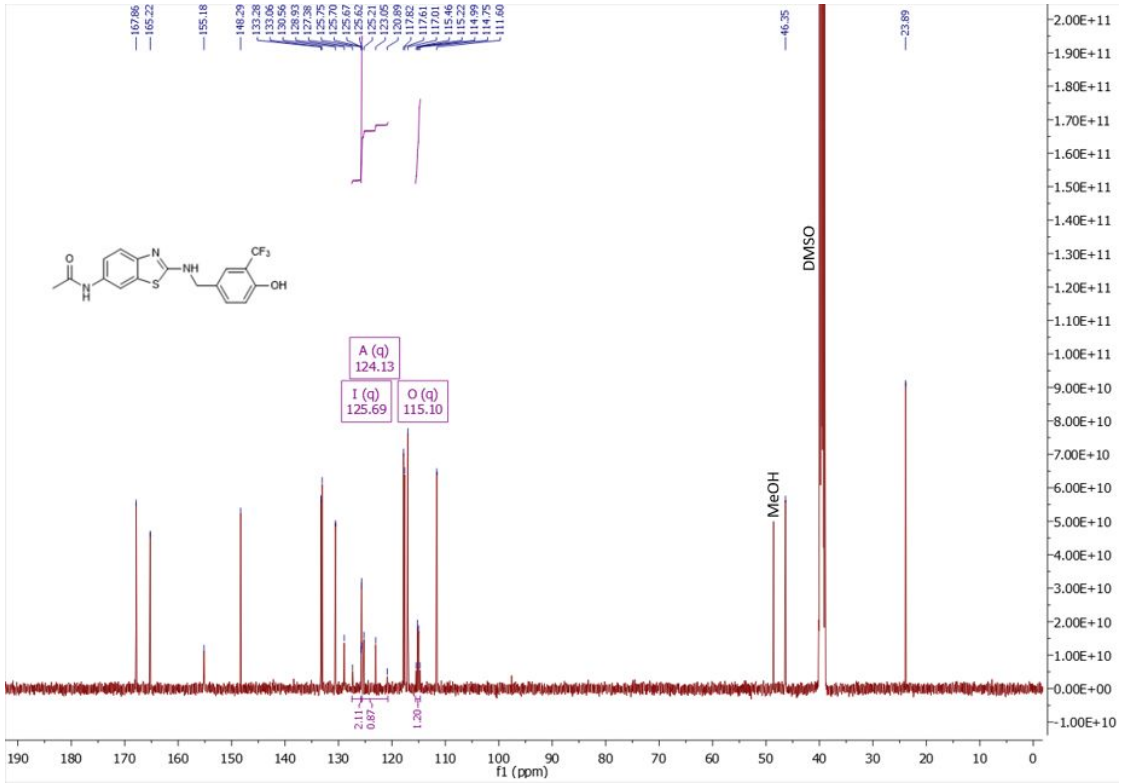

^{1}H NMR spectrum of compound **15** (500 MHz, DMSO-d_6)

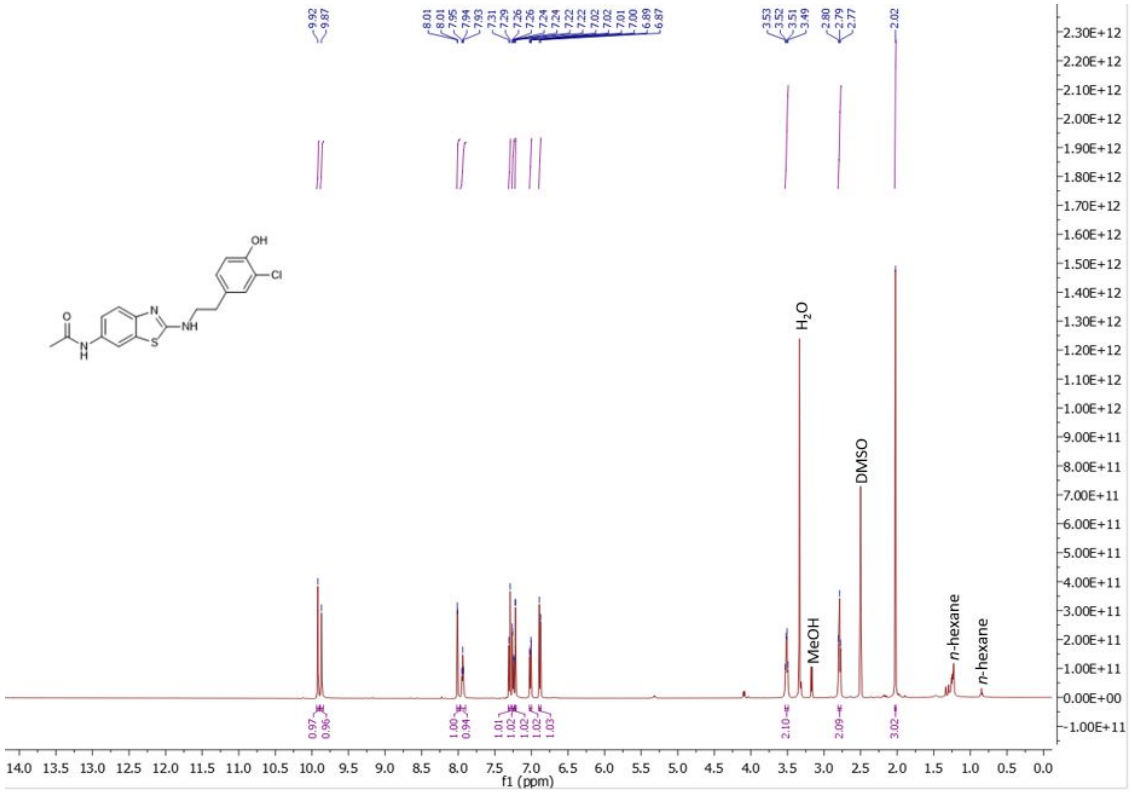

^{13}C NMR spectrum of compound **15** (126 MHz, DMSO-d_6)

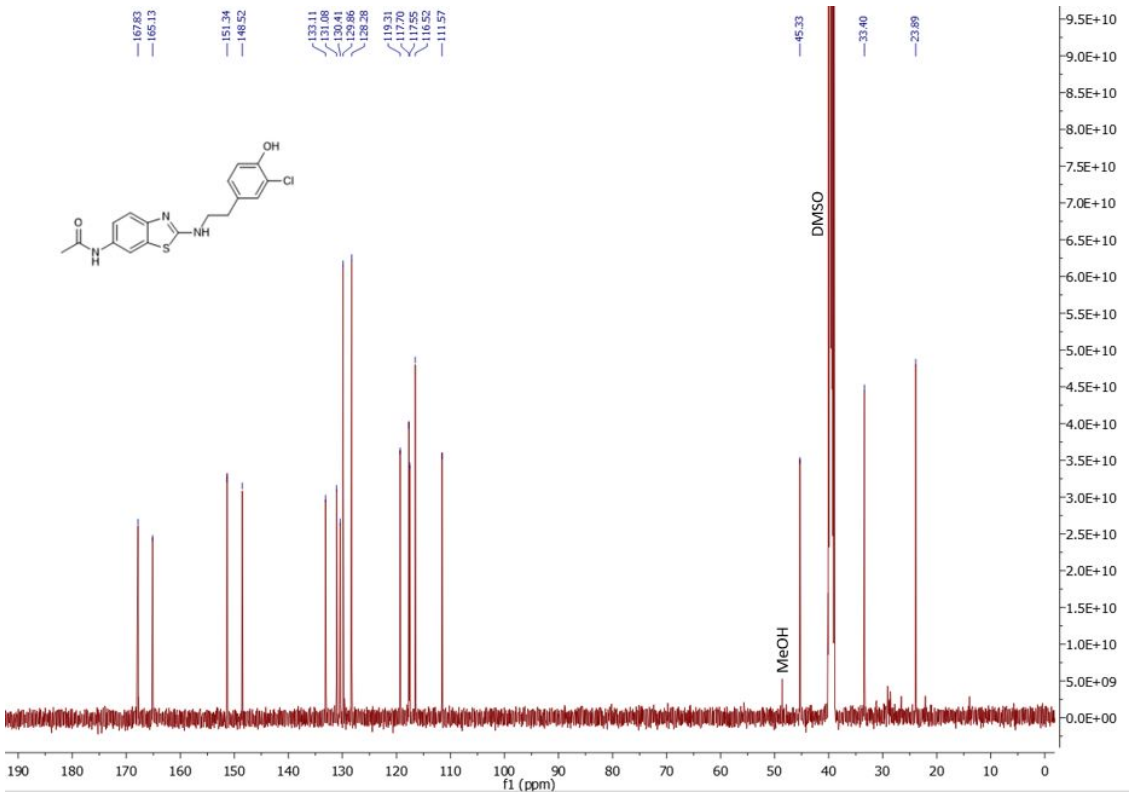

^{1}H NMR spectrum of compound **16** (500 MHz, DMSO-d_6)

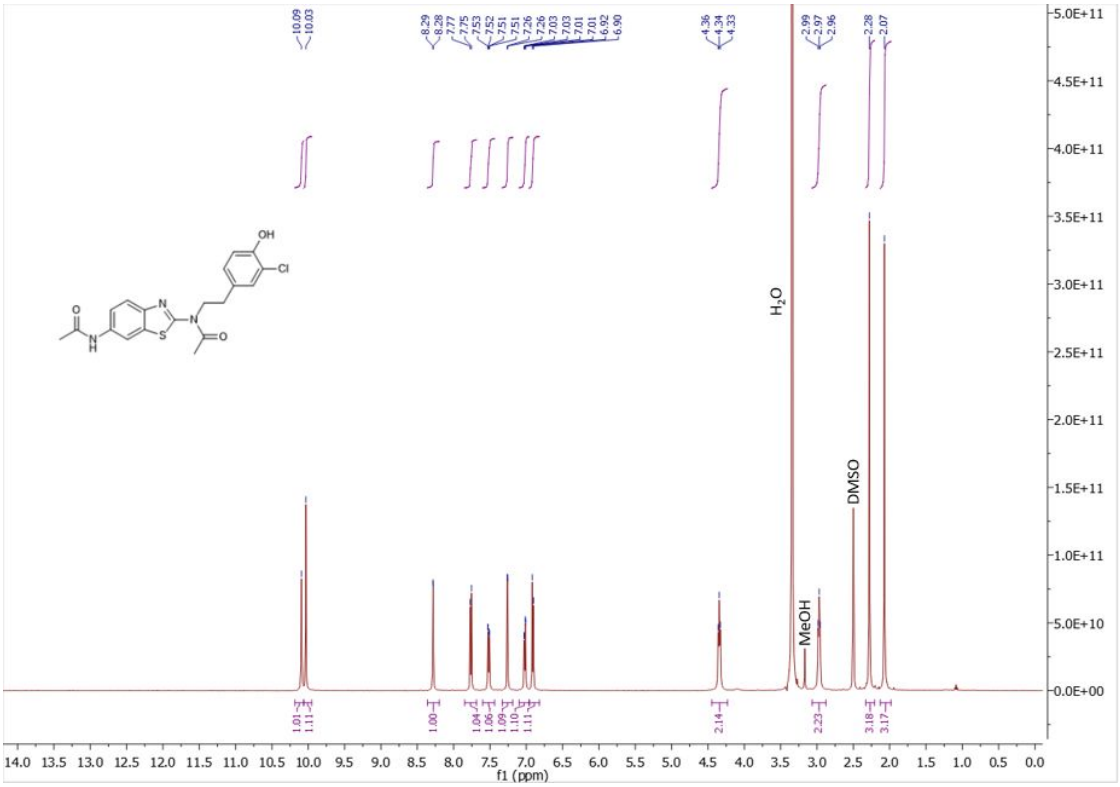

^{13}C NMR spectrum of compound **16** (126 MHz, DMSO-d_6)

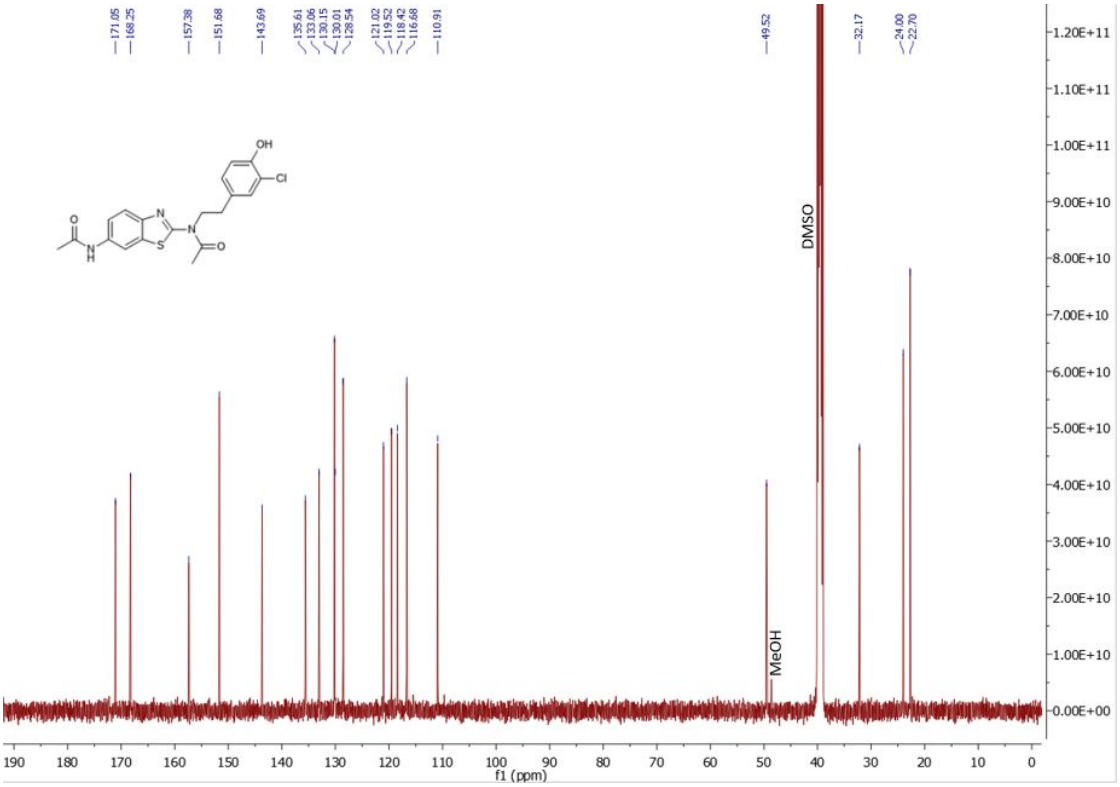

5 HRMS spectra of final products 3–16

HRMS information of compound **3**

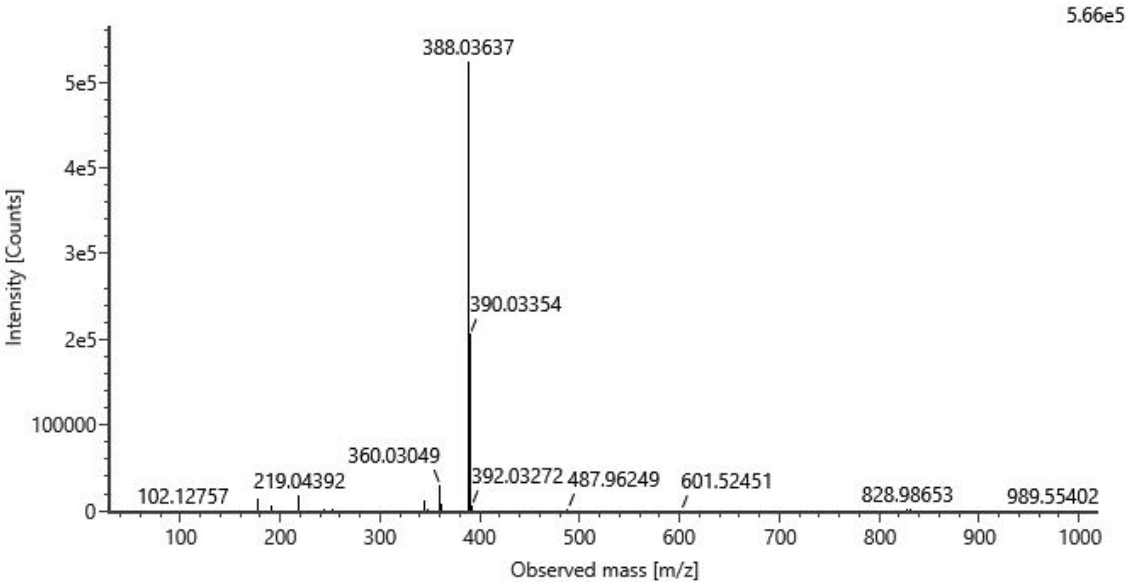

HRMS information of compound **4**

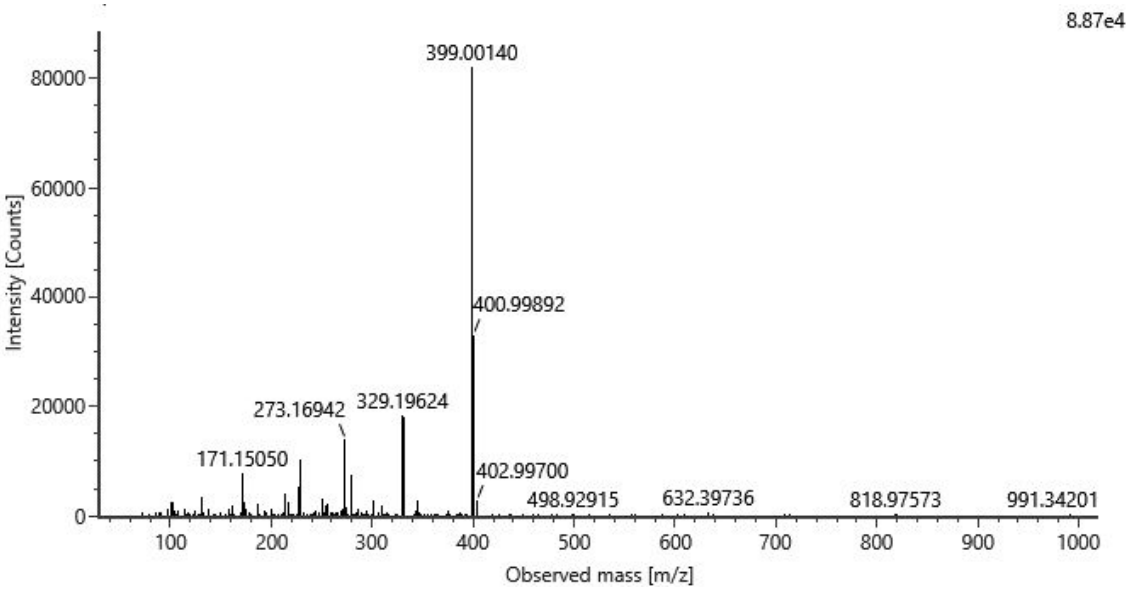

HRMS information of compound **5**

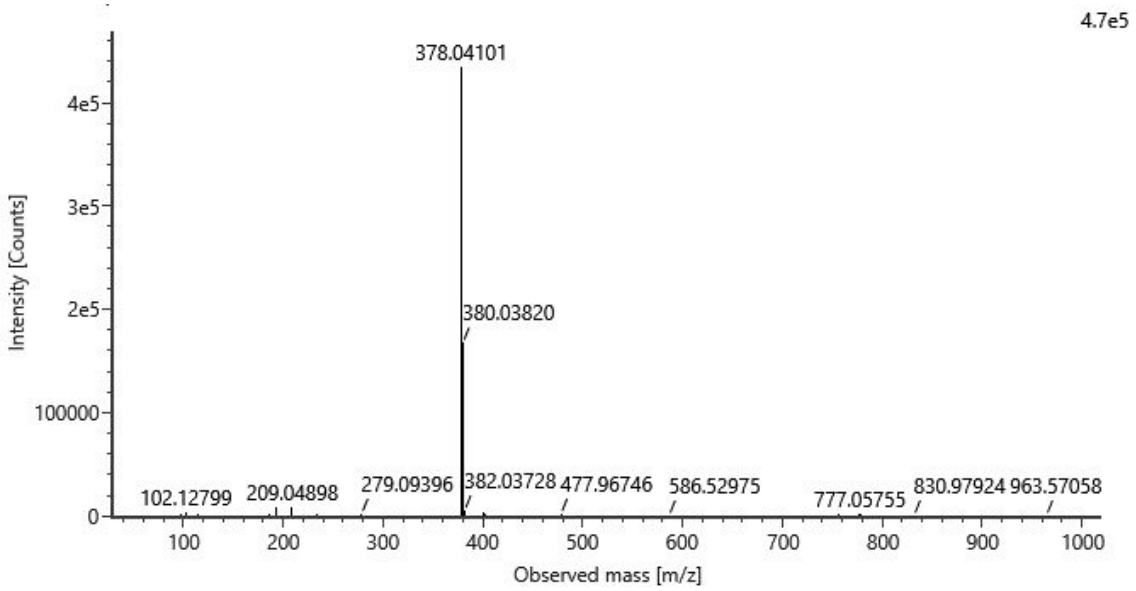

HRMS information of compound **6**

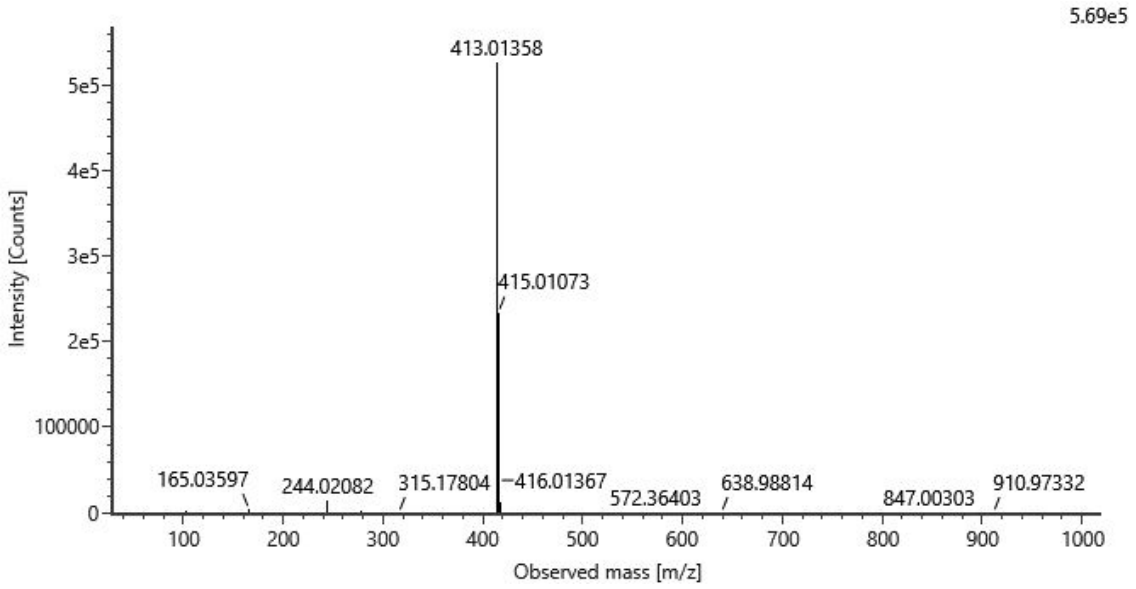

HRMS information of compound **7**

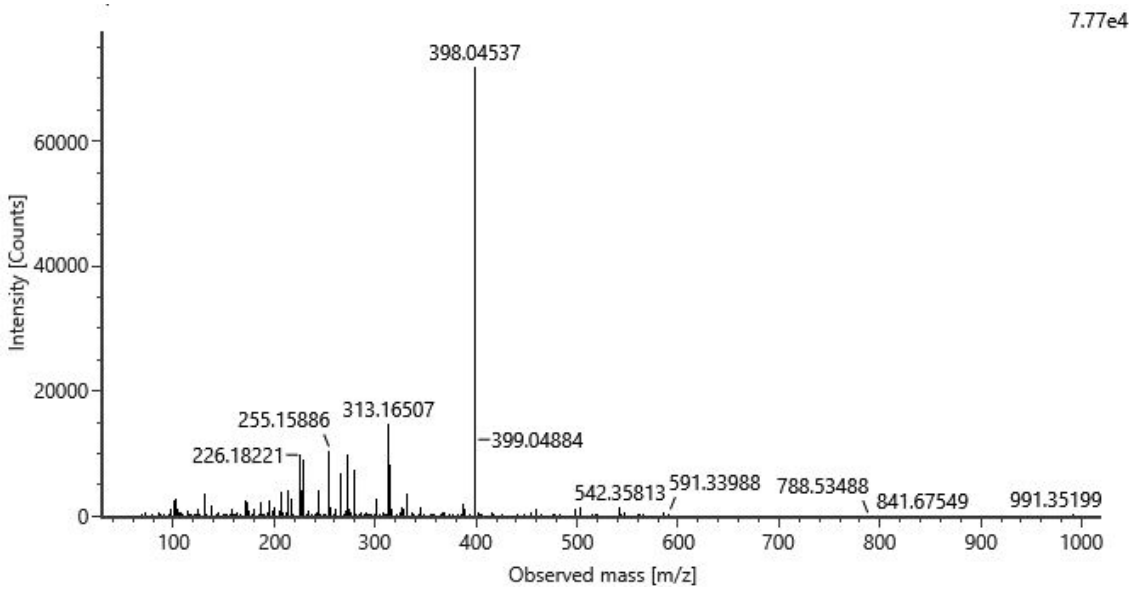

HRMS information of compound **8**

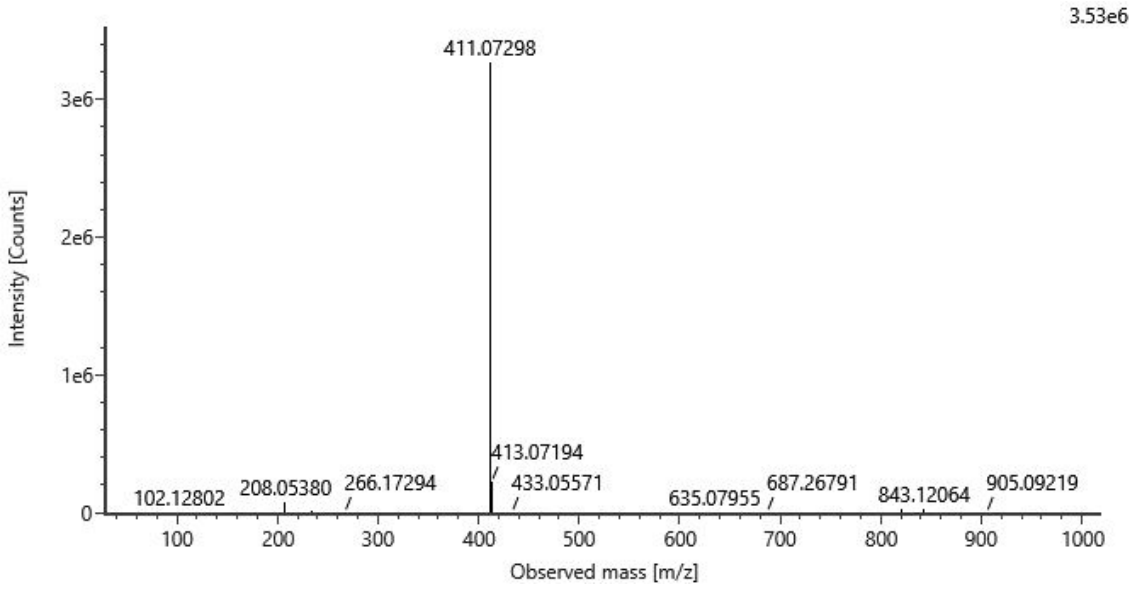

HRMS information of compound **9**

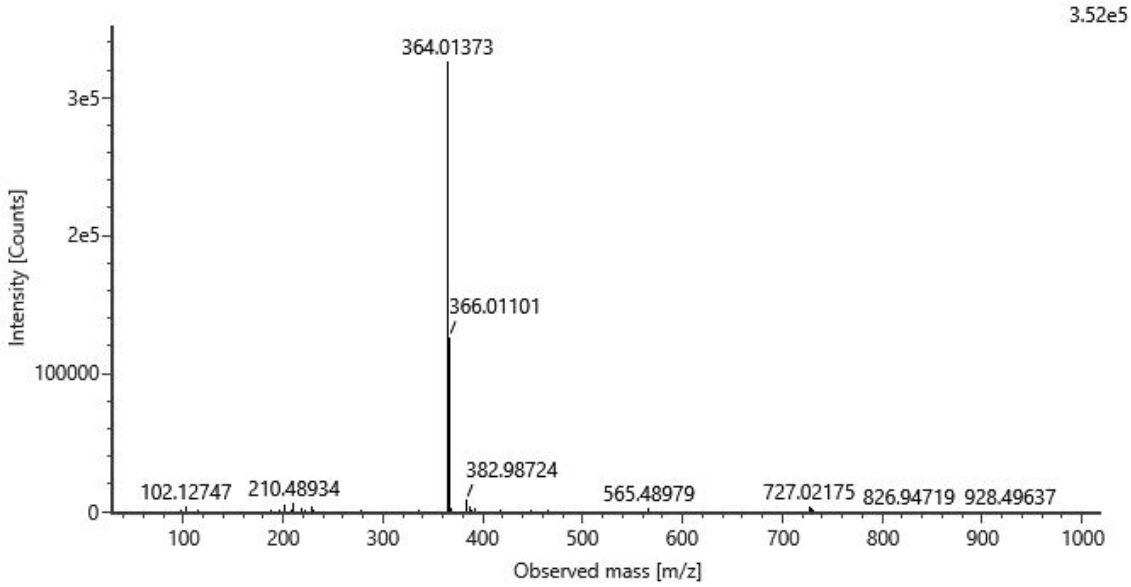

HRMS information of compound **10**

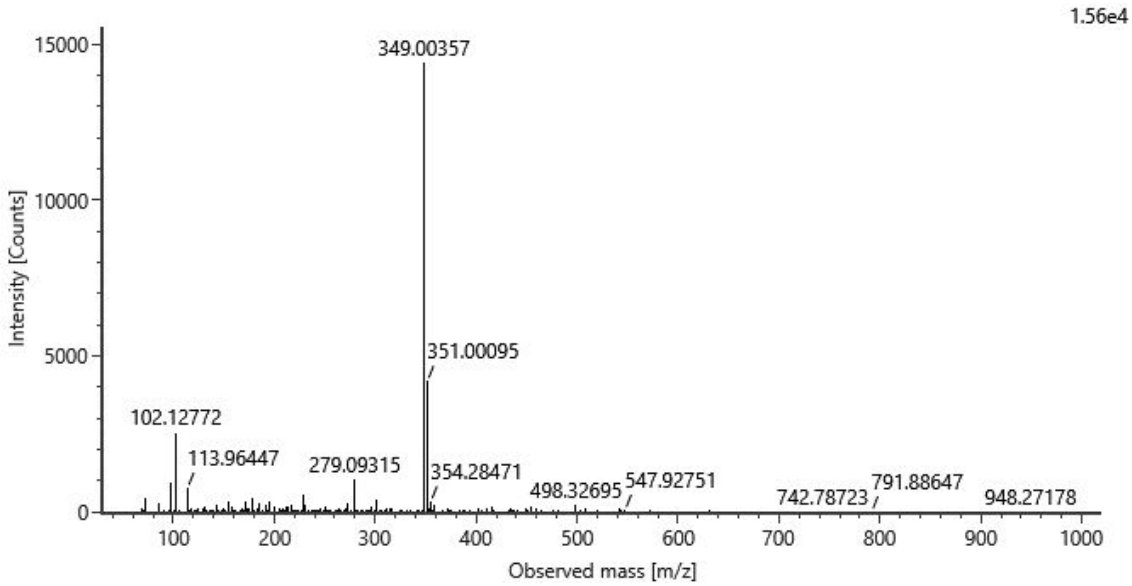

HRMS information of compound **11**

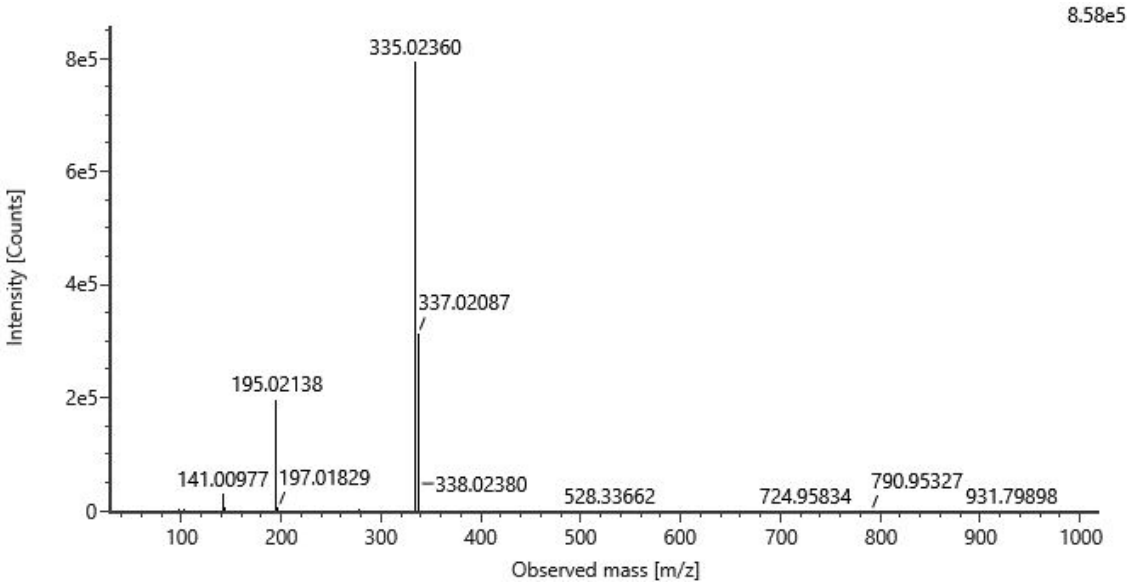

HRMS information of compound **12**

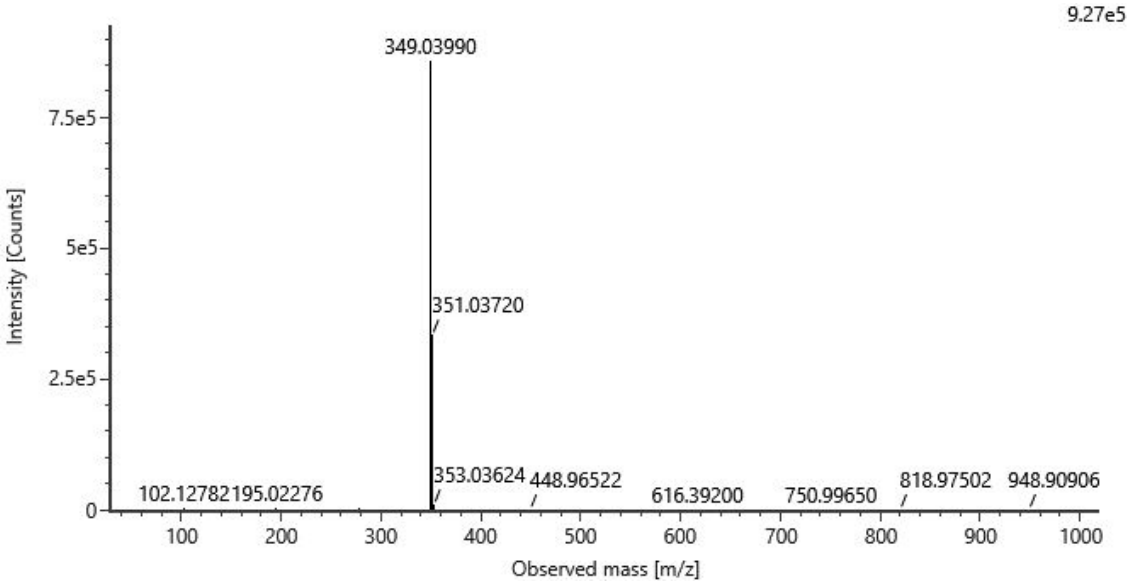

HRMS information of compound **13**

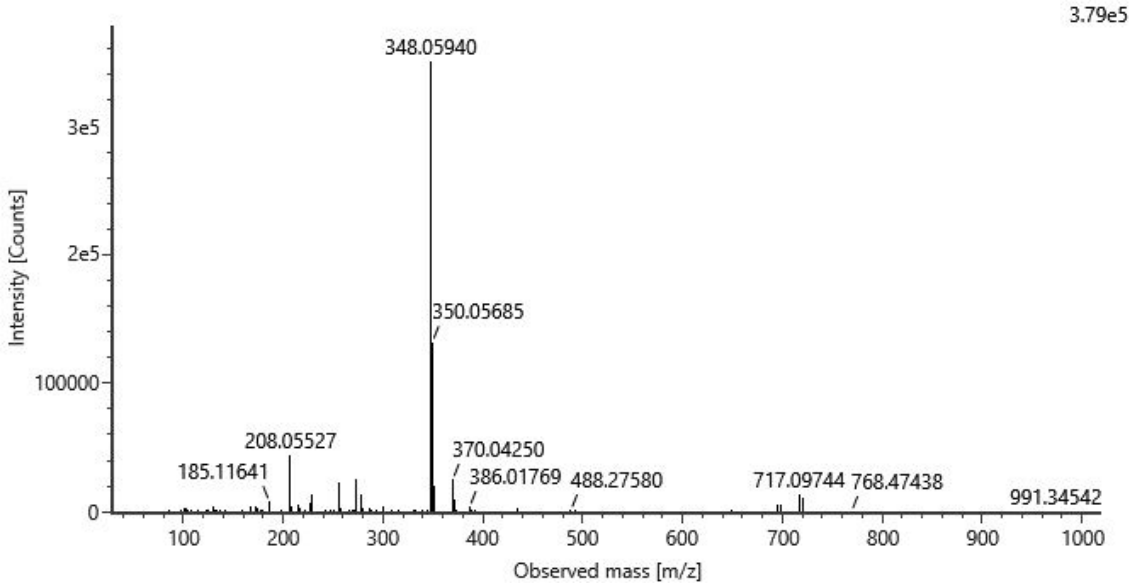

HRMS information of compound **14**

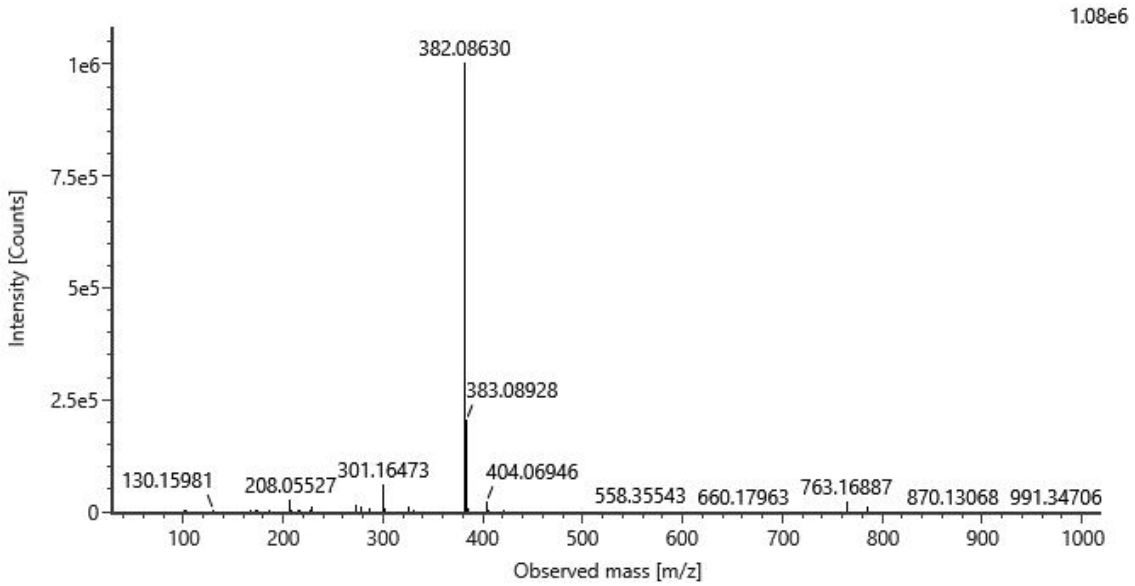

HRMS information of compound **15**

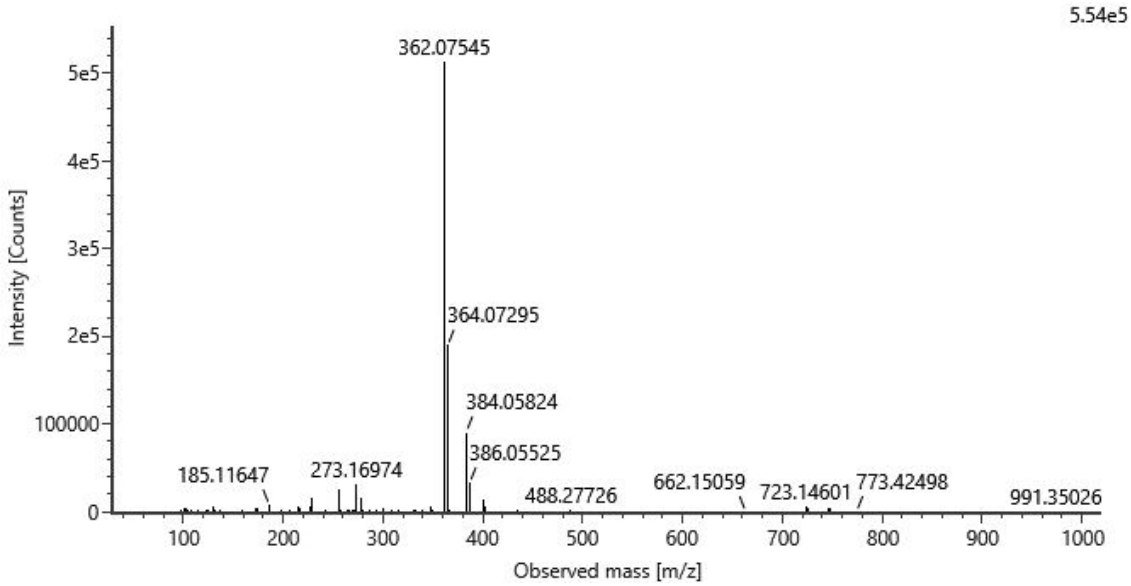

HRMS information of compound **16**

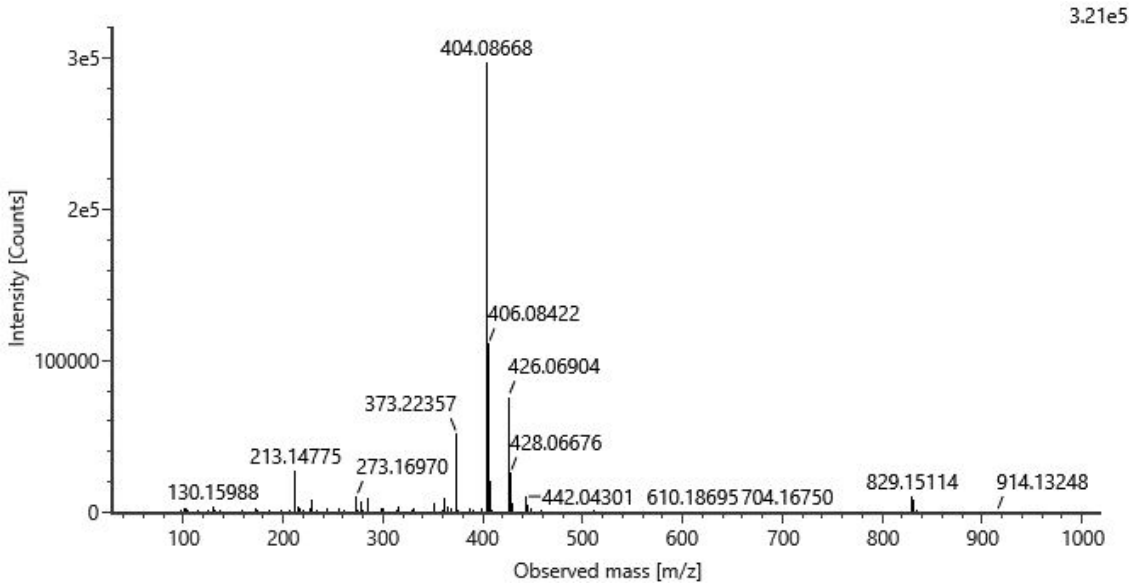

6 Methods of *in vitro* evaluation

6.1 Enzymatic assays

Inhibition screening using AAC substrate

The recombinant His-tagged 17β-HSD10 was expressed in *E. coli* BL21 (DE3) strain and purified as described previously. [1]

For the pilot 10 μM and 1 μM inhibitor screenings, the absorbance assay using acetoacetyl coenzyme A (AAC) as a substrate published by Schmidt et. al.[2] was used with minor changes. Briefly, the reaction mixture of 53 nM recombinant 17β-HSD10 and 320 μM NADH in assay buffer (10 mM Tris-HCl, pH 7.4; 150 mM NaCl; 1 mM dithiothreitol; 0.001% Tween 20; 0.01% bovine serum albumin) was pre-incubated with the tested inhibitor at 10 μM or 1 μM concentration (or DMSO as vehicle control) for 5 minutes at 37 °C. The reaction was started by the addition of 320 μM AAC and the decrease of absorbance at 340 nm was measured for 2 minutes in 10-s intervals. The inhibitors were dissolved in anhydrous DMSO and the final DMSO concentration in the reaction mixture was 2.2% (v/v).

Inhibition screening and IC_{50} determination using E2 or ALLOP substrates

For the 10 μM and 1 μM inhibitor screening and IC_{50} determination, the fluorometric assay using E2 (or ALLOP) as a substrate published previously[1] was used. In brief, the reaction mixture of 45 nM recombinant 17β-HSD10 and 500 μM NAD^+ in assay buffer (100 mM potassium phosphate buffer, pH 8.0) was pre-incubated with the tested inhibitor (or DMSO as vehicle control) for 5 minutes at 37 °C. The reaction was started by the addition of 50 μM E2 (or 20 μM ALLOP) and the increase of fluorescence (Ex/Em = 340/460) was measured for 20 minutes in 30-s intervals. The inhibitors were dissolved in anhydrous DMSO and the final DMSO concentration in the reaction mixture was 2.2 % (v/v).

The IC_{50} measurements were performed as dose-response inhibition at 11 different concentrations of inhibitors (0.004–40 μM) with fixed concentrations of other components of the reaction. Dose-response curves were analysed using non-linear regression analysis and IC_{50} values (± SEM) were determined (GraphPad Prism 8.4.3).

Inhibition Type Determination

The type of inhibition was determined for the most potent inhibitors (compounds **3**, **5**, **6**, and **7**) using E2 as a substrate (methodology mentioned in the previous section). The inhibitors were measured at three different concentrations according to their IC_{50} values in combination with different concentrations of E2 (1.56–75 μM) and a saturated NAD^+ concentration (500 μM). DMSO was used as vehicle control and measured data were analysed using the linearization of Hanes-Woolf (GraphPad Prism 8.4.3).

Differential Scanning Fluorimetry

Melting temperatures (T_m) were determined using Differential Scanning Fluorimetry according to previously published methodology.[1] Briefly, 1.43 μM 17β-HSD10 and 1:1000 SYPRO Orange (Sigma-Aldrich) were mixed in 100 mM potassium phosphate buffer (pH 8.0). The best inhibitors were added at 25 μM or 50 μM final concentration and the interaction was tested without or in the presence of 250 μM NAD^+. DMSO was used as vehicle control. The total reaction volume was 40 μL per tube. The melting curves were monitored in the temperature ramps of 1 °C/min (25–90 °C) using qPCR machine qTower^3 G (Analytik Jena, Ex/Em = 490/575). The melting curves were analysed and melting temperatures were determined using qPCRsoft 4.0 (Analytik Jena). The differences between groups were analysed using the Student's unpaired t-test (GraphPad Prism 8.4.3).

6.2 Cell-based assays

A set of cellular assays were used to evaluate the cytotoxic potential of prepared compounds and target engagement in the living cells. For this purpose, HEK293 cells and HEK293 overexpressing 17β-HSD10 cells (HEK293 17β-HSD10) published previously[1] were used. Cells were maintained in DMEM (Capricorn) supplemented with 10% foetal bovine serum (Gibco), 2 mM L-glutamine, and non-essential amino acids additives (Gibco) at 37 °C in a 5% CO_2 humidified atmosphere. The cells were passaged regularly at 70–80% confluency, and all culture preparations were repeatedly tested for Mycoplasma contamination (MycoAlert Plus, Promega).

Cytotoxicity evaluation

All compounds were tested on HEK293 cells to determine their cytotoxicity effects using the CellTox Green Cytotoxicity Assay kit (Promega). For measurement, 5×10^3 cells per well in 50 μL of culture media were seeded into white solid flat-bottom 96 well microplates (Nunc, 136102) and cultured for 24 hours before the addition of compounds. The compounds were dissolved and further diluted in anhydrous DMSO, and added to the wells at a final concentration of 10 μM, 25 μM, and 50 μM, with a total DMSO concentration in the assay of 1%. The treated cells were cultured for an additional 48 hours, followed by the fluorescence measurement using a Tecan Spark 10M instrument. The CellTox Green Assay procedure was performed according to the manufacturer's protocol. The fluorescence was measured as endpoint readout using 485 nm for excitation and 530 nm for emission wavelengths. The data were normalized between cells treated with 1% DMSO only (vehicle control), and 100 μM valinomycin treated cells (positive control).

Cellular 17β-HSD10 inhibition and IC_{50} determination

The 17β-HSD10 inhibition inside the HEK293 17β-HSD10 cells was performed using (-)-CHANA fluorogenic probe.[3] The cells were seeded at a density of 1×10^4 cells per well in 200 μL of DMEM

without phenol red (Gibco) supplemented with 10% foetal bovine serum (Gibco), 2 mM L-glutamine, non-essential amino acids additives (Gibco) and 4.5 g/L glucose (Sigma) into black 96 clear bottom well plates (Brand, 781971). The cells were incubated for 20 hours following the treatment with the compounds dissolved in anhydrous DMSO or DMSO only (vehicle control). After 2 hours of compound treatment, (-)-CHANA probe was added at the final concentration of 20 μM and the changes in fluorescent intensities were measured immediately after (-)-CHANA addition and 2 hours later. The fluorescence intensities of the CHANK product were taken using the TECAN SPARK 10M instrument (Ex/Em = 380/525 nm). The residual 17β-HSD10 activity was calculated as ΔF between 2 hours and 0 hours after (-)-CHANA treatment and the data were normalized between non-treated HEK293 17β-HSD10 and non-transfected HEK293 controls (using relative response ratio).

The compounds were screened at 10 μM and 25 μM concentrations to detect the ability to penetrate the cells and to influence the 17β-HSD10 enzyme activity inside the cells. For the compounds with residual activity lower than 55% at 10 μM concentration (**4**, **6**, **13**, **14**, **15**, and **16**), the IC_{50} values were measured as a dose-response inhibition at 9 different concentrations of inhibitors (0.3125–40 μM). The data were analysed using GraphPad Prism 8.4.3.

7 Results of *in vitro* evaluation

Table S1: Inhibition screening on purified 17β-HSD10 enzyme. 10 µM and 1 µM screening of the tested compounds against recombinant 17β-HSD10 using AAC and E2 substrates. Values are given as means ± SD (n = 3 for AAC, n = 4 for E2).

17β-HSD10 Activity *in vitro* (%)				
Compound	**AAC assay**		**E2 assay**	
	10 µM	**1 µM**	**10 µM**	**1 µM**
1	12.2 ± 4.0	45.6 ± 0.7	6.8 ± 3.1	62.4 ± 3.4
2	10.0 ± 1.7	43.0 ± 3.0	14.3 ± 3.4	59.7 ± 6.2
3	7.0 ± 5.0	27.9 ± 0.6	0.0 ± 2.2	30.1 ± 1.5
4	9.2 ± 3.5	32.9 ± 2.3	2.5 ± 3.0	30.5 ± 3.0
5	14.0 ± 5.0	45.1 ± 2.8	0.9 ± 1.8	36.8 ± 1.0
6	13.5 ± 2.9	40.9 ± 2.7	0.0	39.5 ± 6.2
7	7.1 ± 2.2	38.5 ± 3.6	4.4 ± 2.7	17.6 ± 1.8
8	2.8 ± 3.2	21.0 ± 2.0	71.3 ± 1.0	40.3 ± 2.6
9	37.1 ± 3.3	87.2 ± 2.4	21.1 ± 2.2	64.8 ± 2.2
10	4.0 ± 3.4	42.4 ± 1.9	0.0	61.1 ± 2.2
11	45.8 ± 5.2	93.2 ± 3.5	20.7 ± 3.4	81.3 ± 2.0
12	6.9 ± 2.7	59.8 ± 1.0	0.0	42.8 ± 6.6
13	26.0 ± 2.0	77.7 ± 2.1	18.0 ± 1.5	65.1 ± 0.3
14	14.2 ± 3.0	60.3 ± 1.3	9.9 ± 1.5	57.2 ± 7.8
15	9.8 ± 2.0	42.0 ± 3.8	5.5 ± 1.9	46.0 ± 4.6
16	27.8 ± 0.7	78.8 ± 4.9	14.6 ± 1.8	55.2 ± 2.8

Table S2: Differential scanning fluorimetry. Melting temperatures (T_m) for 17β-HSD10 were measured at 25 µM and 50 µM inhibitor concentrations in the absence or presence of 250 µM NAD^+ cofactor. Values are given as means ± SD (n = 3).

T_m values (°C)				
	w/o NAD^+		**with NAD^+**	
DMSO	49.9 ± 0.3		54.5 ± 0.1	
Compound	**25 µM**	**50 µM**	**25 µM**	**50 µM**
3	57.3 ± 0.1	59.5 ± 0.2	63.6 ± 0.0	65.1 ± 0.1
5	53.4 ± 0.2	54.2 ± 0.1	59.9 ± 0.1	61.0 ± 0.1
6	53.3 ± 0.3	54.4 ± 0.2	60.9 ± 0.2	62.1 ± 0.1
7	51.2 ± 0.2	52.4 ± 0.2	58.4 ± 0.1	60.0 ± 0.1

Table S3: Cellular cytotoxicity determination (CellTox Green Assay) in HEK293 cells at concentrations 50 µM, 25 µM and 10 µM. Values are given as mean ± SD from two independent measurements performed in triplicates.

Compound	% of Cytotoxicity		
	50 µM Compound	25 µM Compound	10 µM Compound
3	0.46 ± 0.82	0.88 ± 1.34	0.62 ± 2.91
4	1.90 ± 0.24	1.77 ± 1.50	3.31 ± 1.48
5	1.08 ± 0.95	-0.10 ± 1.27	0.37 ± 0.01
6	2.00 ± 2.74	0.73 ± 1.92	1.24 ± 1.30
7	-1.99 ± 1.45	-0.70 ± 2.58	0.45 ± 0.50
8	1.19 ± 0.58	1.05 ± 1.57	3.16 ± 1.81
9	0.12 ± 2.39	-0.01 ± 0.51	1.49 ± 2.70
10	-1.44 ± 1.87	1.10 ± 0.87	1.52 ± 1.70
11	0.24 ± 0.52	1.71 ± 1.01	1.26 ± 1.78
12	-0.08 ± 0.16	0.31 ± 1.08	1.33 ± 0.71
13	6.48 ± 1.35	4.32 ± 1.57	2.87 ± 1.28
14	1.43 ± 2.65	0.53 ± 0.52	0.11 ± 0.11
15	0.65 ± 2.73	0.68 ± 1.56	1.89 ± 1.72
16	1.95 ± 0.49	1.12 ± 0.54	0.42 ± 1.58

Table S4: Cellular inhibitory screening of compounds at concentrations 25 µM and 10 µM using a conversion of (-)-CHANA fluorogenic probe in HEK293 17β-HSD10 cells. Values are given as mean ± SD from two independent measurements performed in triplicates.

Compound	Cellular 17β-HSD10 Activity (%)	
	25 µM Compound	10 µM Compound
3	61.7 ± 1.9	74.6 ± 3.0
4	22.4 ± 0.7	51.7 ± 3.4
5	36.5 ± 2.3	63.5 ± 3.1
6	16.6 ± 1.1	39.1 ± 3.3
7	49.1 ± 2.6	69.0 ± 0.1
8	27.9 ± 0.2	60.5 ± 2.8
9	55.6 ± 0.3	63.8 ± 2.6
10	64.4 ± 1.5	83.9 ± 5.7
11	117.6 ± 5.1	86.4 ± 1.7
12	48.6 ± 5.0	64.9 ± 1.6
13	24.2 ± 3.0	47.5 ± 3.0
14	11.9 ± 1.5	36.6 ± 2.2
15	0.0	30.6 ± 2.5
16	21.6 ± 1.9	54.4 ± 2.4

8 Safety Statement

No unexpected or unusually high safety hazards were encountered during experimental work.

9 References

(1) Schmidt, M.; Vaskova, M.; Rotterova, A.; Fiandova, P.; Miskerikova, M.; Zemanova, L.; Benek, O.; Musilek, K. Physiologically Relevant Fluorescent Assay for Identification of 17β-hydroxysteroid Dehydrogenase Type 10 Inhibitors. *J Neurochem* **2023**, jnc.15917. https://doi.org/10.1111/jnc.15917.

(2) Schmidt, M.; Benek, O.; Vinklarova, L.; Hrabinova, M.; Zemanova, L.; Chribek, M.; Kralova, V.; Hroch, L.; Dolezal, R.; Lycka, A.; Prchal, L.; Jun, D.; Aitken, L.; Gunn-Moore, F.; Kuca, K.; Musilek, K. Benzothiazolyl Ureas Are Low Micromolar and Uncompetitive Inhibitors of 17β-HSD10 with Implications to Alzheimer's Disease Treatment. *Int J Mol Sci* **2020**, *21* (6), 2059. https://doi.org/10.3390/ijms21062059.

(3) Muirhead, K. E. A.; Froemming, M.; Li, X.; Musilek, K.; Conway, S. J.; Sames, D.; Gunn-Moore, F. J. (-)-CHANA, a Fluorogenic Probe for Detecting Amyloid Binding Alcohol Dehydrogenase HSD10 Activity in Living Cells. *ACS Chem Biol* **2010**, *5* (12), 1105–1114. https://doi.org/10.1021/cb100199m.

10.5 Publikace V

Hanzlova, M., Slavikova, B., Morozovova, M., Musilek, K., Rotterova, A., Zemanova, L., Kudova, E., 2024. The C-3 steroidal hemiesters as inhibitors of 17β-hydroxysteroid dehydrogenase type 10. Manuskript v pokročilé fázi recenzního řízení v ACS Omega.

This document is confidential and is proprietary to the American Chemical Society and its authors. Do not copy or disclose without written permission. If you have received this item in error, notify the sender and delete all copies.

The C-3 steroidal hemiesters as inhibitors of 17β-hydroxysteroid dehydrogenase type 10

Journal:	*ACS Omega*
Manuscript ID	ao-2023-10148z.R1
Manuscript Type:	Article
Date Submitted by the Author:	12-Jan-2024

Complete List of Authors:	Hanzlova, Michaela; University of Hradec Kralove Faculty of Science, Department of Chemistry Slavikova, Barbora; Institute of Organic Chemistry and Biochemistry Czech Academy of Sciences, Neurosteroids Morozovova, Marina; Institute of Organic Chemistry and Biochemistry Czech Academy of Sciences, Neurosteroids Musilek, Kamil; University of Hradec Kralove Faculty of Science, Department of Chemistry Rotterova, Aneta; University of Hradec Kralove Faculty of Science, Department of Chemistry Zemanová, Lucie; University of Hradec Kralove Faculty of Science, Department of Chemistry Kudova, Eva; Institute of Organic Chemistry and Biochemistry Czech Academy of Sciences, Neurosteroids

SCHOLARONE™
Manuscripts

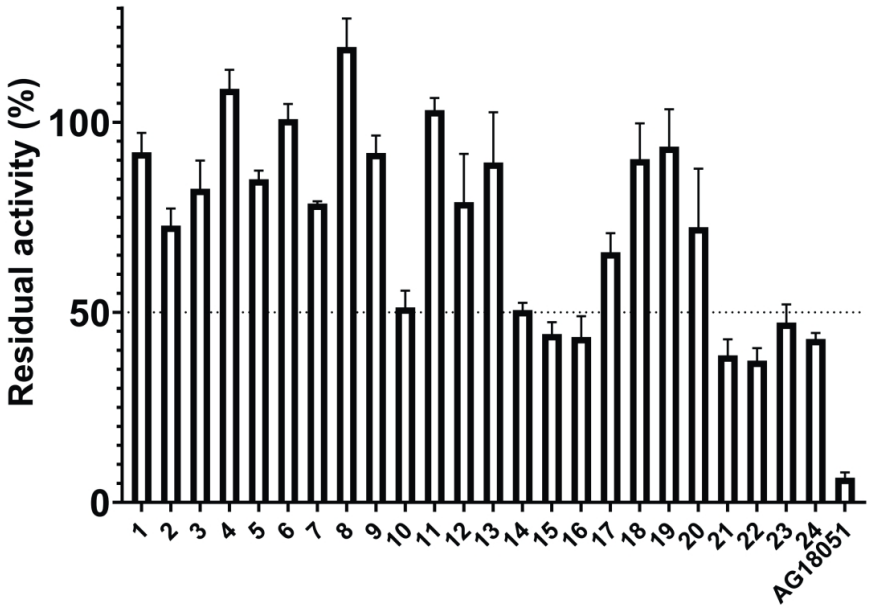

Caption : Figure 1. Evaluation of the inhibitory effect of compounds 1-24 and inhibitor AG18051 (standard) at 10 μM. Values represent means ± SD (n = 4).

220x160mm (300 x 300 DPI)

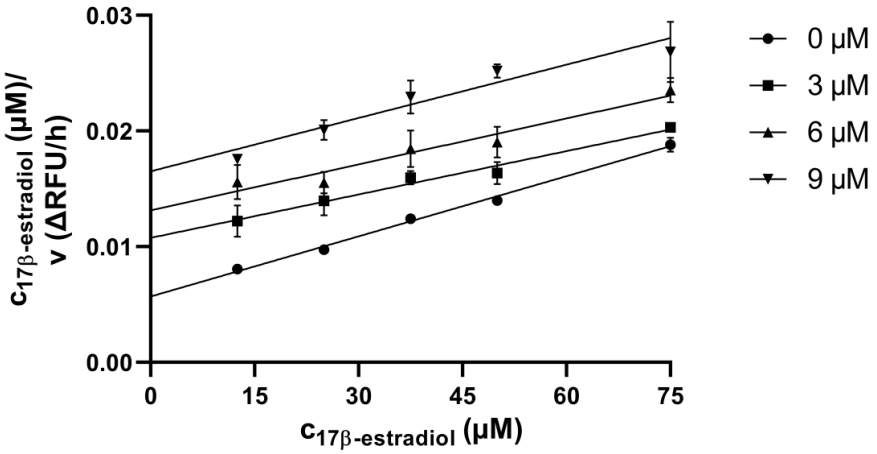

Figure 2: The kinetic inhibition of 17β-HSD10 using com-pound 23 at 0, 3, 6 and 9 μM concentration. Data are shown as mean ± SD (n = 3).

134x73mm (1200 x 1200 DPI)

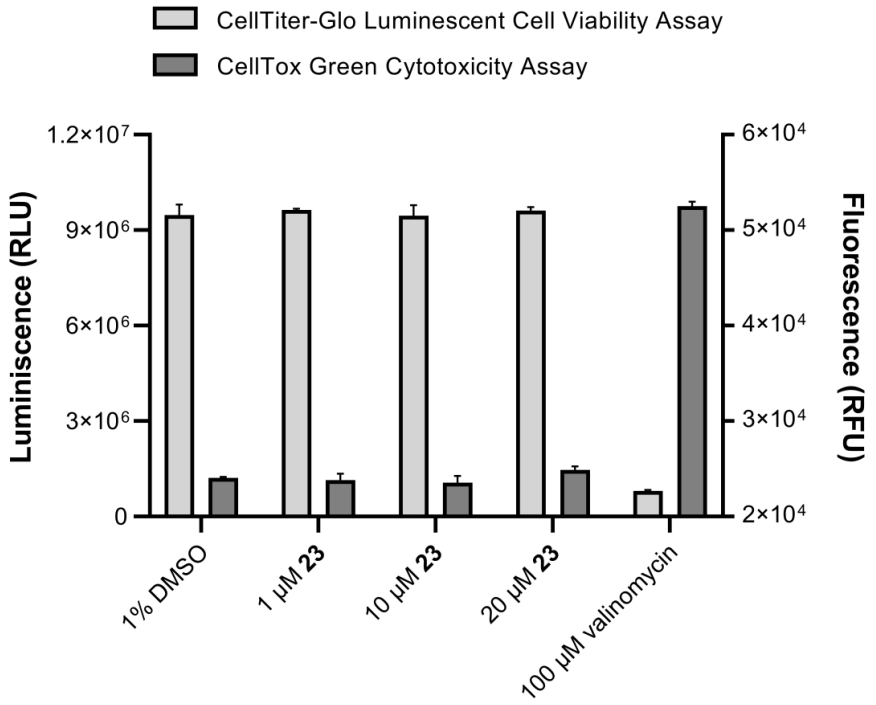

Figure 3: Viability of HEK-293 cells in the presence of compound 23 (measured by CellTiter-Glo Viability Assay) and its cytotoxic effect (measured by CellTox Green Assay). DMSO-treated and valinomycin-treated cells were used as cell viability respectively cytotoxicity controls. Data are presented as mean ± SD (n = 3).

122x99mm (1200 x 1200 DPI)

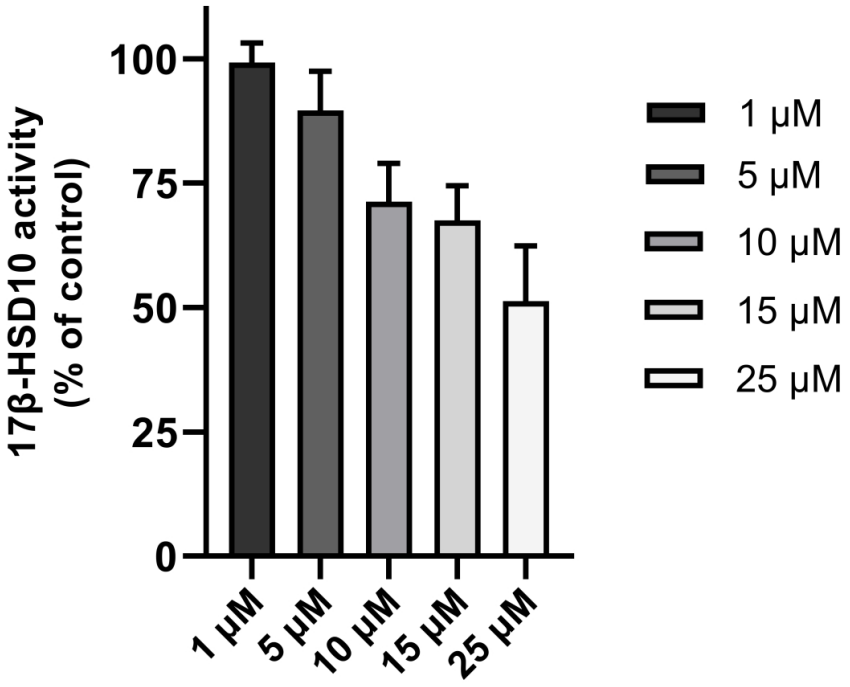

Figure 4: Inhibition of 17β-HSD10 by compound 23 in HEK-293 cellular model overexpressing 17β-HSD10 (HEK-293_HSD10). The activity of 17β-HSD10 was determined using a probe (-)-CHANA as a substrate, and the fluorescence of formed product CHANK was measured. Values are given as mean ± SD from two biological replicates with three technical replicates.

85x73mm (1200 x 1200 DPI)

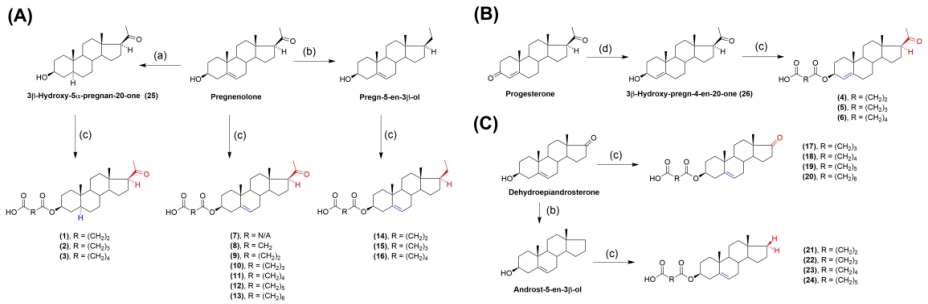

Scheme 1. Synthesis of compounds 1-24. Reaction conditions and reagents: (a) H_2, Pd/C, EtOH/EtOAc; (b) Zn, TMSCl, MeOH, DCM; (c) For compound 7: oxalyl chloride, Et_3N, DCM, DMF. For compound 8: Meldrum's acid, toluene, 80 °C. For compounds 1, 4, 9, 14, 21: succinic anhydride, DMAP, pyridine, 110 °C. For compounds 2, 5,10,15,17, 22: glutaric anhydride, DMAP, pyridine, 110 °C. For compounds 3, 6, 11, 16, 18, 23: adipic acid, EDCI, DIPEA, DMAP, DCM. For compounds 12, 19, and 24: pimelic acid, EDCI, DIPEA, DMAP, DCM. For compounds 13 and 20: suberic acid, EDCI, DIPEA, DMAP, DCM; (d) $NaBH_4$, $CeCl_3.7H_2O$, MeOH.

425x138mm (300 x 300 DPI)

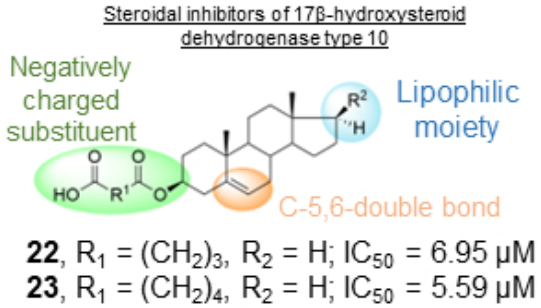

TOC for manuscript

82x44mm (96 x 96 DPI)

The C-3 steroidal hemiesters as inhibitors of 17β-hydroxysteroid dehydrogenase type 10

Michaela Hanzlova[a,†], Barbora Slavikova[b], Marina Morozovova[b], Kamil Musilek[a], Aneta Rotterova[a], Lucie Zemanová[a,*], Eva Kudova[b,*]

[a] University of Hradec Kralove, Faculty of Science, Department of Chemistry, Rokitanskeho 62, 500 03 Hradec Kralove, Czech Republic

[b] Institute of Organic Chemistry and Biochemistry, Czech Academy of Sciences, Flemingovo namesti 2, Prague 6, 166 10, Czech Republic

KEYWORDS 17β-HSD10, inhibitor, steroid, pregnane, structure-activity relationship

ABSTRACT: 17β-HSD10 is a mitochondrial enzyme that catalyzes the steroidal oxidation of a hydroxy group to a keto group and thus is involved in maintaining steroid homeostasis. The druggability of 17β-HSD10 is related to potential treatment for neurodegenerative diseases including Alzheimer's disease or certain types of cancer. Here, steroidal derivatives with an acidic hemiester substituent at position C-3 on the skeleton were designed, synthesized, and evaluated using pure recombinant 17β-HSD10 converting estradiol to estrone. Compounds **22** (IC_{50} = 6.95 ± 0.35 μM) and **23** (IC_{50} = 5.59 ± 0.25 μM) were identified as the most potent inhibitors from the series. Compound **23** inhibited 17β-HSD10 activity regardless of the substrate. It was found not cytotoxic towards the HEK-293 cell line and able to inhibit 17β-HSD10 activity also in the cellular environment. Together, these findings support steroidal compounds as promising candidates for further development as 17β-HSD10 inhibitors.

INTRODUCTION

Human 17β-hydroxysteroid dehydrogenase type 10 (17β-HSD10, SDR5C1 also called ABAD/ERAB or HADH2, UniProt ID Q99714) is a member of the short-chain dehydrogenase/reductase (SDR) superfamily that is expressed in the mitochondrial matrix in a variety of tissues, such as lung, liver, brain and other.[1] The 17β-HSD10 is a so-called moonlighting enzyme that exhibits at least two physiologically relevant functions. First, it is a key component of the ribonuclease P (RNase P) complex that participates in isoleucine metabolism as well as in lipid metabolism.[2] The second essential function reflecting its name is its role in steroid metabolism. 17β-HSD10 catalyzes e.g. NAD^+-dependent oxidation of 17β-estradiol to less active estrone, 3α-androstanediol to more potent 5α-dihydrotestosterone or neurosteroid allopregnanolone to 5α-dihydroprogesterone. Thus, the activity of 17β-HSD10 can influence important cellular processes related to the steroid concentrations such as proliferation, apoptosis, or neural excitability.[3, 4] Finally, the crucial role of 17β-HSD10 in the development of various pathological conditions and diseases should be mentioned. According to the literature, the 17β-HSD10 overexpression may lead to the disturbance in steroid homeostasis proposed as an important factor attributing to the development of various diseases, such as Alzheimer´s disease,[5] prostate cancer,[6, 7] or osteosarcoma.[8] Taken together, the restoration of steroid homeostasis through 17β-HSD10 inhibition is thought to promote neuroprotection and serve as a promising therapeutic approach for the development of novel drug-like molecules.[5, 8, 9]

To date, several groups of 17β-HSD10 inhibitors have been described in the literature. For details, see the review of Vinklarova et al.[10] They can be divided into several groups based on their structure, namely benzothiazole-based ureas, [11-15] pyrazole-pyrimidine compounds,[16, 17] steroidal inhibitors,[18-20] and risperidone or its analogues.[21] Based on the mechanism of action, inhibitors of 17β-HSD10 are designed to either block the catalytic activity of the enzyme or to modulate the interaction of 17β-HSD10 with amyloid-beta (Aβ) that is contributing to Aβ-induced toxicity by promoting mitochondrial dysfunction.

According to the literature, pyrazole-pyrimidine compound AG18051, is a well-known and potent inhibitor of 17β-HSD10.[16] Co-crystallization of AG18051 with human 17β-HSD10 with its NAD^+ cofactor has shown that it forms a covalent adduct with amino acids in the active site. Nevertheless, AG18051 has been further studied,[22] and attempts for rational optimization studies of the structure have been also published.[17] Very recently, a novel benzothiazolylurea inhibitor with similar efficiency and non-competitive mode of action has been described.[15] The most potent steroidal structures that have been described so far are RM-532-46 and D-3,7.[18,20] Interestingly, compounds RM-532-46, D-3,7 as well as benzothiazole-

based ureas inhibitors are nitrogen-containing compounds that potentially can act as a proton-acceptor (a base).[11-13] Therefore, we proposed, synthesized, and tested a series of negatively charged steroids **1**-**24** (**Scheme 1**) for their ability to inhibit the 17β-HSD10 activity.

Synthesis of neurosteroids for the treatment of yet untreatable central nervous system diseases represents a novel and attractive target for the development of drug-like compounds due to their endogenous origin and significantly more inherent nature to humans than e.g. benzothiazole-based ureas or pyrazole-pyrimidine compounds. In addition, recently FDA-approved neurosteroids brexanolone (treatment of post-partum depression)[23, 24] or ganaxolone (treatment of seizures in CDKL5 deficiency)[25] provide evidence of still underappreciated possibilities of neurosteroids in drug development.

RESULTS AND DISCUSSION

Chemistry

The synthesis of compounds **1**-**24** is shown in **Scheme 1**. Compounds **1**-**3** were prepared from commercially available pregnenolone (Steraloids, Newport, RI, USA). Compound 3β-hydroxy-5α-pregnan-20-one **25** was prepared by catalytic hydrogenation with Pd/C of pregnenolone.[26, 27] Compounds **4**-**6** were prepared from commercially available progesterone (Steraloids, Newport, RI, USA). The conjugated carbonyl group of progesterone in position C-3 was selectively reduced by using sodium borohydride in the presence of cerium(III) chloride (Luche reduction) affording compound **26** in 50% yield.[28] Compounds **1**-**24** were prepared by treatment of parent C-3 hydroxyl group with anhydride or carboxylic acid depending on the availability of such reagents. In brief, compounds **1** and **4** were esterified with succinic anhydride in the presence of DMAP in pyridine at 110 °C, affording compounds **25** and **26** in 65% and 40% yield, respectively. Compounds **2** and **5** were prepared from compounds **25** and **26** by treatment with glutaric anhydride in the presence of DMAP in pyridine at 110 °C. Hemiesters **2** (45% yield) and **5** (62% yield) were obtained. The treatment of compounds **25** and **26** with adipic acid, 1-ethyl-3-(3-dimethylaminopropyl)carbodiimide (EDCI), *N*,*N*-diisopropylethylamine (DIPEA) and DMAP in DCM gave hemiesters **3** and **6** (93% and 51% yield). Compounds **7**-**24** were prepared analogously as compounds **1**-**6** according to the literature[29] from pregnenolone, dehydroepiandrosterone, pregn-5-en-3β-ol, and from androst-5-en-3β-ol. Decarbonylation was achieved by Clemmensen reduction mediated by Zn/TMSCl according to the literatere.[30]

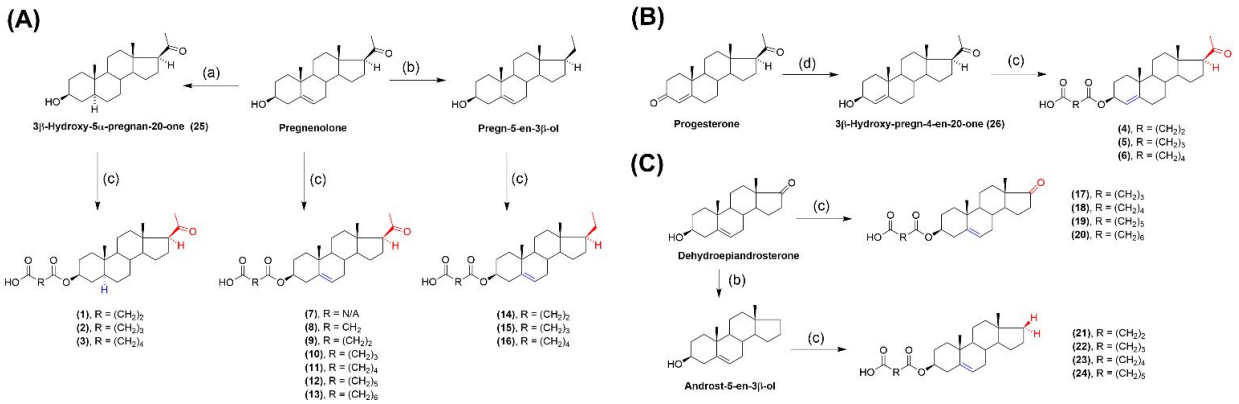

Scheme 1. Synthesis of compounds **1**-**24**. Reaction conditions and reagents: (a) H_2, Pd/C, EtOH/EtOAc; (b) Zn, TMSCl, MeOH, DCM; (c) For compound **7**: oxalyl chloride, Et_3N, DCM, DMF. For compound **8**: Meldrum's acid, toluene, 80 °C. For compounds **1**, **4**, **9**, **14**, **21**: succinic anhydride, DMAP, pyridine, 110 °C. For compounds **2**, **5**,**10**,**15**,**17**, **22**: glutaric anhydride, DMAP, pyridine, 110 °C. For compounds **3**, **6**, **11**, **16**, **18**, **23**: adipic acid, EDCI, DIPEA, DMAP, DCM. For compounds **12**, **19**, and **24**: pimelic acid, EDCI, DIPEA, DMAP, DCM. For compounds **13** and **20**: suberic acid, EDCI, DIPEA, DMAP, DCM; (d) $NaBH_4$, $CeCl_3.7H_2O$, MeOH.

Biological results

The inhibitory effect of compounds **1**-**24** at 10 μM concentration was evaluated *in vitro* using the conversion of estradiol to estrone by purified recombinant 17β-HSD10. As standards, we used the known inhibitor AG18051 as the positive control and the published steroidal compounds[18] namely, pregnenolone, testosterone, dihydrotestosterone, androsterone, epiandrosterone, and dehydroepiandrosterone. Our study has shown that the uncharged steroids that were used as comparators were inactive or displayed a very low inhibitory efficiency in the assay (*Table S1*). These results reflect the results of study of Ayan et al.[18] although they used different (cellular) assay.

Further, we tested three series of steroidal compounds of 20-oxo-pregna(e)ne skeleton that differed at position C-5 by presence/absence of a double bond: *(i)* compounds **1**-**3** with 5α-stereochemistry, *(ii)* unsaturated compounds **4**-**6** with C-4,5 double bond (Δ^4 compounds), *(iii)* unsaturated compounds **7**-**10** with C-5,6 double bond (Δ^5 compounds). In the primary screening, only compound **10** demonstrated an inhibitory ability of approximately 50% at 10 μM concentration (**Figure 1**). Thus, considering the structure of

compound **10**, we have prepared Δ^5 compounds varying with the substituent at position C-17 with C-3 linker of various lengths: *(i)* Δ^5-20-oxo compounds **11**-**13** with longer C-3 linker than compound **10**, *(ii)* Δ^5-20-deoxy compounds **14**-**16** without 20-oxo substituent, *(iii)* Δ^5-17-oxo compounds **17**-**20** belonging to androstane family having C-17 substituent, *(iv)* Δ^5 compounds **21**-**24** without substituent at position C-17.

Interestingly, the structure-activity relationship revealed that compounds with lipophilic substitution at position C-17, namely **14**-**16** and **21**-**24** were the most active compounds in the study. In particular, steroids bearing 20-oxo (**1**-**13**) or 17-oxo substituent (**17**-**20**) demonstrated inhibitory ability ≤50% at 10 μM concentration except for compound **10** which demonstrated approximately ~50% inhibition. In contrast, decarbonylation at position C-20 (**14**-**16**) and position C-17 (**21**-**24**) afforded an inhibitory effect ≥50% at 10 μM concentration (**Figure 1**). Therefore, compounds **10**, **14**-**16**, and **21**-**24** were further described by their IC_{50} values. The results are summarized in **Table 1**. All tested compounds **10**, **14**-**16**, and **21**-**24** displayed inhibition with IC_{50} values varying from 5.59 μM (compound **23**) to 9.94 μM (compound **14**). Dose-response curves for the most potent inhibitors **22** (IC_{50} ~6.95 μM) and **23** (IC_{50} ~5.59 μM) are shown in *Figure S25A,B*. The most potent inhibitor **23** was also tested for its ability to inhibit 17β-HSD10 activity regardless of substrate. In particular, the oxidation of steroid allopregnanolone was also inhibited by compound **23** with IC_{50} ~15.25 μM. The dose-response curve is shown in *Figure S25C*.

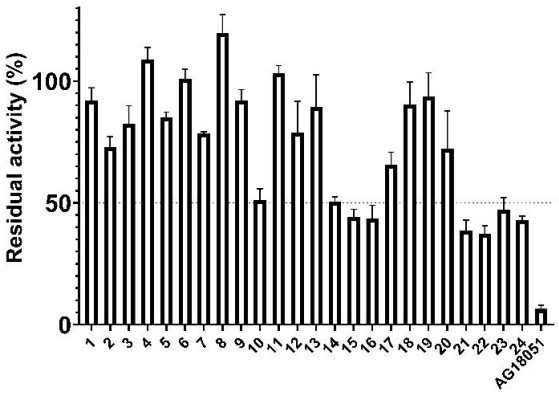

Figure 1. Evaluation of the inhibitory effect of compounds **1**-**24** and inhibitor AG18051 (standard) at 10 μM. Values represent means ± SD (n = 4).

Table 1. IC_{50} values for compounds **10**, **14**-**16**, and **21**-**24**. Values represent means ± SEM (n = 4).

Compound	IC_{50} (μM)
10	16.89 ± 1.33
14	9.94 ± 0.23
15	9.01 ± 0.43
16	9.29 ± 0.28
21	7.33 ± 0.45
22	6.95 ± 0.35
23	5.59 ± 0.25
24	7.17 ± 0.40
AG18051	0.09 ± 0.01[15]

It should be noted that the IC_{50} values determined in our experiments using the purified recombinant 17β-HSD10 cannot be directly compared with other published studies due to the strong dependency of IC_{50} value on various factors of the assay, i.e. the amount of enzyme, particular substrate, or other experimental conditions. For example, steroid inhibitor RM-532-46 has been demonstrated as a strong inhibitor with an IC_{50} value of 0.55 μM in the cellular assay using the HEK-293 cell line.[18] The study of Boutin et al.[19] used a method to a certain extent comparable to our assay (*in vitro* conditions, recombinant enzyme, identical substrate) described compound RM-532-46 with IC_{50} of 610 μM using 17β-estradiol and 235 μM using allopregnanolone as substrates. However, no standard (e.g. AG18051) was used in these studies. Structurally diverse inhibitors of 17β-HSD10 of the benzothiazolyl type have been described as compounds having IC_{50} values in the submicromolar to 1 μM concentration range. Only one compound (**26**) was able to achieve the potency of AG18051, namely a derivative of benzothiazole-based urea with the IC_{50} value of 0.07 μM. Unfortunately, this compound was identified as toxic for the HEK-293 cell line.[15]

The most potent inhibitor from the current series, compound **23** was further evaluated for the type of inhibition. The uninhibited enzymatic reaction (0 μM of **23**) was compared with the enzymatic reaction at three concentrations of compound **23** (3, 6 and 9 μM) using 17β-estradiol as the substrate. We have hypothesized that a compound of steroid origin could demonstrate a competitive mechanism of action. Such inhibitor binds the enzyme preventing the formation of the enzyme-substrate complex. Thus, the substrate concentration does not enhance the inhibitory ability. This hypothesis was confirmed by the kinetic experiment. The obtained data were linearized by using Hanes-Woolf plots (**Figure 2**).

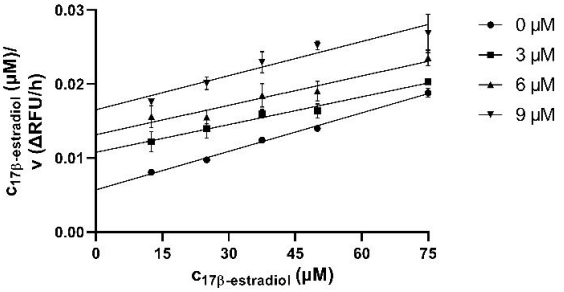

Figure 2: The kinetic inhibition of 17β-HSD10 using compound **23** at 0, 3, 6 and 9 μM concentration. Data are shown as mean ± SD (n = 3).

Considering the expected biological instability of hemiester group and lipophilicity of compounds **14**–**16** and **21**–**24**, the results permeability and plasma stability experiments were included in this study (**Table 2**).[31] According to the

literature, drugs with permeability coefficients greater than 1 x 10^{-6} cm/s in Caco-2 cells are expected to be completely absorbed in humans.[32, 33] Therefore, we conclude that compounds **14–16** and **21–24** display sufficient permeability. Given the presence of the metabolically unstable hemiester moiety, compounds **14–16** and **21–24** were expected to exhibit poor stability in both rat and human plasma. The stability was described as the percentage of parental compound remaining in plasma after 8 h. Surprisingly, all compounds **14–16** and **21–24**[31] demonstrated high stability in human plasma after the 8 h of incubation and mediocre to high stability in rat plasma (**Table 2**). We conclude that such unexpected stability in plasma offers new potential for the structure-activity relationship study targeting stability of hemiester moiety at position C-3.

Table 2. *In vitro* safety assessment and plasma stability of tested compounds **14–16** and **21–24.**

Compound	Caco-2 cell permeability (50 μM)	Rat plasma stability	Human plasma stability
	Papp (cm/s)	% remaining after 8 hours	
14	5.7×10^{-6}	55	100
15	1.9×10^{-6}	99	100
16	1.2×10^{-6}	43	94
21	1.0×10^{-4}	88	99
22	1.2×10^{-5}	57	98
23	3.1×10^{-6}	32	100
24	1.3×10^{-6}	38	100

Finally, because the strongest inhibitor identified *in vitro* compound **23** has a favorable permeability coefficient, its potency to inhibit 17β-HSD10 also at the cellular level was determined**.** First, it was necessary to exclude the possibility that higher concentrations of compound **23** could be unfavourable to cells. The effect of compound **23** on the cellular viability and cytotoxicity of this compound (1, 10, and 20 μM) were determined using CellTiter-Glo viability assay and CellTox Green assay, respectively on human embryonic kidney 293 cells (HEK-293). The data in **Figure 3** shows that compound **23** does not influence HEK-293 viability and is not toxic toward HEK-293 cells line up to concentration 20 μM.

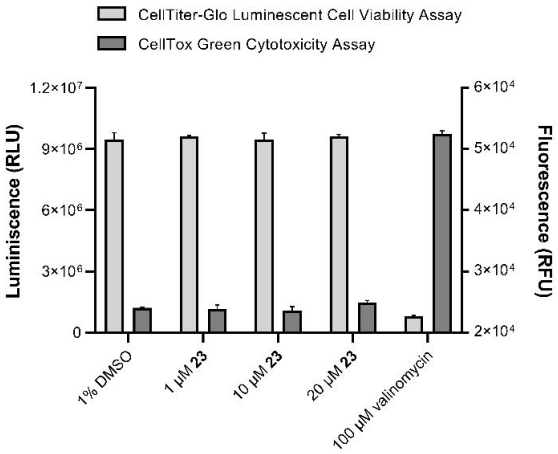

Figure 3: Viability of HEK-293 cells in the presence of compound **23** (measured by CellTiter-Glo Viability Assay) and its cytotoxic effect (measured by CellTox Green Assay). DMSO-treated cells were used as controls for cell viability. Valinomycin-treated cells were used as cytotoxicity controls. Data are presented as mean ± SD (n = 3).

Identical concentrations of compound **23** were used for fluorogenic cellular assay using a special probe (-)-CHANA as a substrate for 17β-HSD10 overexpressed in HEK-293 (HEK-293-HSD10 cell line).[15] These results demonstrate that compound **23** can inhibit 17β-HSD10 in such a more complex system. Its inhibition ability is dose-dependent and the highest concentration used (25 μM) leads to ~50% inhibition of the activity (**Figure 4**). The exact IC_{50} value at the cellular level was not possible to determine because of some method interferences as well as its unknown cytotoxic characteristics. Higher IC_{50} (> 20 μM) is in agreement with the high concentration of 17β-HSD10 in the model cell line.[15]

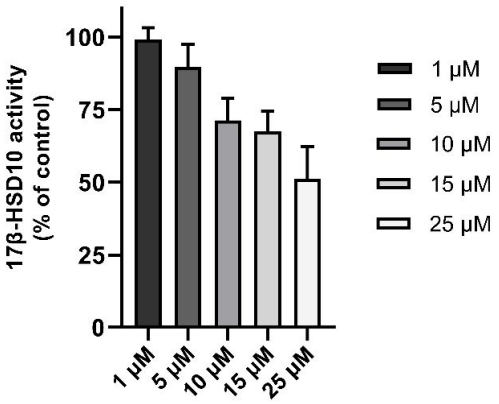

Figure 4. Inhibition of 17β-HSD10 by compound **23** in HEK-293 cellular model overexpressing 17β-HSD10 (HEK-293_HSD10). The activity of 17β-HSD10 was determined using a probe (-)-CHANA as a substrate, and the fluorescence of formed product CHANK was measured.

Values are given as mean ± SD from two biological replicates with three technical replicates.

The results of our study have described the structure-activity relationship for steroids with C-3 hemiester moiety to the inhibitory effect on 17β-HSD10 *in vitro*. We have show the ability of the non-toxic compound **23** to inhibit the target enzyme also on the cellular level, along with cellular permeability and stability in rat and human plasma.

Conclusions

Taken together, from the results of our study using both steroidal standards from Ayan et al.[18] and the standard inhibitor AG18051, it can be concluded that steroidal compounds of the androstane skeleton (**14**-**16** and **22**-**24**) bearing a lipophilic substitution at the position C-17 with a negatively charged hemiester moiety at C-3 of various lengths (C_2-C_7) demonstrate promising *in vitro* inhibitory potential and they could serve as a useful tool for further development of steroidal 17β-HSD10 inhibitors.

MATERIALS AND METHODS

Chemistry. All other commercial reagents and solvents were used without purification. Melting points were determined with a micromelting point apparatus (Hund/Wetzlar, Germany), and are uncorrected. For elemental analysis, PE 2400 Series II CHNS/O Analyzer (Perkin Elmer, MA, USA) was used, with microbalance MX5 (Mettler Toledo, Switzerland). For measurement of optical rotation, AUTOPOL IV (Rudolph Research Analytical, NJ, USA) was used, all samples were measured at 20 °C, at a given concentration in a given solvent at 589 nm. Proton and carbon NMR spectra were measured in a Bruker AVANCE III 400 MHz with chemical shifts given in parts per million (ppm δ, relative to residual $CDCl_3$ peak at 7.260 and 77.160 ppm for 1H and 13C nuclei, respectively). Coupling constants (J) are given in Hz. The HRMS spectra were performed with LTQ Orbitrap XL (Thermo Fischer Scientific, MA, USA) in ESI mode. Thin-layer chromatography (TLC) was performed on silica gel (Merck, 60 μm) and visualized with phosphomolybdic acid/ethanol stain. For flash chromatography, puriFlash 5.250 instrument (Interchim, France) was used, with neutral silica gel (Merck, 40–63 μm) and an ELSD detector. Analytical samples were dried over phosphorus pentoxide at 25 °C/0.25 kPa.

General Procedure I: Synthesis of Steroidal Hemiesters from Anhydrides. A mixture of steroid (1 mmol) and dicarboxylic acid anhydride (6 eq) was dried overnight at 50 °C. Then, dry pyridine (12 mL) and DMAP (0.24 eq) were added. The mixture was stirred at 110 °C for 6 h under an inert atmosphere. The reaction mixture was then poured into water and extracted with DCM. Combined organic extracts were washed with brine and dried over sodium sulfate. Solvents were evaporated, and the residue was purified on a column of silica gel.

General Procedure II: Synthesis of Steroidal Hemiesters from ω-Dicarboxylic Acids. A solution of steroid (1 mmol) in dry DCM (5 mL) was added under an inert atmosphere to a solution of dicarboxylic acid (2 mmol), EDCI (2 mmol), DIPEA (2 mmol), and DMAP (0.24 eq) in dry DCM (10 mL) at 0 °C while stirring. The reaction mixture was stirred at room temperature for 18 h. The solvents were then evaporated and the residue was dissolved with DCM, washed with water, dried over sodium sulfate, and concentrated in vacuo. Purification on a column of silica gel gave the desired steroidal hemiester.

*20-Oxo-5α-pregnan-3β-yl Hemisuccinate (**1**).* Compound **1** was prepared according to *General Procedure I.* Starting from compound 3β-hydroxy-5α-pregnan-20-one **25** (318.5 mg, 1.0 mmol), compound **1** (270 mg, 65%) was obtained as a white solid by column chromatography (30–50% ethyl acetate in petroleum ether): m.p. 196-198 °C (toluene); $[\alpha]_D^{20}$ +70.6 (*c* 0.2, $CHCl_3$). ^{1}H NMR (400 MHz, $CDCl_3$): δ 0.60 (s, 3H, H-18), 0.82 (3H, s, H-19), 2.11 (3H, s, H-21), 2.52 (1H, t, *J* = 8.9, H-17), 2.63 (4H, m, H-2´ and H-3´), 4.72 (1H, tt, J_1 = 11.3, J_2 = 4.9, H-3). ^{13}C NMR (101 MHz, $CDCl_3$): δ 209.96, 177.46, 171.84, 74.34, 63.96, 56.76, 54.20, 44.77, 44.390, 39.15, 36.86, 35.64, 35.59, 34.00, 32.05, 31.68, 29.41, 29.05, 28.58, 27.49, 24.54, 22.94, 21.34, 13.60, 12.35. IR spectrum ($CHCl_3$): 1727, 1716, 1702 (C=O); 1179 (C-O). MS ESI *m/z*: 417.2 (100%, M - 1), 418.3 (32%, M). HR-MS (ESI) *m/z* for $C_{25}H_{37}O_5$ [M - 1] calcd. 417.26465, found 417.26475. For $C_{25}H_{38}O_5$ (418.6) calcd: 71.74%, C; 9.15% H. Found: 71.70%, C; 9.22%, H.

*20-Oxo-5α-pregnan-3β-yl Hemiglutarate **2**.* Compound **2** was prepared according to *General Procedure I.* Starting from compound 3β-hydroxy-5α-pregnan-20-one **25** (318.5 mg, 1.0 mmol), compound **2** (195 mg, 45%) was obtained as a white solid by column chromatography (30–50% ethyl acetate in petroleum ether): m.p. 165-167 °C (EtOAc); $[\alpha]_D^{20}$ 63.9 (*c* 0.310, $CHCl_3$). ^{1}H NMR (400 MHz, $CDCl_3$): δ 0.60 (3H, s, H-18), 0.82 (3H, s, H-19), 1.94 (2H, p, *J* = 7.3, H-3´), 2.11 (3H, s, H-21), 2.36 (2H, t, *J* = 7.3, H-2´), 2.42 (2H, p, *J* = 7.3, H-4´), 2.52 (1H, t, *J* = 9.0, H-17), 4.70 (1H, tt, J_1 = 11.4, J_2 = 4.9, H-3). ^{13}C NMR (101 MHz, $CDCl_3$): δ 209.96, 178.30, 172.58, 73.90, 63.96, 56.76, 54.21, 44.78, 44.39, 39.15, 36.88, 35.65, 35.59, 34.10, 33.72, 33.01, 32.05, 31.68, 28.59, 27.59, 24.54, 22.93, 21.34, 20.08, 13.60, 12.36. IR spectrum ($CHCl_3$): 1722, 1711, 1703 (C=O); 1192 (C-O). MS ESI *m/z*: 431.3 (100%, M - 1), 432.3 (32%, M). HR-MS (ESI) *m/z* for $C_{26}H_{39}O_5$ [M - 1] calcd. 431.28030, found 431.27994. For $C_{26}H_{40}O_5$ (432.6) calcd: 72.19%, C; 9.32% H. Found: 71.95%, C; 9.40%, H.

*20-Oxo-5α-pregnan-3β-yl Hemiadipate (**3**).* Compound **3** was prepared according to *General Procedure II.* Starting from compound 3β-hydroxy-5α-pregnan-20-one **25** (318.5 mg, 1.0 mmol), compound **3** (416 mg, 93%) was obtained as a white solid by column chromatography (20–30% ethyl acetate in petroleum ether): m.p. 127-130 °C (EtOAc); $[\alpha]_D^{20}$ 60.1 (*c* 0.284, $CHCl_3$). ^{1}H NMR (400 MHz, $CDCl_3$): δ 0.60 (3H, s, H-18), 0.82 (3H, s, H-19), 2.11(3H, s, H-21), 2.25-2.41 (4H,

m, H-2´ and H-5´), 2.52 (1H, t, J = 8.9, H-17), 4.70 (1H, tt, J_1 = 11.4, J_2 = 4.9, H-3). ^{13}C NMR (101 MHz, $CDCl_3$): δ 209.94, 178.66, 173.03, 73.73, 63.96, 56.76, 54.22, 44.78, 44.39, 39.16, 36.89, 35.65, 35.60, 34.42, 34.11, 33.63, 32.05, 31.68, 28.60, 27.59, 24.54, 24.21, 22.93, 21.34, 13.60, 12.36. IR spectrum ($CHCl_3$): 1723, 1709, 1704 (C=O); 1191, 1182 (C-O). MS ESI *m/z*: 445.3 (100%, M - 1), 446.3 (30%, M). HR-MS (ESI) *m/z* for $C_{27}H_{41}O_5$ [M - 1] calcd. 445.29595, found 445.29586. For $C_{27}H_{42}O_5$ (446.6) calcd: 72.61%, C; 9.48% H. Found: 72.82%, C; 9.61%, H.

*20-Oxo-pregn-4-en-3β-yl Hemisuccinate **4**.* Compound **4** was prepared according to *General Procedure I.* Starting from compound 3β-hydroxy-pregn-4-en-20-one **26** (316.5 mg, 1.0 mmol), compound **4** (166 mg, 40%) was obtained as a white solid by column chromatography (10–20% ethyl acetate in petroleum ether): m.p. 172-174 °C (EtOAc-*n*-heptane); $[\alpha]_D^{20}$ 64.3 ($_c$ 0.213, $CHCl_3$). ^{1}H NMR (400 MHz, $CDCl_3$): δ 0.63 (s, 3H, H-18), 1.06 (3H, s, H-19), 2.11 (3H, s, H-21), 2.52 (1H, t, J = 8.9, H-17), 2.65 (4H, m, H-2´ and H-3´), 5.22 (1H, m, H-4), 5.26 (1H, m, H-3). ^{13}C NMR (101 MHz, $CDCl_3$): δ 209.80, 177.10, 172.18, 149.41, 119.17, 71.49, 63.82, 56.43, 54.18, 44.24, 38.99, 37.45, 35.99, 35.06, 32.98, 32.23, 31.67, 29.39, 28.98, 25.12, 24.54, 22.94, 21.13, 18.95, 13.51. IR spectrum ($CHCl_3$): 1717, 1700 (C=O); 1659 (C=C); 1184, 1111 (C-O). MS ESI *m/z*: 415.3 (100%, M - 1), 416.3 (30%, M). HR-MS (ESI) *m/z* for $C_{25}H_{35}O_5$ [M - 1] calcd. 415.24900, found 415.24879. For $C_{25}H_{36}O_5$ (416.6) calcd: 72.08%, C; 8.71% H. Found: 72.29%, C; 8.63%, H.

*20-Oxo-pregn-4-en-3β-yl Hemiglutarate **5**.* Compound **5** was prepared according to *General Procedure I.* Starting from compound 3β-hydroxy-pregn-4-en-20-one **26** (316.5 mg, 1.0 mmol), compound **5** (265 mg, 62%) was obtained as a white solid by column chromatography (15–30% ethyl acetate in petroleum ether): m.p. 138-140 °C (EtOAc-n-heptane); $[\alpha]_D^{20}$ 67.4 (*c* 0.224, $CHCl_3$). ^{1}H NMR (400 MHz, $CDCl_3$): δ 0.63 (3H, s, H-18), 1.06 (3H, s, H-19), 1.96 (2H, p, J = 7.3, H-3´), 2.11(3H, s, H-21), 2.39 (2H, t, J = 7.3, H-2´), 2.44 (2H, t, J = 7.3, H-4´), 2.52 (1H, t, J = 8.9, H-17), 5.21 (1H, m, H-4), 5.24 (1H, m, H-3). ^{13}C NMR (101 MHz, $CDCl_3$): δ 209.81, 177.99, 172.89, 149.32, 119.33, 71.08, 63.82, 56.43, 54.20, 44.24, 38.99, 37.45, 35.99, 35.12, 33.68, 32.98, 32.96, 32.25, 31.67, 25.22, 24.54, 22.93, 21.12, 20.05, 18.95, 13.51. IR spectrum ($CHCl_3$): 1722, 1711 (C=O); 1661 (C=C); 1189, 1111 (C-O). MS ESI *m/z*: 429.3 (100%, M - 1), 430.3 (35%, M). HR-MS (ESI) *m/z* for $C_{26}H_{37}O_5$ [M - 1] calcd. 429.26465, found 429.26446. For $C_{26}H_{38}O_5$ (430.6) calcd: 72.53%, C; 8.90% H. Found: 72.34%, C; 8.79%, H.

*20-Oxo-pregn-4-en-3β-yl Hemiadipate **6**.* Compound **3** was prepared according to *General Procedure II.* Starting from compound 3β-hydroxy-pregn-4-en-20-one **26** (318.5 mg, 1.0 mmol), compound **6** (231 mg, 51%) was obtained as a white solid by column chromatography (15–30% ethyl acetate in petroleum ether): m.p. 91-93 °C (EtOAc-*n*-heptane); $[\alpha]_D^{20}$ 60.7 (*c* 0.201, $CHCl_3$). ^{1}H NMR (400 MHz, $CDCl_3$): δ 0.63 (3H, s, H-18), 1.06 (3H, s, H-19), 2.11 (3H, s, H-21), 2.33 (2H, m, H-2´), 2.38 (2H, m, H-5´), 2.52 (1H, t, J = 8.9, H-17), 5.22 (1H, m, H-4), 5.24 (1H, m, H-3). ^{13}C NMR (101 MHz, $CDCl_3$): δ 209.80, 178.39, 173.32, 149.24, 119.42, 70.92, 63.82, 56.43, 54.22, 44.24, 39.00, 37.45, 36.00, 35.14, 34.39, 33.58, 32.98, 32.25, 31.67, 25.23, 24.54, 24.51, 24.24, 22.93, 21.12, 18.94, 13.51. IR spectrum ($CHCl_3$): 1750, 1720, 1709 (C=O); 1661 (C=C); 1183, 1111 (C-O). MS ESI *m/z*: 443.3 (100%, M - 1), 444.3 (34%, M). HR-MS (ESI) *m/z* for $C_{27}H_{39}O_5$ [M - 1] calcd. 443.28030, found 443.28004. For $C_{27}H_{40}O_5$ (444.6) calcd: 72.94%, C; 9.07% H. Found: 72.56%, C; 8.82%, H.

*20-Oxo-pregn-5-en-3β-yl Hemioxalate **7**.* Compound **7** was prepared from pregnenolone according to the literature.[34]

*20-Oxo-pregn-5-en-3β-yl Hemimalonate **8**.* Compound **8** was prepared from pregnenolone according to the literature.[34]

*20-Oxo-pregn-5-en-3β-yl Hemisuccinate **9**.* Compound **9** was prepared from pregnenolone according to the literature.[34]

*20-Oxo-pregn-5-en-3β-yl Hemiglutarate **10**.* Compound **10** was prepared from pregnenolone according to the literature.[34]

*20-Oxo-pregn-5-en-3β-yl Hemiadipate **11**.* Compound **11** was prepared from pregnenolone according to the literature.[34]

*20-Oxo-pregn-5-en-3β-yl Hemipimelate **12**.* Compound **12** was prepared from pregnenolone according to the literature.[34]

*20-Oxo-pregn-5-en-3β-yl Hemisuberate **13**.* Compound **13** was prepared from pregnenolone according to the literature.[34]

*Pregn-5-en-3β-yl Hemisuccinate **14**.* Compound **14** was prepared from 3β-hydroxy-pregn-5-en-20-one according to the literature.[34]

*Pregn-5-en-3β-yl Hemiglutarate **15**.* Compound **15** was prepared from 3β-hydroxy-pregn-5-en-20-one according to the literature.[34]

*Pregn-5-en-3β-yl Hemiadipate **16**.* Compound **16** was prepared from 3β-hydroxy-pregn-5-en-20-one according to the literature.[34]

*17-Oxo-androst-5-en-3β-yl Hemiglutarate **17**.* Compound **17** was prepared from dehydroepiandrosterone according to the literature.[34]

*17-Oxo-androst-5-en-3β-yl Hemiadipate **18**.* Compound **18** was prepared from dehydroepiandrosterone according to the literature.[34]

*17-Oxo-androst-5-en-3β-yl Hemipimelate **19**.* Compound **19** was prepared from dehydroepiandrosterone according to the literature.[34]

*17-Oxo-androst-5-en-3β-yl Hemisuberate **20**.* Compound **20** was prepared from dehydroepiandrosterone according to the literature.[34]

*Androst-5-en-3β-yl Hemisuccinate **21**.* Compound **21** was prepared from androst-5-en-3β-ol according to the literature.[34]

*Androst-5-en-3β-yl Hemiglutarate **22**.* Compound **22** was prepared from androst-5-en-3β-ol according to the literature.[34]

*Androst-5-en-3β-yl Hemiadipate **23**.* Compound **23** was prepared from androst-5-en-3β-ol according to the literature.[34]

*Androst-5-en-3β-yl Hemipimelate **24**.* Compound **24** was prepared from androst-5-en-3β-ol according to the literature.[34]

*3β-Hydroxy-5α-pregnan-20-one **25**.* Compound **25** was prepared from commercially available pregnenolone according to the literature.[26, 27]

*3β-Hydroxy-pregn-4-en-20-one **26**.* Compound **26** was prepared according to the literature.[28] Progesterone (3.14 g, 10.0 mmol) was added with cerium chloride heptahydrate (3.73 g, 10.0 mmol, 1 eq) to an oven-dried three-necked 250 mL round-bottom flask with a thermometer. Methanol (100 mL) was added under argon and the solution was chilled to -20 °C. Sodium borohydride (0.189 g, 5 mmol, 0.5 eq) was then added in bulk. The solution temperature raised briefly up to -16 °C. After 15 minutes, 37 mL acetone was added, and the solution was warmed to ambient temperature. Water (25 mL) was added, and the solvent volume was reduced by approximately 100 mL. Ether was added, along with more water, which caused the solution to become clear and colourless. The aqueous layer was extracted with ether (3 x 30 mL). The organic layers were combined, washed with brine, dried, filtered, and concentrated. The crude material was purified by column chromatography (20−25% ethyl acetate in petroleum ether) affording 1.57 g (50%) of **26**. The purity and identity of compound **26** were confirmed by ^{1}H NMR which was identical with the literature. ^{1}H NMR (400 MHz, $CDCl_3$): δ 0.63 (s, 3 H, s, H-18), 1.05 (3H, s, H-19), 2.11 (3H, s, H-21), 2.51 (1H, t, *J* = 9.0, H-17), 4.12-4.18 (1H, m, H-3), 5.29 (1H, d, *J* = 1.8, H-4). Therefore, compound **26** was used in further synthesis without further characterization.

Biology.

Chemicals. 17β-estradiol, NAD^+, benzonase, lysozyme, and anhydrous DMSO were purchased from Sigma-Aldrich. cOmplete™ EDTA-free protease inhibitor cocktail was obtained from Roche. Allopregnanolone was purchased from Tocris Bioscience. All other chemicals and reagents were of the highest commercially available purity.

Production and purification of human recombinant. 17β-HSD10 was performed as described previously.[11] Briefly, the autoinduction and overexpression were performed at 25 °C for 18 h in E. coli BL21 (DE3) strain. The bacterial pellet resuspended in lysis buffer [50 mM sodium phosphate buffer, 150 mM NaCl, and 10 mM imidazole (pH 8.0) with 1 mg/mL lysozyme, 150 U/mL benzonase, and complet EDTA-free protease inhibitor cocktail] was incubated on ice for 20 min and sonicated (12 × 10 s pulses with 30 s pauses). After centrifugation (16 000× g, 10 min, 4°C), the supernatant was applied to the Ni-NTA agarose resin and incubated on ice for 1 h with gentle stirring. The resin was washed three times with 10 mL of washing buffer I [50 mM sodium phosphate buffer, 150 mM NaCl, and 20 mM imidazole (pH 8.0)], followed by 3 × 10 mL of washing buffer II [50 mM sodium phosphate buffer, 150 mM NaCl, and 40 mM imidazole (pH 8.0)] and elution was performed using elution buffer [50 mM sodium phosphate buffer, 150 mM NaCl, and 250 mM imidazole (pH 8.0)]. The elution buffer was exchanged for storage buffer [71 mM Tris-HCl, 214 mM NaCl (pH 8.0)] using Amicon Ultra-4 Centrifugal Filter Unit (10 000 MWCO). The enzyme was stored at −80 °C. The protein concentration was determined by the Bradford assay and the purity of 17β-HSD10 was confirmed by SDS-PAGE.

Inhibition of 17β-estradiol to estrone transformation. The standard steroids were screened at 1 μM and 10 μM concentrations, and the tested compounds and standard AG18051 were screened at 10 μM concentration to compare the ability to inhibit 17β-HSD10. For compounds with at least 50% inhibition of 17β-HSD10, the IC_{50} values were determined.

Steroid compounds were dissolved in anhydrous DMSO to a concentration of 5 mM and further diluted with DMSO to working concentrations. DMSO was used as a vehicle control and AG18051 was used as a control inhibitor. The enzyme activity was determined fluorometrically at 37 °C in the activity assay buffer [100 mM potassium phosphate buffer (pH 8.0)]. The general reaction mixture (200 μl per well) consisted of 25 μM 17β-estradiol (dissolved in DMSO), 500 μM NAD+ (dissolved in deionized water), 45 nM recombinant 17β-HSD10 and different concentrations of inhibitor (2.2% (v/v) final concentration of DMSO as solvent). Before the addition of substrate, the reaction mixture of enzyme, cofactor and inhibitor in the assay buffer was preincubated for 5 min at 37 °C. The increase of fluorescence (Ex/Em = 340/460 nm) due to the formation of NADH was monitored for 20 min (30 s intervals).

For IC_{50} value determination, dose-response inhibition at 11 different concentrations of inhibitor (0.6-33.75 μM) was determined and the data were analyzed by GraphPad Prism 8.4.3 (GraphPad Software Inc.). All measurements were performed in a tetraplicate.

Inhibition of allopregnanolone to 5α-dihydroprogesterone transformation. Compound **23** was dissolved in anhydrous DMSO to a concentration of 5 mM and further diluted with DMSO to working concentrations. DMSO was used as vehicle control. The enzyme activity was determined as described in the previous section, the only difference was the replacement of 25 μM 17β-estradiol with 20 μM allopregnanolone as 17β-HSD10 substrate. For IC_{50} value determination, dose-response inhibition at 10 different concentrations of inhibitor (0.16-33.75 μM) was determined and the data were analyzed by GraphPad Prism 8.4.3 (GraphPad Software Inc.). All measurements were performed in a tetraplicate.

Inhibition type determination. The type of inhibition of the compound **23** was determined with respect to the substrate 17β-estradiol. The inhibitor was determined at three different concentrations (3, 6, 9 μM) in combination with different concentrations of the 17β-estradiol (12.5-75 μM) and a saturated NAD^+ concentration (500 μM). DMSO was used as vehicle control. The obtained data were analyzed using GraphPad Prism 8.4.3 (GraphPad Software Inc.). All measurements were performed in triplicate.

Luminescent Cell Viability assay and CellTox Green cytotoxicity assay. HEK-293 cells were maintained in DMEM (Capricorn) supplemented with 10% fetal bovine serum (Gibco), 2 mM L-glutamine (Lonza) and non-essential amino acids additives (Gibco) at 37 °C, under a humidified atmosphere of 5% CO_2. Compound **23** was tested on the HEK-293 cell line to determine their cytotoxic

effects and impact on cell viability using CellTox Green (G8741, Promega) and CellTiter-Glo 2.0 kit (G9241, Promega), respectively. The measurements were performed as endpoint methods in the multiplex using a Tecan Spark 10M instrument. For multiplex measurement, 7500 cells were seeded per well in 50 µL of culture media and cultured for 24 h before the addition of selected compounds. Compound **23** was dissolved in anhydrous DMSO, further diluted in DMSO and added to the wells to obtain a final compound concentration of 1 and 10 µM (1 % (v/v) total concentration of DMSO in the reaction). The cells treated with 1% DMSO only were used as a vehicle control and 100 µM valinomycin treatment was used as a positive control. After the treatment, the cells were cultured for an additional 48 hours followed by the multiplex measurement. The measurements were performed in a white solid bottom 96 well microplates following the manufacturer's protocol. The fluorescent CellTox Green Cytotoxicity Assay was determined first (Ex/Em 485/530 nm) followed by the CellTiter-Glo Luminescent Cell Viability Assay with an integration time of 500 ms.

Fluorogenic assay for cellular inhibition of 17β-HSD10. A previously published cell line with overexpressed 17β-HSD10 (HEK-293_HSD10)[15] was used to measure 17β-HSD10 inhibition in the cellular environment. For this purpose, (-)-CHANA fluorogenic probe was used. The cells were seeded at a density of 1×10^4 cells per well in 200 µL of DMEM without phenol red (Gibco) supplemented with 10 % foetal bovine serum (Gibco), 2 mM L-glutamine, non-essential amino acids additives (Gibco) and 4.5 g/L glucose (Sigma) into black clear bottom 96-well plates (Brand, 781971). The cells were incubated for 20 h following the treatment with compound **23** dissolved in anhydrous DMSO or with DMSO only (vehicle control). After 2 hours of compound treatment, (-)-CHANA probe was added at the final concentration of 20 µM. The changes in fluorescent intensities were measured immediately after (-)-CHANA addition and 2 h later. The fluorescence intensities of the CHANK product were taken using the TECAN SPARK 10M instrument (Ex/Em = 380/525 nm). The residual 17β-HSD10 activity was calculated as ΔF between 2 h and 0 h after (-)-CHANA treatment and the data were normalized between non-treated HEK-293_HSD10 and native, non-transfected HEK-293 controls (using relative response ratio). The compound **23** was used at 1, 5, 10, 15 and 25 µM concentrations to detect the ability to penetrate the cells and to influence the 17β-HSD10 enzyme activity inside the cells.

ASSOCIATED CONTENT

Supporting Information

The Supporting Information is available free of charge on the ACS Publications website: ^{1}H and ^{13}C NMR spectra of compounds 1-6 (Figure S1 – Figure S12); HRMS spectra of compounds 1-6 (Figure S13 – Figure S18); LC-MS spectra of compounds 1-6 (Figure S19 – Figure S24); *In vitro* inhibitory potency of the steroidal comparators (Table S1); Dose-response curve for compound **23** and compound **22** (Figure S25) (PDF)

AUTHOR INFORMATION

Corresponding Authors

Eva Kudova – Eva Kudova Junior Research Group, Neurosteroids, Institute of Organic Chemistry and Biochemistry of the Czech Academy of Sciences, Flemingovo namesti 2, Prague 6, 166 10, Czech Republic; orcid.org/0000-0001-7131-5948; Phone: +420 220 183 273; Email: kudova@cas.uochb.cz

Lucie Zemanova – University of Hradec Kralove, Faculty of Science, Department of Chemistry, Rokitanskeho 62, 500 03 Hradec Kralove, Czech Republic; orcid.org/0000-0002-2732-5935; Phone: +420 493 332 776; Email: lucie.zemanova@uhk.cz

Present Addresses

†Michaela Hanzlova present address: Department of Preventive Medicine, Faculty of Medicine in Hradec Kralove, Charles University, Simkova 870, 530 03 Hradec Kralove, Czech Republic.

Author Contributions

The manuscript was written through the contributions of all authors. All authors have approved the final version of the manuscript. BS synthesized all tested compounds, MM evaluated the purity of all tested compounds, MH measured all enzymatic assays, AR measured cellular assays, KM revised the manuscript, EK wrote the manuscript and designed structures for synthesis, LZ wrote the manuscript and supervised all biological experiments.

Funding Sources

This work was supported by the Research Project of the AS CR RVO 61388963 and the University of Hradec Kralove, Faculty of Science, no. SV2103-2022.

ABBREVIATIONS

17β-HSD10, 17β-hydroxysteroid dehydrogenase type 10; AG18051, ((1-azepan-1-yl-2-phenyl-2-(4-thioxo-1,4-dihydropyrazolo [3–d] pyrimidin-5-yl)-ethanone); RM-532-46, {(3α,5α,17α)-3-Hydroxy-3-[4-(3-methoxybenzyl)piperazin-1-yl]methylandrostan-17-one}.

REFERENCES

(1) He, X.-Y.; Merz, G.; Yang, Y.-Z.; Mehta, P.; Schulz, H.; Yang, S.-Y. Characterization and localization of human type10 17b-hydroxysteroid dehydrogenase *Eur J Biochem* **2001**, *268*, 4899-4907.

(2) Wohlfarter, Y.; Eidelpes, R.; Yu, R. D.; Sailer, S.; Koch, J.; Karall, D.; Scholl-Bürgi, S.; Amberger, A.; Hillen, H. S.; Zschocke, J.; et al. ost in promiscuity? An evolutionary and biochemical evaluation of HSD10 function in cardiolipin metabolism. *Cell Mol Life Sci* **2022**, *79* (11), 562.

(3) He, X. Y.; Merz, G.; Mehta, P.; Schulz, H.; Yang, S. Y. Human brain short chain L-3-hydroxyacyl coenzyme A dehydrogenase is a single-domain multifunctional enzyme. Characterization of a novel 17beta-hydroxysteroid dehydrogenase. *J Biol Chem* **1999**, *274* (21), 15014-15019.

(4) Carlson, E. A.; Marquez, R. T.; Du, F.; Wang, Y.; Xu, L.; Yan, S. S. Overexpression of 17β-hydroxysteroid dehydrogenase type 10 increases pheochromocytoma cell growth and resistance to cell death. *BMC Cancer* **2015**, *15*, 166.
(5) Yang, S. Y.; He, X. Y.; Isaacs, C.; Dobkin, C.; Miller, D.; Philipp, M. Roles of 17β-hydroxysteroid dehydrogenase type 10 in neurodegenerative disorders. *J Steroid Biochem Mol Biol* **2014**, *143*, 460-472.
(6) Zhang, A.; Zhang, J.; Plymate, S.; Mostaghel, E. A. Classical and Non-Classical Roles for Pre-Receptor Control of DHT Metabolism in Prostate Cancer Progression. *Horm Cancer* **2016**, *7* (2), 104-113.
(7) Snaterse, G.; van Dessel, L. F.; van Riet, J.; Taylor, A. E.; van der Vlugt-Daane, M.; Hamberg, P.; de Wit, R.; Visser, J. A.; Arlt, W.; Lolkema, M. P.; et al. 11-Ketotestosterone is the predominant active androgen in prostate cancer patients after castration. *JCI Insight* **2021**, *6* (11).
(8) Salas, S.; Jézéquel, P.; Campion, L.; Deville, J. L.; Chibon, F.; Bartoli, C.; Gentet, J. C.; Charbonnel, C.; Gouraud, W.; Voutsinos-Porche, B.; et al. Molecular characterization of the response to chemotherapy in conventional osteosarcomas: predictive value of HSD17B10 and IFITM2. *Int J Cancer* **2009**, *125* (4), 851-860.
(9) Porcu, P.; Barron, A. M.; Frye, C. A.; Walf, A. A.; Yang, S. Y.; He, X. Y.; Morrow, A. L.; Panzica, G. C.; Melcangi, R. C. Neurosteroidogenesis Today: Novel Targets for Neuroactive Steroid Synthesis and Action and Their Relevance for Translational Research. *J Neuroendocrinol* **2016**, *28* (2), 12351.
(10) Vinklarova, L.; Schmidt, M.; Benek, O.; Kuca, K.; Gunn-Moore, F.; Musilek, K. Friend or enemy? Review of 17β-HSD10 and its role in human health or disease. *J Neurochem* **2020**, *155* (3), 231-249.
(11) Schmidt, M.; Benek, O.; Vinklarova, L.; Hrabinova, M.; Zemanova, L.; Chribek, M.; Kralova, V.; Hroch, L.; Dolezal, R.; Lycka, A.; et al. Benzothiazolyl Ureas are Low Micromolar and Uncompetitive Inhibitors of 17β-HSD10 with Implications to Alzheimer's Disease Treatment. *Int J Mol Sci* **2020**, *21* (6), 2059.
(12) Benek, O.; Hroch, L.; Aitken, L.; Dolezal, R.; Guest, P.; Benkova, M.; Soukup, O.; Musil, K.; Kuca, K.; Smith, T. K.; et al. 6-benzothiazolyl ureas, thioureas and guanidines are potent inhibitors of ABAD/17β-HSD10 and potential drugs for Alzheimer's disease treatment: Design, synthesis and in vitro evaluation. *Med Chem* **2017,** 14(7).
(13) Aitken, L.; Benek, O.; McKelvie, B. E.; Hughes, R. E.; Hroch, L.; Schmidt, M.; Major, L. L.; Vinklarova, L.; Kuca, K.; Smith, T. K.; et al. Novel Benzothiazole-based Ureas as 17β-HSD10 Inhibitors, A Potential Alzheimer's Disease Treatment. *Molecules* **2019**, *24* (15).
(14) Benek, O.; Vaskova, M.; Miskerikova, M.; Schmidt, M.; Andrys, R.; Rotterova, A.; Skarka, A.; Hatlapatkova, J.; Zdarova Karasova, J.; Hroch, L.; et al. Development of submicromolar 17β-HSD10 inhibitors and their in vitro and in vivo evaluation. *Eur J Med Chem* **2023**, *258*, 115593.
(15) Schmidt, M.; Vaskova, M.; Rotterova, A.; Benek, O.; Fiandova, P.; Miskerikova, M.; Zemanova, L.; Musilek, K. Physiologically relevant fluorescent assay for identification of 17β-HSD10 inhibitors. *J Neurochem* **2023**, *167* (2), 154-167.
(16) Kissinger, C. R.; Rejto, P. A.; Pelletier, L. A.; Thomson, J. A.; Showalter, R. E.; Abreo, M. A.; Agree, C. S.; Margosiak, S.; Meng, J. J.; Aust, R. M.; et al. Crystal structure of human ABAD/HSD10 with a bound inhibitor: implications for design of Alzheimer's disease therapeutics. *J Mol Biol* **2004**, *342* (3), 943-952.
(17) Morsy, A.; Maddeboina, K.; Gao, J.; Wang, H.; Valdez, J.; Dow, L. F.; Wang, X.; Trippier, P. C. Functionalized Allopurinols Targeting Amyloid-Binding Alcohol Dehydrogenase Rescue Aβ-Induced Mitochondrial Dysfunction. *ACS Chem Neurosci* **2022**, *13* (14), 2176-2190..
(18) Ayan, D.; Maltais, R.; Poirier, D. Identification of a 17β-hydroxysteroid dehydrogenase type 10 steroidal inhibitor: a tool to investigate the role of type 10 in Alzheimer's disease and prostate cancer. *ChemMedChem* **2012**, *7* (7), 1181-1184.
(19) Boutin, S.; Roy, J.; Maltais, R.; Alata, W.; Calon, F.; Poirier, D. Identification of steroidal derivatives inhibiting the transformations of allopregnanolone and estradiol by 17β-hydroxysteroid dehydrogenase type 10. *Bioorg Med Chem Lett* **2018**, *28* (22), 3554-3559..
(20) Boutin, S.; Maltais, R.; Roy, J.; Poirier, D. Synthesis of 17β-hydroxysteroid dehydrogenase type 10 steroidal inhibitors: Selectivity, metabolic stability and enhanced potency. *Eur J Med Chem* **2021**, *209*, 112909.
(21) Dilly, S. J.; Clark, A. J.; Marsh, A.; Mitchell, D. A.; Cain, R.; Fishwick, C. W. G.; Taylor, P. C. A chemical genomics approach to drug reprofiling in oncology: Antipsychotic drug risperidone as a potential adenocarcinoma treatment. *Cancer Lett* **2017**, *393*, 16-21.
(22) Metodieva, V.; Smith, T.; Gunn-Moore, F. The Mitochondrial Enzyme 17βHSD10 Modulates Ischemic and Amyloid-β-Induced Stress in Primary Mouse Astrocytes. *eNeuro* **2022**, *9* (5).
(23) Pinna, G.; Almeida, F. B.; Davis, J. M. Allopregnanolone in Postpartum Depression. *Front Glob Womens Health* **2022**, *3*, 823616.
(24) Cornett, E. M.; Rando, L.; Labbé, A. M.; Perkins, W.; Kaye, A. M.; Kaye, A. D.; Viswanath, O.; Urits, I. Brexanolone to Treat Postpartum Depression in Adult Women. *Psychopharmacol Bull* **2021**, *51* (2), 115-130.
(25) Lamb, Y. N. Ganaxolone: First Approval. *Drugs* **2022**, *82* (8), 933-940.
(26) Hamilton, N. M.; Dawson, M.; Fairweather, E. E.; Hamilton, N. S.; Hitchin, J. R.; James, D. I.; Jones, S. D.; Jordan, A. M.; Lyons, A. J.; Small, H. F.; et al. Novel steroid inhibitors of glucose 6-phosphate dehydrogenase. *J Med Chem* **2012**, *55* (9), 4431-4445.
(27) MacNevin, C. J.; Atif, F.; Sayeed, I.; Stein, D. G.; Liotta, D. C. Development and screening of water-

soluble analogues of progesterone and allopregnanolone in models of brain injury. *J Med Chem* **2009**, *52* (19), 6012-6023.
(28) Tserfas, M. O.; Levina, I. S.; Kuznetsov, Y. V.; Scherbakov, A. M.; Mikhaevich, E. I.; Zavarzin, I. V. Selective synthesis of the two main progesterone metabolites, 3α-hydroxy-5α-pregnanolone (allopregnanolone) and 3α-hydroxypregn-4-en-20-one, and an assessment of their effect on proliferation of hormone-dependent human breast cancer cells. *Russian Chem Bull* **2020**, *69*, 552-557.
(29) Kudova, E.; Chodounska, H.; Slavikova, B.; Budesinsky, M.; Nekardova, M.; Vyklicky, V.; Krausova, B.; Svehla, P.; Vyklicky, L. A New Class of Potent N-Methyl-D-Aspartate Receptor Inhibitors: Sulfated Neuroactive Steroids with Lipophilic D-Ring Modifications. *J Med Chem* **2015**, *58* (15), 5950-5966.
(30) Xu, S.; Toyama, T.; Nakamura, J.; Arimoto, H. One-pot reductive cleavage of exo-olefin to methylene with a mild ozonolysis-Clemmensen reduction sequence. *Tetrahedron Letters* **2010**, *51* (34), 4534-4537.
(31) Matousova, M.; Soucek, R.; Tloustova, E.; Slavikova, B.; Chodounska, H.; Mertlikova-Kaiserova, H.; Kudova, E. Pregn-5-en-3β-ol and androst-5-en-3β-ol dicarboxylic acid esters as potential therapeutics for NMDA hypofunction: In vitro safety assessment and plasma stability. *Steroids* **2019**, *147*, 4-9.
(32) Artursson, P.; Karlsson, J. Correlation between oral drug absorption in humans and apparent drug permeability coefficients in human intestinal epithelial (Caco-2) cells. *Biochem Biophys Res Commun* **1991**, *175* (3), 880-885.
(33) Rubas, W.; Jezyk, N.; Grass, G. M. Comparison of the permeability characteristics of a human colonic epithelial (Caco-2) cell line to colon of rabbit, monkey, and dog intestine and human drug absorption. *Pharm Res* **1993**, *10* (1), 113-118.
(34) Krausova, B.; Slavikova, B.; Nekardova, M.; Hubalkova, P.; Vyklicky, V.; Chodounska, H.; Vyklicky, L.; Kudova, E. Positive Modulators of the N-Methyl-d-aspartate Receptor: Structure-Activity Relationship Study of Steroidal 3-Hemiesters. *J Med Chem* **2018**, *61* (10), 4505-4516.

Table of Contents

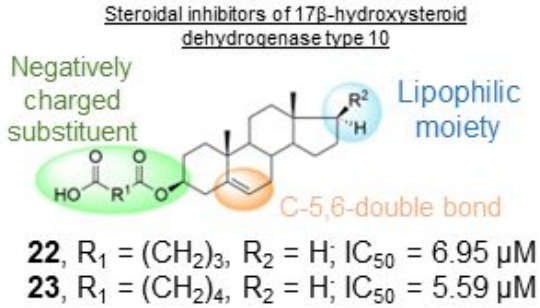

Supporting information

The C-3 steroidal hemiesters as inhibitors of 17β-hydroxysteroid dehydrogenase type 10

Michaela Hanzlova[a,†], Barbora Slavikova[b], Marina Morozovova[b], Kamil Musilek[a], Aneta Rotterova[a], Lucie Zemanová[a,*], Eva Kudova[b,*]

[a]Department of Chemistry, Faculty of Science, University of Hradec Kralove, Hradec Kralove, Czech Republic

[b]Institute of Organic Chemistry and Biochemistry, Czech Academy of Sciences, Flemingovo namesti 2, Prague 6, 166 10, Czech Republic

Table of Contents

1 Chemistry 2

1.1 ^{1}H and ^{13}C NMR spectra of compounds 1-6 2

1.2 HRMS spectra of compounds 1-6 8

1.3 LC-MS analysis of compounds 1-6 11

2 *In vitro* results 21

1 Chemistry

1.1 ^{1}H and ^{13}C NMR spectra of compounds 1-6

Figure S1. ^{1}H NMR spectra of compound **1**

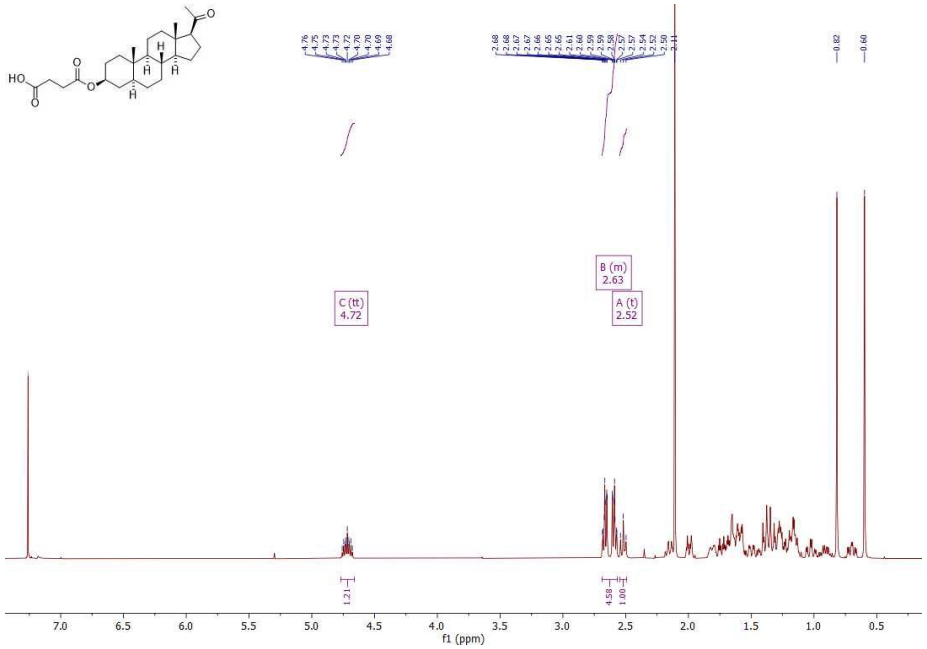

Figure S2. ^{13}C NMR spectra of compound **1**

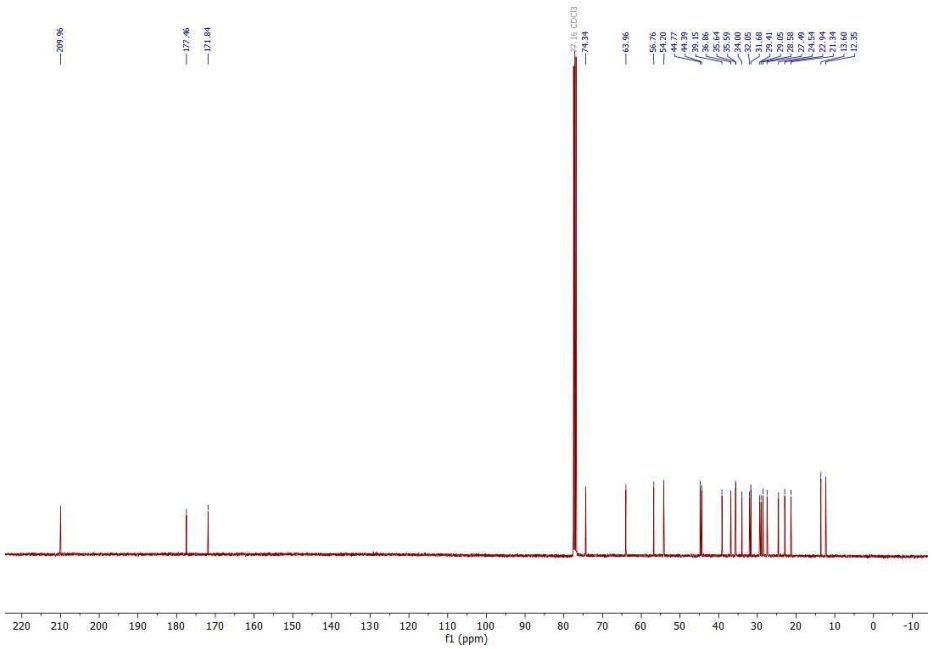

Figure S3. ^{1}H NMR spectra of compound **2**

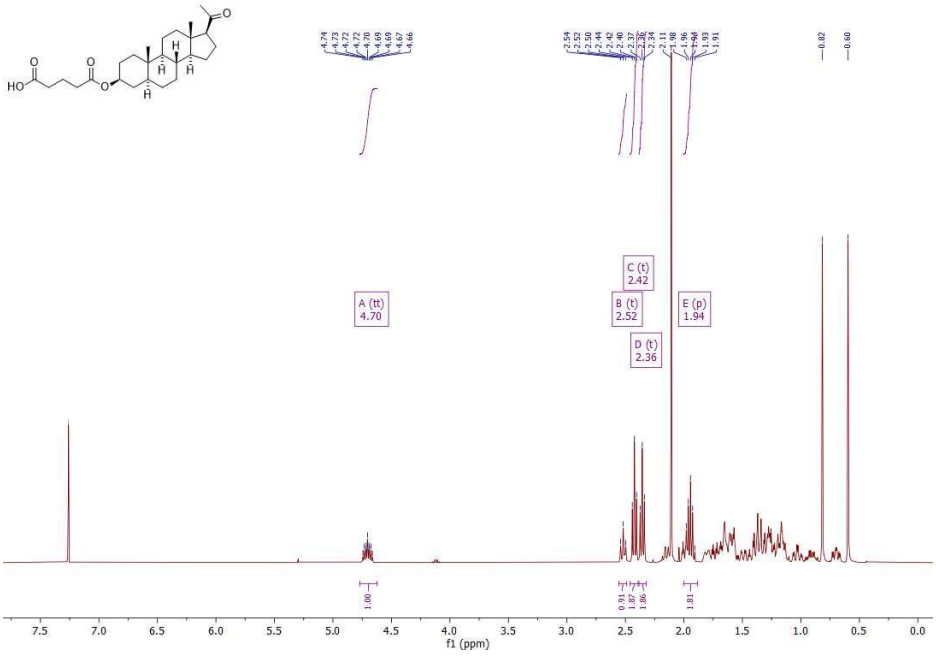

Figure S4. ^{13}C NMR spectra of compound **2**

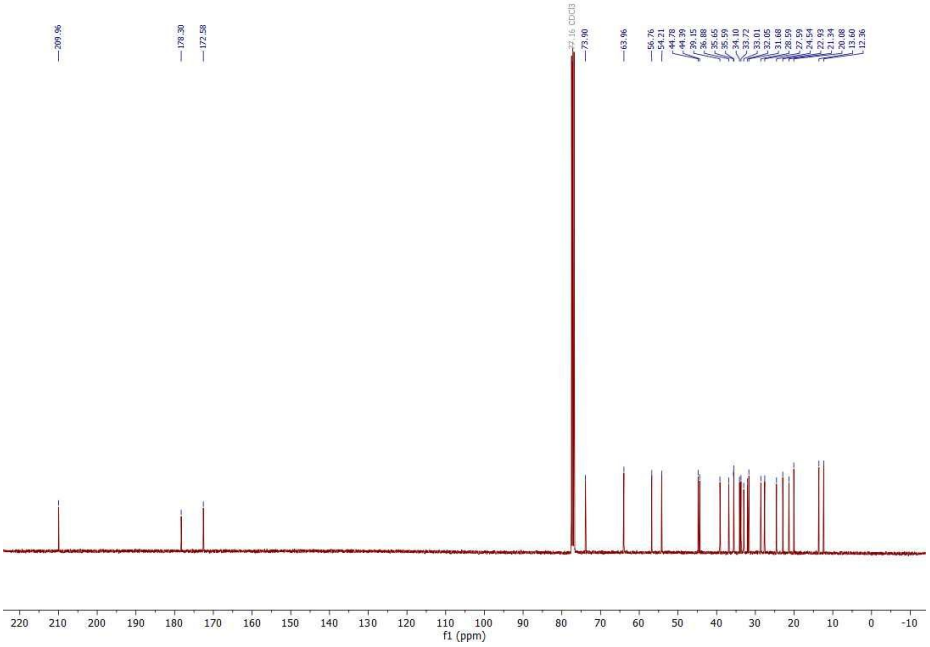

Figure S5. ^{1}H NMR spectra of compound **3**

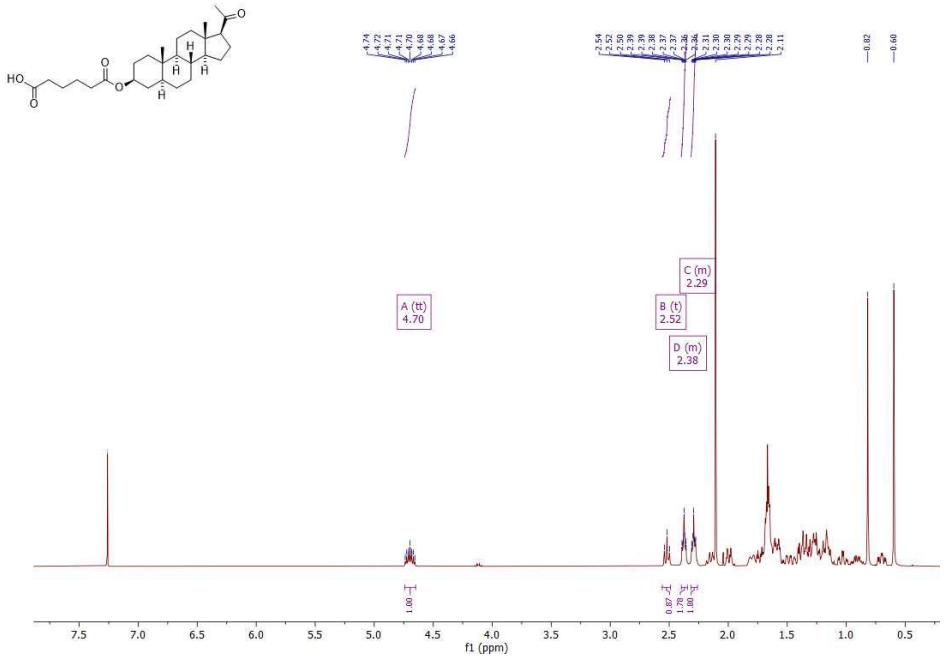

Figure S6. ^{13}C NMR spectra of compound **3**

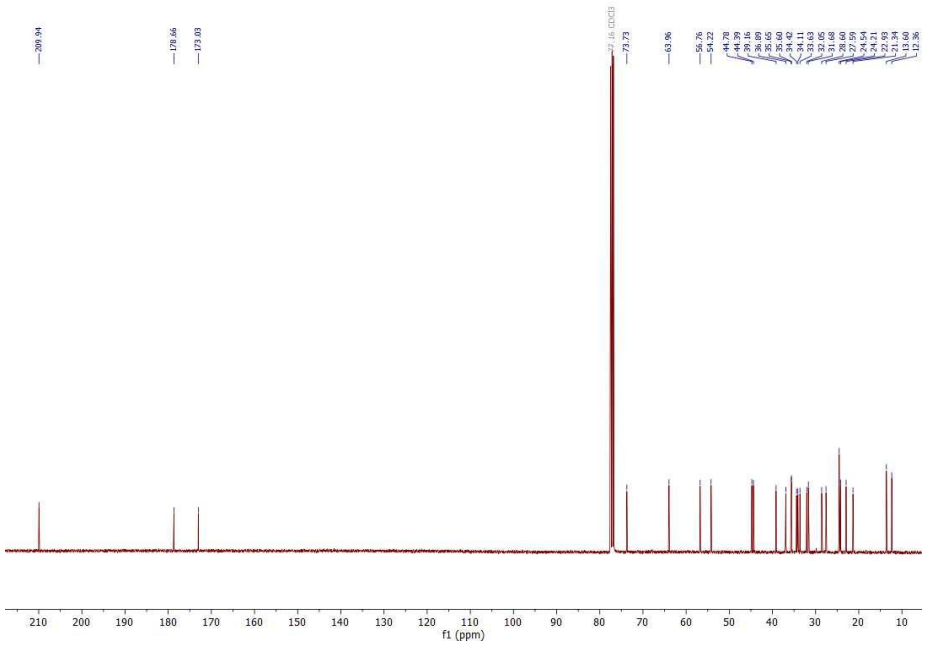

Figure S7. ^{1}H NMR spectra of compound **4**

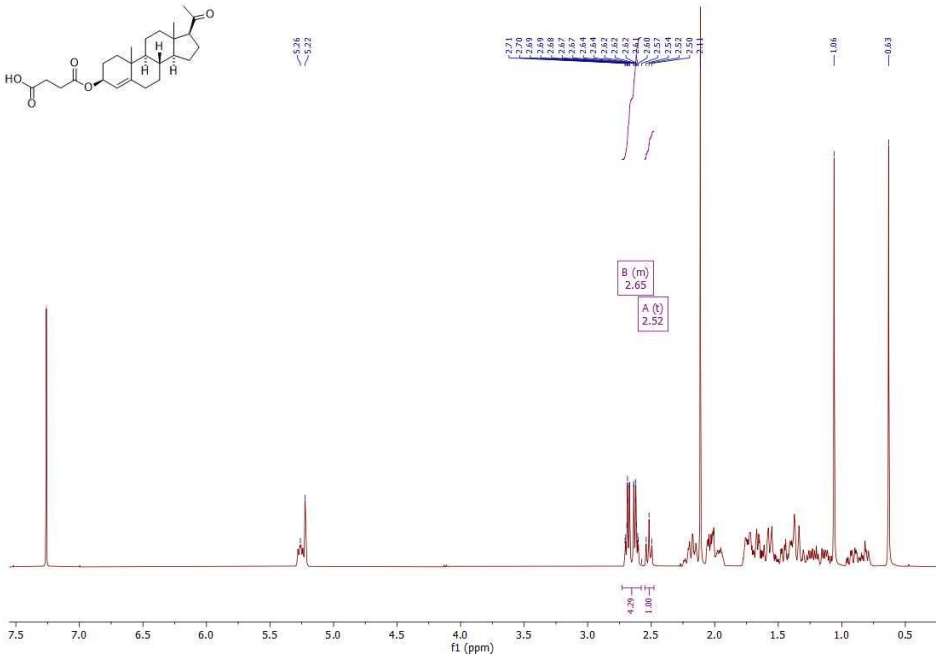

Figure S8. ^{13}C NMR spectra of compound **4**

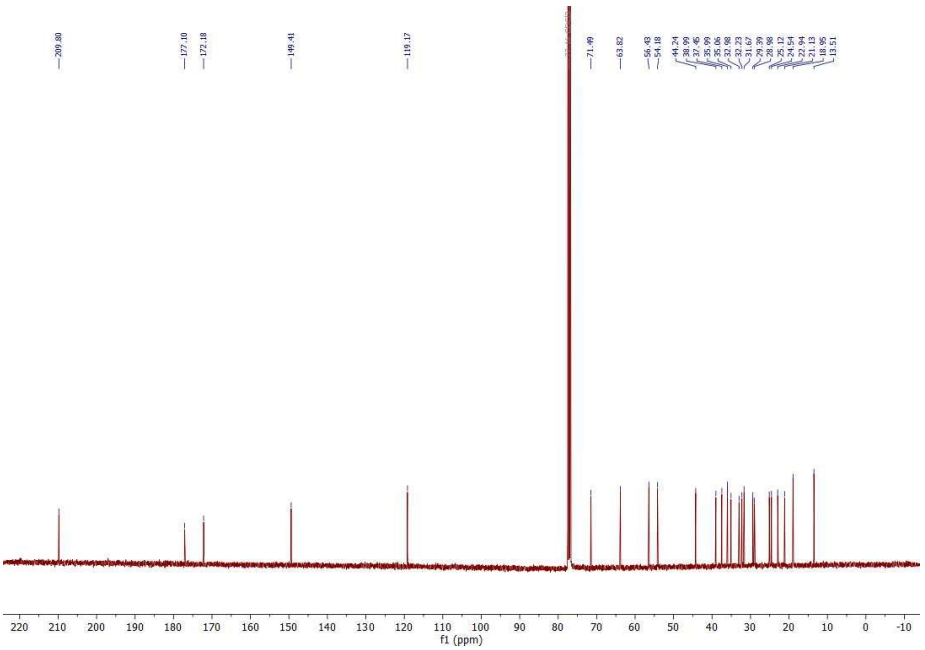

Figure S9. ^{1}H NMR spectra of compound **5**

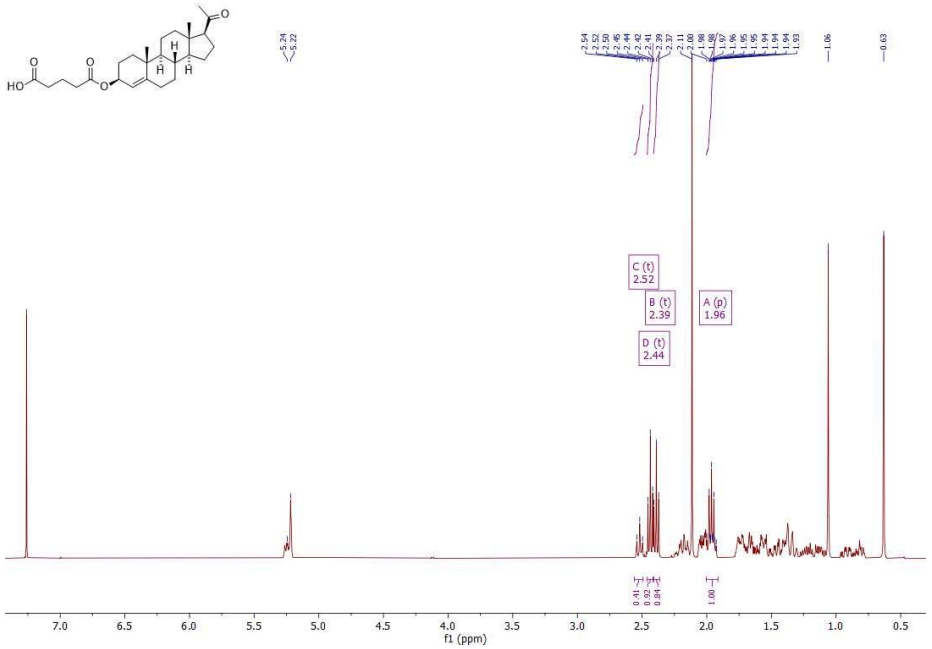

Figure S10. ^{13}C NMR spectra of compound **5**

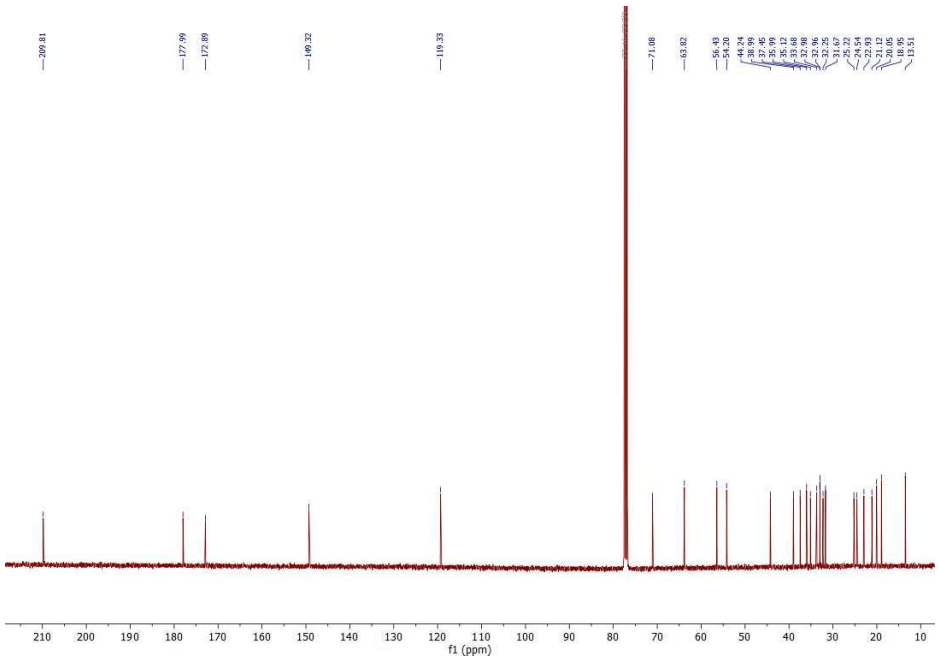

Figure S11. ^{1}H NMR spectra of compound **6**

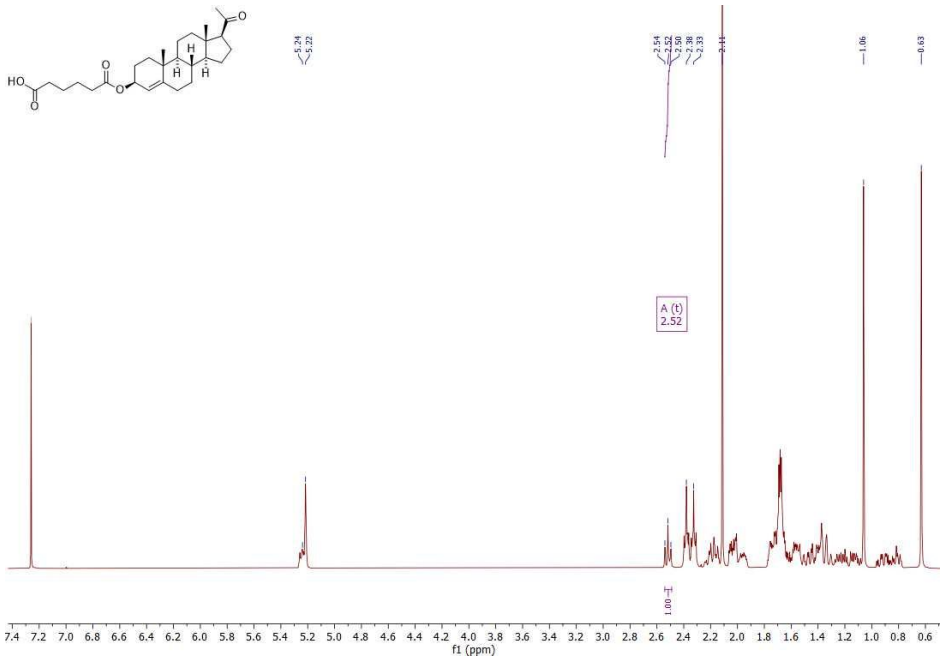

Figure S12. ^{13}C NMR spectra of compound **6**

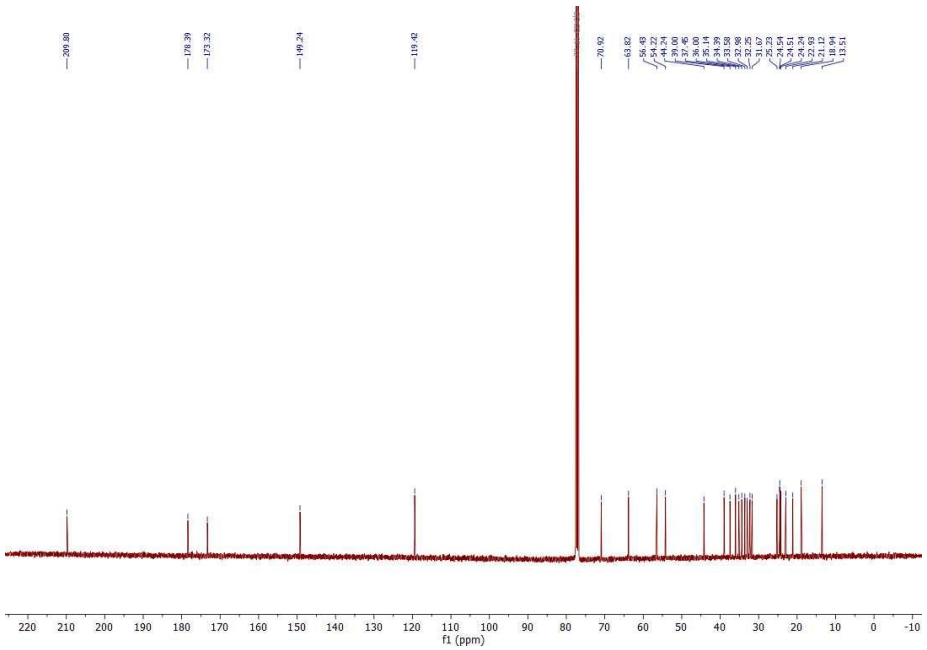

1.2 HRMS spectra of compounds 1-6

Figure S13. HRMS spectra of compound **1**

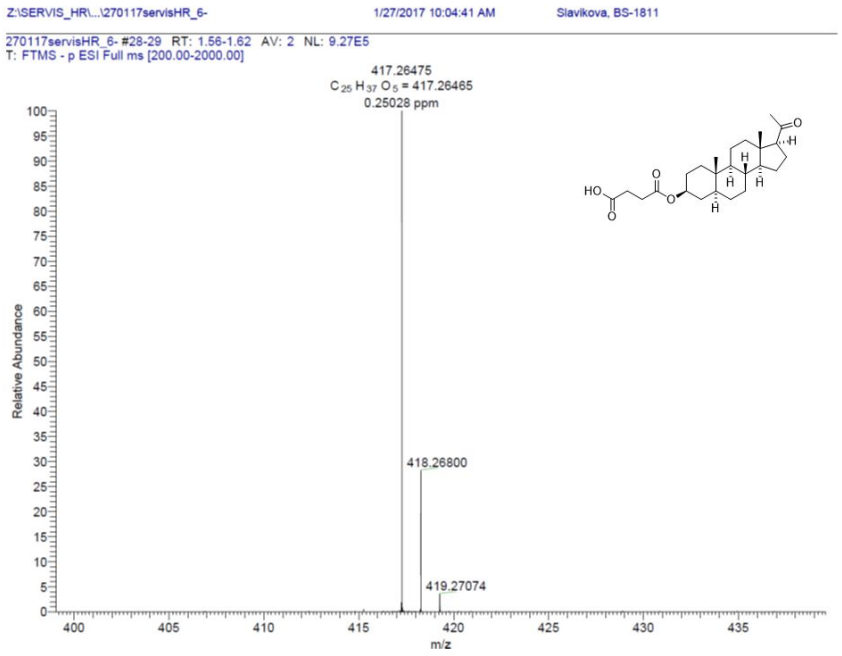

Figure S14. HRMS spectra of compound **2**

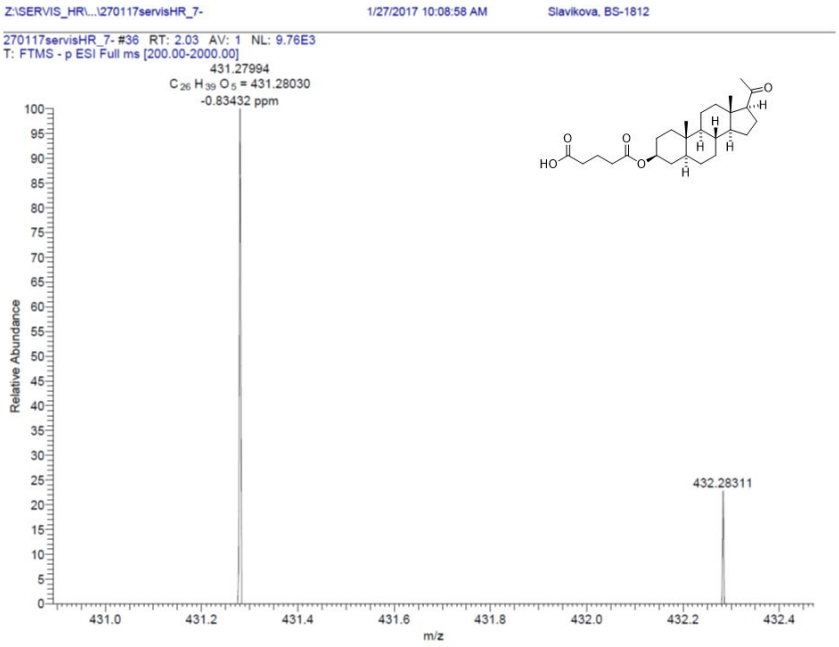

Figure S15. HRMS spectra of compound **3**

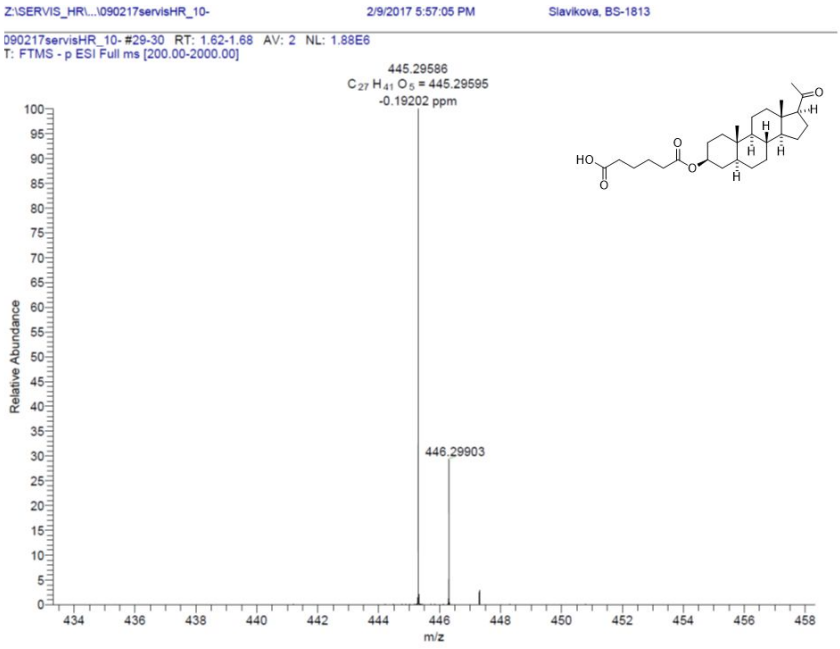

Figure S16. HRMS spectra of compound **4**

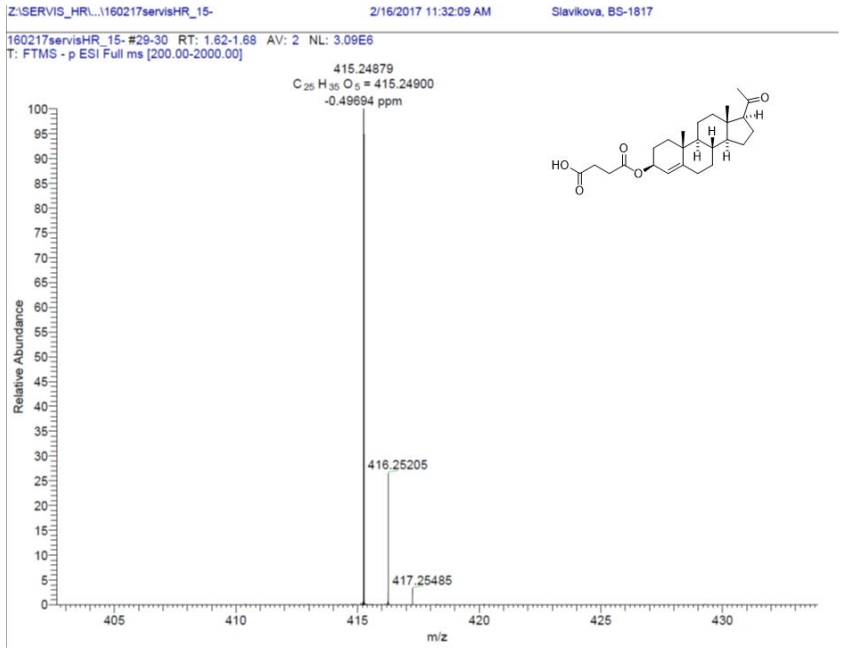

Figure S17. HRMS spectra of compound **5**

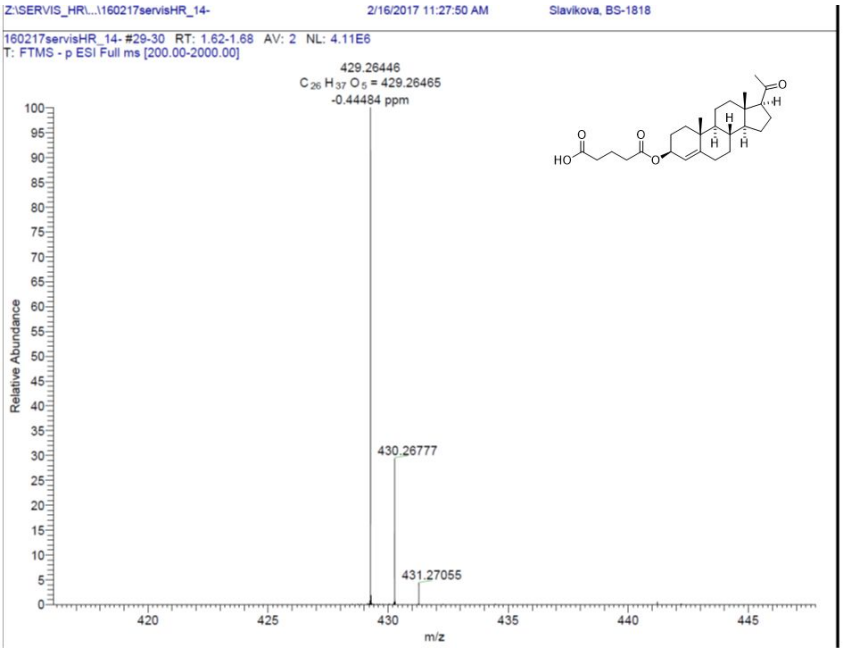

Figure S18. HRMS spectra of compound **6**

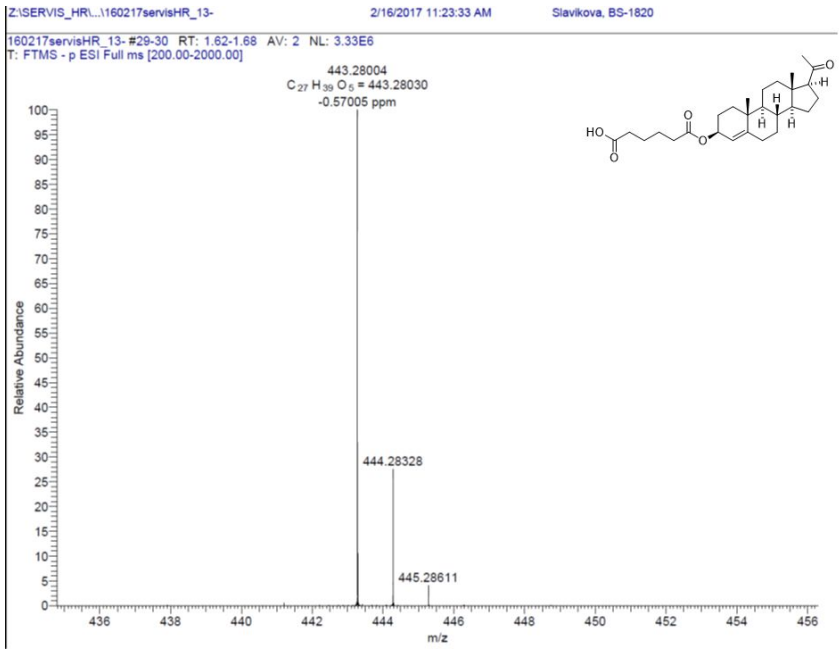

1.3 LC-MS analysis of compounds 1-6

Acetonitrile and methanol were of HPLC gradient grade, purchased from VWR Chemicals (Czech Republic) and Fisher Scientific (USA), formic acid (eluent additive for LC-MS; Fisher Scientific). Water for the HPLC mobile phase was purified by an ultrapure milli-Q water system (3P Synergy UV).

The analytical HPLC measurements were performed on Shimadzu (Tokyo, Japan) Nexera LC-40 equipped with a SCL-40 communication module, a two degasser units DGU- 403 and DGU-405, two LC-40 D X3 dual solvent delivery module, an autosampler and a thermostated column oven CTO-40S. The separation was performed using Shim-pack Scepter C8-120, 1.9 µm, 2.1x100mm (Shimadzu). The mobile phase of water/methanol/formic acid (95/5/1) (A) and acetonitrile (B) was used with isocratic elution. The flow rate of mobile phase was 0.6 ml/min , the temperature of the column was set to 40 °C, and the injection volume was 0.4 µL. An ELSD-LT II, evaporative light scattering detector (ELSD) (Shimadzu, Japan) was utilized for the analysis of the purity. The conditions for the analysis were 60 °C nebulization temperature by nitrogen and 10 the gain factor.

Mass spectrometric detection was performed on a single quadrupole LCMS-2020 (Shimadzu, Japan) with dual ion source by an electrospray ionization (ESI) probe, and simultaneously ionized by an atmospheric pressure chemical ionization (APCI) corona discharge needle located below the ESI outlet. All acquisitions were performed in both positive and negative ionization mode. The nebulizing gas had flow 1.5 L/min, the drying gas was set to 15 L/min, corona needle voltage 4500 V (for positive mode), and a heat block had temperature of 400°C. Full scan mass spectra were acquired from m/z 200-800 . The data was processing by software LabSolutions™.

Figure S19. LC-MS spectra of compound **1**

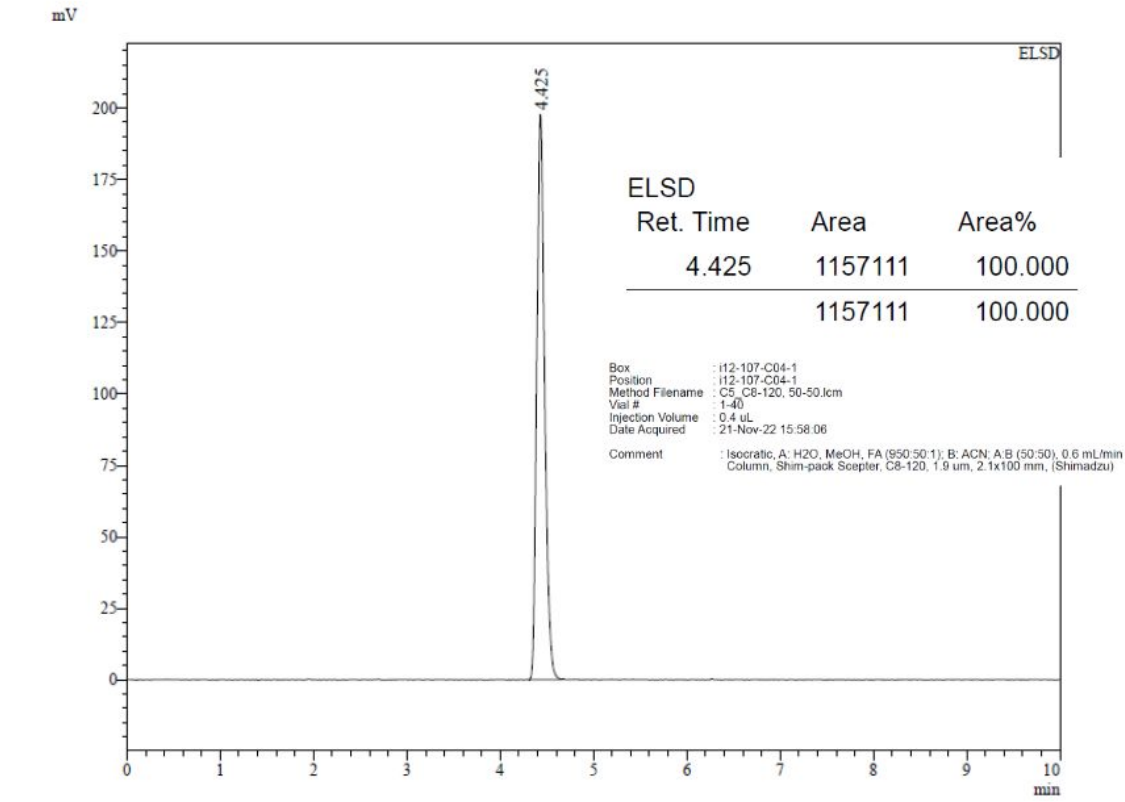

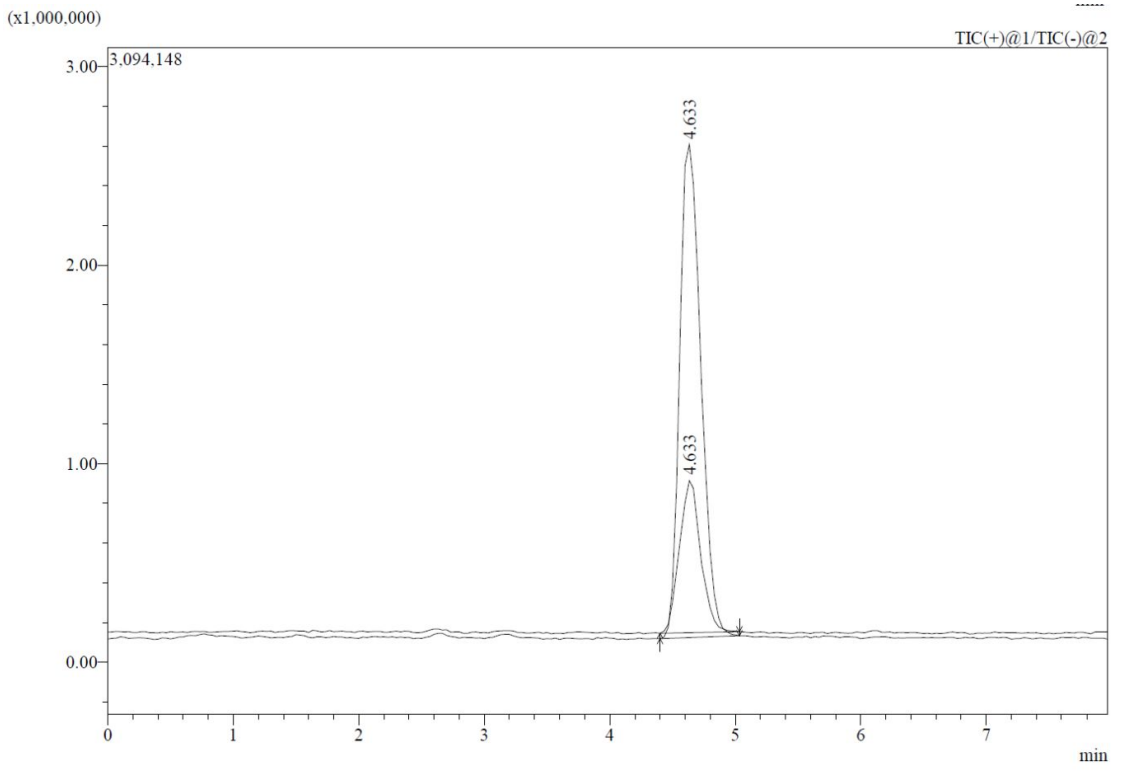

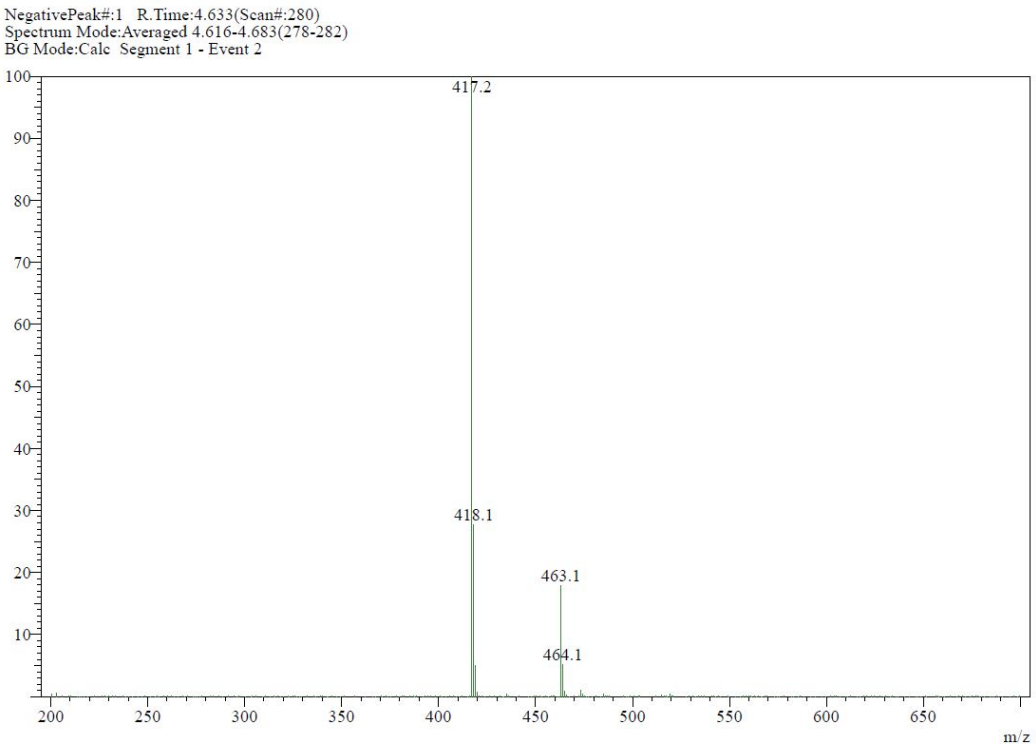

Figure S20. LC-MS spectra of compound **2**

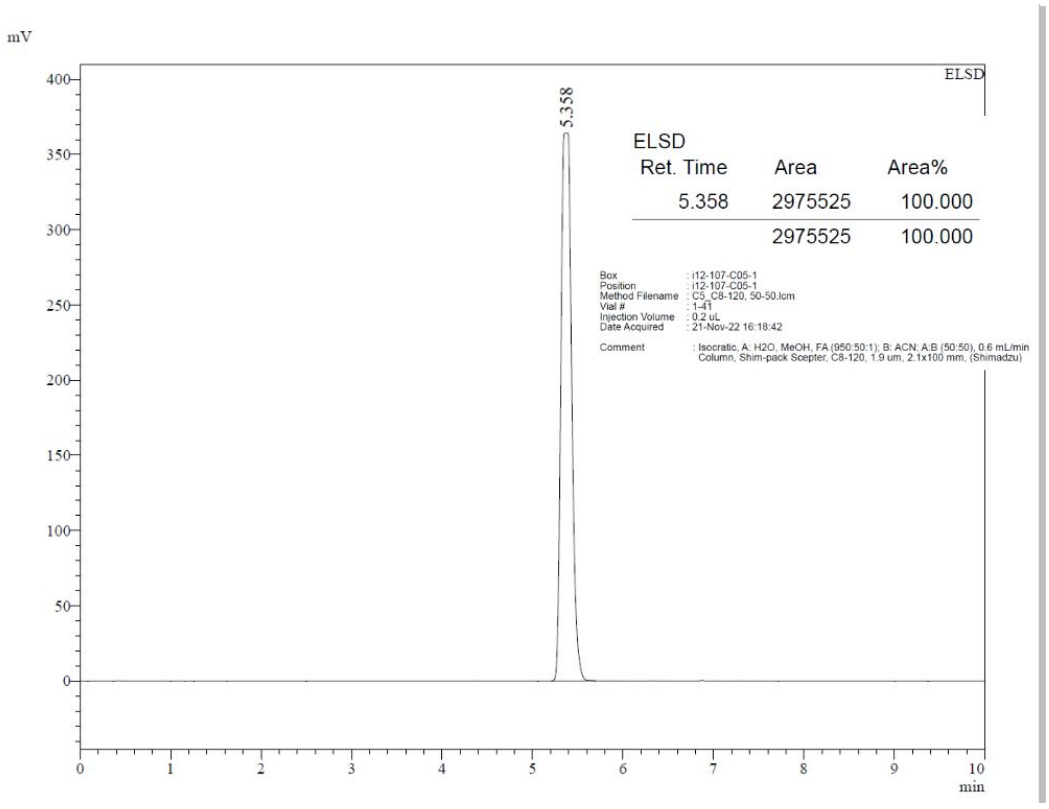

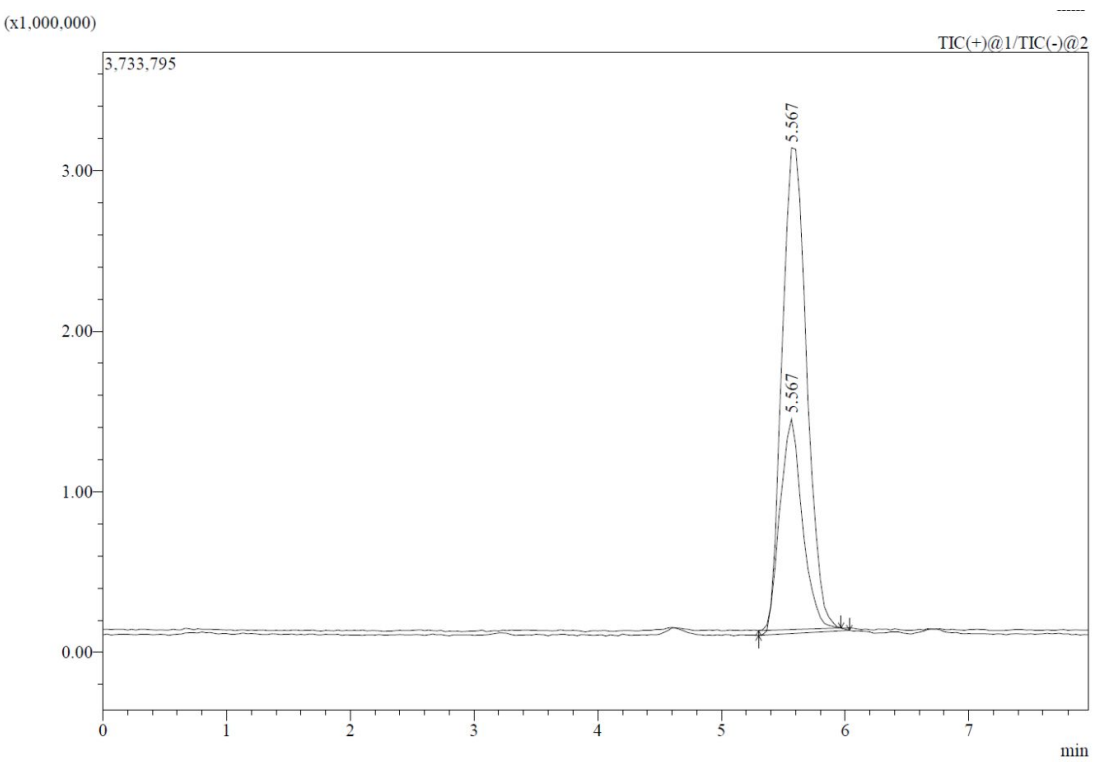

NegativePeak#:1 R.Time:5.567(Scan#:336)
Spectrum Mode:Averaged 5.550-5.616(334-338)
BG Mode:Calc Segment 1 - Event 2
Negative

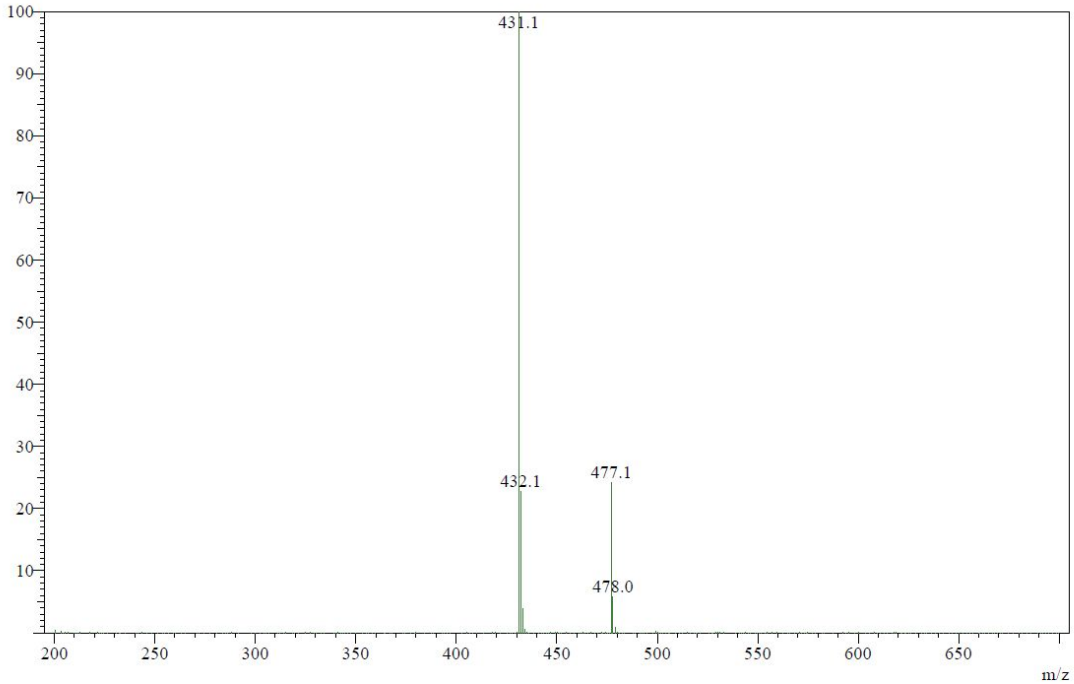

Figure S21. LC-MS spectra of compound **3**

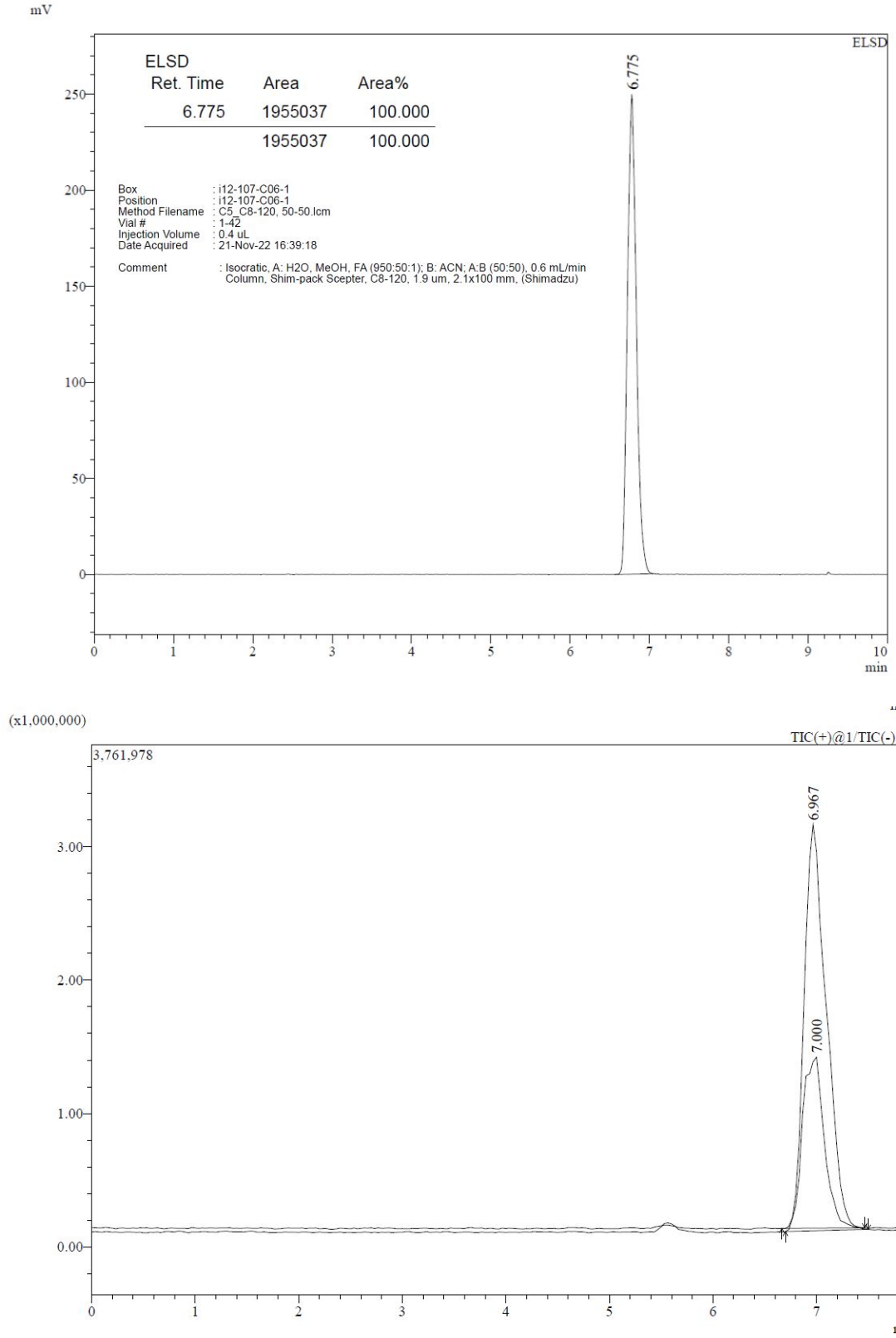

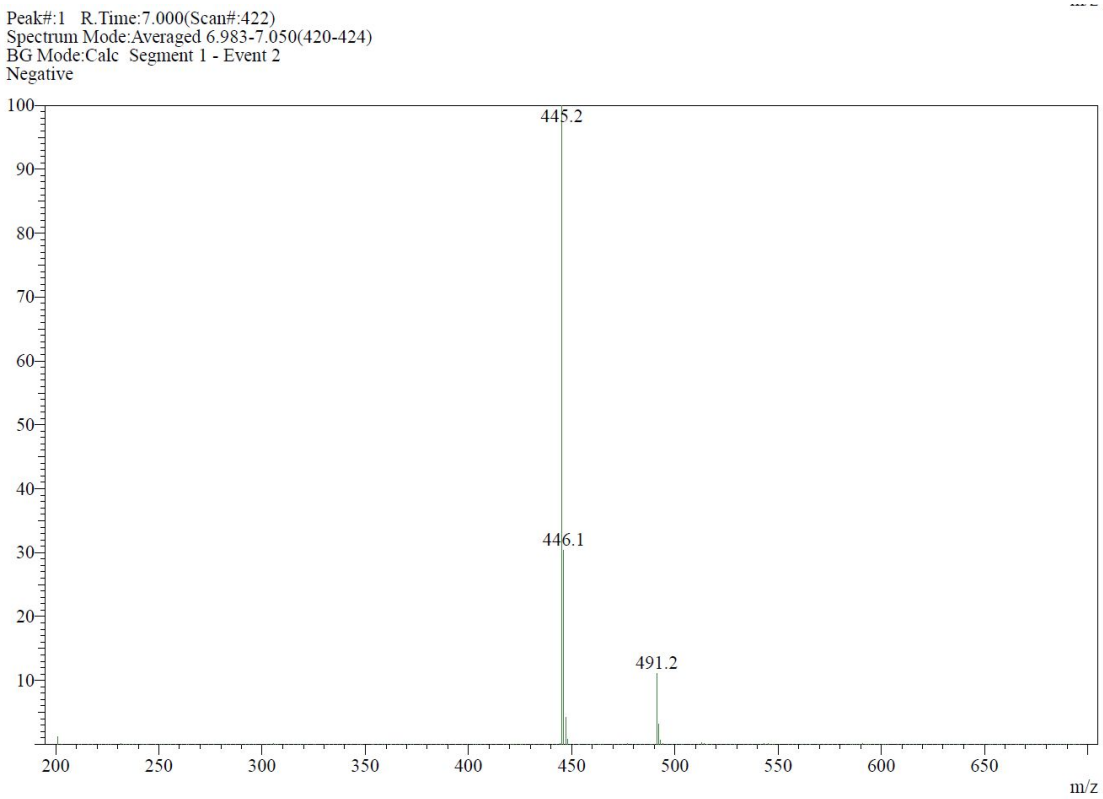

Figure S22. LC-MS spectra of compound **4**

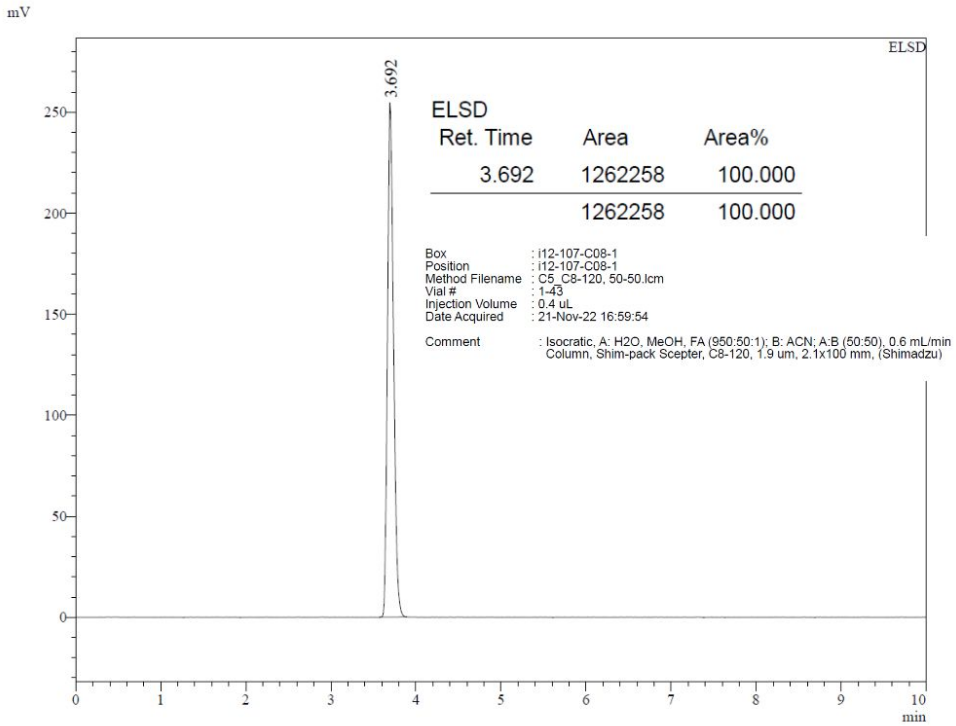

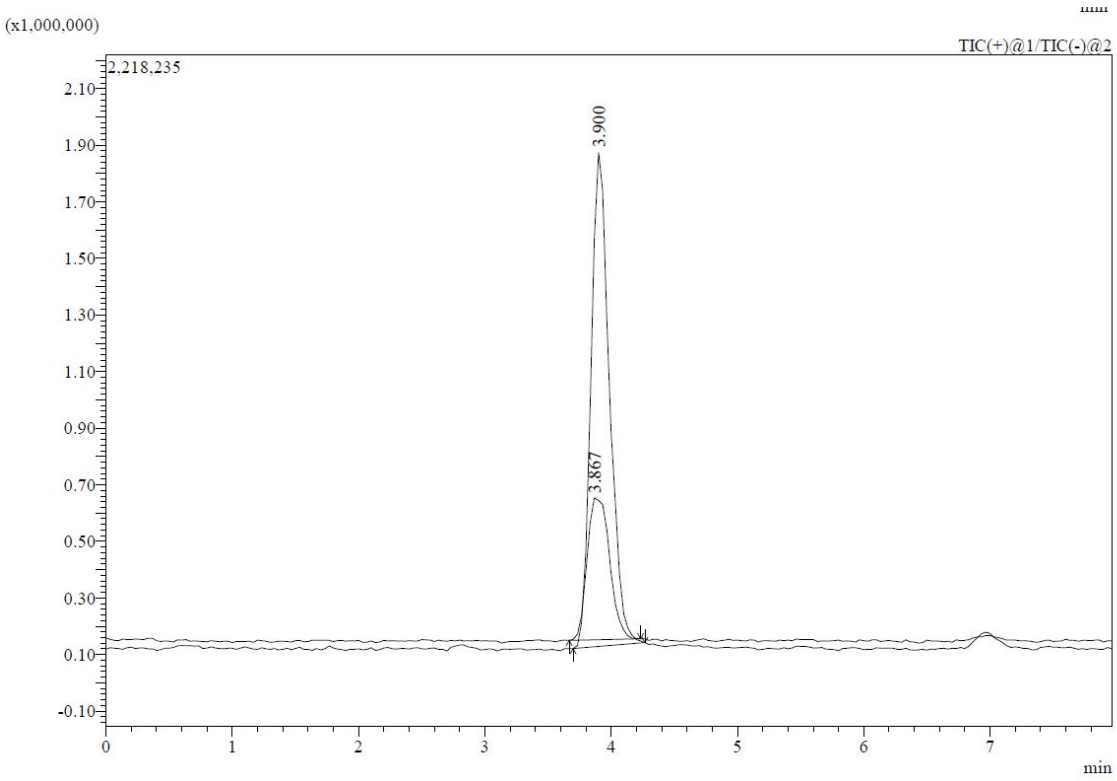

NegativePeak#:1 R.Time:3.867(Scan#:234)
Spectrum Mode:Averaged 3.850-3.916(232-236)
BG Mode:Calc Segment 1 - Event 2

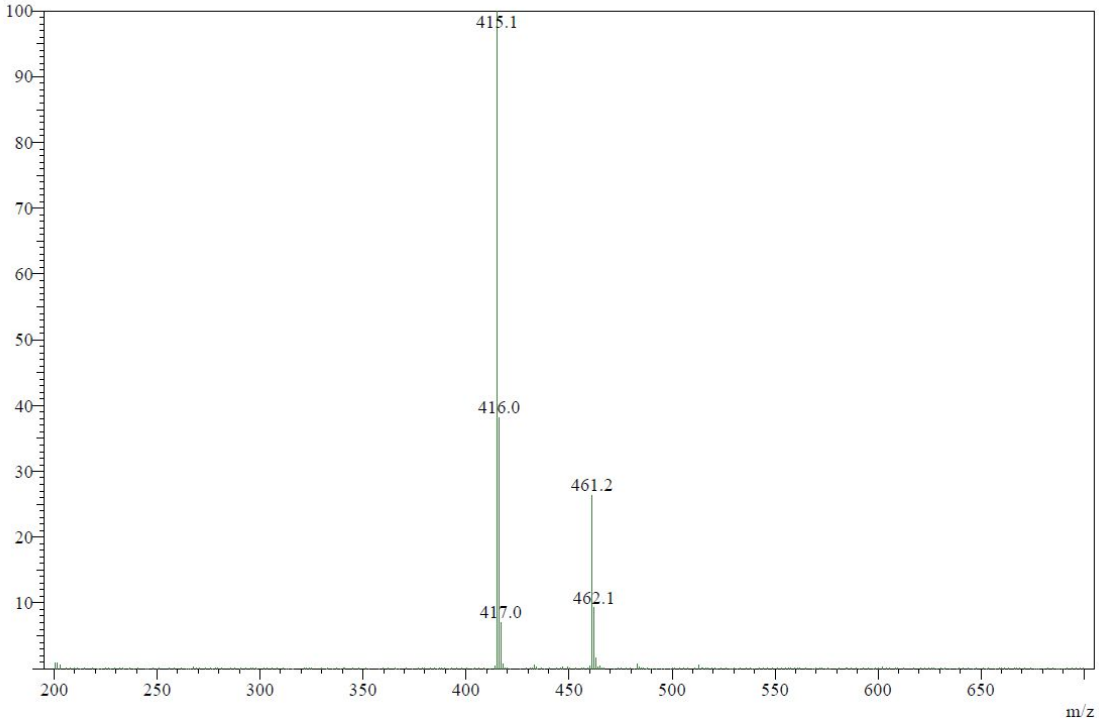

Figure S23. LC-MS spectra of compound **5**

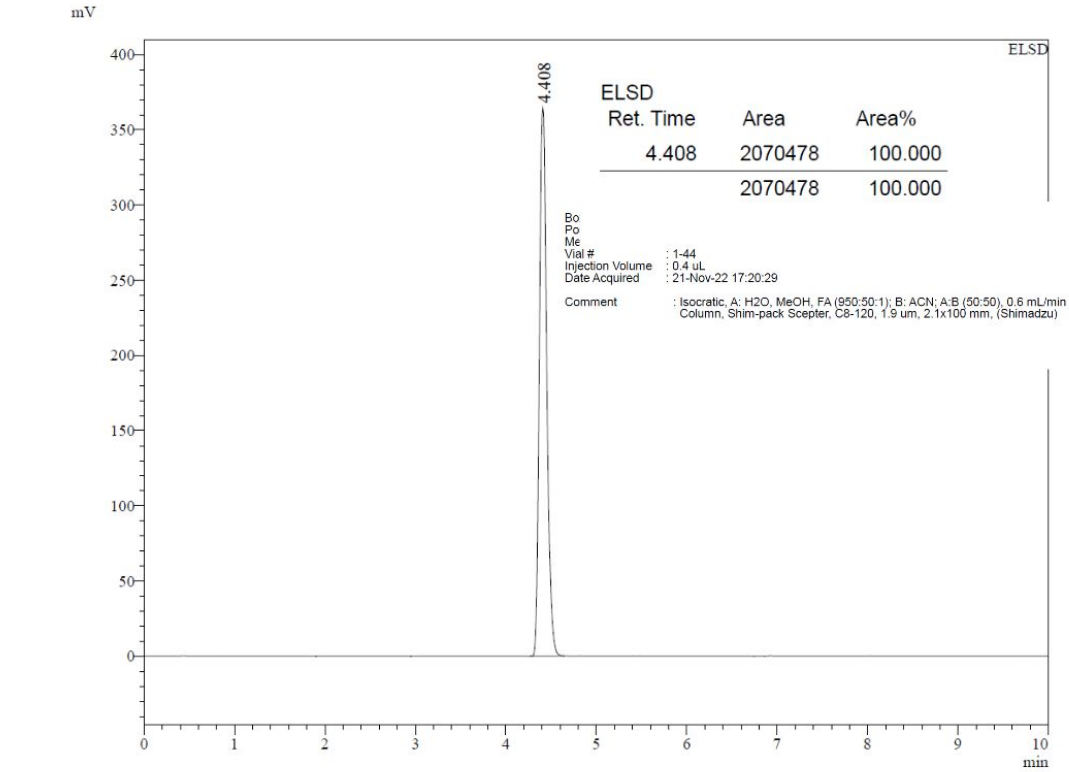

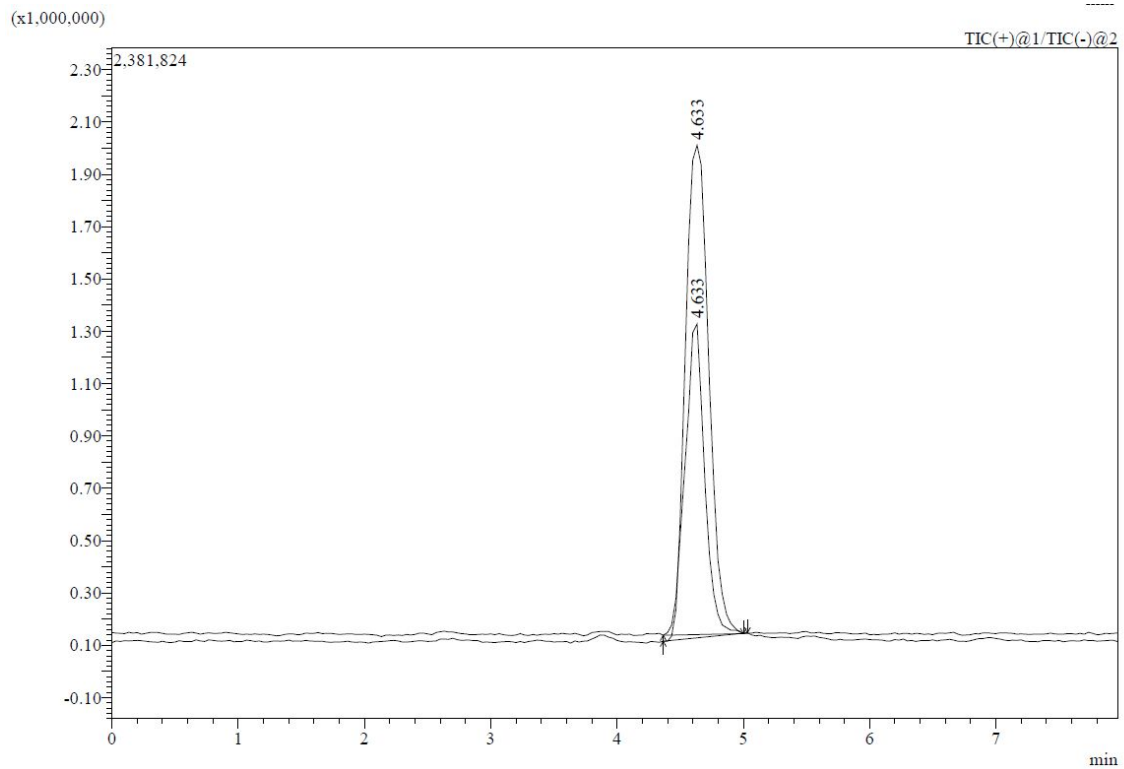

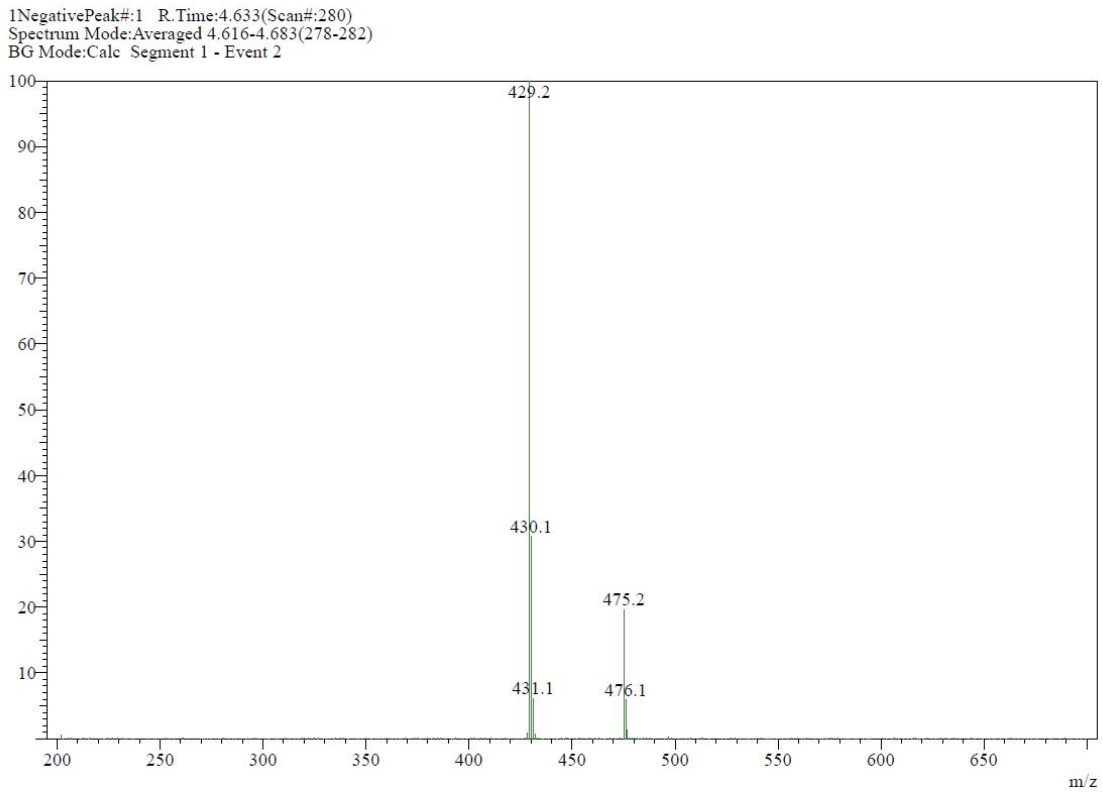

Figure S24. LC-MS spectra of compound **6**

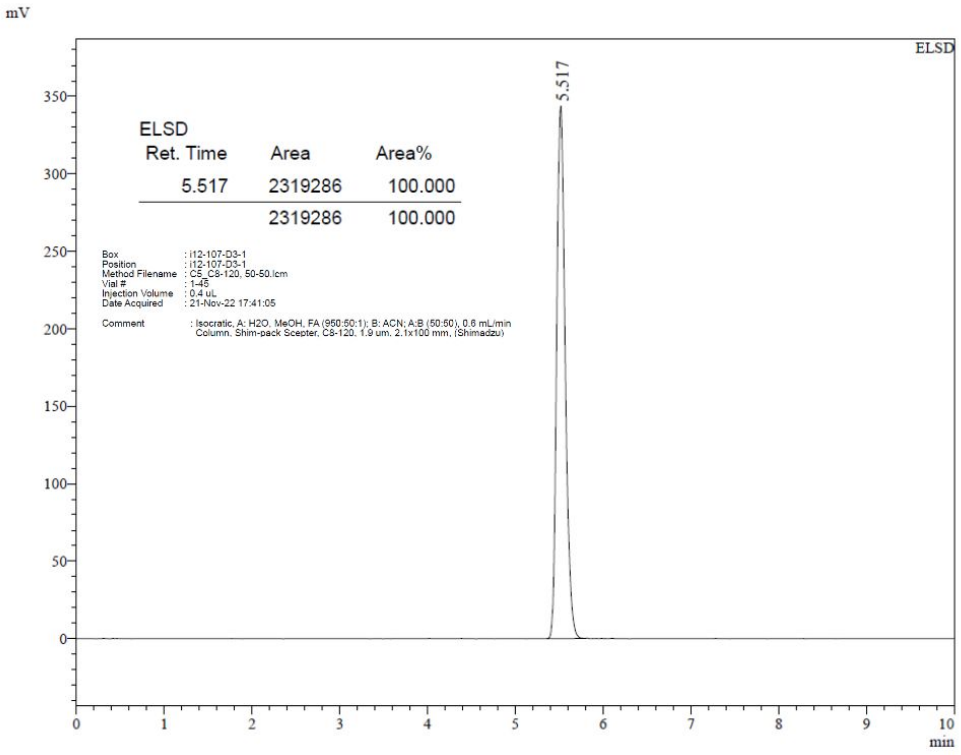

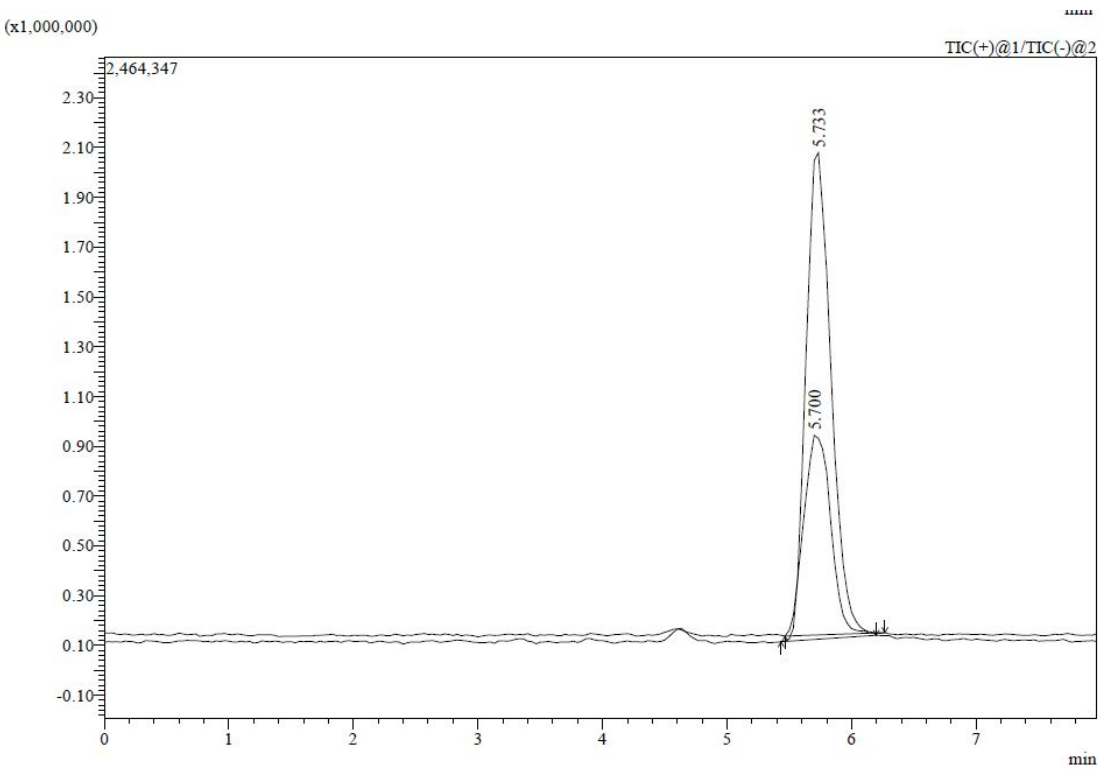

NegativePeak#:1 R.Time:5.700(Scan#:344)
Spectrum Mode:Averaged 5.683-5.750(342-346)
BG Mode:Calc Segment 1 - Event 2

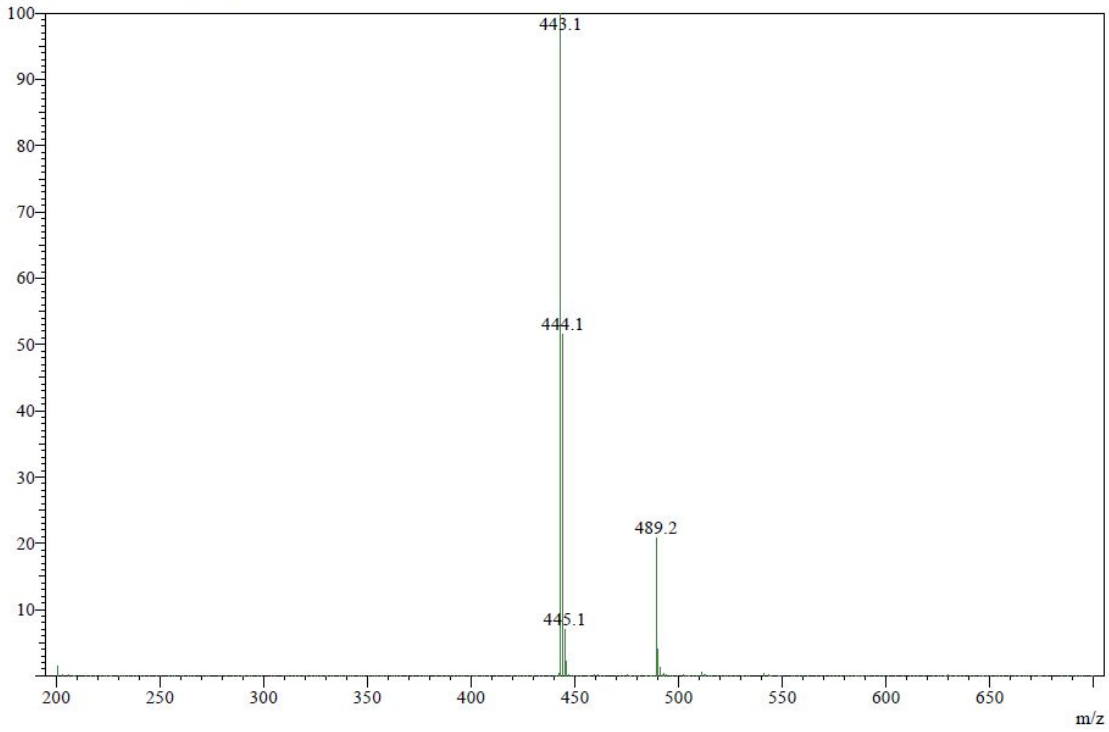

2 *In vitro* results

Table S1. *In vitro* inhibitory ability of the steroidal standards. Inhibition of 17β-HSD10 activity in the presence of the steroids at concentrations of 10 μM and 1 μM using 17β-estradiol as substrate. Values represents means ± SD (n = 4).

Steroid	Inhibition at 10 μM (%) (this study)	Inhibition at 1 μM (%) (this study)	Inhibition at 1 μM (%) Ayan et al. 2012
pregnenolone	5.9 ± 0.8	0.0 ± 3.1	11 ± 2.6
testosterone	15.7 ± 3.8	10.3 ± 5.1	0.0 ± 3.2
dihydrotestosterone	6.3 ± 2.0	0.0 ± 2.2	15 ± 0.8
androsterone	0.0 ± 2.4	3.2 ± 2.2	7.0 ± 5.9
epi-androsterone	7.0 ± 2.5	2.0 ± 4.9	6.0 ± 1.0
dehydroepiandrosterone	6.6 ± 3.5	5.4 ± 3.7	0.0 ± 3.2

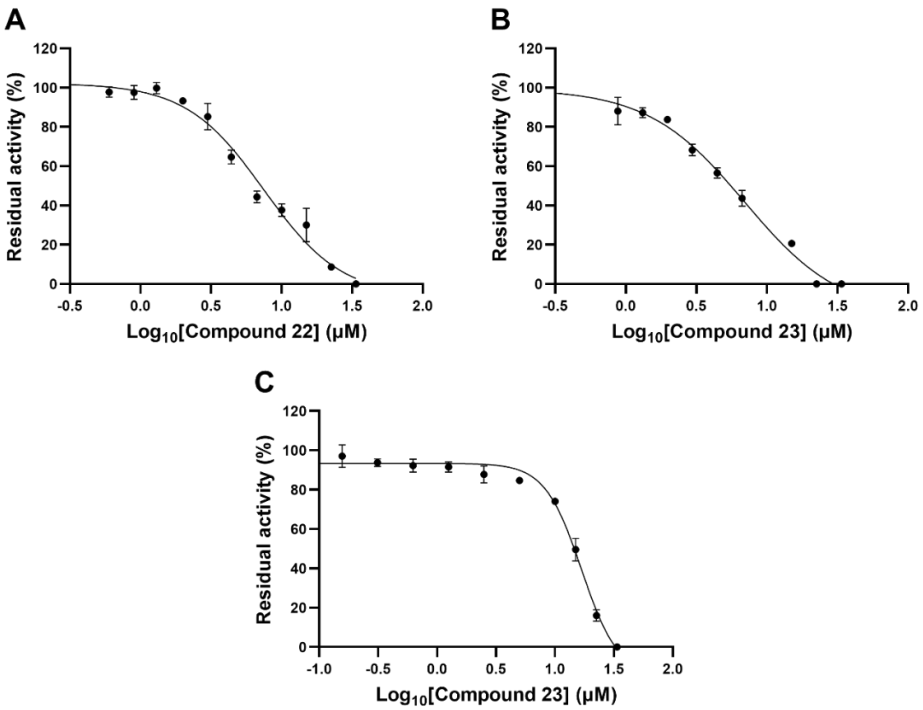

Figure S25. Dose-response curve for compound **23** (A and C) and compound **22** (B). The IC_{50} value with 17β-estradiol as substrate was determined 6.95 ± 0.35 μM for compound **22** (A) and 5.59 ± 0.25 μM for compound 23 (B). The IC_{50} value for compound **23** with allopregnanolone as substrate was determined 15.25 ± 0.39 μM (C). Presented data are shown as mean ± SEM (n = 4).